Divergent Chemistry of Ditetrelynes (E_2R_2, E = Si, Ge) with Late Transition Metals and Low-valent Silicon Precursors

Dissertation

Submitted in fulfillment of the degree

doctor rerum naturalium

(Dr. rer. Nat.)

of

The Faculty of Mathematics and Natural Sciences

of

The Rheinische Friedrich-Wilhelms-University of Bonn

By

Prasenjit Palui, M.Sc.

From Arambagh, West Bengal, India

Bonn, 2024

Prepared with the consent of the Faculty of Mathematics and Natural Sciences of the Rheinische Friedrich-Wilhelms-Universität Bonn.

Thesis committee members:

Prof. Dr. Alexander C. Filippou (Reviewer and Supervisor)

Prof. Dr. Alessandro Bismuto (Reviewer)

Prof. Dr. Matthias Wagner (External Reviewer)

Prof. Dr. Drik Menche (Examiner)

Prof. Dr. Diana Imhof (Examiner)

Work-period of this Doctoral Thesis: October 2018 to June 2023

Date of dissertation defense: 5th June, 2024

Year of Publication: 2024

Acknowledgements

It is a great pleasure to express my sincere gratitude to **Prof. Dr. Alexander C. Filippou** for giving me the opportunity to work in his well-equipped laboratory on this highly challenging research topic and also for his excellent guidance, rigorous training, and helpful advices during the course of my work. I express my deepest respect to him not only for his guidance throughout my Ph.D. career and to proof-read my dissertation, but also for his motivation and inspiration towards my future endeavors. In this context, I would also like to thank Dr. Ujjal Das for his enormous encouragement and support throughout the progress of my dissertation by many valuable suggestions.

I would like to extend my thanks to:

- The NMR department, Dipl.-Ing. Karin Prochnicki, Hannelore Spitz, Ulrike Weynand and Dr. Senada Nozinovic for recording solution NMR spectra and for their guidance in the recording of countless variable temperature measurements.

- Kerstin Kühnel-Lysek, Hannelore Spitz, Anna Martens, Charlotte Rödde and Dr. Sabine Rings for the preparation and measurement of the elemental analysis samples.

- Dr. Gregor Schnakenburg and Charlotte Rödde for the X-ray crystallographic measurements and molecular structure solutions.

- Dr. Gregor Schnakenburg, Jens Rump, and Leonard Maurer for the quantum chemical calculations to make us understand the nature of the electronic structure of my compounds. Additionally, I thank Dr. Gregor Schnakenburg for his patience to go through the whole thesis to proof read it and made valuable corrections and suggestions wherever it required.

- Leonard Maurer and Jens Rump for the UV-Vis and cyclic voltammetry measurements, respectively.

- Dr. Jürgen Tirrée for the competent technical support and for keeping the lab functioning properly.

- All research group members (specially Fabian, Sandeep, Kanishk and Tobias) for the friendly atmosphere and productive scientific and non-scientific discussions.

- The University of Bonn for providing infrastructure and the financial support of this work.

- All my friends, mentors and well wishers for their encouraging words, and constant support.

Expressing my deep gratitude to my family for their unwavering support, care, love, and affection across every phase of my life. Their good wishes, immense patience, and sacrifices have been instrumental in all my studies. A heartfelt thanks to the incredible women in my life, my MOM and PAMPA, whose inspiring love and constant emotional support have truly made all the difference.

Finally, I express my gratitude to the Almighty God, bowing down for granting me the health and energy to successfully complete this work.

The characteristic of scientific progress is our knowing that we did not know

— Gaston Bachelard

Contents

1. Introduction

Carbon, often referred to as the "element of life," is the cornerstone of organic chemistry. Carbon nanotubes, graphene and all the nanomaterials derived from it showed extraordinary electrical, thermal, and mechanical properties, with promising applications in various fields, including electronics and materials science. Silicon is the second most abundant element in the Earth's crust after oxygen, comprising approximately 26.3 % by weight.[1] This abundance makes it a readily available resource for various industrial applications. It is widely used for the production of transistors, diodes and photovoltaic solar cells.[2] The immediate heavier homologue of silicon, germanium is often referred as a "semiconductor pioneer", although in modern electronics, it is less prominent than silicon but played a crucial role in the early development of transistors and the semiconductor industry. It has also found applications in optoelectronic devices such as infrared detectors and optical fibers.[3] Despite the usual common trends observed along a group of the periodic table, it has become evident that the heavier counterparts within the same group exhibit markedly distinct behaviors when compared to their lighter homologues. This phenomenon is particularly pronounced among the group 14 elements.[4] These variations can be attributed to the considerably lower electronegativities of the heavier elements, combined with a growing disparity in the sizes of their respective s and p valence orbitals[4] and resulted an increasing disinclination for these elements to engage in the formation of hybrid orbitals.[5,6]

1.1. Structure and bonding of heavier group-14 alkyne analogues, the "ditetrelynes"

Alkynes are widely known with their distinctive triple bond structure, and used as versatile tools in organic synthesis. It also holds a pivotal position in materials science, contributing to the development of conjugated polymers and organic semiconductors. Their extended π-electron systems making them vital in modern electronic devices like OLEDs.[7]

In contrast to alkynes, synthesis of its heavier counterparts (ditetrelynes, E = Si-Pb) (***Figure 1***) remained very challenging due to the requirement of sterically demanding substituents for the kinetic stabilization of E≡E triple bond. The first heavier homologue of alkyne was reported in 2000 by P. P. Power and co-workers upon isolating the first diplumbyne $Ar^{Tip}PbPbAr^{Tip}$ (Tip = C_6H_2-2,4,6-^{i}Pr$_3$) from the reaction of PbBr(C_6H_3-2,6-Trip$_2$) with $LiAlH_4$.[8] Two years later, the germanium and tin analogues, digermyne $Ar^{Dipp}GeGeAr^{Dipp}$ (Dipp = C_6H_3-2,6-^{i}Pr$_2$)[9] and distannyne

$Ar^{Dipp}SnSnAr^{Dipp}$,[10] were reported by the same group. The series was finally completed in 2004, when Sekiguchi and his co-workers isolated the first disilyne RSiSiR (R = Si{(CH(SiMe$_3$)$_2$^{i}Pr).[11] It is important to highlight that in 2002 Wiberg and co-workers had already hypothesised the existing of such a species, (RSiSiR (R = Si{Si(^{t}Bu)}$_3$Me)),[12,13] however no structural evidence was found.

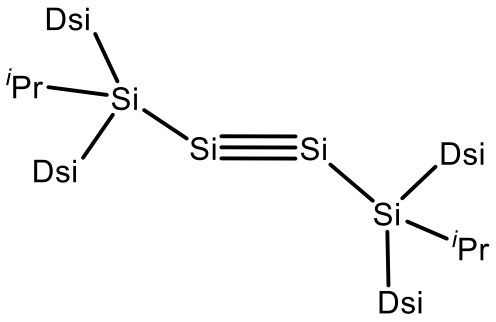

Sekiguchi, 2004

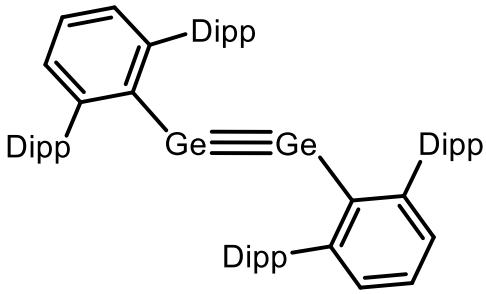

Power, 2002

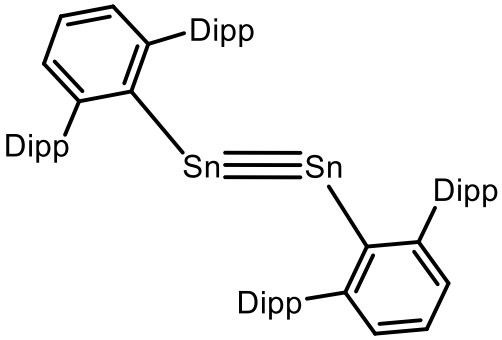

Power, 2002

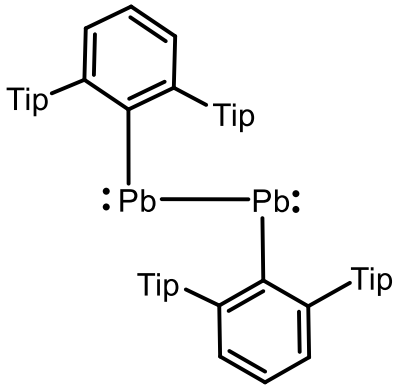

Power, 2000

Dsi = CH(SiMe$_3$)$_2$, Dipp = C$_6$H$_3$-2,6-^{i}Pr$_2$, Tip = C$_6$H$_2$-2,4,6-^{i}Pr$_3$

Figure 1. First examples of the structurally characterized ditetrylines.

The notable structural contrast between alkynes and their heavier group 14 element counterparts can be explained using the Carter-Goddard-Malrieu-Trinquier (CGMT) model (***Figure 2***).[14–16] According to this model, when two E–R (E = C – Pb) fragments combine in a quartet state, a linear structure with a triple bond is observed. Conversely, a trans-bent geometry is observed when two E–R fragments combine in a doublet state.[6] The E–R fragments initially exist in a doublet ground state, and the determination of the geometry of R–EE–R species relies on the energy difference, specifically, it hinges on the energy required to excite two doublet E–R fragments into the quartet state ($2\Delta E_{D\rightarrow Q}$) compared to the energy gained from the emergence of two

π-bonds ($E_{2\pi}$). In broader sense, for the C–R fragments, the energy associated with $E_{2\pi}$ surpasses that of $2\Delta E_{D\rightarrow Q}$, resulting in a linear structure. Conversely, for E–R fragments where E = Si - Pb, the energy $E_{2\pi}$ is lower than $2\Delta E_{D\rightarrow Q}$, leading to the adoption of a trans-bent geometry.

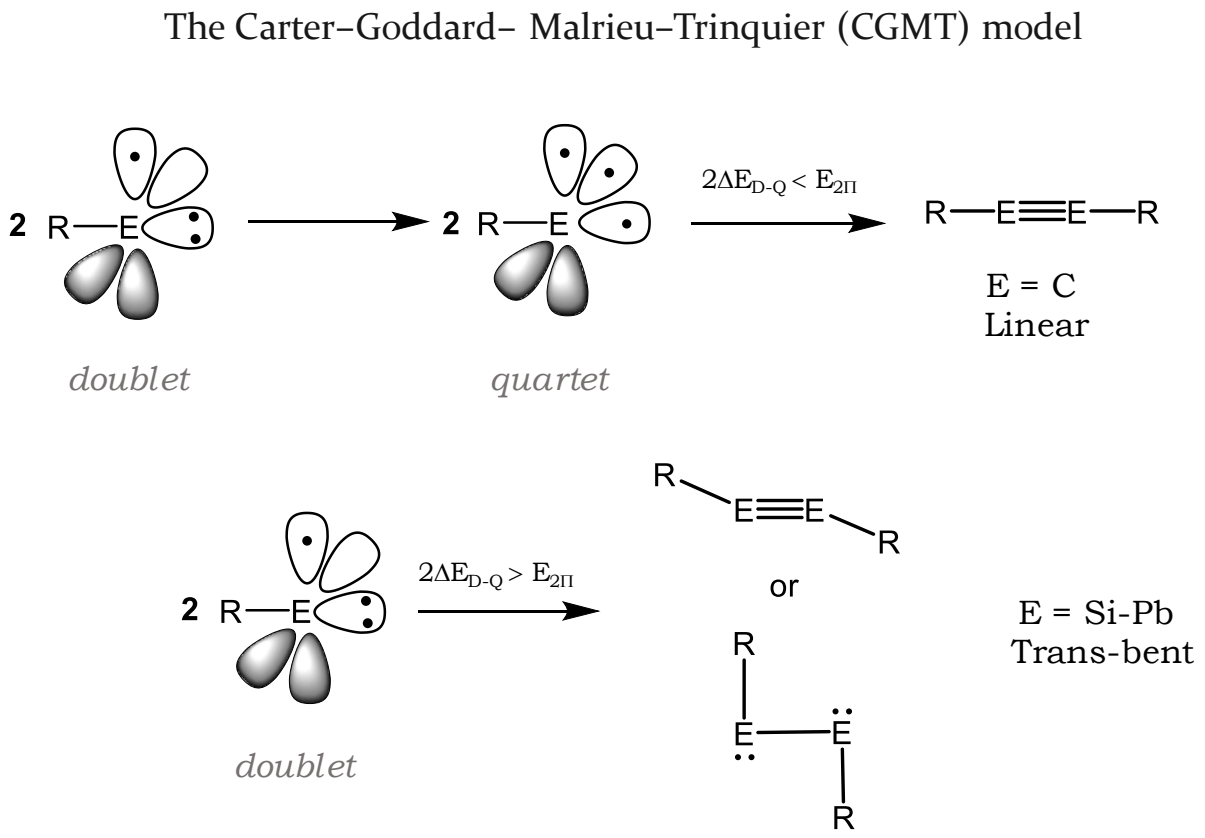

Figure 2. Representation of the contrast between the linear and trans-bent geometries of alkynes and their heavier group 14 element counterparts as per the CGMT model.

The observed deviations in geometry, transitioning from linear to bent structure, in multiply bonded heavy main group element analogues of alkyne, can also be comprehended through a second-order Jahn–Teller (SOJT)[17] perspective (***Figure 3***). The structural distortions are a result of the interaction between the highest occupied molecular orbital (HOMO) and an unoccupied orbital (LUMO+1). This interaction stabilizes the HOMO while simultaneously destabilizing the vacant LUMO+1 orbital, leading to the nonbonding electron density. This excess of electron density triggers geometric distortions due to an interelectronic repulsion. This phenomenon is more pronounced in heavier species due to their generally weaker bonds, which allow for closer molecular-level interactions. This interaction is inversely correlated with the orbital energy difference and depends on the electronegativity of the substituents.[17]

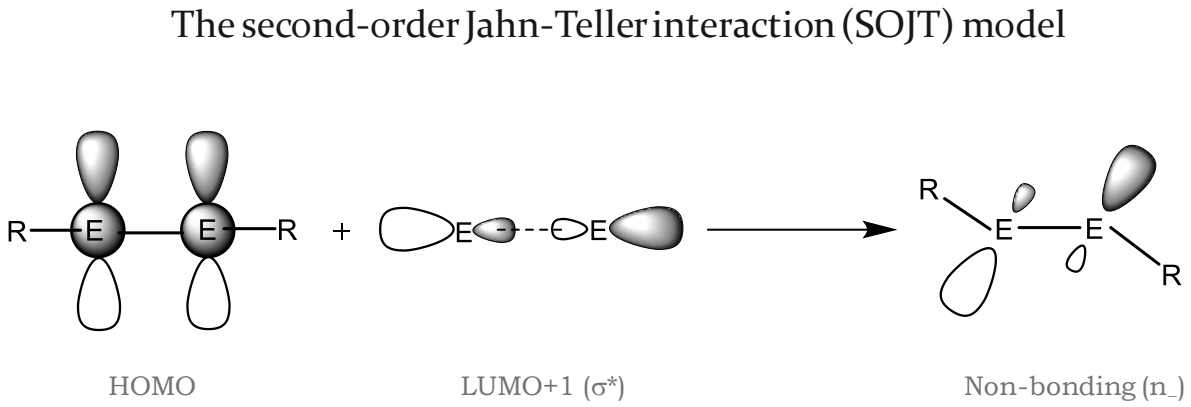

Figure 3. Orbital mixing in heavier alkynes as a result of SOJT interaction.

In the following years, the successful synthesis of compounds bearing similar structural motif extended to a broader range of disilynes,[18–22] digermynes[23–29] and distannynes.[24,28,30–32] Furthermore, investigation on their reactivity demonstrated some notable chemistry including the activation of small molecules,[33] C–C coupling reaction,[22] and even have an example where a digermyne acted as a catalyst in the regioselective cyclotrimerization reaction of terminal alkynes.[34]

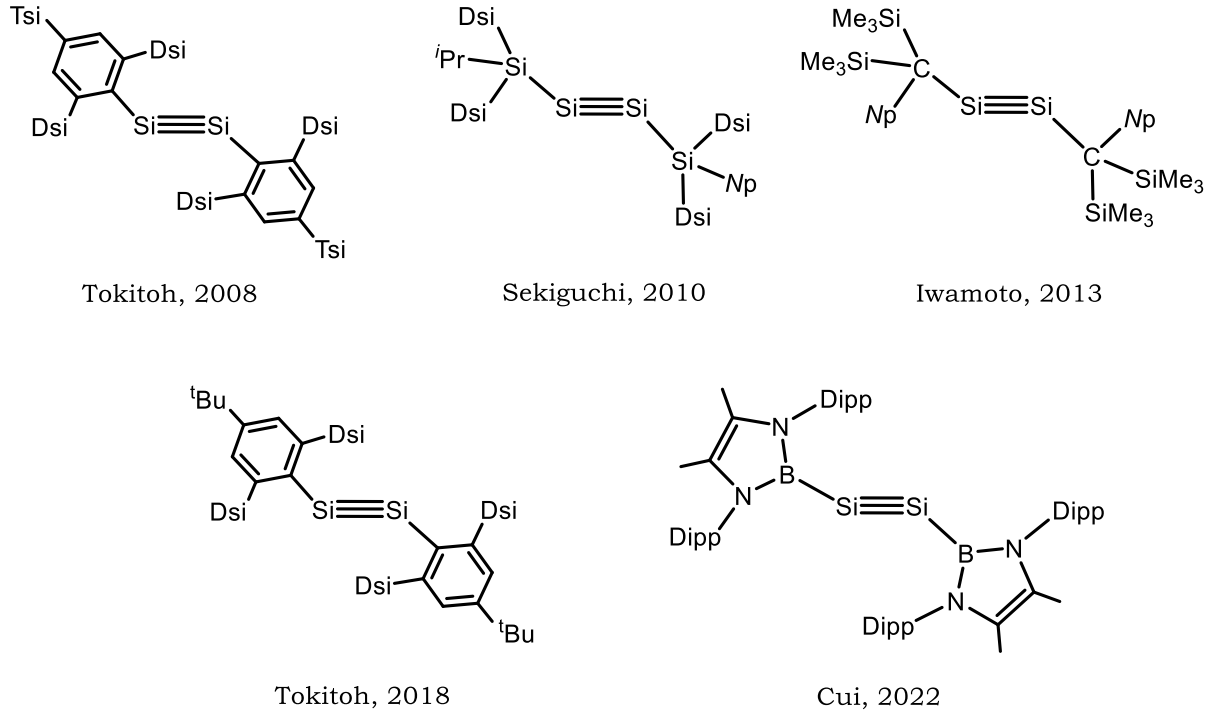

Dsi = $CH(SiMe_3)_2$, Tsi = $C(SiMe_3)_3$, Np = $CH_2{}^tBu$, Dipp = C_6H_3-2,6-$^iPr_2$

Figure 4. Chronological order of evolution of disilynes over the years.

1.2. Unsaturated metallacycles in heavier group-14 chemistry

In carbon chemistry, unsaturated metallacycles or metallacyclopolyenes are known to be involved as reactive intermediates in numerous transition metal mediated stoichiometric and catalytic transformations of alkynes, such as, alkyne hydro-functionalization, C–C coupling reactions, cyclotrimerization, alkyne metathesis and polymerization.[35–39] These metallacycles typically contain unsaturated MC_n rings of the type **I** – **IV** (M = transition metal, n = 2 – 5) and their structure, bonding and reactivity have been extensively studied and thoroughly reviewed attesting them to be an important class of metallacycle.

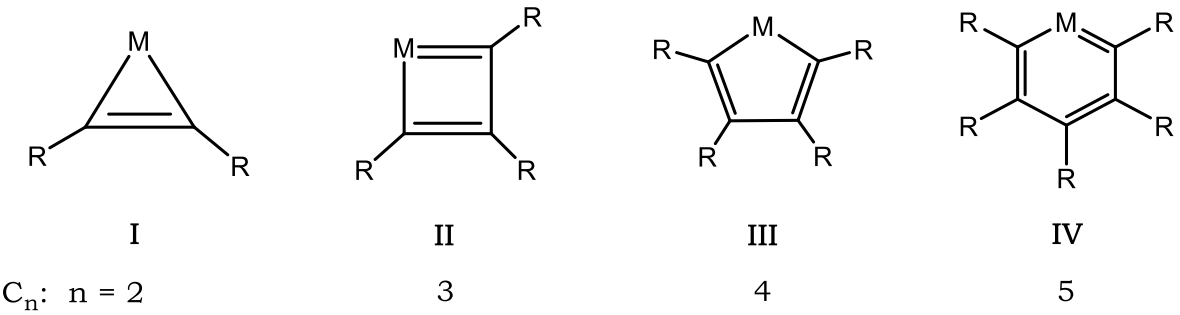

Figure 5. A general representation of metallacyclopolyenes (**I** – **IV**) containing unsaturated MC_n rings (M = any transition metal).

In comparison, chemistry of metallacycles containing M and heavier group 14 elements (E = Si - Pb) as the only hetero ring-atoms are most commonly found in 1-metallacyclotetrelanes, the heavier analogues of metallacycloalkanes and in 1-metalla-2,5-bistetrelacyclopent-3-enes - the heavier analogues of metallacyclopent-3-enes.[40–48] These metallacycles contain $R_2E–M–ER_2$ (R = ring substituent) linkages featuring four coordinated tetrel centers, thus are not considered as metallacyclopolyenes.

Recent developments in coordination chemistry of compounds containing low-valent heavy tetrels have led to the isolation of heavier metallacycles containing three-coordinated tetrel centers in unusual coordination geometry and oxidation states (**I-1** to **I-8**).[49,20,50–56] The current state-of-the-art of low-valent Ge or Si-compounds show that Ge/Si-metallacyclopolyenes featuring RE–M–ER (E = Si, Ge, R = ring substituent) linkage are rather rare, the Ag(I)-complex $[AgGe_2(Ar^{Dipp})_2][SbF_6]$ (Ar^{Dipp} = C_6H_3-2,6-(C_6H_3-2,6-$^i Pr_2$)$_2$) (**I-1**) (***Figure 6***, *top*) represents the example that features a significantly low type-**I** metallacyclic character.

Unsaturated metallacycles reported by other research groups

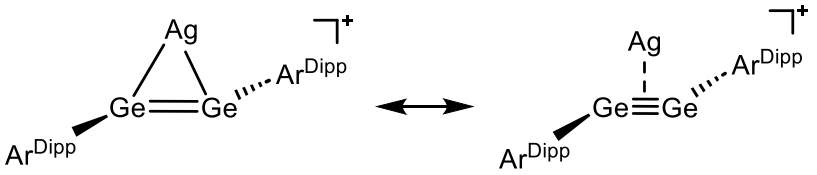

metallacycle (minor) I-1 π-complex (major)

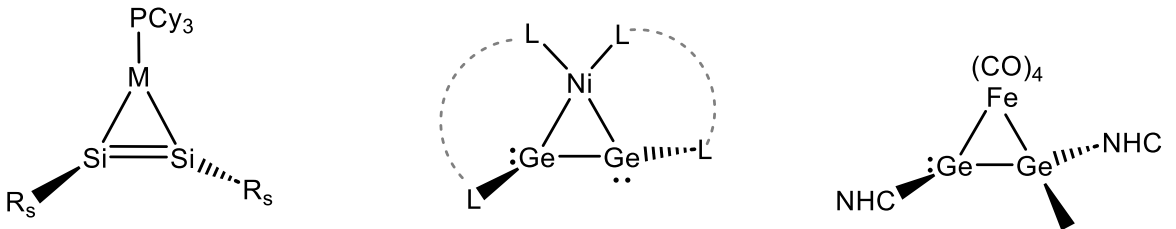

I-2 (M = Pd, Pt) I-3 I-4

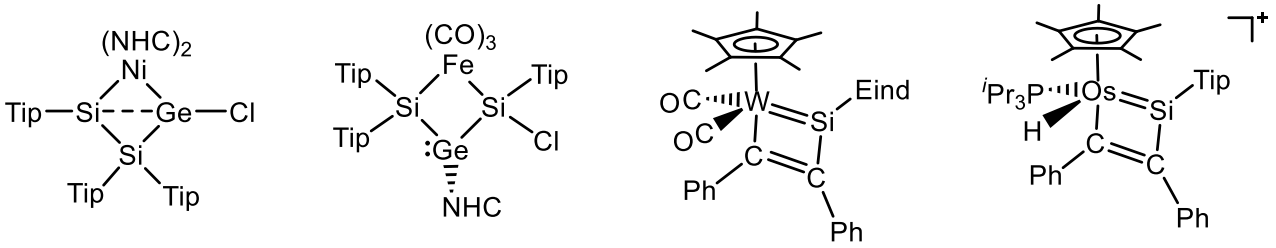

I-5 I-6 I-7 I-8

Contribution from Filippou and coworkers

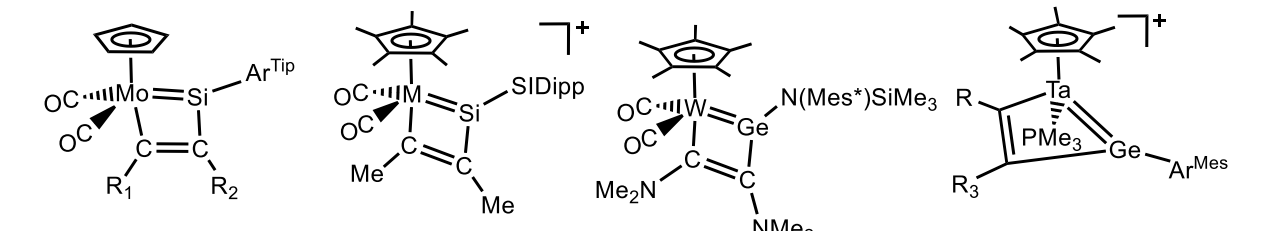

$R_1 = R_2$ = H, Me, Et, NMe_2, NEt_2
R_1 = Ph, R_2 = NMe_2

M = Cr, Mo

R = R_3 = H, Me
R = Me, R_3 = Ph

I-9 I-10 I-11 I-12

Ar^{Dipp} = C_6H_2-2,6-(C_6H_2-2,6-^{i}pr$_2$)$_2$; R_s = $C(SiMe_3)_2(CH_2CMe_3)$; L---L = bis(Si[(N^tBu)$_2$C(Ph)])xanthene; NHC = C[N(^{i}Pr)C(Me)]$_2$; Tip = C_6H_2-2,4,6-^{i}Pr$_3$; Eind = 1,1,3,3,5,5,7,7-octaethyl-s-hydrindacene-4-yl; Ar^{Tip} = C_6H_2-2,6-(C_6H_2-2,4,6-^{i}Pr$_3$)$_2$; SIDipp = 1,3-bis-(2,6-diisopropylphenyl)imidazolidin-2-ylidene; Mes* = C_6H_2-2,4,6-^{t}Bu; Mes = C_6H_2-2,4,6-Me

Figure 6. Metallacycles (**I-1 – I-12**) containing low-valent heavier tetrels; formal charges are not included in the Lewis structures for simplicity; for all the cationic complexes, the corresponding counter anions are not depicted for clarity.

To date, the complex denoted as **I-2** was synthesized by phosphine/disilyne R_s–Si≡Si–R_s (R_s = $C(CH_2{}^tBu)(SiMe_3)_2$)[20] ligand exchange reaction, stand as the sole example of a type-**I** metallacycle containing two low-valent silicon centers. Furthermore, complexes **I-3**[50] and **I-4**[51] can be considered closely related to type-**I** metallacycles. In these compounds the presence of LGe–Ni–GeL (L = imidinatosilylene ligand) and Ge–Fe–Ge linkages are prominent. Within the category of type-**II** metallacycles, except **I-5**[52,53] and **I-6**[54], all others (**I-7** and **I-8**)[55,56] have been documented as products stemming from [2+2]-cycloaddition reaction involving silylidyne or germylidyne complexes with an alkyne. Notably, the majority of these contributions can be attributed to the work of Filippou and co-workers (**I-9** to **I-12**)(***Figure 6***).[i][57–59]

1.3. Transition metal-bistetrylidyne complexes (E = Ge, Sn)

In comparison to metal-carbyne chemistry, metal-bis(carbyne) complexes are exceptionally rare. This can be attributed to their intrinsic susceptibility to undergo carbyne-carbyne coupling reactions,[60–64] a phenomenon that Filippou and co-workers have been previously investigating. Their research revealed that this coupling reaction can be effectively prevented by utilizing aminocarbyne ligands. This pivotal discovery has enabled the successful isolation of the first bis(aminocarbyne) complex, [(η^5-C_5Me_5)W($CNEt_2$)$_2$(CNEt)]BF_4, which exists as a stable solid at ambient temperature.[61]

Nucleophile-induced coupling of two carbyne ligands

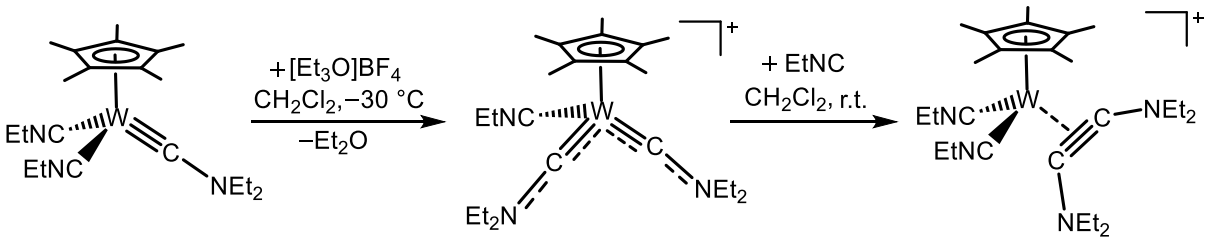

Scheme 1. Metal-centered coupling of two carbyne ligands forming an alkyne complex; the counter anion for both the cationic complexes is BF_4^-.

[i] The metallacycles (**I-9**) were thoroughly characterized and reported in the following doctoral thesis; Oleg Chernov, "Novel Molecular Si(II) Precursors for Synthesis of the First Compounds with Metal-Silicon Triple Bonds", *Dissertation*, Rheinische Friedrich-Wilhelms-Universität Bonn, **2012**.

Despite of the significant progress in molecular chemistry, particularly in the field of transition metal alkylidyne complexes and their extension to heavier carbon homologues,[65–67] it's important to emphasize that the synthesis of transition metal bis(carbyne) complexes are still sustaining with persistent challanges. Moreover, extension of this bis(carbyne) chemistry to the heavier counterparts of carbon still remains a formidable challenge. Since early 2000s, Filippou and co-workers have consistently focussed on developing the chemistry of transition metal-tetrylidyne complexes (tetrel = Si-Pb). Their efforts have led to significant progress in comprehending the syntheses, bonding nature and reactivity of these intriguing species,[65,66] including few steps on bis(tetrylidyne) complexes too.[68,69] Taking the advantage of the reactivity of a mono-tetrylidyne complex ([(η^5-C_5H_5)(PMe_3)$_2$Mo≡$SnAr^{Mes}$]),[ii] the first bis(tetrylidyne) complex was synthesized.

The complex [(η^5-C_5H_5)(PR_3)$_2$Mo≡$SnAr^{Mes}$)] (R = Me, Et) exhibits selective reactivity when reacted with an equimolar quantity of chlorostannylene Sn(Ar^{Mes})Cl. This reaction results in the formation of [(η^5-C_5H_5)(PR_3)$_2$Mo(=SnClAr^{Mes})(≡$SnAr^{Mes}$)], which represents the first documented instance of a transition metal tetrylidene-tetrylidyne complex,[ii] as described in ***Scheme 2***. Further abstracting the halogen using a halide scavenger yielded the first heavier analogue of a metal bis(carbyne) complex, the cationic Mo(0)-bis(stannylidyne complex) [(η^5-C_5H_5)(PR_3)$_2$Mo($SnAr^{Mes}$)$_2$][A].

The first heavier analogue of bis(carbyne) complex

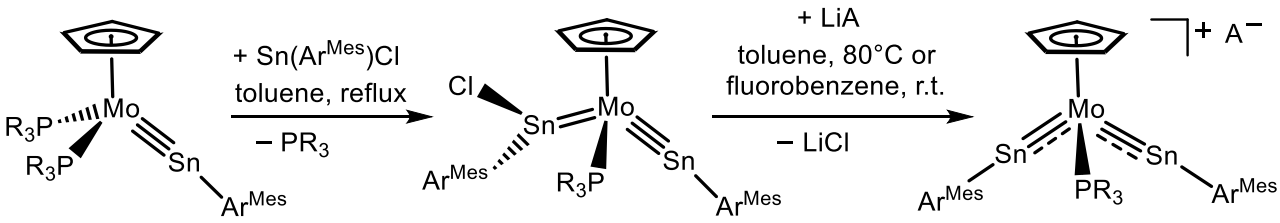

Ar^{Mes} = C_6H_3-2,6-Mes_2, R = Me, Et

A = $Al(OCH(CF_3)_2)_4$, $B(C_6F_5)_4$, $B(C_6H_5$-3,5-$(CF_3)_2)_4$

Scheme 2. Synthesis of a molybdenum stannylidene-stannylidyne complex followed by its halide abstraction yielding a cationic molybdenum(0) bis(stannylidyne) complex.

[ii] The compound is reported in the following doctoral thesis; Christoph Lindlahr, "Neuartige Tetrelaylidinkomplexe der Gruppe 6 mit Trialkylphosphanliganden", *Dissertation*, Rheinische Friedrich-Wilhelms-Universität Bonn, **2014**.

By utilizing a similar synthetic strategy (same as ***Scheme 2***), several Mo or W germylidyne and stannylidyne complexes were employed and led to the successful isolation of numerous heavier analogs of homo- or hetero-bis(carbyne) complexes of group-6 metals (***Figure 7***).[68] However, the progress has been very limited in advancing the field of bis(tetrylidyne) chemistry, whether it involves the cleavage of the triple bond of ditetrelynes at a single metal center or exploring more of the transition bis(tetrylidyne) complexes beyond those in group-6.

Neutral and cationic heavier bis(carbyne) complexes

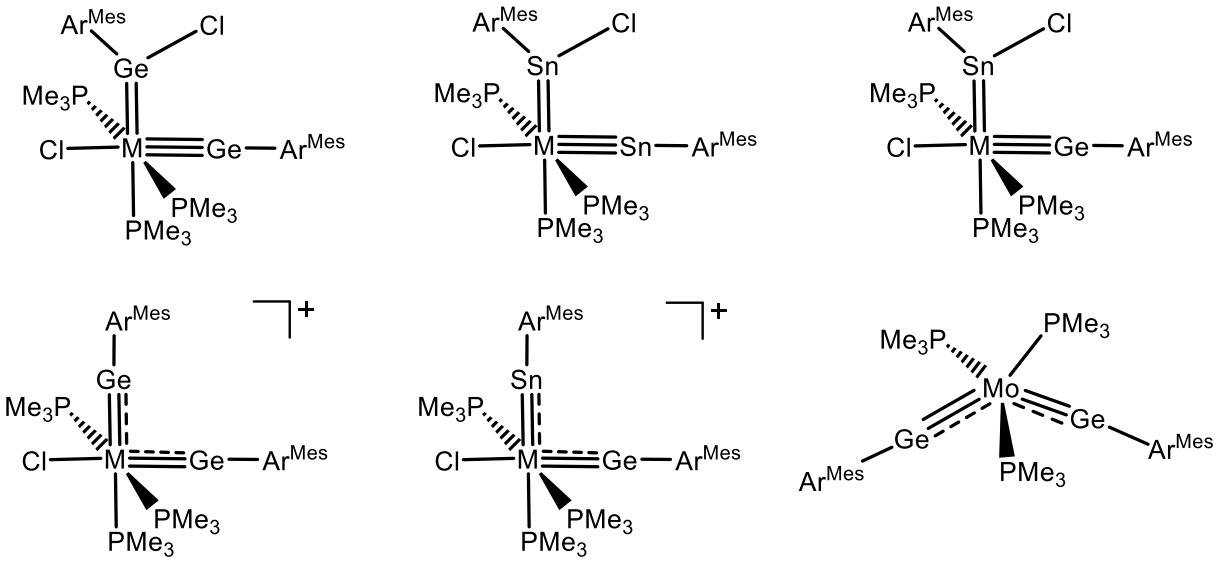

M = Mo,W; Ar^{Mes} = C_6H_3-2,6-Mes_2

Figure 7. Selected examples of heavier analogs of homo- or hetero-(carbene-carbyne) and bis(carbyne) complexes of group-6 metals.

1.4. Metathesis reactions in heavier group-14 multiple bond chemistry

The alkene and the alkyne metathesis reactions have been recognized as one of the cornerstones of organometallic chemistry. They have found extensive applications in the field of organic synthesis and even earned recognition with a Nobel Prize in chemistry in 2005.[70–75] Typically, they necessitate the Schrock or Grubbs type alkylidene or Schrock type alkylidyne complexes as catalysts. Through a sequential [2+2]-cycloaddition and cycloreversion steps (***Figure 8***), these complexes facilitate the transformation of the starting alkene or alkyne into the desired metathesized product.[71,74] In stark contrast, alkane metathesis follows a distinct path. It involves a tandem process combining dehydrogenation and olefin metathesis. In this

sequence, the olefin is first generated through dehydrogenation. Subsequently, the metathesis step takes place with the assistance of a Schrock-type alkylidene complex and finally, the reaction concludes with hydrogenation to yield the desired alkane product.[76] In contrast, the metathesis of the heavier alkene homologues proceeds via an entirely different mechanism, depending on the degree of unsaturation of the E–E bonds. For instance, ditetrelenes ($R_2E{=}ER_2$, E = Si, Ge)[77,78] undergo facile metathesis without the aid of a transition metal catalyst.

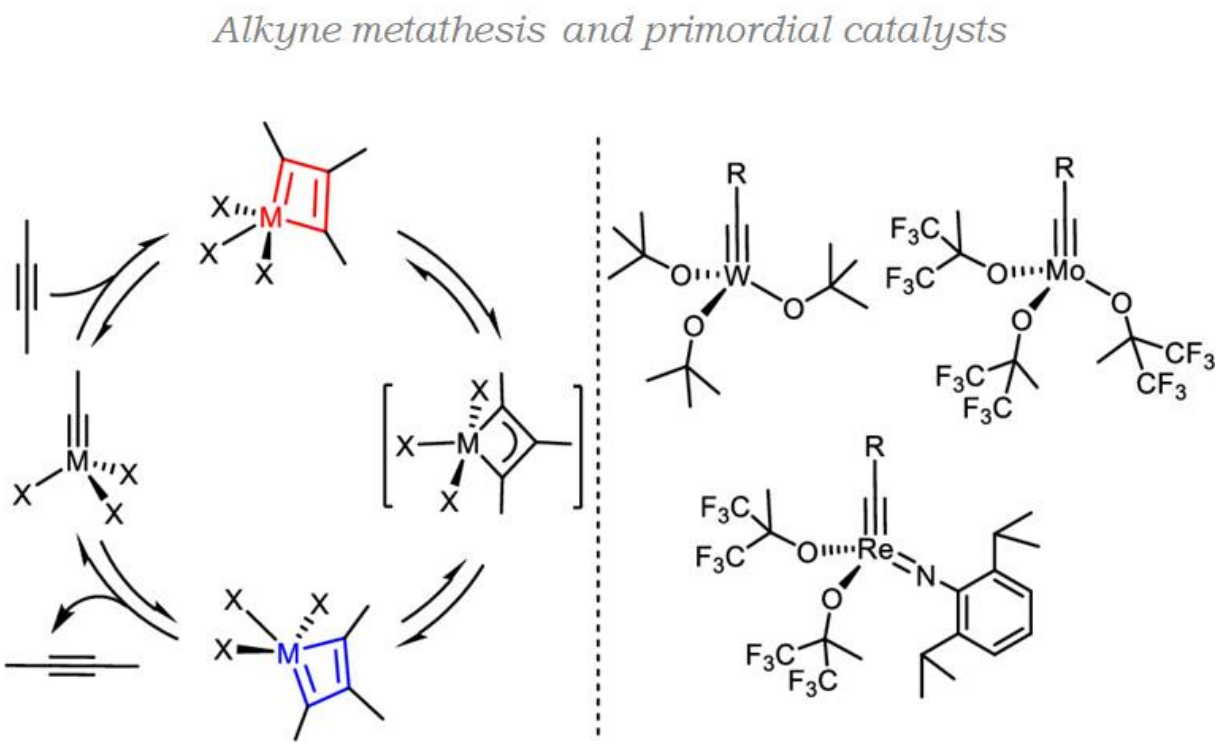

Figure 8. (*left*) General reaction mechanism of alkyne metathesis and (*right*) important catalysts used. The figure was extracted from reference [74].

In comparison to alkenes, ditetrelenes feature much weaker double bonds and are known to dissociate into singlet tetrelenes ($:ER_2$) upon heating or coordination by a Lewis-base.[79,80] In fact, a reversible metathetical exchange of disilenes was observed at ambient temperature in solution, bearing different substituents at the silicon center.[81,82] Furthermore, utilizing a similar concept (an intramolecular Lewis-base stabilization), Ge=Ge double bond metathesis was recently reported (***Figure 9***).[83]
The metathesis of trans-bent ditetrelynes pose a considerably greater. Even with the addition of Lewis bases like DMAP, small NHCs, or RNC, the cleavage of the E≡E bond does not occur. Instead, the reaction leads to the formation of neutral Lewis acid-base adducts or intramolecular C–H activated products, as observed in prior studies.[33] To date, the cleavage of E≡E triple bonds has been exclusively achieved through the reactions involving H_2, alkenes/alkynes, or transition metal (mainly

group-6 metals) complexes.[33,84] Recently, there has been a report on thermally induced metathesis of ditetrelynes (Ar^R)E≡E(Ar^R) (E = Ge – Pb) (R = Dipp, Tip; Dipp = C_6H_3-2,6-^{i}Pr$_3$, Tip = C_6H_2-2,4,6-^{i}Pr$_3$) with the Mo≡Mo triple and Mo–Mo single bonds present in molybdenum complexes $(CO)_2CpMo{\equiv}MoCp(CO)_2$ and $(CO)_3CpMo{-}MoCp(CO)_3$.[85] Despite these exciting advances, that highlight the exciting potential of E≡E bond metathesis, the metathesis of ditetrylynes with low-valent silicon compounds remains elusive.

Reversible Si=Si metathesis, Tamao, 2011

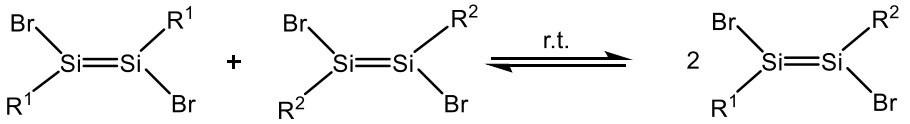

Ge=Ge metathesis, Scheschkewitz, 2021

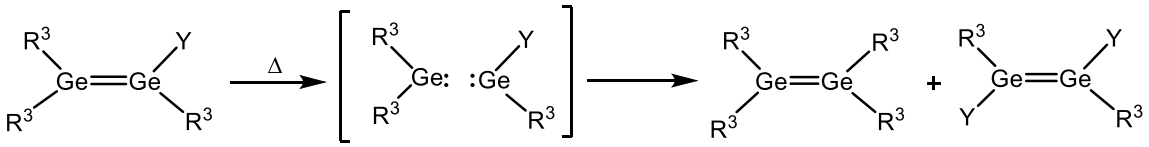

E≡E metathesis with transiton-metals, Power, 2020

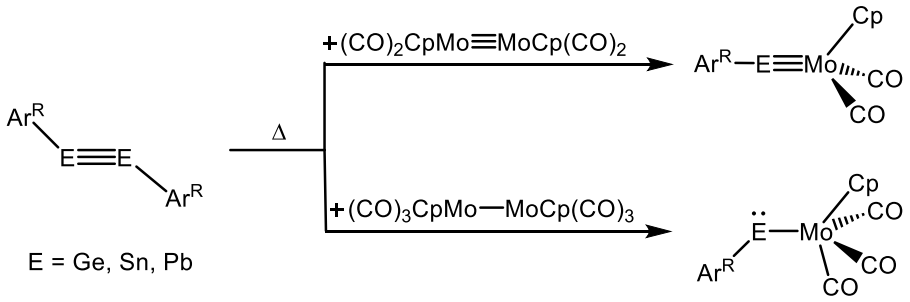

R^1 = Eind = 1,1,3,3,5,5,7,7-octaethyl-s-hydrindacen-4-yl; R^2 = EMind = 1,1,7,7-tetraethyl-3,3,5,5-tetramethyl-s-hydrindacen-4-yl; R^3 = Tip = 2,4,6-^{i}Pr$_3$-C_6H_2; Y = SiR_2(Dma) (R = Me, Ph; Dma = 2-Me_2N-C_6H_4); Ar^R = 2,6-R-C_6H_3 (R = Dipp = 2,6-^{i}Pr$_2$-C_6H_3 or Tip

Figure 9. Reported examples of E=E and E≡E bond metathesis in heavier of group-14 element chemistry.

1.5. Base-supported heteroditetrelynes and their constitutional isomers

The synthesis of homonuclear ditetrelynes proceeds in most cases by reductive dehalogenation of tetrel(II) or tetrel(IV) precursors.[33,86] However, this approach failed so far for the synthesis of heteronuclear ditetrelynes.[87] The only successful methodology has been reported by Filippou and co-workers.[iii] It involves the reaction of a distannyne ($Sn_2Ar^{Dipp}_2$) with one equivalent of germanium(II) halide ($Ar^{Dipp}GeCl$) at ambient temperature, resulting in the formation of the dark purple stannagermyne ($Ar^{Dipp}SnGeAr^{Dipp}$) (***Scheme 3***).

The only base-free heteronuclear ditetrelyne

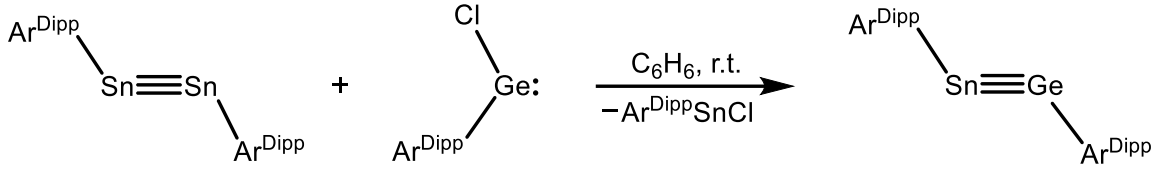

Dark green Orange Dark purple

Ar^{Dipp} = C_6H_3-$Dipp_2$, Dipp = C_6H_3-$^iPr_2$

Scheme 3. Synthesis of a stannagermyne following the cross coupling of a distannyne with a Ge(II) precursor.

The molecular chemistry of silicon and germanium has witnessed a renaissance in recent years, prompted by the recognition that N-heterocyclic carbenes (NHCs) and cyclic (alkyl)(amino)carbenes (CAACs) can be used as exceptionally valuable Lewis bases. These ligands have contributed to the thermodynamic and kinetic stabilization of highly reactive, low-oxidation state silicon and germanium species, which are characterized by intriguing bonding features and promising synthetic potential.[88–95] As base-free heteronuclear ditetrelynes, the base-supported versions are also scarce with the only example emerging recently from the research group of Filippou.[95] Employing the NHC stabilization, the first two-coordinated Si^0-isocyanide compound [(NHC)SiCNR, R = Ar^{Mes}, Mes = C_6H_2-2,4,6-Me_3] was isolated. Reaction with $Ar^{Mes}GeCl$

[iii] The compound ($Ar^{Dipp}Sn{\equiv}GeAr^{Dipp}$) is reported in the following doctoral thesis; David Hoffmann, "Novel synthetic routes for multiple bond formation between Si, Ge,and Sn and the d- and p-block elements", *Dissertation*, Rheinische Friedrich-Wilhelms-Universität Bonn, **2021**.

afforded in a “Si(NHC)” transfer reaction and facilitaed the isolation of the only base-supported heteronuclear ditetrelyne [(NHC)Si(Cl)GeAr^{Mes}] (***Scheme 4***).

Way to the first base-supported heteronuclear ditetrelyne

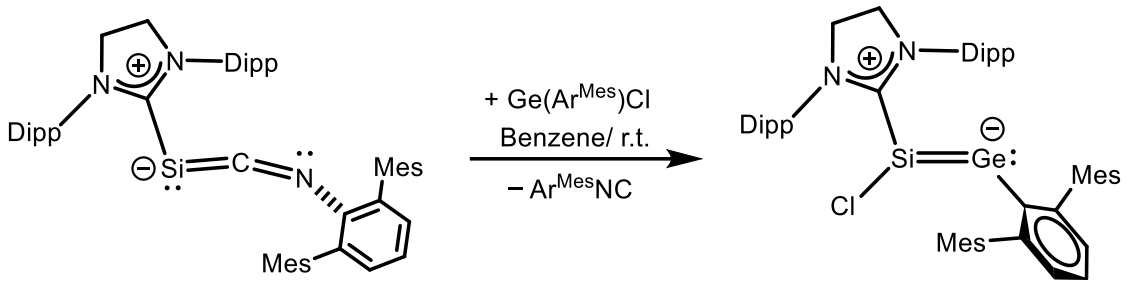

Dipp = C_6H_3-2,6-$^{i}Pr_2$; Mes = C_6H_2-2,4,6-Me_3

Scheme 4. Synthesis of an NHC-supported germasilyne.

Whereas base-supported heteronuclear ditetrelynes are rare, their constitutional isomers, base-supported heteronuclear ditetrela vinylidenes are moderately explored in literature.[iv] The first entry into this highly intriguing class of compound was reported by D. Scheschkewitz et *al.*, presenting a coreduction of Tip_2SiCl_2 and (NHC)$GeCl_2$ (Tip = 2,4,6-$^{i}Pr_3$-C_6H_2; NHC = 1,3-diisopropyl-4,5-dimethylimidazol-2-ylidene (I$^{i}Pr_2Me_2$)) by lithium-naphthanalide leading to the I$^{i}Pr_2Me_2$-stabilized silagermenylidene **I-13** (***Figure 10***).[96] Expanding on this, the same group introduced a similar compound **I-14**[51] using a different approach involving the reduction of (NHC)$GeCl_2$ with a disilenide. Taking advantage of an intramolecular germylene-phosphine Lewis pair a successful synthesis of a phosphine-stabilized germasilenylidene **I-15**[97] has been reported by L. Wesemann *et al.*. The most recent advancement in this field comes from Filippou and co-workers, where the synthesis of the first CAAC-supported germasilenylidene **I-16**[iv] is reported.

[iv] A general overview on NHC- or CAAC-supported heavier group-14 vinylidenes are presented in the following doctoral theses; a) Fabian Gstrein, “Silicon Compounds in Low Oxidation States Supported by a Cyclic (Alkyl)(Amino)Carbene: Synthesis, Structure and Reactivity”, *Dissertation*, Rheinische Friedrich-Wilhelms-Universität Bonn, **2023**, and b) Simon Schwarzwald, “NHC-supported Disilavinylidenes and Oxysilylenes: Synthesis, Characterization and Reactivity Studies”, *Dissertation*, Rheinische Friedrich-Wilhelms-Universität Bonn, **2023**.

Base-supported heavier analogues of hetero vinylidene

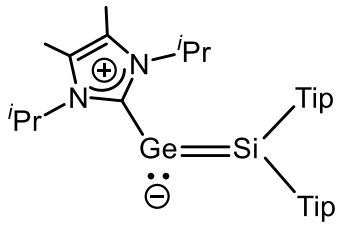

Scheschkewitz, 2013

I-13

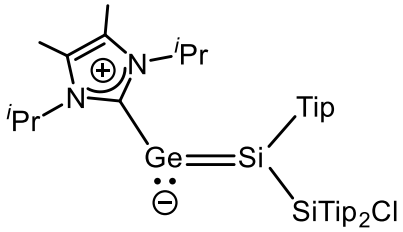

Scheschkewitz, 2014

I-14

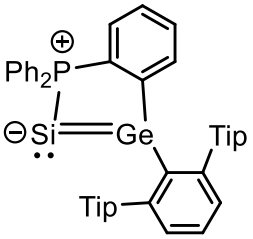

Wesemann, 2019

I-15

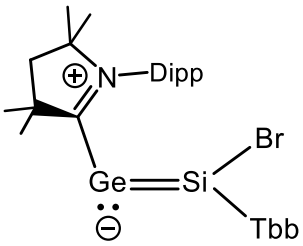

Filippou, 2023

I-16

Tip = C_6H_2-2,4,6-$^{i}Pr_3$, Dipp = C_6H_3-2,6-$^{i}Pr_2$, Tbb = 2,4-Dsi-6-^{t}Bu-C_6H_2

Figure 10. Literature known heavier congeners of hetero vinylidenes.

It is quite surprising that cyclic (alkyl)(amino)carbenes (CAACs) have not seen frequently used in stabilizing heavier group-14 vinylidenes.[96,98,99] CAACs are quite different from usual NHCs and have much enhanced π-accepting abilities.[92,93,100]

1.6. Objective of this work

In modern inorganic chemistry, achieving "gram-scale syntheses" of compounds featuring elements in unusually low oxidation states with unconventional bonding modes continues to be a central goal. Successful isolation of such compounds requires novel synthetic approaches and well-designed sterically demanding substituents to provide kinetic protection. The heavy analogues of alkynes, the "*ditetrelynes*" stand out as notable examples in this category. They exhibit a trans-bent core with a small HOMO–LUMO gap (~2 eV) and partial diradical character. This unusual bonding of ditetrelynes render them intriguing in terms of reactivity, and they have proven effective in small molecule activation, C–C coupling reactions and even in catalysis.

Within this framework, my efforts will concentrate on pioneering new synthetic methodologies for the formation of heavier tetrel–element bonds. The objectives involve compounds featuring the elements Si and Ge within an unsaturated bonding environment. The primary focus is on their comprehensive characterization using standard analytical techniques and correlating the findings with results obtained from quantum chemical calculations.

The key objectives of this work can be summarized as follows: -

- To synthesize and characterize novel unsaturated metallacycles containing low-valent Si and Ge, and explore their further reactivity.

- To synthesize and characterize unprecedented bis(tetrylidene), tetrylidene-tetrylidyne, and bis(tetrylidyne) complexes using the "Ge≡Ge" triple bond cleavage of a digermyne at a single metal center (M = Fe, Co, Ni).

- To synthesize a caac^{Me}-supported heavier tetrel analogue of alkynes using a transition metal free metathesis reaction of "Ge≡Ge" triple bond of a digermyne and explore its unique reactivity.

2. Results and discussion

2.1. Synthesis and properties of digermyne-complexes

As highlighted in the introduction, in contrast to metal-alkyne complexes, there are only few studies on metal-ditetrelyne complexes ($L_nM(E_2R_2)$, E = Si- Pb, and R denotes any bulky group), and their reactivity has yet to be thoroughly investigated. An entry into this field provided the reaction of $CpCo(CO)_2$ with Ge_2Tbb_2 (Tbb = C_6H_2-4-^{t}Bu-2,6-$(CH(SiMe_3)_2)_2$)[101] in *n*-pentane at ambient temperature. The reaction was very fast and was accompanied by evolution of CO gas with an immediate color change from red orange to brown. Monitoring the progress of the reaction by *in-situ* FT-IR and ^{1}H NMR spectroscopy revealed a complete consumption of the starting materials witnin five minutes and a very selective formation of the mono-carbonyl digermyne complex ***rac***-[Cp(CO)Co{η^2-*trans*-Ge_2Tbb_2}] (**1-Co**). A similar reaction was observed with $CpRh(CO)_2$. In this case a colour change from red orange to dark-green was observed leading to the mono-carbonyl digermyne complex ***rac***-[Cp(CO)Rh{η^2-*trans*-Ge_2Tbb_2}] (**1-Rh**). After work up and crystallization of the crude products from Et_2O at −30 °C, **1-Co** was isolated as a brown microcrystalline mono-ether solvate **1-Co•(Et_2O)** in 79 % yield and **1-Rh** as a dark-green crystalline mono-ether solvate **1-Rh•(Et_2O)** in 78 % yield.

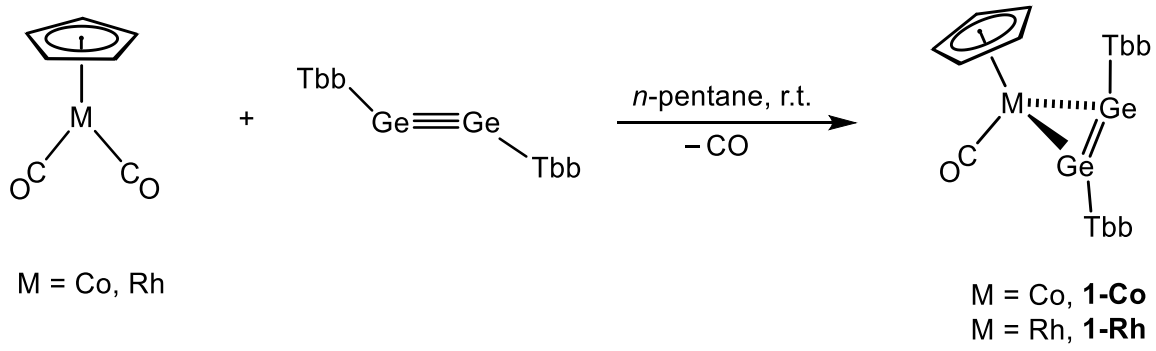

Scheme 5. Synthesis of trans bent-digermyne complexes **1-Co** and **1-Rh**.

Both complexes are extremely air-sensitive, well soluble in dry, de-oxygenated *n*-pentane, benzene and THF. Their solutions in (D_6)benzene show no sign of decomposition for at least one day at ambient temperature. Remarkably, both display a very high thermal stability in the solid state with a decomposition temperature (T_{dec}) of 208 °C and 204 °C for **1-Co** and **1-Rh** respectively, as compared to that of the free digermyne Ge_2Tbb_2 (T_{dec} = 155.0 - 155.7 °C)[101] and the Co-alkyne complexes Cp(CO)Co(η^2-$C_2(SO_2{}^tBu)_2$) (T_{dec} = 110 °C),[102] and Cp(CO)Co(η^2-cyclo-alkyne) (T_{dec} =

120 °C)[v]. This indicates a strong complexation of the Ge_2Tbb_2 with the metal center in line with the structural and spectroscopic data (*vide infra*).

Of particular note, the observed CO/Ge_2Tbb_2 ligand exchange reaction time (t ~5 min) for ~99% conversion at ambient temperature is an example of an unusual reaction kinetics in CO-substitution chemistry of $CpCo(CO)_2$, which is known to undergo slow associative ligand substitutions triggered by $\eta^5 \rightarrow \eta^3$ slippage of the Cp-ring and the kinetics of which is strongly retarded by steric bulk of the entering ligand. Thus, the reaction time (t) is remarkably shorter than the first half-life ($t^{1}_{½}$ = 13 days) of CO/PPh_3 ligand exchange at 40 °C under pseudo-first order condition ($t^{1}_{½} = 1/k[PPh_3]_0$, $k = 4.5\times10^{-6}$ s^{-1}, $[PPh_3]_0$ = 0.2 M)[103] and also astonishingly shorter than the first half-life ($t^{1}_{½}$ = 38 min) of the radio ^{14}CO exchange reaction at 0 °C (k = 0.022 $M^{-1}s^{-1}$, $[CpCo(CO)_2]_0$ = 0.02 M).[104] Moreover, the rate of the CO/Ge_2Tbb_2 ligand exchange reaction (0.02 M Ge_2Tbb_2) is far too fast than the CO-substitution reaction of $CpCo(CO)_2$ with an equimolar amounts of the cyclo-alkyne 3,3,6,6-tetramethyl-1-thiacyclohept-4-yne that requires 24 hours for completion at ambient temperature.[105][v] Assuming an overall second-order kinetics requiring seven half-lives ($t^{n}_{½} = 2^{(n-1)}t^{1}_{½}$, $t^{n}_{½}$ = n^{th} half-life) for 99 % conversion the estimated first half-life ($t^{1}_{½}$) of CO/Ge_2Tbb_2 ligand exchange is $t^{1}_{½}$ = ~2.5 s and that of CO/cyclo-alkyne exchange is $t^{1}_{½}$ = ~12 min. The peculiar electronic features of Ge_2Tbb_2 originating from its *trans*-bent ground state structure is nicely demonstrated by the observed unusually fast CO/Ge_2Tbb_2 ligand exchange despite the presence of very bulky Tbb substituents and a substitutionally quite inert $CpCo(CO)_2$.

Complex **1-Co** is the first 3d-metal ditetrylyne complex to be reported and hence it was thoroughly characterized by single crystal X-ray diffraction (sc-XRD) analysis and multinuclear NMR spectroscopy. Suitable plate shaped dark-brown crystals of **1-Co•(Et_2O)** for sc-XRD analysis were obtained by slow cooling its saturated Et_2O solution at −30 °C. The complex **1-Co•(Et_2O)** crystalizes in the centrosymmetric $P2_1/c$ space group with an unit cell composed of a racemate of structurally identical (***R,R***)-**1-Co** and (***S,S***)-**1-Co** enantiomers with two stereogenic Ge centers (***Figure 11***). The molecular structure of **1-Co** (used hereafter to describe both (***R,R***) and (***S,S***)) features two trigonal pyramidal stereogenic Ge-centers (∑°(∠Ge1) = 306.6°, ∑°(∠Ge2) = 316.8°) located at a short internuclear distance (Ge1−Ge2 = 2.3456(3) Å) and both of which

[v] The Synthesis and characterization of this complex is reported in the following doctoral thesis; B Jessel "Gespannte cyclische Alkine zur Darstellung isolierbarer Zwischenstufen der Acetylenmetathese und der Acetylentrimerisierung mit Iopentadienyldicarbonylcobalt", *Dissertation*, Universität Hamburg, **1984**.

are connected to the Co center *via* a short Co–Ge2 distance (2.3675(4) Å) and a long Co–Ge1 distance (2.5010(4) Å). A strong coordination of the Ge_2Tbb_2 is evident from – i) the Co–Ge1 and Co–Ge2 distances that lie in the typical range of Co–Ge single bond lengths of closed-shell Co(I)-germyl complexes (2.294 Å - 2.525 Å) reported in the Cambridge Structural Database (CSD), ii) the elongation (Δd) of the Ge1–Ge2 distance by 0.12 Å compared to that of the uncoordinated Ge_2Tbb_2 (d(Ge–Ge) = 2.222 Å)[101] and iii) the decrease ($\Delta\phi$) of the skeletal dihedral angle C1–Ge1–Ge2–C25 (ϕ = 155.9(1)°) by 24.1° relative to that of the free Ge_2Tbb_2 (ϕ = 180°). The Ge1–Ge2 distance (2.3456(3) Å) is much longer than those of the digermenes (2.212 Å – 2.296 Å) containing trigonal planar Ge centers ($\sum°(\angle Ge)$ = 355° - 360°), but compares well with those of the CSD reported strongly pyramidalized ($\sum°(\angle Ge)$ = 328° - 345°) *acyclic*-1,2-diaryldigermenes without halogen substituent at Ge (2.303 Å - 2.378 Å), indicating the retention of significant multiple bond character in the coordinated *trans*-Ge_2Tbb_2 ligand. Notably, the Δd and $\Delta\phi$ parameters of **1-Co** (Δd = 0.12 Å, $\Delta\phi$ = 24.1°) is significantly larger than those of the π-digermyne complex [Ag(η^2-*trans*-$Ge_2(Ar^{Dipp})_2$)][SbF_6][49] and comparable to those of the disilyne complex [(PCy_3)Pd(η^2-*trans*-$Si_2(R_s)_2$][20] (Δd = 0.084 Å, $\Delta\phi$ = 45°) suggesting a considerable metallacyclic character in the $CoGe_2$ ring of **1-Co**.

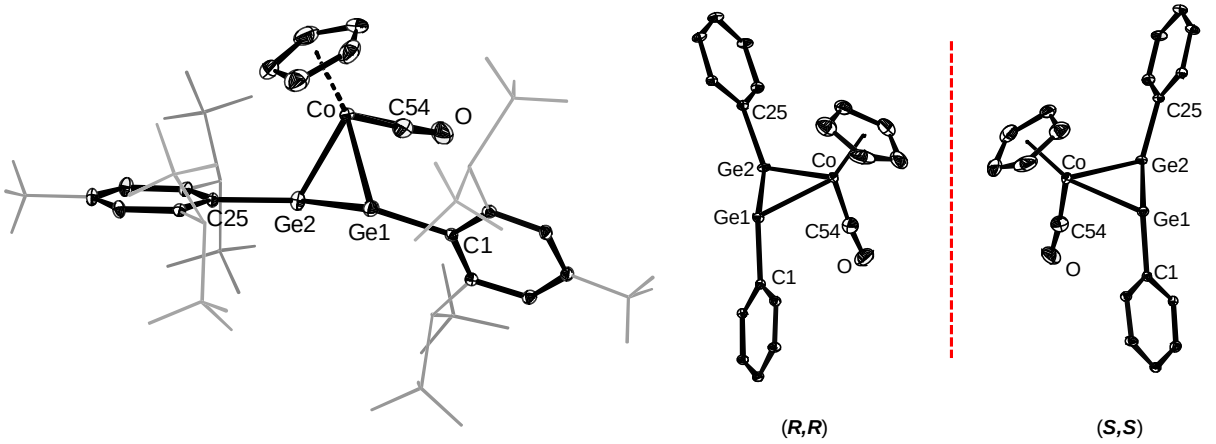

Figure 11. (*left*) DIAMOND plot of the molecular structure of (***R,R***)-**1-Co**. Thermal ellipsoids are set at 30 % probability level. Hydrogen atoms are omitted and the Dsi and ^{t}Bu substituents of the Tbb ligand are presented in wire-frame for clarity. Selected bond lengths [Å], bond angles [°] and torsion angle [°]: Ge1-Ge2 2.3456(3), Co-Ge1 2.5010(4), Co-Ge2 2.3675(4), Co-C54 1.714(3), Co-Ge1-Ge2 58.378(11), C1-Ge1-Ge2 131.41(6), Co-Ge1-C1 116.85(6), Co-Ge2-Ge1 64.097(12), Co-Ge2-C25 117.95(7), C25-Ge2-Ge1 134.83(6), C1–Ge1–Ge2–C25 155.9(1). (*right*) The two enantiomers (***R,R***) and (***S,S***) present in the unit-cell of **1-Co•(Et_2O)**.

The presence of two different Co–Ge distances in **1-Co** leads to an asymmetric η^2-coordination mode of Ge_2Tbb_2 with a %-slippage parameter Ω of 13 % towards Ge2 center calculated from its molecular structure (Ω = 0% (η^2-*sym*) - 100% (η^1-*asym*))[106]

and it is accompanied by a slight twisting of the C_t-Co-CO plane (C_t: Cp-centroid) relative to the Ge1−Ge2 vector giving rise to two different basal angles ∠(C_t-Co-Ge2) of 125.40° and ∠(C_t-Co-Ge1) of 133.89°. The two angles ∠(Ge1-Ge2-C25) (134.83(6)) and ∠(Ge2-Ge1-C1) (131.41(6)°) are very similar to that of the free digermyne Ge_2Tbb_2 (134.46°) and are much smaller than the ∠(E−E'−C^R) angle at the base-free tetrel site (E, E' = Si - Sn) of the mono Lewis-base (L) adducts of homo- and hetero-nuclear ditetrylynes REE'R(L) (98.135° – 120.35°)[95] that contain stereochemically active lone pair localized at the base-free tetrel center, suggesting no buildup of stereochemically active lone-pair with high s-character at the Ge1 center of the coordinated Ge_2Tbb_2 ligand upon slippage towards Ge2 center.

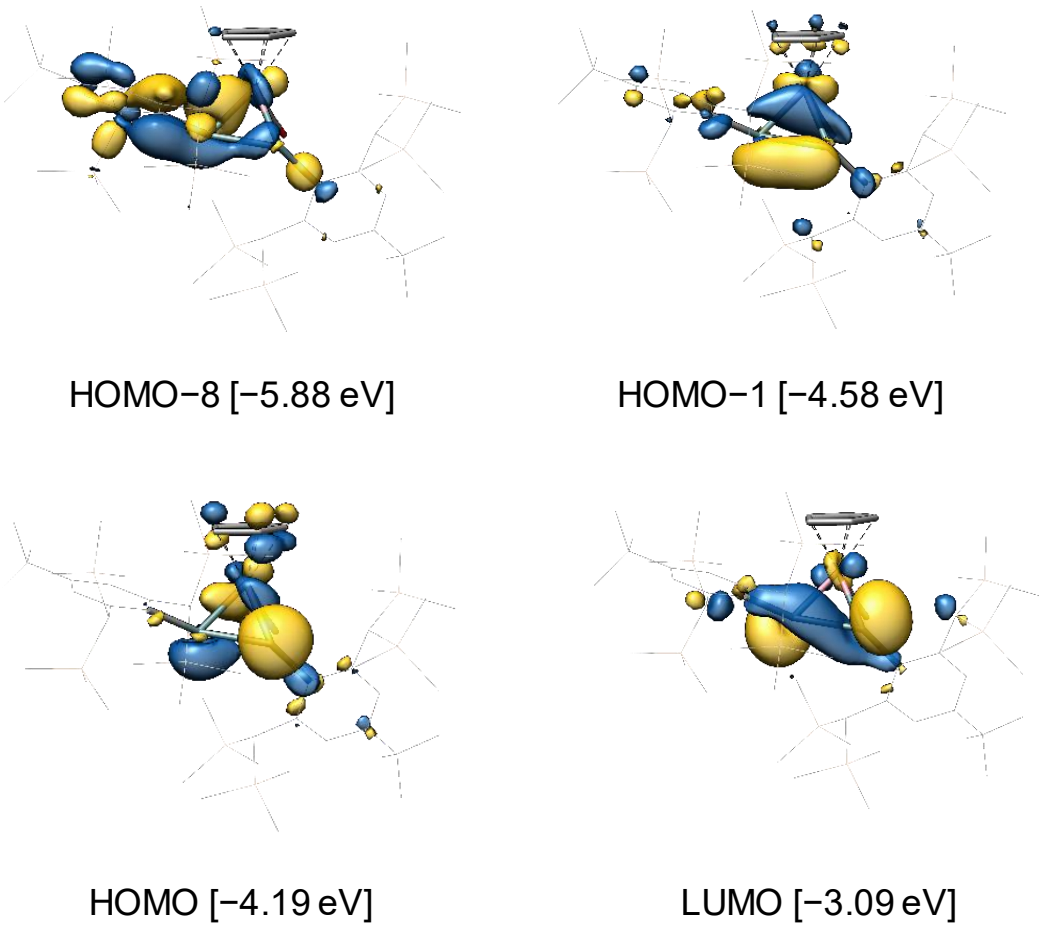

Figure 12. Selected molecular orbitals of (**(*S,S*)-1-Co**)$_{calc}$ and their orbital energies (eV); the isosurface value is set at 0.04 $e^{1/2}$·$Bohr^{-3/2}$.

Quantum chemical calculations (B97-D3(BJ)-ATM/def2-TZVP (level-**I**)) in gas phase revealed that in the potential energy hypersurface (**(*R,R*)-1-Co**)$_{calc}$ with a calculated $(\Delta d)_{calc}$ = 0.18 Å, $(\Delta\phi)_{calc}$ = 20.3° is the global minimum, while the **(*R,R*)-1-CoS**)$_{calc}$ featuring an η^2-*sym* coordination mode of Ge_2Tbb_2 was found to be a local minimum lying at only +5.0 kJ/mol higher in energy suggesting that the digermyne slippage in

(***R,R*)-1-Co**$)_{calc}$ most probably ensues from weak stereoelectronic effects. Taken together, the analysis of the structural parameters of **1-Co** in the solid state confirms an out-of-plane asymmetric η^2-coordiantion of the Ge_2Tbb_2 ligand to the Co-center and the presence of considerable metallacyclic character in the $CoGe_2$ ring with the intact slipped π(Ge−Ge) bond. Accordingly, an analysis of the Kohn-Sham orbitals calculated at the level-**I** computations showed the presence of Co−Ge bonding in the HOMO−8 and HOMO−1, whereas, HOMO and LUMO are mainly Ge-centered orbitals that resemble with the in-plane slipped Ge−Ge π_{in} and π^*_{in} orbitals, respectively.

A default Natural Bond Orbital (NBO) analysis of the model complex ***(R,R)***-[Cp(CO)Co(η^2-*trans*-$Ge_2(Me)_2$)] ((***R,R*)-1-Co^{Me}**$)_{calc}$, which displays very similar structural parameters to that of the (***R,R*)-1-Co**$)_{calc}$, revealed the presence of a Natural Lewis Structure (NLS) featuring a highly polar bond-pair (BD) NBO for the Ge1−Ge2 single bond (occ: 1.86, %pol: 76 (Ge2)) with two remarkably different Ge-NHOs (Ge1: 99% p-NAO, Ge2: 50% s-NAO) and the two Co−Ge bonds (occ: 1.68, 1.71) polarized towards Co with a very similar Ge-NHO (%p-NAO: 95% (Ge1), 81% (Ge2)). These NBOs suggest that the Ge−Ge bond of (***R,R*)-1-Co^{Me}**$)_{calc}$ may be described as the intra-ligand donor-acceptor σ-bond formed from the interaction of the two cobaltagermylene ligands. Thus, a lone-pair (LP) NBO at Ge1 (occ: 1.73, 88% Ge(s)-NAO) and a lone-vacant (LV) NBO at Ge2 (non-Lewis occ: 0.5, 99% Ge(p)-NBO) were accordingly found with a LP→LV *E(2)*-SOPT interaction energy of 77.40 kJ/mol in line with the presence of double donor-acceptor Ge−Ge multiple bond. The polarized Ge−Ge bonds presumably causes the η^2-asymmetric bonding of the Ge_2Tbb_2.

The solution structure of **1-Co** was investigated by NMR spectroscopy. Since **1-Co** crystallizes as a racemate of ***(R,R)*-1-Co** and ***(S,S)*-1-Co** enantiomers, it exists in solution as a racemic mixture, which should render the Tbb substituents diastereotopic, one pointing toward Cp (Ge2 bonded Tbb) and the other away from Cp (Ge1 bonded Tbb), and were arbitrarily assigned as Tbb_X and Tbb_Y, respectively. Therefore, a separate set of signals for Tbb_X and Tbb_Y was expected in the ^{1}H NMR spectrum of **1-Co**. Surprisingly, the ^{1}H NMR spectrum of **1-Co** at 298 K in (D_8)THF displays only one set of broad signals for the two diastereotopic Tbb groups suggesting fast chemical exchange in the NMR time scale, which was studied by variable temperature ^{1}H NMR spectroscopy. Indeed, a separate set of signals is observed for each Tbb substituent in the slow exchange limit spectrum at 233 K (***Figure 13***), e.g. two singlets in an 18 : 18 integration ratio for the $SiMe_3$ groups of Tbb_Y, four singlets in an 9 : 9 : 9 : 9 ratio for Si*Me*$_3$ groups of Tbb_X and one singlet for each of the ^{t}Bu methyl protons of Tbb_X and Tbb_Y at δ = 1.33 ppm and 1.38 ppm. Three

chemical exchange processes were resolved by remeasuring the NMR sample at different temperatures. The first process involves rotation of the Ge–Tbb_X bond with a coalescence at T_{c1} = 263 K of the four $(SiMe_3)_X$ proton signals into a very broad signals, a second T_{c2} at 273 K for the coalescence of ^{t}Bu signals of Tbb_x and Tbb_Y and a third one at T_{c3} = 313 K due to the coalescence of $(SiMe_3)_X$ and $(SiMe_3)_Y$ signals. Finally, in the fast exchange limit spectrum at 313 K a time averaged local C_{2v} symmetry of **1-Co** was observed suggesting that the second and the third processes involve complicated stereodynamics. The barriers for these processes at the respective coalescence temperature calculated by plugging in the Gutowsky-Holm formula $k_{exch} = 2.22\ (\Delta\upsilon_{max})$ (k_{exch} = first order exchange rate constant in Hz, $\Delta\upsilon_{max}$ = peak-to-peak separation in Hz of the two exchanging singlets in the low temperature limit spectrum) in the Eyring-Polanyi equation (assuming the transmission coefficient $\kappa = 1$) were $\Delta G^{\ddagger}_1$ = 54 kJ/mol, $\Delta G^{\ddagger}_2$ = 59 kJ/mol and $\Delta G^{\ddagger}_3$ = 64.5 kJ/mol suggesting that these processes occur non-synchronously. Full line shape analysis using gNMR programme for the first two dynamics processes gave the following activation parameters, first process: $\Delta H^{\ddagger}_1$ = 48.1(±3) kJ/mol, $\Delta S^{\ddagger}_1$ = −25.2(±11) kJ/K, second process: $\Delta H^{\ddagger}_2$ = 66.5(±2) kJ/mol, $\Delta S^{\ddagger}_2$ = 28(±8) kJ/K, whereas, the line-shape analysis for the third process was unsuccessful.

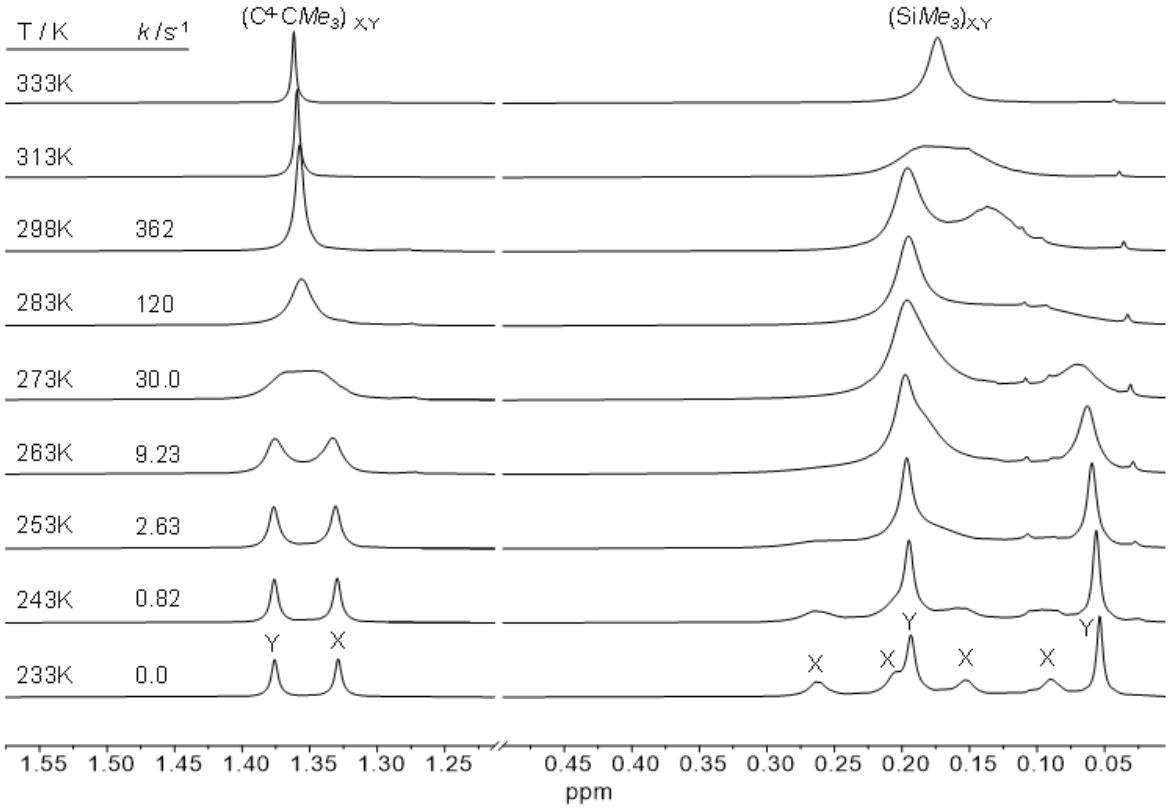

Figure 13. Stack plot of the variable temperature ^{1}H NMR spectra of **1-Co** in (D_8)THF in the temperature range of 233 K to 313 K in 300.1 MHz showing chemical exchange processes along with the first order rate constants (k/s^{-1}) obtained from full line-shape analysis of the C*Me*$_3$ signals.

In order to get a deeper insight into the mechanism of the stereodynamics of **1-Co** the following hypotheses were considered the *trans*-bent structure of Ge_2Tbb_2 renders its two faces prochiral (***Si,Si***) and (***Re,Re***) for the two Ge centers so that the (***R,R***)**-1-Co** ⇌ (***S,S***)**-1-Co** (***Figure 14***) enantiomerization essentially means switching the metal fragment from the (***Si,Si***) face to the (***Re,Re***) face either via a formal rotation of the coordinated Ge_2Tbb_2 ligand around the Ge–Ge vector or through a *trans*→*cis*→*trans* C^{Tbb}-Ge-Ge-C^{Tbb} skeletal torsion, whereas, the topomerization means rotation CpCoCO fragment around the vector that bisects the C_t-Co-C(O) angle (C_t = Cp-centroid). Thus, the topomerization does not lead to enantiomerization because during this process the metal fragment does not swap the prochiral faces of the Ge_2Tbb_2, however, this process would lead to chemical exchange of two ^{t}Bu groups (second process), but not of the two $SiMe_3$ groups of each $CH(SiMe_3)_2$ group (third process), which will remain diastereotopic despite Ge–C^{Tbb} bond rotations. Thus, the local time averaged C_{2V} symmetry of **1-Co** requires (***R,R***)**-1-Co** ⇌ (***S,S***)**-1-Co** enantiomerization, either synchronously (achiral pathway) or non-synchronously (two enantiomeric chiral pathways) as expected for Narcissistic reactions.[107]

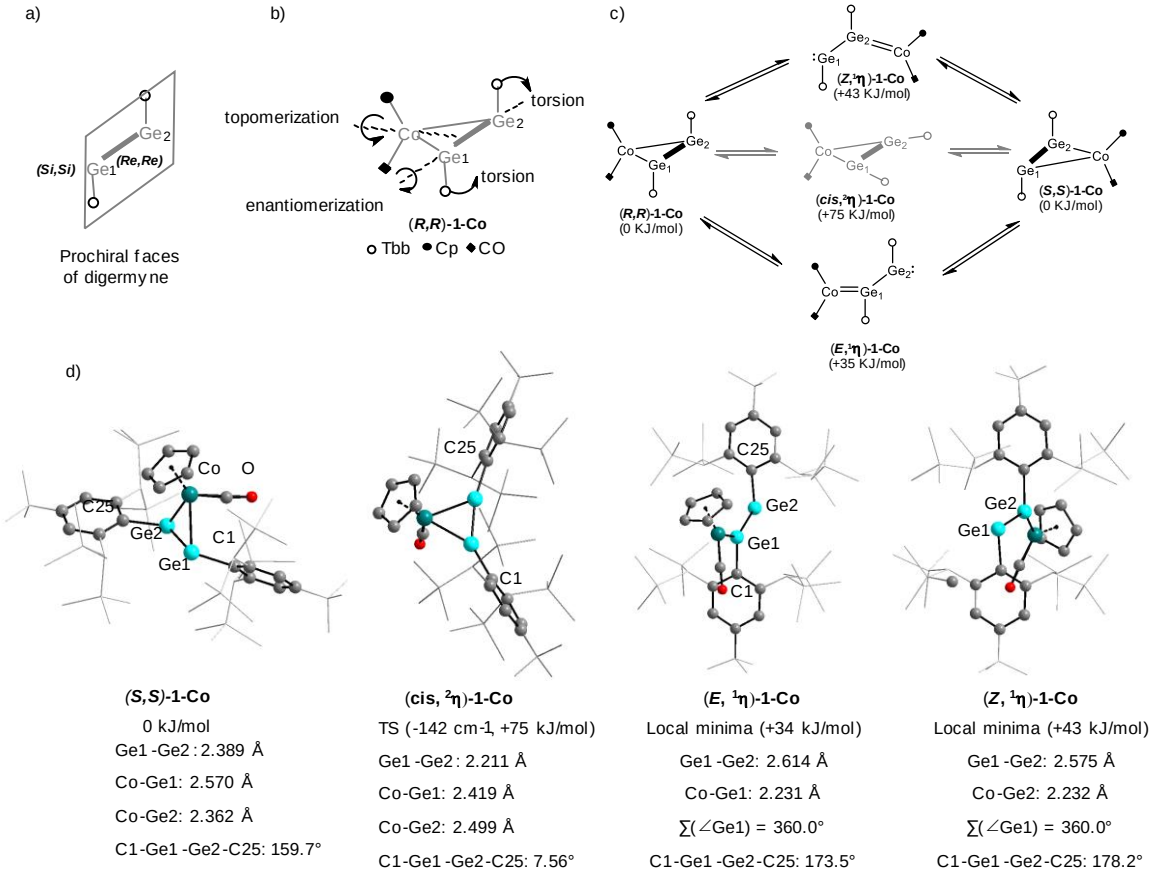

Figure 14. a) prochiral faces of *trans*-Ge_2Tbb_2; b) conceivable stereomutation processes for the chemical exchange of **1-Co**; c) proposed mechanism of (***R,R***)**-1-Co** ⇌ (***S,S***)**-1-Co** enantiomerization of **1-Co** according to the PES scans at the level-I computations; d) selected bonding parameters of the calculated structures.

Several potential energy surface (PES) scans and constrained geometry structure optimizations in the gas phase using level-**I** computations were carried to pre-select candidate structures for the enantiomerization. It was found that the skeletal torsion and the topomerization followed a much higher energy path with Saddle points and un-converged scans than the enantiomerization path via a complete $\eta^2 \rightarrow \eta^1$ digermyne slippage. Thus, the PES scans of the Co-Ge1-Ge2 and Co-Ge2-Ge1 angles of (***R,R*)-1-Co**$)_{calc}$ gave upon complete digermyne slippage the C_s-symmetric germylene-germylidene complexes (***E*,η^1)-1-Co** and (***Z*,η^1)-1-Co** as the local minimum structures lying only +34 kJ/mol and +43 kJ/mol higher in energy than ((***R,R*)-1-Co**$)_{calc}$. Most importantly, during this PES scan the skeletal torsion angle C^{Tbb}-Ge1-Ge2-C^{Tbb} (ϕ) remained almost unchanged (ϕ = 155°– 165°) suggesting minimal mixing between slippage and torsional dynamics. The (***E*,η^1)-1-Co** and (***Z*,η^1)-1-Co** displays a Co=Ge double bond (2.231, 2.231 Å), a trigonal planar Ge center (360°) connected to a dicoordinated Ge-center with V-shaped geometry (108.0, 101.8°) via a Ge−Ge single bond (2.614, 2.575 Å). This means that the enantiomerization may proceed through a $\eta^2 \rightarrow \eta^1$ digermyne slippage. In fact, PES scans of (***E*,η^1)-1-Co** of the C(O)-Co-Ge1-Ge2 torsion angle in clock-wise motion (basically Co=Ge double bond rotation) leads to the formation of the enantiomer ((***S,S*)-1-Co**$)_{calc}$. On the other, the (***cis*,η^2)-1-Co**, which is a plausible intermediate for the enantiomerization via a synchronous torsion appears at a much higher in energy (+75 kJ/mol) than that of (***E*,η^1)-1-Co** and found to be a first order saddle point with an imaginary frequency of −142 cm^{-1}. In conclusion, the $\eta^2 \rightarrow \eta^1$ digermyne slippage is the energetically favored mechanism for the (***R,R*)-1-Co** ⇌ (***S,S*)-1-Co** enantiomerization. The presence of this pathway is also in agreement with the lone-pair character of the in-plane π(Ge−Ge) bond of the coordinated Ge_2Tbb_2 which induces the $\eta^2 \rightarrow \eta^1$ digermyne slippage during the formal rotation of the coordinated Ge_2Tbb_2 ligand around the Ge−Ge vector.

The isostructural **1-Rh** was also characterized by single crystal X-ray diffraction (sc-XRD) analysis and multinuclear NMR spectroscopy. Suitable dark-green crystals of **1-Rh•(Et_2O)** for sc-XRD analysis were obtained by slow cooling its saturated Et_2O solution at −30 °C. The molecular structure of **1-Rh** (***Figure 15***) features two trigonal pyramidal stereogenic Ge-centers (∑(∠Ge1) = 309.2°, ∑(∠Ge2) = 315.2°) located at a short internuclear distance (Ge1−Ge2 = 2.3368(4) Å) and both of which are connected to the Rh center *via* a short Rh−Ge2 distance (2.4700(4) Å) and a long Rh−Ge1 distance (2.5560(4) Å). The Rh−Ge1 and Rh−Ge2 bond distances lie in the typical range of Rh−Ge single bond lengths of closed-shell Rh(I)-germyl complexes (2.335 Å – 2.506Å) reported in the Cambridge Structural Database (CSD) and also compares

well to the reported Rh−Ge single inverse dative bond in [η^5-$C_5Me_5(PMe_3)_2RhGeCl_2$].[108] The elongation (Δd = 0.12 Å) of the Ge1−Ge2 distance as well as the decrement ($\Delta\phi$ = 22.4°) of the skeletal dihedral angle C1−Ge1−Ge2−C25 with respect to that of the free Ge_2Tbb_2 are well comparable to those of **1-Co**.

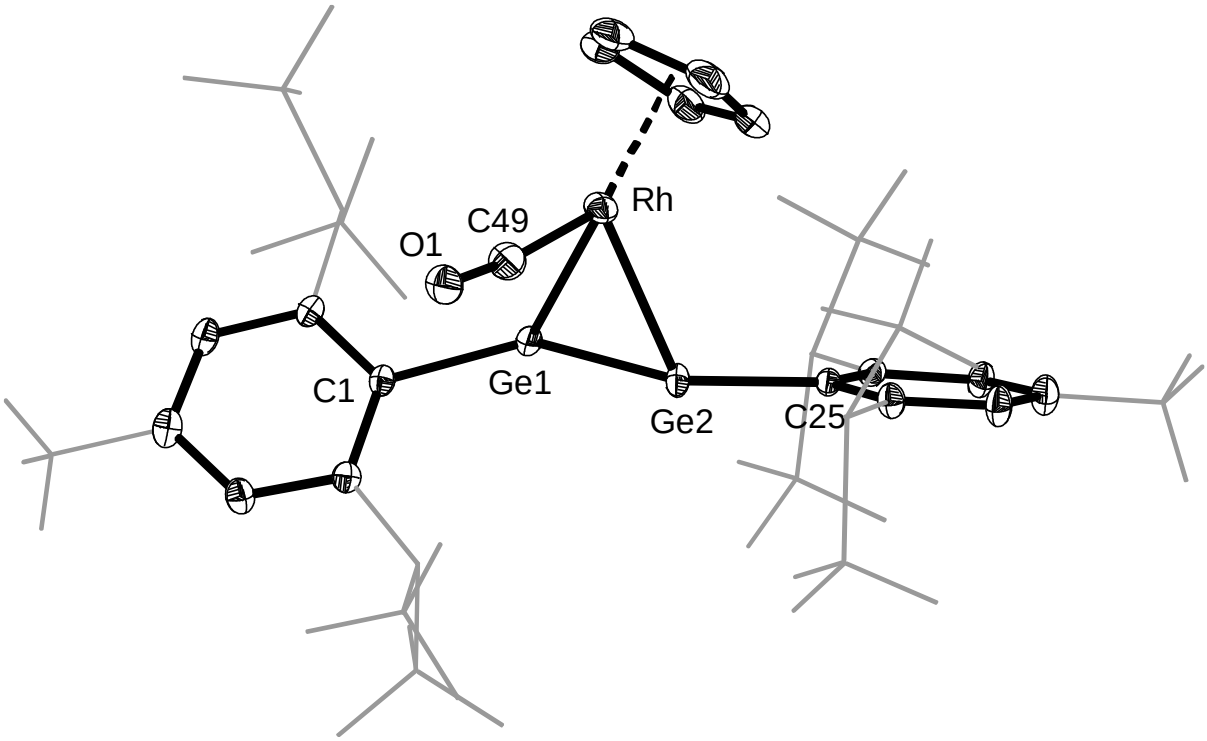

Figure 15. DIAMOND plot of the molecular structure of **1-Rh** Thermal ellipsoids are set at 30 % probability level. Hydrogen atoms are omitted, the Dsi and ^{t}Bu substituents of the Tbb ligand are presented in wire-frame for clarity. Selected bond lengths [Å], bond angles [°]and torsion angle [°]: Rh-Ge1 2.5560(4), Rh-Ge2 2.4700(4), Ge1-Ge2 2.3368(4), Rh-C49 1.828(4), C49-O 1.144(5), Rh-Ge1-Ge2 60.441(12), Rh-Ge1-C1 116.73(8), C1-Ge1-Ge2 132.07(8), Rh-Ge2-Ge1 64.178(13), Rh-Ge2-C25 115.98(8), C25-Ge2-Ge 135.02(8), C1-Ge1-Ge2-C25 157.6(1).

The solution structure of **1-Rh** was investigated by multinuclear NMR spectroscopy, showing resemblances in dynamic behavior to that of **1-Co**, which was also studied by ^{1}H VT-NMR spectroscopy (***Figure 16***), where the Gibbs free energy of activation for the dynamic process was only calculated using the modified Eyring equation.

$$\Delta G^{\ddagger} = 0.01915 \cdot T_c \cdot \left[9.972 + \log\left(\frac{T_c}{\Delta\nu}\right)\right] [\mathrm{kJ\ mol^{-1}}]$$

With T_c, the coalescence temperature ($T_c \approx 293$ K) and $\Delta\nu$ (11.8 Hz) is the chemical shift difference of the exchanging ^{t}Bu singlets in the low-temperature limit spectrum (213 K), where no exchange is assumed to occur (k = 0). The obtained $\Delta G^{\ddagger}$ value of 63.8 kJ/mol compares well with the obtained value for **1-Co** ($\Delta G^{\ddagger}$ = 59 kJ/mol).

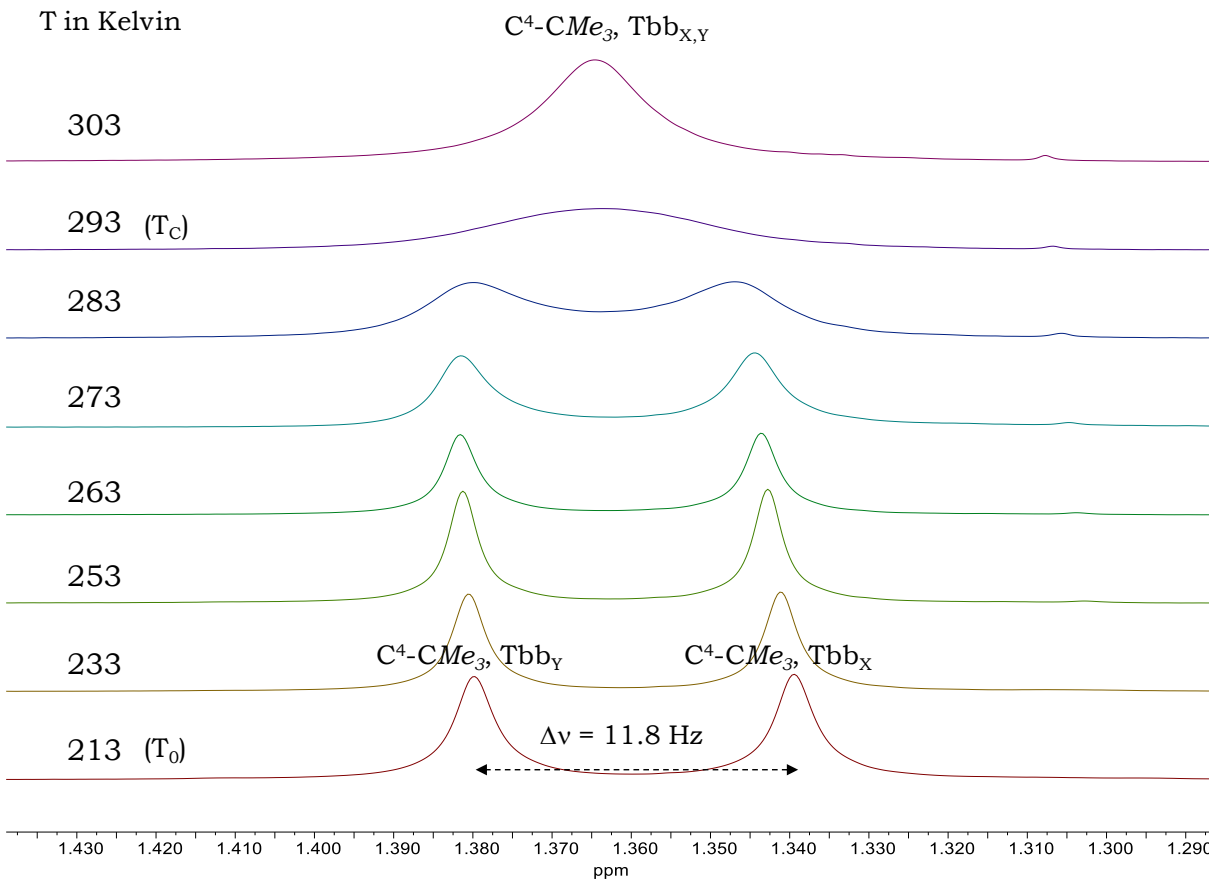

Figure 16. Excerpt of the VT-^{1}H NMR spectra (300.1 MHz) of **1-Rh** in (D_8)THF from 213 K – 298 K showing the exchanging C^4-C*Me*$_3$ signals of the Tbb$_X$ and Tbb$_Y$ substituents.

The structure and bonding analysis of **1-Co** show that both the in-plane and the out-of-plane π-bonds of trans-bent Ge_2Tbb_2 cannot be available for bonding to a single metal center due to stereoelectronic reasons implying that Ge_2Tbb_2 cannot be a four-electron donor ligand in its trans-bent geometry. We surmised that a cis-bend digermyne ligand can act as a four-electron donor and hence might be accessible if a suitable 14-VE metal fragment is chosen. Thus, we speculated that the CO-free digermyne complex CpCo(η^2-*cis*-$Ge_2(Tbb)_2$) (**3-Co**) should have a cis-bent alkyne like bonding mode of the Ge_2Tbb_2 ligand. However, when **1-Co** was heated in boiling toluene or photolyzed in *n*-heptane using a high-pressure Hg-lamp (120 W) the expected decarbonylation product was not formed. Thus, an alternative synthetic route for **3-Co** was planned staring from $CpCo(C_2H_4)_2$. In the first step, $CpCo(C_2H_4)_2$ was converted selectively to bis-bromogermylidene complex $CpCo(GeBrTbb)_2$ (**2-Co**) upon treatment with one equivalent of the dibromodigermene $Ge_2Br_2Tbb_2$ in *n*-pentane at ambient temperature. Complex **2-Co** was isolated after work up as an extremely air and moisture sensitive, dark brownish purple microcrystalline solid in 69 % yield. In the second step, **2-Co** was reduced with two equivalents of KC_8 in benzene at ambient temperature affording after work up the digermyne complex

CpCo(η^2-*cis*-Ge_2(Tbb)$_2$) (**3-Co**) as reddish-brown solid in 63 % yield. Complex **3-Co** is highly air-sensitive dark brown solid and decomposes upon melting at 160 °C.

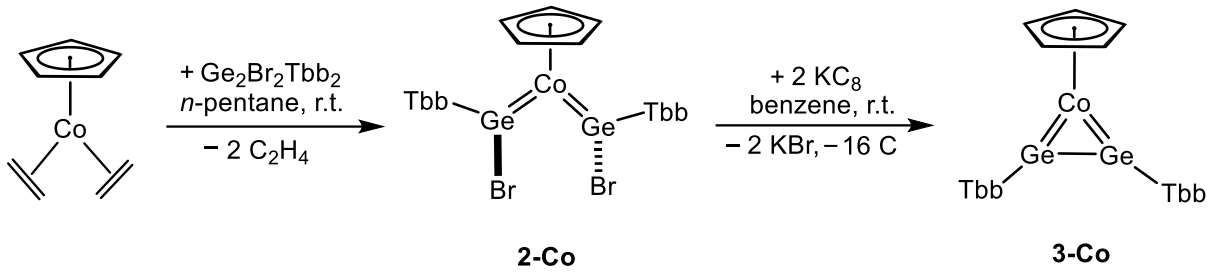

Scheme 6. Synthesis of cis bent digermyne complex **3-Co**.

The complex **2-Co** was comprehensively characterized by multinuclear NMR spectroscopy and single crystal X-ray diffraction (*sc*-XRD) analysis. Suitable plate shaped orange-brown crystals of **2-Co** for *sc*-XRD analysis were obtained by slow cooling its saturated *n*-hexane solution at −60 °C.

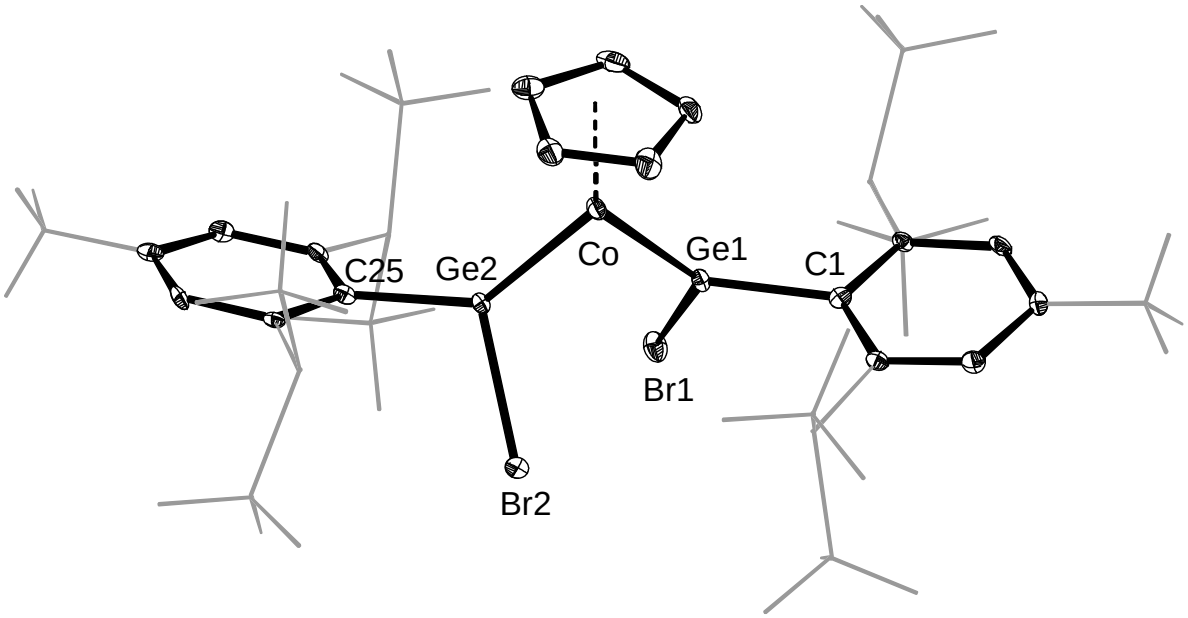

Figure 17. DIAMOND plot of the molecular structure of **2-Co**. Thermal ellipsoids are set at 30 % probability level. Hydrogen atoms are omitted and the Dsi and ^{t}Bu substituents of the Tbb ligand are presented in wire-frame for clarity. Selected bond lengths [Å] and bond angles [°]: Co-Ge1 2.1714(8), Co-Ge2 2.1795(8), Ge1-Br1 2.3750(7), Ge2-Br2 2.3581(6), Co-Ge1-C1 135.32(12), C1-Ge1-Br1 104.29(12), Co-Ge1-Br1 120.12(3), Co-Ge2-C25 138.32(12), Co-Ge2-Br2 115.95(3), C25-Ge2-Br2 105.46(12).

The molecular structure of **2-Co** features two trigonal planar coordinated Ge-centers (∑°(∠Ge1) and ∑°(∠Ge2) each 359.7°) connected to the Co center *via* short Co−Ge distances (2.1714(8) Å) and 2.1795(8) Å), which are very similar to the previously known mono- or bis-germylidene[58] complexes of cobalt made in our group.

The molecular structure of **3-Co** was determined by sc-XRD analysis of the reddish-brown plate shaped single crystals, which were grown by cooling its saturated Et_2O solution at −30 °C. Remarkably, in the molecular structure of **3-Co** the digermyne ligand Ge_2Tbb_2 coordinates to the Co-center *via* an η^2-*symmetric* coordination mode (Ω = 0 %) and adopts a *cis*-bent structure as indicated by the *syn-periplanarity* of the C1−Ge1−Ge2−C25 skeleton (ϕ = 4.3(1)°), in contrast to the *anti-periplanarity* of the C1−Ge1−Ge2−C25 skeleton of **1-Co** (ϕ = 155.9(1)°). Furthermore, the two trigonal planar coordinated Ge-centers (∑∠Ge1 and Ge2) = 359.9° and 359.6°) are connected to the Co-center *via* two short Co−Ge bonds (2.2268(4) Å and 2.2243(4) Å), which are slightly elongated (ca. 0.05 Å) when compared with **2-Co** but ca. 0.19 Å shorter than the Co−Ge2 bond (2.3675(4) Å) of **1-Co**. Finally, the pyramidality angle (the angle between Cp-centroid, Co and the centriod of the 3-memberred ring) (α) is close to 180° leading to a pseudo-C_{2V} symmetry of **3-Co**. Taken together, these structural peculiarities are in line with the 4e-donation mode of the digermyne ligand.

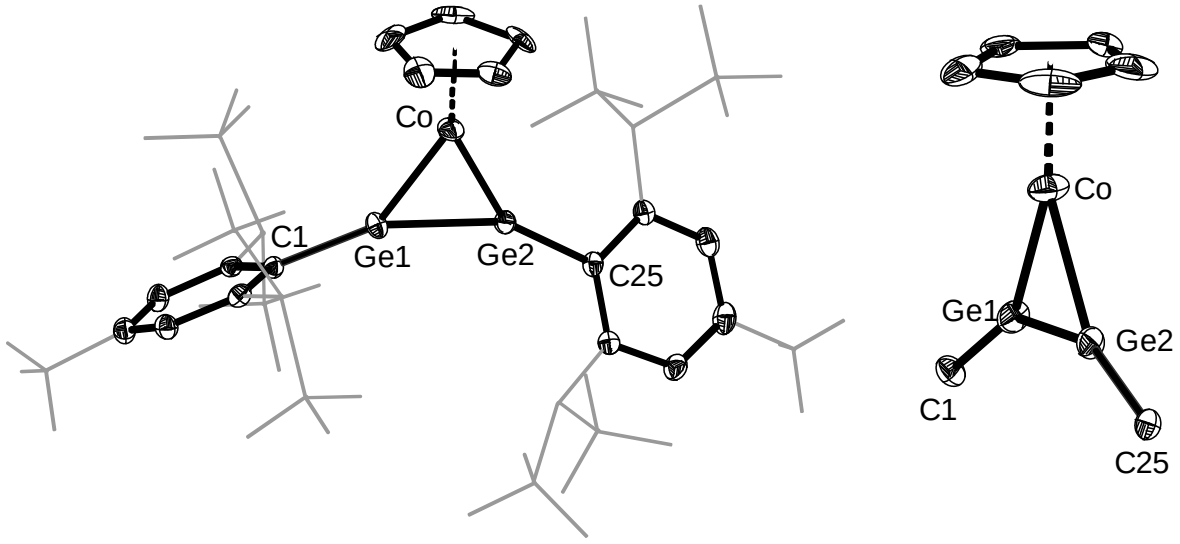

Figure 18. (*left*) DIAMOND plot of the molecular structure of **3-Co**, (*right*) its condensed side view. Thermal ellipsoids are set at 30 % probability level. Hydrogen atoms are omitted and the Dsi and ^{t}Bu substituents of the Tbb ligand are presented in wire-frame for clarity. Selected bond lengths [Å] and bond angles [°]: Ge1-Ge2 2.3137(4), Co-Ge1 2.2268(4), Co-Ge2 2.2223(4), Co-Ge1-Ge2 58.571(12), C1-Ge1-Ge2 155.16(7), Co-Ge1-C1 146.22(7), Co-Ge2-Ge1 58.579(12) , Co-Ge2-C25 150.92(7), C25-Ge2-Ge1 149.91(7).

However, the Ge1−Ge2 distance (2.3137(4) Å) of **3-Co** is slightly shorter than that of **1-Co** (2.3456(3) Å), in which Ge_2Tbb_2 acts as a 2e-donor ligand and the longer Ge1−Ge2 distance is probably caused by the digermyne slippage (Ω = 13 %). Notably, the Ge1−Ge2 distance of **3-Co** is very similar to that of the trigermacyclopropenium cation $[Ge_3(Si^tBu_3)_3]BPh_4]$ (d(Ge−Ge)$_{av}$ = 2.326 Å), in which all the three Ge−Ge distances are crystallographically identical due to the 2π-electron delocalization in

the Ge_3-ring.[109] According to the quantum chemical calculation the $CoGe_2$ ring of **3-Co** is also a 2π-electron system. Complex **3-Co** was also characterized by multinuclear NMR spectroscopy. It displays the correct number of sharp signals in the ^1H and ^{13}C NMR spectra according to its pseudo-C_{2V} symmetric solid-state structure with free rotations of Tbb ligands around the Ge–C^{Tbb} bonds in the NMR time scale and is diamagnetic as expected for an 18-VE two-legged piano stool complex with a strong π-acceptor ligand leading to a large HOMO–LUMO gap.

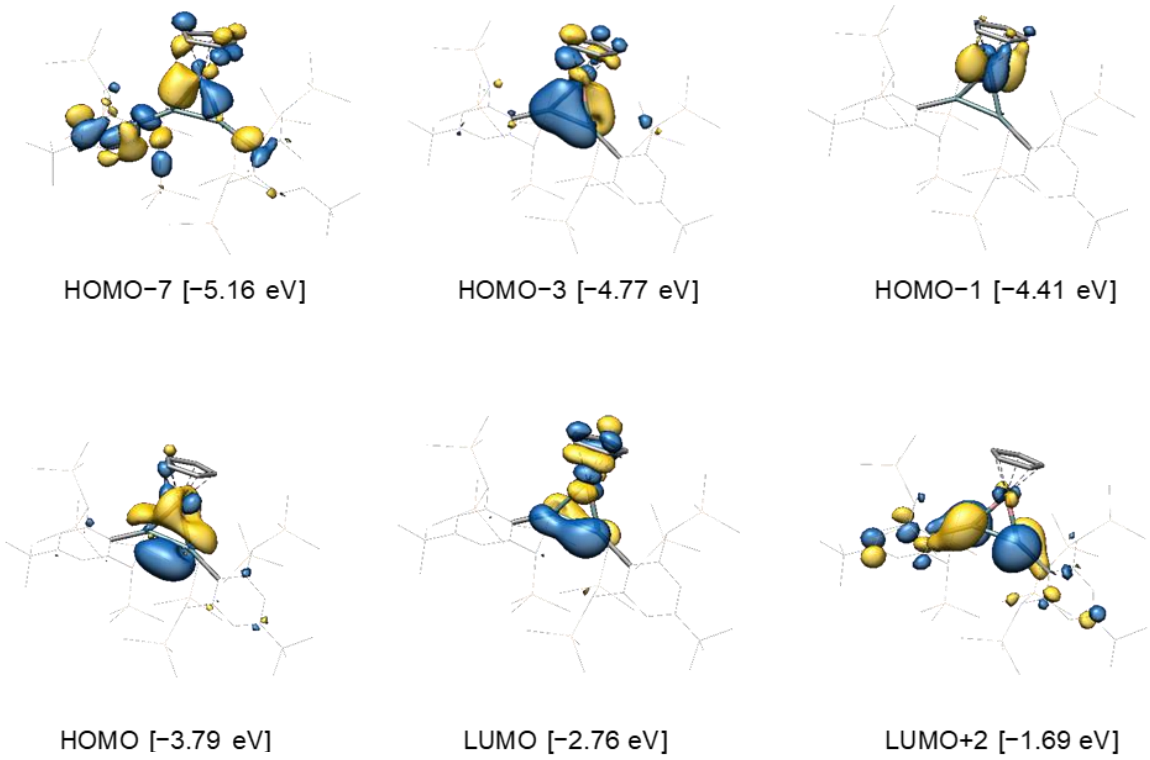

Figure 19. Selected Kohn-Sham MOs of **3-Co$_{calc}$** and their orbital energies (eV); the isosurface value is set at 0.04 $e^{1/2}$·$Bohr^{-3/2}$.

The electronic structure of **3-Co** was studied by NBO analysis of the gas phase optimized minimum energy structure **3-Co$_{calc}$**, which displays structural parameters in good agreement with the solid-state structure. According to the directed NBO analysis the cobalt-digermyne bonding is described by three important donor-acceptor interactions: two Ge_2Tbb_2→Co donations (σ and π_{out}) and one Co→Ge_2Tbb_2 π^*_{in}-back-donation with the respective *E(2)* of 428 kJ/mol, 55 kJ/mol, 38 kJ/mol and the occupancy of the Ge≡Ge NBOs of 1.7e (π_{in}), 1.1e (π_{out}), 0.7e (π^*_{in}), respectively. Thus, the NBO analysis confirms that Ge_2Tbb_2 acts as a four-electron donor ligand. Of note, the π^*_{out}(Ge–Ge) antibonding NBO shows significant non-Lewis occupancy of 0.1e and a Co→Ge_2Tbb_2 δ_{out}-back-donation interaction with an *E(2)* of 59 kJ/mol

(10 % of total *E(2)* of 580 kJ/mol). These interactions are also found the in the following canonical molecular orbitals HOMO, HOMO–3, HOMO–7 and HOMO–1, respectively. Accordingly, the LUMO is a non-bonding orbital due to the presence of Cp-Co-$Ge_2(Tbb)_2$ 3c-4e interaction with a π^*_{out}(Co−Ge) character and the LUMO+2 represents the δ^* orbital. The synergic effects of stronger donation and weaker back-donation is also reflected in the positive natural charge on the Ge_2Tbb_2 ligand (+0.22).

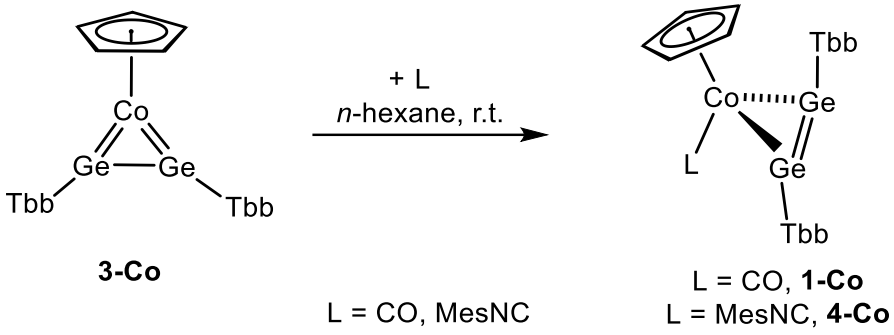

Scheme 7. Reactivity of **3-Co** with small neutral nucleophiles.

The synthetic potential of **3-Co** was first tested with small nucleophiles such as CO and MesNC (***Scheme 7***). When CO gas (0.3 bar) was introduced in to a dark orange-red, *n*-hexane solution of **3-Co** at ambient temperature, the colour of the reaction solution immediately changed to brown. The ^{1}H NMR and FT-IR spectroscopic analysis of the reaction solution confirmed about a quantitative transformation of **3-Co** into **1-Co**. When the similar reaction was performed with one equivalent of MesNC at ambient temperature the reaction solution immediately turned olive green. Analysis of the reaction progress by IR and ^{1}H NMR spectroscopy confirmed the co-ordination of MesNC ligand to the cobalt center [$\tilde{\nu}$ (cm^{-1}) = 2036, ν(CN)] along with a quantitative transformation of **3-Co** [CpCo(η^2-*cis*-Ge_2Tbb_2)] to **4-Co** [CpCo(CNMes)(η^2-*trans*-Ge_2Tbb_2)]. Out of curiosity, when 2 equivalents of MesNC or even more was added in to the *n*-hexane solution of **3-Co** at ambient temperature, the reaction mixture was found to be messy by spectroscopic analysis where the $CpCo(CNMes)_2$[110] was identified as the only Cp containing compound present in the reaction solution along with some unidentified Tbb and Mes containing products.

Compound **4-Co** was isolated as dark-green solid in 69 % yield and comprehensively characterized by spectroscopic and sc-XRD analysis. Suitable single crystals of **4-Co** were obtained by slow cooling its saturated *n*-hexane (olive-green) solution at –10 °C. In solid, the structural parameters are well comparable to that of **1-Co** and are summarized in ***Table 1***.

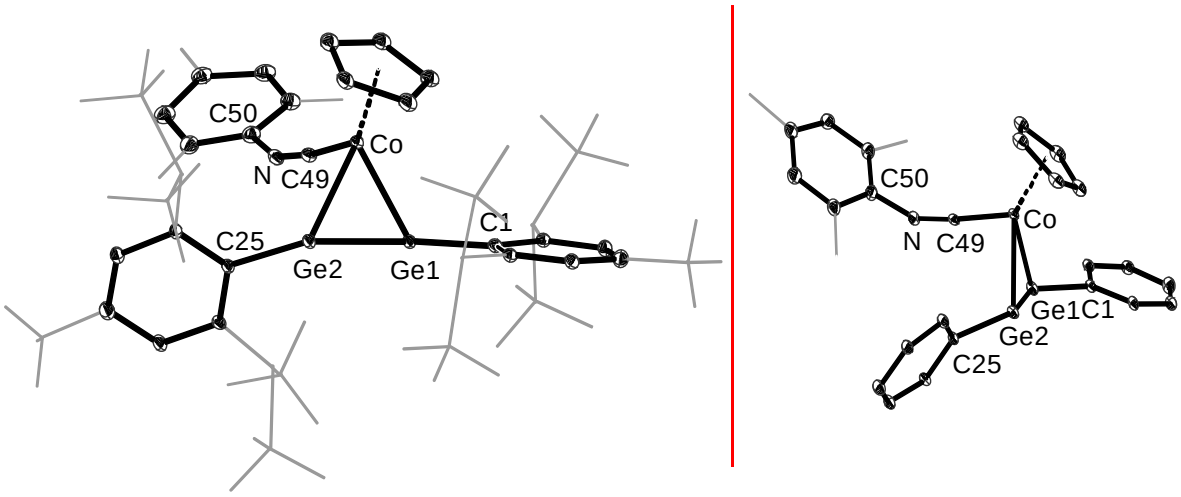

Figure 20. DIAMOND plot of the molecular structure(*left*) of **4-Co** and its side view(*right*). Thermal ellipsoids are set at 30 % probability level. Hydrogen atoms are omitted, the Dsi and ^{t}Bu substituents of the Tbb ligand and C^{2},C^{4},C^{6} methyl groups of Mes ligand are presented in wire-frame for clarity. Selected bond lengths [Å], bond angles [°] and torsion angle [°]: Co-Ge1 2.3209(15), Co-Ge2 2.4709(15), Ge1-Ge2 2.3928(12), Co-C49 1.772(8), C49-N 1.174(10), C1-Ge1-Ge2 133.7(2), Co-Ge1-Ge2 63.21(4), Co-Ge1-C1 119.5(2), C25-Ge2-Ge1 128.4(2), Co-Ge2-Ge1 56.97(4), Co-Ge2-C25 114.3(2), Co-C49-N 173.3(7), C49-N-C50 154.0(8), C1-Ge1-Ge2-C25 –157.41(3).

Table 1. Solid state structural parameters of digermyne complexes.

Comp.	Co-Ge1 (Å)	Ge1-Ge2 (Å)	∑Ge (°)	∠C1-Ge1-Ge2-C25 (°)
1-Co	2.3675(4) & 2.5010(4)	2.3456(3)	306.6 & 316.8	155.9(1)
3-Co	2.2268(4) & 2.2223(4)	2.3137(4)	359.9 & 359.6	4.3(1)
4-Co	2.3209(15) & 2.4709(15)	2.3928(12)	316.6 & 299.7	157.4(3)

The solution structure of **4-Co** was investigated by multinuclear NMR spectroscopy, showing resemblances to that of the ^{1}H NMR spectrum of **1-Co** at 298 K in (D_8)THF. It displays only one set of broad signals for the two diastereotopic Tbb groups and only one set of signals for the Mes group, suggesting fast chemical exchange of the Tbb ligands as well as fast chemical exchange of $C^{3,5}$ protons of the Mes group on the NMR time scale. This chemical exchange processes were studied by variable temperature ^{1}H NMR spectroscopy. In the slow exchange limit spectrum, indeed a separate set of signals was observed for each Tbb substituent. Unlike **1-Co**, the rotation of both Tbb substituents is frozen out on the NMR time scale, probably due to increased steric bulk of the MesNC ligand in place of CO. So, two different broad singlets for each of the $C^{3,5}$ protons for each Tbb ligand as well as one singlet for each

of the ^{t}Bu methyl protons of Tbb_X and Tbb_Y at δ = 1.37 ppm and 1.41 ppm is observed. However, the rotation of the mesityl ligand around N-C^{Mes} bond could not be frozen out.

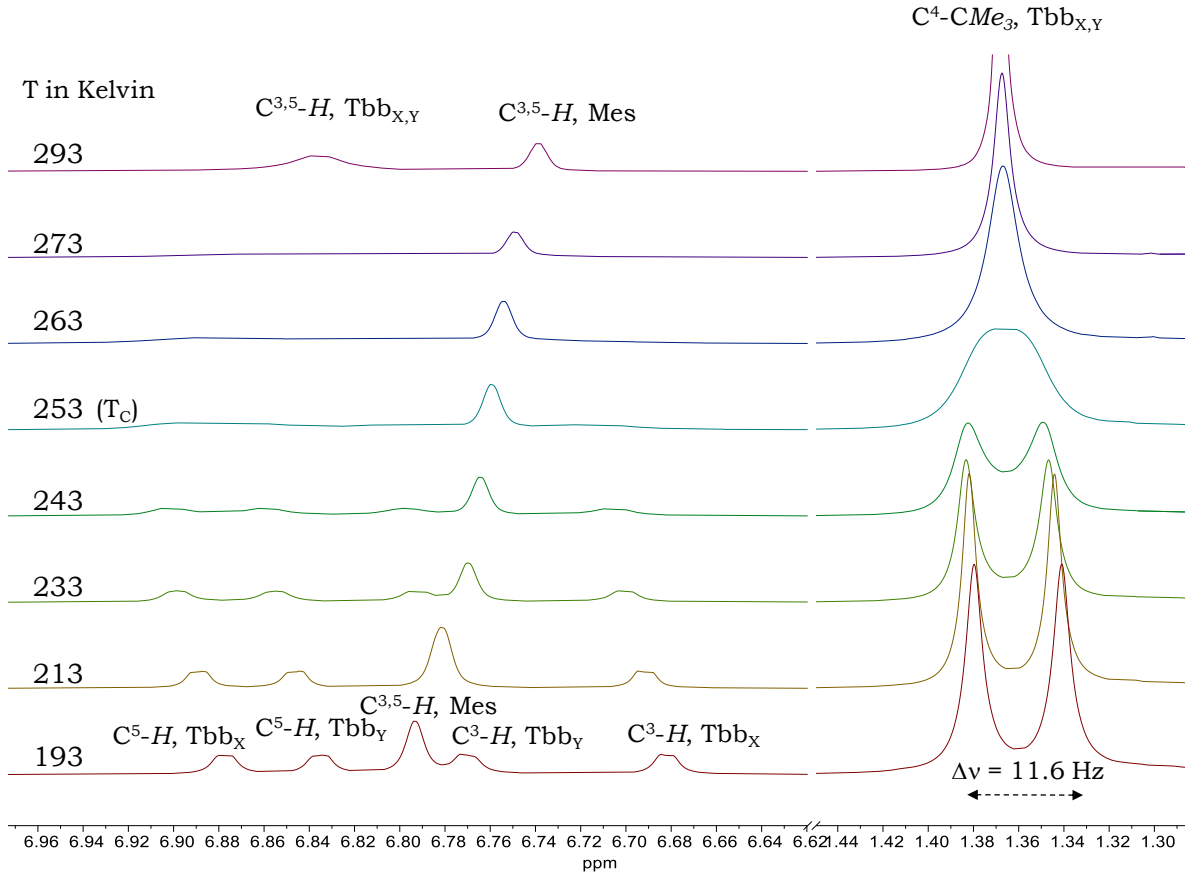

Figure 21. Excerpt of the VT-^{1}H NMR spectra (300.1 MHz) of **4-Co** in (D_8)THF from 193 K – 293 K showing the exchange of C^4-C*Me$_3$* and C^{3,5}-*H* signals of the Tbb_X and Tbb_Y substituents.

The Gibbs free energy of activation for the dynamic process of **4-Co** was similarly calculated as for **1-Rh** using the modified Eyring equation. Where is T_c, the coalescence temperature ($T_c \approx 253$ K) and $\Delta\nu$ (11.6 Hz) is the chemical shift difference of the exchanging ^{t}Bu singlets in the low-temperature limit spectrum (193 K), where no exchange is assumed to occur (k = 0). The obtained $\Delta G^{\ddagger}$ value of 54.8 kJ/mol compared well to that of **1-Co** ($\Delta G^{\ddagger}$ = 59 kJ/mol).

2.2. Unusual cycloaddition chemistry of digermyne complexes

Structural, spectroscopic and computational studies of **1-Co** and **3-Co** suggested that both compounds would undergo Ge-centered reactivity. This hypothesis was first verified by reacting **1-Co** with 2-butyne. In fact, heating a *n*-hexane solution of **1-Co** in the presence of an excess of 2-butyne at 65 °C for 65 hours was accompanied by a gradual color change from brown to dark green. Monitoring the progress of the

reaction by solution FT-IR and ^{1}H NMR spectroscopy revealed the quantitative formation of the carbonyl free 2,5-digerma-cobaltacyclopentatriene **5-Co**.

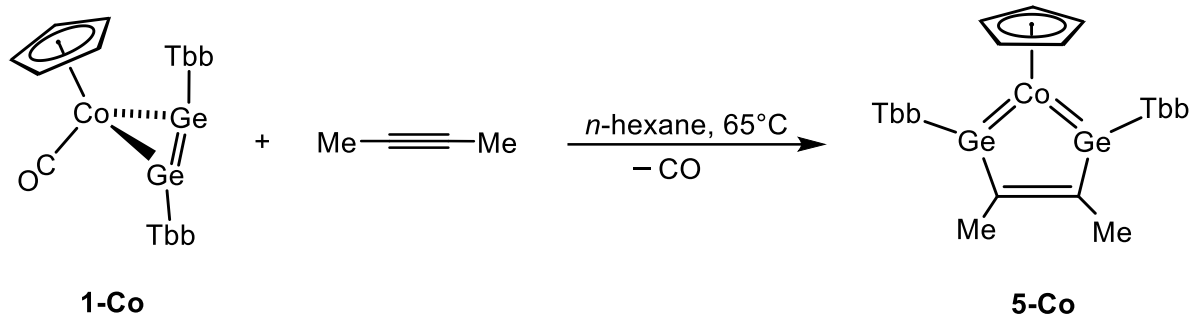

1-Co **5-Co**

Scheme 8. Reactivity of **1-Co** with 2-butyne.

In order to get a comparative reactivity study on *cis*- and *trans*-bent digermyne complexes, **3-Co** was also reacted with 2-butyne and it was found to react much faster than **1-Co**. The reaction of **3-Co** with 2-butyne (10 equiv.) at 65 °C for 5 h led to the formation of **5-Co** along with the digermacyclobutadiene complex **6-Co** [CpCo($Ge_2Tbb_2C_2Me_2$)$_{cbd}$] almost in 1 : 1 molar ratio. Interestingly the molar ratio of these two complexes did not alter even after prolonged heating (24 h) at this temperature.

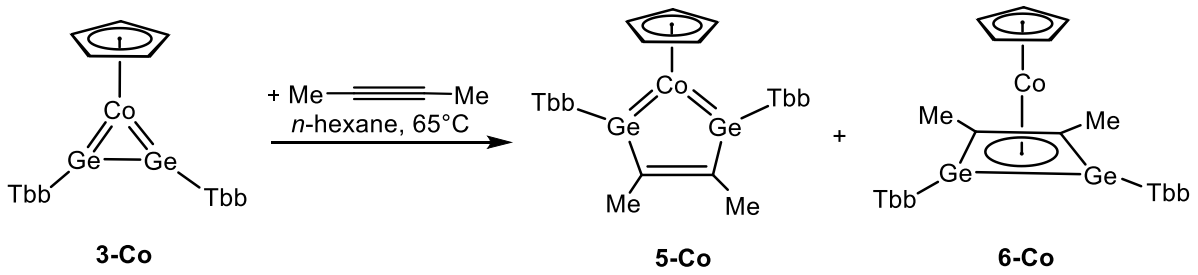

3-Co **5-Co** **6-Co**

Scheme 9. Reactivity of **3-Co** with 2-butyne.

However, when the mixture of **5-Co** and **6-Co** was dissolved in benzene and heated at 80 °C for 34 h a complete and irreversible valence isomerization of **6-Co** to **5-Co** was observed (***Scheme 10*** and ***Figure 22***). Of note, the selectivity of the reaction of **3-Co** with 2-butyne did not change much when the reaction was carried out at sub-zero temperatures. Compound **5-Co** was isolated in 75 % yield as an extremely air-sensitive, but thermally robust (T_{dec} = 260 °C) dark green solid. It is well soluble in *n*-hexane, Et_2O, benzene and toluene at ambient temperature, but insoluble in CH_3CN. Under strict exclusion of air a solution of **5-Co** in (D_6)benzene does not show any sign of decomposition after one week at ambient temperature.

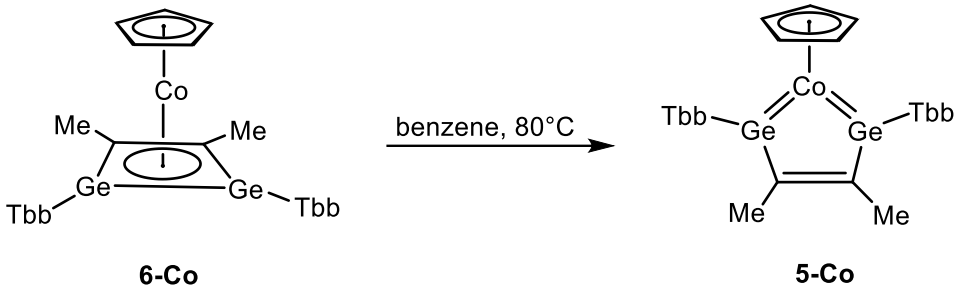

6-Co **5-Co**

Scheme 10. Irreversible valence isomerization of **6-Co** to **5-Co**.

Of note, the heavier tetrel (E = Si-Pb) congeners of metallacyclopolyenes of the general formula $[L_nM\{\kappa^{2(1,3)}\text{-}(CR)_n\}]$(n=3 (metallacyclobutadiene),[36] 4(metallacyclopentadiene, metallacyclopentatriene),[37] 5 (metallabenzene)),[39] are rare, only few monosila- and monogerma-metallacyclobutadienes of Cr,[57] Mo,[i][57] W,[55,58] Ta,[59] and Os[56] have been reported so far. The 2,5-digerma-cobaltacyclopentatriene **5-Co** is the first example of the heavier ditetrel congeners of metallacyclopolyenes to be reported and hence was thoroughly characterized.

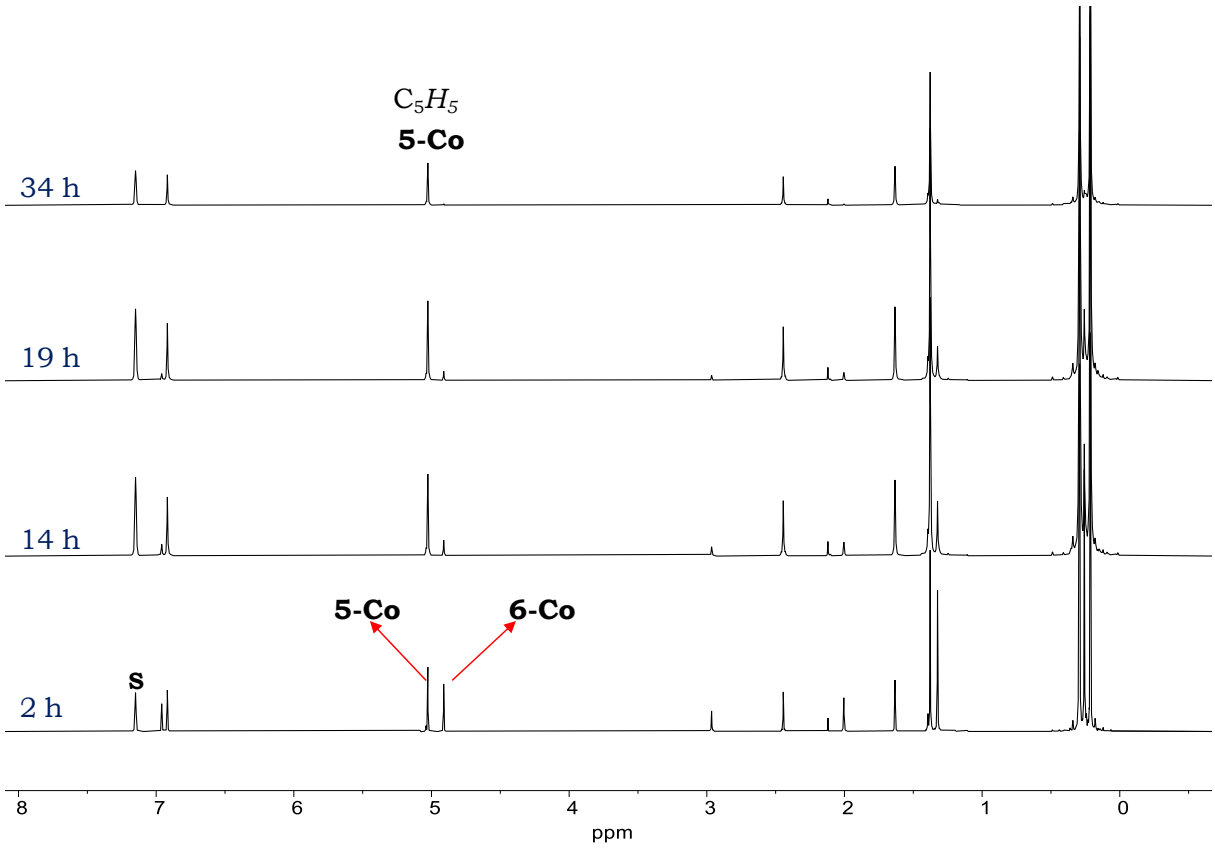

Figure 22. Stack plot of ^{1}H NMR (300.1 MHz) spectra recorded in (D_6)benzene at 298 K during the reaction monitoring of the valence isomerization. S represents the residual proton of deuterated solvent.

The molecular structure of **5-Co** was determined by sc-XRD analysis of the plate shaped green crystals, which were grown by slow evaporation of its saturated Et_2O/CH_3CN (1 : 1, V/V) solution at ambient temperature inside the glove box. Complex **5-Co** crystallizes as a solvate **5-Co•**(1.25 Et_2O, 0.5 CH_3CN) in the P-1 space

group. It features a planar cobaltacycle with the largest atom-to-plane distance of 0.062 Å for Ge1. As expected for closed-shell d^8-$CpML_2$ complexes with large HOMO-LUMO gap (*vide infra*),[111] the metallacyclic ring plane (***Figure 23***) is nearly orthogonal to the Cp plane with a pyramidality angle α of 175.0(1)° The Ge1 and Ge2 atoms are trigonal planar coordinated (∑(∠Ge1,2) = 360°), and the phenyl rings of Tbb are nearly orthogonally arranged with respect to the cobaltacycles (interplane angles of 119.7(1)° (Ge1−Tbb) and 108.2(1)° (Ge2−Tbb)). This spatial arrangement in the crystal lattice gives rise to a pseudo-C_{2v} symmetry of **5-Co** with the C_2-axis being through the C_t-Co-Z vector (***Figure 23***). The Co−Ge1 and Co−Ge2 (2.1791(3) Å, 2.1852(3) Å) distances are quite similar as in **2-Co**, but far too short compared to the Co−Ge single bond lengths of the CSD reported Co(I)-germyl complexes (2.294 Å – 2.525 Å) and are in the range expected for a Co=Ge double bond. The C49−C50 bond length (1.325(2) Å) is a typical localized C=C double bond and the Ge1−C49 and Ge2−C50 distances (1.991(1) Å, 1.975(1) Å) are very similar to those of the Ge1−C1 (1.964(4) Å) and Ge2−C25 (1.974(3) Å) single bonds.

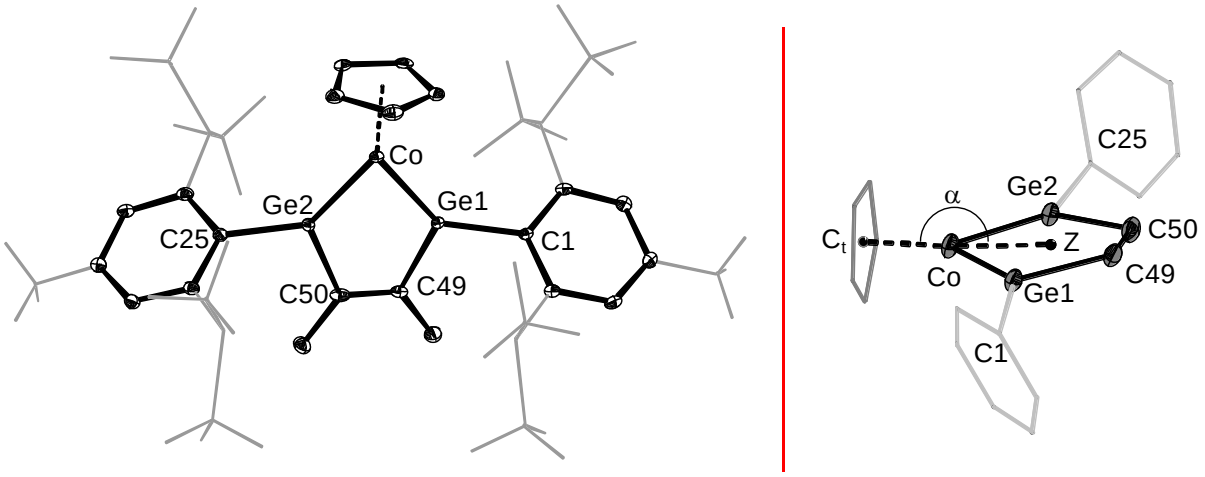

Figure 23. (*left*) DIAMOND plot of the molecular structure of **5-Co**. Thermal ellipsoids are set at 30 % probability level. Hydrogen atoms are omitted and the Dsi and ^{t}Bu substituents of the Tbb ligand are presented in wire-frame for clarity. Selected bond lengths [Å] and bond angles [°]: Ge1-Ge2 2.8996(6), Co-Ge1 2.1902(7), Co-Ge2 2.1836(7), Ge1-C49 1.993(4), Ge2-C50 1.980(4), C49-C50 1.344(5), Co-Ge1-C49 114.86(10), C1-Ge1-C49 103.82(15), Co-Ge1-C1 140.70(11), Co-Ge2-C50 115.46(11), Co-Ge2-C25 137.17(11), C25-Ge2-C50 107.36(15). (*right*) A side-on view of the truncated molecular structure of **5-Co**; α = 175.0(1)°, C_t and Z is the centroid of the Cp and the cobaltacycle, respectively.

The 2,5-*trans*-annular distance of 2.8950(3) Å between the Ge1 and Ge2 atoms is far too long compared to normal Ge−Ge single bonds in digermanes (average: 2.45 Å), but lies well within the sum of van der Waals radii of two Ge atoms (4.22 Å).[112] A CSD search of structures having a Ge···Ge separation of 2.80 Å – 2.90 Å between its two tri-coordinated Ge atoms (without considering the *trans*-annular Ge atom) gave

several structures featuring long Ge···Ge distances, which were ascribed by quantum chemical calculations as a π-single bond,[113] ultra-long σ-bond,[114] part of a multi-centered bond (π(3c-2e)),[115] stretched-bond with singlet diradical character,[116] and even no-bond.[117,118] Thus, the Ge···Ge bond-type of **5-Co** cannot be axiomatically derived from its molecular structure by comparison with the structural data available in the CSD database. To get a deeper insight into the bonding on **5-Co** its electronic structure was analyzed by quantum chemical calculations using level-**I**. Gas phase optimized structure $(\mathbf{5\text{-}Co})_{\mathbf{calc}}$ displays bonding parameters in good agreement with those of the solid-state structure. The pertinent MOs are displayed in ***Figure 24*** and were interpreted by constructing a MO-diagram between the CpCo and $(Ge_2(Tbb)_2C(Me)_2)$ fragments in pseudo-C_{2V} point group. Thus, four symmetry adapted interactions between the fragment orbitals of A_1, B_1, A_2 and B_2 symmetries give rise to HOMO–12, HOMO–4, HOMO–2 and HOMO, respectively. The Co–Ge bonding of $(\mathbf{5\text{-}Co})_{\mathbf{calc}}$ can be described by these four interactions, with HOMO being a 3c-2e π_{out}(Ge–Co–Ge) bond, HOMO-2 a 3c-2e δ_{out}(Ge–Co–Ge) bond, whereas, HOMO-4 and HOMO-14 contribute in the formation of 3c-2e (Ge–Co–Ge) σ-bonds.

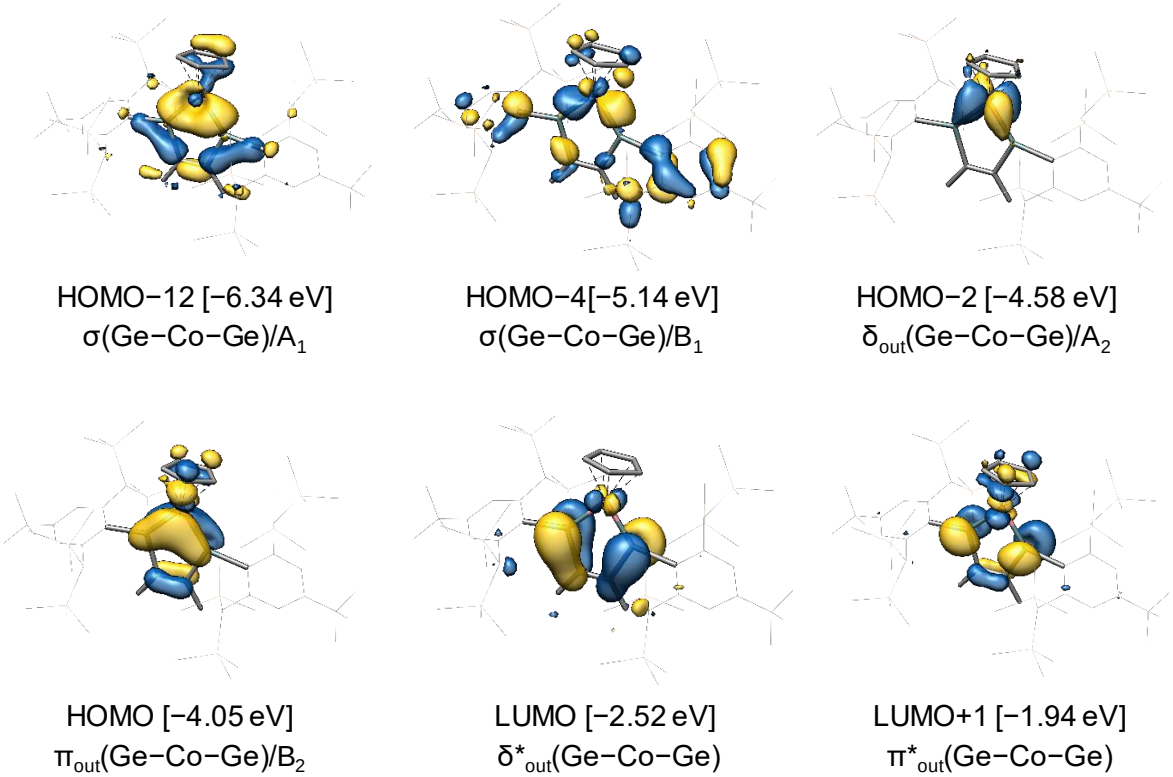

Figure 24. Selected Kohn-Sham MOs of $(\mathbf{5\text{-}Co})_{\mathbf{calc}}$ and their orbital energies (eV); the isosurface value is set at 0.04 $e^{1/2}\cdot Bohr^{-3/2}$ and the symmetry labels are given according to the C_{2V} point group.

Further insight into the electronic structure of $(\mathbf{5\text{-}Co})_{\mathbf{calc}}$ was supplemented by the Natural Bond Orbital (NBO) analyses The local NRT analysis showed that the NRT

space is dominated by no-bond resonance structures. Thus the 18-VE zeroth-order Natural Lewis Structure (NLS) **5-Co-A** was found with the highest contribution of 16 %, whereas, the participation of **5-Co-B** – **5-Co-D** in the resonance hybrid is negligible. A directed NBO analysis using **5-Co-A** gave two units $[CoGe_2(Tbb)_2C_2(Me)_4]^{0.3+}$ and $[Cp]^{0.3-}$ due to the non-participation of the p(Co)-NAO as evident from the natural electronic configuration of Co ($4s^{0.3}3d^{8.7}4p^{0.0}$).[119–121] The cobaltacyclic ring $CoGe_2(Tbb)_2C_2Me_2$ shows high occupancies of all Lewis type valence NBOs (≥1.8e). The pertinent NBOs are the two nearly covalent (63%(Ge)) Co–Ge σ-BD NBOs, two highly polarized (88%(Co)) Co–Ge π_{out}-BD NBOs and a unpolar C=C π_{out}-BD NBO.

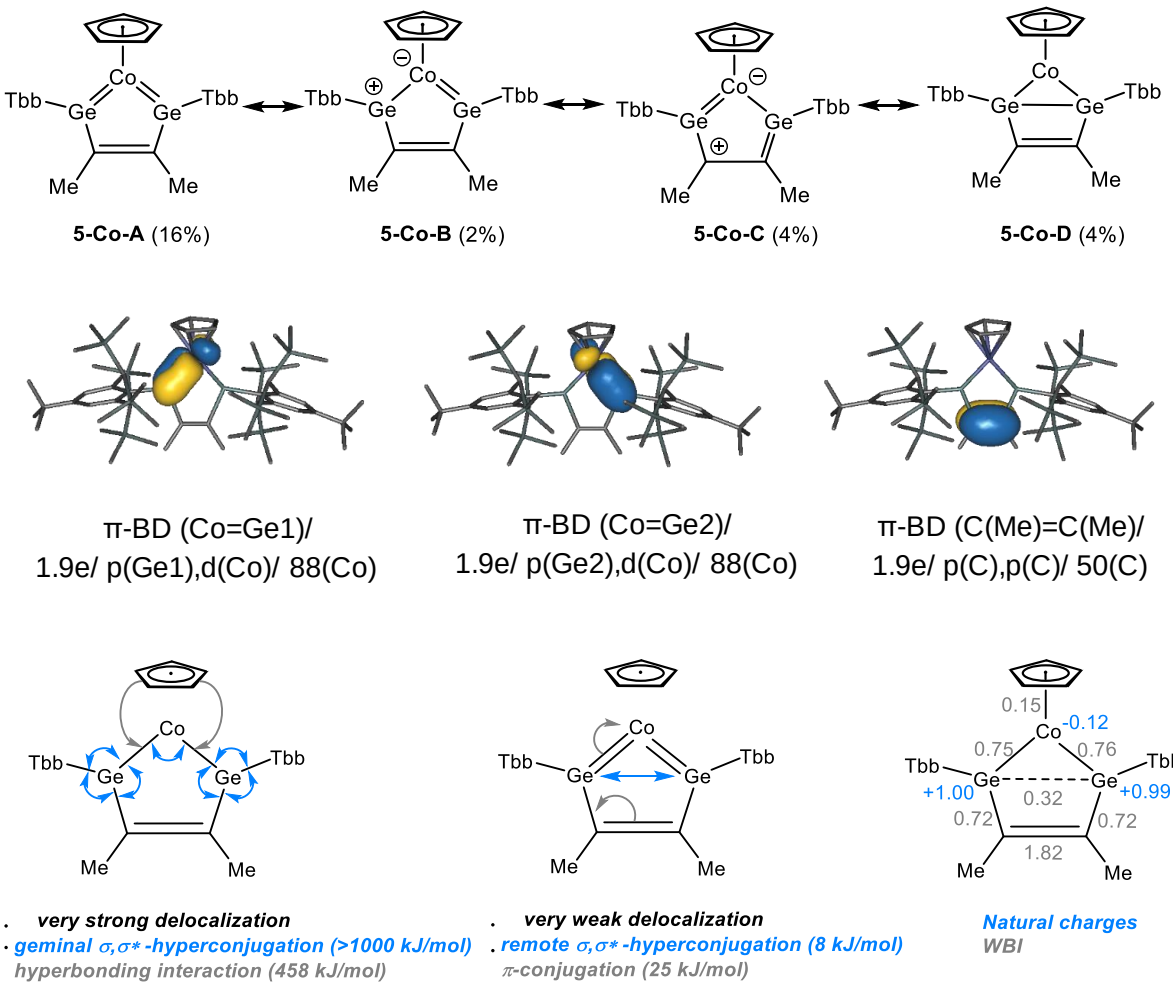

Figure 25. Results of NBO analyses of $(\mathbf{5\text{-}Co})_{calc}$ at the level-I theory: (*top*) main zeroth-order Natural Lewis Structures (NLS); (*middle*) selected Bond-Pair (BD) NBOs (type/ occupancy/ NHO/ % polarization); (*bottom*) selected principal delocalizations, natural charges, and Wiberg Bond Indices (WBI).

A further look at the non-Lewis electrons showed the presence of a total of 2.4e NL-electrons in the cobaltacycles including its four exocyclic ring σ-bonds (average: 0.2e/bond) indicating a highly delocalized structure. Non-Lewis occupancy in an

unsaturated ring generally indicates extensive π-delocalization. However, an analysis of the results of principal delocalizations obtained from the Second Order Perturbation Theory (SOPT) analysis in NBO basis revealed that this is mainly due to four very strong *3c-4e Cp→BD*(Co−Ge) hyper-bonding interactions*[121] ($\sum E(2)$ = 458 kJ/mol) and fourteen *geminal σ,σ*-hyperconjugative interactions*[122] ($\sum E(2)$ > 1000 kJ/mol).

On the other hand, the π-conjugation (C=C↔Co=Ge) and the remote σ(Ge−C^{Tbb})↔σ*(Ge−C^{Tbb}) hyperconjugation was found to be very week with an $\sum E(2)$ of only 25 kJ/mol and 8 kJ/mol respectively. Natural Population (NPA) analysis (*see* ***Figure 25*** (*bottom right*)) showed very high positive natural charge at both the Ge centers (+0.99 and +1.00) and the Co is slightly negative (−0.13) as expected for a rather large Cp→cobaltacycle charge transfer (0.68e) and highly polarized Co=Ge π-bond. The Wiberg Bond Index (WBI) computed in the Natural Atomic Orbital (NAO) basis is 0.32 for the Ge1···Ge2 contact, which is much smaller than that of the Co−Ge (0.75), Ge−C^{ring} (0.74) and Ge−C^{Tbb} (0.72) bonds and also smaller than the WBI of the Ge···Ge interaction in [1,1,1]-pentagermapropellane $Ge_2(GeMes_2)_3$ (0.55 in B3LYP/def2-TZVP level),[116] but considerably larger than the average WBI of Co−C^{Cp} bonds (0.15), suggesting that the sharing of average number of electron pairs between the two Ge centers of (**5-Co**)$_{calc}$ is quite low. Thus, on the basis of WBI the Ge1···Ge2 bond-type could be interpreted as a *weak partially covalent interaction, which is also reflected in the remote* σ(Ge−C^{Tbb})→σ*(Ge−C^{Tbb}) hyperconjugation with a very small *E(2)* value.

In contrast to **5-Co**, the isolation of **6-Co** from the crude reaction mixture proved to be difficult and hence its NMR characterization was carried out using the crude product. All the ^{1}H and $^{13}C\{^{1}H\}$ NMR signals were unequivocally assigned by correlation spectroscopy suggesting the presence of a 1,2-digermacyclobutadiene ligand η^4-coordinated to the Co-center. The most significant chemical shifts were observed in ^{13}C NMR spectra for the ring carbon atoms (C49 and C50 atoms see the molecular structures), which appear as distinct singlets at 86.7 ppm and 164.2 ppm for **6-Co** and **5-Co** respectively. The solution structure of **6-Co** is also in line with its solid-state structure which was determined by sc-XRD analysis of plate-shaped brown crystals, which were grown by slow evaporation of a saturated Et_2O/CH_3CN (4 : 1, V/V) solution at ambient temperature inside the glove box. The salient structural features are the Ge1−Ge2 distance (2.4307(13) Å), which is close to that in a typical Ge−Ge single bond (2.45 Å), a nearly planar Ge_2C_2 core (*interflap* angle C49-Ge1-C50-Ge2 170.09(2)°) with a Co···Cb_t (Cb_t = centroid of the 1,2-digermacyclobutadiene ring) distance of 1.778(2) Å, a *syn-clinal* arrangement of the

C1-Ge1-Ge2-C25 skeleton (ϕ = 70.30(2)°) and a slight tilting of the two ring metal coordinated rings with a tilt angle Cp_t–Co–Cb_t of 168.52(2)° (Cp_t = centroid of the cyclopentadienyl ring).

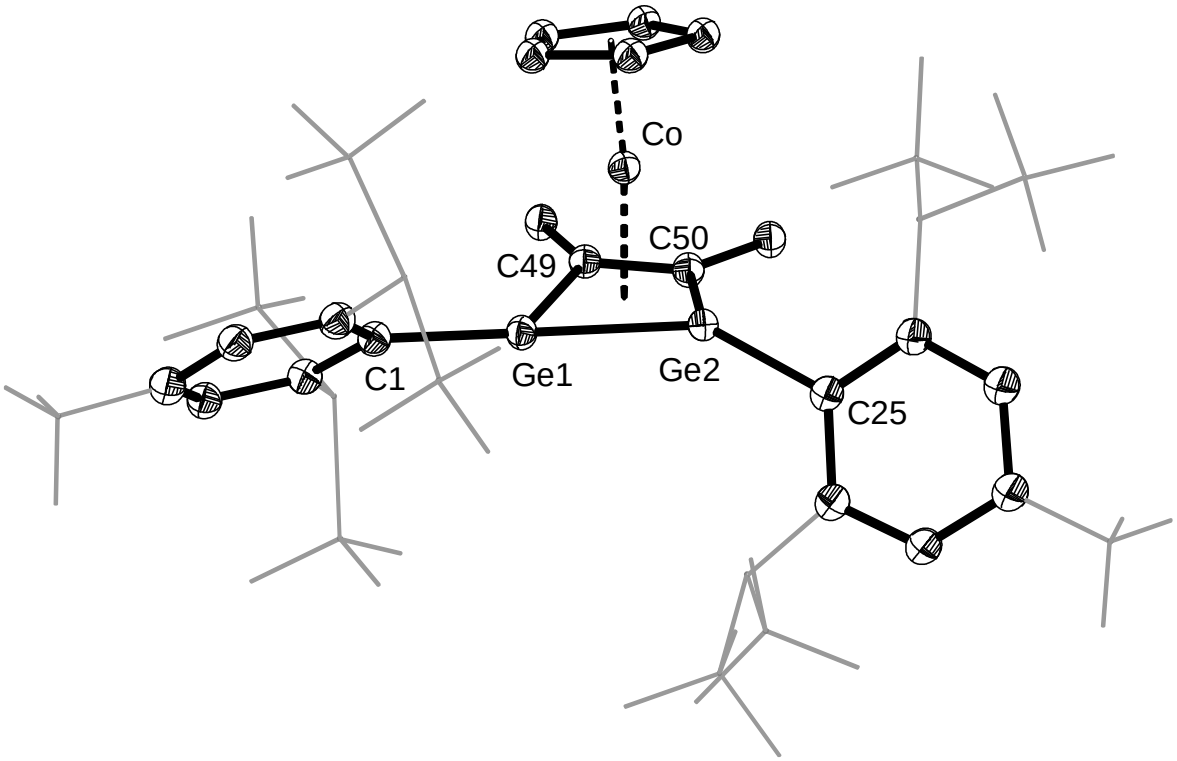

Figure 26. DIAMOND plot of the molecular structure of **6-Co**. Thermal ellipsoids are set at 30 % probability level. Hydrogen atoms are omitted and the Dsi and ^{t}Bu substituents of the Tbb ligand are presented in wire-frame for clarity. Selected bond lengths [Å], bond angles [°] and torsion angle [°]: Co-Ge1 2.5316(17), Co-Ge2 2.3393(15), Co-C49 2.027(10), Co-C50 2.028(10), Ge1-Ge2 2.4307(13), Ge1-C49 1.969(9), Ge2-C50 1.947(9), C49-C50 1.387(13), C1-Ge1-Ge2 152.5(3), C1-Ge1-C49 128.7(4), C49-Ge1-Ge2 74.8(3), C25-Ge2-C50 125.3(4), C25-Ge2-Ge1 148.6(2), C50-Ge2-Ge1 74.0(3), Ge1-C49-C50 103.6(7), Ge2-C50-C49 106.7(7), Ge1-C49-C50-Ge2 –9.1(7).

2.3. Mechanism of the alkyne insertion reaction of 1-Co

The first assumption of an experimental mechanistic pathway for the alkyne insertion reaction of **1-Co** was that the reaction between 1,2-digermacyclobutadiene (**7-Ge**) and $CpCo(CO)_2$ might lead to a selective formation of **5-Co** through the elimination of one equivalent of CO. So, to examine this hypothesis compound **7-Ge** was isolated and characterized (***Scheme 11***).

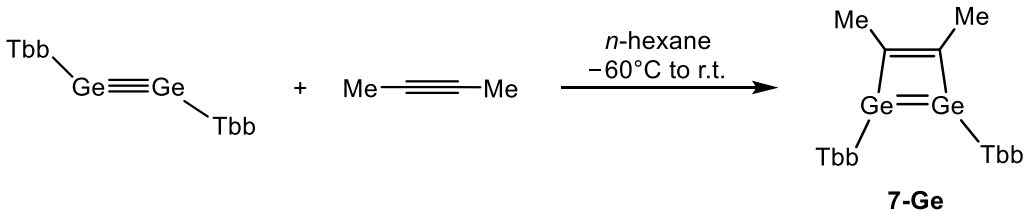

Scheme 11. [2+2]-cycloaddition reaction of Ge_2Tbb_2 with one equivalent of 2-butyne.

To a precooled (–60 °C) orange-red *n*-hexane solution of Ge_2Tbb_2, one equivalent of a stock solution of 2-butyne was added at –60 °C. The reaction solution turned immediately dark-green. Analysis of an aliquot of the reaction solution by ^1H NMR spectroscopy revealing the selective formation of **7-Ge** along with a small amount of **8-Ge** (ca. 7 mol%) and some unreacted Ge_2Tbb_2 (ca. 7 mol%). After a general work-up **7-Ge** was isolated as thermolabile dark green solid in 65 % yield. It is an extremely air-sensitive solid, which decolorizes immediately upon contact with air. It is well soluble in *n*-pentane, benzene, Et_2O and THF at ambient temperature, and converts slowly to an equimolar mixture of Ge_2Tbb_2 and **8-Ge** in solution at ambient temperature. Monitoring of this reaction by ^1H NMR spectroscopy in (D_6)benzene revealed a very slow conversion at 25 °C (ca. 6 mol % after 4 h), which can be accelerated at 70 °C (ca. 40 mol % after 7 h).

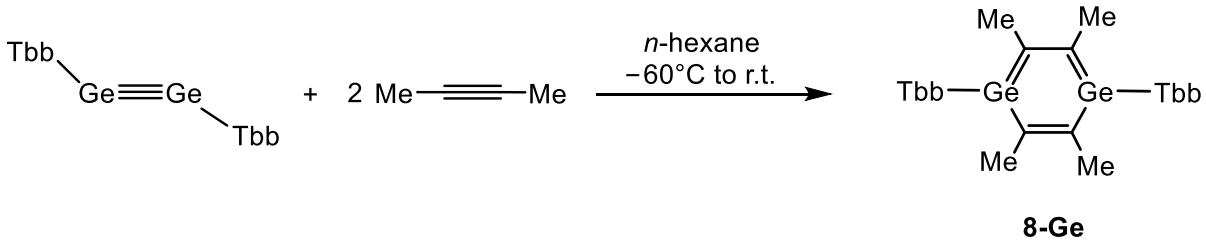

Scheme 12. [2+2+2]-cycloaddition reaction of Ge_2Tbb_2 with two equivalents of 2-butyne.

Using similar conditions, **8-Ge** (***Scheme 12***) was also synthesized from Ge_2Tbb_2 and two equivalents of 2-butyne, proceeded by an immediate colour change to green then within few minutes to orange. ^1H NMR spectroscopic analysis of the reaction solution revealed the selective formation of **8-Ge**, which was isolated after a work-up as an orange solid in 60 % yield. It is moderately air-sensitive but thermally robust solid (T_{dec} = 274 °C) and well soluble in *n*-hexane, benzene, toluene and Et_2O at ambient temperature.

Both compounds (**7-Ge** and **8-Ge**) were characterized using multinuclear NMR spectroscopy, elemental analysis and sc-XRD analysis. Suitable single crystals of **7-Ge** (green plates) were grown upon cooling a saturated *n*-pentane solution at –60 °C and clear orange blocks of **8-Ge•**(*n*-hexane) were obtained after storage of a concentrated *n*-hexane solution at –30°C for one day. The structural parameters of thw two compounds (***Figure 27***) are in quite good agreement with those of 1,2-digermacyclobutadienes [27,123,124] and 1,4-digermabenzenes[125] known in literature.

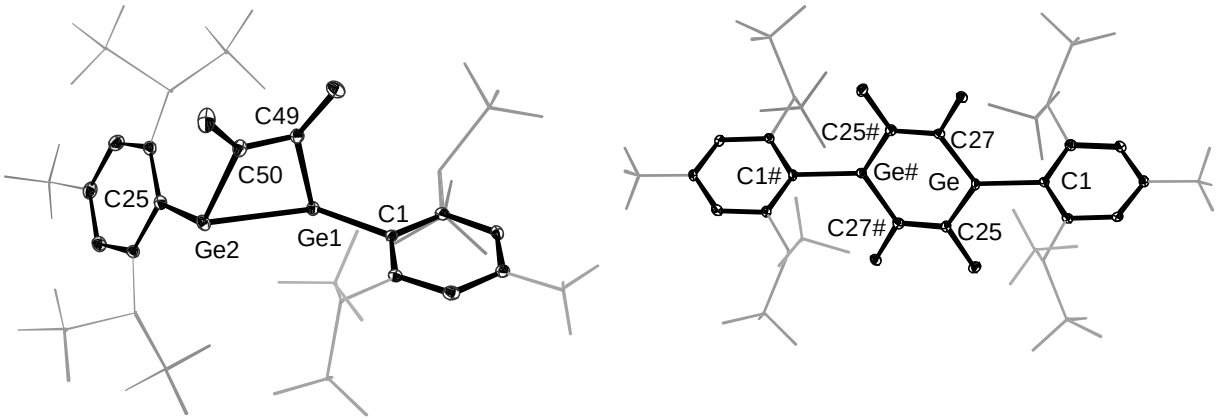

Figure 27. DIAMOND plot of the molecular structure of **7-Ge** (*left*) and **8-Ge** (*right*). Thermal ellipsoids are set at 30 % probability level. Hydrogen atoms are omitted and the Dsi and ^{t}Bu substituents of the Tbb ligand are presented in wire-frame for clarity. Selected bond lengths [Å], bond angles [°] and torsion angle [°]: [**7-Ge**] Ge1-Ge2 2.5591(3), Ge1-C49 1.9151(18), Ge2-C50 2.0652(18), C49-C50 1.360(3), C1-Ge1-Ge2 143.34(5), C49-Ge1-Ge2 81.80(5), C49-Ge1-C1 109.24(7), C25-Ge2-Ge1 108.74(5), C25-Ge2-C50 109.43(7), C50-Ge2-Ge1 63.05(5), Ge1-Ge2-C49-C50 –169.391(5); [**8-Ge**] Ge-C25 1.8659(17), Ge-C27 1.8592(17), C25-C27# 1.395(2), C1-Ge-C25 121.22(7), C1-Ge-C27 120.42(7), C25-Ge-C27 116.30(7).

After isolation of **7-Ge**, its reaction with $CpCo(CO)_2$ was performed at ambient temperature. Upon addition of an orange stock solution of $CpCo(CO)_2$ to a *n*-hexane solution of the 1,2-digermacyclobutadiene, the dark-green colour immediately turned brown. ^{1}H NMR and FT-IR spectroscopic analysis confirmed the formation of **1-Co** and **8-Ge** in an almost 1 : 1 ratio along with unreacted $CpCo(CO)_2$. The solution instability of **7-Ge** leading to a selective conversion to an equimolar mixture of Ge_2Tbb_2 and **8-Ge** is the most probable reason for such an experimental outcome.

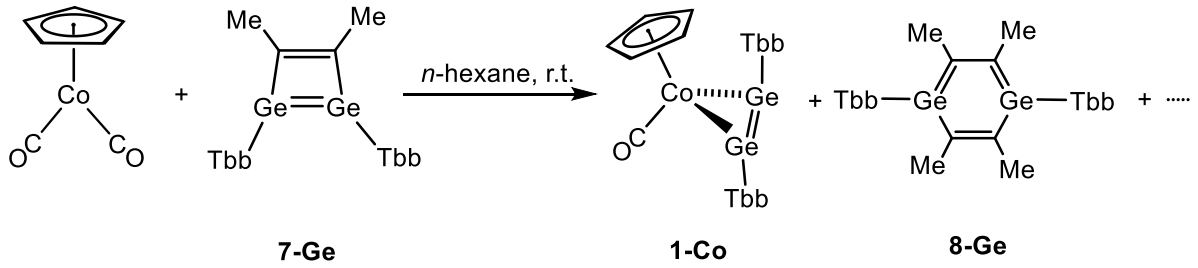

Scheme 13. Reaction of **7-Ge** with $CpCo(CO)_2$.

The most surprising fact about the reaction of **1-Co** with 2-butyne is the high selectivity and mild reaction condition. For example, in the reaction even traces of conceivable products, such as the valence isomers **5-Co** and **6-Co**, the cycloaddition products of digermyne with 2-butyne, i.e. 1,2-digermacyclobutadiene (**7-Ge**) and 1,4-digermabenzene (**8-Ge**) or hexamethylbenzene were not detected. This suggests that a competing alkyne/digermyne exchange reaction of **1-Co** with 2-butyne does not occur, probably indicating that Ge_2Tbb_2 is a stronger ligand than 2-butyne.

In line with this, the carbonyl absorption band of **1-Co** (ν_{CO} (*n*-hexane) = 1956 cm^{-1}) appears at lower energy than that of the alkyne complexes Cp(CO)Co(alkyne) (ν_{CO} = 2017 cm^{-1} ($C_2(SO_2{}^tBu)_2$),[102] 1979 cm^{-1} (1-hexyne),[126] and 1975 cm^{-1} (3,3,6,6-tetrymethyl-1-thaiocyclohept-4-yne).[127] In addition, the analysis of the electronic structure of (**5-Co**)$_{calc}$ (*vide supra*) clearly shows that its frontier orbital controlled [4+2]-cycloaddition reaction with 2-butyne is not thermally allowed forbidding the formation of **8-Ge**. Furthermore, the mild reaction conditions of the alkyne insertion are quite puzzling given the rather low energy carbonyl absorption band of **1-Co** that appears close to that of CpCo(CO)(PMe_3) (ν_{CO} (*n*-hexane) = 1956 cm^{-1}),[128] which does not undergo ligand substitution even under harsh thermal activations. These experimental data led us to surmise that the alkyne insertion of **1-Co** does not proceed via a CO-dissociation mechanism involving a CO-free digermyne complex (**3-Co**) (***Figure 28***).

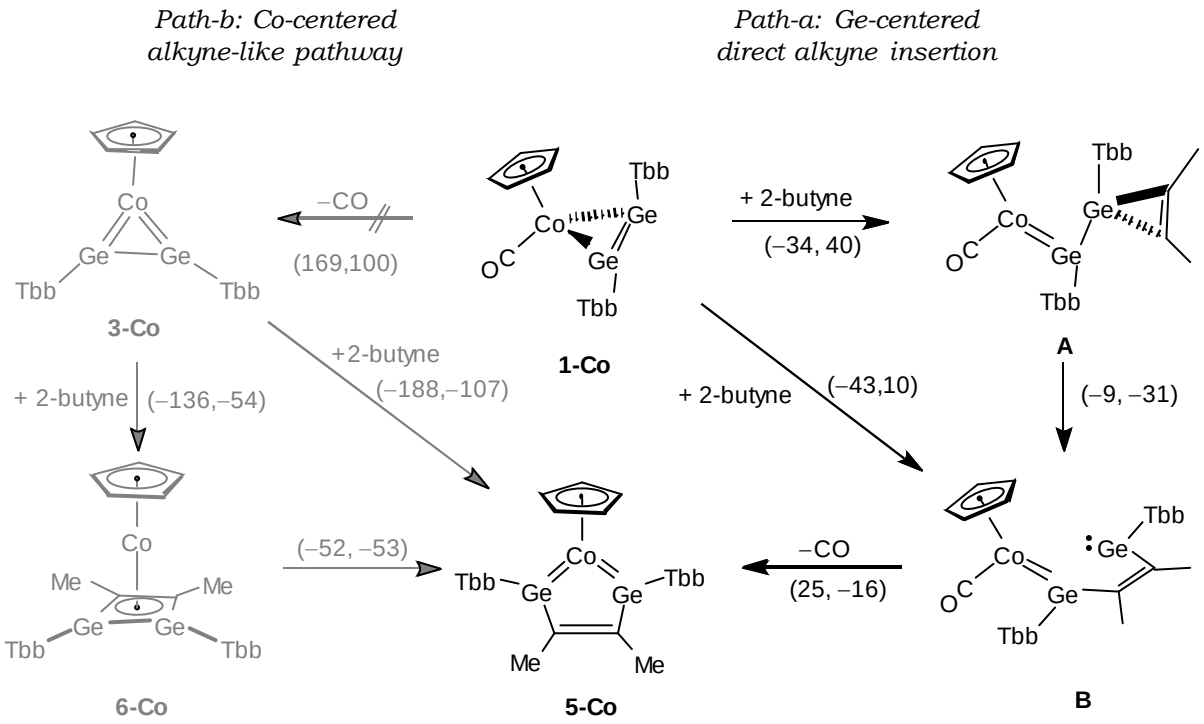

Figure 28. Plausible reaction mechanism of the formation of **5-Co** from **1-Co** and 2-butyne; the calculated reaction electronic and free Gibbs energies (ΔE, ΔG° in kJ/mol) are given in the parentheses with the reaction arrow.

The undertaken reactivity studies together with the physicochemical properties of **1-Co** unequivocally rule out the formation of the CO-free digermyne complex **3-Co** as an intermediate *via* CO loss during the alkyne insertion reaction of **1-Co**. Complex **3-Co**, if formed during this reaction, would be immediately intercepted by 2-butyne to give **6-Co**, which is stable towards valence isomerization to **5-Co** at 60 °C and hence would be observed by *in situ* NMR spectroscopy. However, no intermediate was

observed during the ^{1}H NMR monitoring in the course of the reaction of **1-Co** with 2-butyne. Based on these results, alkyne insertion reaction of **1-Co** most-likely follows an unusual Ge-centered direct alkyne insertion pathway, in which the Co-center acts as a spectator center (path-a, ***Figure 28***), and not a Co-centered alkyne-like pathway after initial CO-dissociation (path-b, ***Figure 28***). The thermodynamics of the overall reaction (**1-Co** + 2-butyne → **5-Co**) is energetically driven with a rather low exergonicity (ΔG° of −7 kJ/mol). In the path-a, 2-butyne inserts into the Ge−Ge bond of the coordinated Ge_2Tbb_2 ligand of **1-Co** forming **B** via **A** akin to the [2+2]-cycloaddition mechanisms of ditetrylynes with alkenes and alkynes.[27,33] Gas phase structural optimizations gave minima energy structures for **A** and **B** with a very low reaction Gibbs free energy of +10 kJ/mol for the **1-Co** + 2-butyne → **B** step. Complex **B** then undergoes intramolecular CO-substitution to form **5-Co** with a reaction Gibbs free energy of only −16 kJ/mol. In path-b, the first CO-dissociation step (**1-Co** → **3-Co**) is energetically highly unfavored (ΔG° = +100 kJ/mol, ΔE= +169 kJ/mol). Thus, the Ge-centered pathway (path-a) is the minimum energy pathway for the [3+2]-dipolar cycloaddition of **1-Co** with 2-butyne. It is noteworthy that CO-free mono-alkyne and bis-alkyne complexes ($CpCo(alkyne)_n$, n = 1, 2) have been implicated as intermediates in the $CoCo(CO)_2$ catalyzed alkyne cyclotrimerization reaction.[129] In contrast, **1-Co** neither catalyzes the cyclotrimerization of 2-butyne, nor it behaves as a classical alkyne complex, but rather as a 1,3-dipole ("$^{(\delta-)}$Ge−Co−Ge$^{(\delta+)}$") underdoing facile [3+2]-dipolar cycloaddition reactions.

2.4. Extension of the cycloaddition chemistry of digermyne complexes with terminal- and amino-alkynes

The scope of the alkyne insertion reaction was further extended to other alkynes. Interestingly, the product formation showed strong dependency on the type of alkynes used. When the CO containing digermyne complexes (**1-Co** or **1-Rh**) were reacted with terminal alkynes (Ph−C≡C−H or Mes−C≡C−H), we have always observed the immediate formation of the corresponding metallacycles **9-Co**, **9-Rh** and **10-Co**. Contrastingly, reacting those terminal alkynes with the CO-free digermyne complex (**3-Co**), an oxidative bond cleavage of (C^{sp}-H) of alkynes was observed, forming the corresponding bis-germylidene complexes (**12-Co** and **13-Co**) (***Scheme 16***).

When a colourless stock solution of phenyl acetylene was added to a brown *n*-hexane solution of **1-Co** at ambient temperature, unlike 2-butyne (where the colour gradually changed to green upon heating at 60 °C), the reaction was accompanied by an immediate colour change from brown to dark-green. Whereas, performing the same reaction with a dark-green *n*-hexane solution of **1-Rh**, no considerable colour change

was observed but in both cases monitoring the reaction progress by ^{1}H NMR spectroscopy after 5 min of stirring at ambient temperature revealed the quantitative transformation of the digermyne complex to the five-membered metallacycle.

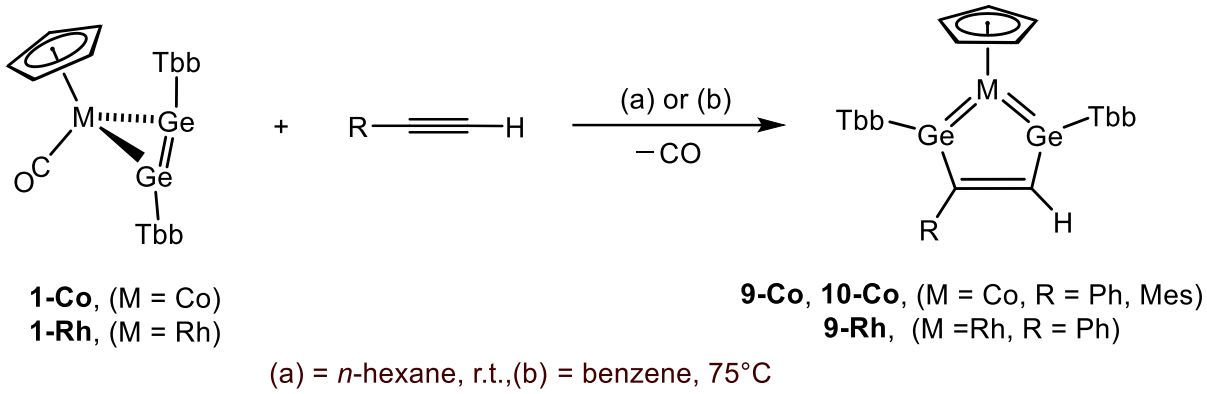

Scheme 14. Reaction of the CO containing digermyne complexes with terminal alkynes.

In contrast to phenyl acetylene, reaction of **1-Co** with mesityl acetylene was extremely slow at ambient temperature. So, a mixture of **1-Co** and mesityl acetylene in 1 : 4 ratio in benzene was taken in benzene heated for 24 hours at 75 °C. The brown reaction solution gradually turned green. ^{1}H NMR spectroscopic analysis of the reaction solution revealed a complete conversion of **1-Co** and the formation of **10-Co** as the main product as well as 1,2-digermabenzene (**11-Ge**) along with very little $CpCo(CO)_2$ and unreacted mesityl acetylene. A CH_3CN/Et_2O work up followed by crystallization obtained **10-Co** in analytically pure form. **10-Co** is a highly air-sensitive, dark-green solid, that is very well soluble in *n*-hexane, benzene, toluene and Et_2O, but insoluble in CH_3CN at ambient temperature. The presence of **11-Ge** in the above experimental outcome was further verified with the isolation of analytically pure **11-Ge**.

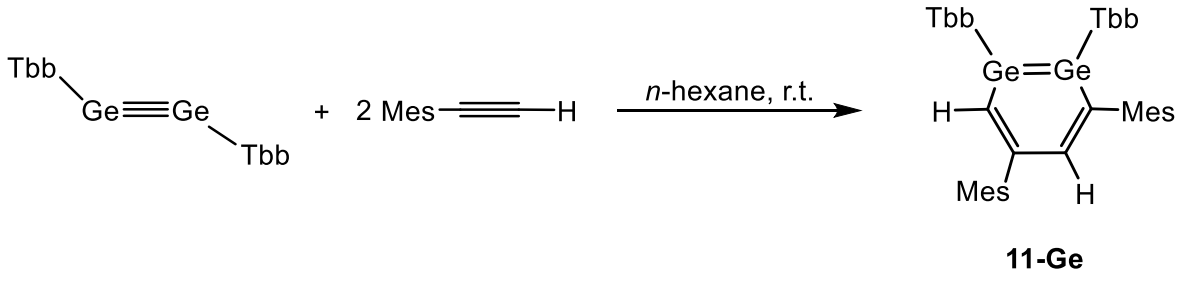

Scheme 15. Synthesis of 1,2-digermabenzene.

The reaction of Ge_2Tbb_2 with mesityl acetylene at ambient temperature selectively formed **11-Ge** (***Scheme 15***) which was isolated after work up as a yellow solid in 50 % yield. In combination with NMR spectroscopy, EA and sc-XRD, all these compounds (**9-Co**, **9-Rh**, **10-Co** and **11-Ge**) were comprehensively characterized.

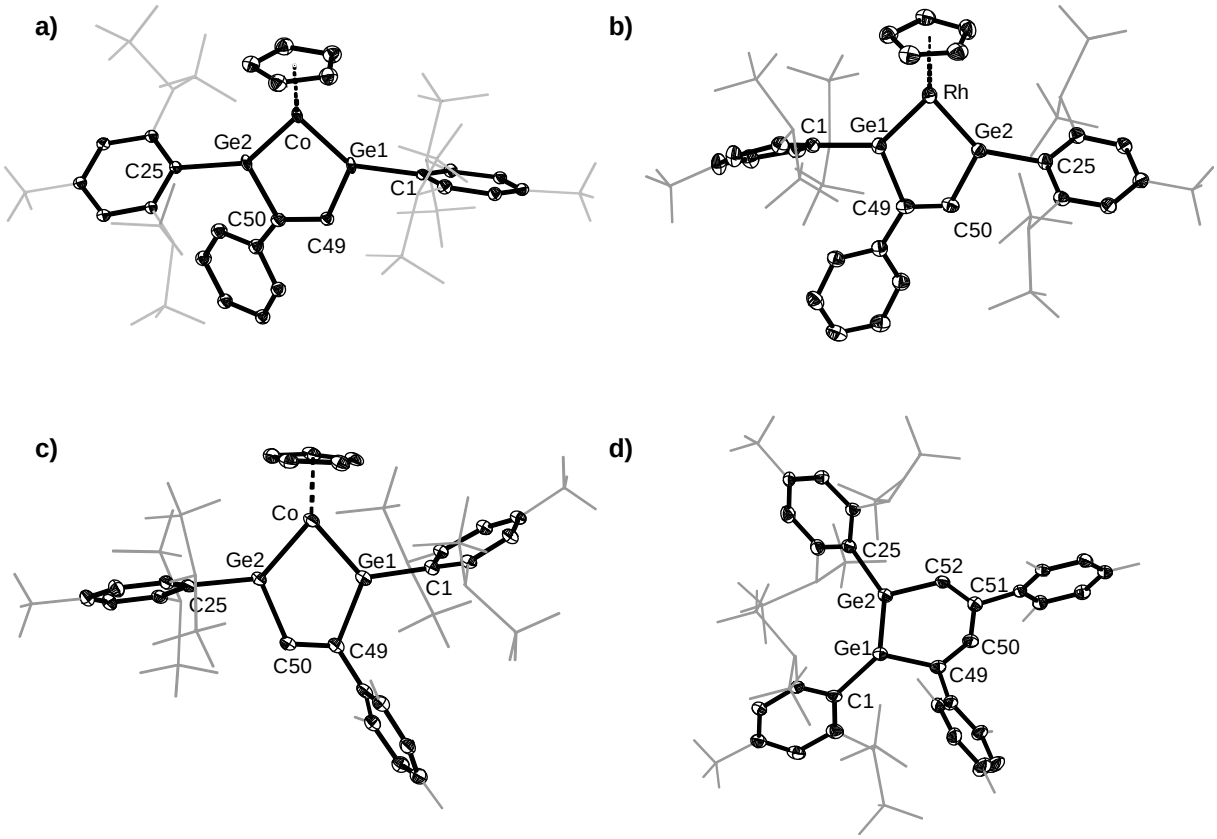

Figure 29. DIAMOND plot of the molecular structures of **9-Co**, **9-Rh**, **10-Co** and **11-Ge**. Thermal ellipsoids are set at 30 % probability level. Hydrogen atoms are omitted, the Dsi and ^{t}Bu substituents of the Tbb ligand and C^{2},C^{4},C^{6} methyl groups of Mes ligand are presented in wire-frame for clarity. Selected bond lengths [Å], bond angles [°], and torsion angles [°]: **a)** Ge1-Ge2 2.8941(6), Co-Ge1 2.1725(7), Co-Ge2 2.1917(7), Ge1-C49 1.968(4), Ge2-C50 2.012(4), C49-C50 1.338(5), Co-Ge1-C1 138.68(11), Co-Ge1-C49 115.04(12), C1-Ge1-C49 106.17(16), Co-Ge2-C25 137.26(11), Co-Ge2-C50 115.40(11), C25-Ge2-C50 107.34(15); **b)** Rh-Ge1 2.2709(7), Rh-Ge2 2.2578(7), Ge1-Ge2 2.9113(8), Ge1-C49 2.026(5), Ge2-C50 1.962(5), C49-C50 1.306(8), Rh-Ge1-C1 135.37(14), Rh-Ge1-C49 116.36(15), C1-Ge1-C49 108.3(2), Rh-Ge2-C25 137.33(15), Rh-Ge2-C50 115.62(17), C25-Ge2-C50 106.9(2); **c)** Co-Ge1 2.1934(12), Co-Ge2 2.1803(11), Ge1-Ge2 2.9213(10), Ge1-C49 2.037(6), Ge2-C50 1.974(6), C49-C50 1.340(9), Co-Ge1-C1 124.28(17), Co-Ge1-C49 114.47(18), C1-Ge1-C49 121.2(2), Co-Ge2-C25 137.39(16), Co-Ge2-C50 114.25(18), C25-Ge2-C50 108.3(2); **d)** Ge1-Ge2 2.3214(10), Ge1-C49 1.918(6), Ge2-C52 1.883(6), C49-C50 1.368(9), C51-C52 1.367(8), C1-Ge1-Ge2 125.60(18), C1-Ge1-C49 124.5(2), C49-Ge1-Ge2 103.70(19), C25-Ge2-Ge1 134.13(19), C25-Ge2-C52 113.1(2), C52-Ge2-Ge1 103.49(18), C1-Ge1-Ge2-C25 58.085(2), C49-Ge1-Ge2-C52 –6.176(2), C49-C50-C51-C52 9.013(4).

Suitable single crystals of **9-Co** (clear dark green plates), **9-Rh** (clear greenish-brown planks) and **10-Co** (clear bluish-green plates) were grown by slow evaporation of saturated Et_2O/CH_3CN (3 : 1, v/v) solutions at ambient temperature inside the glove box, whereas clear yellowish-orange plates of **11-Ge** were obtained upon slow cooling of saturated Et_2O/CH_3CN (5 : 1, v/v) solution at 4 °C. The solid-state structural parameters of the metallacycles **9-Co** and **10-Co** compare well with those of **5-Co**, whereas the structural parameters of **11-Ge** are in good agreement with those of the

1,2-digermabenezene[101] known in literature. Compound **9-Rh** bears the same structural motif as its cobalt congener. It features two trigonal planner coordinated Ge centers (∑∠Ge = 360°) connected to Rh via short bonds (2.2709(7) Å and 2.2578(7) Å), which fit well to the Rh=Ge double bond in previously reported rhodium-germylidene complex [Cp(IDipp)Rh=GeCl{N(Mes*)SiMe$_3$}] [2.2605(4) Å][58] by our group.

As stated earlier, similar reactions of terminal alkynes with **3-Co** do not lead to the cycloaddition product, instead it gets added to the Ge centers via an oxidative cleavage of the alkyne C-H bond, hence the bis-germylidene complexes (**12-Co** or **13-Co**) containing two different germylene units at the cobalt center are formed. Addition of a colourless stock solution of phenyl acetylene to an orange-red *n*-hexane solution of **3-Co** proceeded via an immediate colour change to dark-brown, analyzing the reaction progress by ^{1}H NMR spectroscopy showed selective (~85 %) formation of **12-Co** along with other unknown side products, but traces of **9-Co** were not observed.

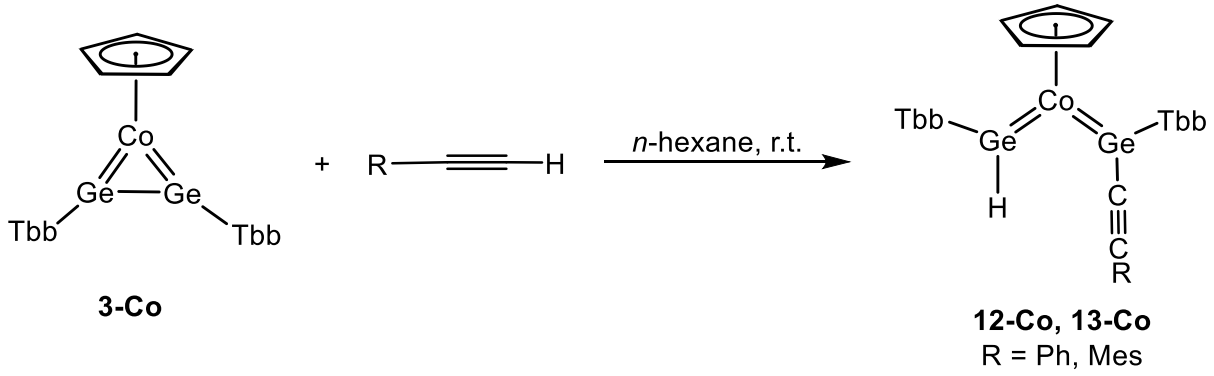

Scheme 16. Terminal alkyne addition to **3-Co** via oxidative cleavage of C^{sp}-H bond.

However, attempts of purifying the product through crystallization failed due to its exceedingly high solubility in common laboratory solvents. After concentrating the crude reaction mixture and upon its controlled storage at –60 °C for a month very few single crystals were obtained. Subsequent X-ray diffraction analysis yielded a low-quality crystal structure, which is depicted in ***Figure 92***, showing the structural motif as bis-germylidene complex where the structural parameters are well comparable to **2-Co**.

The mesityl acetylene reaction with **3-Co** also proceeded immediately as phenyl acetylene. ^{1}H NMR spectroscopic analysis of a reaction aliquot after stirring for 10 min at ambient temperature showed the complete conversion of **3-Co** to **13-Co** and surprisingly some **10-Co** (ca. 10 mole%). Due to the extreme solubility in all different solvents and extreme instability in CH_3CN, several attempts to obtain **13-Co** in pure form by crystallization of the crude product failed and it was only

characterized by spectroscopy. The most distinct ^{1}H NMR signal of these compounds (**12-Co** and **13-Co**) is that of the Ge-H protons, which appears as a singlet in (D_6)benzene at 11.47 and 11.25 ppm, respectively. An absorption (ν_{Ge-H}) band at 1974 cm^{-1} (solid state ATR-IR) was observed in the IR spectrum of **13-Co**, is in line with some of the compounds containing tricoordinate Ge center along with a Ge-H bond (1961 cm^{-1}, 1862 cm^{-1}, 2005 cm^{-1}), reported in literature.[26,130]

So far, in contrast to the used terminal and internal alkynes, the amino-alkyne (Ph−C≡C−NMe_2) reaction with both the digermyne complexes (**1-Co** and **3-Co**) proceeded smoothly and in both cases, a very selective formation of the metallacycle (**14-Co**) was observed.

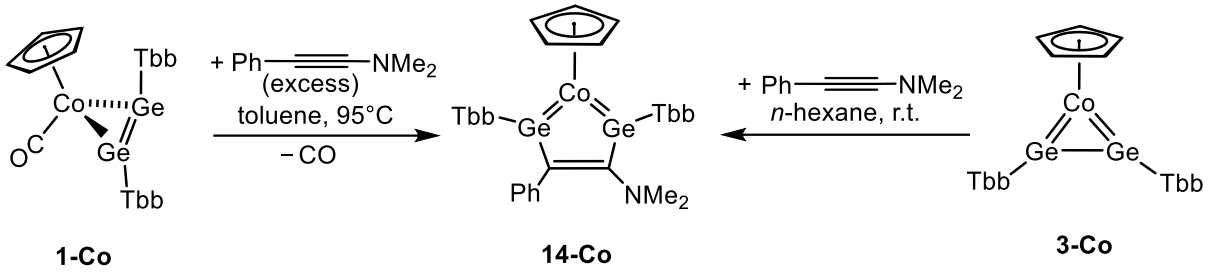

Scheme 17. Reaction of an amino-alkyne with the digermyne complexes.

At ambient temperature no reaction of **1-Co** with the alkyne (Ph−C≡C−NMe_2) was observed. Therefore, a toluene solution of **1-Co** with an excess (10 equiv.) of the amino-alkyne was heated at 95 °C for 24 hours. The reaction proceeded selectively by a gradual colour change of the solution from brown to red-brown. Monitoring the progress of the reaction by ^{1}H NMR spectroscopy revealed very selective formation of **14-Co**. All attempts to isolate **14-Co** in pure form only by crystallization of the crude product from various solvents failed yielding always an oil containing **14-Co** and 1-dimethylamino-2-phenylacetylene. In contrast to **1-Co**, when **3-Co** was reacted with only one equivalent of the alkyne at ambient temperature, an instantaneous darkening (towards red) of the orange-red reaction solution was observed. ^{1}H NMR spectroscopic analysis of an aliquot of the reaction solution revealed a quantitative transformation of **3-Co** to **14-Co**. After a general CH_3CN/Et_2O work up **14-Co** was isolated as an analytically pure solid in 47 % yield. It is a highly air-sensitive, but thermally robust (T_{dec} = 242 °C), dark brown solid, decolorizing immediately upon contact with air. It is very soluble in *n*-pentane, benzene, toluene, Et_2O and THF, but insoluble in acetonitrile at ambient temperature. Suitable single crystals (clear dark brown blocks) of **14-Co** for sc-XRD analysis were obtained upon slow evaporation of a concentrated Et_2O/CH_3CN (1 : 1, v/v) solution inside the glove box. The solid-state

structural motif of **14-Co** is very similar to all above isolated five-membered metallacycles.

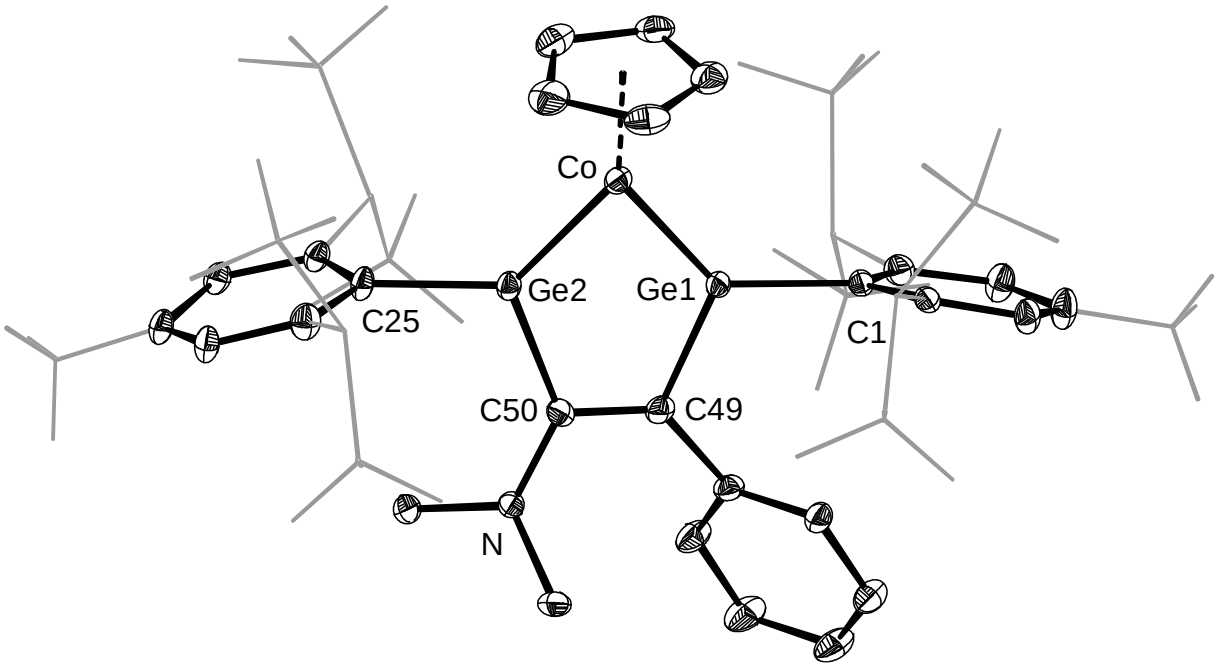

Figure 30. DIAMOND plot of the molecular structure of **14-Co**. Thermal ellipsoids are set at 30 % probability level. Hydrogen atoms are omitted and the Dsi and ^{t}Bu substituents of the Tbb ligand are presented in wire-frame for clarity. Selected bond lengths [Å] and bond angles [°]: Ge1-Ge2 2.8443(8), Co-Ge1 2.1797(10), Co-Ge2 2.1672(11), Ge1-C49 1.979(7), Ge2-C50 2.005(7), C49-C50 1.366(8), Co-Ge1-C1 133.04(19), Co-Ge1-C49 117.02(18), C1-Ge1-C49 109.9(3), Co-Ge2-C25 133.2(2), Co-Ge2-C50 116.75(17), C25-Ge2-C50 110.0(3).

Noteworthy that except **14-Co** which is brownish-red in colour, all other five-membered metallacycles reported above are green. This prompted us to study their solution behavior additionally by UV-Vis spectroscopy. The UV-vis-NIR absorption spectrum of a dark green solution of **5-Co** in toluene shows a characteristic broad band at the longest λ_{max} of 677 nm (ε = 2162 Lmol^{-1}cm^{-1}) with its tail extending up to the NIR region (see section **5.5**). As expected, a large bathochromic shift of +86 nm was observed in the UV-vis spectrum of an orange solution of **14-Co** in toluene with the longest λ_{max} at 763 nm with a very small ε (ca. 300 Lmol^{-1}cm^{-1}) and a strong band at 437 nm (ε = 7565 Lmol^{-1}cm^{-1}) indicating a pronounced auxochromic effect of the NMe_2 group on the π-system of the cobaltacycle **14-Co**, whereas, the longest λ_{max} of **10-Co** (693 nm, ε = 1692 Lmol^{-1}cm^{-1}) is only slightly bathochromically shifted relative to that of **5-Co**. The optical HOMO-LUMO gap (Δ_{opt}) of **5-Co** and **14-Co** calculated from the respective onset of the longest λ_{max} (830 nm for **5-Co**, 863 nm for **14-Co**) to be 1.49 eV and 1.44 eV, respectively, which compares well with the Kohn-Sham gap (Δ_{KS}: 1.53 eV (**5-Co**) and 1.43 eV (**14-Co**)).[131]

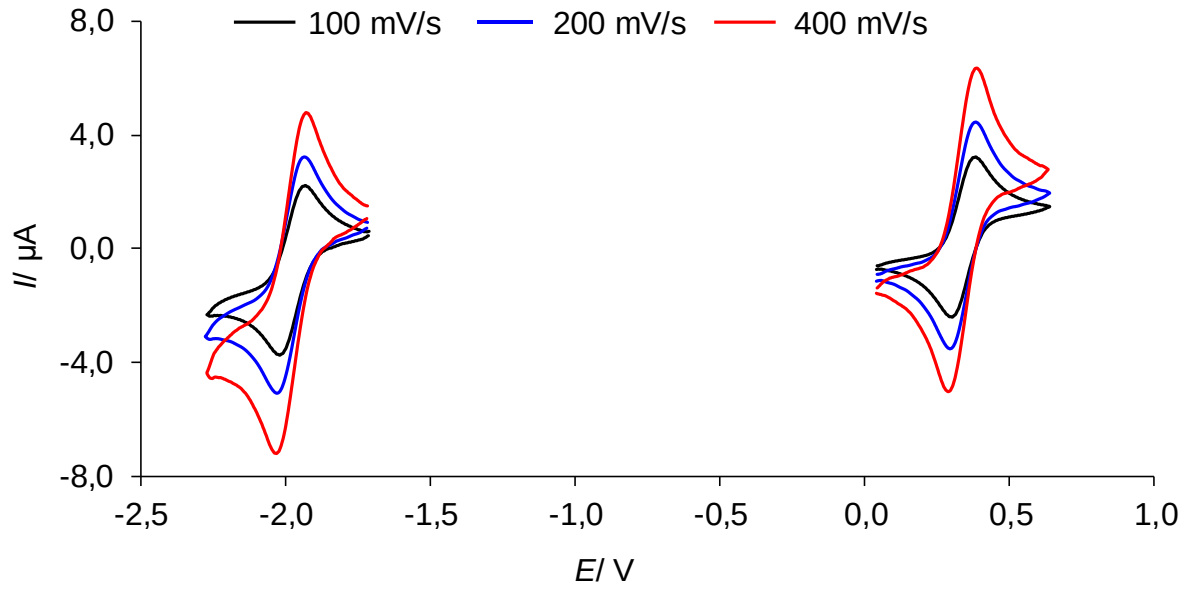

Figure 31. Cyclic voltammogram of **5-Co** showing the quasi-reversible electrochemical processes.

The HOMO-LUMO gap is also consistent with the amphoteric redox properties of **5-Co**. Thus, **5-Co** shows in its cyclic voltammograms (see section **5.4**) a quasi-reversible (E_q-process) voltammetric wave for a one-electron reduction (**5-Co**/**5-Co**$^{\bullet-}$ couple) at a $E_{1/2}$ of –1.983 V (versus $DMFc^{+/0}$) as well as a quasi-reversible wave for a one-electron oxidation (**5-Co**/**5-Co**$^{\bullet+}$ couple) at a $E_{1/2}$ of +0.337 V.

Following the successful reactivity of the digermyne complexes with different alkynes, the reaction of **3-Co** was also tested with an alkene (***Scheme 18***). Treating an orange-red *n*-hexane solution of **3-Co** with an excess of ethylene gas at liquid N_2 temperature and upon warming it up to ambient temperature, the colour of the reaction solution got darkened (towards more brownish). A quantitative conversion of **3-Co** to the cycloadded product (**15-Co**) was confirmed by ^{1}H NMR spectroscopy.

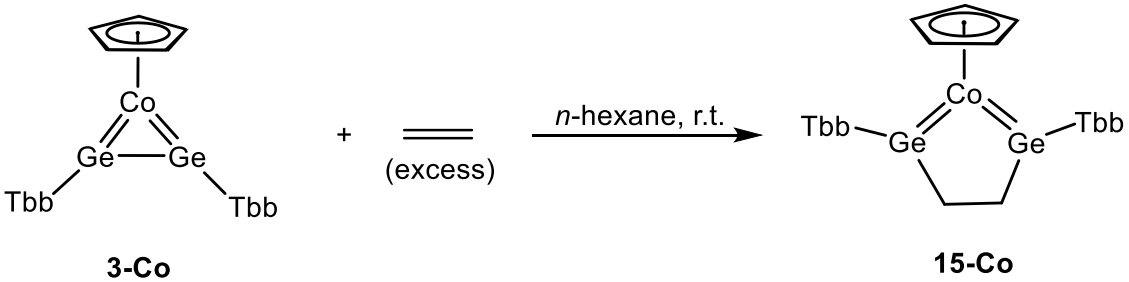

Scheme 18. Reaction of the digermyne complex **3-Co** with ethylene.

Compound **15-Co** was isolated in moderate yield, as an air-sensitive, but thermally robust (T_{dec} = 233 °C), brown solid, which can be stored under argon atmosphere at ambient temperature for several months. The structural motif of **15-Co** is very similar

to those of the unsaturated five-membered metallacycles described above, which was confirmed by sc-XRD analysis of clear block shaped brown crystals of **15-Co**, grown by slow cooling of a concentrated toluene solution in –30 °C.

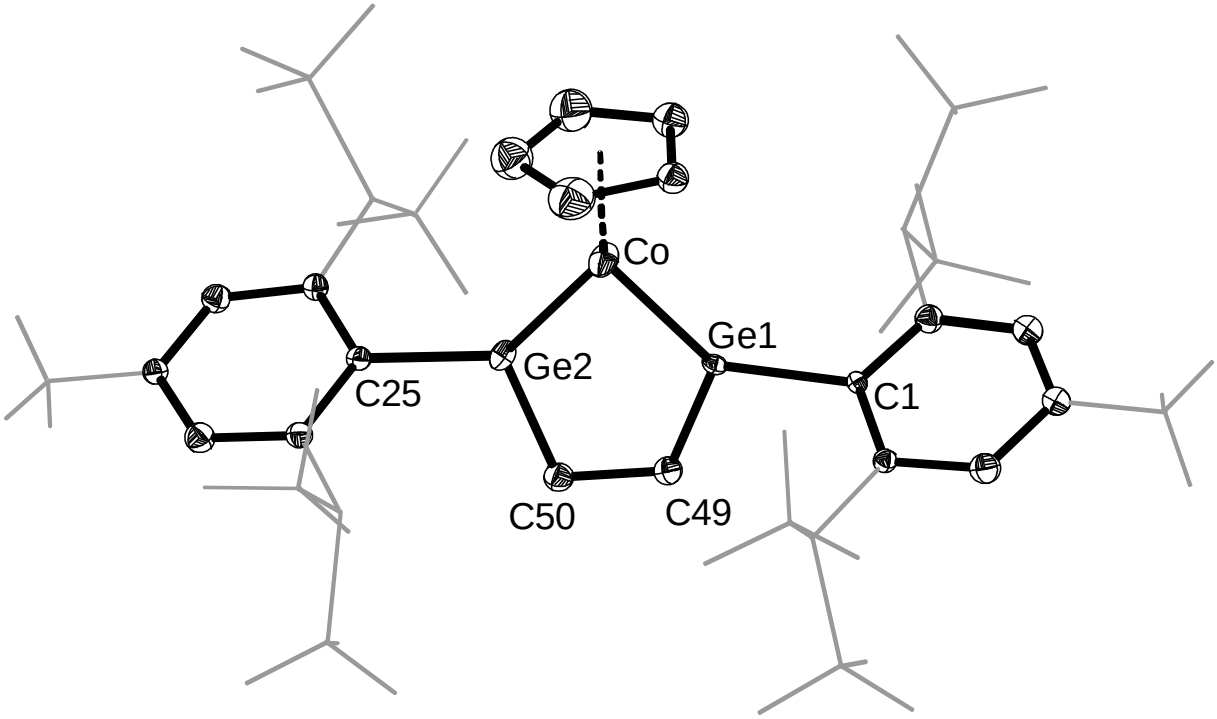

Figure 32. DIAMOND plot of the molecular structure of **15-Co**. Thermal ellipsoids are set at 30 % probability level. Hydrogen atoms are omitted and the Dsi and ^{t}Bu substituents of the Tbb ligand are presented in wire-frame for clarity. Selected bond lengths [Å] and bond angles [°]: Co-Ge1 2.186(2), Co-Ge2 2.191(2), Ge1-C49 1.987(12), Ge2-C50 2.004(17), C49-C50 1.50(2), Ge1-Ge2 2.9120(17), Co-Ge1-C1 133.3(3), C1-Ge1-C49 109.6(5), Co-Ge1-C49 117.0(4), Co-Ge2-C25 136.6(3) , Co-Ge2-C50 117.2(5), C25-Ge2-C50 106.1(6).

The unsaturated five-membered metallacycle (**5-Co**) was proved to be quite inert. Thus, no reactions either at ambient temperature or upon thermal activation were observed with nucleophiles such as dimethyl cyanamide (NMe_2CN), 1-dimethylamino-2-phenylacetylene, or even NHC stabilized silicon dihalide ($SiBr_2$SIDipp). However, **5-Co** reacted with a diazo-alkane (***Scheme 19***). Although, no reaction was observed upon addition of a pale-yellow stock solution of trimethylsilyl diazomethane to a dark-green *n*-hexane solution of **5-Co** at ambient temperature, but upon heating the reaction solution at 60 °C for 16 hours the dark green colour changed to deep red. Monitoring the reaction progress by ^{1}H NMR spectroscopy revealed a complete consumption of **5-Co** and its quantitative transformation to **16-Co**.

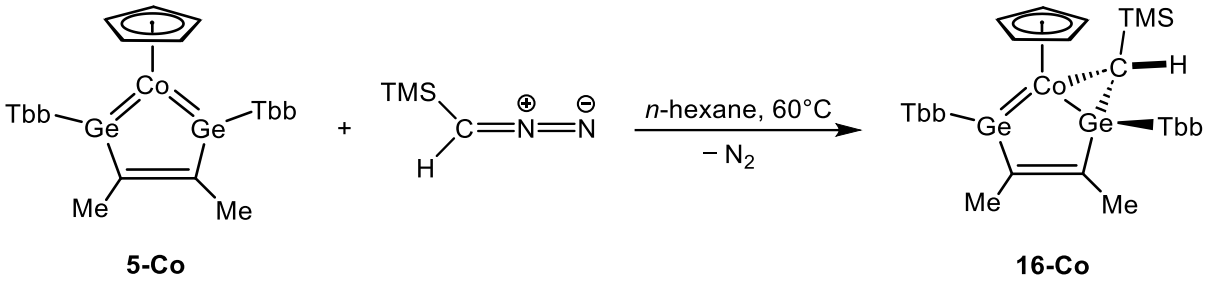

Scheme 19. [2+1]-cycloaddition of **5-Co** with diazoalkane.

After work-up, **16-Co** was isolated in 71 % yield, as an air sensitive but thermally robust (T_{dec} = 208 °C), dark-red solid. It is well soluble in *n*-hexane, benzene and Et_2O, but insoluble in acetonitrile at ambient temperature. The structural motif of **16-Co** was confirmed by sc-XRD analysis of the red cube shaped crystals, grown by slow evaporation of a concentrated Et_2O/CH_3CN (5 : 1, v/v) solution inside the glovebox.

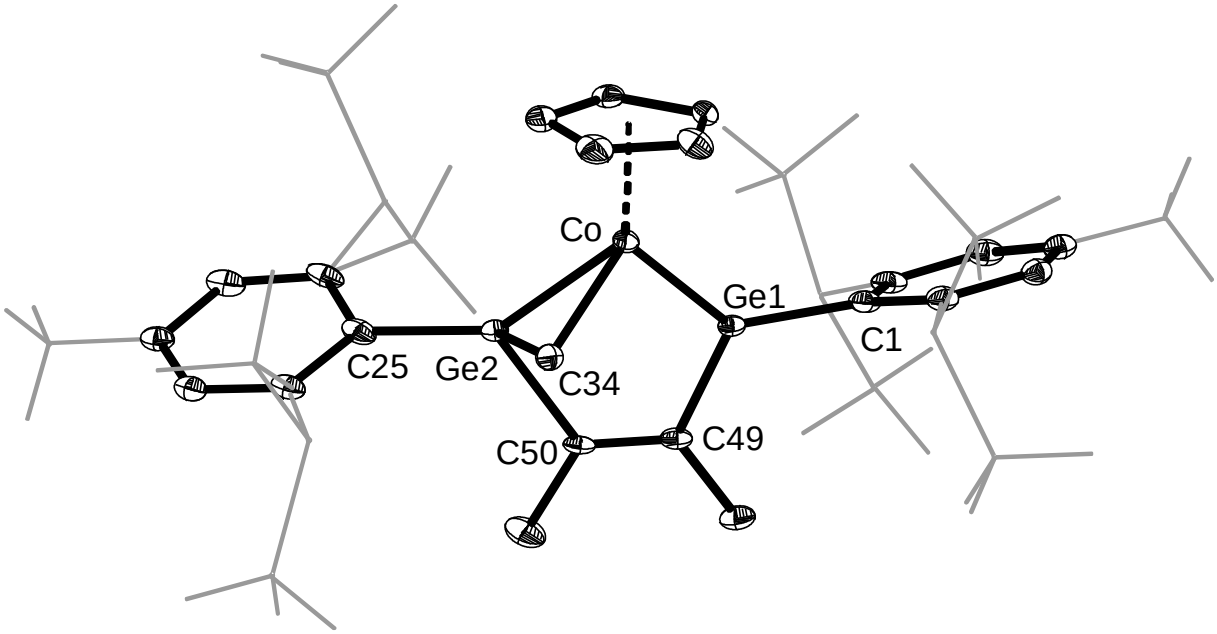

Figure 33. DIAMOND plot of the molecular structure of **16-Co**. Thermal ellipsoids are set at 30 % probability level. Hydrogen atoms and $SiMe_3$ unit on C34 are omitted. The Dsi and ^{t}Bu substituents of the Tbb ligand are presented in wire-frame for clarity. Selected bond lengths [Å] and bond angles [°]: Co-Ge1 2.2272(18), Co-Ge2 2.344(2), Co-C34 2.088(4), Ge2-C34 1.900(5), Ge1-C49 1.936(5), Ge2-C50 1.973(5), C49-C50 1.319(6), Co-Ge1-C1 131.01(13), Co-Ge1-C49 113.83(17), C1-Ge1-C49 114.99(17), Co-Ge2-C34 57.80(14), Co-C34-Ge2 71.81(16).

In the molecular structure of **16-Co** (***Figure 33***), the metal center is connected to one tetra coordinated Ge center via a long bond (2.344(2)Å), which is similar to Co-Ge single bonds found in cobalt-germyl complexes[132] along with a trigonal planner coordinated (∑∠Ge1 = 359.8 °) Ge center via a short bond (2.2272(18) Å), which is almost identical to the Co=Ge double bonds found in **2-Co** or **5-Co**. Basically, **16-Co**

is formal [2+1]-cycloaddition product of the carbene moiety [C(H)TMS] with the Co=Ge double bond of **5-Co** (***Figure 33***). The Ge-C34 (1.900(5) Å) bond length is quite similar to that of some metallo-germanes (contain atleast an alkyl group on tetracoordinated Ge center) found by CSD search and the Co-C34 (2.088(4) Å) bond is in good agreement with the Co-Ge single bonds of the complexes ([(μ-CH_2)$_2${(η^5-C_5Me_5)Co(CO)}$_2$], [(η^5-C_5H_5)Co(CH_2($C H_2$)$_4$$CH_2$)($PPh_3$)]).[133,134] It is noteworthy to mention that an excess addition of the diazoalkane to a solution of isolated **16-Co**, does not lead to any further reaction even at elevated temperature. The solution structure of **16-Co** was also investigated by NMR spectroscopy, which is in line with its C_1 symmetric solid-state structure, carrying two stereogenic centers, where the two Tbb substituents are heterotopic and arbitrarily assigned as Tbb_X (Ge2 bonded) and Tbb_Y (Ge1 bonded), respectively. Indeed, the ^{1}H NMR spectrum of **16-Co** at 298 K in (D_6)benzene displays two separate set of signals for the two diastereotopic Tbb groups. Each of the Tbb groups displays four singlets (for $SiMe_3$, in 9 : 9 : 9 : 9 ratio) and two singlets for Dsi protons, indicating that rotation of the Tbb groups around the Ge-C^{Tbb} bond is frozen out on the NMR time scale.

After the successful development of the $CpM(CO)_2$ (M = Co/Rh) chemistry with Ge_2Tbb_2, the reactivity studies were extended to[$Pd(PCy_3)_2$][vi] or Ni(1,5-COD)$_2$.
So, the reaction of Ge_2Tbb_2 with Ni-(1,5-COD)$_2$ (1 : 1) at ambient temperature indeed proceeded immediately with a colour change from orange-red to orange-brown. ^{1}H NMR spectroscopic analysis of the reaction solution revealed mainly the presence of the [2+2+2]-cycloadded product **17-Ge** (***Scheme 20***) along with very little broad signals of unknown origin.

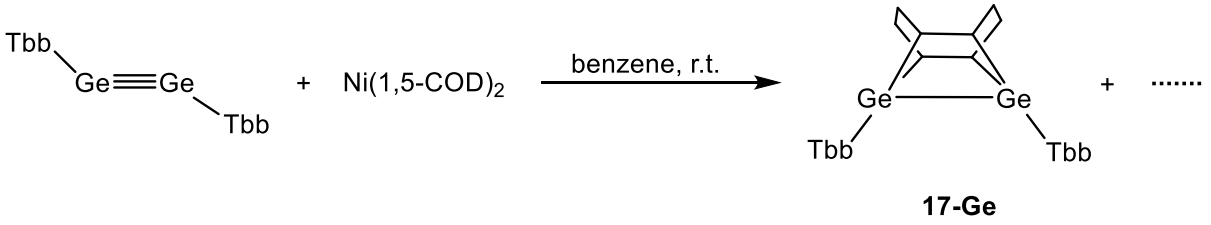

17-Ge

Scheme 20. Reaction of Ge_2Tbb_2 with Ni(1,5-COD)$_2$.

[vi] The reaction outcome of Ge_2Tbb_2 with $Pd(PCy_3)_2$ was a simple complexation of the digermyne unit to the Pd center via one equivalent of PCy_3 being eliminated. It is reported in the following Bachelor thesis of Leon Gomm; 'Bachelorarbeit in Chemie' entitled with "Reaktivität eines Digermins gegenüber Übergangsmetallkomplexen der 10. Gruppe", Rheinischen Friedrich-Wilhelms-Universität Bonn, **2021**.

To verify the formation of **17-Ge**, an independent synthesis was performed from Ge_2Tbb_2 and 1,5-COD (***Scheme 21***) and the compound was isolated in analytically pure form.

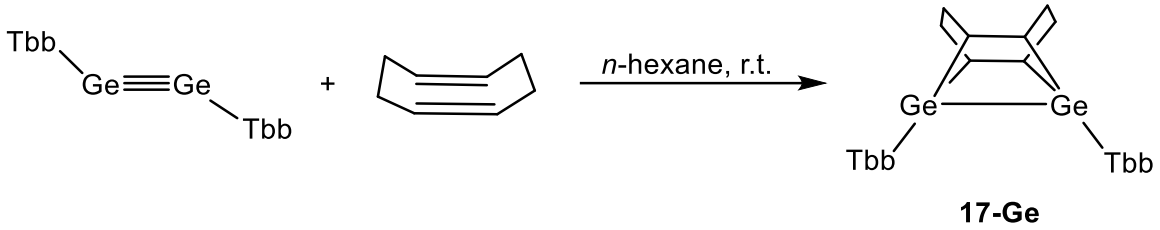

Scheme 21. [2+2+2]-cycloaddition reaction of Ge_2Tbb_2.

Compound **17-Ge** is a thermally robust ($T_{dec.}$ = 242 °C), air-stable, colourless solid, which is very well soluble in *n*-pentane, benzene, and Et_2O but poor soluble in DCM at ambient temperature. Along with spectroscopy and EA, **17-Ge** was also characterized by sc-XRD analysis.

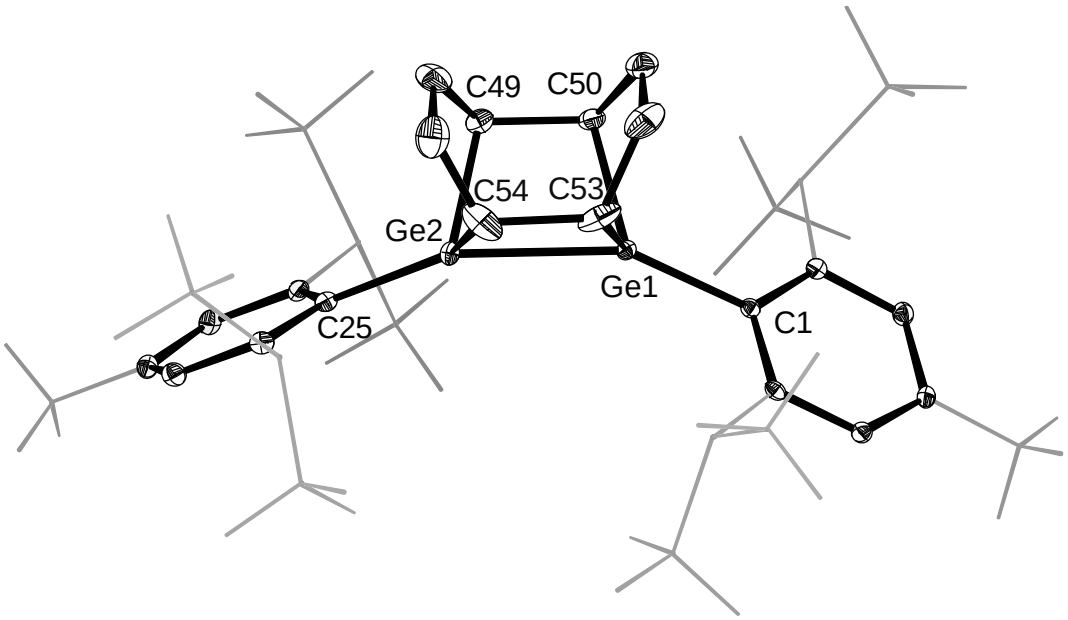

Figure 34. DIAMOND plot of the molecular structure of **17-Ge**. Thermal ellipsoids are set at 30 % probability level. Hydrogen atoms are omitted and the Dsi and ^{t}Bu substituents of the Tbb ligand are presented in wire-frame for clarity. Selected bond lengths [Å] and bond angles [°]: Ge1-Ge2 2.4967(4), Ge1-C50 2.020(3), Ge1-C53 1.981 (3), Ge2-C49 2.003(3), Ge2-C54 2.013(3), C49-C50 1.586(4), C53-C54 1.668(5), C1-Ge1-Ge2 151.32(7), C25-Ge2-Ge1 153.09(7), C50-Ge1-C53 85.50(12), C49-Ge2-C54 84.30(13).

Suitable plate shaped colourless single crystals of **17-Ge** were grown by slow cooling of a saturated Et_2O/DCM solution at 4 °C. The solid-state structural parameters (***Figure 34***) are well agreeing to a similar compound reported by N. Tokitoh *et al.*[135], which was obtained from the reaction of Ge_2Bbt_2 (Bbt = 2,6-$[CH(SiMe_3)_2]_2$-4-$[C(SiMe_3)_3]$-C_6H_2) with an excess of ethylene gas (ca. 1 atm.) at –78 °C.

Apart from the CO substitution reaction by Ge_2Tbb_2, an unexpected reaction was also observed when $CpRh(CO)_2$ was reacted with $Ge_2Br_2Tbb_2$ (***Scheme 22***). A stock solution of the metal complex was added to a yellow-orange *n*-pentane solution of $Ge_2Br_2Tbb_2$ at ambient temperature. Unlike Ge_2Tbb_2, this reaction proceeded slowly (2.5 h) and accompanying with a gradual colour change to dark-orange.

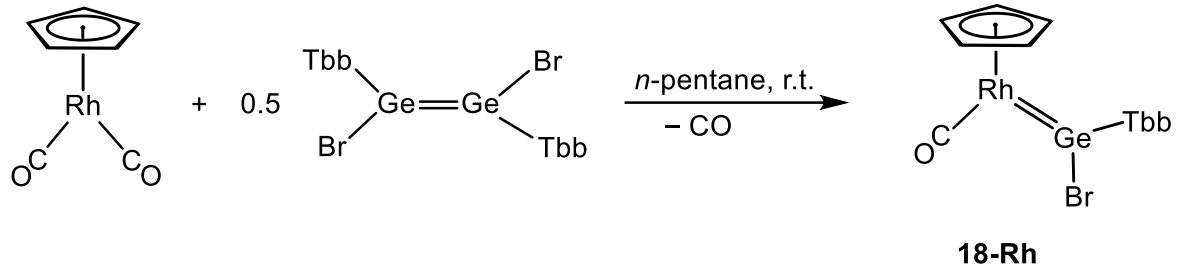

18-Rh

Scheme 22. CO substitution reaction of $CpRh(CO)_2$ by a germylene unit.

^1H NMR and IR spectroscopic analysis of an aliquot of the reaction solution confirmed the selective formation of the mono-carbonyl complex **18-Rh**. After work up and crystallization of the crude product from Et_2O at –30 °C, **18-Rh** was isolated as orange-red solid in 66 % yield. It is a moderately air-sensitive, but thermally robust ($T_{dec.}$ = 180 °C) solid, which is very well soluble in *n*-hexane, benzene, THF, fluorobenzene and Et_2O at room temperature. Under strict exclusion of air, a solution of **18-Rh** in (D_6)benzene shows only a tiny decomposition after 10 hrs of heating at 80 °C. In combination of EA, NMR and IR spectroscopy, **18-Rh** was also characterized by sc-XRD analysis. Suitable single crystals (clear orange blocks) were obtained upon slow cooling a saturated solution in Et_2O at –30 °C overnight. The molecular structure (***Figure 35***) features a trigonal planner coordinated Ge center ($\sum\angle$Ge = 359.1 °) bonded to the Rh center via a short bond (2.2530(12) Å), which is substantially shorter than the reported Rh–Ge bond length (2.501(1) Å) for the complex $[Cp^*(PMe_3)_2RhGeCl_2]$,[108] containing a Rh bound tricoordinated Ge center, but very similar to the observed Rh=Ge double bond in the molecular structure of **9-Rh**. No change in Ge–Br bond distance (2.3648(17)Å) in comparison to its precursor $Ge_2Br_2Tbb_2$ (2.3636(6)Å)[27] was observed. Of note, in a hope for the formation of a cationic Rh-germylidyne complex[58] upon bromide abstraction of **18-Rh**, its reaction with a halide scavenger was tested. No reaction was observed, when **18-Rh** was mixed with one equivalent of $NaB(Ar^F)_4$ [Ar^F = 3,5-$(CF_3)_2$-C_6H_3] in fluorobenzene at ambient temperature.

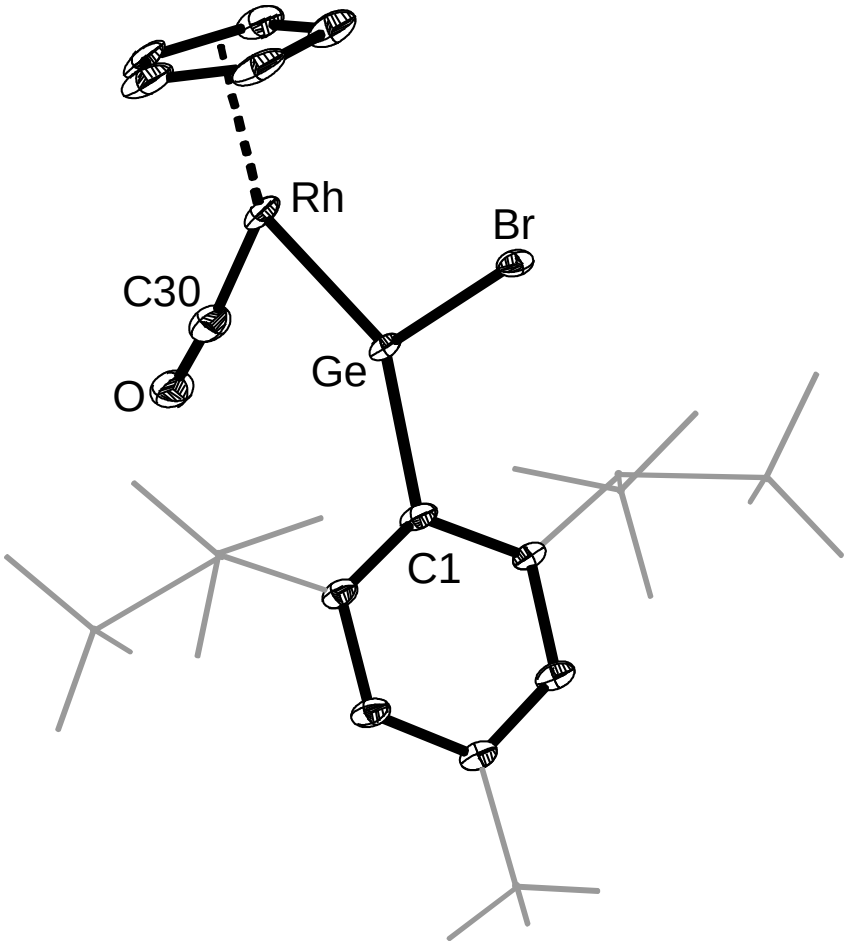

Figure 35. DIAMOND plot of the molecular structure of **18-Rh**. Thermal ellipsoids are set at 30 % probability level. Hydrogen atoms are omitted and the Dsi and ^{t}Bu substituents of the Tbb ligand are presented in wire-frame for clarity. Selected bond lengths [Å], bond angles [°] and torsion angles [°]: Rh-Ge 2.2530(12), Ge-Br 2.3648(17), Rh-C30 1.822(15), C30-O 1.157(17), Rh-Ge-C1 141.1(2), Rh-Ge-Br 112.84(5), C1-Ge-Br 106.0(2), C30-Rh-Ge-Br 171.815(5), C30-Rh-Ge-C1 –12.767(10).

2.5. Metal mediated reversible uptake of CO

Since the isolation of the first disilyne (Si_2R_2, R = singly bonded bulky substituent) in 2004 by Sekiguchi, over the last two decades its chemistry is steadily developing and leading to a plethora of novel silicon compounds with intriguing bonding features and enormous synthetic potential.[136,21,22,33] After successful isolations of all intriguing compounds from digermyne chemistry (**1-Co**-**16-Co,** *vide supra*), the challenging part was to imitate similar chemistry with disilyne. As of the present date, mentioned in the introduction, only two metal-disilyne complexes[20] have been reported, and their reactivity still remains unexplored, probably explaining the defiance in accessing them. Using a similar approach to digermyne chemistry (***Scheme 5***), disilyne (Si_2Tbb_2) was also reacted with [$CpM(CO)_2$, M =Co, Rh] (***Scheme 23***) hoping to obtain disilyne complexes of Co and Rh. However, the outcome was completely different and astonishing.

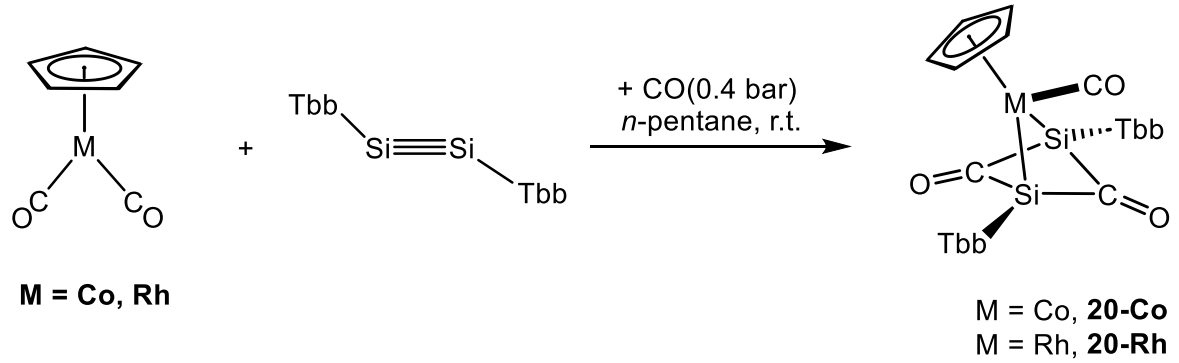

Scheme 23. Reaction of a disilyne with $CpM(CO)_2$ in presence of CO.

When an orange stock solution of $CpCo(CO)_2$ was added dropwise to a golden yellow solution of Si_2Tbb_2 in *n*-pentane at ambient temperature, an immediate reaction was observed with a colour change to red-brown. Upon exposure of the red-brown reaction solution to CO atmosphere, the colour changed to orange within 3 minutes. ^{1}H NMR and solution FT-IR spectroscopic analysis confirmed the complete consumption of disilyne and quantitative formation of **20-Co**. Before introducing the CO gas into the red-brown reaction solution, an aliquot was analyzed by IR and ^{1}H NMR spectroscopy, revealing a complete conversion of Si_2Tbb_2 and giving a mixture of three different products which are depicted in ***Figure 36***. Thereafter, with the CO gas introduced, all these compounds (**19-Co** and **21-Co**) selectively transformed to **20-Co**. However, several attempts of isolating **19-Co** in analytically pure from the crude reaction mixture through crystallization using different solvents or by low temperature washing have failed. So, **19-Co** could only be characterized by IR and multinuclear NMR spectroscopy using the crude reaction mixture. The spectroscopic features (see

section ***4.5.20***) helped to deduce the overall structural motif of the compound (**19-Co**), which compares well to the IR and NMR data of a similar compound **27-Rh** (*vide infra*).

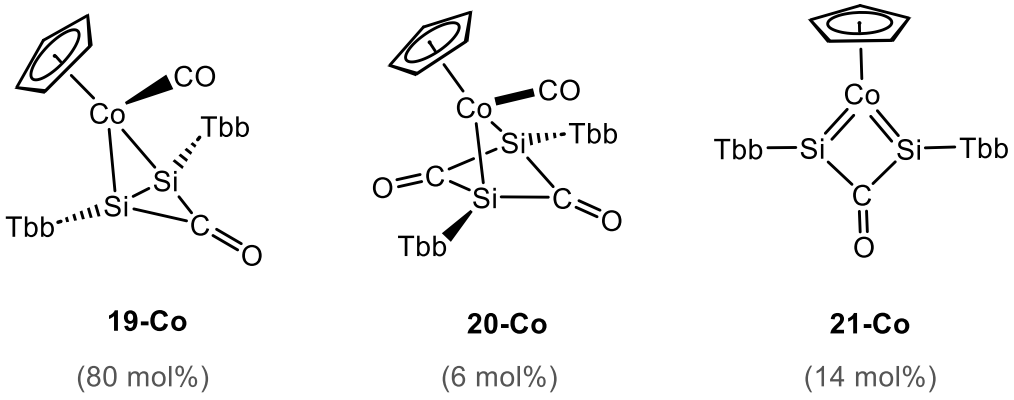

19-Co (80 mol%) **20-Co** (6 mol%) **21-Co** (14 mol%)

Figure 36. The reaction outcome of $CpCo(CO)_2$ with Si_2Tbb_2 at ambient temperature before introducing the CO gas in to the reaction solution.

Performing the similar reaction of Si_2Tbb_2 with $CpRh(CO)_2$, also proceeded very fast with an immediate colour change to red-brown and after introducing CO gas in to the reaction solution, the colour quickly changed to greenish-yellow. Analyzing a reaction aliquot by FT-IR and ^1H NMR spectroscopy confirmed a complete consumption of Si_2Tbb_2 and a very selective formation of **20-Rh**. Unlike the Co-case, before the introduction of the CO gas in to the reaction solution, an aliquot was analyzed by FT-IR and ^1H NMR spectroscopy, revealing the complete conversion of Si_2Tbb_2 and giving a mixture of only two compounds (**20-Rh** and **21-Rh**) in almost 1 : 1 ratio, and upon bringing this mixture in CO atmosphere, it completely converted to **20-Rh**. After work-up both compounds (**20-Co** and **20-Rh**) were isolated in analytically pure form as light-orange and greenish-yellow solids in 79 % and 74 % yields, respectively. It is noteworthy to mention that the compounds **20-Co** and **20-Rh** are examples of bissilyl ketones, which are in general quite uncommon in synthetic chemistry due to facile 1,2-anionic migration of the silyl group (Brook rearrangement),[137] and their structures are poorly studied. So, both compounds were thoroughly characterized by EA, IR and multinuclear NMR spectroscopy along with sc-XRD analysis. Suitable single crystals of **20-Co•0.5 (Et_2O)** (clear light orange prism) and **20-Rh•0.5 (Et_2O)** (clear yellow prism) were grown by slow cooling their respective saturated Et_2O solutions at –30 °C. The molecular structure of **20-Co** (***Figure 37***, *top*) features two distorted tetrahedral coordinated silicon centers connected to the cobalt center via long bonds (Co-Si1 2.3555(10) Å and Co-Si2 2.3633(9) Å), which are very similar to the Co–Si single bonds (~2.36 Å) of mono-silyl complexes of cobalt (**Co^I**) reported in literature.[138–141] However, the Co-Si bonds of **20-Co** are slightly longer than those

reported for (**Co^{III}**)[142,143] mono-and di-silyl complexes and (**Co^{V}**).[144] disilyl complex. Of note, the Co-Si bonds of **20-Co** are much longer than the Co-Si bonds found in silylene complexes of Roesky *et al.* containing either NHC-stabilized dihalosilylene[140] or amidinate-stabilized halosilylene (NHSi)[145] adducts of CpCo(CO). The Si–C bond lengths of **20-Co** (Si1-C26 1.943(3) Å, Si1-C27 1.939(3) Å, Si2-C26 1.939(3) Å, Si2-C27 1.938(4) Å) are significantly elongated than those of Si–C^{Tbb} (1.882(3) Å and 1.873(3) Å) but well comparable to the Si–C bond lengths of disilyl-ketones[146,147] reported in literature. The C–O bond (C26-O2 1.221(4) Å and C27-O1 1.216(4) Å) in the bridging CO groups are slightly elongated compared to that in the terminal CO ligand (C28-O3 1.156(4) Å) (probably hinting the higher back-donation ability of the silyl groups than the metal center), but in good agreement to those of the literature reported disilyl-ketones.[146,147]

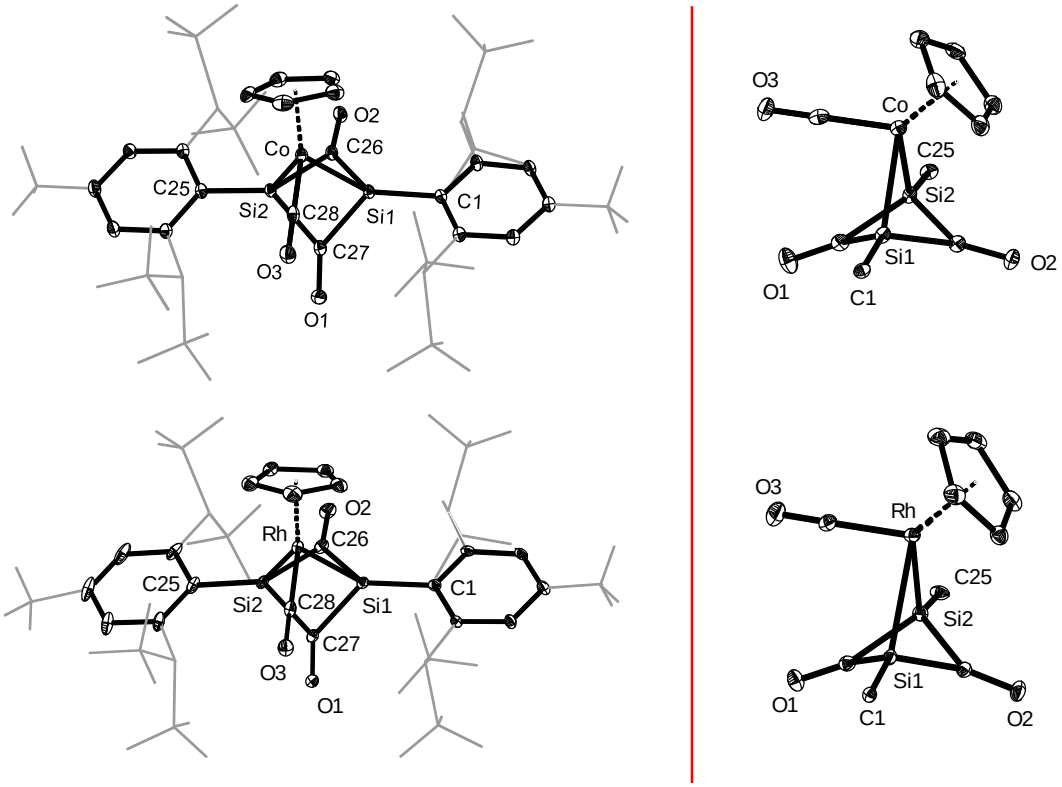

Figure 37. (*left*) DIAMOND plot of the molecular structure of **20-Co** and **20-Rh** and (right) their side view respectively. Thermal ellipsoids are set at 30 % probability level. Hydrogen atoms are omitted, the Dsi and ^{t}Bu substituents of the Tbb ligand are presented in wire-frame for clarity. In the side views except C1 and C25, all other atoms in the Tbb ligands are omitted for clarity. Selected bond lengths [Å], bond angles [°] and torsion angles [°]: **20-Co**: Co-Si1 2.3555(10), Co-Si2 2.3633(9), Si1-Si2 2.6395(11), Si1-C26 1.943(3), Si1-C27 1.939(3), Si2-C26 1.939(3), Si2-C27 1.938(4), C26-Si1-C27 81.99(14), C26-Si2-C27 82.12(14), Si1-Co-Si2 68.02(3), C26-Si1-Si2-C27 –127.157(3); **20-Rh**: Rh-Si1 2.4387(3), Rh-Si2 2.4465(3), Si1-Si2 2.6479(5), Si1-C26 1.9430(13), Si1-C27 1.9453(12), Si2-C26 1.9428(12), Si2-C27 1.9511(12), Rh-C28 1.8431(13), C26-Si1-C27 82.28(5), C26-Si2-C27 82.14(5), Si1-Rh-Si2 65.64(1), C26-Si1-Si2-C27 –127.585(4).

Interestingly, the trans annular Si···Si distance (2.6395(11) Å) is shorter than the sum of the van der Waals radii (4.2 Å)[112] of two Si atoms and even in the range of the longest known Si–Si bonds[148–151] and also very similar to that of some of the binuclear-metal clusters (silicon-cobalt) known in literature.[152]

Compound **20-Rh** (***Figure 37***, *bottom*) is isostructural to **20-Co** and similarly features two distorted tetrahedral coordinated silicon centers connected to the rhodium center via stretched single bonds (Rh-Si1 2.4387(3) Å and Rh-Si2 2.4465(3) Å), which are slightly lomger than the Rh–Si single bonds (~2.38 Å) of mono-and bis-silyl complexes of rhodium (**Rh^{I}**, **Rh^{III}** and **Rh^{V}**) reported in literature.[153–158] The Si–C bond lengths (Si1-C26 1.9430(13) Å, Si1-C27 1.9453(12) Å, Si2-C26 1.9428(12) Å, Si2-C27 1.9511(12) Å), C–O bond lengths (C27-O1 1.2080(15) Å, C26-O2 1.2211(16) Å, C28-O3 1.1421(17) Å) and the trans annular Si···Si distance (2.6479(5) Å) are akin to its cobalt analogue.

Further insight into the structures of **20-Co** and **20-Rh** was provided by multinuclear NMR and IR spectroscopy. The ^{1}H and ^{13}C{^{1}H} NMR data of both complexes suggest a time averaged *C*s-symmetric structure in solution. The symmetry plane bisects the ∠Si1-Rh-Si2 angle, rendering the two silicon centers and Tbb groups enantiotopic. The ^{29}Si{^{1}H} NMR spectra display a characteristic singlet for the silyl silicon atoms at δ = 49.2 ppm and a distinct doublet at 41.95 ppm (^{1}J(^{103}Rh-^{29}Si) = 28 Hz) of **20-Co** and **20-Rh** respectively. The chemical shifts compare well with those of the mono- and bis-silyl complexes of cobalt and rhodium, but are highly down-field shifted as compared to acyl silanes (~–20 ppm)[159] as well as bissilyl ketones (~–40 ppm).[137,146,147]

The bridging carbonyl carbons give rise to two singlets at δ = 224 and 239 ppm in **20-Co**, and two distinct doublets at δ = 228 (^{2}J(^{103}Rh-^{13}C) = 7 Hz) and 241 ppm (^{2}J(^{103}Rh-^{13}C) = 29 Hz) in **20-Rh**. The signals appear in the same range of acyl silanes (δ = 220–240 ppm)[159] but are high-field shifted compared to the disilyl ketone (δ = 260.3 ppm) reported by Sekiguchi *et al.*[147]

The solution IR spectra of **20-Co** and **20-Rh** corroborate well with the solution NMR spectra and solid-state-structure. The solution IR spectrum of **20-Co** in *n*-hexane displays three ν_{CO} absorption bands at 1987 (s), 1663 (m) and 1613 (m) cm^{-1}, and that of **20-Rh** at 2003 (s), 1665 (m) and 1620 (m) cm^{-1}. Notably, the bridging C=O absorption bands for both complexes appear at lower wavenumbers as compared to aliphatic ketones (~1715 cm^{-1}) and the reported disilyl ketone (PhMe$_2$Si)$_2$C=O) (1690 cm^{-1}) by Ichida *et al.*[146] However, one of the two bridging C=O absorption bands (1663 and 1665 cm^{-1} for **20-Co** and **20-Rh**, respectively) are quite similar to

the disilyl ketone (1673 cm^{-1}) reported by Sekiguchi *et al.*[147], which was prepared upon CO insertion (under photolytic conditions) into the Si–Si single bond bond of a silyl-substituted 1,4-Disila(Dewar benzene).

After successful isolation of the complexes **20-Co** and **20-Rh**, the next step was to obtain the observed intermediates **21-Co** and **21-Rh** during the reaction of Si_2Tbb_2 with $CpM(CO)_2$ in pure form. Upon refluxing an orange solution of **20-Co** in toluene for 5 hours, the colour of the reaction solution gradually turned wine-red. ^1H NMR and FT-IR spectroscopic analyses confirmed the complete and quantitative transformation of **20-Co** into the mono-carbonyl-bridged complex **21-Co**.

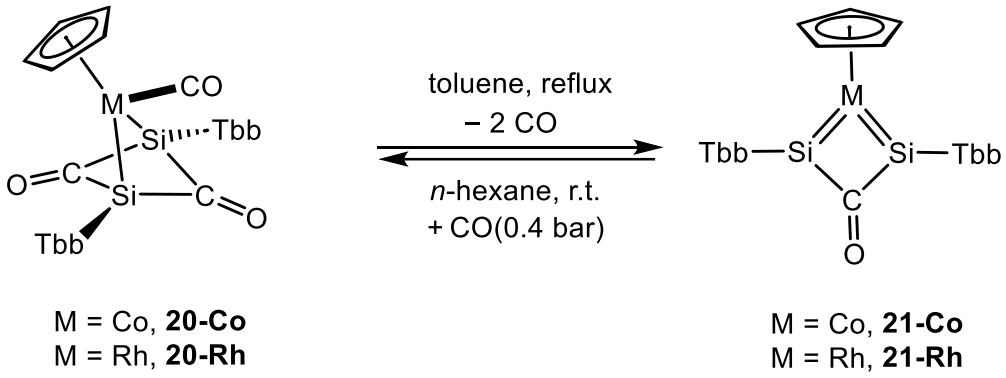

Scheme 24. Reversible uptake of carbon monoxide.

Similarly, refluxing a yellowish-green solution of **20-Rh** in toluene for 5 hours was accompanied by a gradual colour change to yellowish-brown and spectroscopic analyses confirmed the very selective formation of **21-Rh**. After work-up both compounds were isolated in analytically pure form as dark-maroon (**21-Co**) and brown-black solids (**21-Rh**) in 85 % and 68 % yield, respectively. Both compounds are extremely air sensitive, but thermally robust ($T_{dec.}$ = 194 and 208 °C, respectively) solids, decolourizing immediately upon contact to air, and are quite well soluble in aliphatic, aromatic and ethereal solvents at ambient temperature. The two complexes are first examples of metalladisila-cyclobutadienones to be reported, and were comprehensively characterized by EA, NMR and IR spectroscopy along with *sc*-XRD analysis. Suitable single crystals of **21-Co** were grown (orange prisms) upon slow cooling of a concentrated *n*-hexane solution at –20 °C. Its solid-state structure (***Figure 38***) features, two trigonal planar coordinated silicon (∑∠Si1/Si2 = 360°) centers bonding to the cobalt center via short Co–Si bonds (Co-Si1 2.1428(5) and Co-Si2 2.1356(5)), which are shortened by ca. 0.22 Å than those of its precursor (**20-Co**), but fit well to the sum of the double bond covalent radii of cobalt and silicon (ca. 2.10 Å) reported by Pykkö *et al.*[160] However, the Co–Si bonds of **20-Co** are slightly longer (ca. 0.03-0.04 Å) than that reported for a cationic base-free silylene complex

of cobalt (2.121(2) Å),[161] where a bond shortening occurred probably due to the cationic nature of the molecule. Surprisingly, the Co–Si bonds are also slightly longer than those of amidinato-supported or base-stabilized silylene and bis-silylene complexes of Co(I) reported by Stalke *et al.* (2.1143(4) Å)[145] and Driess *et al.* (2.125 and 2.120 Å),[162] respectively, but marginally shorter than an amidinato-stabilized halosilylene (NHSi) complex of Co(I) reported by Khan *et al.* (2.172 Å),[141] and Fenske *et al.* (2.181 Å).[163] The Si–C bond lengths (Si1-C26 1.9476(18), Si2-C26 1.9278(17)), C–O bond length (C26-O 1.204(2)) and the trans annular Si····Si distance (2.6139(6) Å) are very similar to those of its precursor.

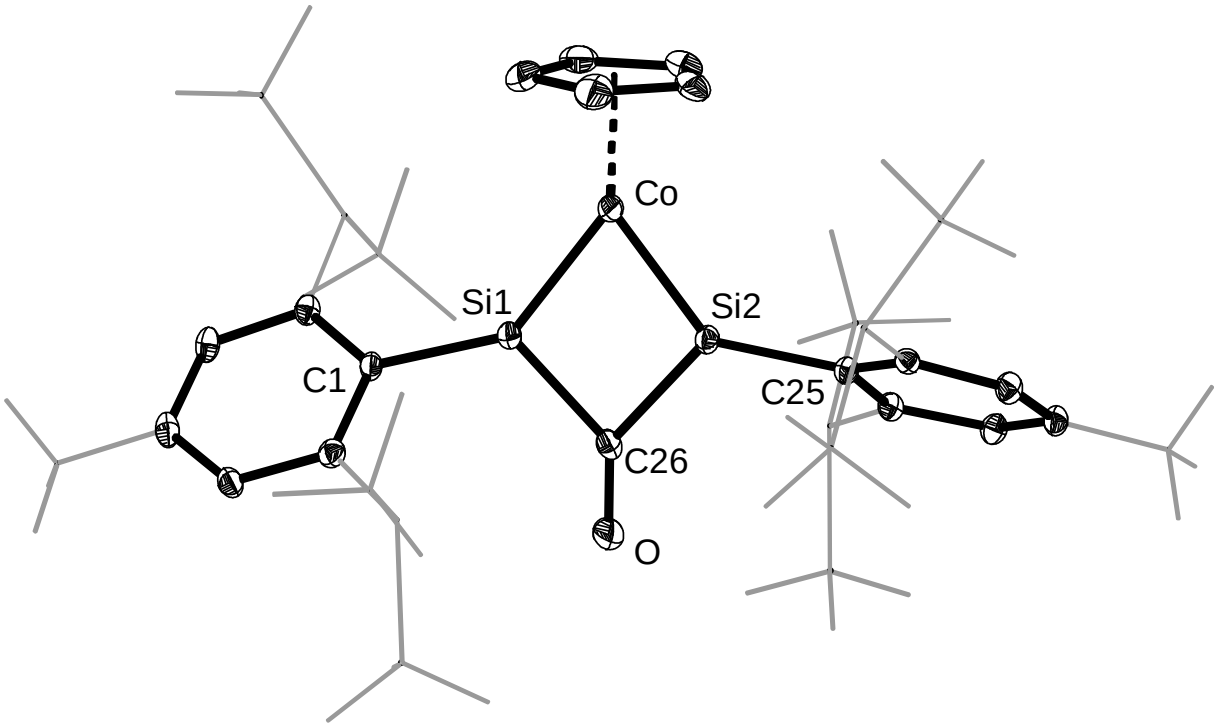

Figure 38. DIAMOND plot of the molecular structure of **21-Co**. Thermal ellipsoids are set at 30 % probability level. Hydrogen atoms are omitted, the Dsi and ^{t}Bu substituents of the Tbb ligand are presented in wire-frame for clarity. Selected bond lengths [Å], bond angles [°] and torsion angle [°]: Co-Si1 2.1428(5), Co-Si2 2.1356(5), Si1-Si2 2.6139(6), Si1-C26 1.9476(18), Si2-C26 1.9278(17), C26-O 1.204(2), Co-Si1-C1 141.07(5), Co-Si1-C26 99.41(5), C1-Si1-C26 119.49(7), Co-Si2-C25 138.80(5), Co-Si2-C26 100.30(5), C25-Si2-C26 120.90(7), Si1-Co-Si2 75.317(19), Co-Si1-Si2-C26 –176.314(4).

The solution structure of the CO bridged bis-silylidene complex **21-Co** was examined by IR and multi-nuclear NMR spectroscopy. In solution, the ^{1}H and ^{13}C{^{1}H} NMR spectra of **21-Co** suggest a time averaged C_{2v} symmetric structure, which well corroborates to its solid-state structure. In the ^{29}Si{^{1}H} NMR spectrum a distinct singlet signal for the tri coordinated Si atoms appears at δ = 291 ppm, which is exceptionally down-field shifted with respect to the aforementioned amidinato-

supported or base-stabilized silylene and bis-silylene complexes Co(I)[141,145,162] or even the cationic base-free silylene complex of cobalt,[161] where in every case the silicon resonance was observed around ca. 50 ppm, probably reflecting the lower coordination number of silicon in **21-Co**. Notably, the silicon resonance of **21-Co** is also low-field shifted compared to that of a reported Ni-silylidene complex (δ = 250.3 ppm) by Filippou *et al.*,[67,68] which contains a Ni=Si double bond. It is noteworthy to mention, that compared to **21-Co**, the CO adduct of silylenes reported by Schulz *et al.* ([L(Br)Ga]$_2$Si-CO, L = HC[C(Me)N(2,6-^{i}Pr$_2$-C$_6$H$_3$)]$_2$)[164] or by Inoue et *al.* [(Me$_3$Si)$_3$Si](^{t}Bu$_3$Si)Si-CO)[165] show extremely high-field shifted signals in ^{29}Si NMR spectra (–256.5 and –228.5 ppm respectively).

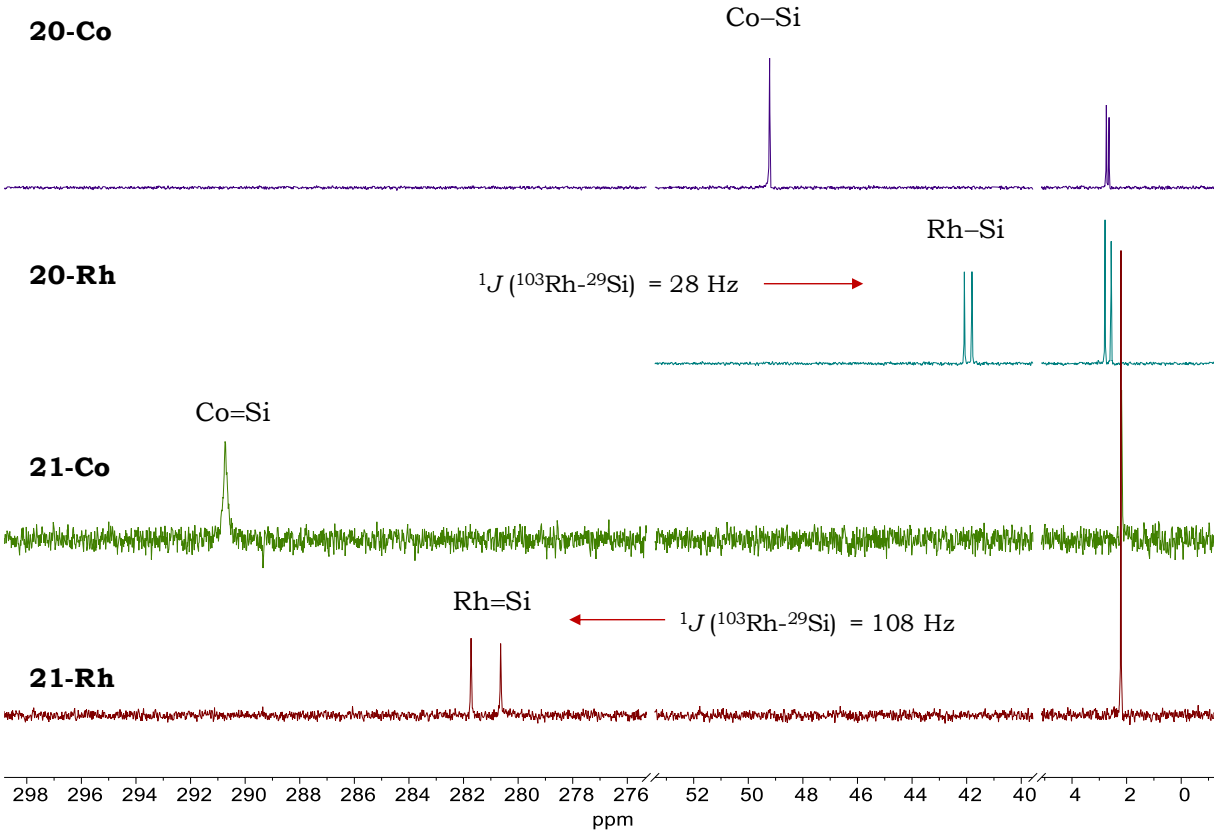

Figure 39. A stack plot of the ^{29}Si{^{1}H} NMR spectra for the compounds **20-Co** to **21-Rh**.

The bridging carbonyl carbon of **21-Co** gives rise to a distinct singlet resonance at δ = 310 ppm, which is highly down-field shifted than its precursor (**20-Co**) and the bissilyl ketone (δ = 260.3 ppm) reported by Sekiguchi *et al.*,[147] but it is quite similar to that reported for the disilyl ketones (PhMe$_2$Si)$_2$C=O (δ = 316 ppm) and (SiMe$_3$)$_2$C=O (δ = 320 ppm) by Ichida *et al.*[146] The CO-resonance of **21-Co** is also significantly (ca. 100 ppm) down-field shifted when compared with those of the above mentioned CO adducts of silylenes[164,165] and the recently reported 1,2-disilicon dicarbonyl complex (δ_{CO} = 220.1 ppm) by Cui *et al.*[22] The IR absorption band of **21-Co** (ν_{CO} = 1615 cm^{-1})

closely resembles to those of the bridging CO absorption bands observed for its precursor, **20-Co**.

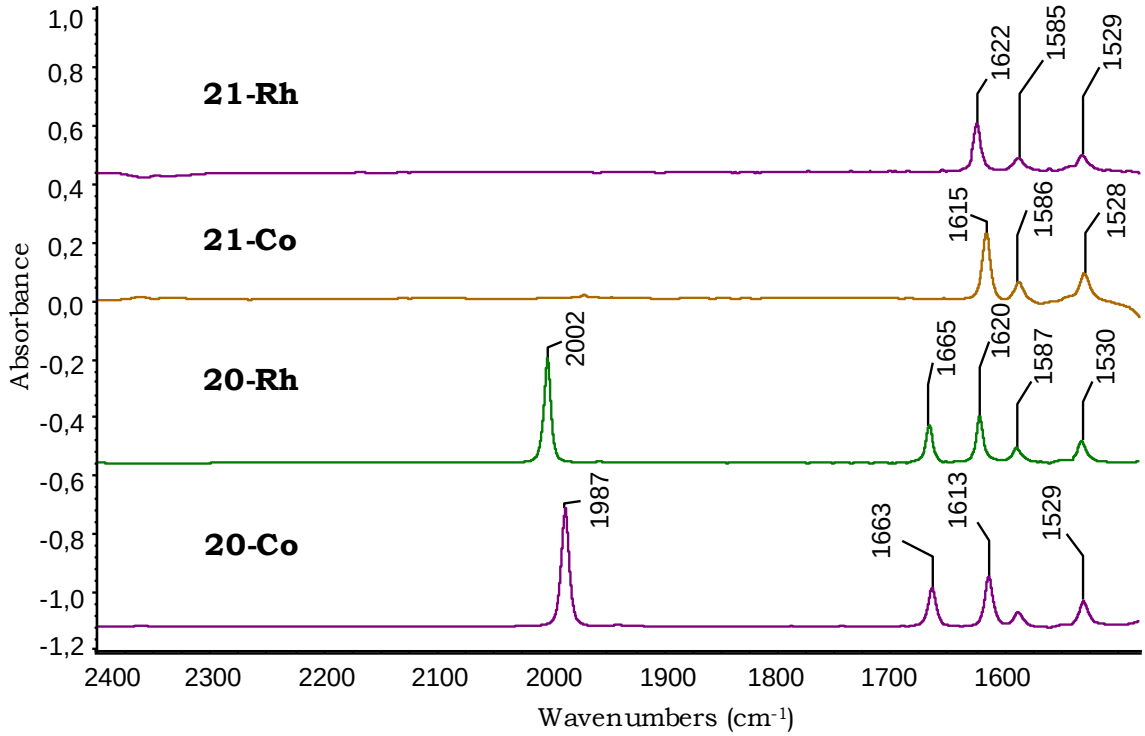

Figure 40. A stack plot of the IR absorption bands for the compounds **20-Co** to **21-Rh** measured in *n*-hexane using an IR cell with CaF_2 windows.

Akin to **21-Co**, suitable single crystals (orangish-brown prisms) of **21-Rh** were obtained upon slow cooling of a saturated *n*-hexane solution at 4 °C and analyzed by *sc*-XRD. It is isostructural (***Figure 41***) to its cobalt analogue and also features two trigonal planar coordinated silicon (∑∠Si1/Si2 = 360°) centers bonded to rhodium via short Rh–Si bonds (Rh-Si1 2.2208(9) and Rh-Si2 2.2072(9)). The Rh–Si bonds are shortened by ca. 0.22 Å compared to its precursor (**21-Rh**), but compare well with the sum of the double bond covalent radii of rhodium and silicon (ca. 2.17 Å) reported by Pykkö *et al.*[160] The Rh–Si bonds of **21-Rh** are considerably shorter than that of a neutral Rh**I**-complex bearing a cyclic amino(bora-ylide)silylene ligand (2.352(1) Å), reported by Kato et *al.*,[166] an iminophosphonamide-supported chlorosilylene ligand (2.2943(7) Å), reported by Nakata *et al.*,[167] and those of cationic Rh**I** complexes bearing N-heterocyclic silylene ligands (~2.30 Å) reported by Pfaltz et *al.*.[168] However, the Rh–Si bonds of **21-Rh** are longer than the Rh–Si bond (2.138(1) Å) of a Rh-metallacyclic silylene reported by Kato *et al.*[169] and a silylene-rhodium complex (2.133(1) Å) reported by Nakata *et al.*[167] The significant reduction in bond length of the Rh–Si single bond of the Rh-metallacyclic Silylene[169] was attributed to a Rh–Si

backdonation interaction (18.31 kcal/mol), which was further validated by second-order perturbation theory.

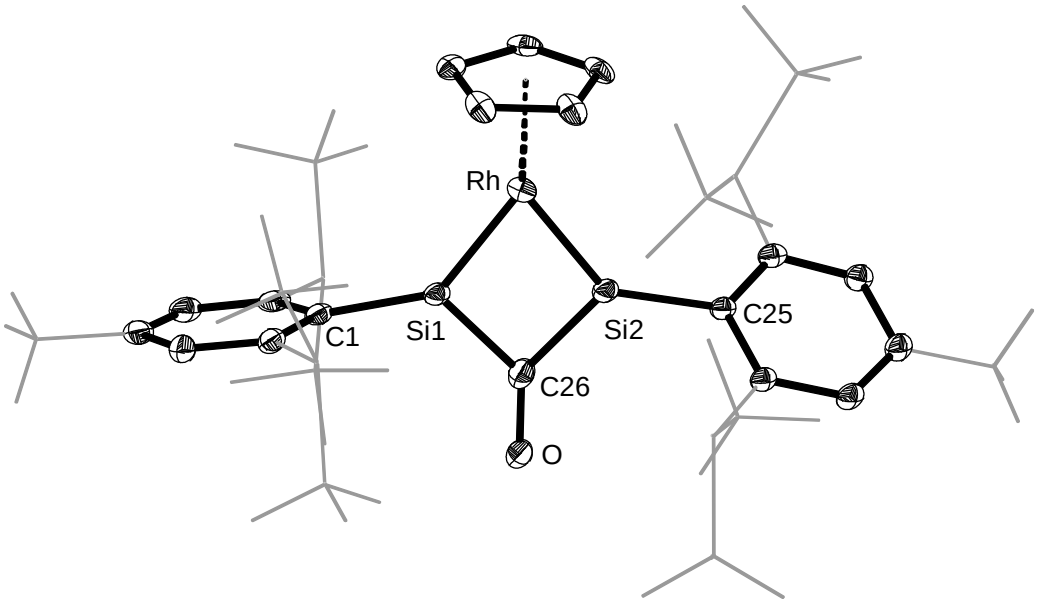

Figure 41. DIAMOND plot of the molecular structure of **21-Rh**. Thermal ellipsoids are set at 30 % probability level. Hydrogen atoms are omitted, the Dsi and ^{t}Bu substituents of the Tbb ligand are presented in wire-frame for clarity. Selected bond lengths [Å], bond angles [°] and torsion angle [°]: Rh-Si1 2.2208(9), Rh-Si2 2.2072(9), Si1-Si2 2.6219(13), Si1-C26 1.931(4), Si2-C26 1.933(4), C26-O 1.264(5), Rh-Si1-C1 136.70(10), Rh-Si1-C26 100.75(12), C1-Si1-C26 122.53(15), Rh-Si2-C25 137.65(10), Rh-Si2-C26 101.18(12), C25-Si2-C26 121.13(15), Si1-Rh-Si2 72.61(3), Rh-Si1-Si2-C26 –179.518(2).

The solution structure of **21-Rh** was also studied by IR and multinuclear spectroscopy. In solution, the IR (in *n*-hexane, ν_{CO} = 1623 cm^{-1}) and NMR spectroscopic feature (δ_{Si} (Rh-Si) = 281.2 ppm and δ_{C}(CO) = 302.4 ppm) of **21-Rh** were very similar to its cobalt analogue **21-Co**.

Table 2. Selected crystallographic and spectroscopic parameters of **20-Co** to **21-Rh**.

Comps.	$d_{(M\text{-}Si)}$ (Å)	δ_{Si}(M–*Si*) (ppm)	δ_{C}(Si-CO-Si) (ppm)	ν_{CO} (Solid) (cm^{-1})
20-Co	2.3555(10) and 2.3633(9)	49.20(s)	204.7 (s), 224.2 (s) and 239.2 (s)	1981, 1661 and 1615
20-Rh	2.4387(3) and 2.4465(3)	41.95(d) (^{1}J(^{103}Rh-^{29}Si) = 28 Hz)	192.79 (d, ^{1}J(^{103}Rh-^{13}C) = 79.3 Hz), 227.91 (d, ^{2}J(^{103}Rh-^{13}C) = 7.3 Hz) and 240.58 (s)	2000, 1666 and 1618
21-Co	2.1428(5) and 2.1356(5)	290.71(s)	309.96 (s)	1613
21-Rh	2.2208(9) and 2.2072(9)	281.19 (d) (^{1}J(^{103}Rh-^{29}Si) = 108 Hz)	302.41 (d, ^{2}J(^{103}Rh-^{13}C) = 32 Hz)	1621

NMR data are given in (D_6)benzene at 298 K.

To gain better insight into the bonding situation around the rhodium and the silicon centers in **21-Rh**, DFT calculations were carried out using the B97-D3(BJ)-ATM/def2-TZVP level of theory. The QT-AIM bonding paths in **21-Rh** ruled out the possibility of having a transannular Si····Si interaction as no bond critical point was found between two silicon centers.

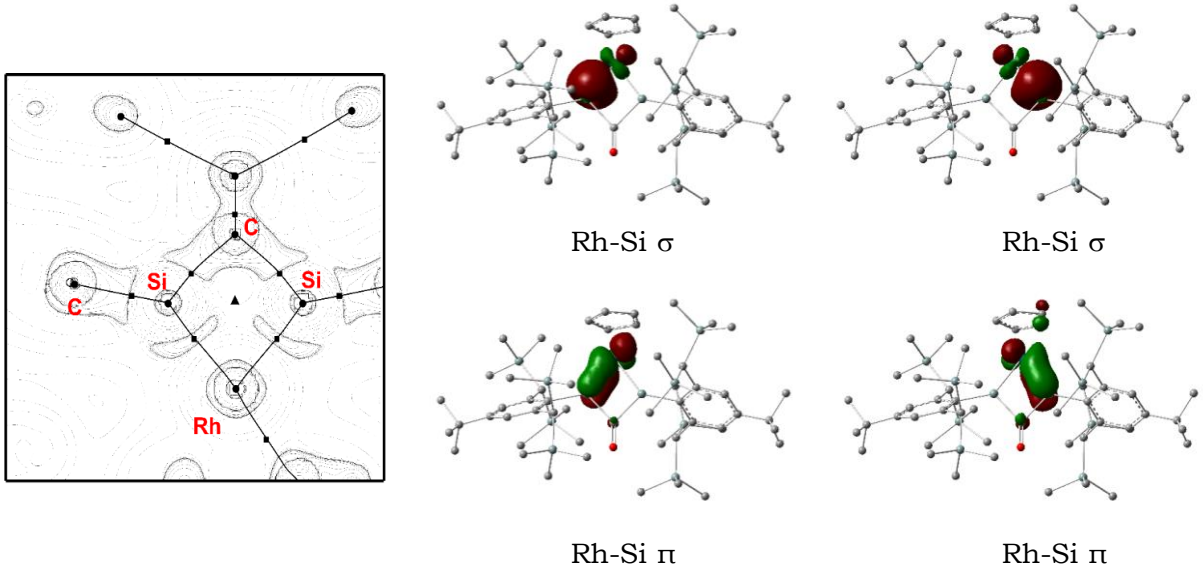

Figure 42. (*left*) Contour plot of the Laplacian of the electron density of **21-Rh** in the Rh–Si–C–Si ring plane. Dots with quadrilateral shape represent bond critical points and the triangular dot represent the ring critical point. (*Right*) Pipek–Mezey-localized molecular orbitals of **21-Rh** and their assigned bond type. Hydrogen atoms are omitted for clarity, and the isosurface value was set to 0.04 $e^{1/2}Bohr^{-3/2}$.

Since the canonical MOs are quite challenging to interpret due to their delocalized nature, the Pipek–Mezey localization scheme was applied to generate localized Pipek–Mezey MOs (LMOs), which found two Rh-Si σ bonds and two corresponding π bonds, supporting well the crystallographic findings. So, taken together compounds **21-Co** and **21-Rh** can be best described as CO bridged bis-silylidene complexes.

2.6. C–C coupling of isocyanides at low-valent silicon centers through skeletal editing

The isolation of this unprecedented class of compounds (**21-Co** and **21-Rh**) in good to high yields offered the chance to study their further reactivity, therefore, a wide range of electrophilic and nucleophilic reagents were screened. But, in most of the cases (diazoalkanes, small azides, nitriles, alkynes, isocyanate, small silane, CO_2, P_4 and $B(tol)_3$) either it was too unselective or totally unreacted. Since, both of these compounds undergo a quantitative CO addition reaction to form back their precursors **20-Co** or **20-Rh**, it prompted to test the reaction with another isoelectronic CO species, an isocyanide. Of note, isocyanides have emerged as advantageous building blocks in synthetic organic chemistry and often used as a non-gaseous CO surrogate.[170] In heavier main group chemistry CO/RNC exchange reactions are reported recently,[164,165] So expectantly, a reaction of **21-Co** with one equivalent MesNC was performed. Indeed, an instantaneous reaction was observed forming mainly **22-Co**, unreacted **21-Co** along with a little amount of an unknown side product. Following this reaction outcome, the reaction was repeated with two equivalents of MesNC.

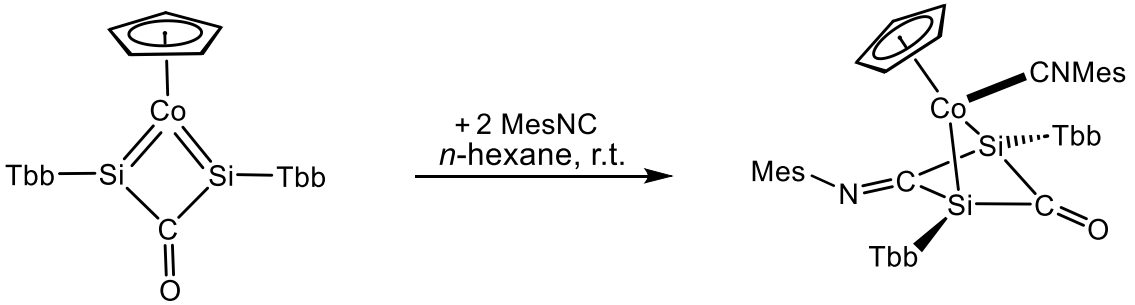

21-Co **22-Co**

Scheme 25. Reactivity of **21-Co** with MesNC.

Dropwise addition of a colourless *n*-hexane solution of MesNC to a wine-red *n*-hexane solution of **21-Co** at ambient temperature was accompanied by an immediate colour change to straw-yellow. NMR and IR spectroscopic analysis of the reaction solution revealed a complete transformation of the starting materials into **22-Co**. After work-up, compound **22-Co** was isolated in analytically pure form in 56 % yield. It is an air-sensitive, but thermally robust ($T_{dec.}$ = 203 °C), brown solid which is well soluble in *n*-hexane, benzene, toluene and Et_2O at ambient temperature.

Curiously, when subjecting **20-Co** to a comparable reaction with two equivalents of MesNC, no observable reaction occurred at ambient temperature. However, upon

thermal activation, only one of the bridging CO groups was replaced by the isocyanide moiety.

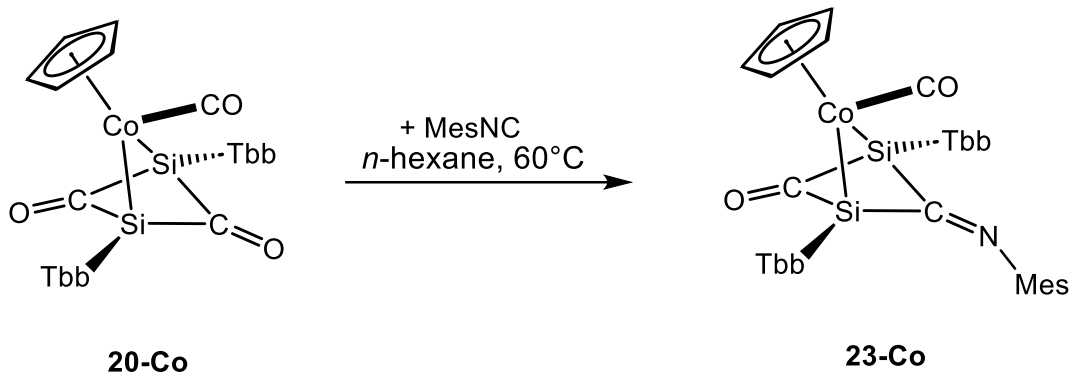

20-Co **23-Co**

Scheme 26. CO/MesNC exchange reaction of **20-Co** upon thermal activation.

Heating an orange reaction solution of **20-Co** with MesNC in *n*-hexane at 60 °C for almost 3.5 days, the colour gradually changed to straw-brown. Monitoring the reaction progress by ^{1}H NMR spectroscopy revealed a 97 % selective conversion of **20-Co** to **23-Co** along with a small amount of unreacted MesNC. After work-up **23-Co** was isolated as analytically pure solid in 79 % yield. It is an air-sensitive, but thermally robust ($T_{dec.}$ = 171 °C), straw-brown solid, which is well soluble in *n*-hexane, benzene, toluene, THF and Et_2O at ambient temperature. Under strict exclusion of air, a solution of **23-Co** in (D_6)benzene does not show any sign of decomposition after one day at ambient temperature. Both compounds (**22-Co** and **23-Co**) were thoroughly characterized by EA, NMR and IR spectroscopy along with *sc*-XRD analysis.

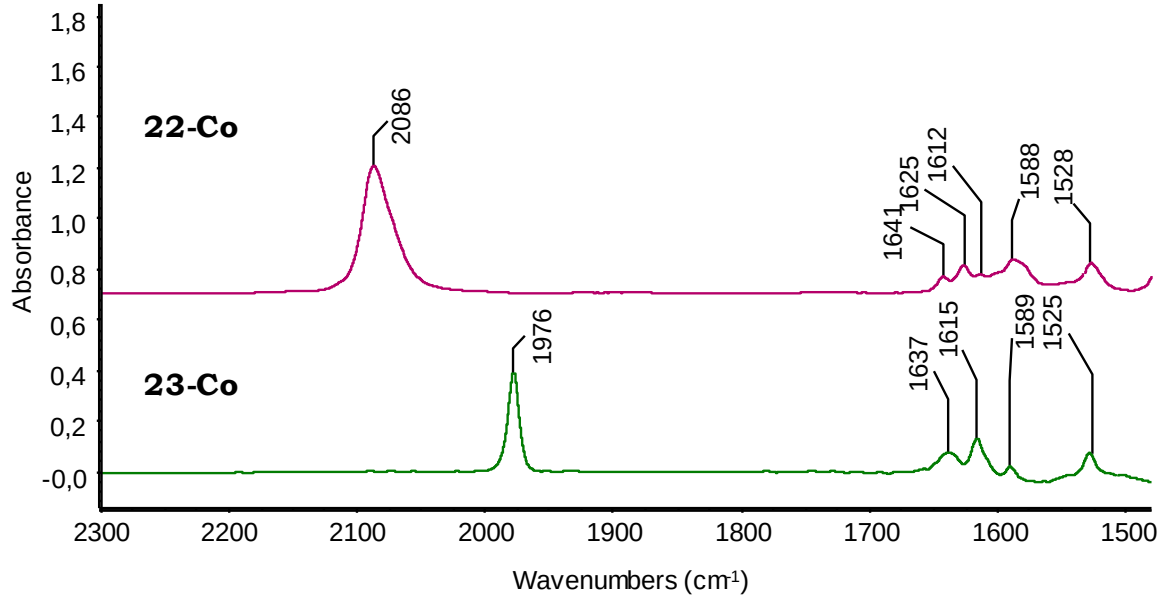

Figure 43. A stack plot of the IR absorption bands of the compounds **22-Co** to **23-Co** measured in THF using an IR cell with CaF_2 window.

Suitable single crystals of **22-Co** (orangish-brown prisms) and **23-Co•C_6H_{14}** (brown blocks) were grown upon slow cooling of concentrated *n*-hexane solutions at –30 °C. In solid state, these molecules are isostructural to **20-Co** (***Figure 44***) and feature similar structural parameters. In solution, the key IR (ν_{CO}) and NMR spectroscopic features (δ_C(CO) and δ_{Si}(Co-Si)) (see ***Table 3***) are quite well fitting to those of **20-Co**. Of note, in addition to CO, these molecules also contain a bis(silyl)imine functionality and in general, the synthetic approach to a bisilyl imine is accomplished either by an isocyanide insertion to Si–Si (mainly disilanes) bond using Pd catalysts[171–173] or by an isocyanide insertion to a Si=Si double bond.[174,175]

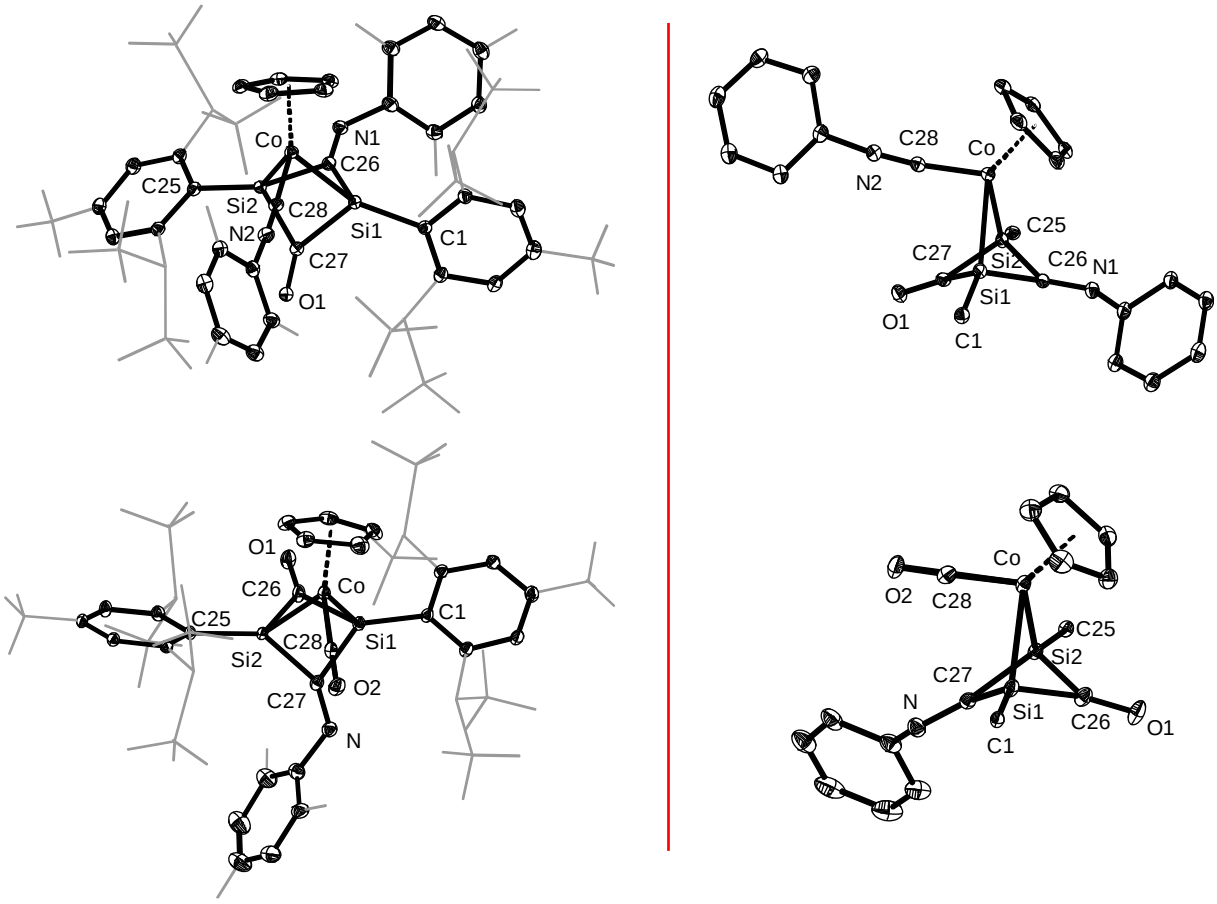

Figure 44. (*left*) DIAMOND plot of the molecular structure of **22-Co and 23-Co** and (*right*) their side view respectively. Thermal ellipsoids are set at 30 % probability level. Hydrogen atoms are omitted, the Dsi and ^{t}Bu substituents of the Tbb ligand and C^2, C^4 and C^6 methyl groups of Mes ligand are presented in wire-frame for clarity. Except C1 and C25 atoms, all other atoms in the Tbb ligands are omitted for clarity. Selected bond lengths [Å], bond angles [°] and torsion angles [°]: **22-Co**: Co-Si1 2.3718(7), Co-Si2 2.3803(7), Si-Si2 2.6158(9), Si1-C26 1.957(2), Si1-C27 1.927(2), Si2-C26 1.952(2), Si2-C27 1.911(2), Co-C28 1.795(2), C26-N1 1.271(3), C28-N2 1.159(3), C26-Si1-C27 83.97(10), C26-Si2-C27 84.55(10), C26-Si1-Si2-C27 130.929(1); **23-Co**: Co-Si1 2.3384(5), Co-Si2 2.4020(5), Si1-Si2 2.6325(6), Si1-C26 1.9268(18), Si1-C27 1.9099(18), Si2-C26 1.9467(18), Si2-C27 1.9872(18), C27-N 1.269(2), C26-Si1-C27 83.08(8), C26-Si2-C27 80.60(7), C26-Si1-Si2-C27 125.878(3).

In the $^{13}C\{^1H\}$ NMR spectra, the bridging isocyanide carbons appear as a distinct singlet at δ = 191.4 and 192.8 ppm for **22-Co** and **23-Co** respectively, which is slightly down-field shifted than those of the aliphatic imines (~160-170 ppm), but marginally high-field shifted than those of bis(silyl)imines reported by Sekiguchi *et al.* (213.6 ppm),[176] Ito *et al.* (217.1 ppm)[171] and Weidenbruch *et al.* (223.3 ppm),[173] respectively. However, it is quite similar to those of the bis-isocyanide adduct of the amidinate chelated halo-silylenes reported by Jones *et al.* (192.3 ppm)[177] and the bis-isocyanide adduct of a cyclotrisilene reported by Scheschkewitz *et al.*(194.2 ppm).[178] In the FT-IR spectra, the observed bridging C=N stretching frequency at 1628 and 1639 cm^{-1} for **22-Co** and **23-Co** respectively, is quite similar to that of the compound reported by Sekiguchi *et al.* (1639 cm^{-1}),[176] but higher as compared to those of reported acyclic and cyclic disilylimines (~1540–1595 cm^{-1}).[172–174]

In order to achieve the isocyanide equivalent compound of **21-Co**, complex **23-Co** was refluxed in *n*-heptane. Upon refluxing for 5 hours, the straw-brown *n*-heptane solution of **23-Co** gradually turned wine red. Analysis of an aliquot of the reaction solution by ^1H NMR spectroscopy in (D_6)benzene revealed complete consumption of **23-Co** and the very selective formation of **24-Co.**

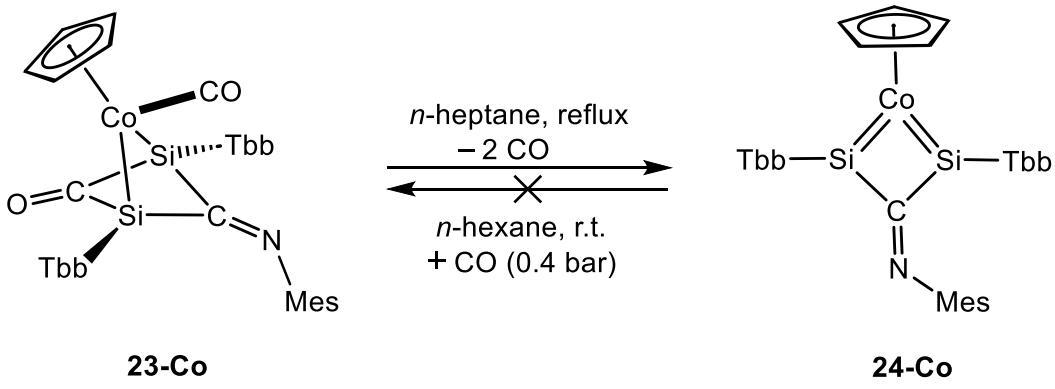

23-Co **24-Co**

Scheme 27. Thermal decarbonylation reaction of **23-Co**.

24-Co was isolated as an analytically pure solid in 72 % yield. It is an extremely air-sensitive, dark-maroon solid, which is highly soluble in *n*-hexane, benzene, toluene and Et_2O at ambient temperature. Unlike **21-Co**, **24-Co** does not react back with CO to form **23-Co**. Instead, the reaction gives a mixture of unknown compounds. Compound **24-Co** was fully characterized using EA, IR, multinuclear NMR spectroscopy and *sc*-XRD analysis. Suitable single crystals (brown blocks) of **24-Co•Et$_2$O** were grown upon slow cooling a saturated Et_2O solution at –30 °C. In solid state, the structural features ($d_{(Co\text{-}Si)}$, $\sum\angle Si$ and $d_{(Si\text{-}CN)}$) are rather similar to its CO

analogue, **21-Co** except the trans annular Si···Si distance (2.5494(6) Å), which got slightly shortened (~0.07 Å) compared with that of **21-Co**.

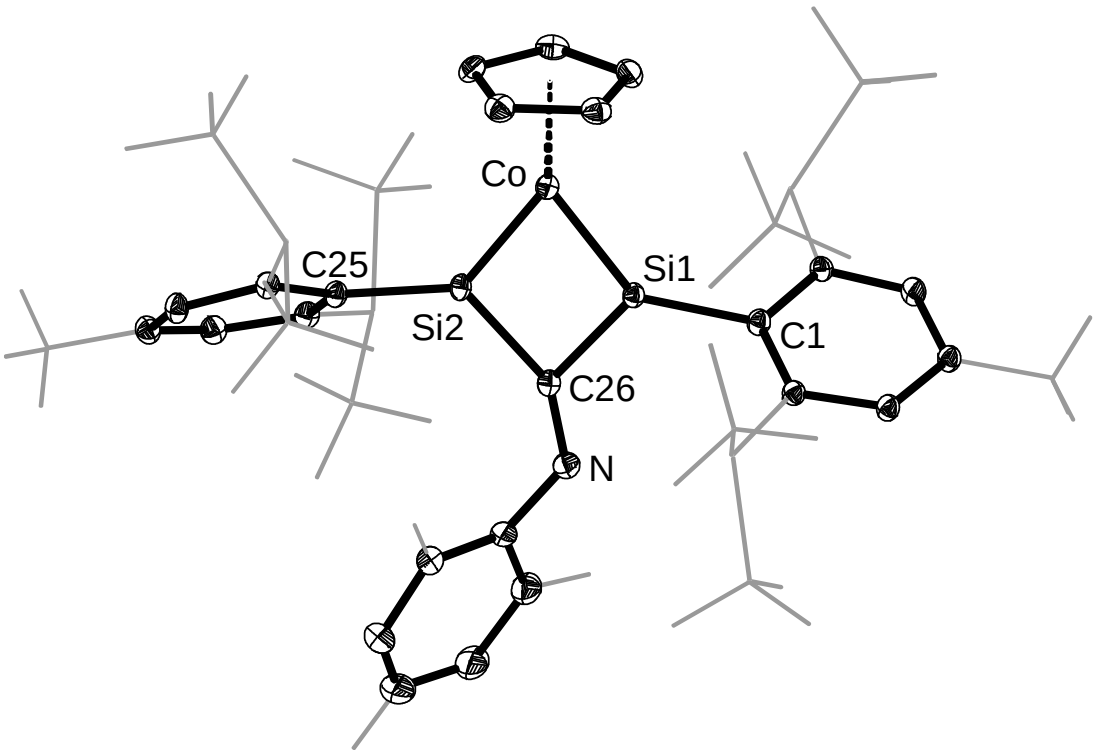

Figure 45. DIAMOND plot of the molecular structure of **24-Co**. Thermal ellipsoids are set at 30 % probability level. Hydrogen atoms are omitted, the Dsi and ^{t}Bu substituents of the Tbb ligand and C^{2},C^{4} and C^{6} methyl groups of Mes ligand are presented in wire-frame for clarity. Selected bond lengths [Å], bond angles [°] and torsion angle [°]: Co-Si1 2.1238(8), Co-Si2 2.1543(8), Si1-Si2 2.5494(10), Si1-C26 1.900(3), Si2-C26 1.938(3), C26-N 1.284(4), Co-Si1-C1 137.34(9), Co-Si1-C26 102.83(8), C1-Si1-C26 119.83(12), Co-Si2-C25 135.37(9), Co-Si2-C26 100.43(8), C25-Si2-C26 124.19(12), Si1-Co-Si2 73.15(3), Co-Si2-Si1-C26 174.254(5).

In solution, the ^{1}H and ^{13}C{^{1}H} NMR spectra of **24-Co** suggest a time averaged C_{2v} symmetric structure. But, unlike **21-Co**, the Si–C^{Tbb} rotations of **24-Co** are hindered on the NMR time scale, probably due to the presence of the bulkier C*NMes* moiety instead of C*O*. Hence, two different Si*Me*$_3$ signals were observed in ^{1}H NMR spectrum of **24-Co** at ambient temperature. In the ^{29}Si{^{1}H} NMR spectrum, a broad ($\Delta\nu_{1/2}$ = 28 Hz) singlet at δ = 269 ppm was observed for the tri coordinated Si atoms, which is way low-field shifted than its precursor (**23-Co**) but ca. 20 ppm high-field shifted as compared to its CO analogue (**21-Co**). Notably, δ_{Si} of **24-Co** is exceptionally low-field shifted than those for Si^{0}-isocyanide (–142 ppm),[95] bis(silaketenimine) (–172.0 ppm)[179] and even the monosilaketenimine (15.9 ppm)[180] reported in literature. In the ^{13}C{^{1}H} NMR spectrum, the isocyanide carbon appears at δ = 238 ppm, which is quite high-field shifted as compared to its CO analogue (**21-Co**) but ca. 45 ppm down field shifted as compared to its precursor, **23-Co**. In the IR

spectrum, the C=N (1610 cm^{-1}) stretching frequency for **24-Co** was observed at lower wavenumber as compared to its precursor.

In seeking to comprehend any potential disparities in reactivity between **21-Co** and **24-Co** the very first reaction was tried with two equivalents of isocyanide in order to generate an analogous tris-isocyanide derivative of **20-Co**. Unexpectedly, no reaction occurred at ambient temperature. However, upon prolonged heating it eventually reacted, albeit with only one equivalent, leading to the formation of the unprecedented C–C coupled product **25-Co**.

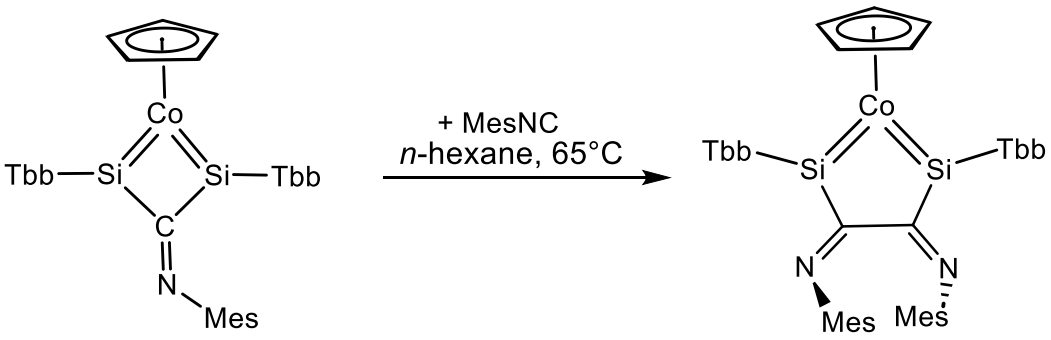

24-Co **25-Co**

Scheme 28. C–C coupling of isocyanides at low-valent silicon center.

When a wine-red *n*-hexane solution of **24-Co** was heated with MesNC (1.1 equiv.) at 65 °C for 90 hours, the colour of the reaction solution gradually changed to red-brown. Analyzing the reaction progress by ^{1}H NMR spectroscopy revealed complete consumption of **24-Co** and very selective formation of **25-Co** (97 mole %) along with 3 mole% of $CpCo(MesNC)_2$ and little unreacted MesNC. After work-up **25-Co** was isolated as an analytically pure solid in 66 % yield. It is an air-sensitive, thermally stable ($T_{dec.}$ = 192 °C), brown-red solid, which is well soluble in *n*-hexane, benzene, THF and Et_2O at ambient temperature. It is worth mentioning that **25-Co** is the very first compound to be reported in heavier main group chemistry, which has been prepared by coupling of isocyanides[175,181] at low-valent silicon centers via *skeletal editing*.[182] Hence, it was comprehensively characterized by EA, IR, multinuclear NMR and sc-XRD analysis. Suitable clear dark planks of **25-Co•2 C_6H_{14}** were obtained upon storing its saturated *n*-hexane solution at 4 °C for 3 days. The solid-state structural parameters (Co-Si1 2.1282(14), Co-Si2 2.1188(14) and ∑∠Si = 360°) are quite well resembling to those of its precursor, except the trans annular Si···Si distance (2.9066(1) Å), which is ca. 0.36 Å elongated compared to that of **24-Co** as a result of ring expansion. The C–C distance ($d_{(C49–C50)}$ = 1.508(6)) of the isocyanide

carbons and Si–C^{iso} (Si1-C49 1.907(5), and Si2-C50 1.902(5)) are well comparable to C–C and Si–C single bonds respectively.

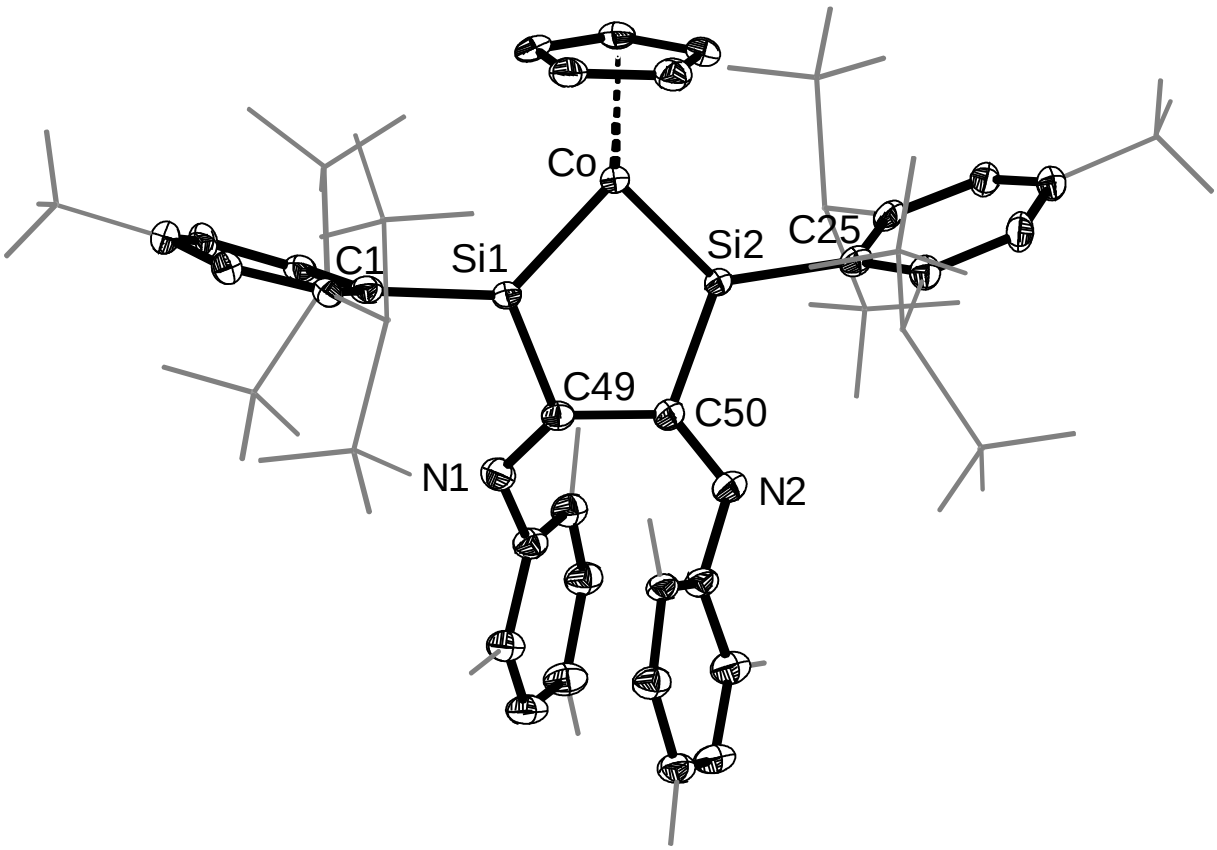

Figure 46. DIAMOND plot of the molecular structure of **25-Co**. Thermal ellipsoids are set at 30 % probability level. Hydrogen atoms are omitted, the Dsi and ^{t}Bu substituents of the Tbb ligand and C^{2},C^{4} and C^{6} methyl groups of Mes ligand are presented in wire-frame for clarity. Selected bond lengths [Å], bond angles [°] and torsion angles [°]: Co-Si1 2.1282(14), Co-Si2 2.1188(14), Si1-Si2 2.9066(1), Si1-C49 1.907(5), Si2-C50 1.902(5), C49-C50 1.508(6), C49-N1 1.296(6), C50-N2 1.294(6), Co-Si1-C49 114.56(15), Co-Si1-C1 129.76(14), C1-Si1-C49 115.3(2), Co-Si2-C50 114.48(15), Co-Si2-C25 127.56(15), C25-Si2-C50 117.4(2), Si1-Co-Si2 86.38(5), N1-C49-C50-N2 –57.1(7), Si1-C49-C50-N2 141.0(4), Si2-C50-C49-N1 144.0(4).

In solution, the ^{1}H and ^{13}C{^{1}H} NMR spectra suggest a time averaged C_2 symmetric structure, where rotation of Tbb groups around the Si–C^{Tbb} bonds are frozen out on the NMR time scale at ambient temperature (***Figure 47***). This leads to homotopic Tbb groups in which both the Dsi groups are diastereotopic. Hence, at ambient temperature, the ^{1}H NMR spectrum of **25-Co** different signals for four different Si*Me*$_3$, two different *Dsi* and two different C^{3,5}-*H* protons were observed. Along with Si–C^{Tbb} rotaion, N–C^{Mes} rotation in **25-Co** has also been stopped, as evidenced from three different C^{2,4,6}-*Me* protons in the ^{1}H NMR spectrum at ambient temperature. In the ^{29}Si{^{1}H} NMR spectrum of **25-Co**, the metal-bound Silicon atoms (286.2 ppm) appear slightly low-field shifted and in the ^{13}C{^{1}H} NMR spectrum the isocyanide carbons (194.3 ppm) appear slightly high-field shifted to those of its precursor, **24-Co**. The IR

spectrum **25-Co** in THF shows a very weak band at 1547 cm^{-1} for the C=N stretching vibration which is lower in wavenumber as compared to **24-Co**.

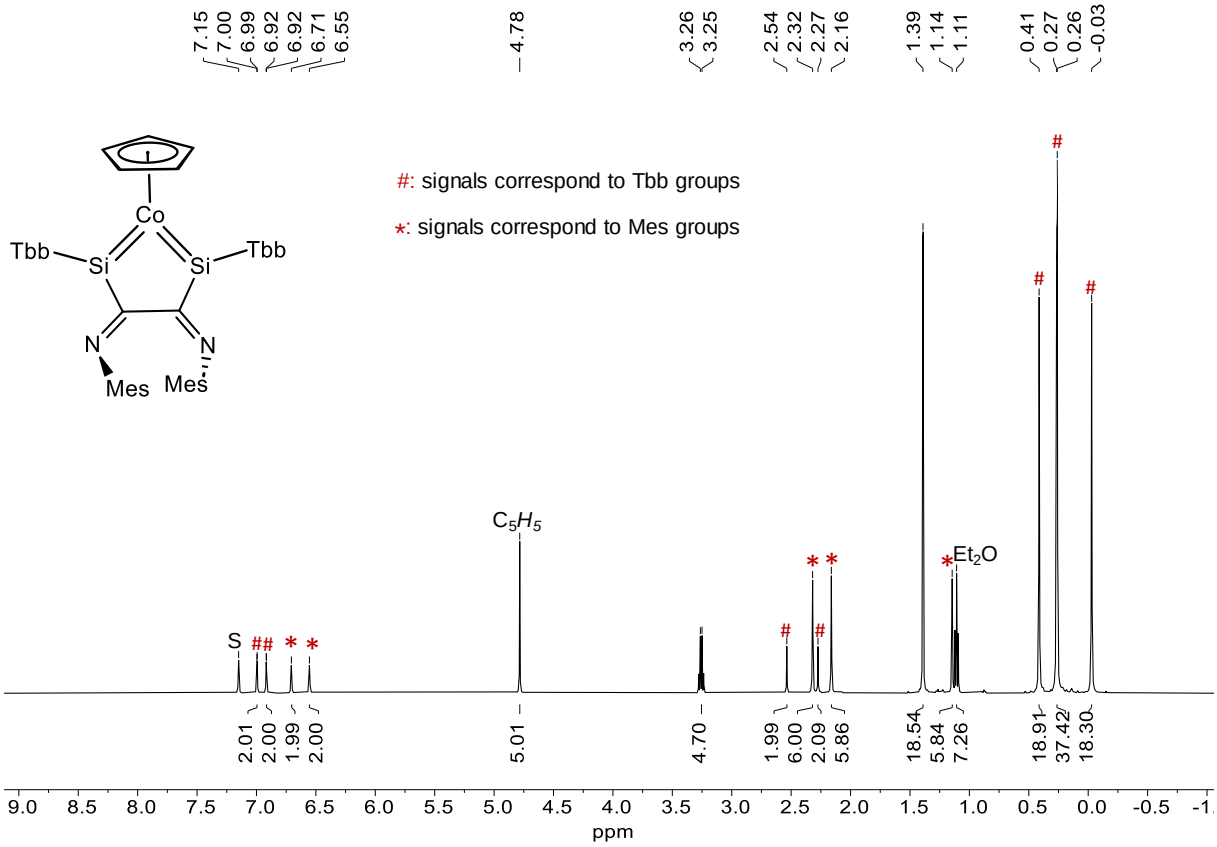

Figure 47. ^{1}H NMR spectrum of **25-Co** in (D6)benzene at 298 K; the residual proton signal of the deuterated solvent is marked with the character S.

Table 3. Selected crystallographic and spectroscopic parameters of **22-Co** to **25-Co**.

Comps.	$d_{(Co–Si)}$ (Å)	δ_{Si}(M–*Si*) (ppm)	δ_{C}(*C*N) (ppm)	δ_{C}(Si-CO-Si) (ppm)	$\nu_{CO/CN}$ (THF) (cm^{-1})
22-Co	2.3718(7) and 2.3803(7)	40.7	191.4	239.0	2086, 1643, 1626, 1612 and 1599
23-Co	2.3384(5) and 2.4020(5)	33.4	192.8	226.8	1978, 1637 and 1615
24-Co	2.1238(8) and 2.1543(8)	269.2	237.8	–	1609
25-Co	2.1282(14) and 2.1188(14)	286.2	194.3	–	1547

All the NMR data are given in (D_6)benzene at 298 K except the δ_{Si} for **22-Co** which is given in (D_8)toluene at 238 K.

2.7. Isolation of the first inverted carbene complexes and the first disilacyclopropenone complex

After the isocyanide chemistry of the unsaturated metallacycle **21-Co**, another intriguing reactivity was observed by introducing a small Lewis acid, $AlMe_3$ (***Scheme 29***). At ambient temperature, the bridging carbonyl ligand in **21-Co** undergoes deoxygenation upon addition of an equimolar amount of $AlMe_3$, resulting in the formation of an unprecedented metal-carbene complex, exhibiting an inverted geometry at the carbene carbon.

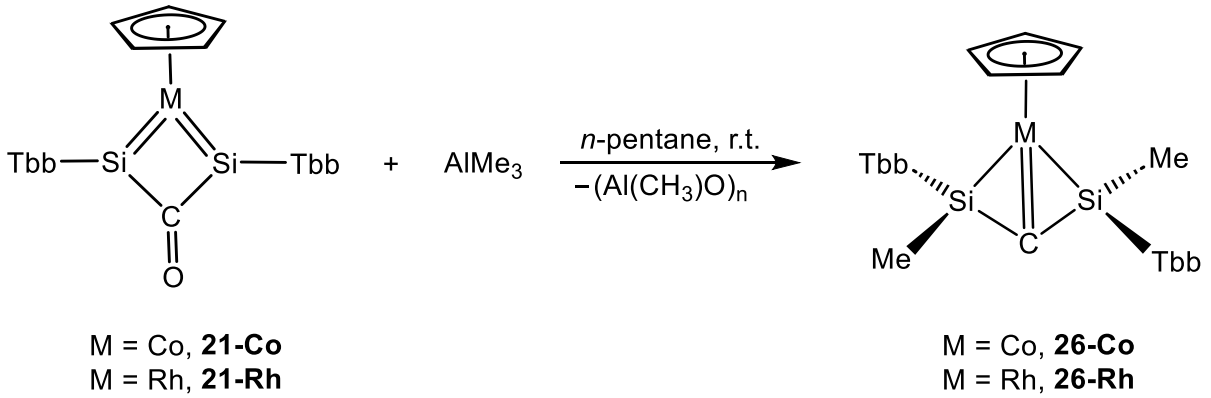

Scheme 29. Synthesis of inverted carbenes via deoxygenation of a bridging carbonyl ligand.

When a colourless stock solution of $AlMe_3$ was added to a wine-red *n*-pentane solution of **21-Co** at ambient temperature, an immediate colour change was observed forming a clear light-green solution. Spectroscopic analysis confirmed the absence of the C=O functionality in the reaction solution and a quantitative formation of **26-Co**. Performing the same reaction with **21-Rh**, a similar outcome was observed except the colour change (purple-brown). Both complexes (**26-Co** and **26-Rh**) were isolated after an acetonitrile/Et_2O work-up as analytically pure solids (green and mink-brown) in 66 % and 72 % yield, respectively. Compounds **26-Co** and **26-Rh** are moderately air sensitive, but thermally stable ($T_{dec.}$ = 208 and 222 °C respectively) solids, which are very well soluble in aliphatic and aromatic solvents, but insoluble in acetonitrile at ambient temperature.

Notably, these molecules represent the first reported examples containing a non-classical metal-carbon double bond, demostrating an inverted geometry at the carbene carbon. While the experimental realization of a similar non-classical double bond at a silicon center was recently revealed by Iwamoto *et al.*,[183] such occurances in carbon chemistry have only been explored *in silico*. So, after isolation of these inverted carbene complexes, a thorough characterization including EA, multinuclear NMR and *sc*-XRD was performed. Suitable single crystals of **26-Co** (clear green planks) and **26-Rh** (clear red planks) were obtained upon slow evaporation of their

respective saturated solutions in 1 : 4 (CH_3CN/Et_2O, v/v) at ambient temperature inside the glove-box.

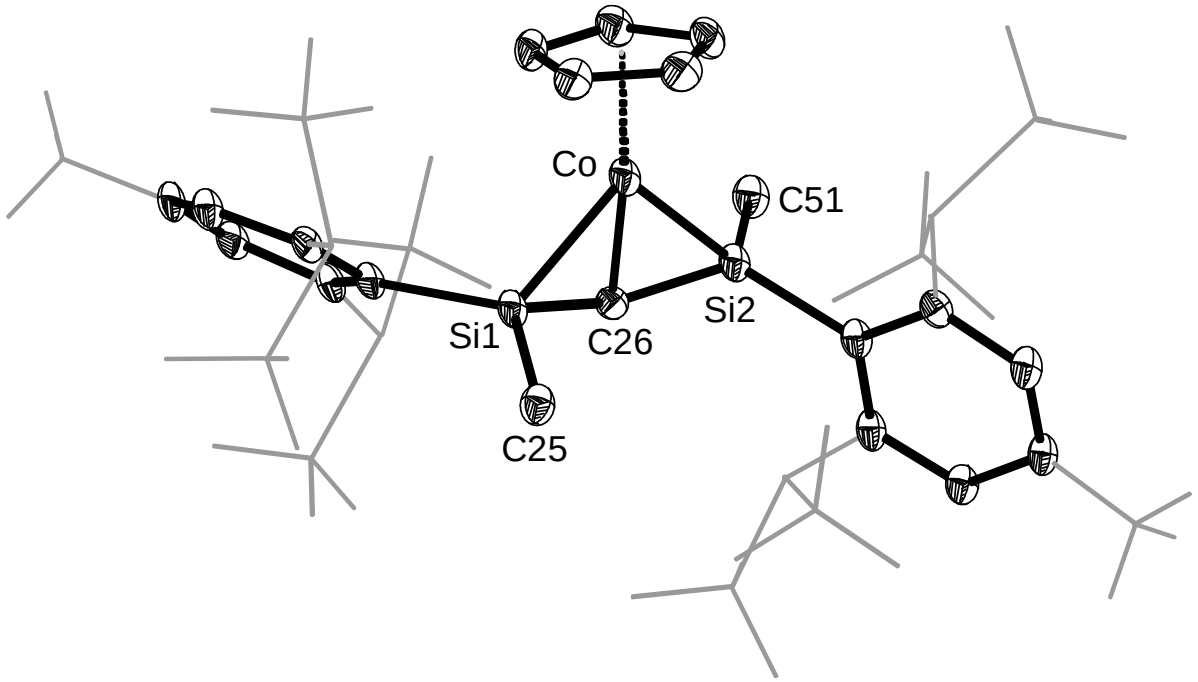

Figure 48. DIAMOND plot of the molecular structure of **26-Co**. Thermal ellipsoids are set at 30 % probability level. Hydrogen atoms are omitted, the Dsi and *t*Bu substituents of the Tbb ligand are presented in wire-frame for clarity. Selected bond lengths [Å], bond angles [°] and torsion angles [°]: Co-Si1 2.293(2), Co-Si2 2.290(2), Co-C26 1.872(6), Si1-C26 1.795(6), Si2-C26 1.765(6), Si1-C26-Si2 150.5(4), Si1-C26-Co 78.0(3), Si2-C26-Co 77.4(2), C1-Si1-C26 124.7(3), C1-Si1-C25 114.8(3), C25-Si1-C26 113.8(3), C27-Si2-C26 124.4(3), C27-Si2-C51 106.2(3), C26-Si2-C51 120.1(3), Si1-Co-C26-Si2 –163.592(6).

The solid state structural features of **26-Co** (***Figure 48***) are as follows, i) two distorted tetrahedrally coordinated silicon centers are present that are bonded to cobalt via Co–Si single bonds (Co-Si1 2.293(2), Co-Si2 2.290(2) Å), which are very close to the sum of single bond covalent radii of cobalt and silicon (~2.27 Å) reported in literature,[160,184] but are slightly shorter (~0.08 Å) than those of the aforementioned bis-silyl complexes **20-Co** and **23-Co**, ii) the tricoordinated carbon (C26) atom is bonded to the cobalt center via a short bond (Co-C26 1.872(6) Å), which lies in the range of Co=C double bond lengths of closed-shell Co(I)-carbene complexes (1.740 Å – 1.989 Å) reported in the Cambridge Structural Database (CSD), iii) two abnormal Si–C bonds (Si1-C26 1.795(6) Å and Si2-C26 1.765(6) Å) are found which are longer than the Si=C double bonds (~1.70 Å) reported for 1-siaallenes,[185–187] but are markedly shorter as compared to normal Si–C single bonds (~1.87 Å) of tetracoordinated silicon centers, iv) a puckered four-membered ring (Co-Si1-C26-Si2) with two silicon centers bending upwards, also evidenced from the torsion angle (Si1-

Co-C26-Si2) of −163.592(6)°. The solution integrity of **26-Co** was verified by multinuclear NMR spectroscopy. Akin to its solid state, in solution, the ^{1}H (***Figure 49***) and ^{13}C{^{1}H} NMR spectra of **26-Co** (***Figure 50***) at ambient temperature feature a time averaged C_2 symmetry with frozen Si–C^{Tbb} rotations on the NMR time scale. In the ^{29}Si{^{1}H} NMR a distinct singlet for the metal bound silicon atoms at δ = 6.6 ppm is observed, which is moderately high-field shifted (~30 ppm) as compared to that of **20-Co**, **22-Co** and **23-Co**. The ^{13}C chemical shift of the carbene carbon (Co=*C*) of **26-Co** (313.8 ppm) is well resembling to that of some Co-carbene complexes (> 300 ppm) known in literature[188] but, considerably low-field shifted than those of Co(I) aminocarbene complexes (~240 ppm) reported by Filippou *et al.*.[189]

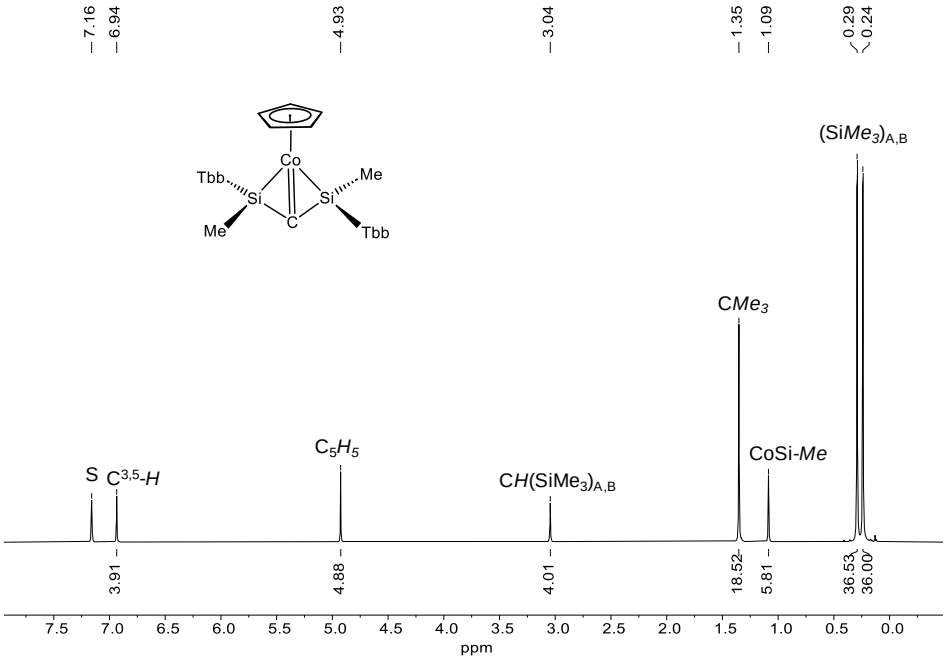

Figure 49. ^{1}H NMR spectrum of **26-Co** in (D6)benzene at 298 K; the residual proton signal of the deuterated solvent is marked with the character S.

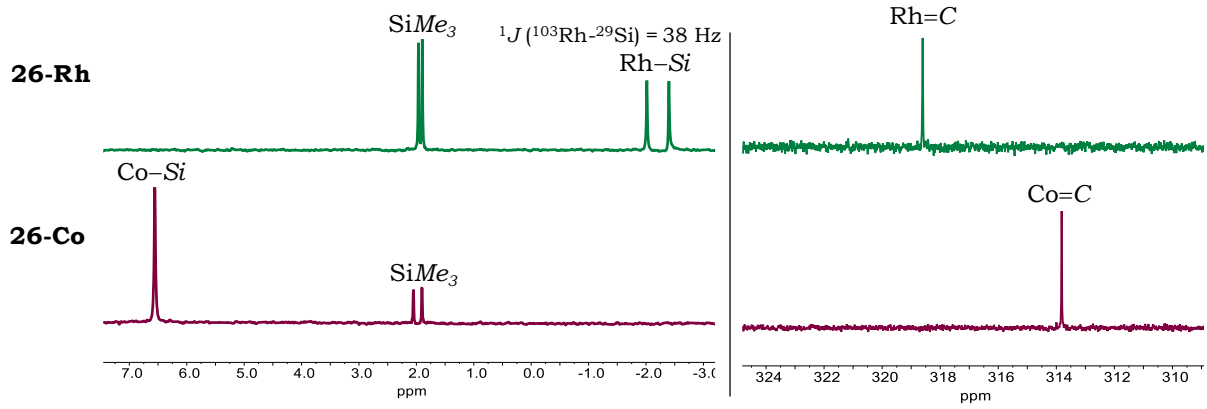

Figure 50. Stack plots of the ^{29}Si{^{1}H} NMR spectra (*left*) and the ^{13}C{^{1}H} spectra carbene resonances (*right*) of the compounds **26-Co** and **26-Rh**.

Compound **26-Rh** (***Figure 51***) is isostructural to **26-Co**. It features two distorted-tetrahedrally coordinated silicon centers bonded to rhodium via Rh–Si single bonds (Rh-Si1 2.3730(4), Rh-Si2 2.3832(4) Å). The Rh–Si bond lengths compare well with the sum of single bond covalent radii of rhodium and silicon (~2.41 Å) reported in literature,[160,184] but are slightly shorter (~0.06 Å) than those of the aforementioned bis-silyl complex **20-Rh**. The tricoordinated carbon (C26) atom is bonded to the metal center via a short bond (Rh-C26 2.0054(13) Å), which is well resembling to the Rh=C double bonds of some closed-shell Rh(I)-carbene complexes (~2.00 Å) reported in the Cambridge Structural Database (CSD) but, markedly longer (ca. 0.12 Å) than those of indenylrhodium-carbene complexes reported by Werner *et al.*.[190] The Si–C bonds (Si1-C26 1.7740(13) Å and Si2-C26 1.7746(13) Å) are short as in the cobalt analogue, and the four-membered ring (Co-Si1-C26-Si2) is puckered with a torsion angle (Si1-Rh-C26-Si2) of 167.386(4).

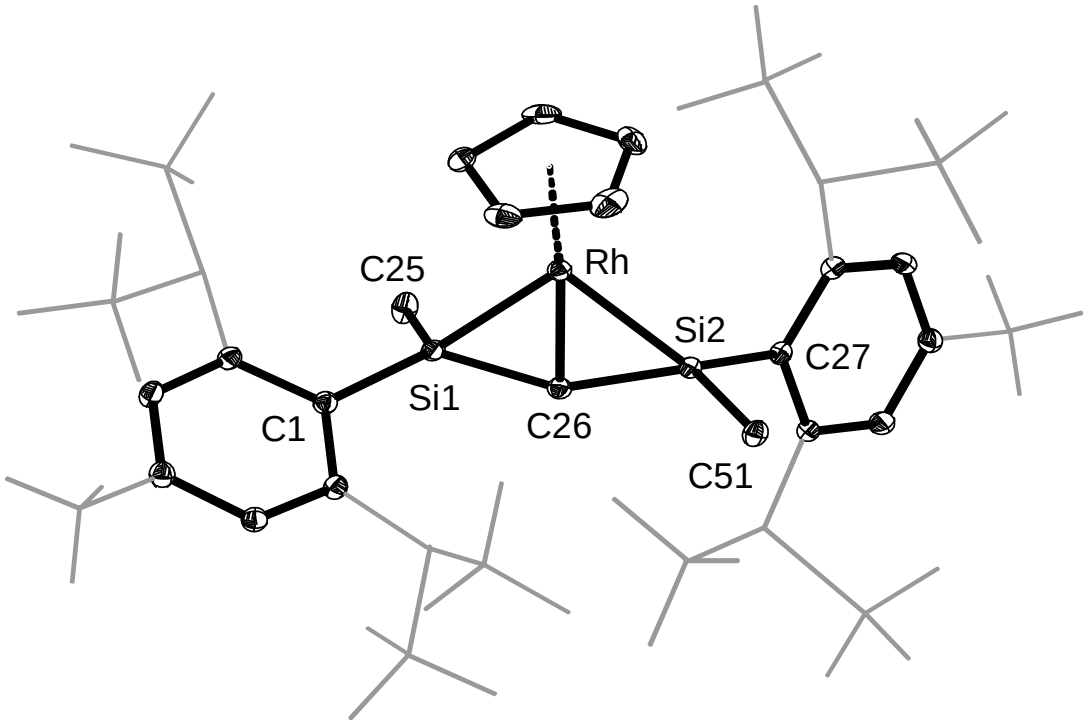

Figure 51. DIAMOND plot of the molecular structure of **26-Rh**. Thermal ellipsoids are set at 30 % probability level. Hydrogen atoms are omitted, the Dsi and ^{t}Bu substituents of the Tbb ligand are presented in wire-frame for clarity. Selected bond lengths [Å], bond angles [°] and torsion angle [°]: Rh-Si1 2.3730(4), Rh-Si2 2.3832(4), Rh-C26 2.0054(13), Si1-C26 1.7740(13), Si2-C26 1.7746(13), Si1-C26-Si2 152.43(8), C1-Si1-C26 123.58(6), C1-Si1-C25 116.97(6), C25-Si1-C26 111.28(6), C27-Si2-C26 123.11(6), C27-Si2-C51 108.35(6), C26-Si2-C51 117.34(6), Si1-Rh-C26-Si2 167.386(4).

The ^{29}Si NMR resonance of the metal bound silicon atoms appears as a sharp doublet at δ = –2.2 ppm ($^{1}J(^{103}\text{Rh}\text{-}^{29}\text{Si})$ = 38 Hz) and is quite high-field shifted as compared to that of **20-Rh**. In the $^{13}C\{^{1}H\}$ NMR spectrum (***Figure 50***) of **26-Rh**, the carbene carbon emerges at δ = 318.6 ppm as a distinct singlet, deviating from the anticipated doublet

due to the absence of ^{103}Rh-^{13}C coupling. This shift is notably down-field compared to that observed in most of the literature-known rhodium-carbene complexes.[190,191] Interestingly, the $\delta_{Carb.}$ closely aligns with [(P^iPr_3)$_2$RhClC(p-Tol)$_2$] ($\delta_{Carb.}$ = 317.0 ppm, ^1J(Rh-C) = 38.1 Hz),[191] but exhibits a considerable high-field shift when compared to a chelating bisphosphine-containing rhodium-carbene complex ($\delta_{Carb.}$ = 355.1 ppm, ^1J(Rh-C) = 31.8 Hz).[192]

In order to get closer insight into the structure and bonding, **26-Rh** was further studied by quantum chemical calculations at the B97-D3(BJ)-ATM/def2-TZVP level of theory. The geometry optimization afforded the minimum structure and a comparison of the structural parameters revealed an excellent agreement between the calculated and the experimental bond lengths and angles obtained for **26-Rh** by X-ray crystallography. The QT-AIM bonding paths in **26-Rh** (***Figure 52***) and its calculated Kohn-Sham MOs ruled out the quandary (originating from very short Si–C$^{carb.}$ bond length) of having a 1,3-disilaallene complex of rhodium. In Kohn-Sham MOs, Rh=C is reflected in HOMO–9 (σ), HOMO–4 (π) and LUMO (π*) whereas HOMO is mainly a metal-centered d orbital.

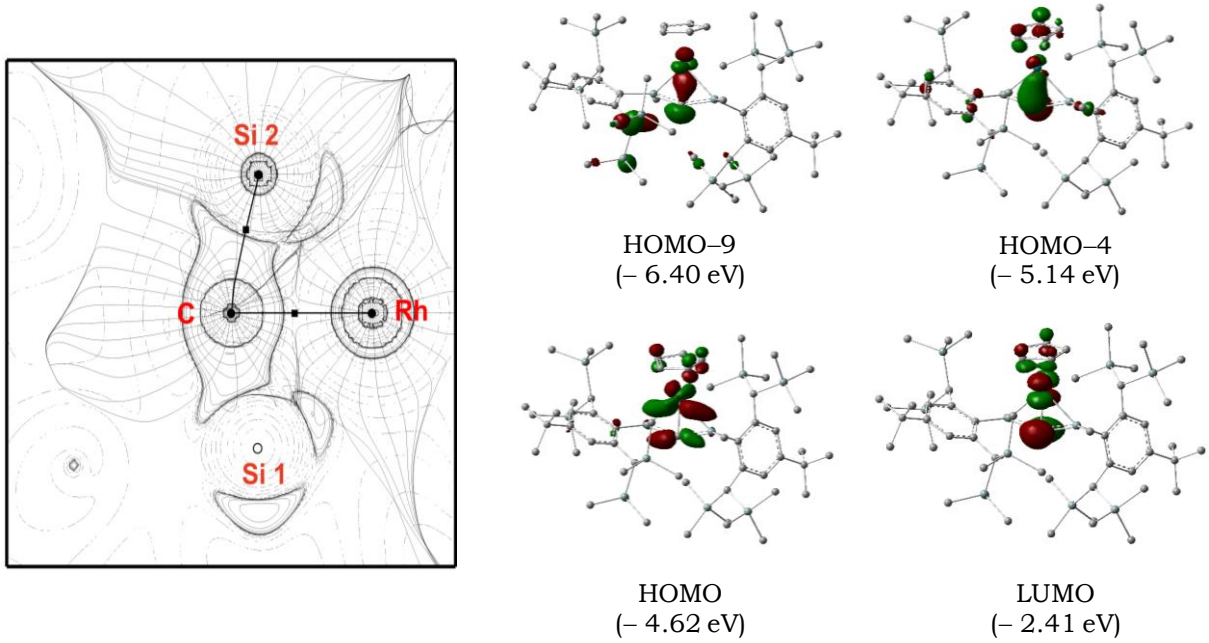

Figure 52. *(left)* Contour plot of the Laplacian of the electron density of **26-Rh** in the Rh–C–Si2 ring plane where the quadrilateral dots represent bond critical points. (*Right*) Selected Kohn-Sham molecular orbitals of **26-Rh**. Hydrogen atoms are omitted for clarity, and the isosurface value was set to 0.04 $e^{1/2}Bohr^{-3/2}$.

Following the exploration of the reactivity of the unsaturated metallacycles **21-Co** and **21-Rh** with small nucleophiles (MesNC) or electrophiles ($AlMe_3$), the reactivity was expanded toward other nucleophiles. It's worth noting that, contrary to transition metal chemistry, in heavier main group chemistry, NHCs (greater in π-acidity than phosphines) are better ligands as compared to phosphines.[193] So distinct a reaction outcome was expected, and shown below.

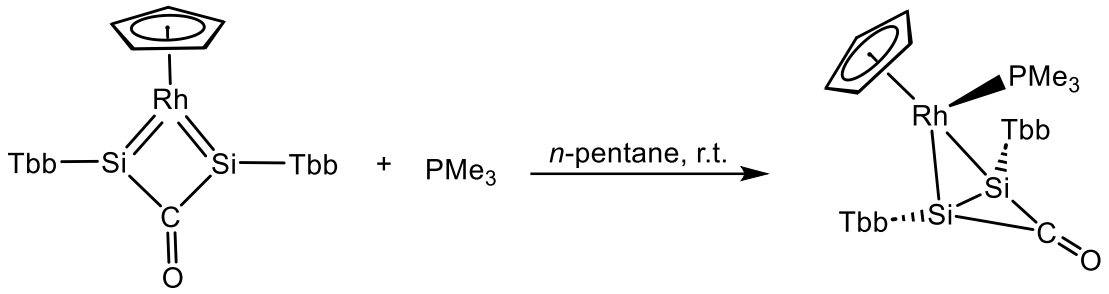

21-Rh **27-Rh**

Scheme 30. Reaction of **21-Rh** with PMe_3 forming the first disilacyclopropenone complex.

Reaction of **21-Rh** with excess of PMe_3 at ambient temperature afforded selectively **27-Rh** (***Scheme 30***), whereas the cobalt analogue (**21-Co**) does not react at all even upon thermal activation.

Infact, an excess of colourless PMe_3 (15 equiv.) was added dropwise to a yellowish-brown *n*-pentane solution of **21-Rh**, the colour immediately turned slightly purple and upon stirring the reaction mixture for 2 hours at ambient temperature, it gradually intensified to dark brownish purple. The ^1H and ^{31}P NMR spectroscopic analyses of the reaction solution confirmed the selective formation of the complex **27-Rh** in addition to little unreacted **21-Rh** (2 mole% with respect to the product). The crude product was worked up by low temperature washings at –30 °C and compound **27-Rh** was isolated as analytically pure solid in 87 % yield. It is an extremely air-sensitive and thermolabile brownish-maroon solid, which is well soluble in *n*-hexane, benzene, toluene, THF and Et_2O at ambient temperature. The melting associated decomposition of **27-Rh** was observed at 185 °C.

At ambient temperature, **27-Rh** dissociates in solution and forms back the starting complex **21-Rh** along with free PMe_3. Monitoring of this process by ^1H NMR spectroscopy in (D_6)benzene revealed a fast conversion at 25 °C (ca. 34 mole % of **21-Rh** after 4.5 h), which surprisingly does not change any further with time, probably indicating the presence of a ligand dissociation equilibrium in solution.

It is noteworthy to mention that compound **27-Rh** is the first example of transition metal-disilacyclopropenone complex to be reported. While in heavier tetrel chemistry,

cyclopropene derivatives[194] are ubiquitous but their transition metal complexes[53] are extremely rare. In contrast to heavier cyclopropenes, the heavier cyclopropenones and their transition metal-complexes have not been realized to date, either experimentally or even in theory. **27-Rh** was characterized by IR and NMR spectroscopy, EA and *sc*-XRD analysis. The molecular structure reveals that the Rh center is bonded to two Si atoms via one short (Rh-Si1 2.3488(4) Å) and one long (Rh-Si2 2.4341(4) Å) bond, which are substantially stretched with respect to the Rh=Si distances found in the molecular structure of its precursor **20-Rh**, but are quite similar to those of **21-Rh**. Importantly, the distance between the bridgehead silicon atoms (Si1-Si2 2.3712(6) Å) is quite similar to the Si–Si single bond lengths (~2.35 Å) in silanes, but ca. 0.25 Å shorter than that of its precursor, and way shorter than that of a Si–Si single π bond reported by Matsumoto *et al.* (2.853(1) Å)[151] and by Iwamoto *et al.* (2.5822(11) Å).[195] Noticeably, the bridgehead Si–Si distance is quite similar to that of tetrasilabicyclo[1.1.0]butane (2.373(3) Å) reported by Masamune *et al.*[148] but considerably shorter than that of a pentasila[1.1.1]propellane (2.636(1) Å) reported by Breher *et al.*.[150]

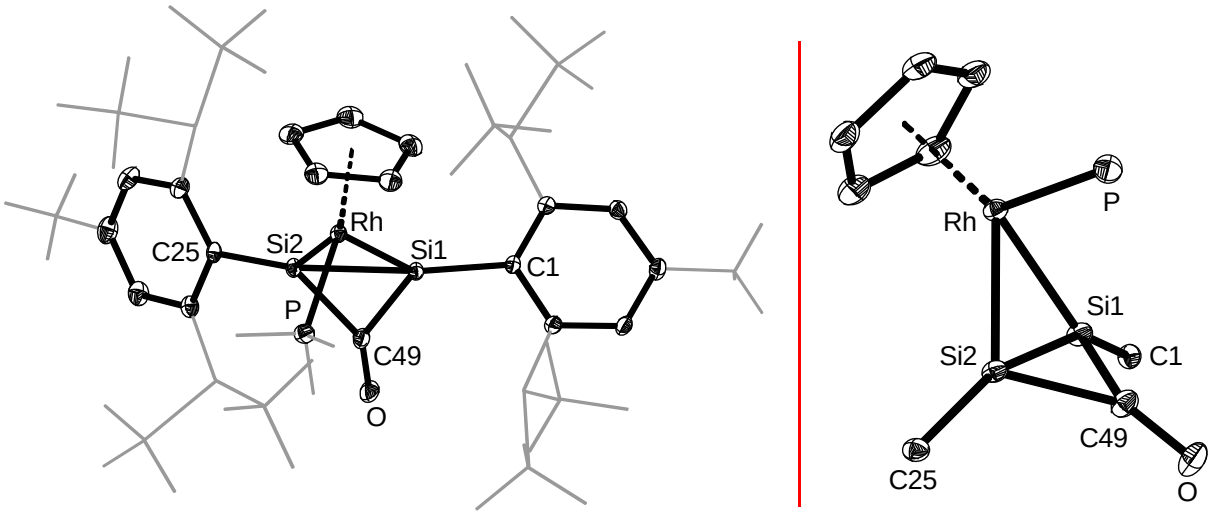

Figure 53. DIAMOND plot of the molecular structure (left) of **27-Rh** and its condensed side view (right). Thermal ellipsoids are set at 30 % probability level. Hydrogen atoms are omitted, the Dsi and ^{t}Bu substituents of the Tbb ligand and methyl groups of PMe_3 are presented in wire-frame for clarity. Selected bond lengths [Å], bond angles [°] and torsion angles [°]: Rh-Si1 2.3488(4), Rh-Si2 2.4341(4), Rh-P 2.2309(5), Si1-Si2 2.3712(6), Si1-C49 1.8481(17), Si2-C49 1.8996(17), C49-O 1.238(2), Rh-Si1-C49 100.70(5), Rh-Si2-C49 96.30(5), C1-Si1-Si2-C25 –3.883(15), Rh-Si2-Si1-C49 133.331(4).

The four membered ring (Rh-Si1-S49-Si2) is puckered as evidenced by the interflap angle (Rh-Si2-Si1-C49) between two triangular rings of 133.331(4)°. This is quite similar to that observed for a disilagermirene-Ni complex (143.83(3)°) reported by Scheschkewitz *et al.*[53] Interestingly, if metal coordination is not considered, the sum

of the bond angles (∑∠Si1 = 328.9° and ∑∠Si2 = 328.0°) in **27-Rh** largely deviate from the expected angle (360°) for being a π-complex according to the Dewar–Chatt–Duncanson,[196] but it is well agreeing to that of the above mentioned disilagermirene-Ni complex (325.70°)[53]. So, upon taking all together the sc-XRD parameters and comparing those to literature, compound **27-Rh** can probably be best described as a disilacyclopropenone-Rh complex, where the disilacyclopropenone unit is bonded to the rohdium center via the sigma component of its Si=Si double bond. The ^{1}H and ^{13}C NMR spectra at ambient temperature clearly suggest a time averaged *C*s symmetric structure with the ^{29}Si{^{1}H} resonance for the bridgehead silicon atoms appearing at δ = 90 ppm (see ***Figure 54***). Notably, the silicon resonance is extremely high-field (ca. 190 ppm) shifted compared with that of its precursor **21-Rh**, but down-field (ca. 50 ppm) shifted as compared to the bis(silyl)complex **20-Rh** and the above mentioned Disilagermirene-Ni complex (34.1 ppm).[53] Interestingly, the silicon resonance is unusually down-field shifted as compared to that of a 1,3-disilabicyclo[1.1.0]butane (–104.2 ppm) reported by Kira *et al.*[197]

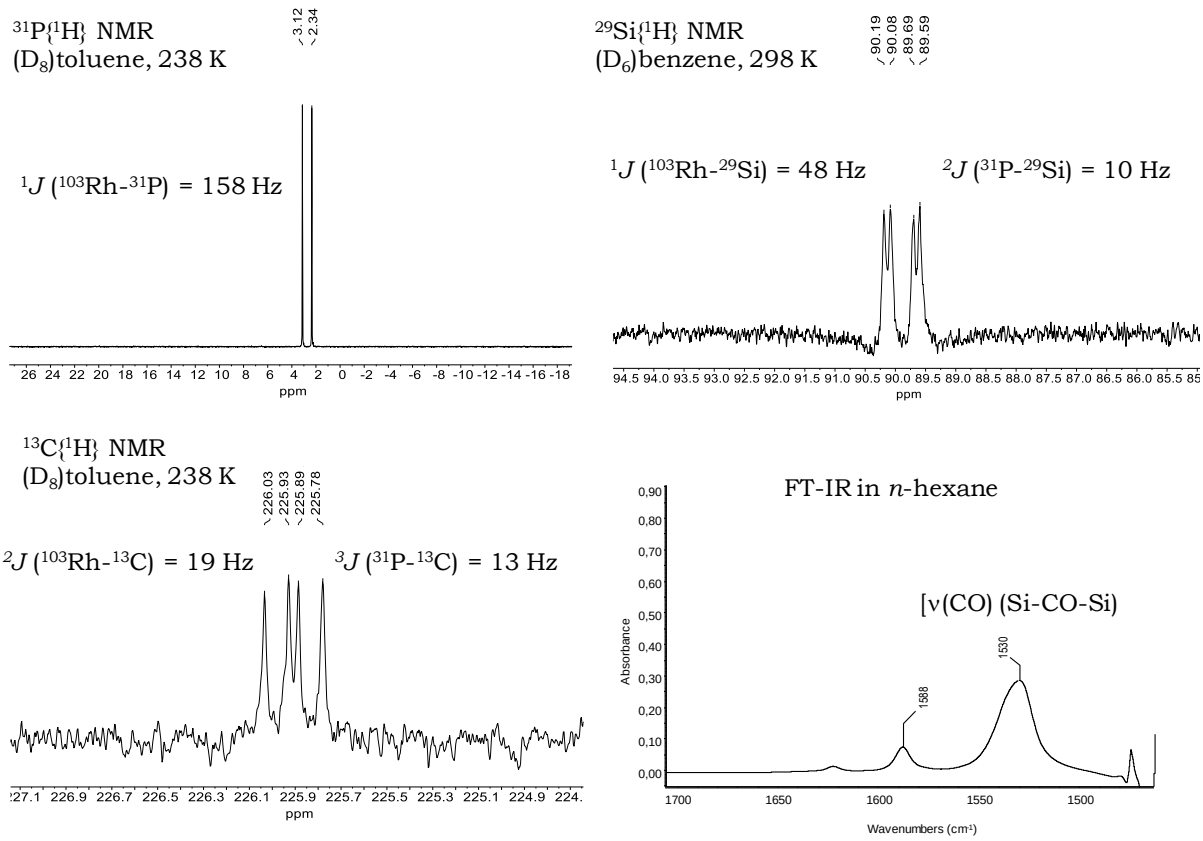

Figure 54. Selected spectroscopic properties of **27-Rh**.

The ^{13}C{^{1}H} resonance for the bridging *C*O appeared at δ = 226 ppm, which is quite similar to those of **20-Rh** (228 and 241 ppm) but quite high-field shifted as compared to its precursor **21-Rh** (302.4 ppm). In the ^{31}P{^{1}H} NMR spectrum the PMe_3 ligand

appears as a clear doublet at δ = 1.82 ppm with a ^{103}Rh-^{31}P coupling of 158 Hz, which is in a typical range of rhodium-PMe_3 complexes.[198,199] In the IR spectra, the CO stretching vibration (1530 cm^{-1}) appears at a lower wavenumber as compared to **20-Rh** (1665 and 1620 cm^{-1}) and **21-Rh** (1615 cm^{-1}).

Unlike PMe_3, the introduction of a small NHC (IMe_4) to **21-Rh** resulted in a coordination to one of the metal-bound silicon centers, yielding **28-Rh** (***Scheme 31***). So, when an off-white Et_2O suspension of IMe_4 was added to a brown solution of **21-Rh** at ambient temperature, the reaction proceeded immediately with a colour change to give a clear purple solution. ^1H NMR spectroscopic analysis of the solution suggested a selective conversion of the starting materials into **28-Rh**. After work up and crystallization of the crude product from *n*-hexane, complex **28-Rh•1.4 C_6H_{14}** was isolated as a black-brown solid in 57 % yield.

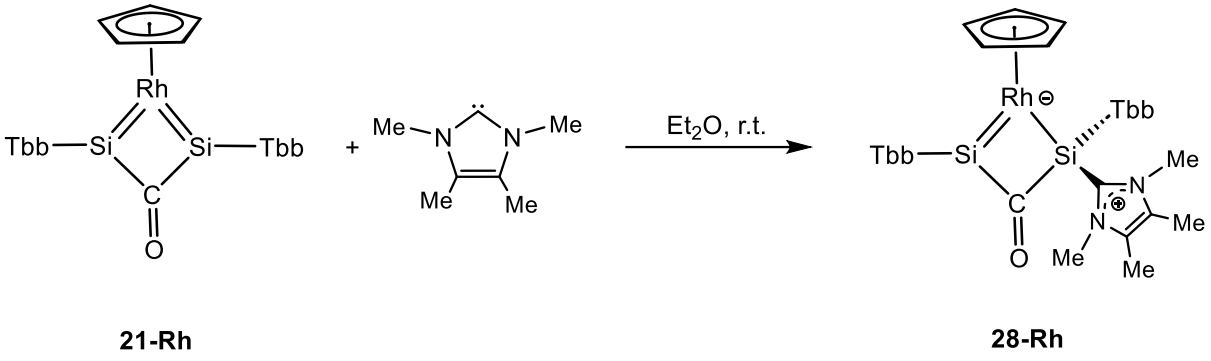

21-Rh **28-Rh**

Scheme 31. Reaction of **21-Rh** with a small NHC.

All attempts to obtain the solvate-free form of **28-Rh•1.4 C_6H_{14}** in fine vacuum failed leading only to partial loss of *n*-hexane and extensive decomposition into some unknown Cp containing products. **28-Rh** is good soluble in THF, Et_2O, aromatic and aliphatic solvents at ambient temperature. Suitable plate shaped (brown) single crystals of **28-Rh•2 Et_2O** were grown by slow evaporation of a saturated Et_2O solution at –30 °C inside the glovebox.

In the solid-state (***Figure 55***), **28-Rh** features one trigonal planar coordinated silicon ($\sum\angle 360°$) bonded to the rhodium center via a short bond (Rh-Si2 2.1944(8) Å), which compares well with the Rh=Si double bond of its precursor **21-Rh** and one distorted tetrahedral coordinated silicon bonded to rhodium via a comparatively longer bond (Rh-Si1 2.3385(7) Å), which is quite similar to the Rh–Si single bonds of **27-Rh**. The Si–C^{NHC} bond length (Si1-C33 1.972(3) Å) is similar to those reported for Si–C single bonds (metal bound tetracoordinated silicon atom containing a small NHC).[200–202] Interestingly, unlike the PMe_3 case, upon coordination of NHC to the silicon center, the trans-annular Si···Si distance (Si1-Si2 2.7522(10) Å) is elongated by ca. 0.13 Å

compared to its precursor **21-Rh**. The quadrilateral ring (Rh-Si-C26-Si2) is almost flat as evidenced by the interflap angle (Rh-Si1-Si2-C26) of 171.441(3)°.

The solution behavior of **28-Rh** was studied by multinuclear NMR spectroscopy and the molecule shows dynamic behavior at ambient temperature, which unfortunately could not be frozen out even at 193 K. Although the expected number of signals were visible in the ^{1}H NMR spectrum of **28-Rh** at 193 K, all the corresponding carbon signals in the $^{13}C\{^{1}H\}$ NMR spectrum were not observed and an unequivocal assignment of all the signals was not possible.

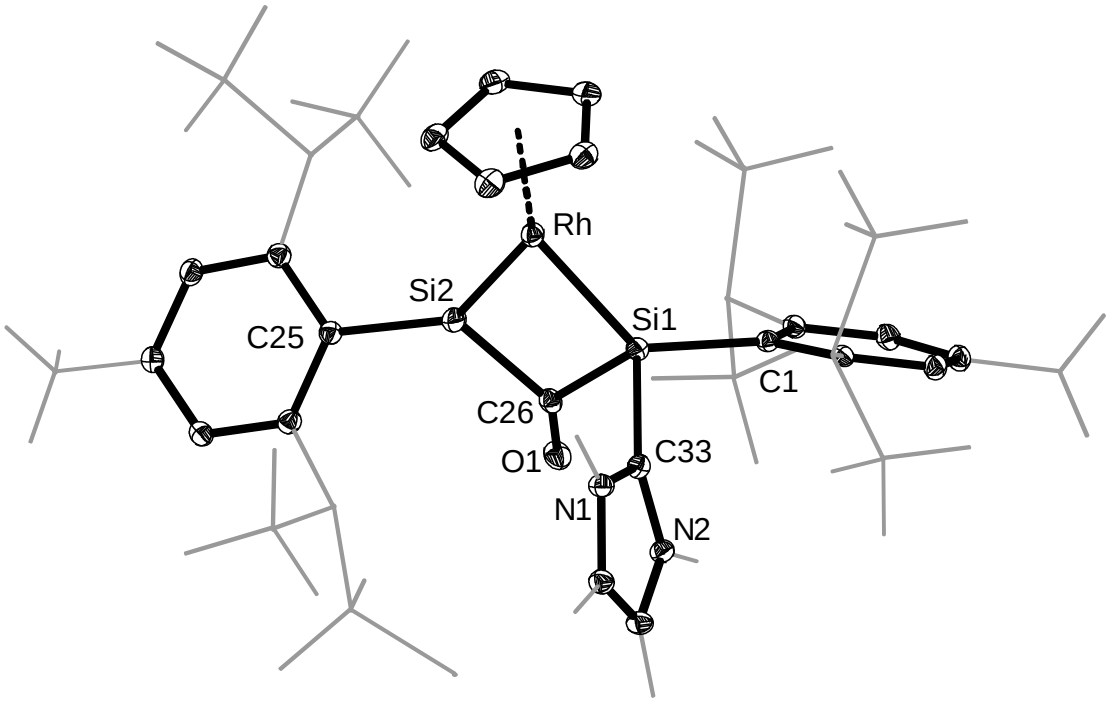

Figure 55. DIAMOND plot of the molecular structure of **28-Rh**. Thermal ellipsoids are set at 30 % probability level. Hydrogen atoms are omitted, the Dsi and ^{t}Bu substituents of the Tbb ligand and methyl groups of IMe$_4$ are presented in wire-frame for clarity. Selected bond lengths [Å], bond angles [°] and torsion angle [°]: Rh-Si1 2.3385(7), Rh-Si2 2.1944(8), Si1-Si2 2.7522(10), Si1-C33 1.972(3), Rh-Si2-C25 139.53(9), C25-Si2-C26 119.13(12), Rh-Si2-C26 101.34(9), Rh-Si1-C1 131.09(9), Rh-Si1-C33 116.16(8), C1-Si1-C33 100.11(11), Rh-Si1-Si2-C26 171.441(3).

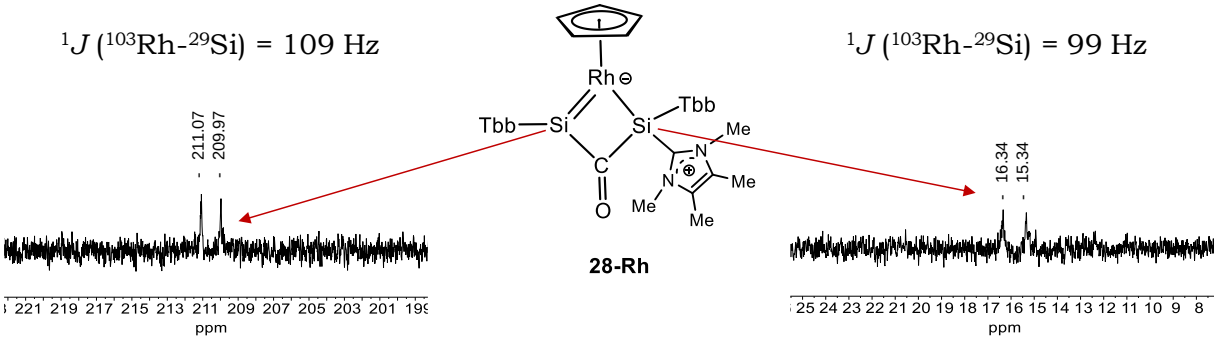

Figure 56. Selected excerpts of the $^{29}Si\{^{1}H\}$ NMR spectrum measured on 99.3 MHz, in (D$_6$)benzene at 298 K.

In the $^{29}Si\{^{1}H\}$ NMR spectrum, the tricoordinated Si atom shows a characteristic broad doublet at δ = 210.5 ppm which is 70 ppm high-field shifted with respect to its precursor **21-Rh** but quite similar to it in terms of coupling constant and the NHC-coordinated Si center appears also as a broad doublet at δ = 15.8 ppm which is ca. 25 ppm high-field shifted than the tetracoordinated Si atoms observed in case of **20-Rh**. So, taken together the NMR spectroscopic data and the structural parameters of **28-Rh**, probably suggesting a new type of metalladisila-cyclobutadienone complex, which is best described by the zwitterionic structure as depicted in ***Scheme 31***.

2.8. Ge≡Ge triple bond cleavage at a single metal center

As quoted earlier, the lower HOMO-LUMO gaps of digermynes (~2 eV) compared to alkynes (~9 – 11 eV) and the Ge-centered ambiphilicity of Ge_2R_2 would lead to novel coordination modes and the very different synergistic donor-acceptor interaction with the transition metals could lead to unique reactivity. The entry into this field was made with a synthetic strategy that requires electronically unsaturated, highly electrophilic metal complexes that contain labile ligands. The 16 VE and 14 VE complexes of late 3d-metals have these features and hence phosphine complexes of Co(I), Ni(II) and Fe(II) were chosen for this study. The ditetrelyne, Ge_2Tbb_2 was selected as the candidate to explore the metal-centered E≡E triple bond activation chemistry and the very first reaction of Ge_2Tbb_2 was tested with $Co(PMe_3)_3Cl$ (***Scheme 32***).

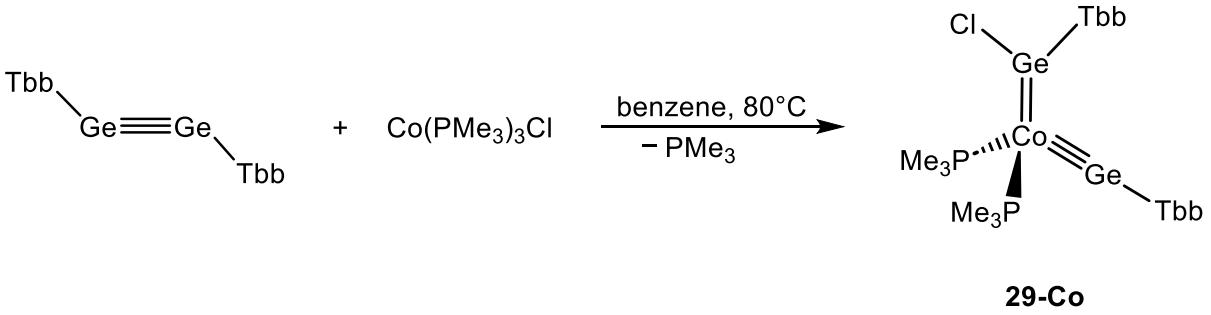

Scheme 32. Synthesis of the first germylidene-germylidyne complex of cobalt.

A dark-blue solution of $[Co(PMe_3)_3Cl]$ in benzene was added to a reddish orange benzene solution of Ge_2Tbb_2 at ambient temperature. The reaction proceeded instantaneously as the colour of the reaction solution immediately turned to dark-brown. A ^1H NMR spectrum of an aliquot of the reaction solution in (D_6)benzene revealed the formation of a mixture of **29-Co**, $[(PMe_3)_3Co{\equiv}GeTbb]$[vii] and a third component[viii] in the approximate ratio of 1 : 2 : 2, which upon further heating at 80 °C for 12 h under periodic vacuum turned barn-red and all intermediates were

[vii] This compound was synthesized and completely characterized internally in our group by T. Deckstein.

[viii] The component is $GeCl(Tbb)(PMe_3)$, which was confirmed upon comparison of the ^1H and $^{31}P\{^1H\}$ NMR data with those of a pure, yellow sample isolated in our group. ^1H and ^{31}P NMR spectroscopic data of $GeCl(Tbb)(PMe_3)$: **^{1}H NMR** (500.1 MHz, (D_6)benzene, 298 K): δ (ppm) = 0.26 (s, 36H, $C^{2,6}$-CH(Si*Me*$_3$)$_2$, Tbb), 1.04 (brs, $\Delta\nu_{1/2}$ = ca. 28 Hz, 9H, P*Me*$_3$), 1.35 (s, 9H, C^4-C*Me*$_3$, Tbb), 2.94 (s, 2H, $C^{2,6}$-C*H*$(SiMe_3)_2$, Tbb), 6.89 (s, 2H, $C^{3,5}$-*H*, Tbb). **^{31}P{^{1}H} NMR** (202.5 MHz, (D_6)benzene, 298 K): δ (ppm) = –30.6 (brs, $\Delta\nu_{1/2}$ = ca. 460 Hz, *P*Me_3).

selectively converted to **29-Co**. After work-up **29-Co** was isolated as a dark red solid in 76 % yield. This reaction suggests that **29-Co** is formed *via* PMe_3 substitution reaction of the germylidyne complex $[(PMe_3)_3Co{\equiv}GeTbb]$. Indeed, **29-Co** was prepared in moderate yield by reacting $[Ge(Tbb)Cl]_2$ with two equivalents of $[(PMe_3)_3Co{\equiv}GeTbb]$ at 80 °C in benzene. Compound **29-Co** is a highly air-sensitive but thermally robust ($T_{melt.}$ = 177 °C), barn-red solid, which is extremely soluble in *n*-hexane, benzene, toluene and diethyl ether, but insoluble in CH_3CN at ambient temperature. A (D_6)benzene NMR sample solution of **29-Co** does not show any sign of decomposition after 3 days at ambient temperature. More interestingly, the germylidyne-germylidene complex **29-Co** could be converted to the bisgermylidene-germylidyne complex **30-Co** upon halide abstraction with $NaB(Ar^F)_4$ (Ar^F = C_6H_3–3,5–$(CF_3)_2$) in fluorobenzene at ambient temperature (***Scheme 33***).

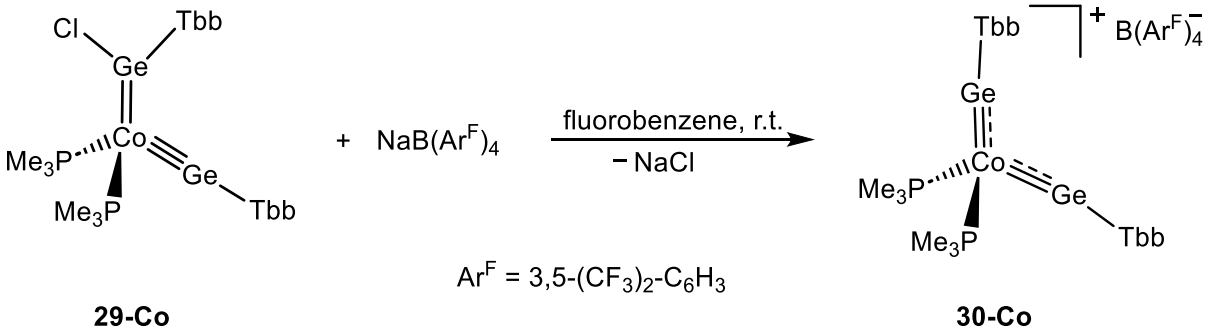

Scheme 33. Synthesis of a cobalt-bisgermylidyne complex upon halide abstraction of **29-Co**.

Infact, when a colourless fluorobenzene solution of $Na[B(Ar^F)_4]$ was added to a barn-red solution of **29-Co** in fluorobenzene at ambient temperature the colour of the reaction mixture turned immediately orange-brown. Spectroscopic analysis revealed the quantitative conversion of **29-Co** to **30-Co**. After work-up **29-Co** was isolated as an analytically pure solid in 85 % yield. It is an air-sensitive wood-brown solid which is well soluble in chlorobenzene, fluorobenzene, dichloromethane and diethyl ether, but almost insoluble in aliphatic solvents at ambient temperature. Remarkably, in contrast to its precursor **29-Co**, the salt **30-Co** decomposes upon melting at lower temperature ($T_{dec.}$ = 122 °C) and shows partial decomposition in solutions of Et_2O, THF and CH_2Cl_2 at ambient temperature.

The solid-state structure of **29-Co•Et_2O** was determined by sc-XRD analysis of clear dark violet crystals, which were grown by slow diffusion of CH_3CN into a saturated Et_2O/CH_3CN solution at ambient temperature inside the glove-box. The molecular structure of **29-Co** (***Figure 57*** *left*) is roughly C_s symmetric with the symmetry plane passing through the planar core composed of the atoms Co, Ge1, Ge2, Cl, C1, and C25 and bisecting the angle ∠(P1−Co−P2). It features a distorted tetrahedral geometry

at the cobalt center (four-coordinate geometry index, τ_4 = 0.82)[203] with the largest angle ∠(Ge1−Co−Ge2) at Co of 126.69(1)° allowing *syn*-coplanar arrangement (C1-Ge-Ge-C25 = 23.01(1)°) of the two bulky Tbb ligands. Most importantly, the distance between the two Ge atoms (3.8399(1) Å) is 1.6 times longer than twice the covalent radius of Ge ($\sum r_1$(Ge,Ge)/Å = 2.44) and comparable to the *transannular* Ge···Ge distance (3.8089(6) Å, WBI = 0.212) in Ge_4(EMind)$_4$ (EMind = 1,1,7,7-tetraethyl-3,3,5,5-tetramethyl-s-hydrindacene-4-yl).[204]

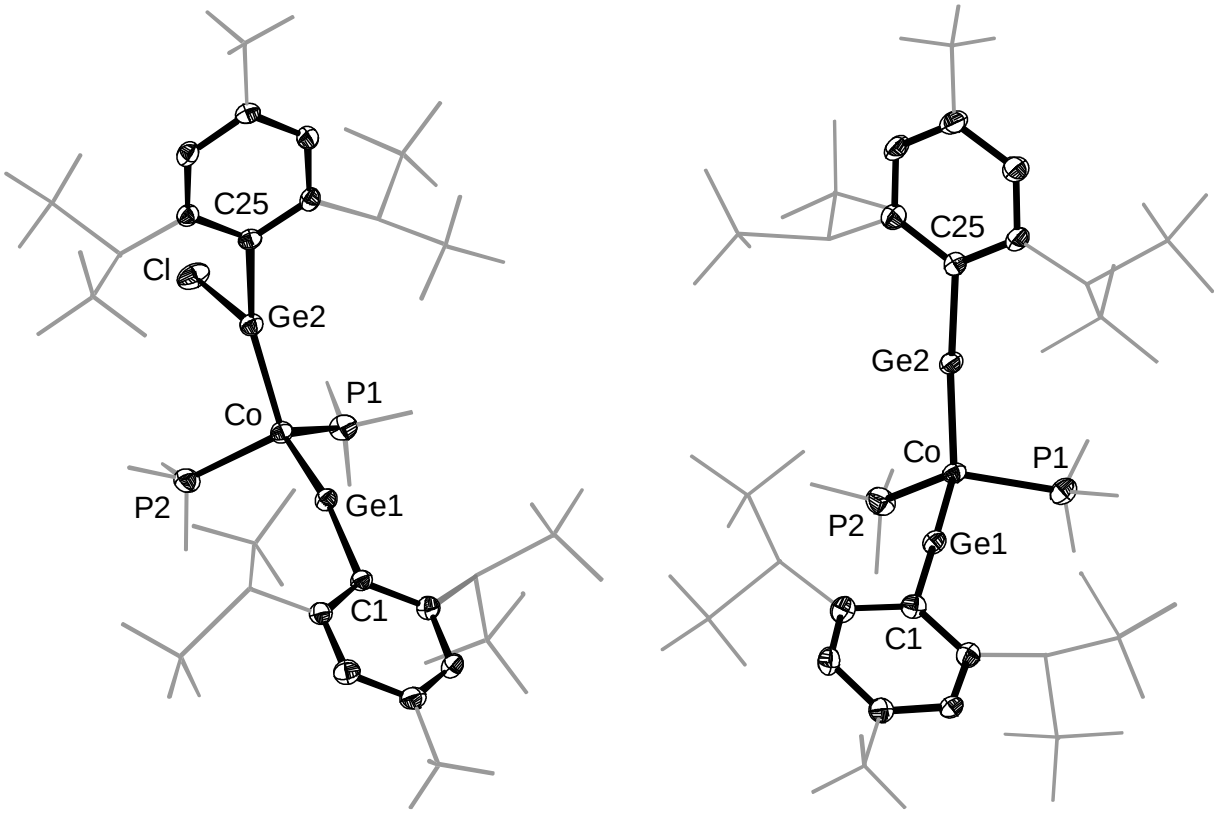

Figure 57. (*left*) DIAMOND plot of the molecular structure of **29-Co** and the cation in **30-Co** (*right*). Thermal ellipsoids are set at 30 % probability level. Hydrogen atoms are omitted, the Dsi and ^{t}Bu substituents of the Tbb ligand and methyl groups of PMe_3 are presented in wire-frame for clarity. Selected bond lengths [Å], bond angles [°] and torsion angle [°]: **29-Co**: Co-Ge1 2.1078(3), Co-Ge2 2.1886(3), Co-P1 2.1658(6), Co-P2 2.1601(6), Ge2-Cl 2.2841(5), Co-Ge1-C1 164.65(6), Co-Ge2-C25 151.08(5), P1-Co-P2 103.20(2), Ge1-Co-Ge2 126.690(14), Ge1-Co-Ge2-Cl –173.582(3); **30-Co**: Co-Ge1 2.1005(6), Co-Ge2 2.0988(5), Co-P1 2.1837(10), Co-P2 2.1976(10), Co-Ge1-C1 179.12(11), Co-Ge2-C25 173.42(10), P1-Co-P2 102.85(4), Ge1-Co-Ge2 110.71(2).

The salient structural features of **29-Co** are i) an almost linear coordinated Ge1 atom in the germylidyne ligand, (∠(Co−Ge−C1)/° = 164.7(1), ii) a very short Co−Ge1 distance of 2.108(1) Å that compares well to the Co≡Ge triple bond length of neutral cobalt-germylidyne complex [$(PMe_3)_3$Co≡Ge–Tbb] (2.102(1) Å)[vii] but is considerably shorter than that of the cationic cobalt-germylidyne complex [(η^5-C_5H_5)(IDipp)CoGe(N(Mes*)$SiMe_3$)][A] featuring a triplet ground state (2.2948(6) Å),[58]

iii) a distorted T-shaped geometry at the trigonal planar coordinated Ge2 atom (∑(Ge2)/° = 360.0) of the germylidene ligand with a very large ∠(Co−Ge2−C25) angle (151.1(1)° and a rather acute angle ∠(C^{Tbb}−Ge−Cl) of 94.66(6)° suggesting that Ge2 atom uses a hybrid orbital of high s-character to form the σ-bond with Co, iv) a short Co−Ge2 distance (2.189(1) Å), which is shorter than the Pyykkös sum of single bond covalent radii of Co and Ge (∑r_1(Co,Ge)/Å = 2.32) and marginally longer than the sum of double bond covalent radii (∑r_2(Co,Ge)/Å = 2.14) indicating Co−Ge2 double bond character.

The molecular structure of the bis-ylidyne complex **30-Co•C_5H_{12}** was also determined by *sc*-XRD analysis of its dark pink crystals, which were grown by slow diffusion of *n*-pentane into a saturated fluorobenzene solution at ambient temperature. The solid-state structure is composed of well separated bis-ylidyne complex cations and borate anions. The complex cation in **30-Co** (***Figure 57*** *right*) is nearly C_{2V} symmetric and features a tetrahedral geometry at the cobalt center (τ_4 = 0.94), that is connected to two almost linearly coordinated Ge atoms via very short Co−Ge bonds (*d*(Co−Ge) = 2.1005(6) and 2.0988(5) Å). Notably, the $(Co-Ge)_{avg.}$ distance is crystallographically identical to that of the neutral Co-germyldiyne complex $[(PMe_3)_3Co{\equiv}Ge–Tbb]$[vii] (see ***Table 4***) and Co−Ge1 distance of its precursor **29-Co**, but ca. 0.09 Å shorter than the Co–Ge2 distance of **29-Co**, indicating the participation of both the p-orbitals of the Ge atoms of the bis-ylidyne complex cation in competing π-bonding with the Co center. The presence of rather strong σ- and π- bonding between the two Ge atoms and Co center is also evident from the very long distance between the two Ge atoms (3.4548(1) Å, which, although remarkably shorter than that of its precursor (3.8399(1) Å (**29-Co**) and lies in the range of transannular distances in $Ge_4(EMind)_4$ (3.8089(6) Å),[204] and excludes (according to the results of the quantum chemical calculations) any Ge····Ge interaction.

Table 4. Selected NMR spectroscopic and structural data of the complexes featuring Co≡Ge bonds

Comps.	δ_{PMe3}/PPM	$d_{(Co–Ge)}$/(Å)	∡Co-Ge-Tbb/(°)	τ_4
$[(PMe_3)_3CoGeTbb]$[vii]	13.2 $\Delta\nu_{1/2}$ = 215 Hz	2.102(1)	174.6(2)	0.93
$[(PMe_3)_2Co(GeClTbb)(GeTbb)]$ (**29-Co**)	6.8 $\Delta\nu_{1/2}$ = 408 Hz	2.108(1) & 2.189(1)	164.7(1) 151.1(1)	0.82
$[(PMe_3)_3Co(GeTbb)_2][B(Ar^F)_4]$ (**30-Co**)	5.6 $\Delta\nu_{1/2}$ = 106 Hz	2.101(1) & 2.099(1)	179.1(1) 173.4(1)	0.94

Multi-nuclear NMR spectroscopy revealed a fluxional behavior of **29-Co** in solution. Infact, the ^{1}H and $^{13}C\{^{1}H\}$ NMR spectra of **29-Co** display only one set of signals for the two Tbb groups, indicating a rapid chloride exchange between the Ge centers. Also, fast rotations of the Co=Ge and Ge–C^{Tbb} bonds lead to a time averaged C_{2v} symmetry which render the Tbb substituents and $SiMe_3$ groups homotopic, even at –80 °C. As expected, **30-Co** displays in solution only one set of signals for the two Tbb groups of the bis-ylidyne ligands. The NMR data suggest a rapid rotation of the Tbb around Ge–C^{Tbb} bond leading to a time avaraged C_{2V} symmetry of the complex cation.

The presence of highly electrophilic Ge centers and the electron-deficient Co center in the bis-germylidyne complex **30-Co** (with respect to a mono-germylidyne complex) suggested its potential involvement in reversible electrochemical processes. In fact, the cyclic voltammogram of **30-Co** in fluorobenzene at ambient temperature (see ***Figure 113*** to ***Figure 116***) displays a reversible one-electron reduction at $E_{1/2}$ = −1.215 V vs. $DMFc^{+/0}$ and a reversible one-electron oxidation at $E_{1/2}$ = +1.316 V vs. $DMFc^{+/0}$. Notably, the oxidation potential is significantly higher than that of the neutral Co-germylidyne [$(PMe_3)_3Co{\equiv}GeTbb$] ($E_{1/2}$ = −0.426 V vs. $DMFc^{+/0}$), indicating a more electron-deficient Co center in **30-Co** compared to the neutral Co-germylidyne complex [$(PMe_3)_3Co{\equiv}GeTbb$].

As next, the reaction of Ge_2Tbb_2 was carried out with a 16VE Ni-complex ($Ni(PMe_3)_2Cl_2$) (a part of this work is included in the bachelor thesis Leon Gomm).[vi] In fact, when a red suspension of $(PMe_3)_2NiCl_2$ in *n*-hexane was added to a stirred orange-red solution of Ge_2Tbb_2 at ambient temperature, the colour of the reaction solution immediately turned purple. Spectroscopic analysis revealed a complete consumption of the starting materials and very selective formation of **31-Ni**, which was isolated after work-up as analytically pure dark-violet solid in 70 % yield.

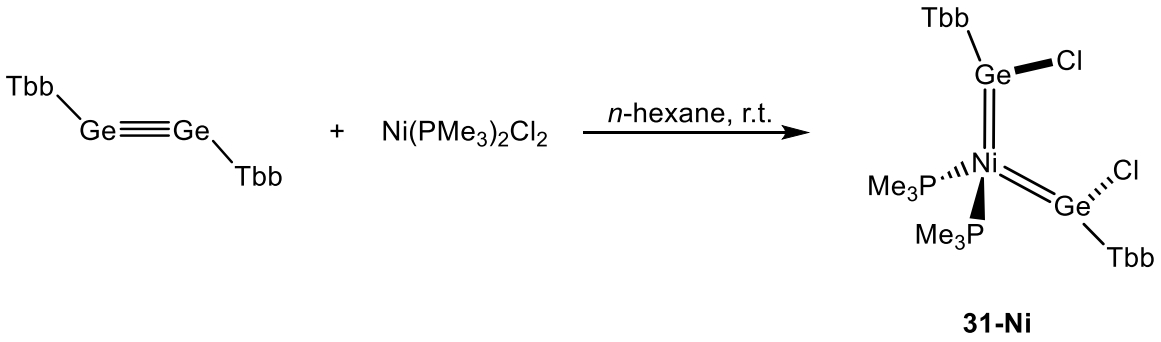

31-Ni

Scheme 34. Cleavage of a digermyne by using a Ni(II)-precursor.

Dark-purple single crystals of **31-Ni** were obtained upon slow crystallization of a saturated *n*-hexane solution at –30 °C and analyzed by sc-XRD. The structural motif

(see ***Figure 93***) in solid state as well as in solution are well described in the above-mentioned bachelor thesis. The structure displays a tetrahedrally coordinated Ni-center, bonded to two trigonal-planar coordinated germanium centers (∑∠Ge = 359.9°) via short bonds (2.2120(7) Å), which compares well to the Ge=Ni double bond of the nickel germylidene complex [$(PMe_3)_3$Ni=Ge(Ar^{Mes})Cl], reported by Filippou *et al.*[67,68]

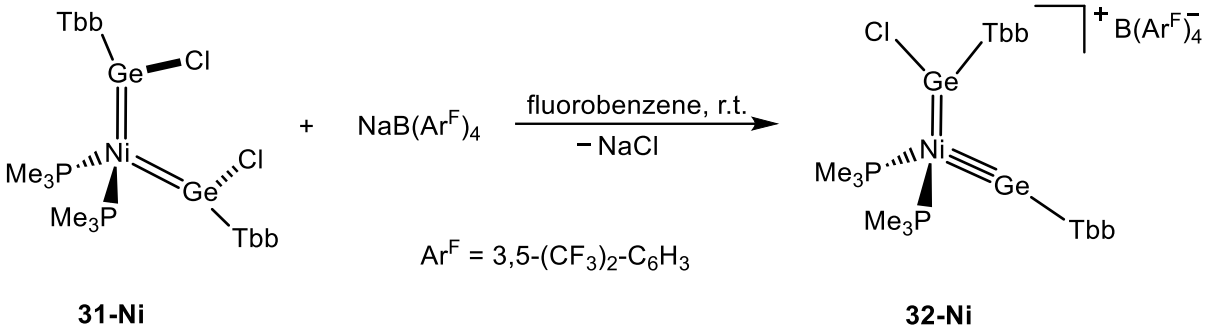

Scheme 35. Synthesis of a cationic germylidene-germylidyne complex of Ni.

More importantly, reacting the Ni-bisgermylidene complex **31-Ni** with a halide scavenger, one chloride can be abstracted forming a cationic Ni-germylidene-germylidyne complex **32-Ni**. In fact, treatment of **31-Ni** with Na[$B(Ar^F)_4$] at ambient temperature proceeded immediately with a colour change from violet to red-brown. Spectroscopic analysis of the reaction solution revealed the quantitative conversion of **31-Ni** to **32-Ni**. Upon working-up the crude reaction mixture, **32-Ni** was isolated as an air-sensitive, thermally stable ($T_{dec.}$ = 156 °C), red-brown solid in 64 % yield. It is well soluble in fluorobenzene, dichloromethane and diethyl ether, but mostly insoluble in aliphats at ambient temperature. Surprisingly, under strict exclusion of air a solution of **32-Ni** in (D_2)dichloromethane does not show any sign of decomposition after at least 24 hours at ambient temperature.

32-Ni is the first nickel ylidene-ylidyne complex to be reported, hence it was comprehensively characterized by elemental analysis and multinuclear NMR spectroscopy. Furthermore, suitable single crystals (clear dark red plates) of **32-Ni** were grown upon slow evaporation of a saturated *n*-hexane/Et_2O solution at ambient temperature, and the molecular structure was determined by single-crystal X-ray diffraction. The solid state structure of the cation in **32-Ni** (***Figure 58***) displays a distorted tetrahedral geometry (τ_4 = 0.88) around the nickel atom, which is bonded to a linearly coordinated Ge1 center (∠Ge = 162.5(2)) and a planar tri-coordinated Ge2 center (∑∠Ge = 360) via short bonds. The Ni–Ge1 bond length (2.1266(12) Å) is almost identical to the Ni≡Ge triple bond of the Ni-germylidyne complex cation ([$(PMe_3)_3$NiGeAr^{Mes}]$^+$, 2.1041(6) Å), reported by Filippou *et al.*,[67,68] whereas the Ni-

Ge2 distance (2.2443(12) Å) is very similar to that of its precursor, but marginally longer (ca. 0.08 Å) than those of Ni-germylidene complexes, reported in literature.[68] The dihedral angle Ge1-Ni-Ge2-Cl –171.406(2)° and the distance between the two Ge atoms (3.9011(1) Å) are very similar to those observed for **29-Co**.

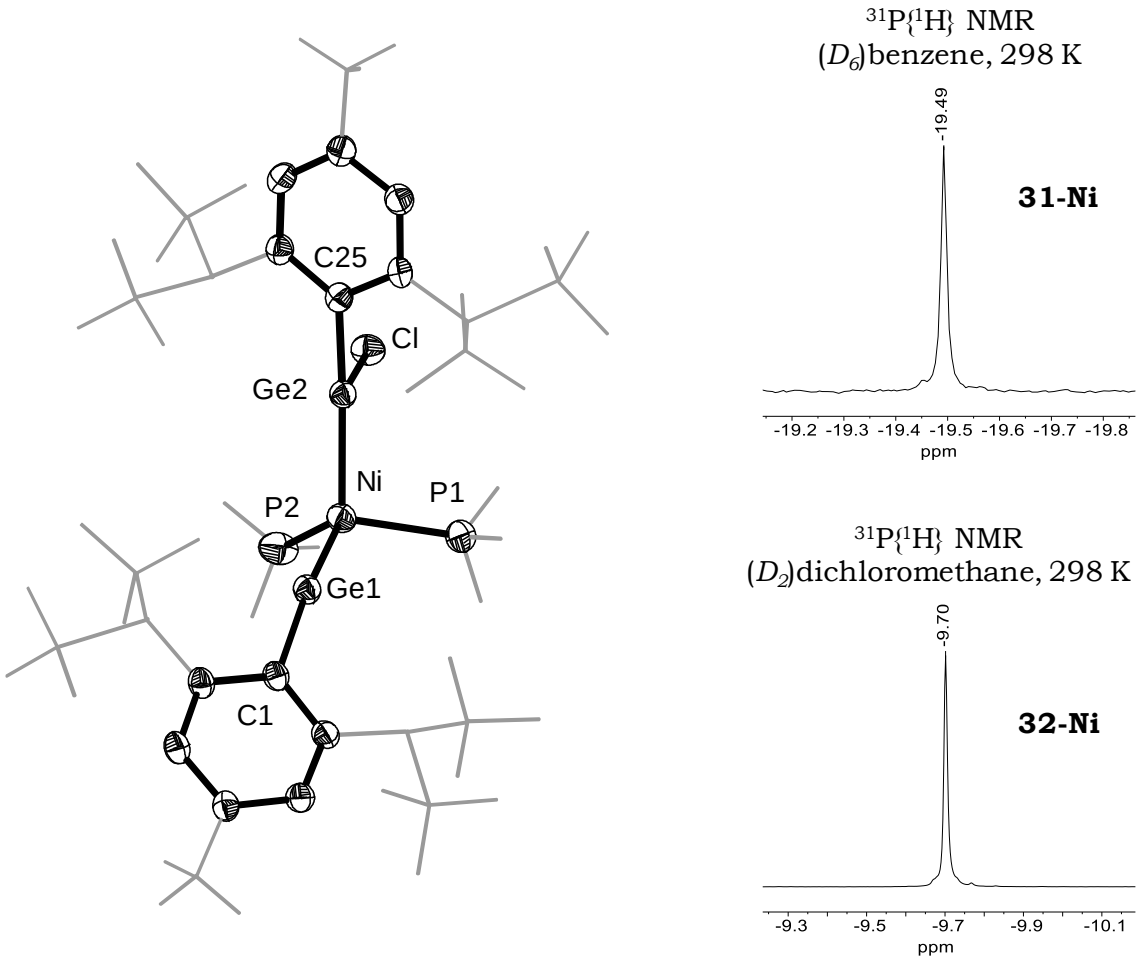

Figure 58. (*left*) DIAMOND plot of the molecular structure of **32-Ni**. Thermal ellipsoids are set at 30 % probability level. Hydrogen atoms are omitted, the Dsi and ^{t}Bu substituents of the Tbb ligand and methyl groups of PMe_3 are presented in wire-frame for clarity. Selected bond lengths [Å], bond angles [°] and torsion angle [°]: Ni-Ge1 2.1266(12), Ni-Ge2 2.2443(12), Ni-P1 2.195(2), Ni-P2 2.187(2), Ge2-Cl 2.2196(17), Ni-Ge1-C1 162.47(17), Ni-Ge2-C25 153.05(17), P1-Ni-P2 110.20(10), Ge1-Ni-Ge2 126.35(5), Ge1-Ni-Ge2-Cl –171.406(2). (*right*) Excerpts of the $^{31}P\{^{1}H\}$ NMR spectra of **31-Ni** and **32-Ni**.

In solution, compound **32-Ni** displays a similar fluxional behavior as **29-Co**. Hence in the ^{1}H and $^{13}C\{^{1}H\}$ NMR spectra of **32-Ni** only one set of signals for the two aryl groups was observed, indicating a rapid chloride exchange between the Ge centers. This leads in combination with rapid rotations of the Tbb groups about the Ge–C^{Tbb} bonds two Tbb substituents as well as the $SiMe_3$ groups of each Dsi substituent homotopic, even at –80 °C. In the $^{31}P\{^{1}H\}$ NMR spectrum of **32-Ni**, the PMe_3 resonance (–9.7 ppm) is appearing low-filed shifted in comparison to that of its precursor **31-Ni** (–19.5 ppm).

Furthermore, the scope of this chemistry was expanded to include iron. According to literature, there are limited reports on the functionality of Fe-tetrel (tetrel = Si-Pb) triple bonds[205] and moreover the experimental realization of Fe-bisylidyne complexes has not been achieved. In this context, the reaction of Ge_2Tbb_2 with $Fe(PMe_3)_2Cl_2$ was studied.

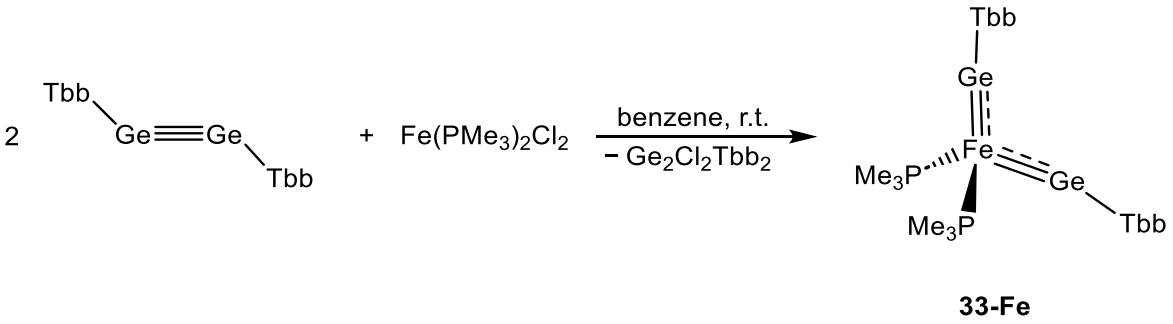

Scheme 36. Cleavage of a digermyne by a Fe(II) precursor.

Addition of benzene to a mixture of the solids Ge_2Tbb_2 and $(PMe_3)_2FeCl_2$ at ambient temperature led instantaneously to a dark-brown suspension. NMR spectroscopic (^1H & ^{31}P) analysis of the reaction solution revealed a complete consumption of Ge_2Tbb_2 and the selective formation of **33-Fe** and $Ge_2Cl_2Tbb_2$ in almost a 1 : 1 molar ratio. After (CH_3CN/Et_2O) work-up, **33-Fe** was obtained as analytically pure solid in 69 % yield. It is a highly air-sensitive, but thermally robust ($T_{dec.}$ = 222 °C) black solid, which is well soluble in *n*-hexane, benzene, toluene and diethyl ether, but insoluble in acetonitrile at ambient temperature.

Compound **33-Fe** is the first bis-germylidyne complex of iron to be reported and it was comprehensively characterized by EA, NMR spectroscopy, CV and sc-XRD analysis. Suitable plate shaped single crystals of **33-Fe•Tol** were grown upon slow diffusion of CH_3CN into a saturated Tol/CH_3CN solution of **33-Fe** at ambient temperature. In solid state molecular structure (***Figure 59***), **33-Fe** features a slightly distorted tetrahedral coordination (τ_4 = 0.92) at the metal center, which is connected to two linearly coordinated (∠Ge1 = 174.9(1)° and ∠Ge2 = 175.0(1)°) Ge centers via short bonds. The Fe–Ge (2.1137(7) and 2.1153(8) Å) bond lengths of **33-Fe** are identical to the Fe≡Ge triple bond found in a cationic iron-germylidyne (2.1198(4) Å) complex $[(depe)_2Fe{\equiv}Ge(2,6\text{-}Mes_2\text{-}C_6H_3)][GeCl_2(2,6\text{-}Mes_2\text{-}C_6H_3)]$.[205]

As expected, **33-Fe** displays in solution only one set of signals for the two Tbb groups of the bis-ylidyne ligands. The ^1H and $^{13}C\{^1H\}$ NMR data further suggest a rapid rotation of the Tbb around Ge–C^{Tbb} bond leading to a time avaraged C_{2V} symmetry of the complex cation.

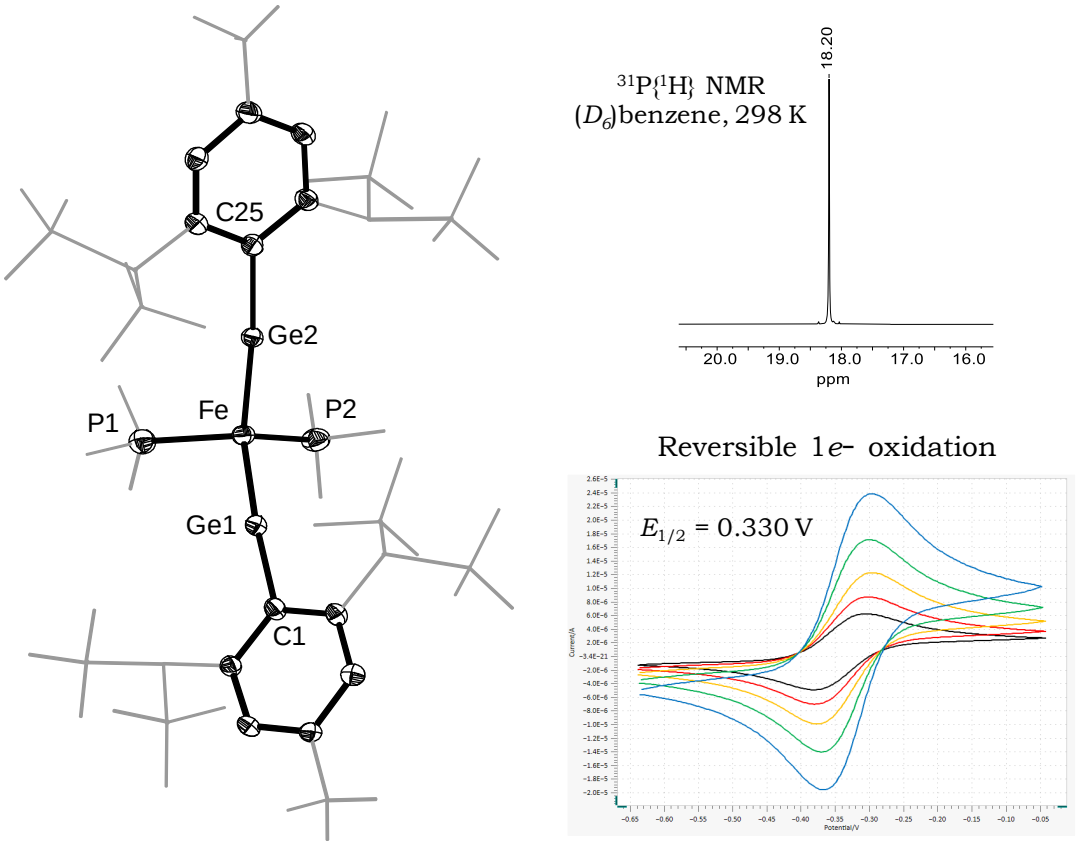

Figure 59. (*left*) DIAMOND plot of the molecular structure of **33-Fe**. Thermal ellipsoids are set at 30 % probability level. Hydrogen atoms are omitted, the Dsi and ^{t}Bu substituents of the Tbb ligand and methyl groups of PMe_3 are presented in wire-frame for clarity. Selected bond lengths [Å] and bond angles [°]: Fe-Ge1 2.1137(7), Fe-Ge2 2.1153(8), Fe-P1 2.1734(14), Fe-P2 2.1726(14), Fe-Ge1-C1 174.89(12), Fe-Ge2-C25 175.00(12), P1-Fe-P2 104.07(6), Ge1-Fe-Ge2 123.29(4); (*right top*) $^{31}P\{^1H\}$ NMR spectrum of **33-Fe** at 298 K; (*right bottom*) the Cyclic voltammograms of **33-Fe** at different scan rates. A reversible oxidation at $E_{1/2}$ = −0.330 V vs. $DMFc^{+/0}$ is observed.

The PMe_3 resonance (18.2 ppm) in the $^{31}P\{^1H\}$ NMR spectrum is appearing low-field shifted as compared to the aforementioned cobalt and nickel complexes (**30-Co** and **32-Ni**). Unlike **30-Co**, the bis-germylidyne complex **33-Fe** shows only reversible oxidations. In fact, it features two reversible voltammetric responses at the $E_{1/2}$ = 0.330 V vs. $DMFc^{+/0}$ and 0.910 V vs. $DMFc^{+/0}$ for the **33-Fe**/**33-Fe**$^{\bullet+}$ and **33-Fe**$^{\bullet+}$/**33-Fe**$^{2+}$ redox couple, respectively.

The low oxidation potential ($E_{1/2}$ = 0.330 V vs. $DMFc^{+/0}$) (see section ***5.4***) of **33-Fe** prompted me experimentally to isolate the corresponding radical-cation and indeed reacting **33-Fe** with equimolar amount of $[Cp_2Fe][B(Ar^F)_4]$ (***Scheme 37***) resulted in the formation of **34-Fe**.

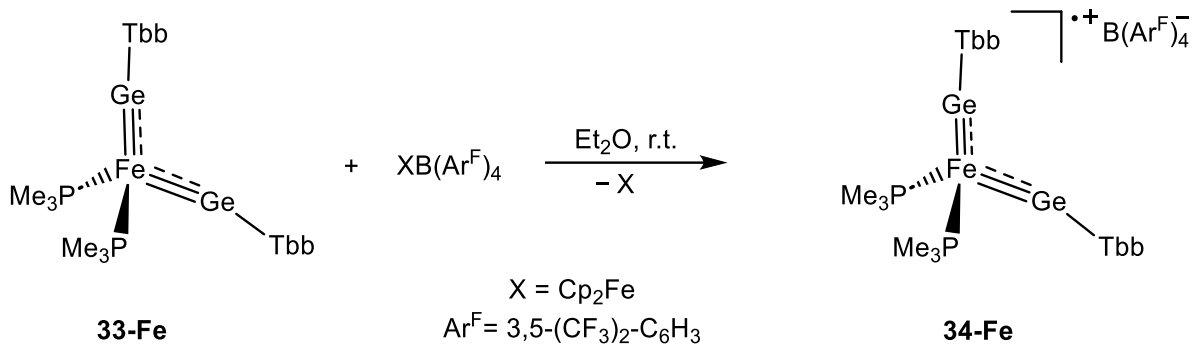

33-Fe **34-Fe**

Scheme 37. One electron oxidation of the Fe-bisgermylidyne complex to its radical cation.

In fact, when a solution of $[Cp_2Fe][B(Ar^F)_4]$ was added dropwise at ambient temperature to a stirred brown solution of **33-Fe** in Et_2O, no considerable colour change was observed. The absence of any signal in the $^{31}P\{^1H\}$ NMR spectrum suggested a complete consumption of **33-Fe**. After work-up of the reaction mixture, **34-Fe** was obtained as an analytically pure solid in 71 % yield. It is an air-sensitive, thermally stable ($T_{dec.}$ = 180 °C), wood-brown solid which is partially soluble in *n*-hexane, but very well soluble in diethyl ether and fluorobenzene at ambient temperature.

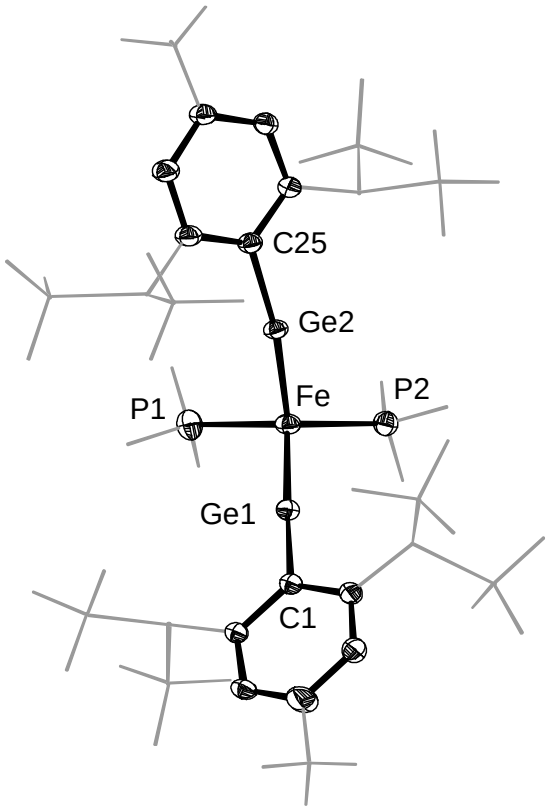

Figure 60. DIAMOND plot of the molecular structure of the cation in **34-Fe**. Thermal ellipsoids are set at 30 % probability level. Hydrogen atoms are omitted, the Dsi and ^{t}Bu substituents of the Tbb ligand and methyl groups of PMe_3 are presented in wire-frame for clarity. Selected bond lengths [Å] and bond angles [°]: Fe-Ge1 2.1349(6), Fe-Ge2 2.1293(6), Fe-P1 2.2713(11), Fe-P2 2.2951(10), Fe-Ge1-C1 176.19(10), Fe-Ge2-C25 170.72(10), P1-Fe-P2 106.94(4), Ge1-Fe-Ge2 117.48(2).

Unfortunately, **34-Fe** was not characterized by EPR spectroscopy, but the EA, magnetic susceptibility measurement and *sc*-XRD analysis abetted the structural integrity of the molecule. Suitable single crystals (clear dark-brown prism) of **34-Fe** were grown by slow cooling a saturated Et_2O/*n*-hexane solution at 4 °C and analyzed by X-ray diffraction.

Table 5. solid-state structural parameters of neutral and cationic iron-bisgermylidyne complexes.

Comps.	Fe–Ge/ (Å)	Fe–P/ (Å)	∠Ge/ (°)	Ge1–Fe–Ge2 /(°)	P1–Fe–P2 /(°)	τ_4
33-Fe	2.113(1) and 2.115(1)	2.173(1) and 2.173(1)	174.9(1) and 175.0(1)	123.3(1)	104.1(1)	0.92
34-Fe	2.135(1) and 2.129(1)	2.271(1) and 2.295(1)	176.2(1) and 170.7(1)	117.5(1)	106.9(1)	0.93

The molecular structure of **34-Fe** is composed of well separated bis-ylidyne complex cation and borate anion. The cation (***Figure 60***) is isostructural (τ_4 = 0.93) to its neutral precursor **33-Fe** (***Table 5***), with no considerable changes in the Fe–Ge bond lengths (Fe-Ge1 2.1349(6), Fe-Ge2 2.1293(6) Å) and angles at the dicoordinated Ge centers (176.19(10) and 170.72(10) °). However, a significant elongation of the Fe–P bonds of the **34-Fe** by ca. 0.1 Å compared of its precursor **33-Fe** is observed.

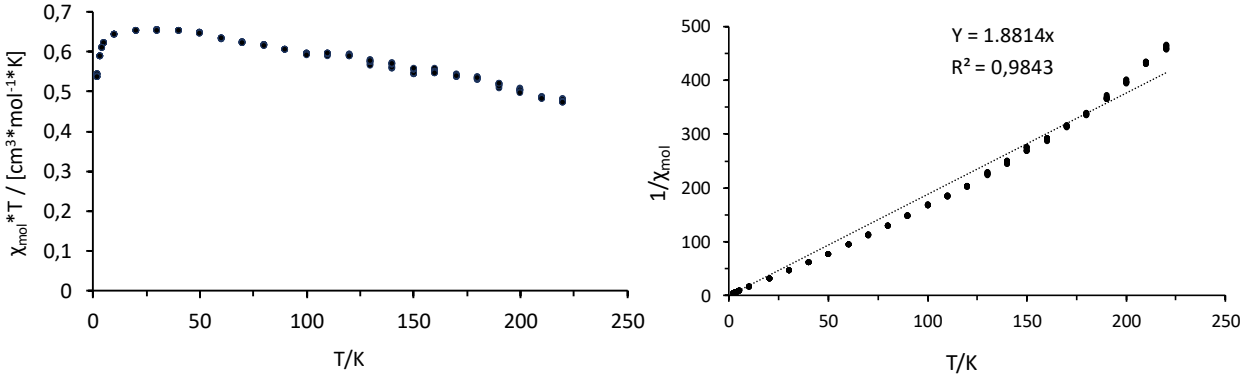

Figure 61. Magnetic susceptibility data of **34-Fe** measured by the VSM (Vibrating Sample Magnetometer) method. (*Left*) plot of molar susceptibility (χ_m) vs temperature (T), (*right*) variation of ($1/\chi_m$) with temperature (T).

$$\mu_{eff} = 2.828 \times (\chi_m \times T)^{1/2} \text{ (B.M)}$$

$$1/\chi_m = (2.828/\mu_{eff})^2 \times T$$

$$\text{Slope} = (2.828/\mu_{eff})^2$$

Magnetic susceptibility measurements of solid **34-Fe** from 2–250 K suggest the presence of a paramagnetic compound with one unpaired electron. A plot of the reciprocal molar magnetic susceptibility against the absolute temperature shows a linear correlation as expected for a paramagnetic compound following Curie's law (***Figure 61***). Calculation of the effective magnetic moment from the slope of the line obtained after linear regression ($R^2 = 0.9843$) yielded $\mu_{eff} = 2.06\ \mu_B$ (μ_B = Bohr magneton = $9.27400968(20) \times 10^{-24}$ J T^{-1}). The value is slightly higher than the expected value derived from the spin-only formula for one unpaired electron ($\mu_{eff} = 1.73\ \mu_B$).

2.9. Metathetical exchange of Si(I) and Ge(I) centers: synthesis and reactivity of a caac^{Me} supported germasilyne

Earlier reactivity studies in our group had shown that the disilicon(I) dihalides $Si_2X_2(NHC^1)_2$ (X = Cl, Br, I) (NHC^1 = IDipp = :C[N(Dipp)CH]$_2$),[206–208] are exceptional starting materials for the synthesis of many novel hypovalent silicon compounds.[207,208] Since these compounds feature a highly reactive Si−Si σ-bond I envisioned that metathesis with ditetrelynes (Tbb)Ge≡Ge(Tbb) would provide a direct synthetic access to NHC-supported germasilynes, featuring a Si−X bond for further functionalization. The first representative of this class was isolated recently by our group using the silicon(0)-isocyanide compound (NHC^2)Si═C═N–Ar^{Mes} (NHC^2 = SIDipp = :C[N(Dipp)CH_2]$_2$, Ar^{Mes} = 2,6-dimesitylphenyl) as (NHC)Si unit transfer reagent in a reaction with Ge(Ar^{Mes})Cl.[95]

However, studying of the reaction of $Si_2X_2(NHC^1)_2$ with Ge_2Tbb_2 showed only decomposition in solution upon heating to $SiX_2(NHC^1)$ and free NHC^1 carbene. Notably, $SiBr_2(NHC^1)$ did not to react with Ge_2Tbb_2 even at 110 °C in toluene. So, I anticipated that the ylidic character of the silicon-carbene bond could be tuned by using the cyclic (alkyl)(amino)carbenes (CAAC), which in contrast to classical NHCs do not only provide superior π-accepting capabilities, but also less sterical protection.[92,93] To consummate this hypothesis compounds like $SiBr_2(caac^{Me})$, $Si_2Br_2(caac^{Me})_2$ and even $Si_2(caa^{Me})_2$ were independently synthesized in our lab and the auspicious synthetic potential of these highly reactive precursors was densely studied.[iv]

A remarkable redox reaction was observed between $SiBr_2(caac^{Me})$ and Ge_2Tbb_2 in benzene at ambient temperature (***Scheme 38***). Monitoring of the reaction solution by ^{1}H NMR spectroscopy revealed the formation of an equimolar mixture of the caac^{Me}-supported germasilyne ($caac^{Me}$)Si(Br)=Ge(Tbb) (**35-Si**) and Ge(Tbb)Br,[27] where the poor solubility of the $Ge_2Br_2Tbb_2$ in aliphatic and aromatic solvents prevented the isolation of **35-Si** in an analytically pure form.

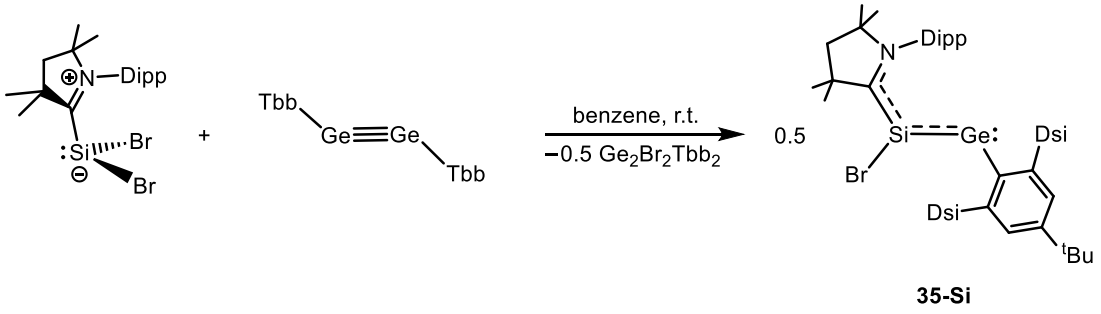

35-Si

Scheme 38. Formation of the caac^{Me}-supported germasilyne **35-Si** from $SiBr_2(caac^{Me})$ and Ge_2Tbb_2.

Then the reaction of the Si(I) dimer (***rac*-Si**) with Ge_2Tbb_2 was studied (***Scheme 39***). Indeed, treatment of $Si_2Br_2(caac^{Me})_2$ with 1.4 equivalents of TbbGe ≡ GeTbb at 90 °C over the course of 4 hours led to a color change of the solution from red-purple to greenish-blue. Analysis of the reaction solution by ^{1}H NMR spectroscopy in (D_6)benzene revealed the selective formation of the caac^{Me}-supported germasilyne **35-Si**, which was isolated in 61 % yield after crystallization from *n*-hexane as an extremely air sensitive dark blue solid in analytically pure form. The excess of 0.4 equivalents of digermyne in the metathesis reaction was needed, in order to ensure full conversion, since digermyne Ge_2Tbb_2 was shown to unselectively decompose upon prolonged heating in benzene or toluene solution.

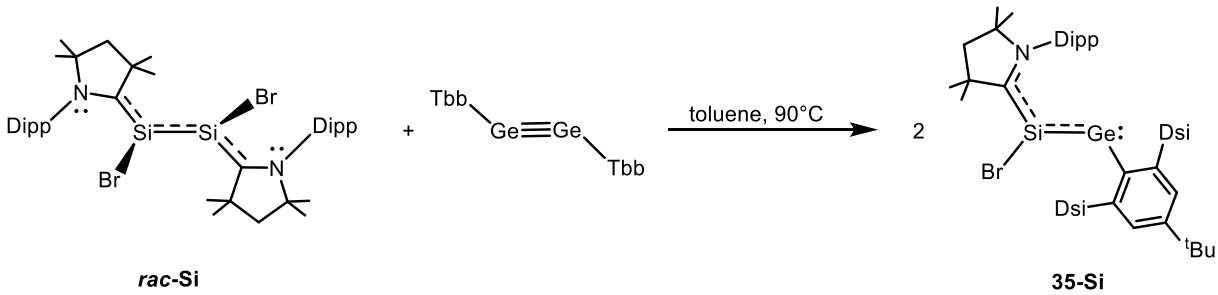

***rac*-Si** **35-Si**

Scheme 39. Reaction of Si(I)-dimer (***rac*-Si**) and Ge_2Tbb_2 yielding the caac^{Me}-supported germysilyne.

Looking for a more atom economic way to synthesize the compound **35-Si**, an alternative two-step method (***Scheme 40***) was developed starting from the Si(II) precursor $SiBr_2(caac^{Me})$. Reaction of 2 equivalents of $SiBr_2(caac^{Me})$ with one equivalent of (*E*)-Tbb(Br)Ge=Ge(Br)Tbb resulted in a color change of the solution from red to yellow-brown. Monitoring the reaction mixture by ^{1}H-NMR spectroscopy revealed the selective formation of the adduct (caac^{Me})$SiBr_2$–Ge(Br)Tbb (**36-Si**). Remarkably, no bromine shift to the three coordinated germanium center could be observed, which may be attributed to the stronger Si–Br bond ($\Delta_f H^0$ = –416 (±8) kJ/mol in $SiBr_4$), compared to the Ge–Br bond ($\Delta_f H^0$ = –306(±6) kJ/mol in $GeBr_4$).[209,210] Unfortunately, attempts to isolate **36-Si** in analytically pure form failed due to its extreme sensitivity, its brown-crystals turning easily colourless during the isolation by filtration at –30 °C. But, upon very careful handling, single crystals of **36-Si** could be grown from the crude reaction mixture in *n*-pentane at –30 °C and its molecular structure was determined by X-ray crystallography. The silylene adduct features a trigonally pyramidalized germylene center (∑∠(Ge) = 314.3°) which is connected to the (caac^{Me})$SiBr_2$ moiety via a Si–Ge single bond (2.474(2) Å) (see the section ***5.3*** and ***Figure 94*** for more details).

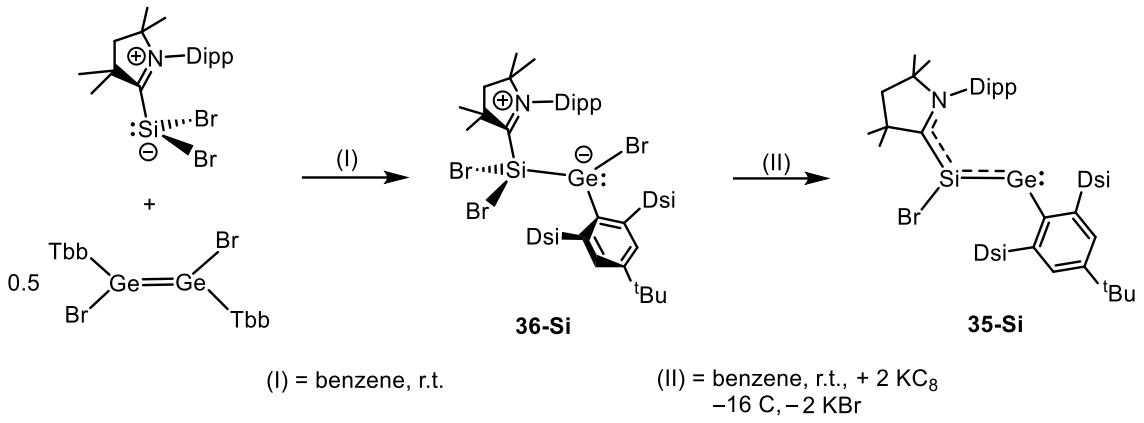

Scheme 40. Synthesis of **35-Si** via an oxidative coupling followed by a reduction.

Reduction of the *in-situ* generated **36-Si** with 2 equivalents of KC_8 for 16 hours of stirring at ambient temperature led to a gradual colour change to turquoise. Thereafter, compound **35-Si** was isolated after crystallization from *n*-hexane as a highly air sensitive, dark-blue microcrystalline solid in 65 % yield. It is very well soluble in toluene, benzene, Et_2O, THF and *n*-hexane at ambient temperature and decomposes upon melting at 132–134 °C.

The analogous NHC compound (**37-Si**) was obtained following the reported Si-NHC transfer reaction of (SIDipp)SiCNAr^{Mes} with tetrel (II) halide(***Scheme 41***).[95]

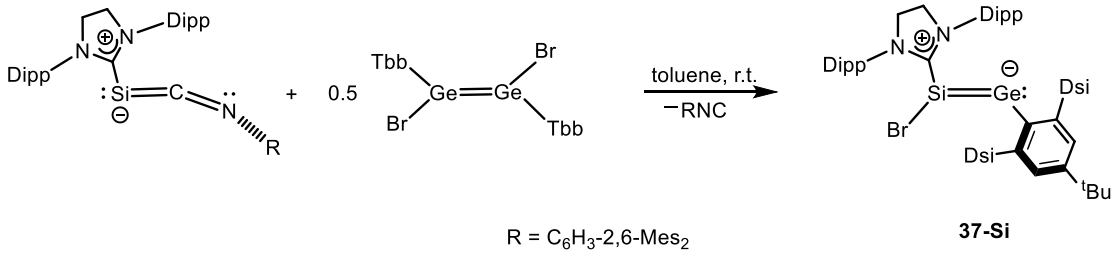

Scheme 41. Synthesis of the NHC-analogous compound of **35-Si**.

In fact, stirring of a mixture of purple (SIDipp)SiCNAr^{Mes} and orange-yellow $Ge_2Br_2Tbb_2$ in toluene at ambient temperature for 5 hours led to a dark-blue suspension. Which was shown by ^{1}H NMR spectroscopy in (D_6)benzene to contain an equimolar mixture of **37-Si** and free Ar^{Mes}NC. Work-up of the reaction afforded **37-Si** as deep purple-black, analytically pure powder in 63 % yield. It is an extremely air sensitive solid, decolorizing immediately upon contact with air. In contrast to **35-Si**, it is sparingly soluble in *n*-hexane, moderately soluble in Et_2O and well soluble in toluene, benzene and THF at ambient temperature. A full characterization of both compounds was done using multinuclear NMR spectroscopy, EA and *sc*-XRD analysis. Suitable single crystals of **35-Si·(C_5H_{12})** (bluish-green blocks) were obtained upon slow cooling a saturated *n*-pentane solution at –30 °C, whereas, reddish-brown

prisms of **37-Si·0.5 (Et_2O, C_6H_{14})** were grown upon slow cooling a saturated *n*-hexane/Et_2O solution at 4 °C.

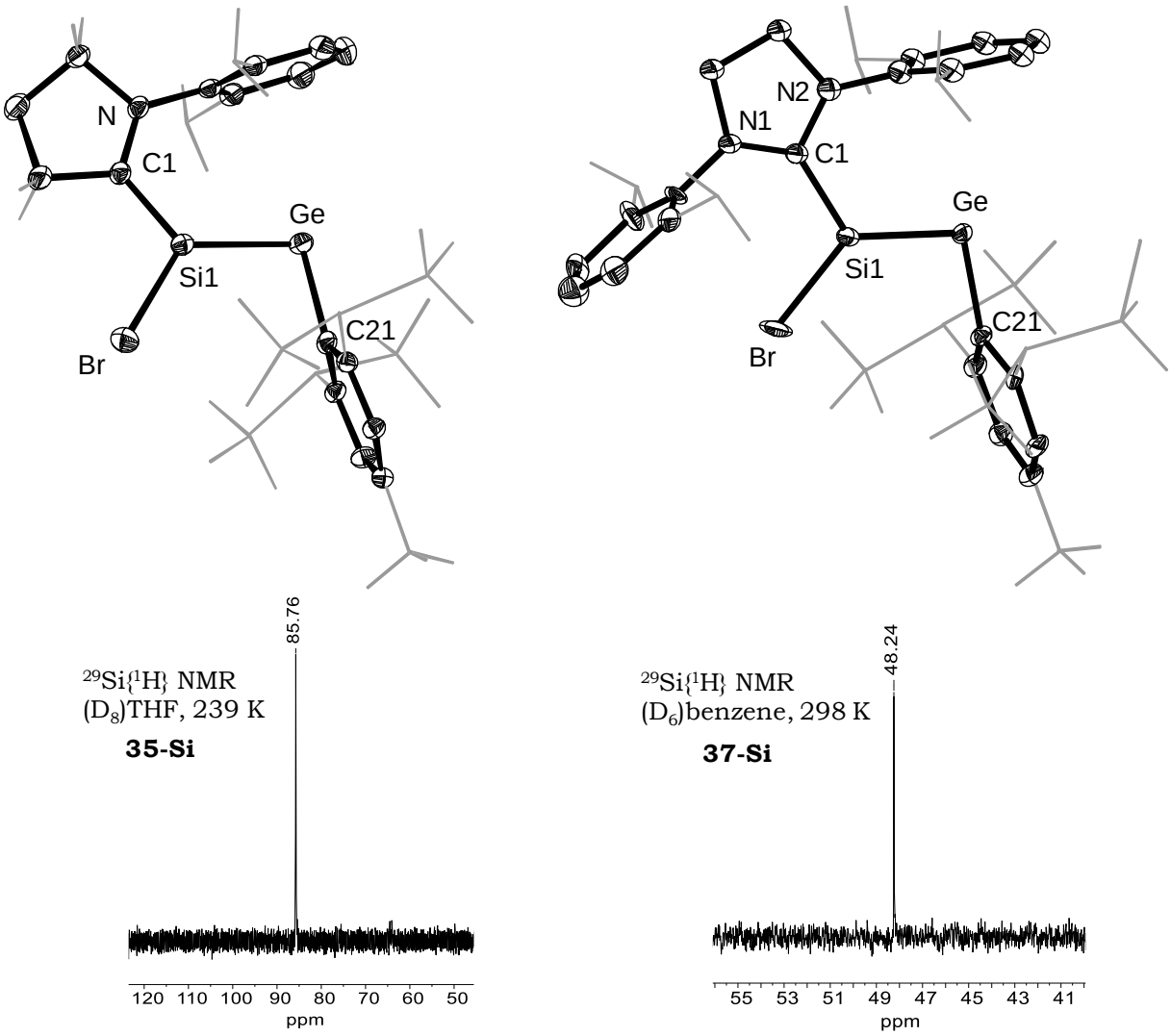

Figure 62. (*top*) DIAMOND plot of the molecular structure of **35-Si** (*top left*) and **37-Si** (*top right*). Thermal ellipsoids are set at 30 % probability level. Hydrogen atoms are omitted, the Dsi and ^{t}Bu substituents of the Tbb ligand, the ^{i}Pr substituents of the Dipp group and the $C^{3,5}$ methyl groups of $caac^{Me}$ are presented in wire-frame for clarity. Selected bond lengths [Å], bond angles [°] and torsion angle [°]: (**35-Si**): Ge-Si1 2.3265(13), Si1-C1 1.829(4), C1-N 1.336(5), Si-Br 2.2752(14), C1-Si1-Ge 126.97(15), C1-Si1-Br 109.33(15), Ge-Si1-Br 123.56(6), Si1-Ge-C21 100.62(12), C21-Ge-Si1-Br –0.294(2), C1-Si1-Ge-C21 –175.562(2), N-C1-Si1-Ge –9.987(3): (**37-Si**): Si1-Ge 2.2726(16), Si1-C1 1.880(5), C1-N1 1.343(7), C1-N2 1.363(6), Si1-Br 2.2404(15), C1-Si1-Ge 121.38(17), C1-Si1-Br 108.36(17), Br-Si1-Ge 130.21(7), Si1-Ge-C21 101.30(15), N2-C1-Si1-Ge –6.081(8), N2-C1-Si1-Br 176.084(5), C1-Si1-Ge-C21 –176.728(4), Br-Si1-Ge-C21 0.581(6); (*bottom*) selected excerpt of the $^{29}Si\{^1H\}$ NMR spectrum of **35-Si** (*bottom left*) and **37-Si** (*bottom right*), respectively.

At first glance the molecular structure of **35-Si** appears remarkably similar to the NHC-supported analogue **37-Si** and the reported germasilyne [$(NHC^2)ClSi{=}Ge(Ar^{Mes})$] (**37-Si´**).[95] All compounds have (a) a planar C^{carb}–Si–Ge–C^{Ar} skeleton with a *trans*-

bent geometry, as evidenced by the torsion angles 175.56(1)° (**35-Si**), –176.73(1)° (**37-Si**) and –179.93(7)° (**37-Si´**), respectively, (b) contain a trigonal planar coordinated silicon center (∑∠(Si1) = 359.9° which is connected to a bent, di-coordinated germanium atom (∠(C^{Ar}–Ge–Si) = 100.6(1)°(**35-Si**), 101.3(1)° (**37-Si**) and 100.9(1)°(**37-Si´**), and (c) the CAAC or NHC carbene is arranged coplanar to the molecular core, as evidenced by the dihedral angle (N–C^{carb}–Si1–Ge) of –9.9(1))°(**35-Si**), –6.1(1)°(**37-Si**) and –3.6(1)°(**37-Si´**)), allowing a significant delocalization of the Si=Ge π-bond over the C^{carb}–Si–Ge moiety in these molecules. Interestingly, the Si–C^{carb} bond length in **35-Si** (1.829(4) Å) is shorter compared to **37-Si** (1.880(5) Å) and **37-Si´** (1.877(2) Å), which is in line with a significant elongation of the N–C^{carb} bond in **35-Si** (1.336(5) Å), as compared to **37-Si** (1.343(7) and 1.363(6) Å) and **37-Si´** (1.351(2) and 1.358(2) Å). Likewise, the Si–Ge bond of **35-Si** (2.3265(13) Å) is dramatically elongated, when compared to that of **37-Si** (2.2726(16) Å) and **37-Si´** (2.275(9) Å). In fact, the Si–Ge bond in **35-Si** lies exactly in between that of typical Si=Ge double bonds present in silagermene $(SitBu_3)_2Si{=}Ge(Mes)_2$ (2.2769(8) Å)[211] and Si–Ge single bonds 2.383–2.416 Å in silagermanes.[212] These findings suggest a greater Si=C^{carb} double bond character in **35-Si**, as compared to its NHC analogues and the higher contribution of a silenyl-germylene resonance structure (***Figure 63***) in **35-Si**, which can be attributed to the greater π-acceptance of CAAC in comparison to the NHC ligand. This was verified by an NRT analysis.

In solution, ^{1}H, $^{13}C\{^{1}H\}$ and $^{29}Si\{^{1}H\}$ NMR spectra of **35-Si** in (D_6)benzene are well corroborating to its C_S-symmetric solid-state structure. The $^{29}Si\{^{1}H\}$ NMR spectrum of **35-Si** in (D_8)THF at 239 K displays a resonance at δ = 85.7 ppm for the tricoordinated Si atom, which is considerably low-field shifted as compared to the NHC analogue **37-Si** (48.2 ppm), but has a similar chemical shift as **37-Si´** (81.8 ppm).

The electronic structure of **35-Si** was investigated by quantum chemical calculations at the B97-D3(BJ)-ATM/def2-TZVP level of theory. Geometry optimization afforded a gas phase minimum structure **35-Si$_{calc.}$** displaying bond lengths and angles in agreement with its solid-state molecular structure. Natural bond orbital analysis (***Table 6***) of the wave function of **35-Si$_{calc.}$** led to a leading natural Lewis structure (NLS) with localized bond pair NBOs for the Si–C^{carb}, Si–Ge, Si–Br and Ge–C^{Tbb} σ-bonds, one π(Si–Ge) bond and a lone pair NBO at the two-coordinated germanium center. All σ-bonds and the lone pair NBO feature a high Lewis occupancy above 1.88 e^{-}. Considerable delocalization is evidenced by the low occupancy of the Si–Ge

π-bond (1.39 e^-), which is strongly polarized to the silicon atom (72 %). The remaining electron density can be found in the π*(N–C^{carb}) NBO (0.63 e^-).

Table 6. Selected results of the natural bond orbital (NBO), natural resonance theory (NRT) and natural population (NPA) analyses of **35-Si**. A local subset including the Si, Ge, Br, C^{CAAC}, N and C^{Tbb} atoms was employed for the NRT analysis.

NBO A–B	occ.[a]	NHO A,B[b] pol., hyb.	WBI[c] A–B	NRT-BO[d] tot/cov/ion	atom/ group	q/Σq[e]
σ(Si–Br)	1.97	26, $sp^{4.7}$, 74, $sp^{4.2}$	0.8	0.9/0.5/0.4	Si	+0.53
σ(Si–C^{CAAC})	1.95	25, $sp^{2.4}$, 75, $sp^{1.6}$	1.1	1.4/0.9/0.5	Ge	+0.36
σ(Si–Ge)	1.93	63, $sp^{0.9}$, 37, p	1.3	1.2/0.8/0.4	Br	−0.35
π(Si–Ge)	1.39	72, p, 28, p			$caac^{Me}$	−0.12
σ(Ge–C^{Tbb})	1.93	28, $sp^{8.9}$, 72, $sp^{2.6}$	0.8	0.9/0.5/0.4	Tbb	−0.42
LP(Ge)	1.88	$sp^{0.2}$				
π*(N–C)^{CAAC}	0.63	27, p, 74, p				

[a]: occ.= occupancy in e^-; [b]: NHO = Natural Hybrid Orbital, pol. (polarization) = $(C_i)^2 \cdot 100\%$, where C_i = coefficient of NHO; [c]: Wiberg bond index; [d]: total, covalent and ionic NRT bond order; [e]: q = NPA charge of the atom, Σq = total NPA charge of the group.

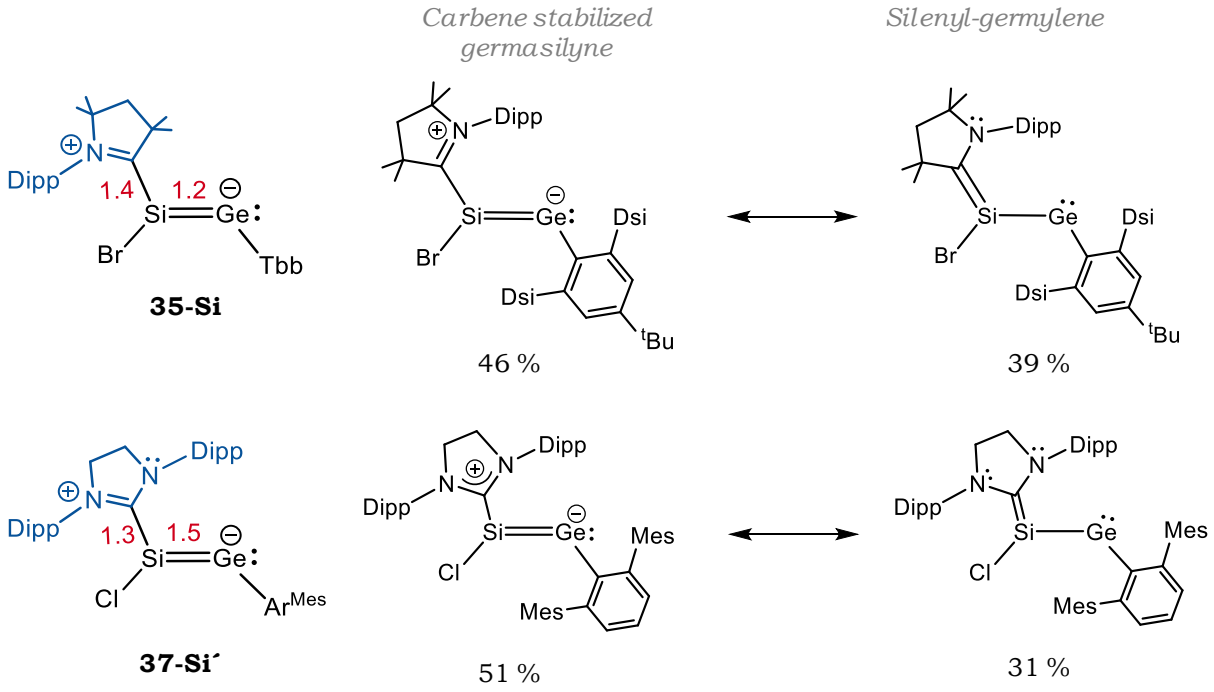

Figure 63. (*left*) NRT bond orders of selected bond lengths and (*right*) most dominant NRT resonance structures of **35-Si**, in comparison to similar NHC-stabilized compound **37-Si´**.

In addition, the NRT bond orders in **35-Si** suggest considerable double bond character in the Si–C^{carb} (1.4) and Si–Ge (1.2) bonds. The dominant NRT resonance structures of **35-Si** provide an insight into the electronic structure (***Figure 63***). In fact, it can be best described as a hybrid of a $caac^{Me}$-stabilized germasilyne (46 %) and silenyl-germylene (39 %).

Although the electronic structure of **35-Si** resembles the structure of **37-Si´**, slight differences can be seen in the results of the NRT-BO analysis. Overall the Si–C^{carb} σ-bond of the three-cooridinated silicon center in **35-Si** features more sp^2-character ($sp^{2.4}$), similar to that of silenes, whereas in **37-Si´** the silicon center features more sp^3-character ($sp^{2.9}$). In addition, the bond order of the Si–C^{carb} bond in **35-Si** (1.4) is marginally higher as compared to that of **37-Si´** (1.3). whereas more double bond character is pronounced in the Si–Ge bond of **37-Si´** (1.5) than that of **35-Si** (1.2). This is also in line with the contribution percentage of the most dominant NRT-resonance structures, where in **35-Si** both silagermyne (46 %) and silenyl-germylene (39 %) structures are contributing almost equally, but in **37-Si´**, the contribution of the carbene-stabilized germasilyne (51 %) remains greater than the silenyl-germylene (31 %) resonance structure.[95]

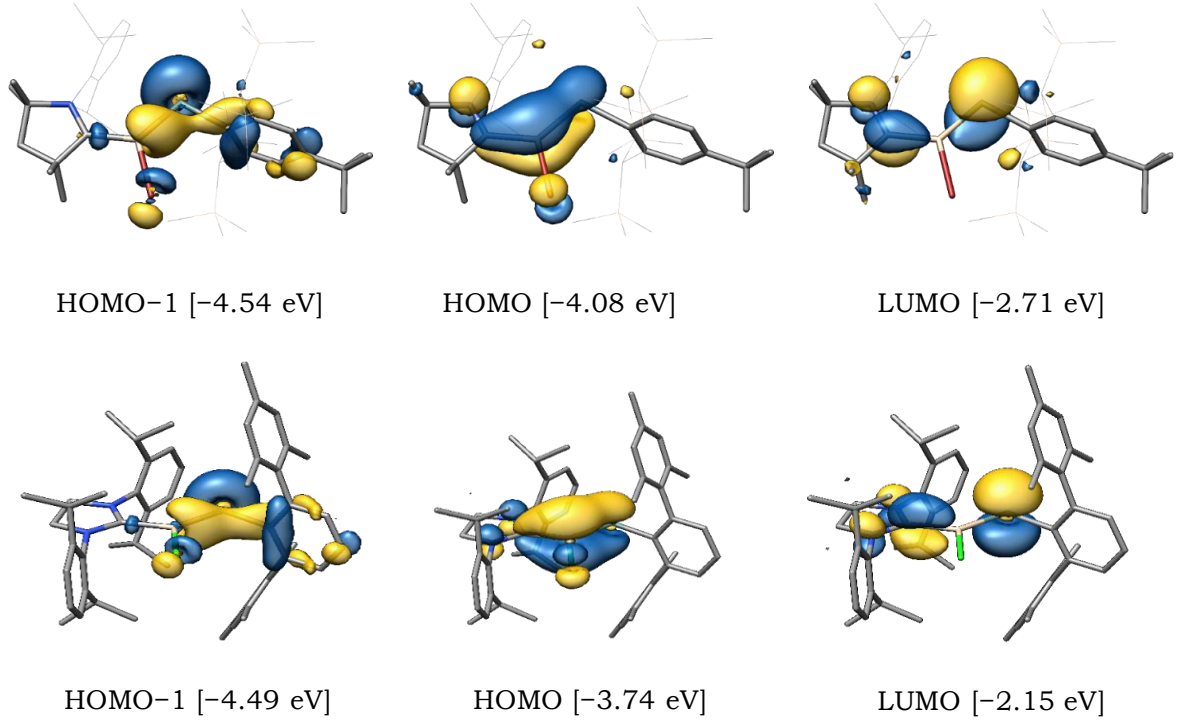

Figure 64. Selected Kohn-Sham molecular orbitals of **35-Si** (*top*) and **37-Si´** (*bottom*) with their orbital energies in eV. Hydrogen atoms are omitted for clarity. The isosurface value is set to 0.04 $e^{1/2}{\cdot}Bohr^{-3/2}$.

The NBO results are reflected in the frontier orbitals of **35-Si** and are well consistent with the reported NHC analogous compound (**37-Si´**). The HOMO−1 contains mainly the lone pair at the Ge atom, the HOMO corresponds to the 3c–2e π_{oop}(C^{carb}–Si–Ge)-

bond and the LUMO corresponds to the empty p orbital at the Ge atom with some antibonding π_{oop}(Si–C^{carb}) contribution.

The compound **35-Si** features many reactive sites, such as the Si–Br bond, an empty p orbital on Ge atom or even the displaceable CAAC group, opening up many potential reaction pathways. A thorough study on the synthetic potential of the molecule **35-Si** was consummated and furthermore, several astonishing compounds were isolated. The very first success was a salt metathesis reaction with a small organolithium reagent, Mes-Li. When a colourless suspension of Mes-Li in Et_2O was added to a greenish-blue Et_2O solution of **35-Si** at ambient temperature, no considerable colour change was observed. However, the reaction proceeded almost quantitatively forming **38-Si**, as evidenced by ^{1}H NMR spectroscopic analysis of a reaction aliquot. Work-up led to the isolatation of **38-Si** as an analytically pure solid in 86 % yield. It is an extremely air sensitive, but thermally robust ($T_{melt.}$ = 207 °C), dark-blue solid turning immediately colourless upon contact with air. It is highly soluble in toluene, benzene, Et_2O, and *n*-hexane at ambient temperature.

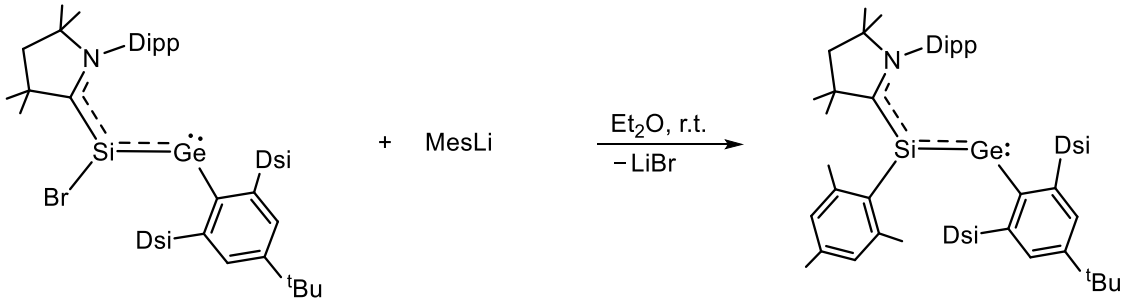

35-Si **38-Si**

Scheme 42. Halide substitution reaction of **35-Si** using Mes-Li.

Compound **38-Si** was fully characterized. Suitable single crystals of **38-Si** (greenish-blue blocks) for sc-XRD analysis were obtained upon slow cooling a saturated *n*-hexane solution at 4 °C. **38-Si** is isostructural to its precursor **35-Si**, where the distances, Si–Ge (2.3439(4) Å), Si–C^{carb} (1.8499(15) Å), the sum of angles at the three coordinated silicon center (∑∠(Si1) = 360 °) and the dihedral angle (φ, N–C^{carb}–Si1–Ge = 10.9(1)°) have similar values as **35-Si**. However, the angle at the germanium center (∠(C^{Tbb}–Ge–Si) = 110.97(4)°), is slightly expanded (ca. 10°) compared to its precursor, probably as a result of an increased steric repulsion between the Mes and the Tbb group. The solution structure of **38-Si** was investigated by multinuclear NMR spectroscopy at 298 K in (D_6)benzene, and it is well corroborating to its C_S-symmetric structure in the solid-state. Interestingly, the tricoordinated Si atom appears as a

distinct singlet at δ = 105.4 ppm in the $^{29}Si\{^{1}H\}$ NMR spectrum, which is considerably low-field shifted (ca. 20 ppm) than that of its precursor.

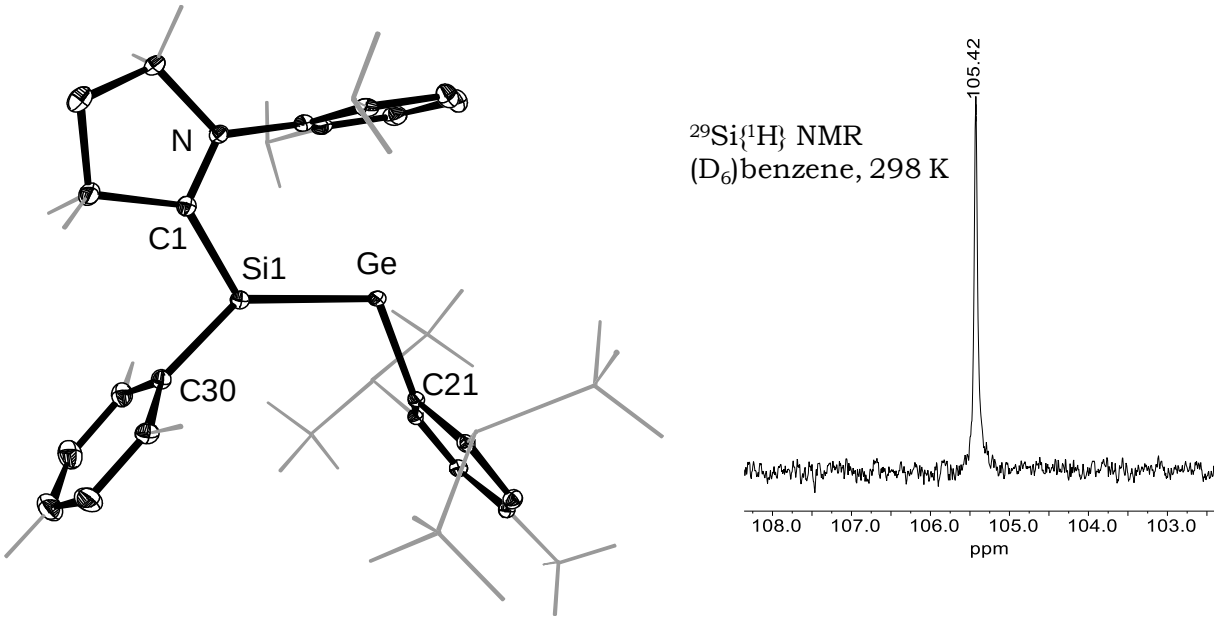

Figure 65. (*left*) DIAMOND plot of the molecular structure of **38-Si**. Thermal ellipsoids are set at 30 % probability level. Hydrogen atoms are omitted, the Dsi and ^{t}Bu substituents of the Tbb ligand, the ^{i}Pr substituents of the Dipp group, the $C^{2,4,6}$ methyl groups of Mes ligand and $C^{3,5}$ Methyl groups of $caac^{Me}$ are presented in wire-frame for clarity. Selected bond lengths [Å], bond angles [°] and torsion angles [°]: Si1-Ge 2.3439(4), Si1-C1 1.8499(15), Si1-C30 1.9028(15), C1-N 1.3583(18), C1-Si1-Ge 118.28(5), C1-Si1-C30 109.77(6), C30-Si1-Ge 131.93(5), Si1-Ge-C21 110.97(4), C1-Si1-Ge-C21 177.771(1), N-C1-Si1-Ge 10.908(3), N-C1-Si1-C30 –170.512(2), C30-Si1-Ge-C21 –0.443(2); (*right*) an excerpt of the $^{29}Si\{^{1}H\}$ NMR spectrum of **38-Si**.

After the successful halide substitution reaction, expectantly a reaction of **35-Si** was performed with a halide scavenger (***Scheme 43***) to obtain the corresponding cationic germasilyne (***Figure 67*** (d)). When a colourless solid of $NaB(Ar^{F})_4$ was added to a greenish-blue solution of **35-Si** in fluorobenzene at ambient temperature, a reaction proceeded slowly with a gradual colour change from greenish-blue to ink-blue.

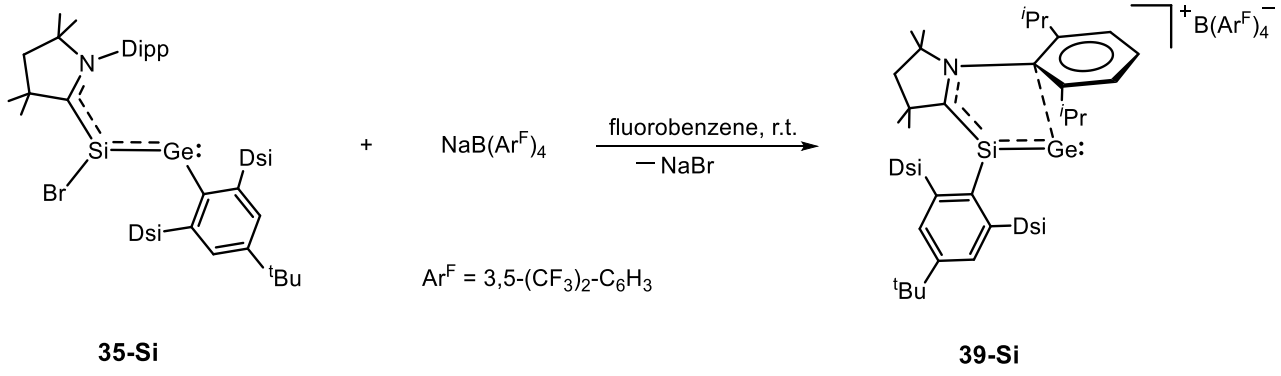

35-Si **39-Si**

Scheme 43. Halide abstraction reaction of **35-Si** forming the cationic vinylidene **39-Si**.

Analyzing the reaction progress by ^{1}H No-D NMR spectroscopy, revealed a complete consumption of **35-Si** and a quantitative formation of the unprecedented cationic mix-vinylidene **39-Si** via 1,2-migration of the Tbb ligand. After work-up compound **39-Si** was isolated as analytically pure solid in 88 % yield. It is an extremely air sensitive, dark-blue solid, turning immediately colourless upon contact with air. The melting associated decomposition of **39-Si** was observed at 171 °C. It is very well soluble in fluorobenzene, Et_2O and dichloromethane, but insoluble in aliphatic solvents at ambient temperature and surprisingly, a sample solution of **39-Si** in (D_2)dichloromethane shows minute decomposition after 8 hours at ambient temperature. Notably, compound **39-Si** is the first base-free silicon-germanium mixed vinylidene to be reported hence, it was comprehensibly characterized. Suitable single crystals of **39-Si** as clear dark-blue plates were grown by slow diffusion of *n*-pentane into a saturated fluorobenzene solution at ambient temperature.

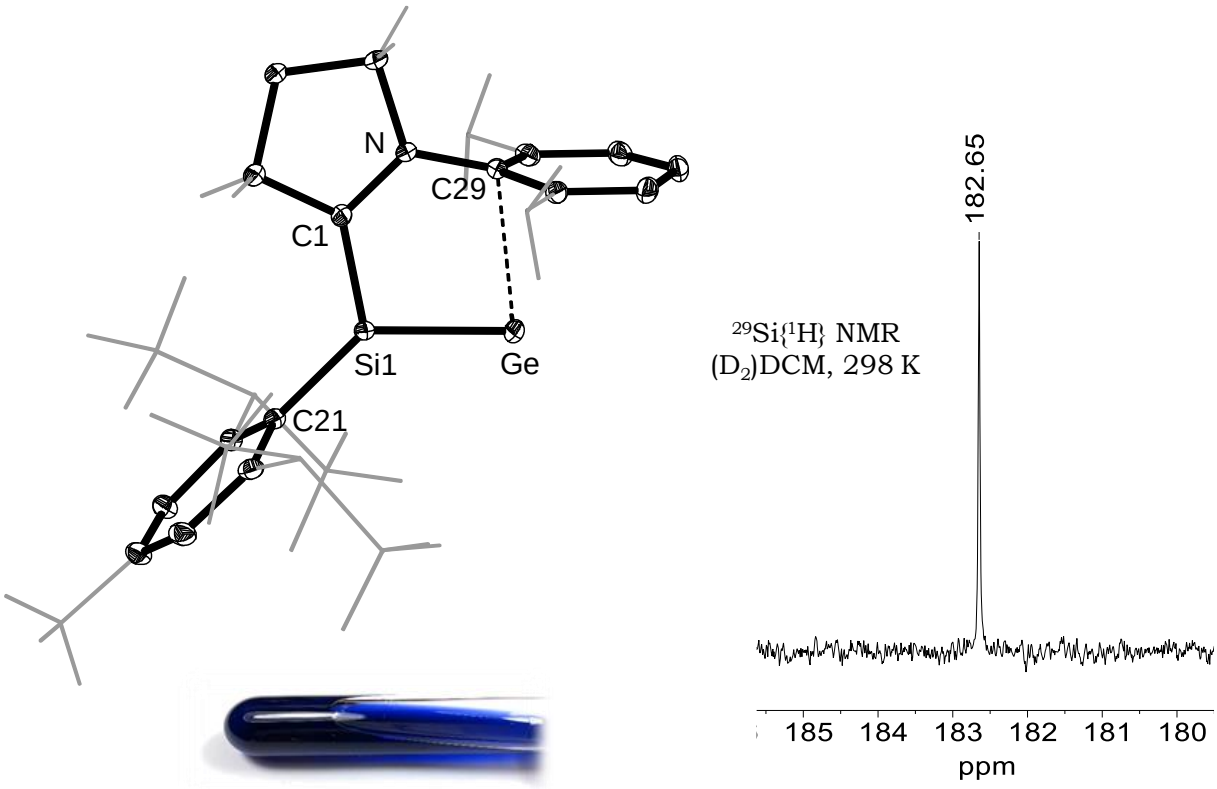

Figure 66. (*left top*) DIAMOND plot of the molecular structure of the cation in **39-Si**. Thermal ellipsoids are set at 30 % probability level. Hydrogen atoms are omitted, the Dsi and ^{t}Bu substituents of the Tbb ligand, the ^{i}Pr substituents of the Dipp group and the$C^{3,5}$ methyl groups of caac^{Me} are presented in wire-frame for clarity. Selected bond lengths [Å], bond angles [°] and torsion angles [°]:Si1-Ge 2.3057(5), Si1-C1 1.7928(18), C1-N 1.361(2), Ge-C29 2.4873(17), C1-Si1-Ge 103.71(6), C1-Si1-C21 121.61(8), C21-Si1-Ge 134.60(6), N-C1-Si1-Ge –2.702(2), N-C1-Si1-C21 –179.794(2); (*left bottom*) picture of a sample solution of **39-Si** in fluorobenzene at ambient temperature; (*right*) an excerpt of the ^{29}Si{^{1}H} NMR spectrum of **39-Si**.

The solid-state molecular structure of **39-Si** (***Figure 66***) features a "one-coordinated" Ge center that is bonded to a trigonal planar coordinated Si center (∑∠Si1 = 359.9°) via a short bond (Si1–Ge 2.3057(5) Å). Interestingly, the Si–Ge and the Si–C^{carb} distances are slightly shortened when compared to those of its precursor. However, the coplanarity of the carbene moiety to the molecular core is even higher than that in its precursor **35-Si**, as evidenced by the dihedral angle of (φ, N-C1-Si1-Ge) –2.7(1))°, and leads as evidenced by the dominant NRT resonance structure (***Figure 67*** (b)), to a significant delocalization of the Si=Ge π-bond over the C^{carb}–Si–Ge moiety. Of note, in the molecular structure of **39-Si**, the $caac^{Me}$-Dipp substituent resides over the "one-coordinated" Ge center leading to a short contact (Ge-C29) of 2.4873(17) Å, which is considerably shorter (ca. 0.4 Å) than that found for the "one-coordinated" Ge center in the diboryl digermavinylidene, $[(HCDippN)_2B]_2GeGe$, reported by Aldrige *et al.*[213] but longer than the covalent Ge–C single bonds (~2.00 Å). The short contact (Ge-C29) 2.4873(17) Å suggests the donor-acceptor stabilizing interaction of the Dipp π-system with the vacant in-plane p orbital at the Ge center.

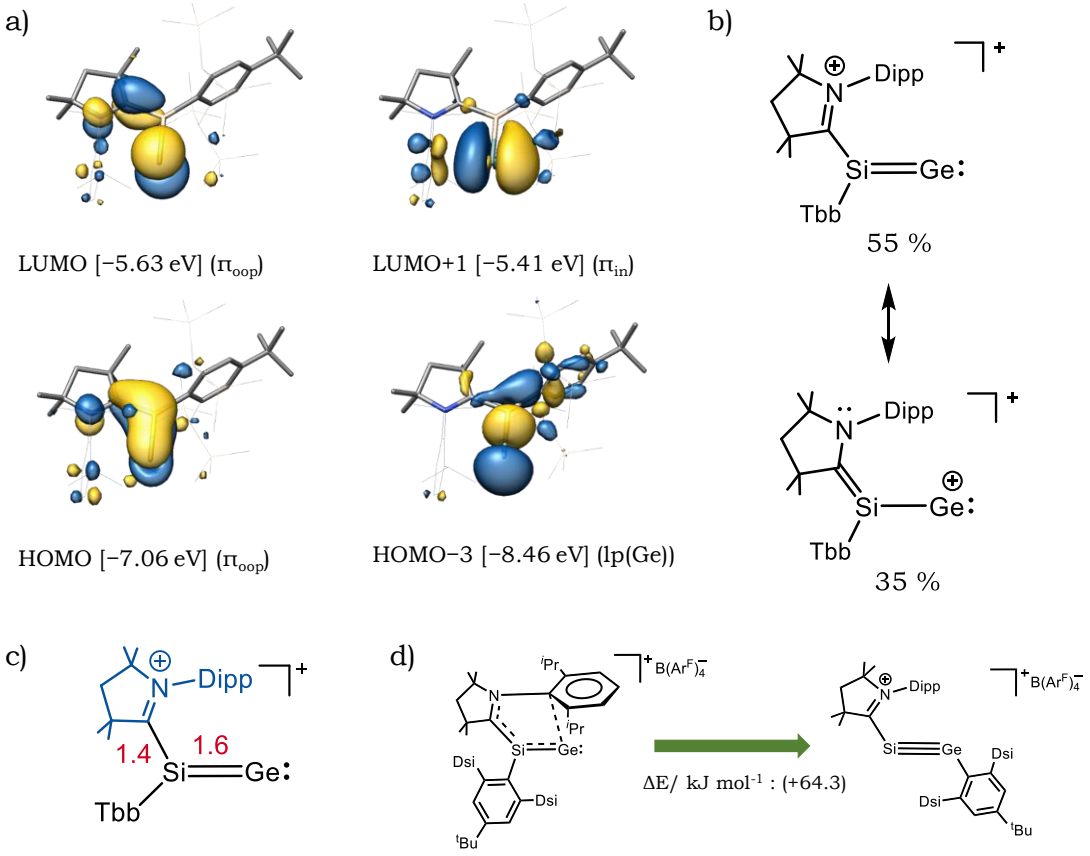

Figure 67. Theoretical results of the cation in **39-Si**: (a) selected kohn-Sham molecular orbitals and their orbital energies in eV, the isosurface value is set to 0.04 $e^{1/2}$·$Bohr^{-3/2}$; (b) most dominant NRT resonance structures; (c) NRT bond orders of selected bond lengths; (d) the energy difference between the vinylidene and the alkyne isomers.

The structute of **39-Si** in solution was verified by multinuclear NMR spectroscopy and the ^{1}H and $^{13}C\{^{1}H\}$ NMR spectra confirm the C_s symmetric solid-state structure of **39-Si**. The Si–C^{Tbb} rotation is frozen out on the NMR time scale at ambient temperature, as evidenced from the appearance of two singlets for the diastereotopic $SiMe_3$ groups. In the $^{29}Si\{^{1}H\}$ NMR spectrum of **39-Si**, the silicon resonance (182.7 ppm) for the tricoordinated silicon atom is significantly down-field shifted when compared to its precursor but appears in close position to those of triarylsilylium ions (~220 ppm) reported in literature.[214]

Table 7. Selected results of the natural bond orbital (NBO), natural resonance theory (NRT) and natural population (NPA) analyses of **39-Si**. A local subset including the Si, Ge, C^{carb}, N and C^{Tbb} atoms was employed for the NRT analysis.

NBO A–B	occ.[a]	NHO A,B[b] pol., hyb.	WBI[c] A–B	NRT-BO[d] tot/cov/ion	atom/ group	q/Σq[e]
σ(Si–C^{carb})	1.95	25, $sp^{2.8}$; 75, $sp^{1.5}$	1.0	1.4/0.9/0.5	Si	+0.72
σ(Si–Ge)	1.93	59, $sp^{1.6}$; 41, $sp^{7.6}$	1.4	1.6/1.3/0.3	Ge	+0.43
π(Si–Ge)	1.47	62, p; 38, p				
σ(Si–C^{Tbb})	1.95	25, $sp^{2.8}$; 75, $sp^{1.5}$	0.8	0.9/0.6/0.3	$caac^{Me}$	+0.11
LP(Ge)	1.96	$sp^{0.1}$			Tbb	−0.26
LV(Ge)	0.17	p				
π*(N–C)^{CAAC}	0.54	27, p; 73, p				

[a]: occ.= occupancy in e^{-}; [b]: NHO = Natural Hybrid Orbital, pol. (polarization) = $(C_i)^2 \cdot 100\%$, where C_i = coefficient of NHO; [c]: Wiberg bond index; [d]: total, covalent and ionic NRT bond order; [e]: q = NPA charge of the atom, Σq = total NPA charge of the group.

Further insight into the electronic structure of **39-Si** was provided by quantum chemical calculations at the B97-D3(BJ)-ATM/def2-TZVP level of theory. Geometry optimization afforded a gas phase minimum structure **39-Si$_{calc.}$** displaying good agreement with the experimental solid-state structure. Selected molecular orbitals of **39-Si** are depicted in the ***Figure 67*** (a), where the HOMO−3 contains parts of a σ(Si–Ge) bond and a lone pair at Ge. In the HOMO a 3c-2e^{-} π bond between Si, Ge and C^{carb} is visible, similar to that of its precursor. The LUMO corresponds to a π* orbital with a main contribution of the out of plane vacant p orbital at Ge. Whereas the LUMO+1 shows a vacant in-plane p orbital at the Ge center, that is destabilized through an anti-bonding interaction with the π-system of Dipp. The NRT analysis (***Figure 67*** (c)) reproduces the 3c-2e^{-} bond with total NRT bond orders of 1.4 and 1.6

for the Si–C^{carb} and Si–Ge bonds, respectively, in comparison to the found single bond for Si–C^{Tbb} (0.9). Notably, the WBI of the Si–C^{carb} bond (1.0) is larger than that of the Si–C^{Tbb} bond (0.8). The NRT analysis also shows a resonance hybrid that mostly consists out of two structures (***Figure 67*** (b)). This is reflected in the NBO results of the leading resonance formula which reveals a high occupation for the σ(Si–C^{carb}), σ(Si–Ge) and σ(Si–C^{Tbb}) bonds of 1.95, 1.93 and 1.95 e^-, respectively, but a low occupation for the π(Si–Ge) NBO with only of 1.47 e^-. A considerable electron density is found in the π*(N^{carb}–C^{carb}) orbital indicating the extensive π-electron delocalization implied by the NRT resonance structure. Interestingly, the in-plane lone valence p-orbital at the germanium atom shows a non-Lewis occupancy of 0.17 e^-, indicating the Dipp→Ge donor-acceptor interaction according to a SOPT analysis within the NBO framework.

Compound **35-Si** could be selectively reduced by $2e^-$ using KC_8 to isolate the potassium silenide **40-Si**. When, KC_8 was added to a vigorously stirred greenish-blue solution of **35-Si** in benzene at ambient temperature, the colour of the reaction mixture turned immediately dark green. A complete consumption of **35-Si** and selective formation of **40-Si** along with some minor unknown side products, was confirmed by spectroscopic analysis. After working-up the reaction mixture, **40-Si** was isolated in analytically pure form in 69 % yield. It is an extremely air sensitive, dark green, pyrophoric solid. It is sparingly soluble in aliphatic solvents and very well soluble in benzene, toluene, and Et_2O at ambient temperature. The melting associated decomposition of **40-Si** was observed around 178 °C.

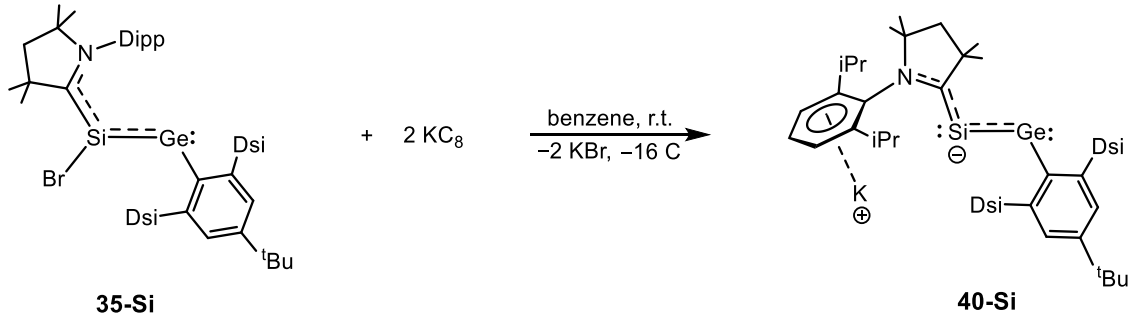

Scheme 44. $2e^-$ reduction of **35-Si** yielding a potassium silenide.

Slow evaporation of a concentrated benzene solution of **40-Si** inside the glovebox resulted in few single crystals of **40-Si•C_6H_6** as clear dark-green planks. Subsequent X-ray diffraction analysis yielded a low-quality crystal structure showing a coordination polymer. The molecular structure (***Figure 68*** (a)) of **40-Si** features C_s-symmetry and a trigonal planar coordinated silicon(0) center where the sum of angles at silicon center (∑∠(Si1) = 358°) is similar to that of the potassium silenides

synthesized and reported by our group[iv] and the lithium silenides (∑∠(Si) = 359.6–360.0 ° (see compounds **40-IV** and **40-V** in ***Figure 69***) reported by Apeloig *et al.*[215,216]

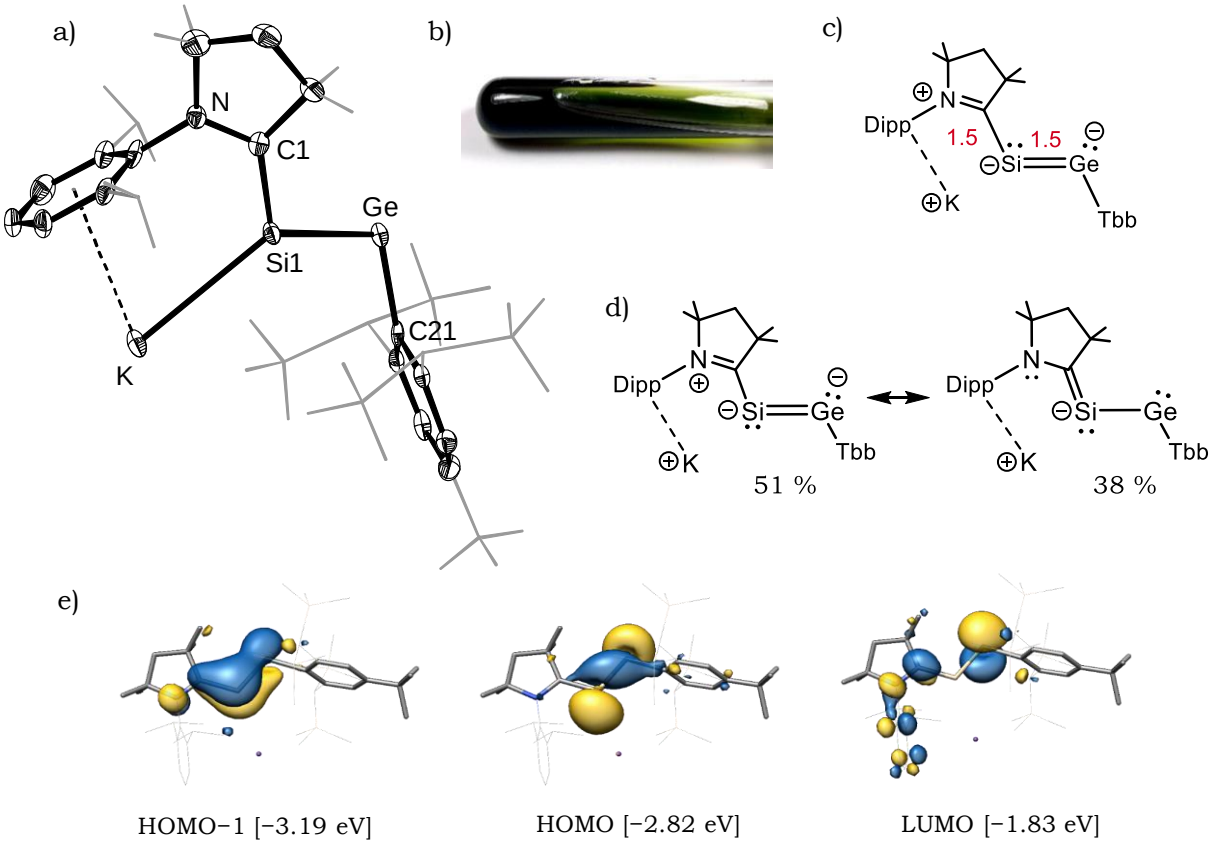

Figure 68. The experimental and the theoretical results of the silenide **40-Si**: (a) DIAMOND plot of the molecular structure, thermal ellipsoids are set at 30 % probability level. Hydrogen atoms are omitted, the Dsi and ^{t}Bu substituents of the Tbb ligand, the ^{i}Pr substituents of Dipp group and the C^{3,5} methyl groups of caac^{Me} are presented in wire-frame for clarity. Selected bond lengths [Å], bond angles [°] and torsion angles [°]: Si1-Ge 2.346(3), Si1-C1 1.865(11), Si1-K 3.442(3), C1-N 1.349(11), C1-Si1-Ge 104.8(3), C1-Si1-K 120.4(3), K-Si1-Ge 132.79(12), Si1-Ge-C21 103.4(2), C1-Si1-Ge-C21 171.935(17), N-C1-Si1-Ge 158.629(23), N-C1-Si1-K –7.031(32), K-Si1-Ge-C21 –24.993(23); (b) picture of a sample solution of isolated **40-Si** in benzene; (c) NRT bond orders of selected bond lengths; (d) most dominant NRT resonance structures; (e) selected Kohn-Sham MOs.

The $d_{(Si–Ge)}$ (2.346(3) Å) and $d_{(Si-Ccarb)}$ (1.865(11) Å) distances are slightly elongated as compared to those of its precursor (**35-Si**), but quite similar to that of the mesityl substituted germasilyne (**38-Si**). The Si–C^{carb} bond (1.865(11) Å) is longer than that of the potassium-silenide [(caac^{Me})Si(K)Si(SiMe$_3$)$_3$; 1.809(2) Å][iv] reported by our group, and also longer than those of the lithium silenides (d(Si–C^{carb}) = 1.762(3) – 1.778(3) Å)) reported by Apeloig *et al.*[215,216] The Si–K distance (3.442(3) Å) is comparatively longer than that of [(caac^{Me})Si(K)Si(SiMe$_3$)$_3$; 3.298(3) Å][iv] but lies in the typical range of potassium silanides (d(Si–K) = 3.37 – 3.42 Å),[217] probably implying

a covalent bonding between Si and K atoms. In addition, the potassium atom is further supported by the π-interaction of the Dipp aromatic ring $d(C^{ring}–K)$ = 3.370(11) – 3.537(11) Å of the caac^{Me}-ligand. The C^{ring}–K distances are very similar to those of silanylidene and germanylidene anions ($d(C^{ring}–K)$ = 3.044(2) – 3.510(2) Å)) described by Roesky *et al.*[218]

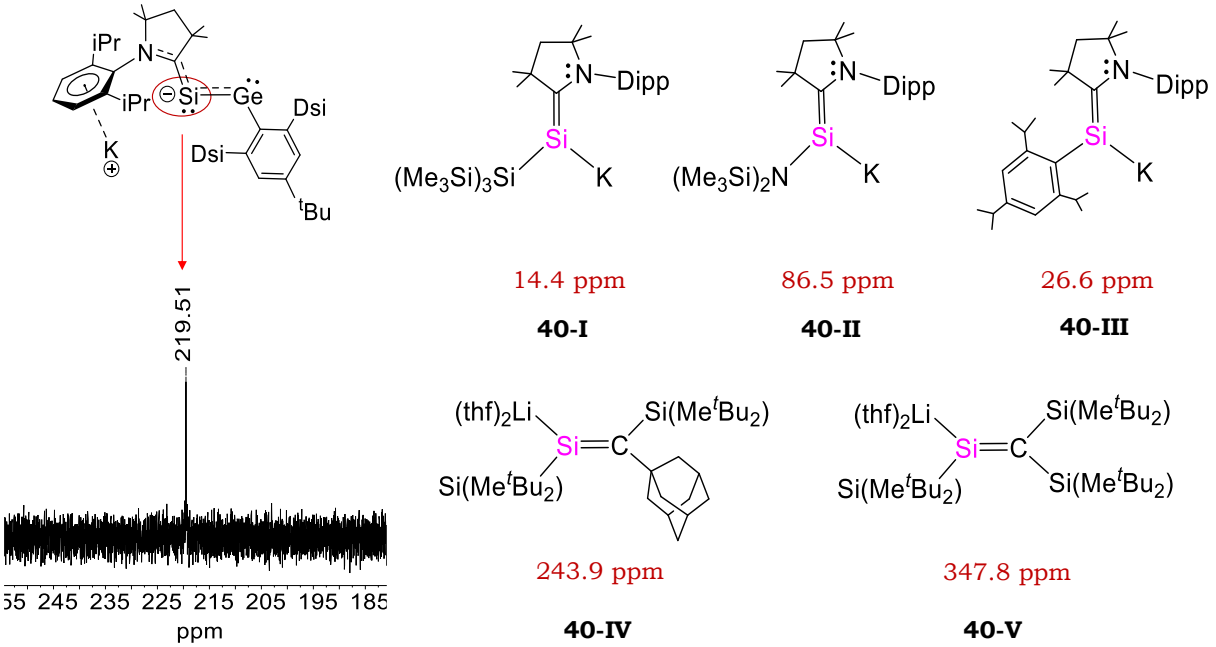

Figure 69. (*left*) An excerpt of the $^{29}Si\{^{1}H\}$ NMR spectrum of **40-Si** measured in (D_6) benzene at 298 K; (*right*) selected potassium and lithium silenides with their respective silicon resonance given below.

In the $^{29}Si\{^{1}H\}$ NMR spectrum of **40-Si** in (D_6)benzene, the silenic silicon appears as a distinct singlet at δ = 219.5 ppm, which is drastically down-field shifted compared with those reported in our group (**40-I**, **40-II**)[iv] and by Roesky *et al.* (**40-III**)[218] but considerably high-field shifted when compared to those for the lithium silenides (**40-IV**, **40-V**), reported by Apeloig *et al.*[215,216] Noteworthy to mention that the spectroscopic features such as the NMR chemical shifts or UV/vis absorption bands, and even the colour of silenides are strongly dependent on the nature of the silenide, whether it is solvent separated ion pair (SSIP) or a contact ion pair(CIP).[215]

The electronic structure of **40-Si** was investigated by quantum chemical calculations at the B97-D3(BJ)-ATM/def2-TZVP level of theory. Geometry optimization afforded a gas phase minimum structure and that is in good agreement with the experimental X-ray structure. Selected molecular orbitals of **40-Si** are depicted in ***Figure 68*** (e), and similar to its precursor **35-Si**. The Ge centered empty p orbital is appearing as LUMO, whereas the 3c-2e⁻ π bond between Si, Ge and C^{carb} atoms is represented by HOMO−1. Interestingly, the HOMO corresponds to the symmetric combination of the lone-pair orbitals of Si and Ge atoms. NRT analysis (***Figure 68*** (c & d)) shows that

two resonance structures contribute mainly to the resonance hybrid leading to NRT bond orders of 1.5 each for the Si–C^{carb} and Si–Ge bonds.

The reactivity of compound **35-Si** with a metallates was also studied. No reaction of **35-Si**, with Li[CpMo(CO)$_3$] was observed at ambient temperature, but upon thermal activation the germylidyne complex **41-Mo** (***Scheme 45***) formed selectively. Interestingly, analysis of the reaction solution by ^{1}H NMR spectroscopy did not provide any evidence for a $caac^{Me}$-Si containing product. Most probably $Si_2(caac^{Me})_2$ was eliminated, which is known to decompose at elevated temperature. Isolation of **41-Mo** in analytically pure form from this reaction mixture was not performed.

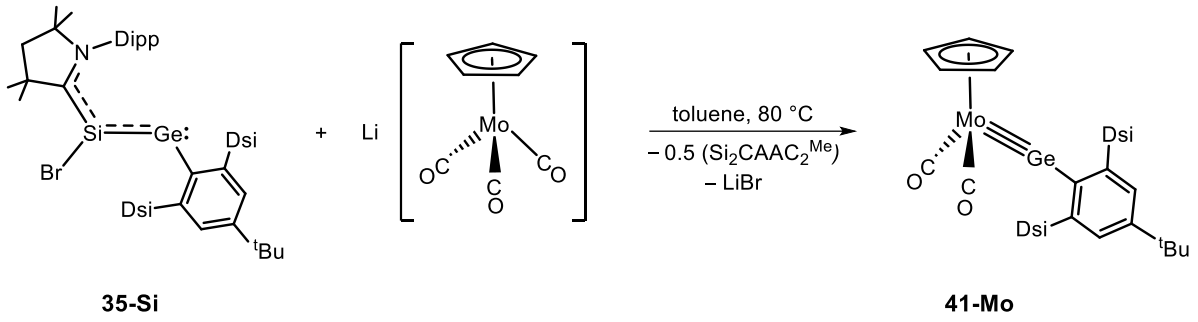

Scheme 45. Reaction of **35-Si** with a molybdenum metallate yielding a Mo-germylidyne complex.

To verify the outcome of the above reaction, the germylidyne complex **41-Mo** was independently prepared from (*E*)-Tbb(Br)Ge=Ge(Br)Tbb. First for this, when a colourless suspension of Li[CpMo(CO)$_3$] in toluene was treated with a yellow-orange solid of $Ge_2Br_2Tbb_2$ at ambient temperature (***Scheme 46***), no considerable colour change was observed, therefore the reaction mixture was heated at 80 °C for 2 hours. During this time, the reaction mixture gradually turned to a dark red suspension. Spectroscopic analysis of the reaction mixture revealed a complete consumption of the starting materials and a very selective formation of **41-Mo**, which was isolated after work-up as dark-red solid in 57 % yield.

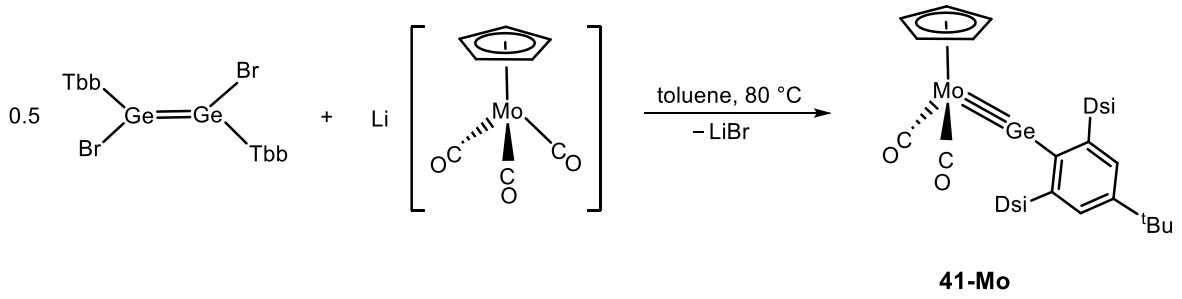

Scheme 46. Synthesis of the germylidyne complex **41-Mo** using a Ge(II) precursor.

Compound **41-Mo** is moderately air sensitive and a thermally robust ($T_{melt.}$ = 183 °C), dark-red solid, which can be stored under argon atmosphere at ambient temperature for several years. It is very well soluble in Et_2O, THF, *n*-hexane, benzene and toluene at ambient temperature. **41-Mo** was fully characterized by EA, IR and NMR spectroscopy. Additionally, clear orange block single crystals of **41-Mo** were grown upon slow cooling a saturated *n*-hexane solution at –30 °C and analyzed by sc-XRD. The solid-state structural parameters (***Figure 70*** *left*) as well as the spectroscopic features compare well with Cp-containing Mo-germylidyne complexes prepared earlier in our group.[219]

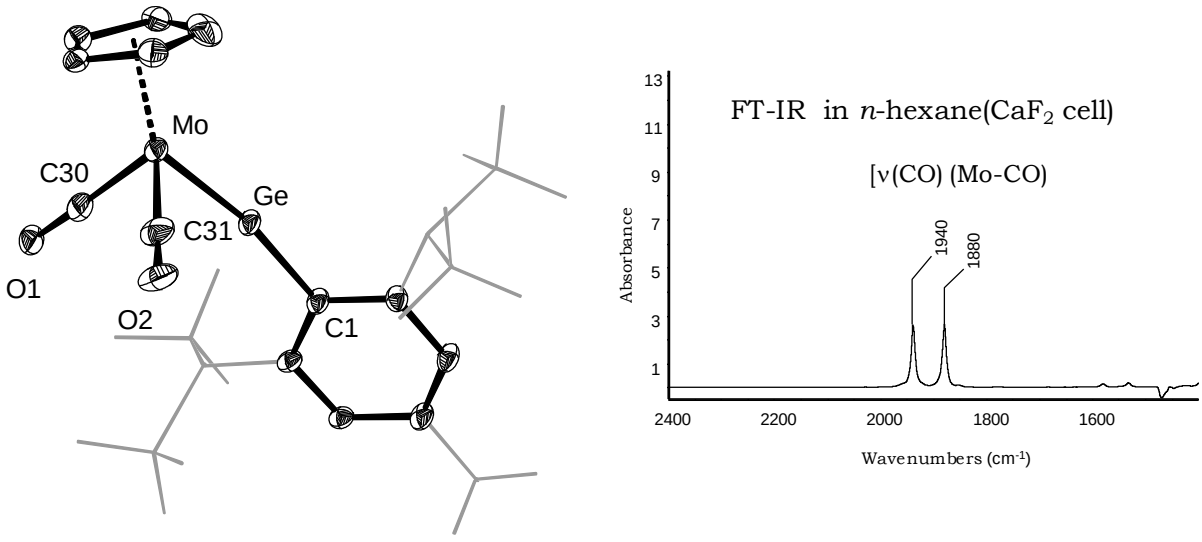

Figure 70. (*left*) DIAMOND plot of the molecular structure of **41-Mo**. Thermal ellipsoids are set at 30 % probability level. Hydrogen atoms are omitted, the Dsi and ^{t}Bu substituents of the Tbb group are presented in wire-frame for clarity. Selected bond lengths [Å] and bond angles [°]: Mo-Ge 2.2765(8), Mo-C30 1.942(8), Mo-C31 1.942(9), Mo-Ge-C1 166.5(2); (*right*) an FT-IR spectrum of isolated **41-Mo** measured in *n*-hexane using an IR cell of CaF_2 windows.

Considering the outcome of the reactions of Ge_2Tbb_2 with $SiBr_2(caac^{Me})$ and $Si_2Br_2(caac^{Me})_2$ further prompted me to carry out a synproportionation reaction of the disilicon(0) precursor, $Si_2(caac^{Me})_2$ with $Ge_2Br_2Tbb_2$, in the hope to obtain the $caac^{Me}$ supported germasilyne **35-Si** (***Scheme 47***). Surprisingly, the experimental outcome was totally different, and only the Lewis acid-base adduct **42-Ge** was witnessed in a reaction in which the soluble Si-containing products could not be detected.

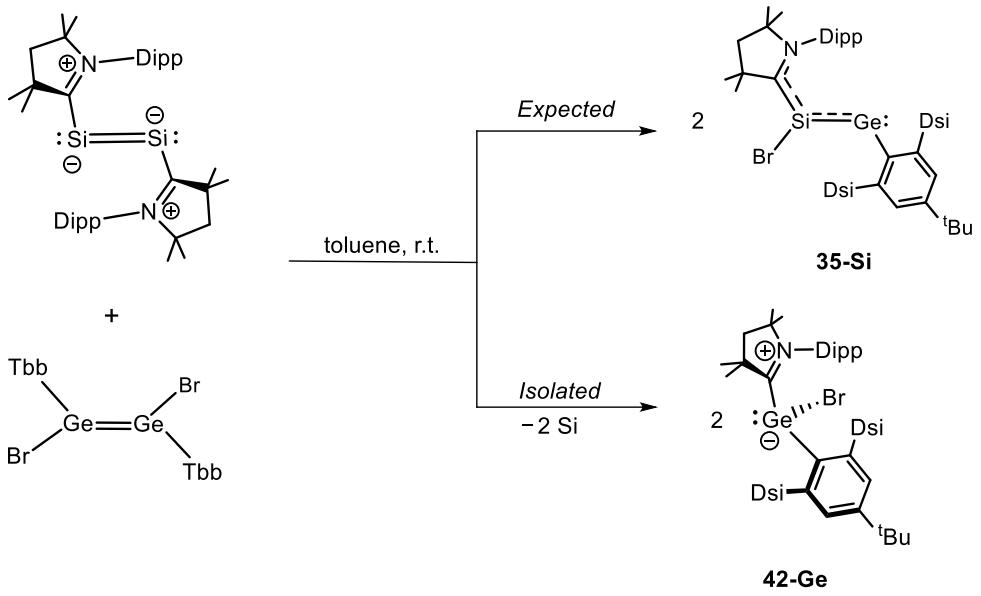

Scheme 47. Reaction of disilicon(0) precursor with $Ge_2Br_2Tbb_2$.

In fact, a dark purple toluene solution of $Si_2(caac^{Me})_2$ was added dropwise to a stirred yellow-orange suspension of $Ge_2Br_2Tbb_2$ in toluene at ambient temperature, the reaction proceeded fast with an immediate colour change first to dark green and then within 2-3 min it changed to orange-red. ^{1}H NMR spectroscopic analysis of the reaction solution revealed a complete consumption of the starting materials and selective formation of **42-Ge** along with some minor by products of unknown composition. Working up the reaction solution followed by crystallization of the crude product yielded analytically pure **42-Ge** in 52 % yield. The same compound could be also obtained upon reacting $caac^{Me}$ with $Ge_2Br_2Tbb_2$ at ambient temperature (***Scheme 48***). In fact, when a colourless benzene solution of $caac^{Me}$ was dropwise added to a stirred yellow-orange suspension of $Ge_2Br_2Tbb_2$ in benzene at ambient temperature, the suspension immediately turned to a clear orange-red solution. Analyzing the reaction solution by ^{1}H NMR spectroscopy revealed a complete consumption of the starting materials and the selective formation of **42-Ge**. Work-up followed by crystallization of the crude product from a Et_2O / THF mixture at –30 °C afforded **42-Ge** as orange-red crystals.

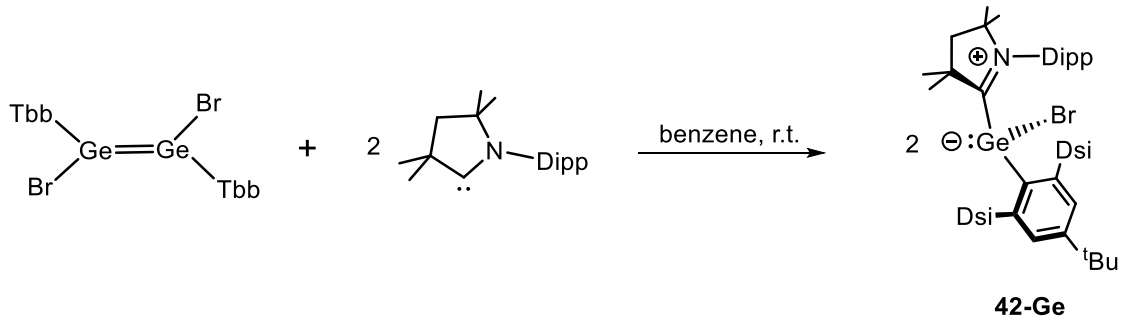

Scheme 48. Synthesis the $caac^{Me}$ adduct of TbbGeBr.

Compound **42-Ge** is an air sensitive, orange-red solid, which is well soluble in Et_2O, THF, *n*-hexane, benzene and toluene at ambient temperature. Under strict exclusion of air, a sample solution of **42-Ge** in (D_6)benzene under heating at 80 °C for 3 hrs. does not show any sign of decomposition. Apart from the EA, and NMR characterization, suitable single crystals (orangish-red planks) of **42-Ge** were grown via slow cooling of a saturated solution in Et_2O : THF (1.5 : 1, v/v) mixture at –30 °C, and were also analyzed by sc-XRD.

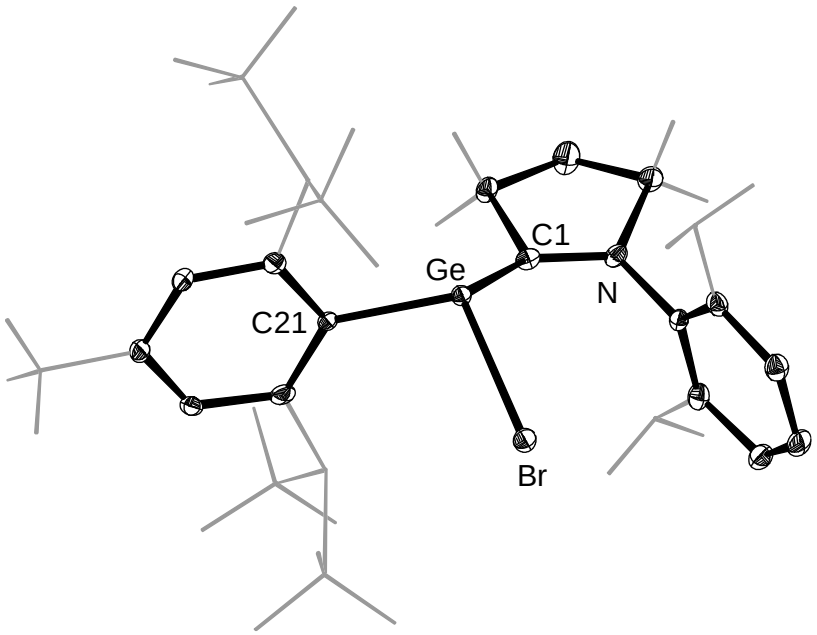

Figure 71. DIAMOND plot of the molecular structure of **42-Ge**. Thermal ellipsoids are set at 30 % probability level. Hydrogen atoms are omitted, the Dsi and ^{t}Bu substituents of the Tbb ligand, the ^{i}Pr substituents of Dipp group and the $C^{3,5}$ methyl groups of caac^{Me} are presented in wire-frame for clarity. Selected bond lengths [Å], bond angles [°] and torsion angles [°]: Ge-C1 2.033(3), Ge-C21 2.055(3), Ge-Br 2.4210(5), C1-N 1.330(3), C21-Ge-Br 103.46(7), C21-Ge-C1 116.83(11), C1-Ge-Br 102.20(7), N-C1-Ge-Br –53.745(13), N-C1-Ge-C21 –165.839(11).

The solid-state structure of compound **42-Ge** (***Figure 71***) reveals a trigonal-pyramidal Ge center ($\sum\angle$Ge = 322.5°) with a Ge–C^{CAAC} bond length of 2.033(3) Å, closely resembling that of the Ge–C^{Tbb} bond (2.055(3) Å). This alignment is consistent with previously reported carbene adducts of germylenes,[220–223] wherein the germanium center is expected to adopt a pyramidal geometry due to the presence of a stereochemically active lone pair. However, in solution, the C_1-symmetric solid-state structure of **42-Ge** is not retained. This is evident from the ^{1}H and $^{13}\{^1H\}$ NMR spectra, which exhibit only one set of symmetric signals for both the Tbb and caac^{Me} ligands, respectively, and suggest a facile pyramidal inversion of **42-Ge** in solution.

2.10. Emulating the alkyne–vinylidene rearrangement in the context of heavier main group chemistry

Presuming that the cationic sila-germavinylidene **39-Si** holds a considerable synthetic potential, several reactions were tested. However, most of the test reactions (with e.g. $Ar^{Mes}Li$, 2-butnye, 1-dimethylamino-2-phenylacetylene, $Ar^{Mes}GeCl$, $Ar^{Mes}SnCl$, metallates, $TMSC(H)N_2$, CO, KC_8 and so on), remained either unreacted or mainly unselective. Finally, the halide transfer reagent (NEt_4Br) was found to react with **39-Si** leading to **43-Si**, which is a constitutional isomer of **35-Si** (***Scheme 49***).

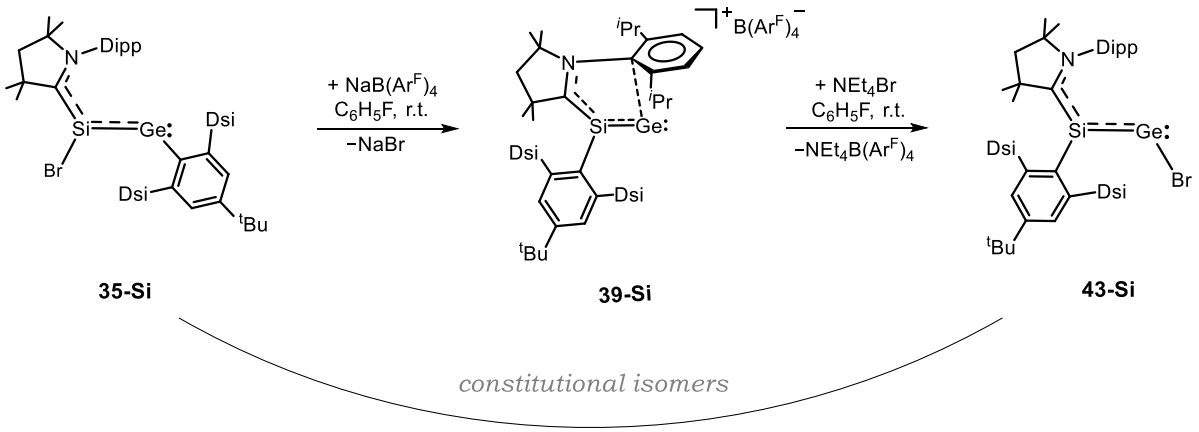

Scheme 49. Reaction of the vinylidene **39-Si** with NEt_4Br.

In fact, when an ink-blue fluorobenzene solution of **39-Si** was treated with one equivalent of NEt_4Br at ambient temperature, the colour of the reaction solution gradually changed from blue to greenish-blue and finally to pine-green. After 4 hours of stirring, analysis of an aliquot of the reaction solution by ^1H no-D NMR spectroscopy revealed a complete consumption of the starting materials and the selective formation of **43-Si**. Following an acetonitrile/Et_2O work-up compound **43-Si** was obtained as an analytically pure solid in 87 % yield. It is an air sensitive pine-green solid, which is very well soluble in Et_2O, THF, *n*-hexane, benzene and toluene, but insoluble in acetonitrile at ambient temperature. Suitable plate shaped single crystals of **43-Si** were grown upon slow evaporation of its saturated Et_2O/CH_3CN solution at ambient temperature inside the glove box.

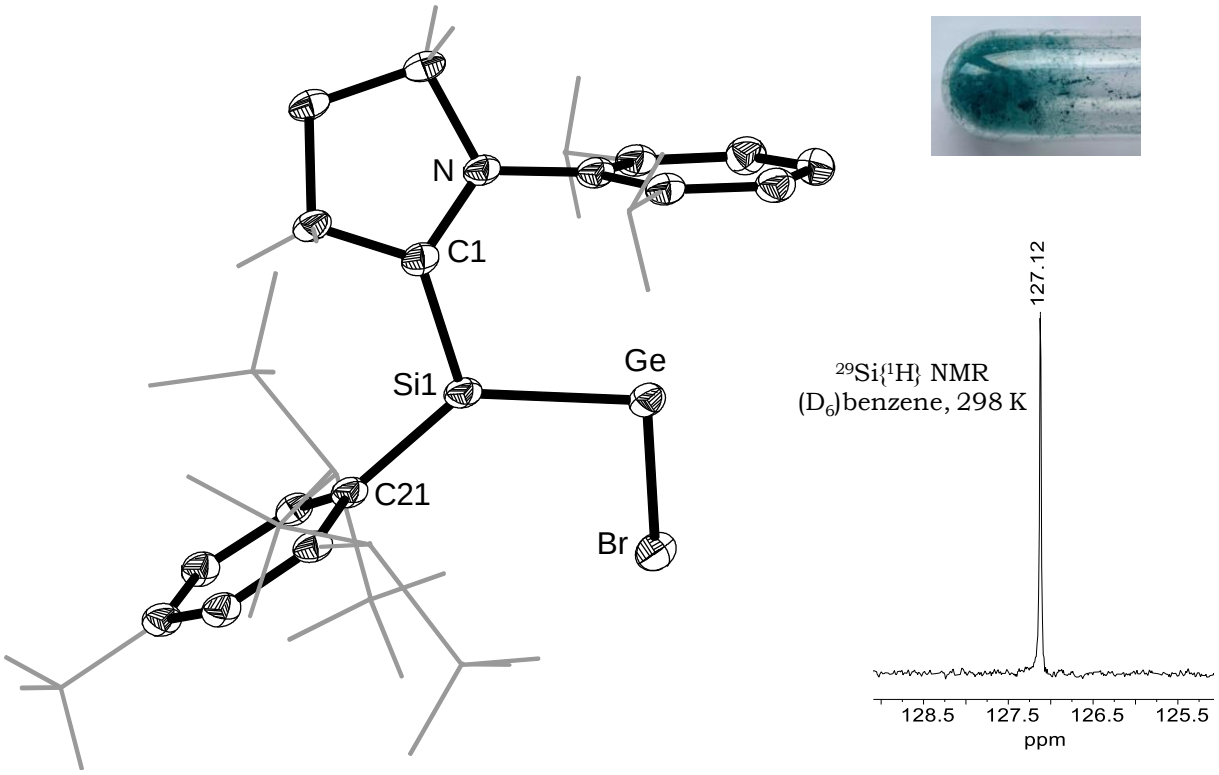

Figure 72. (*left*) DIAMOND plot of the molecular structure of **43-Si**. Thermal ellipsoids are set at 30 % probability level. Hydrogen atoms are omitted, the Dsi and ^{t}Bu substituents of the Tbb ligand, the ^{i}Pr substituents of Dipp group and the C^{3,5} methyl groups of caac^{Me} are presented in wire-frame for clarity. Selected bond lengths [Å], bond angles [°] and torsion angle [°]: Ge-Si1 2.3556(9), Si1-C1 1.830(3), C1-N 1.359(4), Ge-Br 2.4419(5), C1-Si1-Ge 112.62(11), C1-Si1-C21 114.15(14), Ge-Si1-C21 133.22(10), Si1-Ge-Br 100.00(3), N-C1-Si1-Ge 8.038(3), C1-Si1-Ge-Br –155.367(2), N-C1-Si1-C21 –170.716(2), C21-Si1-Ge-Br 23.015(3); (*right top*) a picture of the isolated solid of **43-Si**; (*right bottom*) an excerpt of the ^{29}Si{^{1}H} spectrum of isolated **43-Si** measured at 298 K.

The molecular structure of **43-Si** (***Figure 72*** *left*) resembles to its isomer **35-Si**. It features (a) a trigonal planar coordinated silicon center ($\sum\angle$(Si1) = 360°) connected to a bent, di-coordinated germanium atom ($\angle$(Br–Ge–Si) = 100.0(1)°), (b) a coplanar arrangement of the carbene to the molecular core, as evidenced by the torsion angle (N^{carb}–C^{carb}–Si–Ge) of 8.1(1)°), and (c) an anticlinal C^{carb}–Si–Ge–Br skeleton as shown by the torsion angle of 155.4(1)°, which is ca. 20° lower than that of **35-Si**. Interestingly, the Si–C^{carb} bond of **43-Si** (1.830(3) Å) remains same as compared to that of **35-Si**, whereas the Si–Ge bond (2.3556(9) Å) is modestly elongated, when compared to **35-Si**.

In solution, the ^{1}H, ^{13}C{^{1}H} and ^{29}Si{^{1}H} NMR spectra of **43-Si** in (D$_6$)benzene are well corroborating its C_S-symmetric molecular structure found in the solid-state. However, unlike the Ge–C^{Tbb} rotation of its isomer **35-Si**, the Si–C^{Tbb} rotation is frozen out on the NMR time scale, hence, two singlets are observed for the diastereotopic SiMe$_3$ groups. The ^{29}Si{^{1}H} NMR spectrum of **43-Si** in (D$_6$)benzene at 298 K displays a

resonance at δ = 127.1 ppm for the tricoordinated Si atom, which is considerably low-field shifted compared with **35-Si** (85.8 ppm) and its NHC analogue **37-Si** (48.2 ppm).

An astonishing observation was made when a toluene solution of **43-Si** was heated at 105 °C for 1 hour. The colour of the solution gradually changed from green to dark-blue. The spectroscopic analysis of the reaction solution revealed a complete and quite selective conversion of **43-Si** to **44-Si** (***Scheme 50***) along with some minor unknown side products. Working-up of the reaction solution followed by crystallization from *n*-pentane allowed the isolation of dark blue crystals of **44-Si** in NMR spectroscopically pure form. Notably, the compound **44-Si** was previously prepared in our group following a different approach and all analytical and structural data (X-ray) are reported in the PhD thesis of F. Gstrein.[iv] **44-Si** is an air sensitive, pyrophoric dark blue solid which can be stored inside the glove box at ambient temperature for several months. It is well soluble in Et_2O, *n*-hexane, benzene and toluene at ambient temperature.

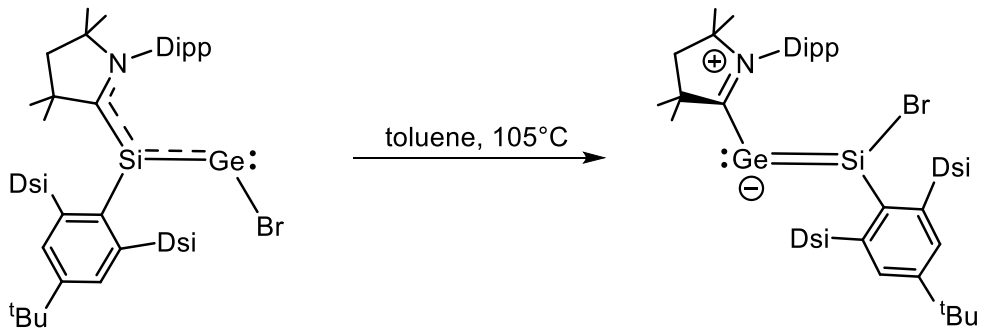

43-Si **44-Si**

Scheme 50. Formal transformation of a germasilyne to its constitutional isomer, a germasilavinylidene.

It is worth noting that the reaction described above represents a unique occurrence in low-valent heavier tetrel chemistry. In this reaction, formally a caac^{Me}-supported ditetrelyne transforms into its vinylidenic isomer.This is the reverse reaction of the Fritsch–Buttenberg–Wiechell (FBW) rearrangement witnessed in carbon chemistry.[224–227] The $^{29}Si\{^1H\}$ NMR spectrum of **44-Si** in (D_6)benzene at 298 K displays a resonance at δ = 120.4 ppm (***Figure 73***) for the tricoordianted Si atom, which is quite similar, when compared to that of its precursor.

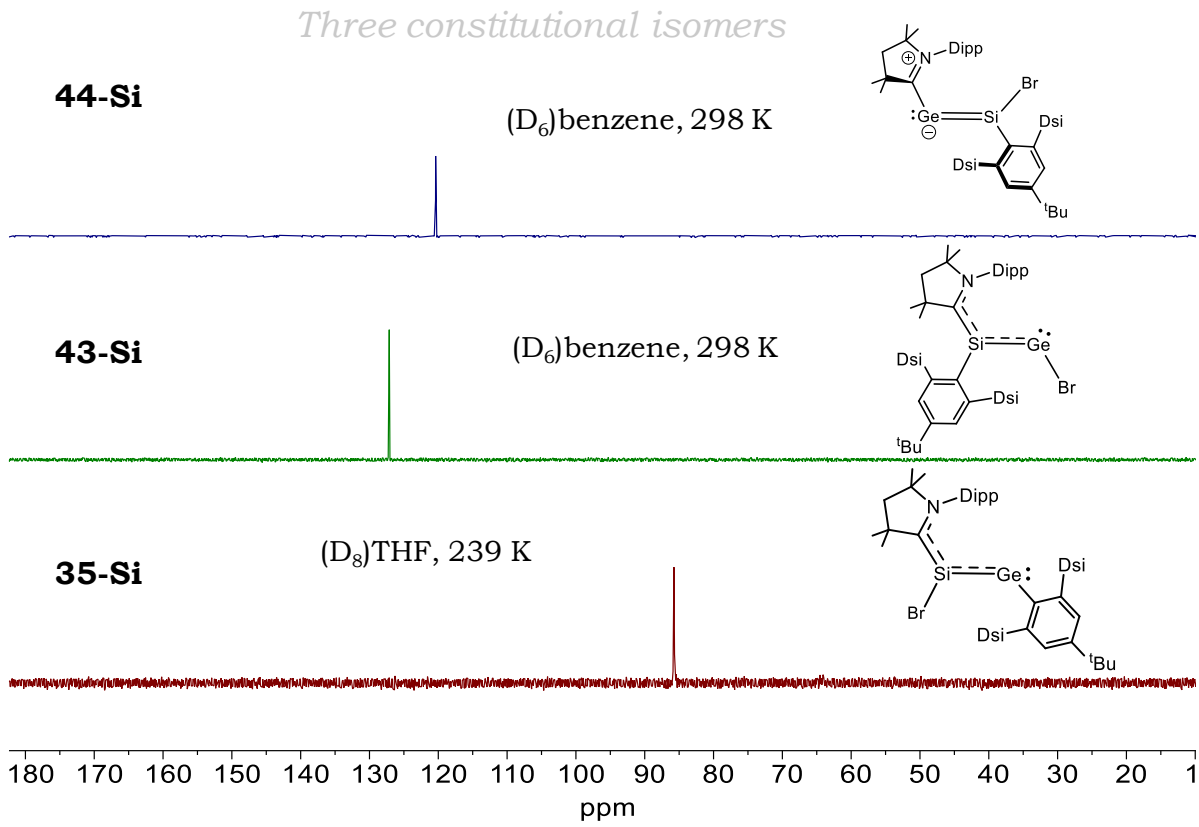

Figure 73. A stack plot of the selected excerpts of the $^{29}Si\{^{1}H\}$ NMR spectra of the compounds **35-Si**, **43-Si** and **44-Si**.

While **39-Si** did not react with CO, its non-gaseous surrogate, an isocyanide (MesNC), selectively reacted and produced an isocyanide adduct of the cationic vinylidene (***Scheme 51***). In fact, when a colourless fluorobenzene solution of MesNC was added into an ink blue solution of **39-Si** at ambient temperature, the colour of the reaction solution immediately changed to cyan. ^{1}H NMR spectroscopy revealed a complete and selective transformation of **39-Si** into **45-Si**. After work-up of the reaction solution, **45-Si** was obtained as an analytically pure solid in 91 % yield.

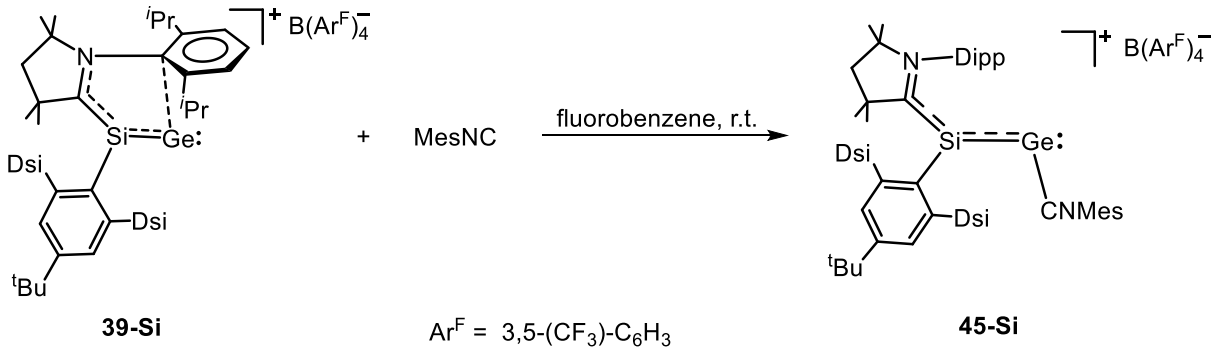

Scheme 51. Reaction of the cationic vinylidene with MesNC forming the isocyanide adduct **45-Si**.

Compound **45-Si** is an air-sensitive cyan solid that exhibits good solubility in solvents such as Et_2O, fluorobenzene, and dichloromethane, but it is insoluble in aliphatic

solvents at ambient temperature. Its melting point associated with decomposition is 157°C. Under strict exclusion of air, a solution of **45-Si** in (D_2)dichloromethane shows minimal decomposition after 5 hours at ambient temperature. The spectroscopic and single-crystal X-ray diffraction (sc-XRD) characterization facilitated a comprehensive elucidation of the molecular attributes. Suitable block-shaped single crystals of **45-Si•C_6H_6** were obtained upon slow cooling of a saturated benzene/fluorobenzene solution at 4 °C.

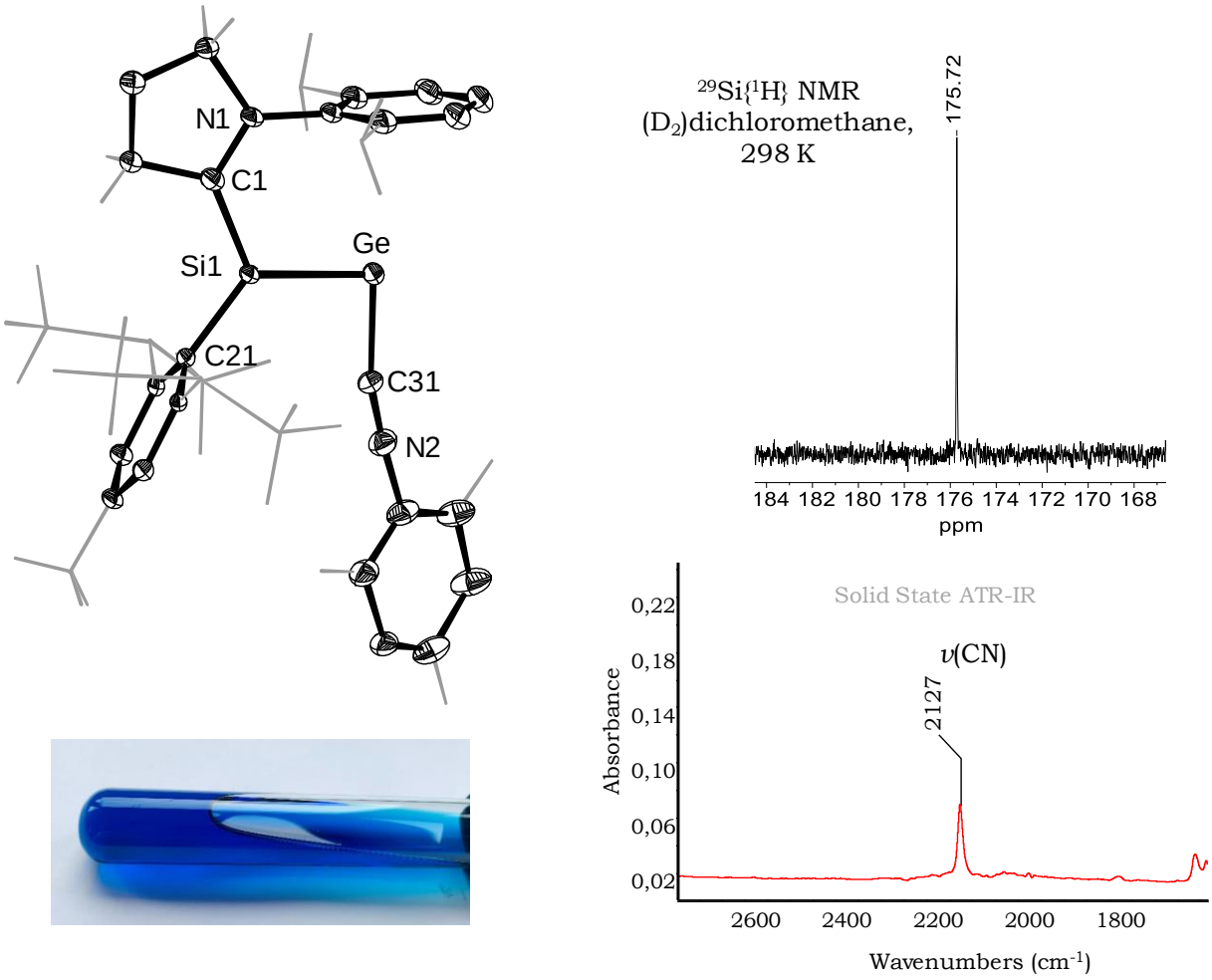

Figure 74. (*top left*) DIAMOND plot of the molecular structure of **45-Si**. Thermal ellipsoids are set at 30 % probability level. Hydrogen atoms are omitted, the Dsi and ^{t}Bu substituents of the Tbb ligand, the ^{i}Pr substituents of Dipp group, the $C^{2,4,6}$ methyl groups of Mes ligand and the $C^{3,5}$ methyl groups of $caac^{Me}$ are presented in wire-frame for clarity. Selected bond lengths [Å], bond angles [°] and torsion angles [°]: Si1-Ge 2.2908(14), Si1-C1 1.887(5), C1-N1 1.348(6), Ge-C31 2.008(5), C31-N2 1.181(7), C1-Si1-Ge 113.46(17), C1-Si1-C21 120.2(2), C21-Si1-Ge 126.36(15), Si1-Ge-C31 91.08(15), N1-C1-Si1-Ge –6.414(2), N1-C1-Si1-C21 172.735(1); (*top right*) an excerpt of the $^{29}Si\{^1H\}$ NMR spectrum of **45-Si** measured at 298 K; (*bottom left*) a sample solution of isolated **45-Si** in fluorobenzene; (*bottom right*) an excerpt of the solid state ATR-IR spectrum of **45-Si**.

The solid-state structural parameters (***Figure 74*** *top left*), **45-Si** shows considerable elongation of the Si–C^{carb} (1.887(5) Å) bond when compared to that of its precursor, but the Si–Ge distance (2.2908(14) Å) remains nearly unchanged. The angle at the Ge center (Si1-Ge-C31 91.08(15)°) reflects the orthogonal coordination of the isocyanide molecule, resulting from interaction of the lone pair of C^{iso} with the in-plane empty p orbital at Ge of **39-Si**. The Ge–C^{iso} bond length (Ge-C31 2.008(5) Å) is consistent with a typical Ge–C single bond and is quite similar to that observed in a previously reported germanium-isocyanide complex (2.075(3) Å) described by Power *et al.*[228] In the solid-state ATR-IR spectrum of **45-Si** (***Figure 74*** *bottom right*), the CN stretching vibration is observed at a wavenumber of 2127 cm^{-1}. Interestingly, this value is even higher than that of free MesNC molecule, which has a CN stretching vibration at a wavenumber of 2112 cm^{-1}. This difference in wavenumbers can likely be attributed to the absence of backdonation from germanium (Ge) to the π* orbital of the C≡N bond in the isocyanide molecule.

The tricoordinated silicon (Si) atom in **45-Si** appears as a distinct singlet in the $^{29}Si\{^{1}H\}$ NMR spectrum at a chemical shift (δ_{Si}) of 175.7 ppm. Notably, this chemical shift is similar to that observed in its precursor **39-Si**. This similarity suggests that the local electronic environment around the tricoordinated Si atom remains largely unchanged from the precursor compound.

The gas phase structure of the cation in **45-Si** was obtained after structure optimization starting from the X-ray structure. The silicon atom keeps the trigonal-planar orientation (∑∠(Si1) = 360.0°), as the MesNC ligand attacks the in-plane p-orbital at Ge in **39-Si**, forming a bond with a Ge–C distance of 200.5 pm. By this, the electron lone-pair of Ge is preserved, which leads to a rather narrow Si–Ge–C^{iso} angle of 90.3°. Other features of **39-Si**, like the co-planar and orthogonal arrangements of the $caac^{Me}$ and Tbb substituents to the C^{carb}–Si–C^{Tbb}–Ge plane, respectively, are also retained in **45-Si**. The isonitrile unit is not fully linear as the Ge–C–N angle amounts to 162.6°.

The analysis of the molecular orbitals of the cation in **45-Si$_{calc}$** shows again the 3c-2e⁻ π-bond between C^{carb}, Si and Ge in the HOMO, with a slightly larger contribution between Si and Ge. The LUMO is a π*(Ge–Si) orbital mainly mainly localized at Ge with some Ge–C^{iso} π-bonding contributions, and some Si–C^{carb} π-bonding contribution. The remaining lone pair at Ge is splited into the HOMO−3 and HOMO−2 and lies in-plane, as already discussed above.

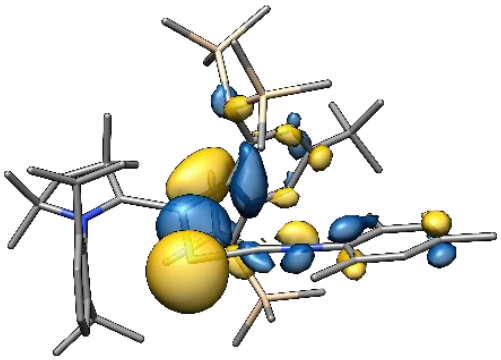

HOMO−3 [−8.06]

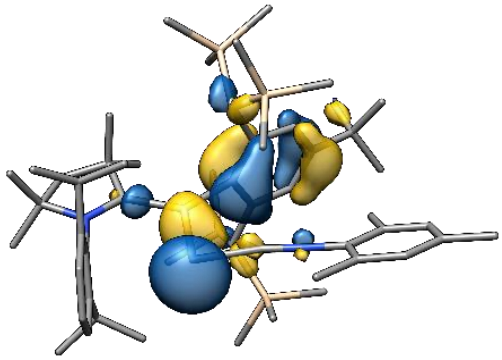

HOMO−2 [−7.47]

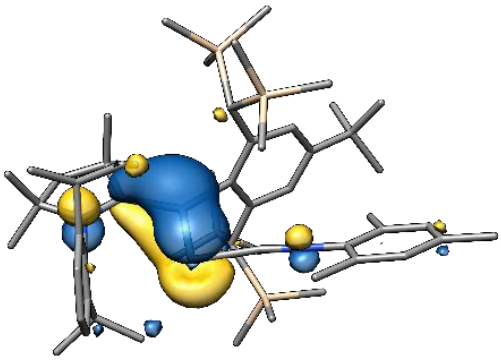

HOMO [−6.84]

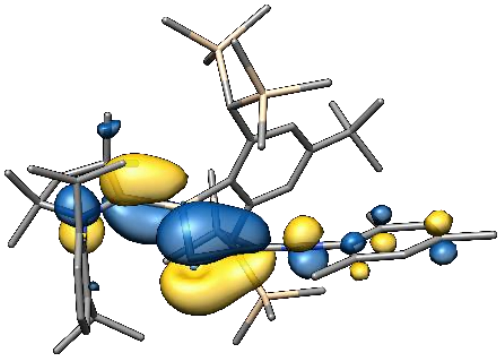

LUMO [−5.66]

Figure 75. Selected molecular orbitals of cation in **45-Si$_{calc}$** and their orbital energies in eV. The isosurface value is set to 0.04 $e^{1/2}$ $Bohr^{-3/2}$.

Table 8. Selected structural and NMR spectroscopic parameters of the caac^{Me} containing compounds included in this thesis.

Comp.	d(Si–Ge)/ Å	d(Si–C^{carb})/ Å	d(N–C^{carb})/ Å	∠(Ge)/(°)	φ[a]/(°)	$\delta_{(Si caac^{Me})}$/ ppm	$\delta_{(C^{carb})}$/ ppm	$\delta_{(N)}$/ ppm
35-Si	2.3265(13)	1.829(4)	1.336(5)	100.62(12)	–9.987(3)	85.7	208.4	177.0
38-Si	2.3439(4)	1,8499(15)	1.3583(18)	110.97(4)	10.908(3)	105.4	208.6	171.6
39-Si	2.3057(5)	1.7928(18)	1.361(2)	-	–2.702(2)	182.7	235.6	193.8
40-Si	2.346(3)	1.865(11)	1.349(11)	103.4(2)	158.629(23)	219.5	234.8	166.8
43-Si	2.3556(9)	1.830(3)	1.359(4)	100.00(3)	8.038(3)	127.1	211.1	157.9
44-Si	2.249(1)	-	1.318(3)	105.5(1)	136.4(2)[b]	120.4	255.4	205.5
45-Si	2.2908(14)	1.887(5)	1.348(6)	91.08(15)	–6.414(2)	175.7	218.9	209.4

(a): the dihedral angle defined as (∠N–C^{carb}–Si1–Ge); (b): the torsion angle defined as (∠N–C^{carb}–Ge–Si1).

2.11. Extension of titanium-tetrylidyne chemistry

As part of an ongoing project involving titanium silylidyne and titanium germylidyne chemistry, I conducted the synthesis of some ylidyne complexes[229] (***Scheme 52***) and investigated their reactivity with small nucleophiles such as PMe_3 and isocyanide. The germylidyne complex **47-Ti** bearing a Ge-bonded Tbb substituent was synthesized following the same procedure as previously described for the Ar^{Mes} analogue by our group.[230] It was successfully isolated as an analytically pure solid with a yield of 71%. Like its Si analogue **46-Ti**, compound **47-Ti** is highly air sensitive dark-brown, thermally robust solid ($T_{melt.}$ = 185 °C). It is well soluble in *n*-hexane and highly soluble in benzene and THF at ambient temperature.

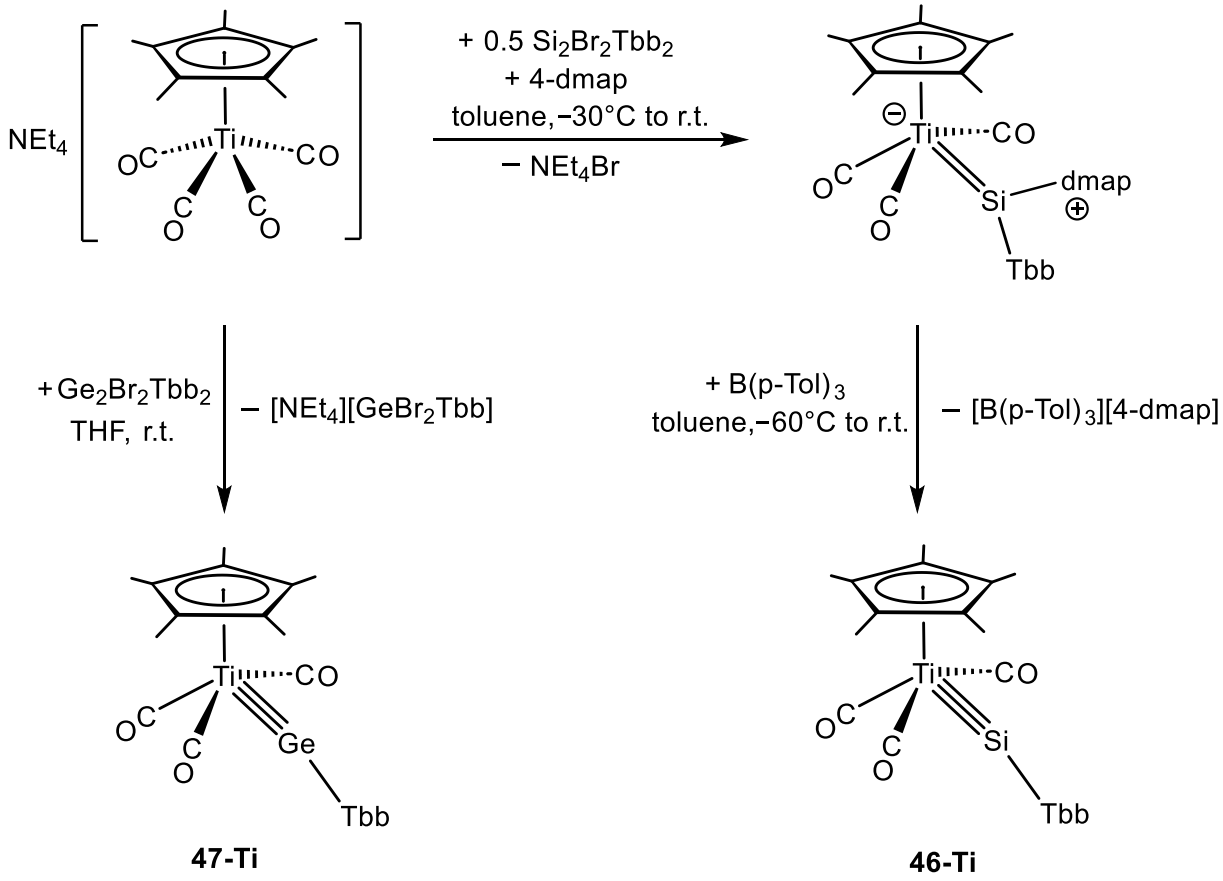

Scheme 52. Synthesis of titatnium silylidyne (**46-Ti**) and titanium germylidyne (**47-Ti**) following the existing procedures in our group.

Suitable single crystals (clear reddish-violet blocks) of **47-Ti** were obtained upon slow evaporation of a saturated *n*-pentane solution at –30 °C inside the glove-box freezer. The crystallographic parameters of **47-Ti** match precisely with those previously described for the titanium germylidyne complex featuring a Ar^{Mes} substituent.[230]

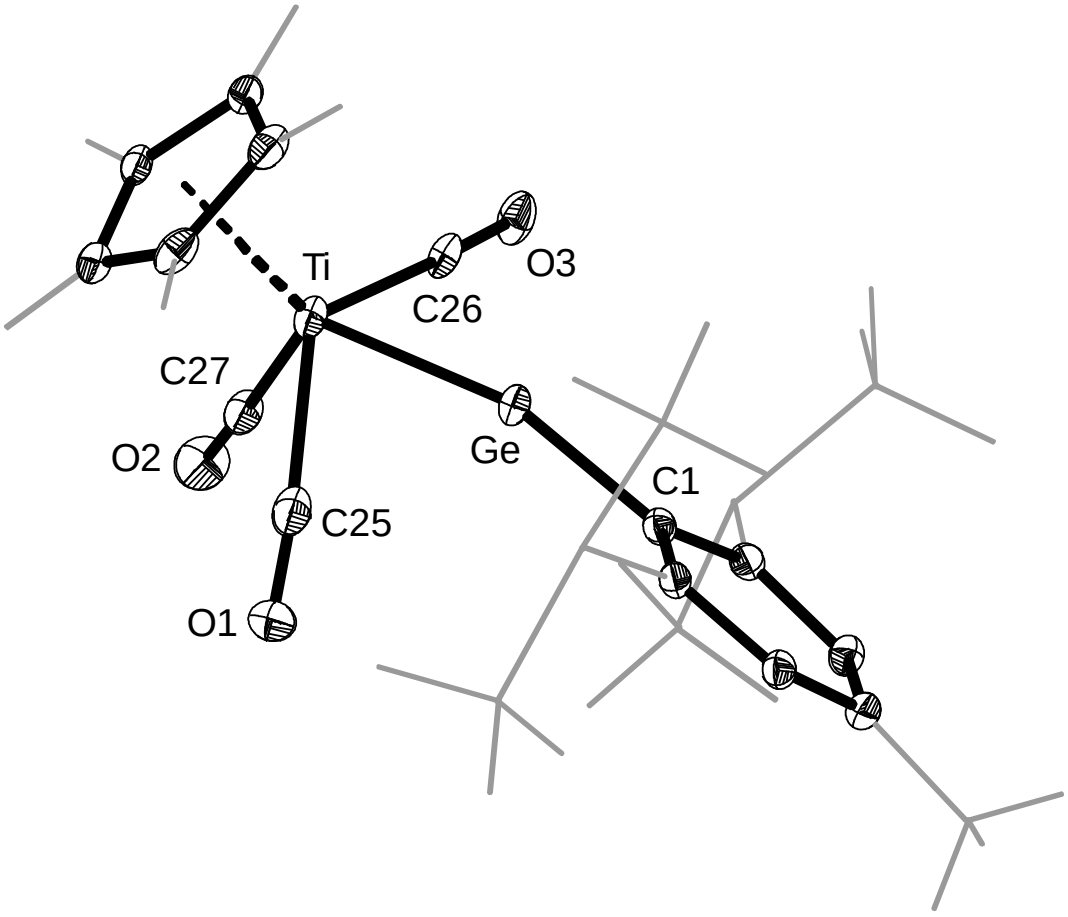

Figure 76. DIAMOND plot of the molecular structure of **47-Ti**. Thermal ellipsoids are set at 30 % probability level. Hydrogen atoms are omitted, the Dsi and ^{t}Bu substituents of the Tbb ligand and the methyl groups of Cp* ligand, are presented in wire-frame for clarity. Selected bond lengths [Å] and bond angles [°]: Ti-Ge 2.3260(4), Ti-C25 2.039(3), Ti-C26 2.064(3), Ti-C27 2.067(3), C25-O1 1.159(3), Ge···C25 2.479(2), Ti-Ge-C1 162.64(6), C25-Ti-Ge 68.86(6), C26-Ti-Ge 75.77(6), C27-Ti-Ge 111.16(7).

Following the successful isolation of compounds **46-Ti** and **47-Ti**, I proceeded with their subsequent reaction with PMe_3, leading to the isolation of mono PMe_3-substituted titanium tetrylidyne complexes, **48-Ti** and **49-Ti** (***Scheme 53***).

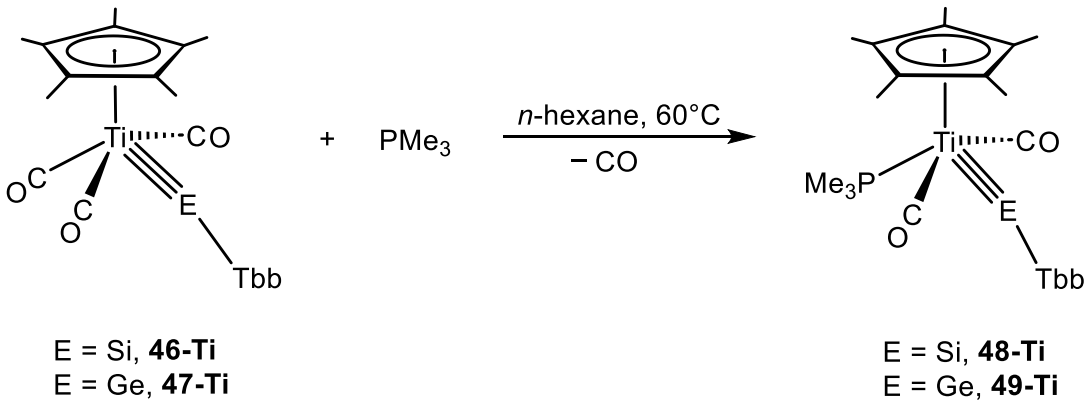

E = Si, **46-Ti**
E = Ge, **47-Ti**

E = Si, **48-Ti**
E = Ge, **49-Ti**

Scheme 53. CO substitution reaction of Ti-tetrylidyne complexes by a PMe_3 ligand.

When a brownish-purple solution of **46-Ti** and PMe_3 (1.04 equiv.) in *n*-hexane was heated at 60 °C in a closed Schlenk tube, the colour of the reaction solution gradually changed to dark red. In both cases, a quantitative reaction was observed as evidenced by the presence of only one singlet resonance in the $^{31}P\{^1H\}$ NMR spectra ($\delta(^{31}P)$ = 14.4 (**48-Ti**), 11.2 ppm (**49-Ti**). After work-up and crystallization of the crude products from *n*-pentane both compounds were obtained as analytically pure solids in good yield. Compounds **48-Ti** and **49-Ti** are extremely air sensitive dark red solids, decolorizing immediately upon contact with air. They are well soluble in *n*-hexane, diethyl ether, benzene and toluene at ambient temperature. The melting associated decomposition of **48-Ti** occurs at 185 °C, and that of **49-Ti** occurs at 224 °C.

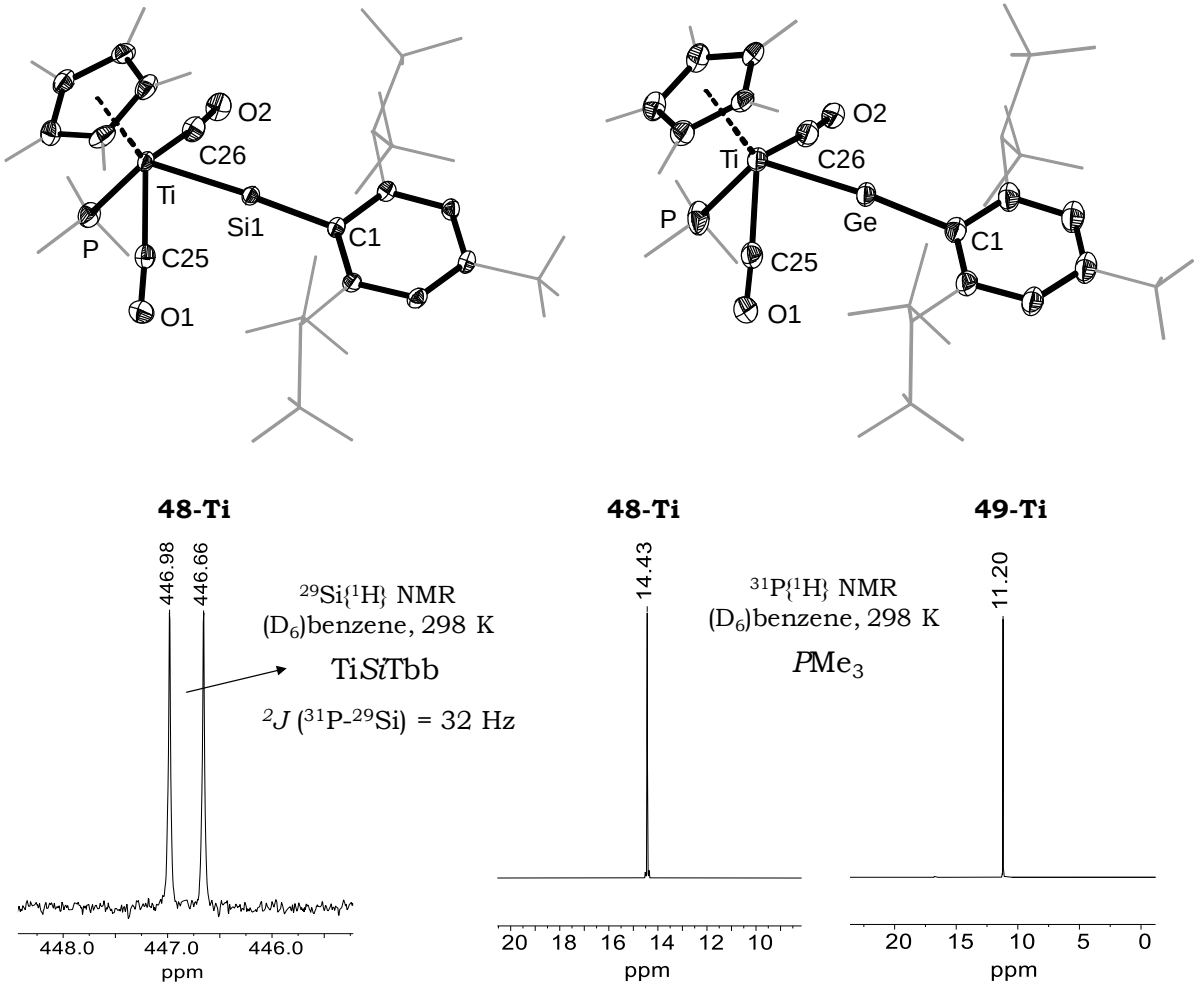

Figure 77. DIAMOND plot of the molecular structure of **48-Ti** (*top left*) and **49-Ti** (*top right*). Thermal ellipsoids are set at 30 % probability level. Hydrogen atoms are omitted, the Dsi and ^{t}Bu substituents of the Tbb ligand, the methyl groups of Cp* and PMe_3 ligands are presented in wire-frame for clarity. Selected bond lengths [Å] and bond angles [°]: **48-Ti**: Ti-Si1 2.2879(5), Ti-P 2.5581(6), Ti-C25 2.017(2), Ti-C26 2.010(2), Ti-Si1-C1 175.79(6), C25-Ti-Si1 72.01(5), C26-Ti-Si1 72.10(5), P-Ti-Si1 110.35(2); **49-Ti**: Ti-Ge 2.3223(7), Ti-P 2.5455(12), Ti-C25 2.031(4), Ti-C26 2.030(4), Ti-Ge-C1 175.08(10), C25-Ti-Ge 74.41(10), C26-Ti-Ge 72.29(10), P-Ti-Ge 112.36(4); (*bottom left*) an excerpt of the $^{29}Si\{^1H\}$ NMR spectrum of **48-Ti**; (*bottom middle and right*) $^{31}P\{^1H\}$ NMR spectra of **48-Ti** and **49-Ti**, respectively.

In combination with EA, NMR and IR spectroscopy, **48-Ti** and **49-Ti** were also characterized by sc-XRD. Suitable single crystals of **48-Ti** (clear red plates) and **49-Ti** (clear red blocks) were grown upon slow cooling of their respective saturated *n*-hexane solutions at –30 °C.

The molecular structure of **48-Ti** unequivocally confirmed the substitution of the diagonal carbonyl ligand by a trimethyl phosphane ligand with the silicon center adopting a nearly linear coordination as evidenced by the ∠Ti-Si1-C1 bond angle of 175.79(6)°and featuring a short Ti–Si1 bond length of 2.2879(5) Å. Notably, these bonding parameters closely align with those observed in its precursor **46-Ti** (Ti-Si1 2.2845(6) Å and ∠Ti-Si1-C1 162.94(6), see section ***5.3***) and the Ti-silylidyne complex (η^5-C_5Me_5)$(CO)_3$Ti≡Si(Eind) (Ti-Si1 2.2979(5) Å and ∠Ti-Si1-C1 166.32(6)), reported in the PhD thesis of N. Wienkenhöver.[229] Similarly, the structural data of the germylidyne complex **49-Ti** (Ti-Ge 2.3223(7) Å and Ti-Ge1-C1 175.08(10)°), resemble well to those found for the Ti-germylidyne complex [Cp*$(CO)_2PMe_3$Ti≡$GeAr^{Mes}$] reported in the PhD thesis of A. Lülsdorf.[230] Characteristic IR [ν(CO)] absorption bands (***Figure 78***) for **48-Ti** (ν_{CO} = 1834, 1780 cm^{-1}) and **49-Ti** (ν_{CO} = 1851, 1802 cm^{-1}) were observed in the attenuated total reflection (ATR) IR spectra.

The ^{29}Si NMR spectrum of **48-Ti** shows a distinct doublet at 446.8 ppm($^2J(^{31}P$-^{29}Si) = 32 Hz), which is even more low-field shifted than its precursor **46-Ti** (433.8 ppm). Notably, the δ_{Si} for **46-Ti** and **48-Ti** are the most deshielded ^{29}Si NMR signals observed so far for silylidyne complexes.

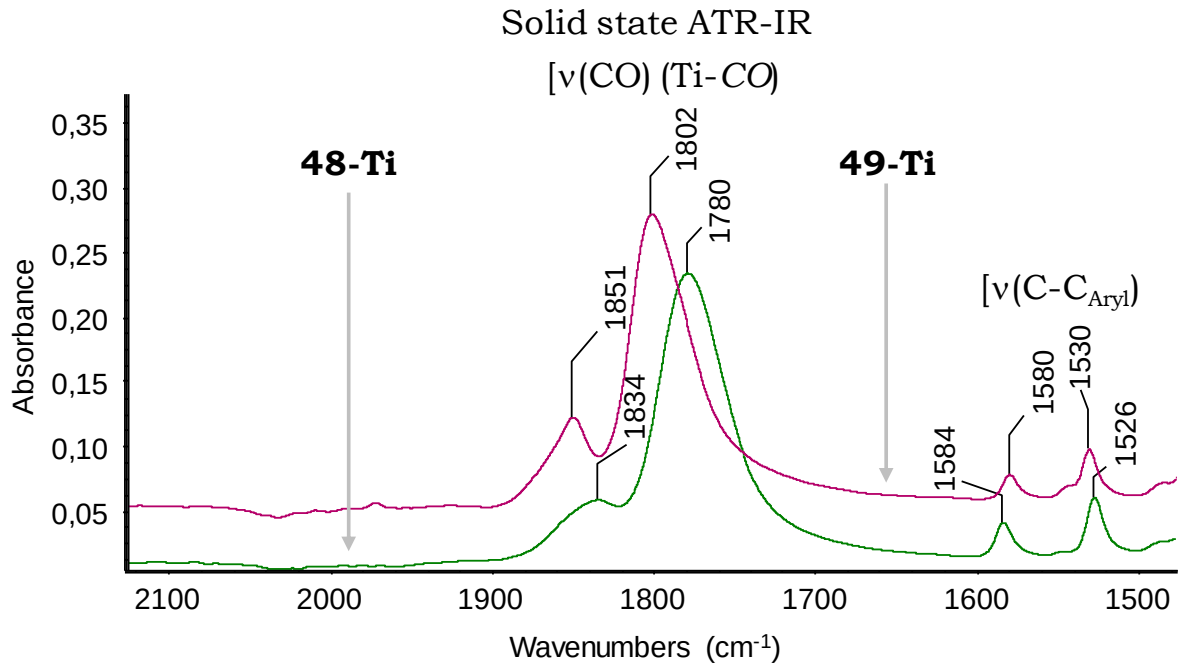

Figure 78. A stack plot of excerpts of the ATR-IR spectra of pure **48-Ti** and **49-Ti**, showing the CO stretching vibrations.

Another successful reaction involving **47-Ti** occurred with MesNC, affording the selective formation of complex **50-Ti**. When a brown reaction solution of **47-Ti** with two equivalents of MesNC in *n*-hexane was heated at 50 °C for 30 hrs. The brown color the solution gradually turned to dark green. Analysis of the reaction solution by IR and ^{1}H NMR spectroscopy revealed a complete consumption of **47-Ti** and the selective formation of the monocarbonyl-diisonitrile complex **50-Ti**.

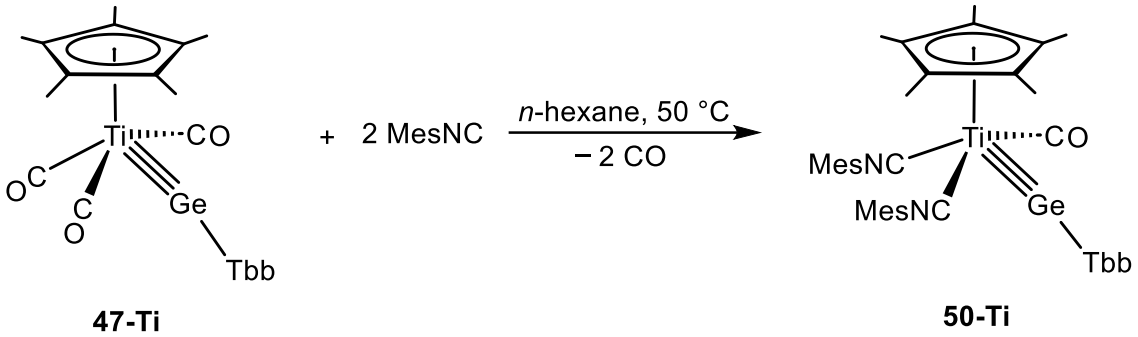

47-Ti **50-Ti**

Scheme 54. Substitution of two CO ligands by isocyanides.

After work-up and a crystallization of the crude product from Et_2O at –60 °C, **50-Ti** was isolated as an analytically pure solid in 56 % yield. It is a highly air sensitive dark green solid, decolorizing immediately upon contact with air. It is well soluble in *n*-hexane, diethyl ether, benzene and toluene, but insoluble in acetonitrile at ambient temperature. Compound **50-Ti** exhibits reduced thermal stability compared to its precursor **47-Ti**, as evidenced by its lower melting-associated decomposition point, which occurs at 118 °C. Analysis of the block-shaped dark green crystals, formed after slow cooling of a saturated CH_3CN/Et_2O (1 : 1, v/v) solution, with single-crystal X-ray diffraction (*sc*-XRD) revealed an overall C_1-symmetric structure of **50-Ti** with one MesNC ligand occupying the diagonal position relative to the germylidyne ligand. The Ti-Ge bond length (2.3442(15) Å) and the angle at the Ge center (∠Ti–Ge–C1 158.18(18)°) in **50-Ti** remained almost similar to those of its precursor **47-Ti** (2.3260(4) Å and 162.64(6)°). Akin to the solid-state, **50-Ti** also exhibits (according to the ^{1}H and ^{13}C{^{1}H} NMR spectra) a C_1-symmetric structure in solution with rapid rotation of the Ge–C^{Tbb} and both N–C^{Mes} bonds on the NMR timescale. In the ^{13}C{^{1}H} spectrum of **50-Ti**, two different isocyanide carbon resonances appear as distinct singlets at 204.4 and 207.8 ppm (see ***Figure 79***) respectively. They appear at a similar position as the isocyanide resonance of the germylidyne complex $[Cp^*(CO)_2(Ar^{Mes}NC)Ti{\equiv}GeAr^{Mes}]$[230] at 200.3 ppm. Interestingly, the $CO_{lat.}$ resonance is observed at a chemical shift of 290.4 ppm, which is even more down-field shifted than those of **49-Ti** (280.9 ppm) and its precursor **47-Ti** (268.1 ppm). In the IR spectrum

of **50-Ti**, the observed CN stretching vibrations (2054 and 2029 cm^{-1}) are in good agreement with that of [Cp*$(CO)_2$($Ar^{Mes}NC$)Ti≡GeAr^{Mes}] (2049 cm^{-1}).[230]

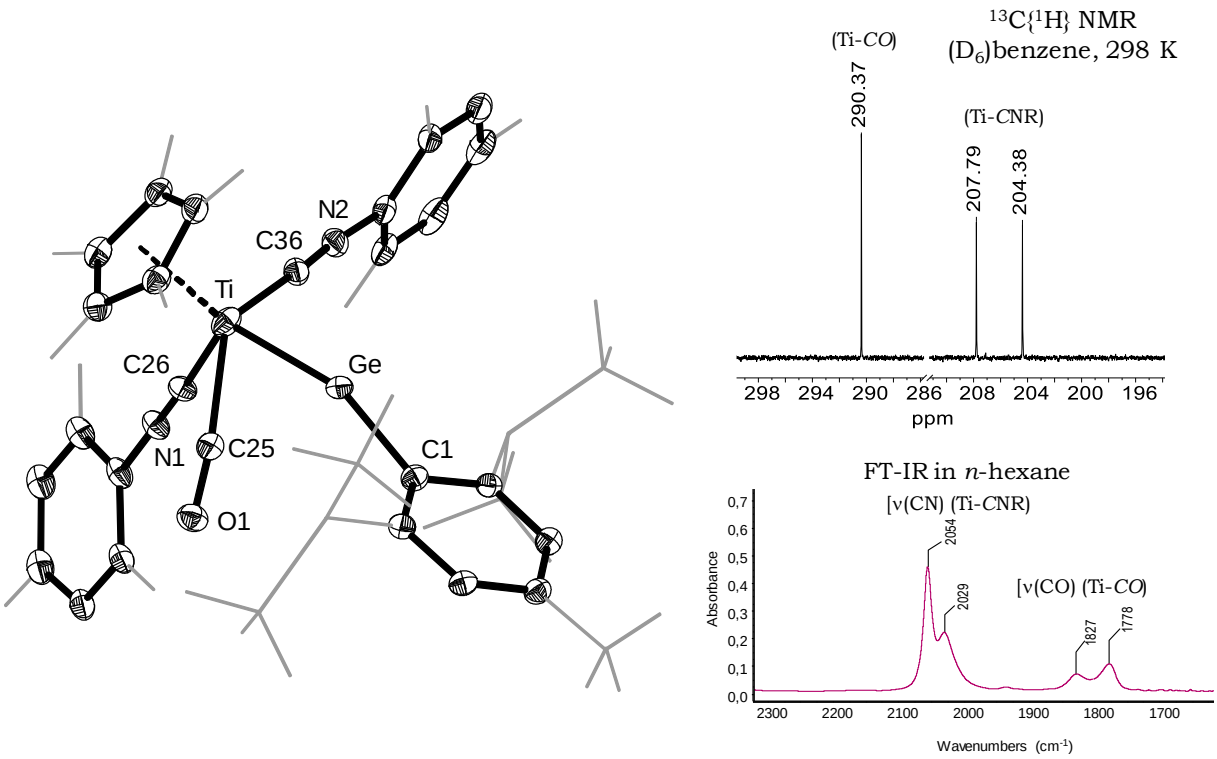

Figure 79. (*left*) DIAMOND plot of the molecular structure of **50-Ti**. Thermal ellipsoids are set at 30 % probability level. Hydrogen atoms are omitted, the Dsi and ^{t}Bu substituents of the Tbb ligand, the methyl groups of Cp* and Mes ligands are presented in wire-frame for clarity. Selected bond lengths [Å] and bond angles [°]: Ti-Ge 2.3442(15), Ti-C25 2.099(7), Ti-C26 2.134(5), Ti-C36 2.105(6), C26-N1 1.165(6), C36-N2 1.165(7), Ge···C25 2.378(7), Ti-Ge-C1 158.18(18), Ti-C26-N1 177.3(4), Ti-C36-N2 178.9(5), C25-Ti-Ge 64.4(2), C26-Ti-Ge 110.44(15), C36-Ti-Ge 92.10(16); (*top right*) a selected excerpt of the $^{13}C\{^1H\}$ NMR spectrum of **50-Ti**; (*bottom right*) an excerpt of the FT-IR spectrum the isolated **50-Ti** in *n*-hexane showing the stretching vibrations of CO and isocyanides.

2.12. Ambiphilic reactivity of E_2Tbb_2(E = Si, Ge)

Given the reported reactivity of ditetrelynes with small isocyanides,[136,231] it's reasonable to anticipate that small phosphines could also form adducts with ditetrelynes. This anticipation stems from the presence of a low-lying in-plane π* orbitals in ditetrelynes, suggesting a potential for bonding with electron-rich molecules such as phosphines. Indeed, the reaction of disilyne and digermyne with PMe_3 yielded their respective mono-phosphine adducts.

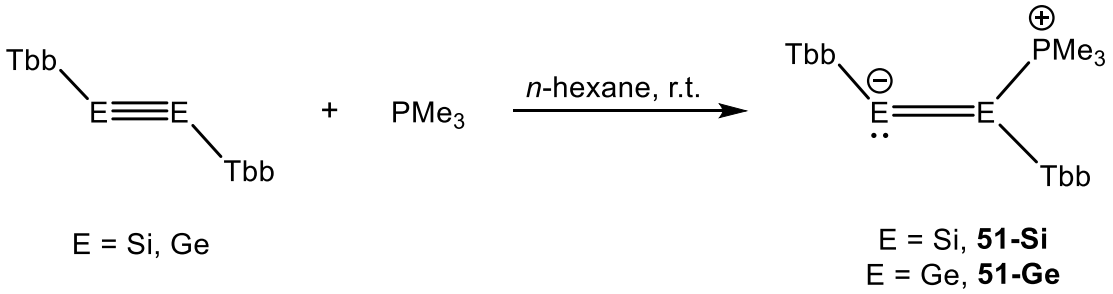

Scheme 55. Synthesis of the PMe_3 adducts of Si_2Tbb_2 and Ge_2Tbb_2.

Upon addition of PMe_3 to a yellow *n*-hexane solution of Si_2Tbb_2 at ambient temperature, the color of the reaction solution immediately changed to dark orange. Analysis of the reaction solution by ^1H NMR and ^{31}P NMR spectroscopy in (D_6)benzene revealed the selective formation of **51-Si**. Upon concentrating the reaction solution followed by storing at –10 °C overnight, the fluffy feather like orange mass of **51-Si** was isolated as analytically pure solid in 59 % yield. Similarly, the germanium analogue **51-Ge** was also obtained as pure solid in 92 % yield. Both compounds are highly air-sensitive, orange-red (**51-Si**) and reddish-brown (**51-Ge**) solids, decolorizing immediately upon exposure to air. Both are well soluble in *n*-hexane, diethyl ether, benzene and toluene at ambient temperature. The melting associated decomposition of **51-Si** occurs at 147 °C and of **51-Ge** at 165 °C. It's worth noting that mono-phosphane adducts do not undergo further reactions, even when an excess of PMe_3 is present. Compounds **51-Si** and **51-Ge** are the first phosphane-stabilized dimetallynes to be reported, and were thoroughly characterized. Suitable single crystals for sc-XRD analysis of **51-Si•Et_2O** (clear orange plates) were grown by slow cooling of a saturated diethyl-ether solution at –10 °C, and red blocks of **51-Ge•2** (**C_5H_{12}**) were grown by slow cooling of a saturated *n*-pentane solution at –30 °C. The molecular structure of **51-Si** (***Figure 80***, *top left*) features a planar core consisting of the atoms P, Si1, C1, and Si2 wherein a trigonal-planar coordinated Si center (∑∠(Si1) = 360°) is linked to a bent, dicoordinated silicon atom through a Si=Si bond (2.241(2) Å). Notably, the PMe_3 group aligns coplanarly with the molecule's core,

as indicated by the torsion angle (P-Si1-Si2-C25) of –0.7(1)°. As a result, compound **51-Si** exhibits similarities to the caac^{Me}/NHC-supported germasilynes (**35-Si**, **37-Si**, and **38-Si**) mentioned earlier, but clearly differs from other NHC-supported ditetrylynes in which the NHC five-memberred rings are twisted out of the planar core of the molecules.[95,232] The Si=Si bond distance of 2.241(2) Å and the angle (Si1-Si2-C25) of 112.18(18)° at the dicoordinated Si center align closely with values reported for base-supported disilynes.[95,232]

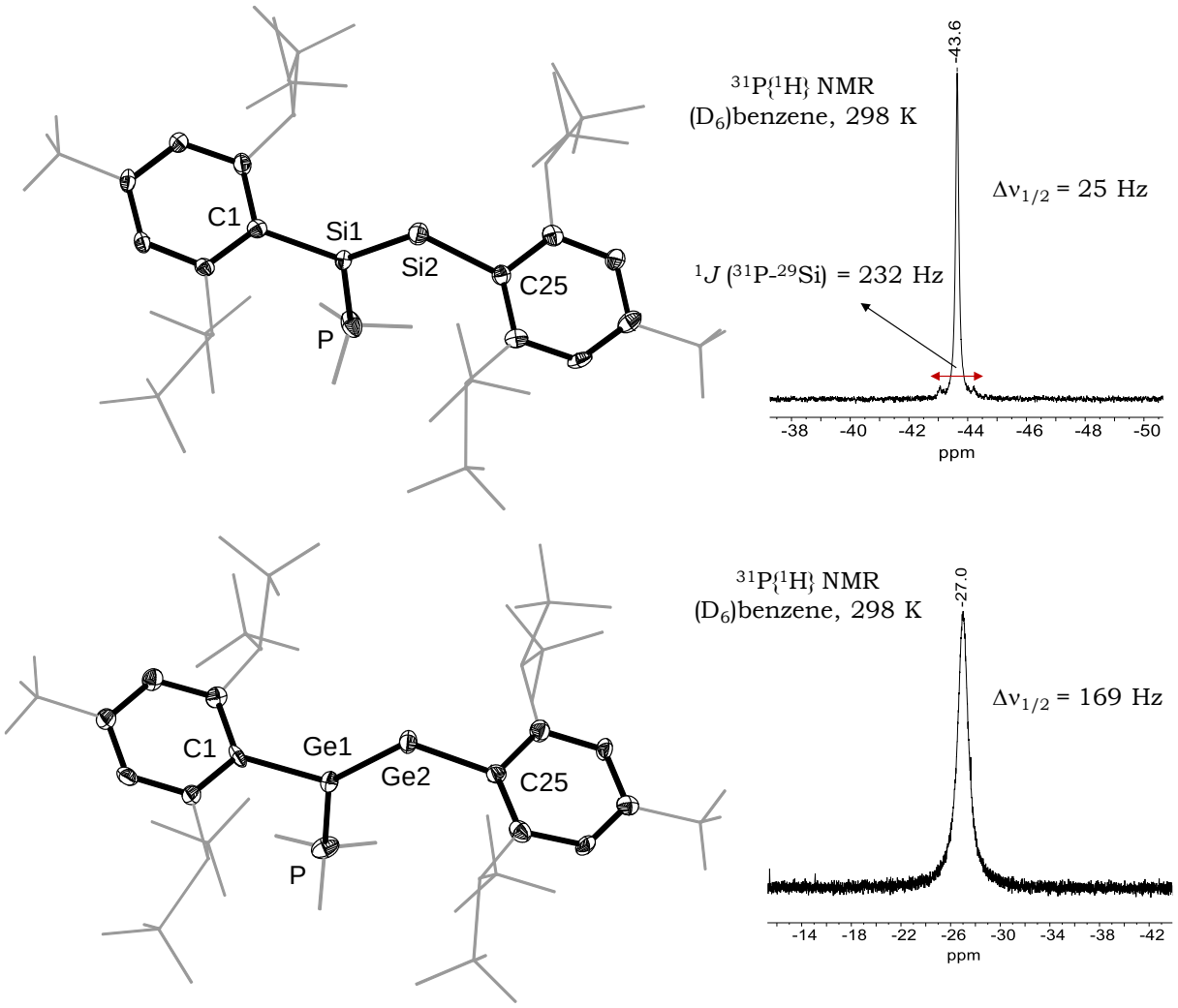

Figure 80. DIAMOND plot of the molecular structure of **51-Si** (*top left*) and **51-Ge** (*bottom left*). Thermal ellipsoids are set at 30 % probability level. Hydrogen atoms are omitted, the Dsi and ^{t}Bu substituents of the Tbb ligand and the methyl groups of PMe_3 are presented in wire-frame for clarity. Selected bond lengths [Å], bond angles [°] and torsion angles [°]: **51-Si**: Si1-Si2 2.241(2), Si1-P 2.227(3), C1-Si1-Si2 123.79(18), C1-Si1-P 107.71(18), P-Si1-Si2 128.50(9), Si1-Si2-C25 112.18(18), C1-Si-Si-C25 179.9(1), P-Si1-Si2-C25 –0.7(1); **51-Ge**: Ge1-Ge2 2.3167(15), Ge1-P 2.352(3), C1-Ge1-Ge2 122.1(3), C1-Ge1-P 101.1(3), Ge2-Ge1-P 136.52(11), Ge1-Ge2-C25 113.2(3), C1-Ge1-Ge2-C25 –176.8(1), P-Ge1-Ge2-C25 –3.9(1); (*top right*) $^{31}P\{^{1}H\}$ NMR spectrum of **51-Si** measured at 298 K; (*bottom right*) $^{31}P\{^{1}H\}$ NMR spectrum of **51-Ge** measured at 298 K.

Compound **51-Ge** (***Figure 80***, *botton left*) is isostructural to its silicon analogue **51-Si** and also features a planar core consisting of the atoms P, Ge1, C1, and Ge2, wherein a trigonal-planar coordinated Ge center ($\sum\angle$(Ge1) = 359.7°) is linked to a bent, dicoordinated germanium atom through a Ge=Ge bond (2.3167(15) Å). The PMe_3 group aligns coplanarly with the molecule's core, as indicated by the torsion angle (P-Ge1-Ge2-C25) of –3.9(1)°. As a result, compound **51-Ge** exhibits resemblances to a similar structure of ^{t}BuNC-coordinated digermyne[123] but clearly differs from other NHC-supported digermynes in which the NHC central rings are rotated out of the planar core of the molecules.[95,213] The Ge=Ge bond distance of 2.3167(15) Å and the angle (Ge1-Ge2-C25) of 113.2(3)° at the dicoordinated Ge center closely match with values reported for base-supported digermynes.[95,123,213]

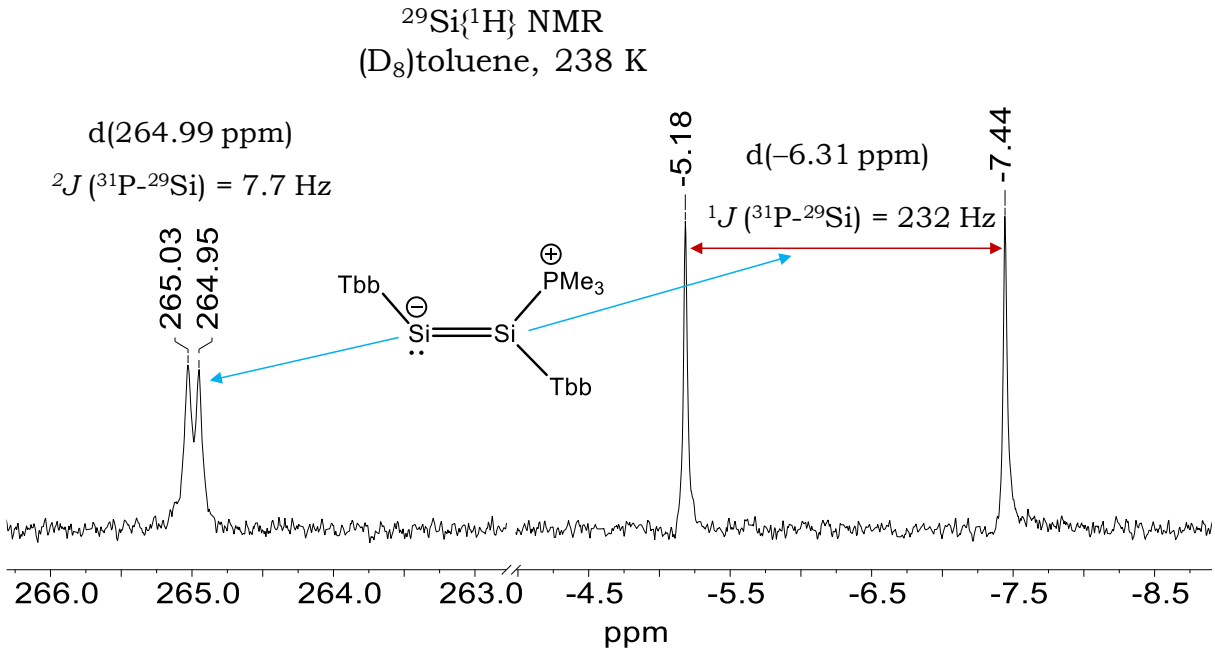

Figure 81. Selected excerpts of the $^{29}Si\{^1H\}$ NMR (99.4 MHz) spectrum of **51-Si** in (D_8)toluene, measured at 238 K.

$Si_2Tbb_2(PMe_3)$ (**51-Si**) exhibits an averaged C_s symmetric structure in solution, in which both heterotopic Tbb substituents are arranged orthogonally to the planar core of the molecule composed of the atoms P, C^{Tbb}–Si–Si–C^{Tbb}. The Tbb substituents are fixed in this position due to hindered rotation around the respective Si–C^{Tbb} bonds. Therefore, two sets of signals are observed for the Tbb substituents in the ^1H and $^{13}C\{^1H\}$ NMR spectra of $Si_2Tbb_2(PMe_3)$ in (D_8)toluene at 238 K. With increasing temperature, a site exchange of the heterotopic Tbb substituents was observed by VT ^1H and $^{31}P\{^1H\}$ NMR spectroscopy (***Figure 82***) originating from the PMe_3 dissociation in solution. At 298 K, the $^{29}Si\{^1H\}$ NMR spectrum of **51-Si**, displays for the PMe_3

bound Si atom a broad doublet at δ_{Si} = –7.38 ppm with a coupling constant ($^{1}J(^{31}P-^{29}Si)$) of 232 Hz, while the dicoordinated Si atom appears as an exceptionally broad singlet at δ_{Si} = 268.8 ppm. The signal broadening is likely a result of a slightly hindered rotation of Si–C^{Tbb} bonds at 298 K, that is frozen out when the temperature is lowered leading to sharp NMR signals. Interestingly, the δ_{Si} values of **51-Si** (***Figure 81***) closely match to those of the reported NHC-disilyne complexes [(IMe$_4$)(R)Si=SiR (R = Si^{i}Pr(CH(SiMe$_3$)$_2$)$_2$: δ = 28.7 and 276.3 ppm; R = Tbb: δ = 21.1 and 203.3 ppm].[95,232]

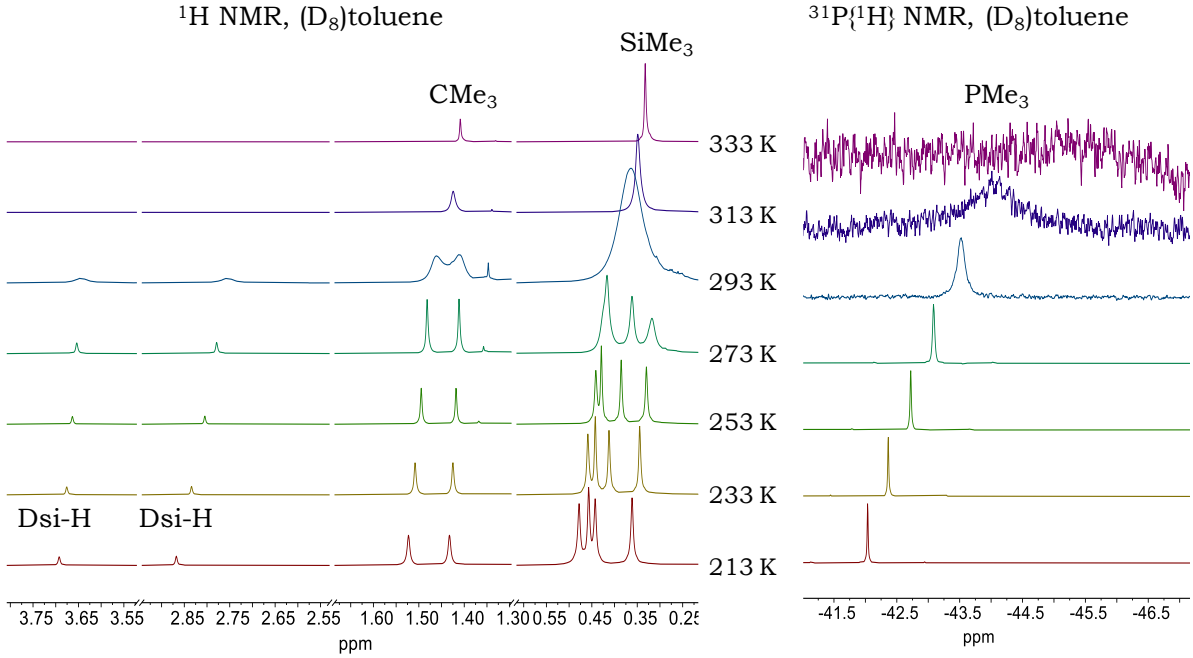

Figure 82. (*left*) excerpts of the VT ^{1}H NMR spectra (300.1 MHz) of Si$_2$Tbb$_2$(PMe$_3$) in (D$_8$)toluene; (*right*) VT-^{31}P{^{1}H} NMR spectra (121.5 MHz) of Si$_2$Tbb$_2$(PMe$_3$) in (D$_8$)toluene.

Similarly, **51-Ge** also shows dynamics in solution as evidenced by the variable temperature (VT) ^{1}H NMR and ^{31}P{^{1}H} NMR spectra in the temperature range of 213 – 343 K. In the slow exchange limit ^{1}H NMR spectrum of **51-Ge** at 213 K two sets of NMR signals are observed for the two heterotopic Tbb substituents, i.e. two singlets for the CMe$_3$ groups, two singlets for the methine protons of the disyl substituents, two singlets of the C^{3,5}-bonded aryl protons and four singlets for the SiMe$_3$ groups (see ***Figure 83***). In line with the solid-state structure of Ge$_2$Tbb$_2$(PMe$_3$), the number and relative intensity of the ^{1}H NMR signals suggest a time-averaged C_s symmetric structure of Ge$_2$Tbb$_2$(PMe$_3$) in solution with both heterotopic Tbb substituents being arranged orthogonally to the planar core of the molecule composed of the atoms P, C^{Tbb}–Ge–Ge–C^{Tbb}. They show moreover that both Tbb substituents are fixed in this position due to hindered rotation around the respective Ge–C^{Tbb} bonds. The fixed

orthogonal orientation of the two Tbb substituents leads to enantiotopic disyl groups in each Tbb substituent and diastereotopic $SiMe_3$ groups in each disyl substituent resulting in a total of four $SiMe_3$ singlets with the integral ratio of 18 : 18 : 18 : 18 protons at 213 K. With increasing temperature, the two singlets for the CMe_3 groups, broaden, shift towards one another, merge into a broad signal and appear in the fast exchange limit ^{1}H NMR spectrum of **51-Ge** at 343 K as a sharp singlet. A similar change was observed with increasing temperature for two singlet signals of the methine protons of the disyl substituents, the two singlet signals of the $C^{3,5}$-bonded aryl protons and the four singlet signals of the $SiMe_3$ groups. The dynamic behavior of **51-Ge** can be rationalized by assuming a dissociation equilibrium between $Ge_2Tbb_2(PMe_3)$ and its dissociation products Ge_2Tbb_2 and PMe_3 (i.e. $Ge_2Tbb_2(PMe_3) \rightleftharpoons Ge_2Tbb_2 + PMe_3$). A rapid equilibration and a shift of the equilibrium to the dissociation products occurs with increasing temperature.

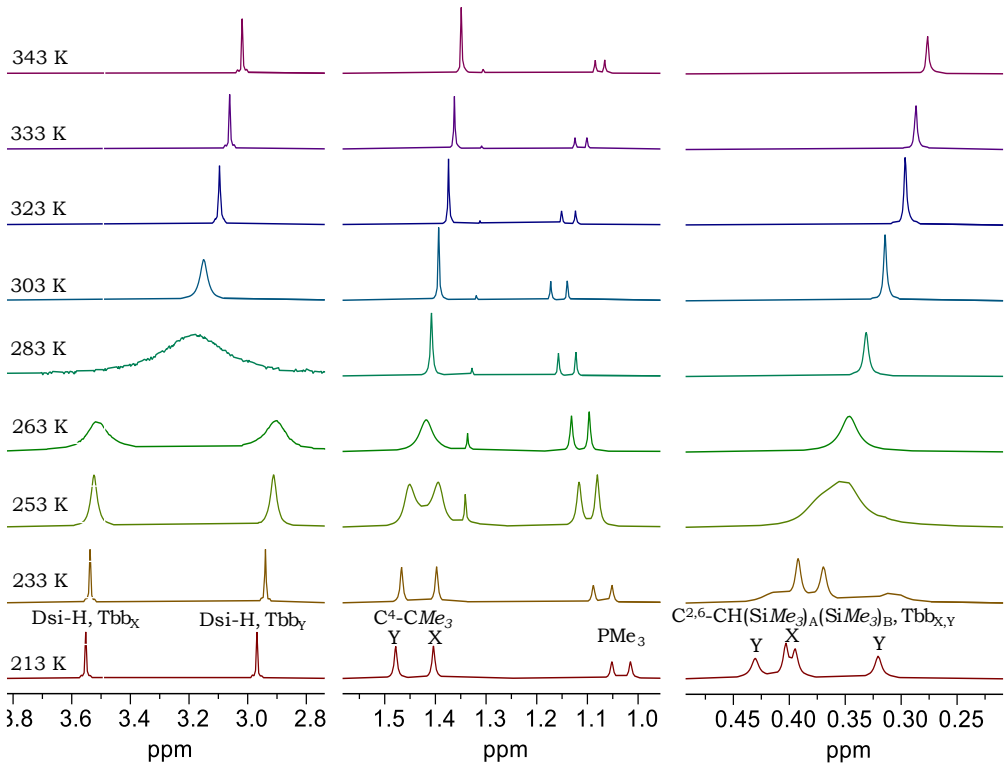

Figure 83. Selected excerpts of the VT-^{1}H NMR spectra (300.1 MHz) of **51-Ge** in (D_8)toluene.

Evidence for this was provided by the VT $^{31}P\{^1H\}$ NMR spectra (see ***Figure 84***) showing a considerable high field shift of the ^{31}P NMR signal from –24 ppm at 213 K to –40.2 ppm at 343K. i.e. toward the position of free PMe_3 (δ_P = –61.9 ppm), and the VT ^{1}H NMR spectra showing a lowering of the $^2J(^{31}P\text{-}^1H)$ coupling constant of PMe_3 from 11.0 Hz at 213 K to 5.6 Hz at 343 K, i.e. toward the value of free PMe_3 ($^2J(^{31}P\text{-}^1H)$ = 2.5 Hz). The same rationale can be applied to explain the dynamic behavior of **51-Si** in solution.

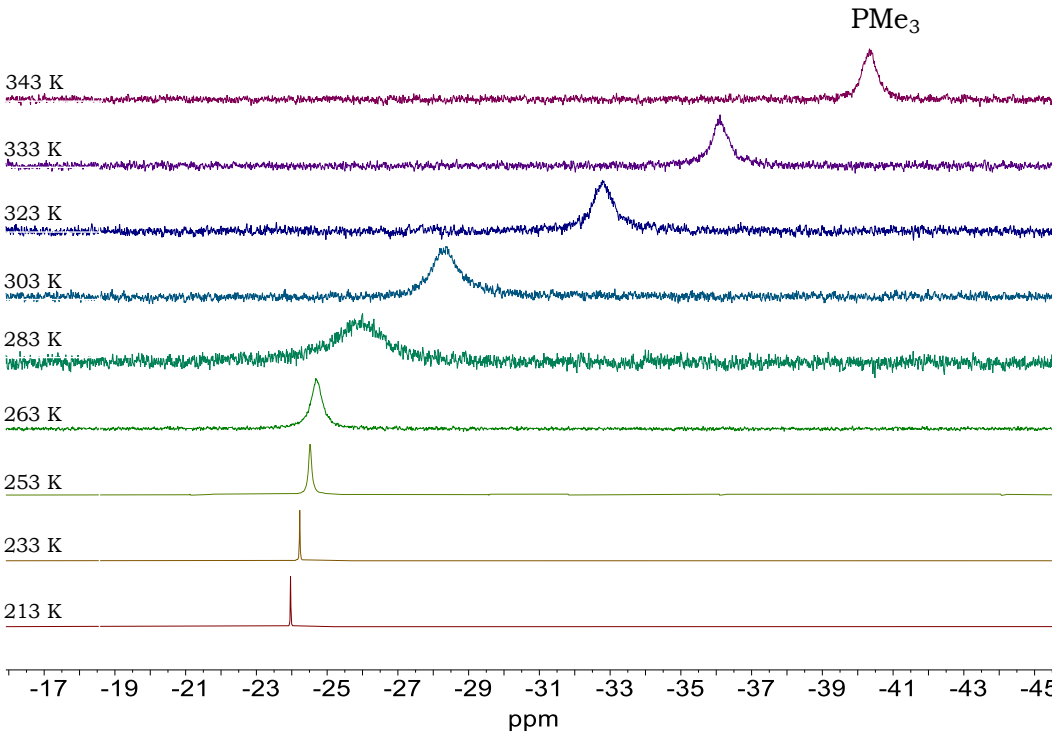

Figure 84. VT $^{31}P\{^{1}H\}$ NMR spectra (121.5 MHz) of **51-Ge** in (D_8)toluene.

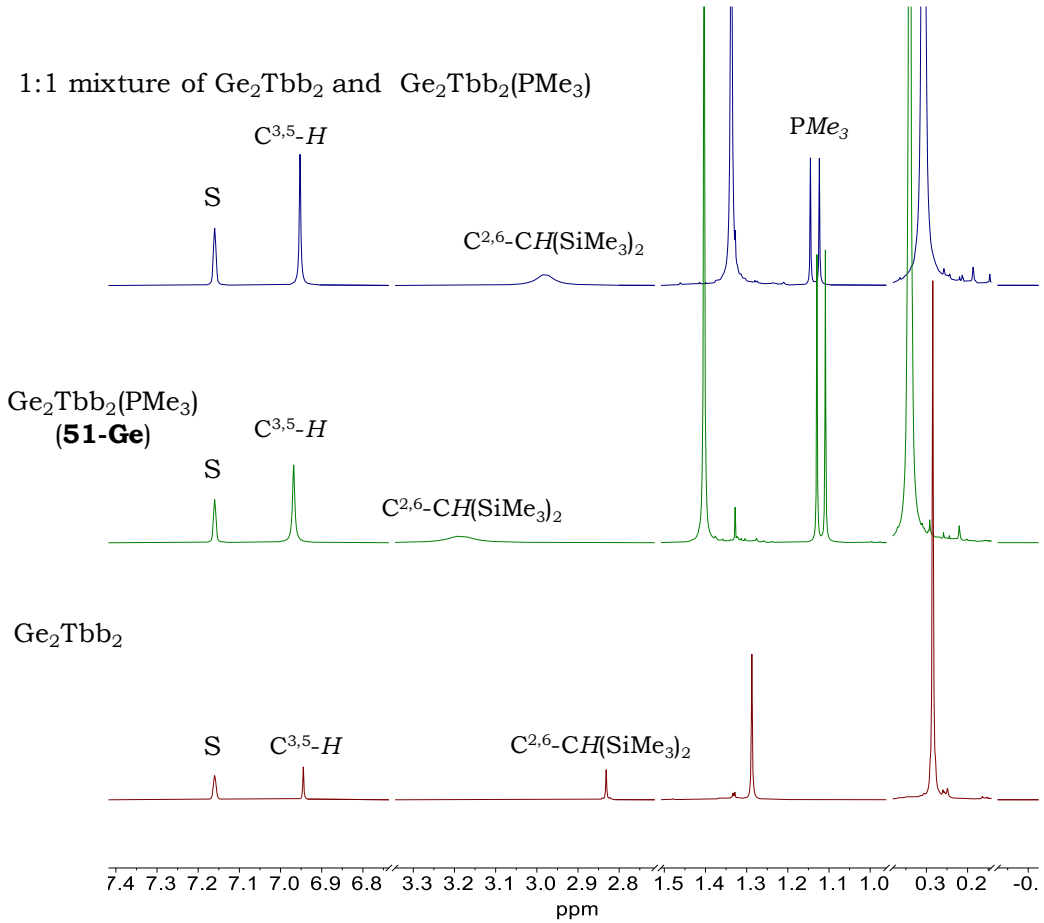

Figure 85. A stack plot of the ^{1}H NMR spectra (500.1 MHz) in (D_6)benzene at 298 K of (*top*) a 1:1 mixture of Ge_2Tbb_2 + PMe_3 ; (*middle*) $Ge_2Tbb_2(PMe_3)$ and (*bottom*) Ge_2Tbb_2. The residual proton signal of the deuterated solvent is marked with the letter S.

Further evidence for an equilibrium between $Ge_2Tbb_2(PMe_3)$ and its dissociation products Ge_2Tbb_2 and PMe_3 was provided by a comparison of the ^1H NMR spectrum of a 1 : 1 molar mixture of $Ge_2Tbb_2(PMe_3)$ and Ge_2Tbb_2 with those of the pure components (see ***Figure 85***). The ^1H NMR spectrum of a 1 : 1 molar mixture of $Ge_2Tbb_2(PMe_3)$ and Ge_2Tbb_2 displays only one set of signals for the Tbb group appearing at an intermediate position of those of the pure components. This suggests a rapid transfer of PMe_3 between $Ge_2Tbb_2(PMe_3)$ and Ge_2Tbb_2 via PMe_3 dissociation and reassociation.

In contrast to the outcome observed in the PMe_3 reaction, when Si_2Tbb_2 was treated with a Lewis acid such as $AlMe_3$, it did not result in the typical formation of a Lewis acid-base adduct. Instead, one of the Al–Me bonds was added to the Si–Si multiple bond of disilyne, leading to the formation of the Al–disilenide, **52-Si**.

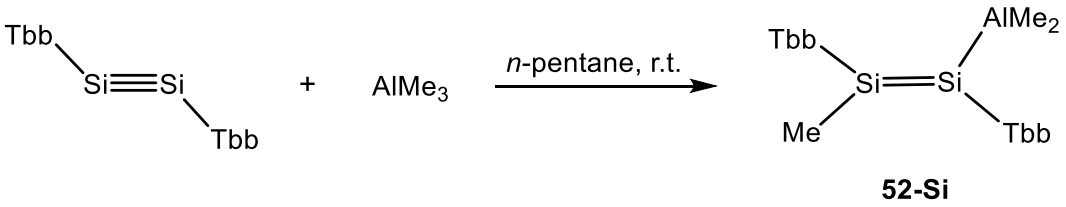

Scheme 56. Reaction of disilyne with a Lewis acid $AlMe_3$.

In fact, when a stock solution of $AlMe_3$ was added dropwise to a golden yellow *n*-pentane solution of Si_2Tbb_2 at ambient temperature, the colour of the reaction solution was immediately changed to lemon yellow. Spectroscopic analysis of the reaction solution revealed a complete consumption of Si_2Tbb_2 and quantitative formation of **52-Si**. After work-up followed by crystallization of the crude product from *n*-pentane, **52-Si** was isolated as analytically pure solid in 43 % yield. It is moderately sensitive to air, and exists as a thermally stable, lemon-yellow solid with a decomposition temperature ($T_{dec.}$) of 166 °C. It exhibits good solubility and stability in *n*-hexane, diethyl ether, benzene, and toluene. However, when dissolved in tetrahydrofuran at ambient temperatures, it undergoes slow and unselective decomposition. In combination with EA, multinuclear NMR spectroscopy, compound **52-Si** was also characterized by sc-XRD analysis of plate-shaped single crystals, which were grown by slow cooling its saturated *n*-pentane solution at –30 °C.

The molecular structure of **52-Si** (***Figure 86***) features a planar core consisting of the atoms C1, Si1, Al, Si2, C51 and C25, wherein two trigonal-planar coordinated silicon atoms ($\sum\angle$(Si1,2) = 359.9°,360.0°) are linked to each other via a Si=Si double bond (2.1677(9) Å). The Si=Si double bond of **52-Si** is slightly shorter than that of (*E*)-(Br)TbbSi=SiTbb(Br) (2.2220(16) Å).[82] However, it aligns perfectly with the Si=Si

double bond of (*E*)-(Me)TbbSi=SiTbb(Me) (2.157(2) Å) reported in the Bachelor thesis of M. Krumpholz[ix] and also falls within the standard range for Si=Si double bonds, which typically spans from 2.138 Å[233,234] to 2.360 Å,[12] as reported in the Cambridge Structural Database (CSD) repository. The Si–Al distance of 2.4199(9) Å in **52-Si** aligns perfectly with the theoretically calculated Si–Al single bond length of 2.42 Å based on Pyykkö's covalent radii.[184] Furthermore, the Si–Al bond of **52-Si** compare well with those of aluminium silyls (~2.42 Å)[235,236] found ba a CSD search.

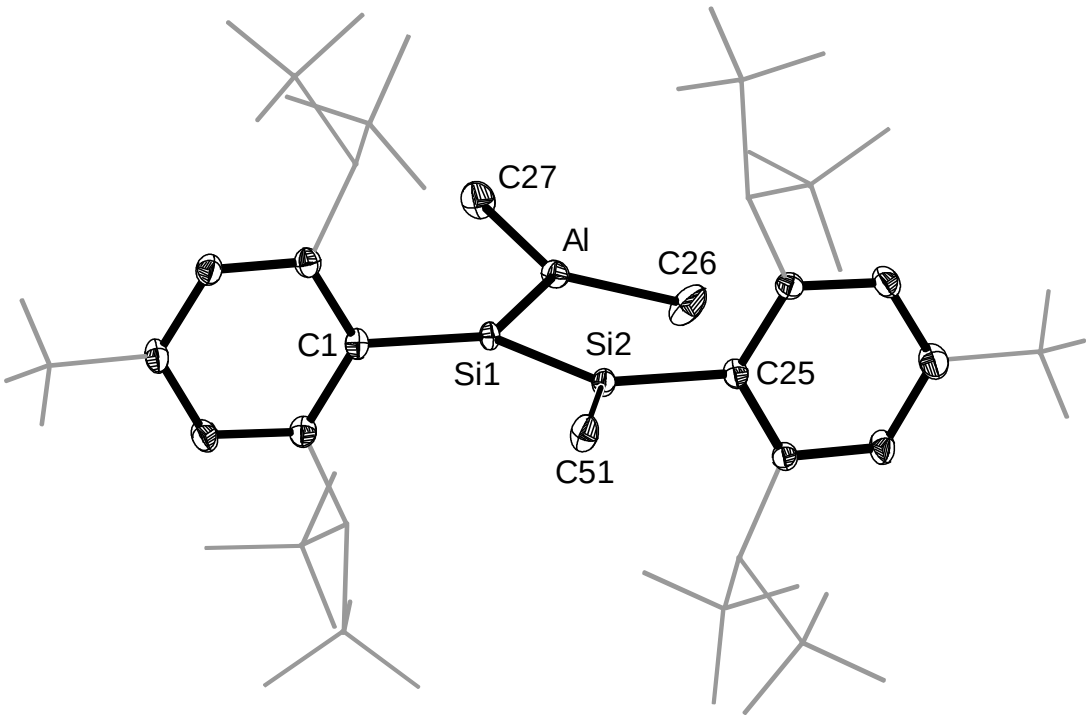

Figure 86. DIAMOND plot of the molecular structure of **52-Si**. Thermal ellipsoids are set at 30 % probability level. Hydrogen atoms are omitted and the Dsi and ^{t}Bu substituents of the Tbb ligand are presented in wire-frame for clarity. Selected bond lengths [Å], bond angles [°] and torsion angles [°]: Si1-Si2 2.1677(9), Si1-Al 2.4199(9), Si2-C51 1.876(3), C1-Si1-Si2 120.00(7), C1-Si1-Al 127.38(8), Al-Si1-Si2 112.60(3), Si1-Si2-C25 121.14(8), Si1-Si2-C51 126.60(9), C25-Si2-C51 112.26(11), C1-Si1-Si2-C25 –179.467(4), Al-Si1-Si2-C51 179.225(4), Al-Si1-Si2-C25 –0.779(5), C1-Si1-Si2-C51 0.537(7).

Akin to its solid-state structure, **52-Si** possesses also a *Cs*-symmetric structure in solution, where the both heterotopic Tbb substituents are orthogonally locked to the planar core of the molecule composed of the atoms Al, C51 and C^{Tbb}-Si-Si-C^{Tbb}. This fixed orthogonal orientation leads to enantiotopic disyl groups in each Tbb

[ix] Synthesis and complete characterization of the compound is reported in the following bachelor thesis; Marcel Krumpholz, "Reaktivitätsstudien von Disilenen mit Si(II)-Halogeniden", *Bachelorarbeit in Chemie*, Rheinischen-Friedrich-Wilhelms-Universität Bonn, **2016**.

substituent and diastereotopic $SiMe_3$ groups in each disyl substituent resulting in a total of four $SiMe_3$ singlets with the integral ratio of 18 : 18 : 18 : 18. In the $^{29}Si\{^1H\}$ NMR spectrum of **52-Si** (***Figure 87***), two distinct singlets corresponding to the two heterotopic silicon atoms are observed. One broadened singlet appears at 45.8 ppm ($\Delta\nu_{1/2}$ = 12 Hz), indicating the presence of the silicon atom associated with aluminium (Al). The broadening of this resonance can be attributed to the quadrupolar moment of the ^{27}Al nucleus. In contrast, the silicon atom linked to the methyl (Me) group displays a sharp singlet at 145.0 ppm.

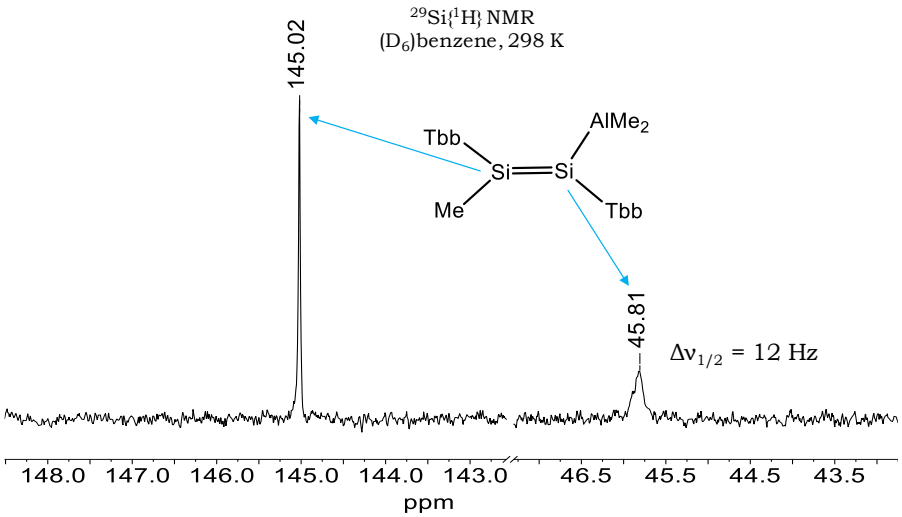

Figure 87. Excerpts of the $^{29}Si\{^1H\}$ NMR spectrum of **52-Si** measured in (D6)benzene at 298 K.

It's worth mentioning that the silicon resonances of **52-Si** are different from those disilenes, such as (*E*)-(Br)TbbSi=SiTbb(Br) (84.12 ppm),[82] (*E*)-(Me)TbbSi=SiTbb(Me) (73.79 ppm),[ix] $(Tip)_2Si=Si(Tip)_2$ (53.4 ppm),[237] and even the Li-disilenide, $Li(Tip)Si=Si(Tip)_2$ (94.5 and 100.5 ppm) reported by Scheschkewitz *et al.*[238] These variations in chemical shifts indicate the differences in the local electronic environments of the two heterotopic silicon atoms in these compounds.

Interestingly, Ge_2Tbb_2 also reacted rapidly with $AlMe_3$ at ambient temperature. However, spectroscopic analysis (^1H NMR) of the reaction solution indicated the presence of a mixture of at least three different Tbb containing components. Unfortunately, no specific species from this mixture could be isolated even after careful crystallization.

3. Summary and Outlook

3.1. Summary

In the present thesis, the diverse and versatile reactivity of disilyne (Si_2Tbb_2) and digermyne (Ge_2Tbb_2) toward transition metals was extensively explored, resulting in a plethora of novel reactions with intriguing follow-up chemistry to unprecedented products. Furthermore, the unusual reactivity of a caac^{Me}-supported germasilyne was explored, and the chemistry of the complexes featuring Ti≡Si and Ti≡Ge triple bonds was extended.

The first part of the thesis (*section* **2.1** to **2.4**) deals with the syntheses and reactivity of digermyne complexes of cobalt and rhodium. The reaction of $CpM(CO)_2$ (M = Co, Rh) with Ge_2Tbb_2 provided an easy access to the digermyne complexes **1-Co** and **1-Rh** (***Scheme 57***). Attempt to convert **1-Co** to the CO-free digermyne complex **3-Co** by thermal or photochemical decarbonylation failed, but **3-Co** could be selectively obtained in two-step synthesis from $CpCo(C_2H_4)_2$. The first step involved a ligand exchange reaction with $Ge_2Br_2Tbb_2$ leading to the bis-bromogermylidene complex **2-Co**, which was then reduced with KC_8 to yield the targeted digermyne complex **3-Co**. **3-Co** reacts with CO or MesNC to give **1-Co** and **4-Co**, respectively.

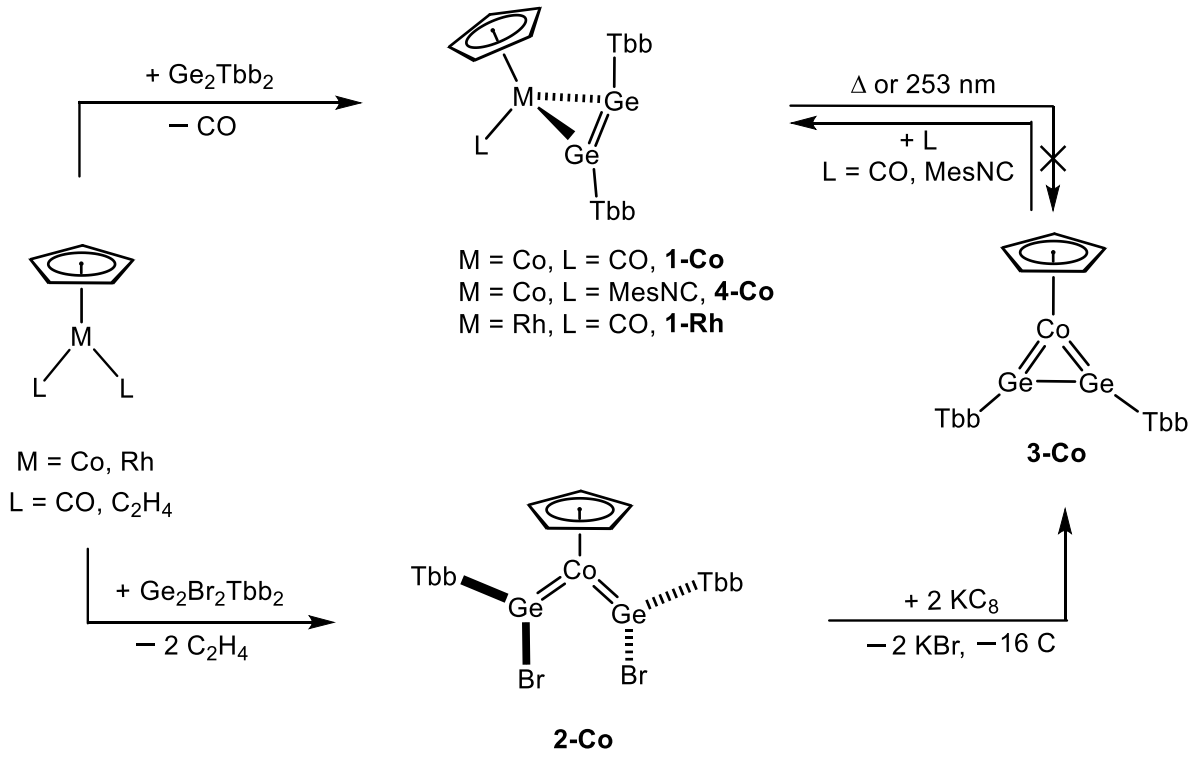

Tbb = 2,4-Dsi$_2$-4-^{t}Bu-C_6H_2, Mes = 2,4,6-Me_3-C_6H_2

Scheme 57. Synthesis of 3-memberred unsaturated metallacycles, the digermyne complexes.

In **1-M** (M = Co, Rh) and **4-Co** digermyne acts as a 2e- donor ligand via the out-of-plane oriented π-bond leading to a trans-orientation of the Tbb groups and two stereogenic trigonal pyramidal coordinated Ge centers. In comparison, the digermyne ligand acts in **3-Co** as a 4e- donor ligand leading to a cis-orientation of the Tbb groups and two trigonal planar coordinated Ge centers. **1-Co** and **3-Co** display different reactivity towards alkynes. **1-Co** reacts with various alkynes yielding in all cases after Ge–Ge bond cleavage to unprecedented 1,3-digermametallacyclopentatrienes (**5-Co**, **10-Co** and **14-Co**). In comparison, the outcome of the reactions of **3-Co** depends strongly on the alkyne. Thus, **3-Co** reacts with 2-butyne to give a mixture of **5-Co** and the 1,2-digermacyclobutadiene complex **6-Co**, the latter thermally converting to **5-Co**, whereas reaction of **3-Co** with mesitylacetylene leads to the bis-germylidene complex **13-Co**. Finally, the reaction of **3-Co** with Ph–C≡C–NMe_2 gives the same product **14-Co** as **1-Co**.

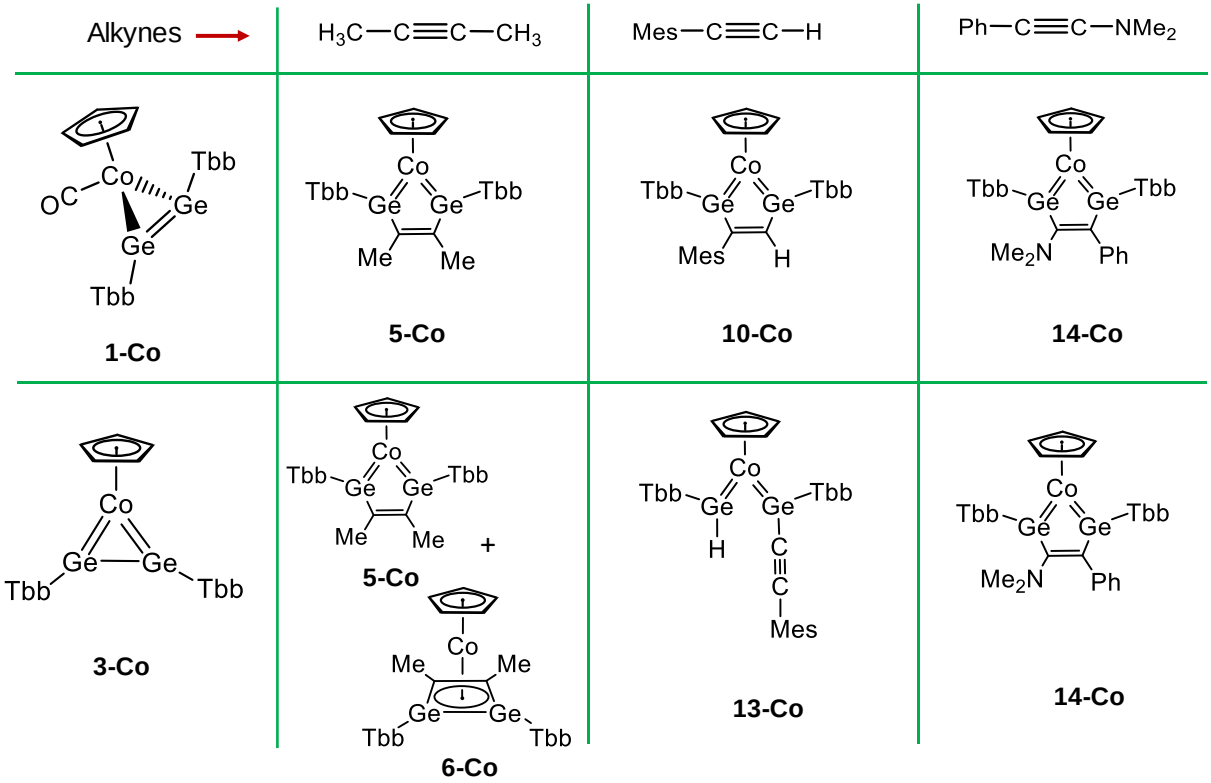

Figure 88. The reaction outcomes of the digermyne complexes **1-Co** and **3-Co** when subjected to various alkynes.

A comparative studies of the reactivity of Si_2Tbb_2 with $CpM(CO)_2$ (M = Co, Rh) presented in *sections* **2.5** to **2.7**, unraveled distinctly different reaction pathways leading to novel Si–CO coupling products upon Si–Si bond cleavage. Thus, reaction

of $CpM(CO)_2$ in CO atmosphere yielded the 1,3-disilacyclobutandione complexes, **20-Co** and **20-Rh**, which upon thermal decarbonylation are converted to the 1,3-disilametallacyclobutadienones **21-Co** and **21-Rh**, respectively. The reactivity of **20-Co** and **21-Co** with MesNC was explored, leading to the unprecedented 1,3-disilacyclobutan-2-on-4-imine complexes, **22-Co** and **23-Co** (***Scheme 58***). Notably, compounds **20-M**, **22-Co** and **23-Co** are reminiscent of propellanes and therefore can be called metalladisilapropellanes. Thermal decarbonylation of **23-Co** yielded **24-Co**, the imine analogue of **21-Co**, which gives with MesNC in an unexpected C–C coupling reaction, the metalacyclic bis-silylidene complex **25-Co**.

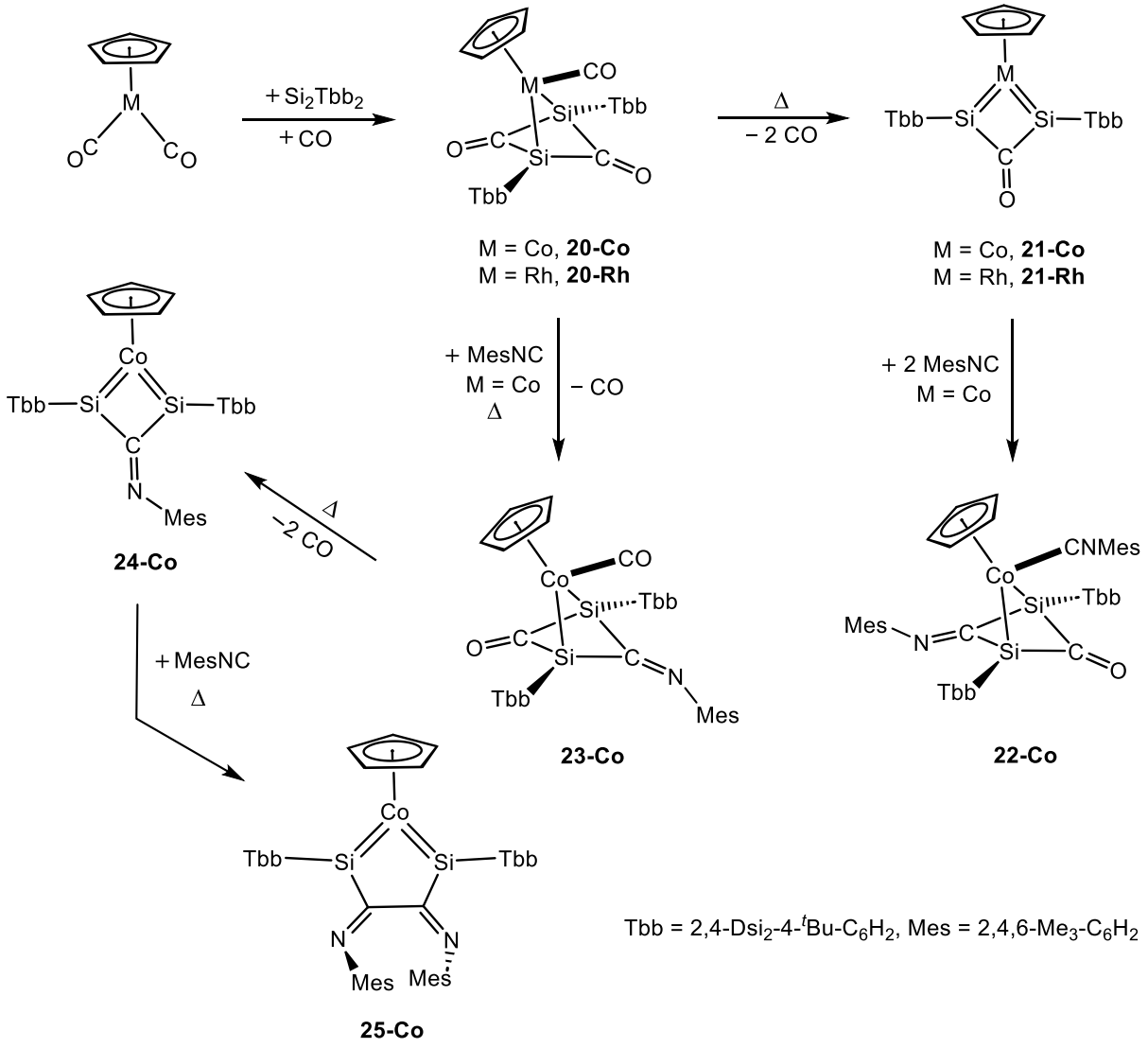

Scheme 58. Compounds synthesized from the follow-up chemistry of Si_2Tbb_2 with $CpM(CO)_2$, where M = Co or Rh.

The complexes **21-M** (M = Co, Rh) exhibit interesting follow-up chemistry (***Scheme 59***). The deoxygenative methylation of **21-M** with $AlMe_3$ afforded the carbene complexes **26-M**, featuring an inverted geometry at the carbene-carbon. The reaction

of **21-Rh** with PMe_3 resulted in a metal-centered Si–Si coupling reaction, forming the disilacyclopropenone complex **27-Rh**. Additionally, the addition of the N-heterocyclic carbene (IMe_4) at one of the silicon centers produced the 1,3-disilarhodacyclobutenone **28-Rh**.

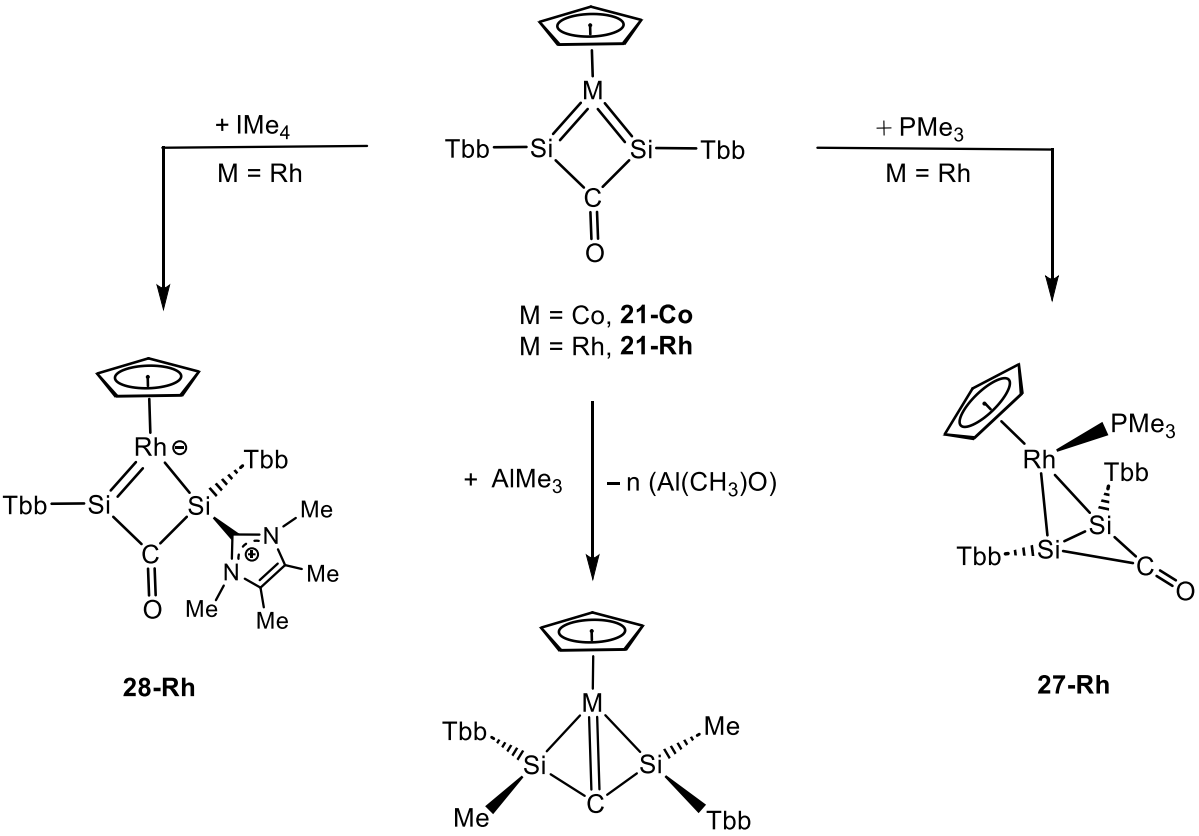

Tbb = 2,4-Dsi_2-4-^{t}Bu-C_6H_2, IMe_4 = 1,3,4,5-tetramethylimidazol-2-ylidene

Scheme 59. Reactivity of **21-M** (M = Co or Rh) with Lewis acid and Lewis bases.

In *Section* **2.8**, a series of novel Fe-, Co-, and Ni-centered Ge≡Ge triple bond cleavage reactions of Ge_2Tbb_2 are presented, yielding unprecedented germylidene-germylidyne (**29-Co**), bis-germylidene (**31-Ni**), and bis-germylidyne (**33-Fe**) complexes. Chloride abstraction from **29-Co** and **31-Ni** yielded the cobalt bis-germylidyne complex cation **30-Co** and the nickel germylidene-germylidyne complex cation **32-Ni**, whereas 1e$^-$ oxidation of **33-Fe** gave the open-shell iron bis-germylidyne complex cation **34-Fe** (***Scheme 60***).

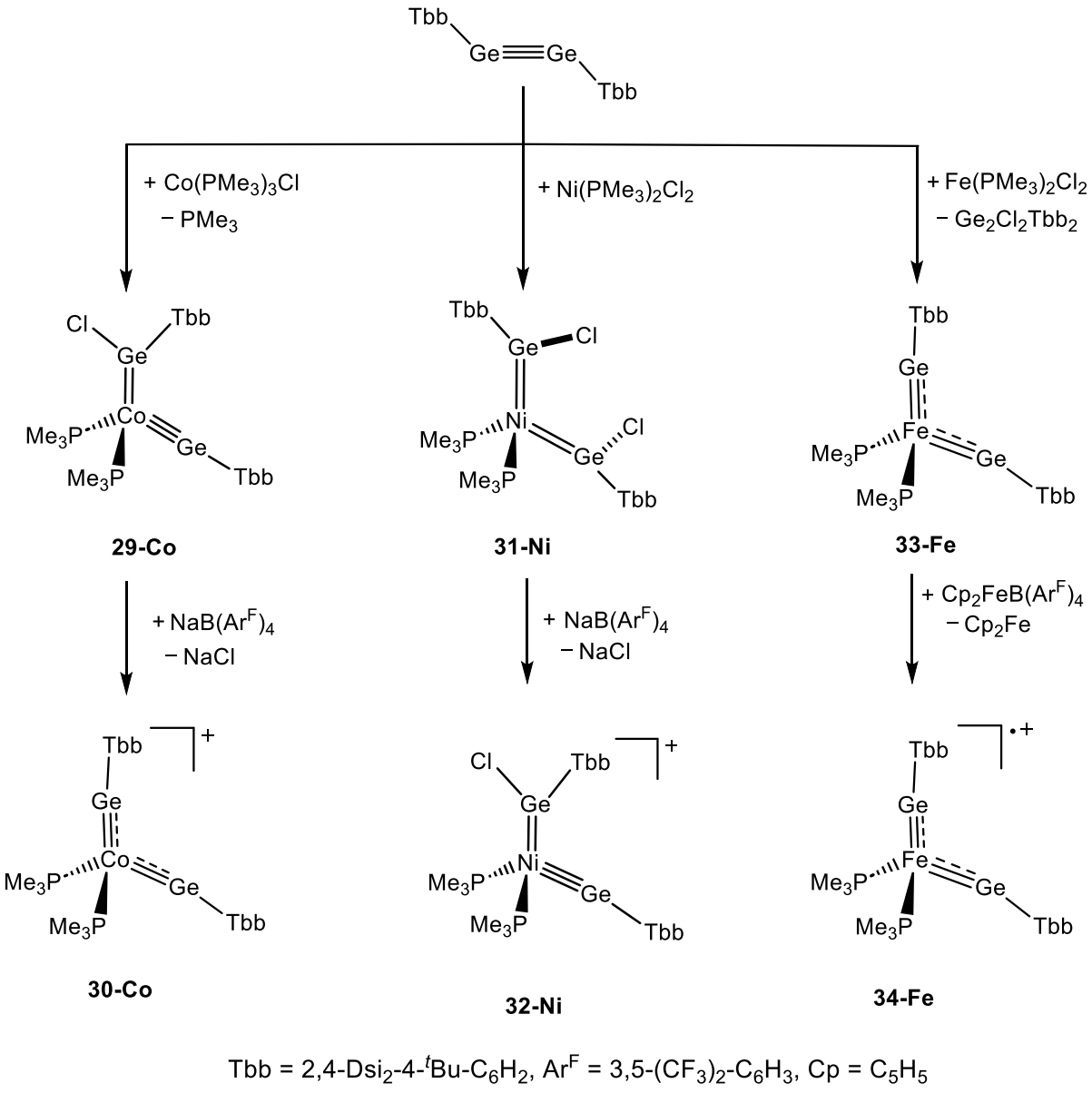

Tbb = 2,4-Dsi$_2$-4-^{t}Bu-C$_6$H$_2$, Ar^F = 3,5-(CF$_3$)$_2$-C$_6$H$_3$, Cp = C$_5$H$_5$

Scheme 60. Synthesis of germylidene-germylidyne, bis-germylidene and bis-germylidyne complexes. For all the cationic complexes the corresponding anion is B(Ar^F)$_4$ and omitted for clarity.

Sections **2.9** and **2.10** are denoted to the reactivity of Ge_2Tbb_2 towards caac^{Me}-supported Si(II) and Si(I) bromides. In fact, the reduction of $SiBr_2$(caac^{Me}) by the digermyne yielded the caac^{Me}-supported germasilyne **35-Si**. However, germasilyne **35-Si** can also be obtained from Si_2Br_2(caac^{Me})$_2$ (***rac*-Si**) and Ge_2Tbb_2 in a reaction involving a metathetical exchange of the GeTbb and SiBr(caac^{Me}) fragments in the reactants. **35-Si** is also accessible from $SiBr_2$(caac^{Me}) and $Ge_2Br_2Tbb_2$. The first reaction involves the formation of the Lewis acid-base adduct **36-Si**, which is then reduced with KC_8 to give the targeted compound (***Scheme 61***).

Metathesis without a transition metal

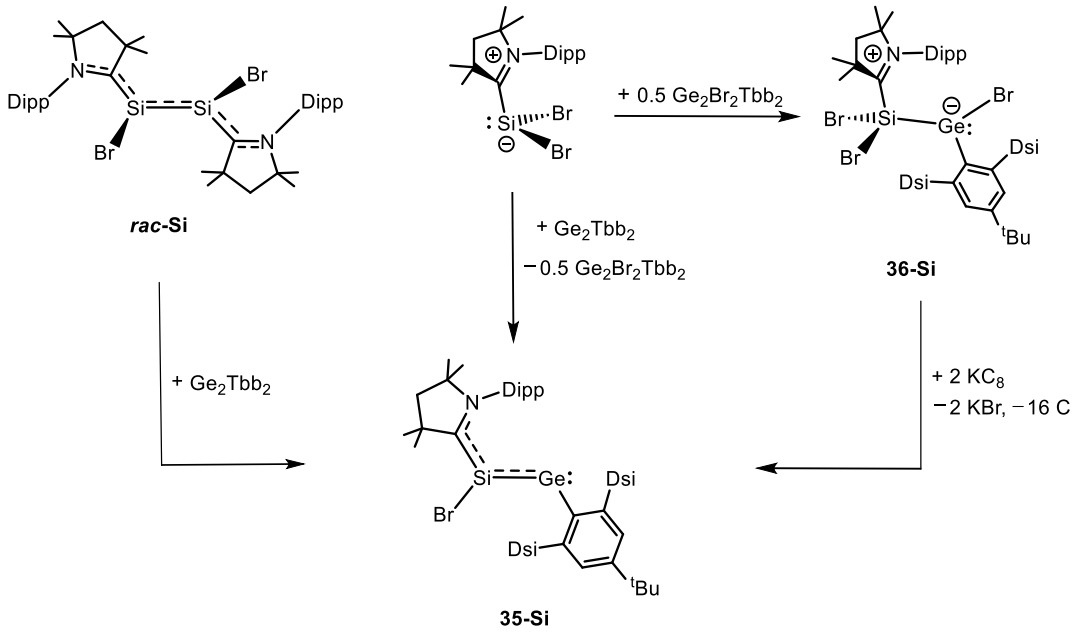

Scheme 61. Synthesis of a caac^{Me}-supported germasilyne.

Compound **35-Si** displays unusual reactivity (***Scheme 62***). Thus bromide abstraction with NaB(Ar^F)$_4$ was accompanied by migration of the Ge-bonded Tbb group to Si, yielding the cationic 1-silagermavinylidene, **39-Si**. It contains an electrophilic Ge center, and transformed upon bromide addition to the caac^{Me}-supported germasilyne **43-Si**, a constitutional isomer of **35-Si**, in which the Tbb and Br groups have been exchanged. An isomerization of **43-Si** occurs upon heating to give the caac^{Me}-supported 1-silagermavinylidene **44-Si**. The reaction is inverse-reminiscent of the Fritsch-Buttenberg-Wiechell (FBW) rearrangement observed in carbon chemistry and involves a migration of caac^{Me} from Si to Ge and of Br atom from Ge to Si.

Inverse reminiscent of the FBW-rearrangement

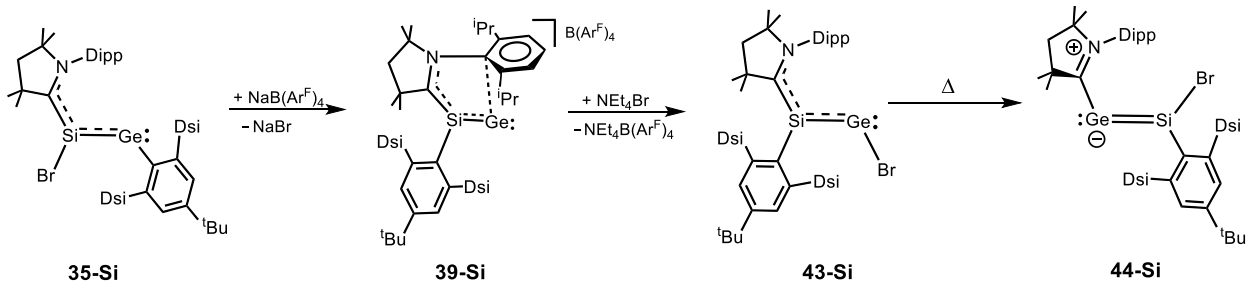

Scheme 62. Synthesis of the constitutional isomer of **35-Si**, **43-Si** and its caac^{Me}/Br-rearrangement reaction.

In *section* **2.11** of this thesis the ligand-exchange chemistry of titanium germylidyne and silylidyne complexes was explored leading to isolation and full characterization of the complexes **48-Ti**, **49-Ti** and **50-Ti** (***Figure 89***, *top*). Finally in *section* **2.12**, the synthesis, full characterization, and dynamics of the PMe_3-adducts of E_2Tbb_2 (E = Si, **51-Si** and E = Ge, **51-Ge**) is presented and the carboalumination of the disilyne Si_2Tbb_2 with $AlMe_3$ is reported leading to the Al-disilenide **52-Si** (***Figure 89***, *bottom*).

Extension of the Ti-ylidyne chemistry

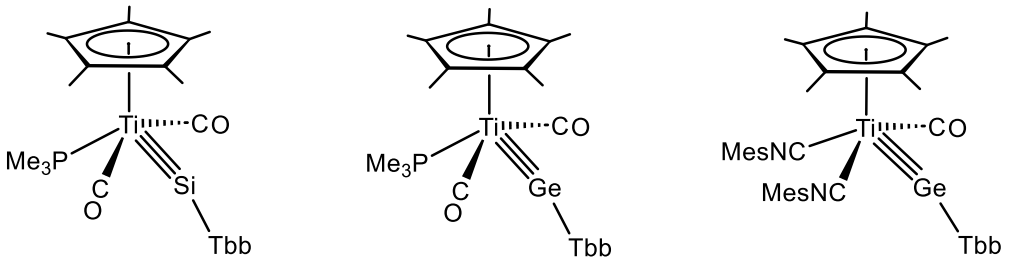

48-Ti **49-Ti** **50-Ti**

Outcomes of the ambiphilic reactivity of ditetrelynes

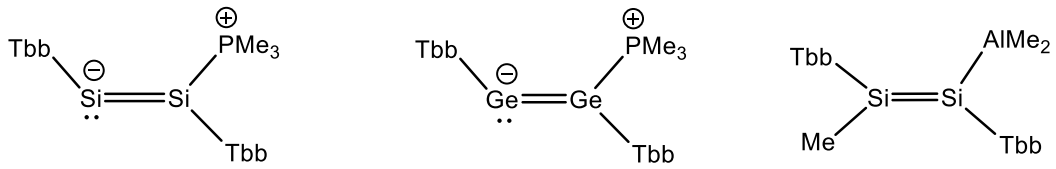

51-Si **51-Ge** **52-Si**

Figure 89. (*top*) Products isolated from the reactivity of Ti-ylidynes; (*bottom*) products isolated from the ambiphilic reactivity of digermyne and disilyne.

3.2. Outlook

The reactions of **1-Co** and **3-Co** with alkynes suggest a 1,3-dipolar reactivity of the coordinated digermyne ligands. In fact, the follow-up studies of **3-Co** shows that, it reacts with ketones, isocyanates and CO_2 to give interesting [3+2]-cycloaddition products, whereas reactions with RN_3 and diazoalkanes give [3+1]-cycloaddition products (***Scheme 63***).

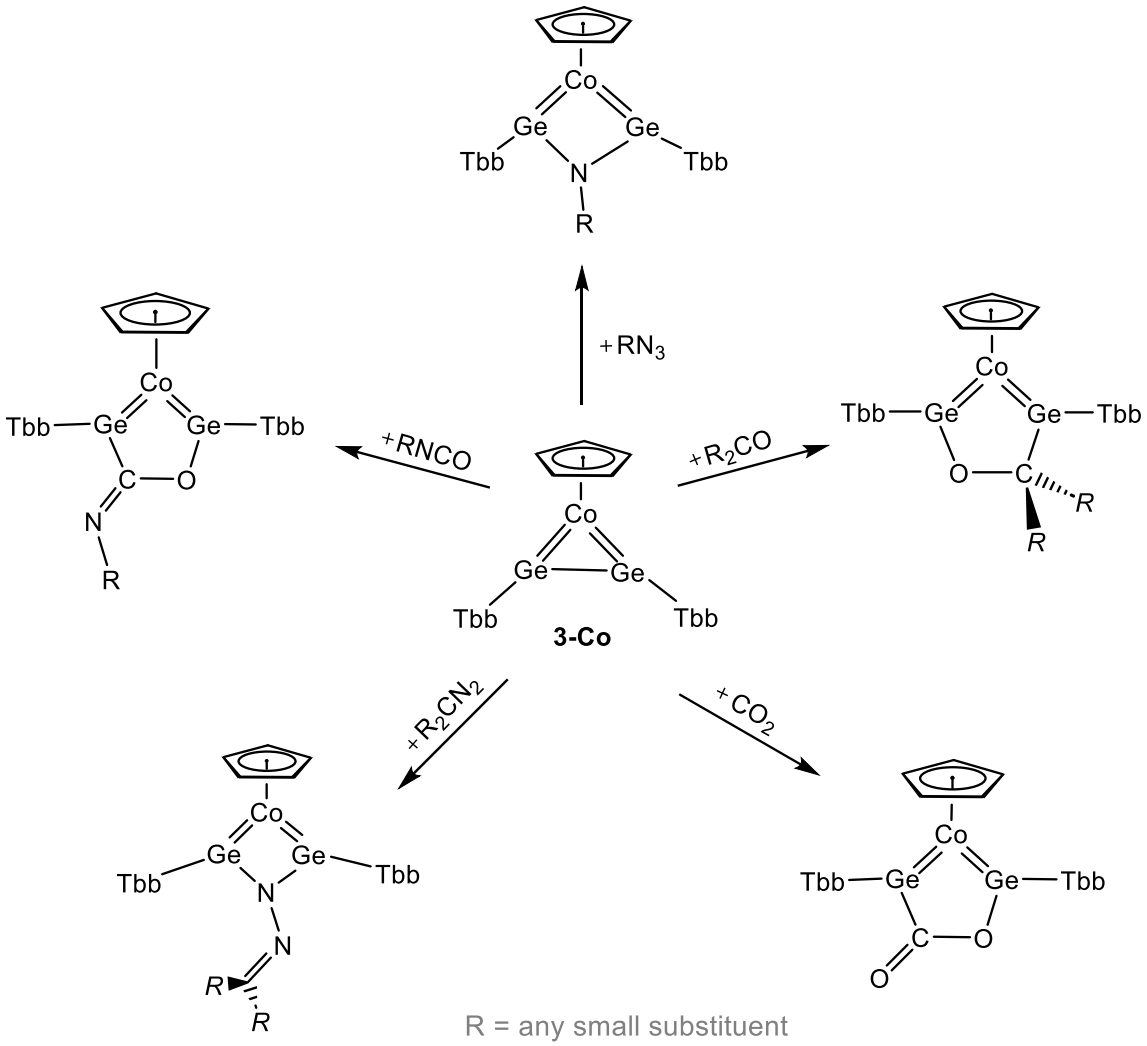

Scheme 63. Reaction outcomes of the digermyne complex **3-Co** with 1,3-dipolar reagents.

Similarly, the follow-up chemistry of 1,3-disilametallacyclobutadienones (**21-Co** and **21-Rh**) or the imine analogue (**24-Co**) might be interesting. Therefore, it would be particularly appealing to further investigate the reactivity of these complexes and gain better understanding of the electronic structure of these molecules. The study could be enhanced by conducting a comparative analysis of the redox behavior of these complexes through cyclic voltammetry, aiming to access the corresponding 1e-reduction product (***Figure 90***).

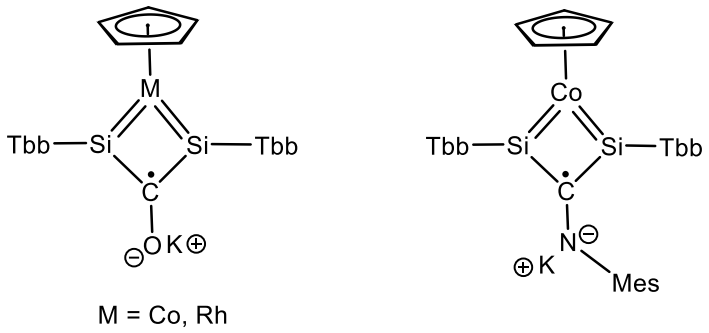

Figure 90. Feasible radical anions of the unsaturated four-membered metallacycles.

The open-shell chemistry of the Fe bis-germylidyne complex cation (**34-Fe**) might be explored (see a in ***Figure 91***). In this context, 1e- reduction of the 18-VE cobalt bis-germylidyne complex cation (**30-Co**) is reversible leading to an open-shell bis-germylidyne complex, the structure and reactivity of which remains to be explored (see b in ***Figure 91***).

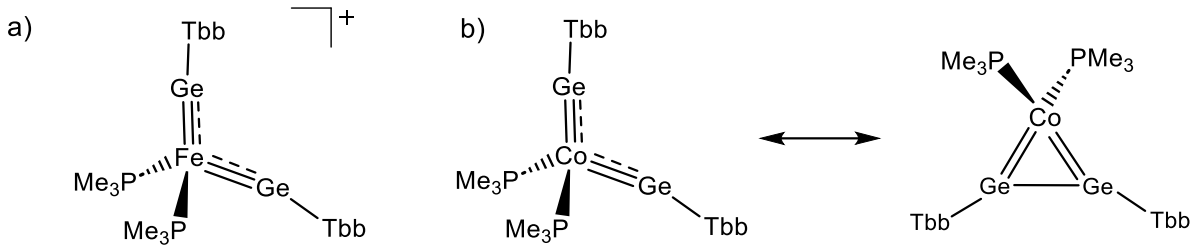

Figure 91. Feasible open shell neutral cobalt bis-germylidyne complex.

Finally, starting from the cationic sila-germavinylidene **39-Si**, germylenes could be accessed in nucleophilic substitution reactions with $NEt_4[EBr_2Ar^R]$ [E = Ge, Sn], which then might give upon reduction the unsymmetrical digermynes or stanna-germynes (***Scheme 64***).

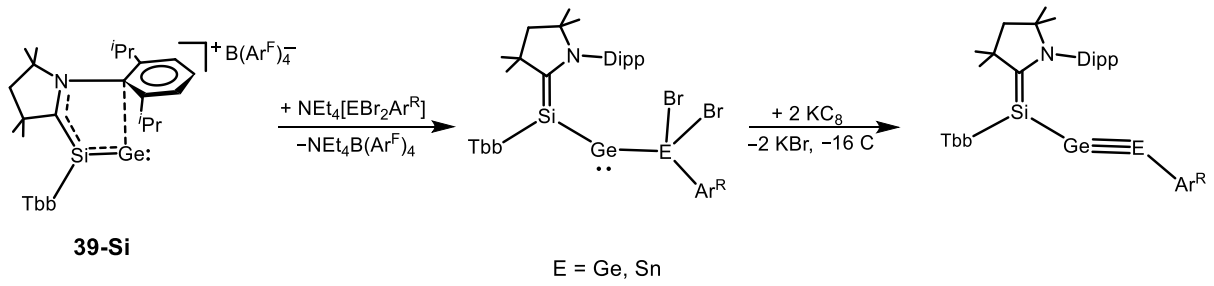

Ar^F = 3,5-(CF_3)-C_6H_3, Ar^R =C_6H_3-Mes_2, Mes = C_6H_2-2,4,6-Me_3

Scheme 64. A plausible approach to synthesize a base free heavier heteroalkyne.

4. Experimental Section

4.1. General Part

All experiments were carried out under strict exclusion of air and moisture in an atmosphere of argon using Schlenk or glove box techniques. Argon was commercially received with a purity of ≥ 99.998 % and passed through a gas purification system composed of two consecutive columns to remove traces of oxygen and water. The first column was filled with the BTS copper catalyst R3−11G from BASF and operating at ca. 80 °C, whereas the second column was filled with 4 Å molecular sieves and kept at room temperature. All glassware was cleaned by storage in a KOH/isopropanol bath for 2 – 3 days, followed by thoroughly washing with tap water, then storage in the dilute HCl bath for 1 – 2 hours and finally cleaned with tap water, acetone and distilled water. All cleaned glassware was dried in a drying oven at approximately 110 °C and baked in fine vacuum (10^{-2} mbar) prior to use. Stainless steel transfer and filter cannulas (∅ = 1 or 2 mm) were used for the transfer of liquids and filtrations through Glass Microfiber filters (GF/B) from Whatman™ filters respectively. Fritted glass (porosity: *P3*) was used for the filtrations carried out inside the glove boxes.
All solvents were dried upon refluxing over suitable drying agents, were purged several times with argon during reflux and distilled under argon. The following drying agents were used for the solvents:

Solvents	Prior storage over	Predrying agents	Drying agents
n-hexane, *n*-pentane and PE		Na-wire	sodium-wire/tetraglyme (0.5 vol%)
Tetrahydrofuran (THF)[a]	KOH	Na-wire	Na-wire/benzophenone dianion (Na2[Ph2CO])[a]
Dimethoxyethane (DME)[a]	KOH	Na-wire	Na-wire/benzophenone dianion ($Na_2[Ph_2CO]$)
Diethyl ether (Et_2O)[a]	KOH	Na-wire	Na-wire/benzophenone dianion ($Na_2[Ph_2CO]$)
Benzene, toluene		Na-wire	Na-wire
Chloroform ($CHCl_3$)		Sicapent	CaH_2
Dichloromethane (CH_2Cl_2)[b]	$CaCl_2$	Sicapent	CaH_2
Fluorobenzene[C]		CaH_2	$LiAlH_4$[C]

[a]: THF, DME and Et2O are typically dried by distillation over Na/benzophenone ketyl ($Na_2[Ph_2CO]$), see references [239] and [240]. For the synthesis and characterization of $Na_2[Ph_2CO]$ see [241]. [b]: Commercially available dichloromethane (CH_2Cl_2) depending on the supplier contained either traces of ethanol or amylenes, which were removed upon extraction of the solvent with sulfuric acid and water. Therefore, a thoroughly drying procedure needed to be carried out, involving the distillation from two sicapent predryer flasks. [c]: Commercially available fluorobenzene contained traces of acetone, which were removed upon stirring the predried solvent over $LiAlH_4$ for atleast 3 h and freshly trap to trap recondensed prior to use.

After distillation all solvents were degassed by freeze-pump-thaw cycles and stored in glove boxes in SCHOTT DURAN® laboratory glass bottles. For extremely air sensitive compounds, the solvents *n*-pentane and benzene were stirred over night over KC_8 and filtered inside the glovebox prior to use. For air-stable compounds, commercially available solvents were used without purification.

4.2. Analytical Methods

4.2.1. IR Spectroscopy

IR spectra of solutions were recorded on a Nicolet 380 or Vector 22 FT-IR spectrometer in the range of 2400 – 1500 cm^{-1} using a cell of either NaCl or CaF_2 windows. IR spectra of the pure solids were recorded on a Bruker Alpha FT-IR spectrometer in the range of 4000 – 400 cm^{-1} in the glovebox using the platinum single reflection diamond ATR module. The following abbreviations were used for the intensities of absorption bands: vs = very strong, s = strong, m = medium, w = weak, vw = very weak, sh = shoulder, br = broad.

4.2.2. NMR Spectroscopy

The NMR spectra were recorded either on a Bruker Avance 300 MHz or a Bruker Avance IIID 500 MHz NMR spectrometer in dry deoxygenated deuterated solvents, using Ø = 5 mm NMR tubes equipped with J. Young valves. The deuterated solvents were dried by stirring over sodium-potassium alloy ((D_6)benzene, (D_8)toluene, (D_8)THF) or CaH_2 ((D_2)dichloromethane degassed and then trap-to-trap condensed and stored over molecular sieves (4 Å) in Schlenk flasks equipped with J. Young valves. The ^{1}H and $^{13}C\{^{1}H\}$ NMR spectra were calibrated against the residual proton and natural abundance ^{13}C resonances of the deuterated solvent relative to tetramethyl silane set at δ = 0 ppm ((D_6)benzene: δ_H = 7.15 ppm and δ_C = 128.0 ppm; (D_8)toluene: δ_H = 2.08 ppm and δ_C = 20.43 ppm; (D_8)THF: δ_H = 1.73 ppm and δ_C = 25.3 ppm; (D_2)dichloromethane: δ_H = 5.32 ppm and δ_C = 53.8 ppm), respectively. The recently reported ^{1}H no-D NMR method was employed at the Bruker Avance IIID 500 MHz NMR spectrometer and was used for monitoring reaction mixture solutions in benzene(C_6H_6), fluorobenzene (C_6H_5F) and *m*-difluorobenzene (C_6H_4-1,3-F_2).[242] The $^{31}P\{^{1}H\}$ and ^{29}Si NMR spectra were calibrated using the ^{2}H frequency of the deuterated solvent (lock frequency) and the frequency ratio value $\Xi(^{31}P)$ = 40.480742 and $\Xi(^{29}Si)$ = 19.867187 as recommended by IUPAC for H_3PO_4 (85% aqueous solution), and $SiMe_4$ (φ(volume fraction) = 1% in (D_1)chloroform) respectively as external reference.[243] The ^{15}N NMR spectra were calibrated using the ^{2}H frequency of the deuterated solvent (lock frequency) and the frequency ratio value

$\Xi(^{15}N)$ = 10.132912 as recommended by IUPAC for neat liquid ammonia as external reference.[243] All lock frequencies were calibrated internally against the ^{1}H NMR signals of the solution of tetramethylsilane (δ_H = 0 ppm) with a volume fraction of ≤ 1 % in the corresponding degassed deuterated solvent. The ^{15}N NMR signals of the compounds were obtained by inverse detected 2D NMR (^{1}H-^{15}N HMBC pulse sequence) experiments. The following abbreviations were used for the forms and multiplicities of the NMR signals: s − singlet, d − doublet, t − triplet, sept − septet, m − multiplet, br − broad. The full width at half maximum of broad signals was designated with $\Delta\nu_{1/2}$ and is given in Hz. All coupling constants are given in Hz as absolute values regardless of their signs. The ^{1}H and ^{13}C NMR signals of all compounds were assigned by a combination of ^{1}H-^{1}H COSY, ^{1}H-^{13}C HMQC and HMBC experiments.

4.2.3. X-ray Crystallography

Typically, crystals for the X-ray diffraction analysis were filtered from their supernatant solution at the temperature of crystallization and covered with Fomblin Y® lubricant to protect from air and moisture. A crystal suitable for the measurement was selected on a microscope and transferred to the diffractometers. The data collection was performed on Bruker X8-Kappa ApexII, Bruker D8-Venture, STOE IDPS-2T and STOE STADIVARI diffractometers using either graphite monochromated Mo-K_α radiation (λ = 0.7107 Å) or Cu- K_α radiation (λ = 1.54178 Å). The diffractometers were equipped with a low-temperature device (Oxford Cryostream 700er series, 100.0 K). Intensities were measured by fine-slicing ω and φ-scans and corrected for background, polarization and Lorentz effects. An absorption correction by integration was applied for all data sets.[x] The structures were solved by direct methods and refined anisotropically by the least-squares procedure implemented in the SHELX program system.[xi] Hydrogen atoms except the silicon/germanium-bonded hydrogen atom were included using the riding model on the bound carbon atoms. The silicon/germanium-bonded hydrogen atom was found on the difference Fourier map and anisotropically refined. Selected crystallographic refinement data are listed in section **5.2**. The sample handling and measurement was done by the central X-ray crystallographic facility of the Institute.

[x] SADABS, 2009/2, AXS, 2009.

[xi] G. M. Sheldrick, SHELXS97 and SHELXL97, University of Göttingen, Germany, 1997.

4.2.4. Elemental Analysis

The C, H, N analyses were carried out in triplicate for each sample using an Elementar Vario Micro elemental analyzer. The individual C, H and N values did not differ by more than ± 0.3 %, and the mean C, H, N values are given for each compound. The sample handling and measurement was done by the central EA facility of the Institute.

4.2.5. Melting Point Determination

The melting points were determined of analytically pure samples in duplicate using a Büchi melting point apparatus M-560, which was calibrated by using the following melting points standards: 4-nitrotoluene (52.5 +/– 0.2 °C at 0.5 °C/min), diphenylacetic acid (147.7 +/– 0.2 °C at 0.5 °C/min), caffeine (236.5 +/– 0.2 °C at 0.5 °C/min), and potassium nitrate (334.5 +/– 0.2 °C at 0.5 °C/min). The samples were sealed in glass capillaries under vacuum and heated once with a gradient of 10 °C/min for a rough determination of the melting point or temperature of starting decomposition. Heating of the second and third samples was then repeated with a gradient of 2 °C/min starting 25 °C below the temperature of melting or decomposition determined in the first experiment. The onset temperature of melting or decomposition of the samples is given without correction for the temperature gradient. The thermally treated samples were cooled to ambient temperature and analyzed either by No-D ^{1}H NMR spectroscopy[242] in fluorobenzene or ^{1}H/^{31}P NMR spectroscopy in (D_6)benzene to elucidate whether decomposition had occurred.

4.2.6. Cyclic Voltammetry

The cyclic voltammetry studies were performed using a Metrohm Autolab PGSTAT100N potentiostat/galvanostat (compliance voltage = 100 V), further equipped with a SCAN250 true linear scan generator module and an ADC10M ultra-fast sampling module. The results were analyzed with the NOVA software version 2.1.5. All experiments were carried out inside a glove box under argon in a gas-tight, specially designed full-glass three-electrode electrochemical cell at ambient temperature. The electrochemical cell used for the CV experiments was composed of a glassy-carbon disk electrode (Ø = 2 mm) as a working electrode (WE), a Pt wire (Ø = 1 mm) as a counter electrode (CE) and a second Pt wire (Ø = 1 mm) as a reference electrode (RE). All potentials are given relative to the half-wave potential ($E_{1/2}$) of the redox couple $[Fe(C_5Me_5)_2]^{+/0}$ ($DMFc^{+/0}$), which was determined at the end of the experiment under the same experimental condition.[244] The CV experiments were carried out in fluorobenzene using 1.3 mmol/L of the analyte and 60 mmol/L

$[N(^{n}Bu)_4][Al(OC(CF_3)_3)_4$[245,246] as conductivity salt. An automatic ohmic drop (iR-drop) compensation for the uncompensated resistance (R_u) of the electrolyte solution existing between the WE and RE was applied for all voltammograms by experimentally determining the R_u during the experiments. The assignment of electrochemical processes as oxidation or reduction was done by comparing the $E_{1/2}$ values of the redox couple with the open circuit potential (OCP) of the analyte, which is defined as the equilibrium potential of the solution of analyte and electrolyte at zero current flow and was determined before the experiment. An $E_{1/2}$ greater than OPC indicates electrochemical oxidation and an $E_{1/2}$ lower than OPC indicates electrochemical reduction process of the analyte. The electrochemical processes - reversible (E_r), quasi-reversible (E_q), irreversible (E_i) and a reversible electrochemical process coupled with irreversible chemical reaction (E_rC_i) were distinguished according to the criteria given in reference [247,248].

4.2.7. UV-Vis NIR Spectroscopy

The UV-Vis-NIR spectra of analytically pure compounds were recorded on a Thermo Scientific Evolution 300 spectrometer in a special designed quartz cuvette under inert conditions. The sample solutions were prepared inside the glove box using pure samples and extremely dry and degassed toluene. The measurements were performed using three different path lengths (d = 1 mm, 5 mm and 10 mm) and four different concentrations (ranging from 400 µmol L^{-1} to 10 µmol L^{-1}) at ambient temperature. the extinction coefficient (ε) were determined by plotting absorbance to concentration of the appropriate absorbance band, and determining the gradient of the linear regressed line through the data points using Microsoft Excel programme.

4.3. List of compounds prepared according to literature

Compound	Experimenter	Reference
$GeBr_2$•(1,4-dioxane)	Filippou group members	[249]
Tbb-Br	Filippou group members	[250,251]
$[TbbGeBr]_2$	Palui	[101]
Ge_2Tbb_2	Palui	[101]
$[TbbSiBr]_2$	Filippou group members	[82]
Si_2Tbb_2	Palui/Tomer	[21]
$SiBr_4$	Gstrein	[xiii]
$caac^{Me}$	Gstrein	[xiii]
$SiBr_2(caac^{Me})$	Palui/Gstrein	[xiii,ix]
$Si_2Br_2(caac^{Me})_2$	Palui/Gstrein	[xiii]
KC_8	Palui/Kumar/Gstrein	[252,253]
$Na[B(C_6H_3\text{-}3,5\text{-}(CF_3)_2)_4]$	Tewes/Kumar	[254,255]
MesLi	Gstrein	[256]
$[Rh(CO)_2Cl]_2$	Palui/Tomer	[257,258]
$CpRh(CO)_2$	Palui	[259]
$Co(PMe_3)_3Cl$	Palui	[260]
$Ni(PMe_3)Cl_2$	Palui/Gomm	[261]
$Fe(PMe_3)_2Cl_2$	Filippou group members	[262]
$NEt_4[Cp^*Ti(CO)_4]$	Palui/Tomer	[230]
IMe_4	Filippou group members	[263]
PMe_3	Filippou group members	[264]
MesNC	Filippou group members	[265]

4.4. List of commercially available reagents

Compound	Supplier	Purification
n-butyl lithium (1.6 M in *n*-hexane)	Chemetall	used as received
tert.-butyl lithium (1.9 M in *n*-pentane)	Acros	used as received
$AlMe_3$ (2 M in Tol)	Sigma-aldrich	used as received
Mesityl acetylene	TCI	used as received
Phenyl acetylene	Fluka	Stirring over K_2CO_3 followed by a distillation
2-butyne	ABCR	Stirring over CaH_2 followed by a trap to trap condensation
1,5-cyclooctadiene	TCI	Stirring over CaH_2 followed by a trap to trap condensation
$CpCo(CO)_2$	ABCR	used as received
$Ni(COD)_2$	Sigma-aldrich	used as received
CO (99.9997 %)		Air Liquide
C_2H_4 (99.5 %)		Air Liquide
naphthalene	Across	Sublimation at 70 °C
Trimethylsilyldiazomethane (2 M in *n*-hexane)	Sigma-aldrich	used as received
TlCp	Sigma-aldrich	Sublimation at 60 °C

4.5. Syntheses and Analytical/Spectroscopic data of Compounds

4.5.1. [CpCo(CO)Ge_2Tbb_2] (**1-Co**)

A dark red stock solution (0.348 M in *n*-hexane) of $CpCo(CO)_2$ (0.99 mL, 0.345 mmol, 1.03 equiv.) was added slowly to a stirred reddish orange solution of Ge_2Tbb_2 (350 mg, 0.334 mmol, 1 equiv.) in 20 mL of *n*-hexane at ambient temperature. The colour of the reaction solution immediately turned brown. The reaction solution was stirred at ambient temperature and the progress of the reaction was followed by FT-IR spectroscopy and ^{1}H NMR spectroscopy. After 5 min the IR spectrum of the reaction solution indicated the selective formation of the mono-carbonyl complex **1- Co** (ν(CO) = 1956 cm^{-1}) in addition to little unreacted $CpCo(CO)_2$ (ν(CO) = 2031 and 1971 cm^{-1}). Analysis of an aliquot of the reaction solution by ^{1}H NMR spectroscopy in (D_6)benzene revealed a complete consumption of Ge_2Tbb_2 and the selective formation of **1-Co** along with little TbbH (ca. 5 mol%).[xii] The reaction solution was worked up by evaporating the solvent to dryness in vacuum followed by crystallization of the brown crude product from Et_2O (4 mL) at −60 °C. The resulting brown microcrystals were isolated by filtration at −60 °C and dried under fine vacuum at 0 °C for 30 min to afford the mono-ether solvate **1-Co•Et_2O**. Yield: 305 mg (0.24 mmol, 72 % from Ge_2Tbb_2).

Attempts to obtain the solvate-free form upon drying of **1-Co•Et_2O** in fine vacuum for 6 hrs. at ambient temperature or at 60 °C for 4 hrs. failed leading only to partial loss of Et_2O and extensive decomposition.

Properties: Compound **1-Co•Et_2O** is a highly air-sensitive, brown solid turning immediately pale green upon contact with air. It can be stored under argon atmosphere at ambient temperature for several months. **1-Co•Et_2O** is very well soluble in *n*-pentane, benzene, toluene, Et_2O and THF at room temperature. Under

---

[xii] 3,5-bis(bistrimethyl(silyl)methyl)-1-*tert*-butylbenzene (TbbH) was identified by NMR spectroscopy upon comparison with an authentic sample, which was obtained as a white solid after quenching of LiTbb with H_2O followed by work-up. NMR spectroscopic data of TbbH: ^{1}H NMR (500.1 MHz, (D_6)benzene, 298 K): δ (ppm) = 0.12 (s, 36H, $C^{3,5}$-C(Si*Me*$_3$)$_2$), 1.31 (s, 9H, C^1-C*Me*$_3$), 1.40 (s, 2H, $C^{3,5}$-C*H*(SiMe$_3$)$_2$), 6.42 (br, $\Delta\nu_{1/2}$ = 20 Hz, 1H, C^4-*H*), 6.79 (brs, $\Delta\nu_{1/2}$ = 7 Hz, 2H, $C^{2,6}$-*H*). ^{13}C NMR (125.8 MHz, (D_6)benzene, 298 K): δ (ppm) = 0.47 (s, 12C, $C^{3,5}$-CH(Si*Me*$_3$)$_2$), 29.8 (s, 2C, $C^{3,5}$-*C*H(SiMe$_3$)$_2$), 31.6 (s, 3C, C^1-C*Me*$_3$), 34.4 (s, 1C, C^1-*C*Me$_3$), 121.3 (brs, $\Delta\nu_{1/2}$ = 72 Hz, 2C, *C*^{2,6}-H), 127.1 (br s, $\Delta\nu_{1/2}$ > 100 Hz, *C*^{4}-H), 142.5 (s, 2C, *C*^{3,5}-CH(SiMe$_3$)$_2$), 150.6 (s, 1C, *C*^{1}-CMe$_3$).

strict exclusion of air, solutions of **1-Co•Et$_2$O** in (D_6)benzene and (D_8)THF are stable for at least one week without any sign of decomposition. However, heating of these solutions at 60 °C for few hours leads to unselective decomposition.

Elemental analysis: 1-Co•Et$_2$O ($C_{58}H_{113}CoGe_2O_2Si_8$, 1271.35 g mol^{-1}): calcd./%: C 54.79, H 8.96; found/%: C 53.98, H 8.87; **Melting Point:** 208 °C (dec.).

IR (Et_2O): $\tilde{\nu}$ (cm^{-1}) = 1953 (s) [ν(CO)], 1582 (w) and 1528 (w) [ν(CC)$_{aryl}$].
IR (*n*-hexane): $\tilde{\nu}$ (cm^{-1}) = 1956 (s) [ν(CO)], 1583 (w) and 1528 (w) [ν(CC)$_{aryl}$].
ATR-IR (solid): $\tilde{\nu}$ (cm^{-1}) = 2950 (m), 2898 (w), 2865 (w), 2739 (vw), 1959 (s) [ν(CO)], 1580 (w) and 1526 (w) [ν(CC)$_{aryl}$], 1476 (vw), 1461 (vw), 1413 (vw, sh), 1392 (m), 1361 (vw), 1350 (vw), 1245 (s), 1212 (vw), 1167 (w), 1122 (w), 1077 (vw), 1021 (w), 996 (w), 984 (w), 955 (w), 947 (w), 935 (w), 882 (m), 833 (vs), 801 (s), 770 (sh), 760 (s), 736 (m), 718 (m), 684 (s), 661 (m), 641 (w), 623 (w), 610 (w), 577 (w), 553 (w), 519 (m), 487 (w), 466 (vw), 412 (m).
^{1}H NMR (500.1 MHz, (D_6)benzene, 298 K): δ (ppm) = 0.26, 0.31 (each br, $\Delta\nu_{1/2}$ = 10 Hz and 19 Hz, 72H, 8 × Si*Me$_3$*, *2* × C^{2,6}-CH(Si*Me$_3$*)$_A$(Si*Me$_3$*)$_B$, 2 × Tbb), 1.37 (s, 18H, 2 × C*Me$_3$*, 2 × Tbb), ca. 1.57* (very broad, 2H, C^{2,6}-C*H*(Si*Me$_3$*)$_A$(Si*Me$_3$*)$_B$, Tbb$_X$), 2.45 (very br, ca. $\Delta\nu_{1/2}$ = 91 Hz, 2H, C^{2,6}-C*H*(SiMe$_3$)$_A$(SiMe$_3$)$_B$, Tbb$_Y$), 4.92 (s, 5H, C$_5$*H$_5$*), 6.95 (br, $\Delta\nu_{1/2}$ = 14 Hz, 4H, 2 × *C^{3,5}-H*, 2 × Tbb); the full width of half maximum ($\Delta\nu_{1/2}$) of the very broad signal marked with an asterisk (*) could not be exactly determined due to its partial overlap with the singlet signal of the C*Me$_3$* groups at δ = 1.37 ppm.
^{1}H-NMR (500.1 MHz, (D_8)THF, 298 K): δ (ppm) = 0.14, 0.20 (each br, $\Delta\nu_{1/2}$ = 38 Hz and 10 Hz, 72H, 8 × Si*Me$_3$*, *2* × C^{2,6}-CH(Si*Me$_3$*)$_A$(Si*Me$_3$*)$_B$, 2 × Tbb), 1.36 (s, 18H, 2 × C*Me$_3$*, 2 × Tbb), 2.29 (very br, $\Delta\nu_{1/2}$ = 91 Hz, 2H, C^{2,6}-C*H*(SiMe$_3$)$_A$(SiMe$_3$)$_B$, Tbb$_Y$), 4.84 (s, 5H, C$_5$*H$_5$*), 6.82 (s, 4H, 2 × *C^{3,5}-H*, 2 × Tbb); the very broad methine proton signal of the C^{2,6}-C*H*(SiMe$_3$)$_A$(SiMe$_3$)$_B$ group of Tbb$_X$ substituent was not observed and is most probably obscured by the singlet signal of the C*Me$_3$* groups at δ = 1.36 ppm.
^{1}H-NMR (300.1 MHz, (D_8)THF, 213 K): δ (ppm) = 0.05 (s, 18H, 2 × SiMe$_3$, C^{2,6}-CH(Si*Me$_3$*)$_A$, Tbb$_Y$), 0.09 (s, 9H, SiMe$_3$, *C^2*-CH(Si*Me$_3$*)$_A$, Tbb$_X$), 0.15 (s, 9H, SiMe$_3$, C^6-CH(Si*Me$_3$*)$_A$, Tbb$_X$), 0.19 (s, 18H, 2 × SiMe$_3$, C^{2,6}-CH(Si*Me$_3$*)$_B$, Tbb$_Y$), 0.20 (s, 9H, SiMe$_3$, C^2-CH(Si*Me$_3$*)$_B$, Tbb$_X$), 0.26 (s, 9H, SiMe$_3$, C^6-CH(Si*Me$_3$*)$_B$, Tbb$_X$), 0.99 (s, 1H, C^2-C*H*(SiMe$_3$)$_A$(SiMe$_3$)$_B$, Tbb$_X$), 1.33 (s, 9H, C^4-C*Me$_3$* Tbb$_X$), 1.38 (s, 9H, C^4-C*Me$_3$*, Tbb$_Y$),1.62 (s, 1H, C^6-C*H*(SiMe$_3$)$_A$(SiMe$_3$)$_B$, Tbb$_X$), 2.43 (br, $\Delta\nu_{1/2}$ = 19 Hz, 2H, C^{2,6}-C*H*(SiMe$_3$)$_A$(SiMe$_3$)$_B$, Tbb$_Y$), 4.83 (s, 5H, C$_5$*H$_5$*), 6.67 (br d, ^{4}*J*(H,H) = 2 Hz, 1H, C^3-*H*, Tbb$_X$), 6.79 (s, 2H, C^{3,5}-*H*, Tbb$_Y$), 6.84 (br d, ^{4}*J*(H,H) = 2 Hz, 1H, C^5-*H*, Tbb$_X$).

$^{13}C\{^1H\}$ NMR (125.8 MHz, (D_8)THF, 298 K): δ (ppm) =1.7 (s, 24C, 8 × $SiMe_3$, $C^{2,6}$-$CH(SiMe_3)_A(SiMe_3)_B$, 2 × Tbb), 31.5 (s, 6C, 2 × C^4-CMe_3, 2 × Tbb), 34.3 (br, $\Delta\nu_{1/2}$ = 26 Hz, 4C, 2 × $C^{2,6}$-$CH(SiMe_3)_A(SiMe_3)_B$, 2 × Tbb), 35.1 (s, 2C, 2 × C^4-CMe_3, 2 × Tbb), 88.5 (s, 5C, C_5H_5), 122.8 (s, 4C, 2 × $C^{3,5}$-H, 2 × Tbb), 147.7 (very br, $\Delta\nu_{1/2}$ = ca. 240 Hz, 2 × C^1, 2 × Tbb), 150.7 (very br, $\Delta\nu_{1/2}$ = ca. 57 Hz, 2C, 2 × C^4, 2 × Tbb), 203.1 (very br, $\Delta\nu_{1/2}$ = 30 Hz, 1C, CO); the signal of the $C^{2,6}$-$CH(SiMe_3)_A(SiMe_3)_B$ carbon atoms was not detected.

$^{13}C\{^1H\}$ NMR (75.5 MHz, (D_8)THF, 213 K): δ (ppm) = 1.0 (s, 3C, C^2-$CH(SiMe_3)_A$, Tbb_X), 1.40 (s, 3C, C^2-$CH(SiMe_3)_B$, Tbb_X), 1.45 (br, 6C, $C^{2,6}$-$CH(SiMe_3)_A(SiMe_3)_B$, Tbb_Y), 1.9 (s, 3C, C^6-$CH(SiMe_3)_A$, Tbb_X), 2.5 (s, 3C, C^6-$CH(SiMe_3)_B$, Tbb_X), 31.42 (s, 3C, C^4-CMe_3, Tbb_Y), 31.48 (s, 3C, C^4-CMe_3, Tbb_X), 33.1 (s, 1C, C^2-$CH(SiMe_3)_A(SiMe_3)_B$,Tbb_X), 33.7 (br, $\Delta\nu_{1/2}$ = 19 Hz, 2C, 2 × C^2-$CH(SiMe_3)_A(SiMe_3)_B$, Tbb_Y), 34.7 (s, 1C, C^6-$CH(SiMe_3)_A(SiMe_3)_B$, Tbb_X), 35.04 (s, 1C, C^4-CMe_3, Tbb_Y), 35.09 (s, 1C, C^4-CMe_3, Tbb_X), 88.7 (s, 5C, C_5H_5), 122.35 (s, 1C, 1 × C^5-H (Tbb_X)), 122.39 (br, 2C, $C^{3,5}$-H, (Tbb_Y)), 123.1 (br, $\Delta\nu_{1/2}$ = 5 Hz, 1C, C^3-H, Tbb_X), 144.7 (s, 1C, C^6, Tbb_X), 146.9 (s, 1C, C^2, Tbb_X), 147.7 (s, 2C, $C^{2,6}$, Tbb_Y), 148.9 (s, 1C, C^1, Tbb_Y), 150.0 (s, 1C, C^4, Tbb_X), 150.7 (s, 1C, C^4, Tbb_Y), 152.5 (s, 1C, C^1, Tbb_X), 203.1 (br, $\Delta\nu_{1/2}$ = 9 Hz, 1C, CO).

4.5.2. [CpRh(CO)Ge_2Tbb_2] (1-Rh)

To a stirred orange solution of Ge_2Tbb_2 (0.700 mg, 0.670 mmol, 1 equiv.) in 30 mL of *n*-hexane, a stock solution (0.393 M in n-hexane) of $CpRh(CO)_2$ (1.74 mL, 0.683 mmol, 1.02 equiv.) was added dropwise at ambient temperature. The colour of the reaction solution immediately changed to dark green. The reaction solution was stirred at ambient temperature and the progress of the reaction was followed by FT-IR spectroscopy and ^1H NMR spectroscopy. After 5 min the IR spectrum of the reaction solution indicated the selective formation of the complex **1-Rh** (ν(CO) = 1972 cm^{-1}) in addition to little unreacted $CpRh(CO)_2$. Analysis of an aliquot of the reaction solution by ^1H NMR spectroscopy in (D_6)benzene revealed a complete consumption of Ge_2Tbb_2 and very selective formation of **1-Rh**. The reaction solution was worked up by evaporating the solvent to dryness in vacuum followed by crystallization of the dark green crude product from Et_2O (8 mL) at −60 °C. The resulting dark green crystals were isolated by filtration at −60 °C and dried under fine vacuum at 0 °C for 45 min to afford the mono-ether solvate **1-Rh•Et_2O**. Yield: 687 mg (0.522 mmol, 78 % from Ge_2Tbb_2).

Attempts to obtain the solvate-free form upon drying of **1-Rh•Et$_2$O** in fine vacuum for 5 hrs. at ambient temperature or at 60 °C for 2 hrs. failed leading only to partial loss of Et_2O and minute decomposition.

Properties: Compound **1-Rh•Et$_2$O** is a highly air-sensitive, dark green solid, turning immediately colourless upon contact with air. It can be stored under argon atmosphere at –30 °C for several months. **1-Rh•Et$_2$O** is well soluble in *n*-pentane, benzene, toluene, Et_2O and THF at room temperature. Under strict exclusion of air, solutions of **1-Rh•Et$_2$O** in (D_6)benzene and (D_8)THF are stable for at 24 hrs. without any sign of decomposition.

Elemental analysis: 1-Rh•Et$_2$O ($C_{58}H_{113}Ge_2O_2RhSi_8$, 1315.33 g mol^{-1}): calcd./%: C 52.96, H 8.66; found/%: C 52.76, H 8.75; **Melting Point:** 204 °C (dec.).

IR (*n*-hexane): $\tilde{\nu}$ (cm^{-1}) = 1972 (s) [ν(CO)], 1582 (w), 1540 (w, sh) and 1528 (w) [ν(CC)$_{aryl}$].
IR (THF): $\tilde{\nu}$ (cm^{-1}) = 1966 (s) [ν(CO)], 1582 (w), 1541 (w, sh) and 1528 (w) [ν(CC)$_{aryl}$].
ATR-IR (solid): $\tilde{\nu}$ (cm^{-1}) = 3060 (vw, br), 2960 (m, sh), 2950 (m), 2898 (w, br), 2865 (w, br), 2738 (vw, br), 1974 (s), 1966 (s) and 1930 (vw, br) [ν(CO)], 1580 (w), 1540 (vw, sh) and 1527 (w) [ν(CC)$_{aryl}$], 1475 (w, br), 1462 (vw, br, sh), 1414 (vw, br, sh), 1392 (m), 1361 (w), 1254 (m, sh), 1245 (s), 1213 (vw, br), 1169 (w), 1169 (w, sh), 1122 (w), 1077 (vw), 1021 (vw), 1013 (vw), 999 (vw), 983 (vw, sh), 953 (w), 947 (w), 934 (w), 883 (m), 855 (s, sh), 833 (vs), 822 (vs, sh), 779 (s), 772 (s, sh), 760 (s), 737 (m), 719 (m), 684 (s), 661 (m), 641 (w), 624 (w), 609 (vw), 587 (bw, br), 553 (vw, br), 543 (vw, br), 506 (w, sh), 496 (w), 474 (w), 416 (w).
^{1}H NMR (500.1 MHz, (D_6)benzene, 298 K): δ (ppm) = 0.26, 0.29, 0.30 and 0.34 (each s, br, $\Delta\nu_{1/2}$ = 17 Hz, 7 Hz, 17 Hz and 15 Hz, 72H, 8 × Si*Me$_3$, 2* × C^{2,6}-CH(Si*Me$_3$*)$_A$(Si*Me$_3$*)$_B$, 2 × Tbb), 1.34 (s, 18H, 2 × C*Me$_3$*, 2 × Tbb), 1.88 (br, $\Delta\nu_{1/2}$ = 35 Hz, 2H, C^{2,6}-C*H*(SiMe$_3$)$_A$(SiMe$_3$)$_B$, Tbb), 2.84 (s, br, $\Delta\nu_{1/2}$ = 16 Hz, 2H, C^{2,6}-C*H*(SiMe$_3$)$_A$(SiMe$_3$)$_B$, Tbb), 5.38 (d, ^2J (^{103}Rh-^{1}H) = 0.3 Hz, 5H, C_5H_5), 6.85 and 6.98 (s, br, $\Delta\nu_{1/2}$ = 20 Hz and s, br, $\Delta\nu_{1/2}$ = 16 Hz, 4H, 2 × *C^{3,5}-H*, 2 × Tbb).
^{1}H-NMR (400.1 MHz, (D_8)THF, 298 K): δ (ppm) = 0.10 and 0.20 (s, br, $\Delta\nu_{1/2}$ = 8 Hz and s, 72H, 8 × Si*Me$_3$, 2* × C^{2,6}-CH(Si*Me$_3$*)$_A$(Si*Me$_3$*)$_B$, 2 × Tbb), 1.33 (s, br, $\Delta\nu_{1/2}$ = 12 Hz, 18H, 2 × C*Me$_3$*, 2 × Tbb), 2.69 (s, br, $\Delta\nu_{1/2}$ = 17 Hz, 2H, C^{2,6}-C*H*(SiMe$_3$)$_A$(SiMe$_3$)$_B$, 2 × Tbb), 1.71** (very br, 2H, C^{2,6}-C*H*(SiMe$_3$)$_A$(SiMe$_3$)$_B$, 2 × Tbb), 5.29 (d, ^2J (^{103}Rh-^{1}H) = 0.4 Hz, 5H, C_5H_5), 6.77 and 6.80 (sh, very br and s, br, $\Delta\nu_{1/2}$ = 15 Hz, 4H, 2 × *C^{3,5}-H*, 2 × Tbb). ** this signal is appearing underneath of the deuterated solvent.

^{1}H-NMR (300.1 MHz, (D_8)THF, 193 K): δ (ppm) = 0.07, 0.11, 0.18 and 0.22 (each s, 72H, 8 × Si*Me*$_3$, *2* × C^{2,6}-CH(Si*Me*$_3$)$_A$(Si*Me*$_3$)$_B$, 2 × Tbb$_{X,Y}$), 1.31 and 1.35 (each s, 18H, 2 × C*Me*$_3$, 2 × Tbb$_{X,Y}$), 1.55 (s, 1H, C^2-C*H*(SiMe$_3$)$_{A,B}$, Tbb$_X$), 1.70 (s, 1H, C^6-C*H*(SiMe$_3$)$_{A,B}$, Tbb$_X$), 5.26 (s, 5H, C_5H_5), 6:63 (d, ^4J (^{1}H-^{1}H) = 1.4 Hz, 1H, C^3-*H*, Tbb$_x$), 6.76 (s, 2H, C^{3,5}-*H*, Tbb$_Y$), 6.77 (sh, br, 1H, C^5-*H*, Tbb$_x$). ***Signal corresponds to C^{2,6}-C*H*(SiMe$_3$)$_{A,B}$ of is not detected.

^{13}C{^{1}H} NMR (125.8 MHz, (D_6)benzene, 298 K): δ (ppm) = 1.6 (s, br, $\Delta\nu_{1/2}$ = 23 Hz, 24C, 8 × Si*Me*$_3$, *2* × C^{2,6}-CH(Si*Me*$_3$)$_A$(Si*Me*$_3$)$_B$, 2 × Tbb), 31.3 (s, 6C, 2 × C*Me*$_3$, 2 × Tbb), 33.8 (s, br, $\Delta\nu_{1/2}$ = 12 Hz, 2C, C^{2,6}-*C*H(SiMe$_3$)$_A$(Si*Me*$_3$)$_B$, Tbb), 34.0 (very br, 2C, C^{2,6}-*C*H(SiMe$_3$)$_A$(Si*Me*$_3$)$_B$, Tbb), 34.5 (s, br, $\Delta\nu_{1/2}$ = 14 Hz, 2C, 2 × *C*Me$_3$, 2 × Tbb), 92.31 (d, ^1J (^{103}Rh-^{13}C) = 2.4 Hz, 5C, C_5H_5), 122.2 (s, 4C, *C*^{3,5}-H, 2 × Tbb), 147.6** (s, br $\Delta\nu_{1/2}$ = 13 Hz), 148.0** (s, br, $\Delta\nu_{1/2}$ = 16 Hz), 150.2 (s, 2C, *C*^{4}, 2 × Tbb), 151.4**(s, br, $\Delta\nu_{1/2}$ = 16 Hz), 192.81 (d, ^1J (^{103}Rh-^{13}C) = 84 Hz, 1C, Rh-*C*O). **Carbon atoms are not assigned because of non-detection of any cross peak in (^{13}C-^{1}H)-HMBC experiment.

^{13}C{^{1}H} NMR (75.5 MHz, (D_8)THF, 193 K): δ (ppm) = 1.0, 1.4, 1.8 and 2.4 (each m, br, 24C, 8 × Si*Me*$_3$, *2* × C^{2,6}-CH(Si*Me*$_3$)$_A$(Si*Me*$_3$)$_B$, Tbb$_{X,Y}$), 31.37 and 31.43 (each br, each $\Delta\nu_{1/2}$ = 9.4 Hz, 6C, 2 × C*Me*$_3$, 2 × Tbb$_{X,Y}$), 33.5 (s, br, $\Delta\nu_{1/2}$ = 5.4 Hz, 1C, C^2-*C*H(SiMe$_3$)$_{A,B}$, Tbb$_X$), 34.6 (s, br, $\Delta\nu_{1/2}$ = 7 Hz, 1C, C^6-*C*H(SiMe$_3$)$_{A,B}$, Tbb$_X$), 35.0 and 35.1 (each s, 2C, 2 × *C*Me$_3$, 2 × Tbb$_{X,Y}$), 93.01 (d, ^1J (^{103}Rh-^{13}C) = 1.8 Hz, 5C, C_5H_5), 122.0 (s, 1C, *C*^{5}-H, Tbb$_X$), 123.1 (s, 1C, *C*^{3}-H, Tbb$_X$), 144.7 (s, 1C, *C*^{2}, Tbb$_X$), 146.7 (s, 1C, *C*^{6}, Tbb$_X$), 147.5 (s, 2C, *C*^{2,6}, Tbb$_Y$), 148.1 (s, br, $\Delta\nu_{1/2}$ = 6 Hz, *C*^{1}, Tbb$_Y$), 150.3 and 150.4 (each s, 2C, *C*^{4}, Tbb$_{X,Y}$), 152.18 (s, 1C, *C*^{1}, Tbb$_X$), 193.14 (d, ^1J (^{103}Rh-^{13}C) = 83 Hz, 1C, Rh-*C*O).***signals correspond to *C*^{3,5}-H of Tbb$_Y$ was not detected.

4.5.3. [CpCo(GeBrTbb)$_2$] (2-Co)

$Ge_2Br_2Tbb_2$ (425 mg, 0.353 mmol, 1 equiv.) was suspended in 10 mL of *n*-hexane and a dark orange solution of $CpCo(C_2H_4)_2$ (64 mg, 0.353 mmol, 1 equiv.) in 2 mL of *n*-hexane was added to the suspension at ambient temperature. The colour of the reaction mixture turned black-purple immediately. After 1 h of stirring at ambient temperature, a ^{1}H NMR spectrum of an aliquot of the black-purple reaction solution was recorded revealing the quantitative formation of **2-Co**. All volatiles were then removed under reduced pressure to give a dark purple residue, which was crystallized from *n*-hexane (4 mL) at −60 °C. The dark purple microcrystals of **2-Co** grown after one day were isolated by filtration at −60 °C and dried in a fine vacuum for 2 hrs. at 40° C. Yield: 325 mg (0.244 mmol, 69 % from $Ge_2Br_2Tbb_2$).

Properties: Compound **2-Co** is an extremely air-sensitive, black-purple solid that decolorizes immediately upon contact with air. It is very well soluble in *n*-hexane, benzene, toluene and Et_2O to give black-purple solutions.

Elemental analysis: 2-Co ($C_{53}H_{103}Br_2CoGe_2Si_8$, 1329.03 g mol^{-1}): calcd./%: C 47.90, H 7.81; found/%: C 47.45, H 7.93 %; **Melting Point:** 192 °C (dec.).

^{1}H NMR (500.1 MHz, (D_6)benzene, 298 K): δ (ppm) = 0.32 (s, 72H, 2 × $C^{2,6}$-CH(Si*Me*$_3$)$_2$, 2 × Tbb), 1.29 (s, 18H, 2 × C^4-C*Me*$_3$, 2 × Tbb), 2.69 (s, 4H, 2 × $C^{2,6}$-C*H*(SiMe$_3$)$_2$, 2 × Tbb), 4.95 (s, 5H, C_5*H*$_5$), 6.86 (s, 4H, 2 × $C^{3,5}$-*H*, 2 × Tbb).
^{13}C{^{1}H} NMR (125.8 MHz, (D_6)benzene, 298 K): δ (ppm) = 1.5 (s, 24C, 2 × $C^{2,6}$-CH(Si*Me*$_3$)$_2$, 2 × Tbb), 30.3 (s, 4C, 4C, 2 × $C^{2,6}$-*C*H(SiMe$_3$)$_2$, 2 × Tbb), 31.2 (s, 6C, 2 × C^4-C*Me*$_3$, 2 × Tbb), 34.6 (s, 2C, 2 × C^4-*C*Me$_3$, 2 × Tbb), 79.5 (s, 5C, *C*$_5$H$_5$), 122.1 (s, 4C, 2 × *C*^{3,5}-H, 2 × Tbb), 145.5 (s, 4C, 2 × *C*^{2,6}, 2 × Tbb), 152.6 (s, 2C, 2 × *C*^{4}, 2 × Tbb), 155.5 (s, 2C, 2 × *C*^{1}, 2 × Tbb).

4.5.4. [CpCo(Ge$_2$Tbb$_2$)] (3-Co)

Complex **2-Co** (400 mg, 0.30 mmol, 1 equiv.) was dissolved in 15 mL of benzene and KC_8 (82 mg, 0.61 mmol, 2.02 equiv.) was added in one portion at ambient temperature. The reaction mixture was stirred for 16 hrs. at room temperature. During this period the colour of the reaction solution changed gradually from black-purple to reddish-brown. ^{1}H NMR spectroscopic analysis of an aliquot of the reaction mixture revealed the complete and selective conversion of **2-Co** to **3-Co**. The reddish-brown solution was separated from the black insoluble part and evaporated to dryness in vacuo. The brown mass was dissolved in 3 mL of *n*-hexane and the solution was stored for one day at −60 °C. The dark brown crystals obtained were separated by filtration and dried for 3 hrs. at 40 °C in vacuo. Yield: 220 mg (0.188 mmol, 63 % from **2-Co**).

Properties: Compound **3-Co** is an air-sensitive, red brown solid and it is very well soluble in *n*-hexane, benzene, toluene and Et_2O. A sample solution of **3-Co** in (D_6)benzene does not show any sign of decomposition after 4 days at ambient temperature.

Elemental analysis: 3-Co ($C_{53}H_{103}CoGe_2Si_8$, 1169.22 g mol^{-1}): calcd./%: C 54.44, H 8.88; found/%: C 54.52, H 8.92; **Melting Point:** 160 °C (dec.).

^{1}H NMR (500.1 MHz, (D_6)benzene, 298 K): δ (ppm) = 0.27 (s, 72H, 2 × $C^{2,6}$-CH(Si*Me*$_3$)$_2$, 2 × Tbb), 1.39 (s, 18H, 2 × C^4-C*Me*$_3$, 2 × Tbb), 2.23 (s, 4H, 2 × $C^{2,6}$-C*H*($SiMe_3$)$_2$, 2 × Tbb), 4.87 (s, 5H, C_5*H*$_5$), 7.00 (s, 4H, 2 × $C^{3,5}$-*H*, 2 × Tbb).
^{13}C{^{1}H} NMR (125.8 MHz, (D_6)benzene, 298 K): δ (ppm) = 1.3 (s, 24C, 2 × $C^{2,6}$-CH(Si*Me*$_3$)$_2$, 2 × Tbb), 31.4 (s, 6C, 2 × C^4-C*Me*$_3$, 2 × Tbb), 33.1 (s, 4C, 4C, 2 × $C^{2,6}$-*C*H($SiMe_3$)$_2$, 2 × Tbb), 34.6 (s, 2C, 2 × C^4-*C*Me_3, 2 × Tbb), 75.1 (s, 5C, *C*$_5$H$_5$), 121.8 (s, 4C, 2 × *C*^{3,5}-H, 2 × Tbb), 143.4 (s, 2C, 2 × *C*^{1}, 2 × Tbb), 147.2 (s, 4C, 2 × *C*^{2,6}, 2 × Tbb), 152.3 (s, 2C, 2 × *C*^{4}, 2 × Tbb).

4.5.5. [CpCo(MesNC)Ge$_2$Tbb$_2$] (4-Co)

To a stirred red brown solution of **3-Co** (470 mg, 402 mmol, 1 equiv.) in 10 mL of *n*-hexane, a stock solution (0.1737 M in *n*-hexane) of MesNC (2.31 mL, 0.402 mmol, 1 equiv.) was added dropwise at ambient temperature. The colour of the reaction solution immediately turned olive green. After 5 min of stirring at ambient temperature, analysis of an aliquot of the reaction mixture by ^{1}H NMR spectroscopy revealed complete consumption of starting materials and quantitative formation of **4-Co**. The reaction was worked up by evaporating the solvent to dryness in vacuo. The dark green mass was redissolved in 1.7 mL of Et_2O and kept at –30 for 2 days. Dark green microcrystals of **4-Co** were separated from its mother liquor by filtration at –30 °C and dried for 3.5 hrs.in fine vacuum at 40 °C. Yield: 362 mg (0.275 mmol, 68.5 % from **3-Co**).

Properties: Compound **4-Co** is an air-sensitive, dark green solid and it is very well soluble in *n*-hexane, benzene, toluene and Et_2O. An olive green sample solution of **4-Co** in (D_6)benzene does not show any sign of decomposition after 2 days at ambient temperature.

Elemental analysis: 4-Co ($C_{63}H_{114}CoGe_2NSi_8$, 1314.42 g mol^{-1}): calcd./%: C 57.57, H 8.74, N 1.06; found/%: C 57.39, H 8.89, N 1.12; **Melting Point:** 215 °C (dec.).

IR (*n*-hexane): $\tilde{\nu}$ (cm^{-1}) = 2036 (m, br) [ν(CN)], 1581 (vw), and 1526 (vw) [$\nu(CC)_{aryl}$].
IR (THF): $\tilde{\nu}$ (cm^{-1}) = 2038 (m, br) [ν(CN)], 1581 (vw), and 1525 (vw) [$\nu(CC)_{aryl}$].
ATR-IR (solid): $\tilde{\nu}$ (cm^{-1}) = 2958 (m, sh), 2950 (m), 2898 (w), 2864 (w, sh), 2817 (vw, br), 2763 (vw, br), 2043 (m, sh), 2022 (s, br) and 1967(w) [ν(CN)], 1581 (w), 1540 (vw, br) and 1527 (w) [$\nu(CC)_{aryl}$], 1475 (w), 1461 (w, sh), 1392 (m), 1360 (w), 1348 (vw, sh), 1257 (m), 1244 (s), 1208 (w), 1171 (w), 1157 (w), 1024 (w), 999 (w), 947 (w, br), 933 (w, sh), 884 (m), 856 (m, sh), 834 (vs), 798 (m, sh), 761 (m), 738 (w), 716 (w), 683 (m,

br), 662 (w), 641 (vw), 623 (vw), 610 (vw), 590 (vw, br), 552 (vw), 520 (w), 503 (vw), 478 (vw), 443 (vw), 414 (w).

^{1}H NMR (500.1 MHz, (D_6)benzene, 298 K): δ (ppm) = 0.25 (s, br, $\Delta\nu_{1/2}$ = 38 Hz, 72H, 2 × $C^{2,6}$-CH(Si*Me*$_3$)$_2$, 2 × Tbb), 1.42 (s, 18H, 2 × C*Me*$_3$, 2 × Tbb), 1.92 (s, 3H, C^4-*Me*, Mes), 2.10 (s, 6H, $C^{2,6}$-*Me*, Mes), 5.03 (s, 5H, C_5H_5), 6.52 (s, 2H, $C^{3,5}$-*H*, Mes), 7.00 (s, br, $\Delta\nu_{1/2}$ = 18.5 Hz, 4H, $C^{3,5}$-*H*, 2 × Tbb). **Signal corresponds to $C^{2,6}$-C*H*(SiMe$_3$)$_2$ was not detected.

^{1}H NMR (300.1 MHz, (D_8)THF, 298 K): δ (ppm) = 0.10 (s, br, $\Delta\nu_{1/2}$ = 18 Hz, 72H, 2 × $C^{2,6}$-CH(Si*Me*$_3$)$_2$, 2 × Tbb), 1.37 (s, 18H, 2 × C*Me*$_3$, 2 × Tbb), 2.01 (s, 6H, $C^{2,6}$-*Me*, Mes), 2.16 (s, 3H, C^4-*Me*, Mes), 4.78 (s, 5H, C_5H_5), 6.74 (s, 2H, $C^{3,5}$-*H*, Mes), 6.84 (s, br, $\Delta\nu_{1/2}$ = 6 Hz, 4H, 2 × $C^{3,5}$-*H*, 2 × Tbb), **Signal corresponds to $C^{2,6}$-C*H*(SiMe$_3$)$_2$ was not detected.

^{1}H NMR (300.1 MHz, (D_8)THF, 193 K): δ (ppm) = –0.03, 0.00, 0.01, 0.09, 0.17, 0.29 and 0.30 (each s, br, each ca. $\Delta\nu_{1/2}$ = 4 Hz, 72H, 2 × $C^{2,6}$-CH(Si*Me*$_3$)$_{A,B}$, Tbb$_{X,Y}$), 0.87 (s, 1H, C^2-C*H*(SiMe$_3$)$_{A,B}$, Tbb$_X$), 1.34 and 1.38 (each s, 18H, 2 × C*Me*$_3$, Tbb$_{X,Y}$), 1.96 (s, 6H, $C^{2,6}$-*Me*, Mes), 2.01 (s, 1H, C^6-C*H*(SiMe$_3$)$_{A,B}$, Tbb$_X$), 2.16 (s, 3H, C^4-*Me*, Mes), 2.45 (s, 1H, C^2-C*H*(SiMe$_3$)$_{A,B}$, Tbb$_Y$), 3.64 (s, 1H, C^6-C*H*(SiMe$_3$)$_{A,B}$, Tbb$_Y$), 4.77 (s, 5H, C_5H_5), 6.69 (s, br, $\Delta\nu_{1/2}$ = 4.4 Hz, 1H, C^3-*H*, Tbb$_X$), 6.78 (s, br, $\Delta\nu_{1/2}$ = 4.1 Hz, 1H, C^3-*H*, Tbb$_Y$), 6.79 (s, br, $\Delta\nu_{1/2}$ = 3.6 Hz, 1H, $C^{3,5}$-*H*, Mes), 6.84 (s, br, $\Delta\nu_{1/2}$ = 4.8 Hz, 1H, C^5-*H*, Tbb$_Y$), 6.88 (s, br, $\Delta\nu_{1/2}$ = 4.5 Hz, 1H, C^5-*H*, Tbb$_X$).

^{13}C{^{1}H} NMR (125.8 MHz, (D_6)benzene, 298 K): δ (ppm) = 1.8 (s, br, $\Delta\nu_{1/2}$ = 46 Hz, 8 × Si*Me*$_3$, 2 × $C^{2,6}$-CH(Si*Me*$_3$)$_2$, 2 × Tbb), 20.1 (s, 2C, $C^{2,6}$-*Me*, Mes), 20.9 (s, 1C, C^4-*Me*, Mes), 31.4 (s, 6C, 2 × C*Me*$_3$, 2 × Tbb), 34.6 (s, 2C, 2 × *C*Me$_3$, 2 × Tbb), 87.8 (s, 5C, *C*$_5$H$_5$), 122.4 (s, br, $\Delta\nu_{1/2}$ = 21 Hz, 4C, 2 × *C*^{3,5}-H, 2 × Tbb), 128.8 (s, 2C, *C*^{3,5}-H, Mes), 129.7 (s, 1C, *C*^{1}, Mes), 133.9 (s, 2C, *C*^{2,6}, Mes), 135.5 (s, 1C, *C*^{4}, Mes), 149.5 (s, 2C, 2 × *C*^{4}, 2 × Tbb).172.9** (very br, 1C, MesN*C*), ** the full width of half maximum ($\Delta\nu_{1/2}$) could not be exactly determined, ***signals correspond to *C*^{2,6}-*C*H(SiMe$_3$)$_2$ and *C*^{1} of the Tbb ligand were not detected.

^{13}C{^{1}H} NMR (75.5 MHz, (D_8)THF, 193 K): δ (ppm) = 0.87 (s, 3C, C^6-CH(Si*Me*$_3$)$_A$(SiMe$_3$)$_B$, Tbb$_Y$), 0.93 (s, 3C, C^2-CH(Si*Me*$_3$)$_A$(SiMe$_3$)$_B$, Tbb$_X$), 1.6 (s, 3C, C^2-CH(Si*Me*$_3$)$_A$(SiMe$_3$)$_B$, Tbb$_Y$), 1.7 (s, 3C, C^6-CH(Si*Me*$_3$)$_A$(SiMe$_3$)$_B$, Tbb$_X$), 1.8 (s, 3C, C^2-CH(SiMe$_3$)$_A$(Si*Me*$_3$)$_B$, Tbb$_Y$), 2.1 (s, 3C, C^6-CH(SiMe$_3$)$_A$(Si*Me*$_3$)$_B$, Tbb$_X$), 2.42 (s, 3C, C^2-CH(SiMe$_3$)$_A$(Si*Me*$_3$)$_B$, Tbb$_X$), 2.43 (s, 3C, C^6-CH(SiMe$_3$)$_A$(Si*Me*$_3$)$_B$, Tbb$_Y$), 20.4 (s, 2C, $C^{2,6}$-*Me*, Mes), 21.2 (s, 1C, C^4-*Me*, Mes), 30.7 (s, br, $\Delta\nu_{1/2}$ = 4.2 Hz, 1C, C^6-*C*H(SiMe$_3$)$_A$(SiMe$_3$)$_B$, Tbb$_Y$), 31.5 and 31.6 (each s, br, each ca. $\Delta\nu_{1/2}$ = 5 Hz, 6C, 2 × C*Me*$_3$, Tbb$_{X,Y}$), 33.5 (s, br, $\Delta\nu_{1/2}$ = 4.7 Hz, 1C, C^2-*C*H(SiMe$_3$)$_A$(SiMe$_3$)$_B$, Tbb$_Y$), 34.0 (s, br, $\Delta\nu_{1/2}$ = 4.4 Hz, 1C, C^6-

*C*H(SiMe$_3$)$_A$(SiMe$_3$)$_B$, Tbb$_X$), 35.0 and 35.2 (each s, 2C, 2 × *C*Me$_3$, Tbb$_{X,Y}$), 88.0 (s, 5C, *C*$_5$H$_5$), 122.1 (m, br, *C*^{3}-H, Tbb$_Y$), 122.4 (m, br, *C*^{5}-H, Tbb$_X$), 122.6 (m, br, *C*^{3}-H, Tbb$_X$), 123.3 (m, br, *C*^{5}-H, Tbb$_Y$), 129.2 (s, br, $\Delta\nu_{1/2}$ = 5 Hz, 2C, *C*^{3,5}-H, Mes), 129.7 (s, *C*^{1}, Mes), 134.4 (s, 2C, *C*^{2,6}-Me, Mes), 136.3 (s, 1C, *C*^{4}-Me, Mes), 143.7 (s, 1C, *C*^{6}, Tbb$_X$), 146.2 (s, 1C, *C*^{2}, Tbb$_Y$), 146.9 (s, 1C, *C*^{2}, Tbb$_X$), 148.7 (s, *C*^{6}, Tbb$_Y$), 149.4 and 149.6 (each s, 2C, *C*^{4}, Tbb$_{X,Y}$), 150.1 (s, 1C, *C*^{1}, Tbb$_Y$), 154.0 (s, 1C, *C*^{1}, Tbb$_X$), 172.4** (very br, 1C, MesN*C*). ** the full width of half maximum ($\Delta\nu_{1/2}$) could not be exactly determined.

4.5.6. [CpCo(Ge$_2$Tbb$_2$C$_2$Me$_2$)] (5-Co).

Complex **1-Co•Et$_2$O** (170 mg, 0.134 mmol, 1 equiv.) was dissolved in 30 mL of *n*-hexane in a 200 mL Schlenk tube. An excess of 2-butyne (0.40 mL, 5.1 mmol, 39 equiv.) was added to the brown solution at ambient temperature without any apparent change in colour. The Schlenk tube was sealed and the reaction solution heated at 60 °C. The reaction solution first slowly took on a greenish-brown hue and then gradually turned green. The progress of the reaction was followed by IR and ^{1}H NMR spectroscopy showing a slow and selective conversion of **1-Co** to **5-Co**, which was completed within 65 hrs. Afterwards all volatiles were removed in vacuo. The resulting dark green residue was redissolved in Et$_2$O (2 mL) and the solution stored at −60 °C for 3 days. The dark green crystals of **5-Co** obtained were isolated by filtration at −60 °C and dried for 1 h at 40 °C in a fine vacuum. Yield: 119 mg (0.10 mmol, 75 % from **1-Co•Et$_2$O**).

Properties: Compound **5-Co** is a highly air-sensitive, dark green solid and well soluble in *n*-hexane, benzene, toluene and Et$_2$O at ambient temperature, but insoluble in Acetonitrile. Under strict exclusion of air a solution of **5-Co** in (D$_6$)benzene does not show any sign of decomposition after one week at ambient temperature.

Elemental analysis: 5-Co (C$_{57}$H$_{109}$CoGe$_2$Si$_8$, 1223.31 g mol^{-1}): calcd./%: C 55.96, H 8.98; found/%: C 55.58, H 8.96; **Melting Point:** 260 °C (dec.).

^{1}H NMR (500.1 MHz, (D$_6$)benzene, 298 K): δ (ppm) = 0.22 (s, 36H, 2 × C^{2,6}-CH(Si*Me$_3$)$_A$, 2 × Tbb), 0.29 (s, 36H, 2 × C^{2,6}-CH(Si*Me$_3$)$_B$, 2 × Tbb), 1.38 (s, 18H, 2 × C^4-C*Me$_3$*, 2 × Tbb), 1.64 (s, 6H, C$_2$*Me$_2$*), 2.45 (s, 4H, 2 × C^{2,6}-C*H*(SiMe$_3$)$_2$, 2 × Tbb), 5.03 (s, 5H, C$_5$*H$_5$*), 6.92 (s, 4H, 2 × C^{3,5}-*H*, 2 × Tbb).

^{13}C{^{1}H} NMR (125.8 MHz, (D$_6$)benzene, 298 K): δ (ppm) = 1.6 (s, 12C, 2 × C^{2,6}-CH(Si*Me$_3$)$_A$*, 2 × Tbb), 1.8 (s, 12C, 2 × C^{2,6}-CH(Si*Me$_3$)$_B$*, 2 × Tbb), 19.7 (s, 2C, 2 × *Me,* C$_2$*Me$_2$*), 29.2 (s, 4C, 2 × C^{2,6}-*C*H(SiMe$_3$)$_2$), 31.4 (s, 6C, 2 × C^4-C*Me$_3$*, 2 × Tbb), 34.5 (s,

2C, 2 × C^{4}-*C*Me$_3$, 2 × Tbb), 80.8 (s, 5C, *C*$_5$H$_5$), 122.6 (s, 4C, 2 × *C*^{3,5}-H, 2 × Tbb), 146.1 (s, 4C, 2 × *C*^{2,6}, 2 × Tbb) 150.5 (s, 2C, *2* × *C*^{4}, 2 × Tbb), 150.7 (s, 2C, 2 × *C*^{1}, 2 × Tbb), 164.2 (s, 2C, *C*$_2$Me$_2$).

4.5.7. [CpCo(Ge$_2$Tbb$_2$C$_2$Me$_2$)$_{cbd}$] (6-Co)

A red-brown solution of **3-Co** (705 mg, 0.603 mmol, 1 equiv.) in 15 mL of *n*-hexane was treated with 2-butyne (0.47 mL, 6.0 mmol, 10 equiv.) at ambient temperature. The reaction mixture was heated in an oil bath at 60 °C for 5 hrs. The colour of the reaction solution slowly changed to brownish-green. An aliquot of the reaction solution was studied by ^{1}H NMR spectroscopy and showed the complete consumption of **3-Co** and a quite selective formation of a mixture of **5-Co** and **6-Co** in the molar ratio of 1.1 : 1. Subsequently all volatiles were removed in vacuo. The resulting dark brown residue was dissolved in 2.5 mL of Et$_2$O and the solution stored at −60 °C overnight. The dark brown microcrystals obtained were isolated by filtration at −60 °C and dried for 2 hrs. at 40 °C in a fine vacuum. ^{1}H NMR spectroscopic analysis of the microcrystals showed a 1.03 : 1 mixture of **5-Co** and **6-Co**. Yield: 580 mg (0.474 mmol, 79 % from **3-Co**).

The NMR spectroscopic data of **6-Co** given below were derived from the NMR spectra of the mixture of **5-Co** and **6-Co** after comparison with the NMR spectra of pure **5-Co.**

^{1}H NMR (500.1 MHz, (D$_6$)benzene, 298 K): *δ* (ppm) = 0.26 (s, 36H, 2 × C^{2,6}-CH(Si*Me$_3$)$_A$, 2 × Tbb), 0.29 (s, 36H, 2 × C^{2,6}-CH(Si*Me$_3$)$_B$, 2 × Tbb), 1.32 (s, 18H, 2 × C^{4}-C*Me$_3$*, 2 × Tbb), 2.00 (s, 6H, C$_2$*Me$_2$*), 2.96 (s, 4H, 2 × C^{2,6}-C*H*(SiMe$_3$)$_2$, 2 × Tbb), 4.91 (s, 5H, C$_5$*H$_5$*), 6.96 (s, 4H, 2 × C^{3,5}-*H*, 2 × Tbb).

^{13}C{^{1}H} NMR (125.8 MHz, (D$_6$)benzene, 298 K): *δ* (ppm) = 1.8 (s, 12C, 2 × C^{2,6}-CH(Si*Me$_3$)$_A$*, 2 × Tbb), 1.9 (s, 12C, 2 × C^{2,6}-CH(Si*Me$_3$)$_B$*, 2 × Tbb), 21.7 (s, 2C, 2 × *Me,* C$_2$*Me$_2$*), 31.2 (s, 6C, 2 × C^{4}-C*Me$_3$*, 2 × Tbb), 32.2 (s, 4C, 2 × C^{2,6}-*C*H(SiMe$_3$)$_2$), 34.4 (s, 2C, 2 × C^{4}-*C*Me$_3$, 2 × Tbb), 81.4 (s, 5C, *C*$_5$H$_5$), 86.7 (s, 2C, *C*$_2$Me$_2$), 122.2 (s, 4C, 2 × *C*^{3,5}-H, 2 × Tbb), 134.9 (s, 2C, *2* × *C*^{1}, 2 × Tbb), 150.0 (s, 4C, 2 × *C*^{2,6}, 2 × Tbb), 150.3 (s, 2C, 2 × *C*^{4}, 2 × Tbb).

4.5.8. Ge$_2$Tbb$_2$C$_2$Me$_2$ (7-Ge)

Ge$_2$Tbb$_2$ (250 mg, 0.239 mmol, 1 equiv.) was dissolved in 20 mL of *n*-hexane and the orange solution was cooled to −60 °C. A 0.126 M stock solution of 2-butyne in *n*-hexane (1.9 mL, 0.239 mmol, 1.0 equiv.) was slowly added by syringe to the solution of Ge$_2$Tbb$_2$ at −60 °C. Upon addition the colour of the reaction solution immediately

turned dark green. The solution was stirred for 1 h at −60 °C and then slowly warmed to room temperature. An aliquot of the dark green reaction solution was analyzed by ^{1}H NMR spectroscopy revealing the selective formation of **7-Ge** along with a small amount of **8-Ge** (ca. 7 mol%) and some unreacted Ge_2Tbb_2 (ca. 7 mol%). All volatiles were removed under vacuum and the resulting green residue was dissolved in *n*-pentane (3 mL). The solution was stored at −60 °C for 2 days to yield green crystals of **7-Ge**, which were isolated by filtration at −60 °C and dried for 1 h at ambient temperature in a fine vacuum. Yield: 170 mg (0.155 mmol, 65 % from Ge_2Tbb_2).

Properties: Compound **7-Ge** is an extremely air-sensitive, dark green solid, which decolorizes immediately upon contact with air. It is well soluble in *n*-pentane, benzene, Et_2O and THF at ambient temperature, and converts slowly to an equimolar mixture of Ge_2Tbb_2 and **8-Ge** in solution at ambient temperature. Monitoring of this reaction by ^{1}H NMR spectroscopy in (D_6)benzene revealed a very slow conversion at 25 °C (ca. 6 mol % after 4 h), which can be accelerated at 70 °C (ca. 40 mol % after 7 h).

Elemental analysis: 7-Ge ($C_{52}H_{104}Ge_2Si_8$, 1099.29 g mol^{-1}): calcd./%: C 56.81, H 9.54; found/%: C 56.48, H 9.62; **Melting Point:** 225 °C (dec.).

^{1}H NMR (300.1 MHz, (D_6)benzene, 298 K): δ (ppm) = 0.24 (s, 72H, 2 × C^{2,6}-CH(Si*Me$_3$*)$_2$, 2 × Tbb), 1.36 (s, 18H, 2 × C^4-C*Me$_3$*, 2 × Tbb), 2.02 (s, 6H, 2 × Me, C$_2$*Me$_2$*), 2.38 (s, 4H, 2 × C^{2,6}-C*H*(SiMe$_3$)$_2$, 2 × Tbb), 6.95 (s, 4H, 2 × C^{3,5}-*H*, 2 × Tbb).

^{1}H NMR (500.1 MHz, (D_8)THF, 298 K): δ (ppm) = 0.11 (s, 72H, 2 × C^{2,6}-CH(Si*Me$_3$*)$_2$, 2 × Tbb), 1.32 (s, 18H, 2 × C^4-C*Me$_3$*, 2 × Tbb), 1.99 (s, 6H, 2 × Me, C$_2$*Me$_2$*), 2.22 (s, 4H, 2 × C^{2,6}-C*H*(SiMe$_3$)$_2$, 2 × Tbb), 6.80 (s, 4H, 2 × C^{3,5}-*H*, 2 × Tbb).

^{13}C{^{1}H} NMR (125.8 MHz, (D_8)THF, 298 K): δ (ppm) = 1.4 (s, 24C, 2 × C^{2,6}-CH(Si*Me$_3$*)$_2$, 2 × Tbb), 20.1 (s, 2C, 2 × *Me*, C$_2$*Me$_2$*), 31.6 (s, 6C, 2 × C^4-C*Me$_3$*, 2 × Tbb), 32.1 (s, 4C, 2 × C^{2,6}-*C*H(SiMe$_3$)$_2$, 2 × Tbb), 35.0 (s, 2C, 2 × C^4-*C*Me$_3$, 2 × Tbb), 122.6 (s, 4C, 2 × *C^{3,5}*-H, 2 × Tbb), 148.1 (s, 2C, 2 × *C^1*, 2 × Tbb),148.8 (s, 4C, 2 × *C^{2,6}*, 2 × Tbb),151.5 (s, 2C, 2 × *C^4*, 2 × Tbb), 203.7 (s, 2C, *C$_2$*Me$_2$).

4.5.9. $Ge_2Tbb_2C_4Me_4$ (8-Ge)

A reddish orange solution of Ge_2Tbb_2 (300 mg, 0.29 mmol, 1 equiv.) in 20 mL of *n*-hexane was cooled to −60 °C and a stock solution of 2-butyne (4.8 mL of 0.126 M stock solution in *n*-hexane, 0.60 mmol, 2.1 equiv.) was added slowly by syringe in to it. The colour of the reaction solution immediately turned to dark green and then to orange within few minutes. The reaction solution was stirred for 30 min at −60 °C and then warmed to room temperature. ^{1}H NMR spectroscopic analysis of an aliquot

of the orange reaction solution revealed the selective formation of **8-Ge**. All volatiles were then removed under reduced pressure to give a bright orange residue, which was crystallized from Et_2O (3 mL) at −30 °C. The orange block like crystals of **8-Ge** obtained after one day were isolated by filtration at −30 °C and dried in fine vacuum for 1 h at ambient temperature. Yield: 199 mg (0.17 mmol, 60 % from Ge_2Tbb_2).

Properties: Compound **8-Ge** is a moderately air-sensitive orange solid, which is very well soluble in *n*-hexane, benzene, toluene and Et_2O at ambient temperature.

Elemental analysis: 8-Ge ($C_{56}H_{110}Ge_2Si_8$, 1153.38 g mol^{-1}): calcd./%: C 58.32, H 9.61; found/%: C 58.26, H 9.64; **Melting Point:** 274°C (dec.).

^{1}H NMR (500.1 MHz, (D_6)benzene, 298 K): δ (ppm) = 0.12 (s, 72H, 2 × $C^{2,6}$-CH(Si*Me*$_3$)$_2$, 2 × Tbb), 1.37 (s, 18H, 2 × C^4-C*Me*$_3$, 2 × Tbb), 2.43 (s, 4H, 2 × $C^{2,6}$-C*H*(SiMe$_3$)$_2$, 2 × Tbb), 2.66 (s, 12H, 2 × C_2*Me*$_2$), 7.00 (s, 4H, 2 × $C^{3,5}$-*H*, 2 × Tbb).
^{13}C{^{1}H} NMR (125.8 MHz, (D_6)benzene, 298 K): δ (ppm) = 1.1 (s, 24C, 4 × $C^{2,6}$-CH(Si*Me*$_3$)$_2$, 2 × Tbb), 22.9 (s, 4C, 2 × C_2*Me*$_2$), 31.3 (s, 6C, 2 × C^4-C*Me*$_3$, 2 × Tbb), 32.7 (s, 4C, 4C, 2 × $C^{2,6}$-*C*H(SiMe$_3$)$_2$, 2 × Tbb), 34.4 (s, 2C, 2 × C^4-*C*Me$_3$, 2 × Tbb), 122.3 (s, 4C, 2 × *C*^{3,5}-H, 2 × Tbb), 132.3 (s, 2C, 2 × *C*^{1}, 2 × Tbb), 150.3 (s, 4C, 2 × *C*^{2,6}, 2 × Tbb), 150.7 (s, 2C, 2 × *C*^{4}, 2 ×Tbb), 158.3 (s, 4C, 2 × *C*$_2$Me$_2$).

4.5.10. [CpCo(Ge$_2$Tbb$_2$C$_2$HPh)] (9-Co)

A solution of phenylacetylene (16 mg, 0.157 mmol, 1 equiv.) in 1 mL of *n*-hexane was added dropwise to a brown solution of **1-Co•Et$_2$O** (200 mg, 0.157 mmol, 1 equiv.) in 15 mL of *n*-hexane at ambient temperature. The colour of the reaction solution turned immediately dark green. After stirring for 10 min an aliquot of the reaction solution was analyzed by ^{1}H NMR spectroscopy showing a complete and selective conversion of **1-Co** to **9-Co**. All volatiles were removed in vacuo and the crude product was crystallized from *n*-hexane (2.4 mL) at −30 °C overnight. The dark green crystals of **9-Co** were isolated by filtering off the mother liquor at −30 °C using a filter cannula and then dried at 60 °C for 1.5 hrs. under fine vacuum. Yield: 160 mg (0.126 mmol, 80 % from **1-Co•Et$_2$O**).

Properties: Compound **9-Co** is a highly air-sensitive dark green solid. It is well soluble in *n*-hexane, benzene, toluene and Et_2O at ambient temperature, but insoluble in CH_3CN. Under strict exclusion of air, a solution of **9-Co** in (D_6)benzene does not show any sign of decomposition after one day at ambient temperature.

Elemental analysis: **9-Co** ($C_{61}H_{109}CoGe_2Si_8$, 1271.36 g mol^{-1}): calcd./%: C 57.63, H 8.64; found/%: C 57.50, H 8.71; **Melting Point:** 234°C (dec.).

^{1}H NMR (500.1 MHz, (D_6)benzene, 298 K): δ (ppm) = 0.07 (s, 18H, $C^{2,6}$-CH(Si*Me$_3$*)$_A$, Tbb_X), 0.17 (s, 18H, $C^{2,6}$-CH(Si*Me$_3$*)$_A$, Tbb_Y), 0.28 (s, 18H, $C^{2,6}$-CH(Si*Me$_3$*)$_B$, Tbb_X), 0.29 (s, 18H, $C^{2,6}$-CH(Si*Me$_3$*)$_B$, Tbb_Y), 1.37 (s, 9H, C^4-C*Me$_3$*, Tbb_Y), 1.38 (s, 9H, C^4-C*Me$_3$*, Tbb_X), 2.40 (s, ^2J(^{29}Si,^{1}H) = 9.5 Hz, 2H, $C^{2,6}$-C*H*($SiMe_3$)$_{A,B}$, Tbb_Y), 2.67 (s, ^2J(^{29}Si,^{1}H) = 9.3 Hz, 2H, $C^{2,6}$-C*H*($SiMe_3$)$_{A,B}$, Tbb_X), 5.10 (s, 5H, C_5H_5), 6.88 (s, 2H, $C^{3,5}$-*H*, Tbb_X), 6.90 (m, 3H, $C^{3,5}$-*H* and C^4-*H*, Ph), 6.95 (s, 2H, $C^{3,5}$-*H*, Tbb_Y), 7.21 (m, 2H, $C^{2,6}$-*H*, Ph), 7.54 (s, 1H, *H*CCPh).

^{13}C{^{1}H} NMR (125.8 MHz, (D_6)benzene, 298 K): δ (ppm) = 1.0 (s, 6C, $C^{2,6}$-CH(Si*Me$_3$*)$_B$, Tbb_Y), 1.2 (s, 6C, $C^{2,6}$-CH(Si*Me$_3$*)$_A$, Tbb_Y), 1.5 (s, 6C, $C^{2,6}$-CH(Si*Me$_3$*)$_B$, Tbb_X), 1.8 (s, 6C, $C^{2,6}$-CH(Si*Me$_3$*)$_A$, Tbb_X), 29.1 (s, ^1J(^{29}Si,^{13}C) = 41 Hz, 2C, $C^{2,6}$-*C*H($SiMe_3$)$_{A,B}$, Tbb_X), 30.4 (s, ^1J(^{29}Si,^{13}C) = 41 Hz, 2C, $C^{2,6}$-*C*H($SiMe_3$)$_{A,B}$, Tbb_Y), 31.4 (s, 6C, C^4-C*Me$_3$*, $Tbb_{X,Y}$), 34.56 and 34.58 (s each, 1C each, C^4-*C*Me_3, $Tbb_{X,Y}$), 80.6 (s, 5C, *C*$_5$H$_5$), 121.7 (s, 2C, *C*^{3,5}-H, Tbb_Y), 123.0 (s, 2C, *C*^{3,5}-H, Tbb_X), 127.9* (s, 1C, *C*^{4}-H, Ph), 128.4 (s, 2C, *C*^{3,5}-H, Ph), 128.6 (s, 2C, *C*^{2,6}-H, Ph), 139.9 (s, 1C, *C*^{1}, Ph), 145.3 (s, 2C, *C*^{2,6}, Tbb_X), 145.9 (s, 2C, *C*^{2,6}, Tbb_Y), 150.2 (s, 1C, *C*^{1}, Tbb_Y), 150.9 and 151.3 (s each, 1C each, *C*^{4}, $Tbb_{X,Y}$), 153.8 (s, 1C, *C*^{1}, Tbb_X), 159.9 (s, 1C, H*C*CPh), 168.4 (s, 1C, HC*C*Ph); *: this signal is masked by of that the deuterated solvent and was detected in the HMBC experiment.

4.5.11. [CpRh(Ge$_2$Tbb$_2$C$_2$HPh)] (9-Rh)

A solution of phenylacetylene (20 mg, 0.190 mmol, 1 equiv.) in 3 mL of *n*-hexane was added dropwise to a dark green solution of **1-Rh•Et$_2$O** (250 mg, 0.190 mmol, 1 equiv.) in 20 mL of *n*-hexane at ambient temperature. The colour of the reaction solution did not change. After stirring for 10 min at ambient temperature, an aliquot of the reaction solution was analyzed by ^{1}H NMR spectroscopy showing a complete and selective conversion of **1-Rh** to **9-Rh**. All volatiles were removed in vacuo and the crude product was crystallized from *n*-hexane (3 mL) at −30 °C overnight. The dark green crystals of **9-Rh** were isolated by filtering off the mother liquor at −30 °C using a filter cannula and then dried at 50 °C for 2 hrs. under fine vacuum. Yield: 175 mg (0.133 mmol, 70 % from **1-Rh•Et$_2$O**).

Properties: Compound **9-Rh** is extremely air-sensitive dark green solid. It is well soluble in *n*-hexane, benzene, toluene and Et_2O at ambient temperature. Under strict exclusion of air, a solution of **9-Rh** in (D_6)benzene does not show any sign of decomposition after one day at ambient temperature.

Elemental analysis: **9-Rh** ($C_{61}H_{109}Ge_2RhSi_8$, 1315.33 g mol^{-1}): calcd./%: C 55.70, H 8.35; found/%: C 55.79, H 8.23; **Melting Point:** 237°C (dec.).

^{1}H NMR (500.1 MHz, (D_6)benzene, 298 K): δ (ppm) = 0.07 (s, 18H, $C^{2,6}$-CH(Si*Me$_3$*)$_A$(SiMe$_3$)$_B$, Tbb$_Y$), 0.18 (s, 18H, $C^{2,6}$-CH(Si*Me$_3$*)$_A$(SiMe$_3$)$_B$, Tbb$_X$), 0.29 (s, 18H, $C^{2,6}$-CH(SiMe$_3$)$_A$(Si*Me$_3$*)$_B$, Tbb$_X$), 0.30 (s, 18H, $C^{2,6}$-CH(SiMe$_3$)$_A$(Si*Me$_3$*)$_B$, Tbb$_Y$), 1.37 (s, 18H, 2 × C*Me$_3$*, Tbb$_{X,Y}$), 2.23 (s, ^2J (^{29}Si-^{1}H) = 9.5 Hz, 2H, $C^{2,6}$-C*H*(SiMe$_3$)$_{A,B}$, Tbb$_X$), 2.58 (s, ^2J (^{29}Si-^{1}H) = 9.5 Hz, 2H, $C^{2,6}$-C*H*(SiMe$_3$)$_{A,B}$, Tbb$_Y$), 5.51 (d, ^2J (^{103}Rh-^{1}H) = 0.6 Hz, 5H, C$_5$*H$_5$*), 6.87 (s, 2H, $C^{3,5}$-*H*, Tbb$_Y$), 6.90 (m, 2H, $C^{3,5}$-*H*, Ph), 6.93 (s, 2H, $C^{3,5}$-*H*, Tbb$_X$), 6.94 (m, 1H, C^4-*H*, Ph), 7.26 (m, 2H, $C^{2,6}$-*H*, Ph), 8.06 (s, 1H, CPhC*H*).
^{13}C{^{1}H} NMR (125.8 MHz, (D_6)benzene, 298 K): δ (ppm) = 1.0 (s, 6C, $C^{2,6}$-CH(Si*Me$_3$*)$_A$(SiMe$_3$)$_B$, Tbb$_X$), 1.1 (s, 6C, $C^{2,6}$-CH(SiMe$_3$)$_A$(Si*Me$_3$*)$_B$, Tbb$_X$), 1.6 (s, 6C, $C^{2,6}$-CH(SiMe$_3$)$_A$(Si*Me$_3$*)$_B$, Tbb$_Y$), 1.8 (s, 6C, $C^{2,6}$-CH(Si*Me$_3$*)$_A$(SiMe$_3$)$_B$, Tbb$_Y$), 29.2 (s, ^1J(^{29}Si-^{13}C) = 42 Hz, 2C, $C^{2,6}$-*C*H(SiMe$_3$)$_{A,B}$, Tbb$_Y$), 30.5 (s, ^1J(^{29}Si-^{13}C) = 42 Hz, 2C, $C^{2,6}$-*C*H(SiMe$_3$)$_{A,B}$, Tbb$_X$), 31.38 and 31.39 (each s, 6C, 2 × C*Me$_3$*, Tbb$_{X,Y}$), 34.5 and 34.6 (each s, 2C, 2 × *C*Me$_3$, Tbb$_{X,Y}$), 84.1 (d, ^1J (^{103}Rh-^{13}C) = 3.7 Hz, 5C, *C$_5$*H$_5$), 121.6 (s, 2C, *C^{3,5}*-H, Tbb$_X$), 123.1 (s, 2C, *C^{3,5}*-H, Tbb$_Y$), 128.0* (s, 1C, *C^4*-H, Ph), 128.5 (s, 2C, *C^{3,5}*-H, Ph), 128.8 (s, 2C, *C^{2,6}*-H, Ph), 139.8 (s, 1C, *C^1*, Ph), 145.5 (s, 2C, *C^{2,6}*, Tbb$_Y$), 146.0 (s, 2C, *C^{2,6}*, Tbb$_X$), 149.94 (d, ^2J (^{103}Rh-^{13}C) = 8 Hz, 1C, *C^1*, Tbb$_X$), 151.0 and 151.5 (each s, 2C, 2 × *C^4*, Tbb$_{X,Y}$), 153.52 (d, ^2J (^{103}Rh-^{13}C) = 8 Hz, 1C, *C^1*, Tbb$_Y$), 164.28 (d, ^2J (^{103}Rh-^{13}C) = 8.5 Hz, 1C, PhC*C*H), 173.90 (d, ^2J (^{103}Rh-^{13}C) = 11 Hz, 1C, Ph*C*CH). **: this signal is masked by of that the deuterated solvent and was detected in the HMBC experiment.

4.5.12. [CpCo(Ge$_2$Tbb$_2$C$_2$HMes)] (10-Co)

A brown solution of **1-Co•Et$_2$O** (700 mg, 0.551 mmol, 1 equiv.) in 15 mL of benzene was treated with mesitylacetylene (318 mg, 2.21 mmol, 4 equiv.) and then heated at 75 °C. The colour of the reaction solution gradually turned to dark green. After heating for 24 hrs. an aliquot of the green reaction solution was taken and analyzed by ^{1}H NMR spectroscopy. This showed a complete conversion of **1-Co** and the formation of **10-Co** as the main product as well as the 1,2-digermabenzene (**11-Ge**), some $CpCo(CO)_2$ and unreacted mesitylacetylene. Subsequently all volatiles were removed in vacuo. The dark-green crude product was washed with 10 mL of CH_3CN : Et_2O (1:1, v/v) mixture to remove the unreacted alkyne, then dissolved in1.5 mL of *n*-hexane and the solution stored at −60 °C for two weeks. The resulting dark green precipitate was isolated by filtering off the green mother liquor at −60 °C using a filter cannula and then dried in vacuo for 1 h at 60 °C. ^{1}H NMR spectroscopic analysis of the obtained mass showed that **10-Co** was contaminated with ca.

7 mole % of **11-Ge**. Analytically pure **10-Co** was obtained upon recrystallization of the solid from 0.6 mL of Et_2O at −30 °C. Yield:180 mg (0.137 mmol, 25 % from **1-Co•Et$_2$O**).

Properties: Compound **10-Co** is a highly air-sensitive, dark-green solid, and very well soluble in *n*-hexane, benzene, toluene and Et_2O at ambient temperature, but insoluble in CH_3CN. Under strict exclusion of air, a solution of **10-Co** in (D_6)benzene does not show any sign of decomposition after one day at ambient temperature.

Elemental analysis: 10-Co ($C_{64}H_{115}CoGe_2Si_8$, 1313.44 g mol^{-1}): calcd./%: C 58.52, H 8.83; found/%: C 58.69, H 8.98; **Melting Point:** 213°C (dec.).

^{1}H NMR (500.1 MHz, (D_6)benzene, 298 K): δ (ppm) = 0.11 (s, 18H, C^{2,6}-CH(Si*Me$_3$*)$_A$, Tbb$_X$), 0.14 (s, 18H, C^{2,6}-CH(Si*Me$_3$*)$_A$, Tbb$_Y$), 0.31 (s, 18H, C^{2,6}-CH(Si*Me$_3$*)$_B$, Tbb$_Y$), 0.33 (s, 18H, C^{2,6}-CH(Si*Me$_3$*)$_B$, Tbb$_X$), 1.32 (s, 9H, C^4-C*Me$_3$*, Tbb$_X$), 1.34 (s, 9H, C^4-C*Me$_3$*, Tbb$_Y$), 2.07 (s, 3H, C^4-*Me*, Mes), 2.30 (s, 6H, C^{2,6}-*Me*, Mes), 2.31 (s, ^2J(^{29}Si,^{1}H) = 8.8 Hz, 2H, C^{2,6}-C*H*(SiMe$_3$)$_{A,B}$, Tbb$_X$), 2.34 (s, ^2J(^{29}Si,^{1}H) = 9.2 Hz, 2H, C^{2,6}-C*H*(SiMe$_3$)$_{A,B}$, Tbb$_Y$), 4.92 (s, 5H, C$_5$*H$_5$*), 6.67 (s, 2H, C^{3,5}-*H*, Mes), 6.76 (s, 1H, *H*CCMes), 6.84 (s, 2H, C^{3,5}-*H*, Tbb$_X$), 6.91 (s, 2H, C^{3,5}-*H*, Tbb$_Y$).

^{13}C{^{1}H} NMR (125.8 MHz, (D_6)benzene, 298 K): δ (ppm) = 1.0 (s, 6C, C^{2,6}-CH(Si*Me$_3$*)$_A$, Tbb$_Y$), 1.3 (s, 6C, C^{2,6}-CH(Si*Me$_3$*)$_B$, Tbb$_Y$), 2.0 (s, 6C, C^{2,6}-CH(Si*Me$_3$*)$_A$, Tbb$_X$), 2.7 (s, 6C, C^{2,6}-CH(Si*Me$_3$*)$_B$, Tbb$_X$), 20.8 (s, 1C, C^4-*Me*, Mes), 23.6 (s, 2C, C^{2,6}-*Me*, Mes), 29.4 (s, ^1J(^{29}Si,^{13}C) = 42 Hz, 2C, C^{2,6}-*C*H(SiMe$_3$)$_{A,B}$, Tbb$_X$), 30.1 (s, ^1J(^{29}Si,^{13}C) = 42 Hz, 2C, C^{2,6}-*C*H(SiMe$_3$)$_{A,B}$, Tbb$_Y$), 31.28 and 31.30 (s each, 3C each, C^4-C*Me$_3$*, Tbb$_{X,Y}$), 34.43 and 34.52 (s each, 1C each, C^4-*C*Me$_3$, Tbb$_{X,Y}$), 81.5 (s, 5C, *C$_5$*H$_5$), 122.2 (s, 2C, *C^{3,5}*-H, Tbb$_Y$), 123.0 (s, 2C, *C^{3,5}*-H, Tbb$_X$), 129.1 (s, 2C, *C^{3,5}*-H, Mes), 133.3 (s, 2C, *C^{2,6}*-Me, Mes), 135.2 (s, 1C,*C^4*, Mes), 142.4 (s, 1C, *C^1*, Mes), 145.4 (s, 2C, *C^{2,6}*, Tbb$_X$), 145.8 (s, 2C, *C^{2,6}*, Tbb$_Y$), 150.1 (s, 1C, *C^1*, Tbb$_Y$), 150.3 (s, 1C, *C^4*, Tbb$_X$), 150.9 (s, 1C, *C^4*, Tbb$_Y$), 155.1 (s, 1C, *C^1*, Tbb$_X$), 159.6 (s, 1C, HC*C*Mes), 175.1 (s, 1C, HC*C*Mes)

4.5.13. $Ge_2Tbb_2C_4H_2Mes_2$ (11-Ge)

A reddish orange solution of Ge_2Tbb_2 (250 mg, 0.239 mmol, 1 equiv.) in 5 mL of *n*-hexane was treated with a solution of mesitylacetylene (103 mg, 0.71 mmol, 3 equiv.) in 2 mL of *n*-hexane at ambient temperature. The colour of the reaction solution immediately changed to orange-yellow. After stirring for 10 min an aliquot of the reaction solution was analyzed by ^{1}H NMR spectroscopy. This showed a complete conversion of Ge_2Tbb_2 to **11-Ge** and a Tbb-containing by-product of unknown composition. The reaction solution was evaporated to dryness in vacuo. The crude

product was dissolved in 2 mL of Et_2O, and 0.9 mL of CH_3CN was added dropwise to the stirred Et_2O solution to precipitate **11-Ge**. The yellow precipitate was isolated by filtering off the yellow mother liquor using a filter cannula, then washed with 2 mL of Et_2O at ambient temperature and dried at 65 °C for 5 h under fine vacuum. Yield: 160 mg (0.120 mmol, 50 % of Ge_2Tbb_2).

Properties: Compound **11-Ge** is a moderately air-sensitive, yellow solid, which is highly soluble in benzene and toluene and moderately soluble in *n*-hexane and Et_2O at ambient temperature, but insoluble in CH_3CN.

Elemental analysis: 11-Ge ($C_{70}H_{122}Ge_2Si_8$, 1333.62 g mol^{-1}): calcd./%: C 63.04, H 9.22; found/%: C 62.94, H 9.40; **Melting Point:** 248°C (dec.).

^{1}H NMR (500.1 MHz, (D_6)benzene, 298 K): δ (ppm) = 0.00 (s, 18H, ($C^{2,6}$-CH(Si*Me*$_3$)$_A$, Tbb_X), 0.09 (s, 18H, ($C^{2,6}$-CH(Si*Me*$_3$)$_A$, Tbb_Y), 0.18 (s, 18H, ($C^{2,6}$-CH(Si*Me*$_3$)$_B$, Tbb_Y), 0.20 (s, 18H, ($C^{2,6}$-CH(Si*Me*$_3$)$_B$, Tbb_X), 1.31 and 1.32 (s each, 9H each, C^4-C*Me*$_3$, $Tbb_{X,Y}$), 2.17 (s, 3H, C^4-*Me*, Mes_P), 2.21 (s, 3H, C^4-*Me*, Mes_Q), 2.32 (s, 6H, $C^{2,6}$-*Me*, Mes_Q), 2.41 (br s, $\Delta\nu_{1/2}$ = 16 Hz, 2H, $C^{2,6}$-C*H*(SiMe$_3$)$_{A,B}$, Tbb_X), 2.50 (s, 6H, $C^{2,6}$-*Me*, Mes_P), 3.14 (br s, $\Delta\nu_{1/2}$ = 16 Hz, 2H, $C^{2,6}$-C*H*(SiMe$_3$)$_{A,B}$, Tbb_Y), 6.86 (s, 2H, $C^{3,5}$-*H*, Mes_P), 6.88 (s, 2H, $C^{3,5}$-*H*, Mes_Q), 6.98 (s, 2H, $C^{3,5}$-*H*, Tbb_Y), 7.05 (s, 2H, $C^{3,5}$-*H*, Tbb_X), 7.45 (d, $^4J(^1H,^1H)$ = 1.8 Hz, 1H, *H*-C^4-C^3-Mes_P), 8.29 (d, $^4J(^1H,^1H)$ = 1.8 Hz, 1H, *H*-C^6-C^5-Mes_Q).
^{13}C{^{1}H} NMR (125.8 MHz, (D_6)benzene, 298 K): δ (ppm) = 1.1 (s, 6C, $C^{2,6}$-(Si*Me*$_3$)$_A$, Tbb_Y), 2.1 (s, 6C, $C^{2,6}$-(Si*Me*$_3$)$_A$, Tbb_X), 2.8 (s, 6C, $C^{2,6}$-(Si*Me*$_3$)$_B$, Tbb_Y), 3.2 (s, 6C, $C^{2,6}$-(Si*Me*$_3$)$_B$, Tbb_X), 20.8 (s, 1C, C^4-*Me*, Mes_P), 21.1 (s, 1C, C^4-*Me*, Mes_Q), 21.2 (s, 2C, $C^{2,6}$-*Me*, Mes_Q), 25.3 (br s, $\Delta\nu_{1/2}$ = 17 Hz 2C, $C^{2,6}$-*Me*, Mes_P), 31.2 and 31.4 (each s, 6C, C^4-C*Me*$_3$, $Tbb_{X,Y}$), 31.8 (br s, $\Delta\nu_{1/2}$ = 18 Hz, 2C, $C^{2,6}$-*C*H(SiMe$_3$)$_{A,B}$, Tbb_X), 32.6 (br s, $\Delta\nu_{1/2}$ = 23 Hz, 2C, $C^{2,6}$-*C*H(SiMe$_3$)$_{A,B}$, Tbb_Y), 34.5 and 34.6 (s each, 1C each, C^4-*C*Me$_3$, $Tbb_{X,Y}$), 123.1 (s, 2C, *C*^{3,5}-H, Tbb_X), 123.4 (s, 2C, *C*^{3,5}-H, Tbb_Y), 128.7 (s, 2C, *C*^{3,5}-H, Mes_Q), 130.3 (br s, $\Delta\nu_{1/2}$ = 21 Hz, 2C, *C*^{3,5}-H, Mes_P), 134.0 (s, 2C, *C*^{2,6}-Me, Mes_P), 134.5 (s, 2C, *C*^{2,6}-Me, Mes_Q), 135.2 (s, 1C, *C*^{4}-Me, Mes_P), 135.6 (s, 1C, *C*^{4}-Me, Mes_Q), 137.4 (s, 1C, *C*^{1}, Tbb_X), 141.1 (s, 1C, H-*C*^{4}-C^3-Mes_P), 142.5 (s, 1C, *C*^{1}, Tbb_Y), 144.8 (s, 1C, *C*^{5}-Mes_Q), 145.9 (s, 1C, *C*^{1}, Mes_Q), 146.4 (s, 1C, *C*^{1}, Mes_P), 148.7 (s, 2C, *C*^{2,6}, Tbb_Y), 150.6 (s, 2C, *C*^{2,6}, Tbb_X), 150.8 and 151.0 (s each, 1C each, *C*^{4}, $Tbb_{X,Y}$), 153.7 (s, 1C, H-*C*^{6}-C^5-Mes_Q), 167.4 (s, 1C, *C*^{3}-Mes_P).

4.5.14. [CpCo{(GeHTbb)(GeCCMesTbb)}] (13-Co)

A 0.58 M stock solution of mesitylacetylene in *n*-hexane (0.74 mL, 0.429 mmol, 1 equiv.) was added to a red-brown solution of **3-Co** (500 mg, 0.428 mmol, 1 equiv.)

in 15 mL of *n*-hexane at ambient temperature. The reaction solution immediately darkened to reddish brown. After stirring for 10 min an aliquot of the reaction solution was analyzed by ^{1}H NMR spectroscopy. This showed the complete conversion of **3-Co** to **13-Co** and some **10-Co** (ca. 10 mole%). The solution was evaporated to dryness in vacuo yielding a brown, sticky solid. Several attempts to obtain **13-Co** in pure form by crystallization of the crude product from various organic solvents failed and as it is characterized by spectroscopy. ^{1}H NMR spectroscopic analysis of the product showed the presence of **13-Co**, **10-Co** and very-little mesitylacetylene in the approximate molar ratio of 22 : 2.8 : 1.

IR (solid): $\tilde{\nu}$ (cm^{-1}) = 2952 (m), 2900 (w), 2868 (vw), 2787 (vw), 2107 (w) [ν(C≡C)], 1974 (br) [ν(Ge−H)], 1610 (vw), 1584 (w), 1531 (w), 1476 (w), 1462 (w), 1425 (w), 1393 (w), 1361 (vw), 1246 (s), 1216 (w), 1164 (w), 1112 (vw), 1006 (w), 954 (m), 936 (w), 882 (m), 832 (vs), 759 (s), 740 (w), 684 (m), 662 (w), 623 (w), 608 (w), 574 (w), 552 (w), 506 (w), 466 (w), 451 (w), 438 (m), 49 (m).

IR (*n*-hexane): $\tilde{\nu}$ (cm^{-1}) = 2109 (m) [ν(C≡C)], 1980 (br) [ν(Ge−H)], 1610 (w) [ν(CC)$_{aryl}$], 1584 (m) [ν(CC)$_{aryl}$], 1541 (m) [ν(CC)$_{aryl}$], 1531 (m) [ν(CC)$_{aryl}$].

^{1}H NMR (500.1 MHz, (D$_6$)benzene, 298 K): δ (ppm) = 0.17 (s, 36H, C^{2,6}-CH(Si*Me$_3$*)$_2$, Tbb$_X$), 0.27 (s, 36H, C^{2,6}-CH(Si*Me$_3$*)$_2$, Tbb$_Y$), 1.35 (s, 9H, C^{4}-C*Me$_3$*, Tbb$_X$), 1.38 (s, 9H, C^{4}-C*Me$_3$*, Tbb$_Y$), 2.01 (s, 3H, C^{4}-*Me*, Mes), 2.24 (s, ^{2}J(^{29}Si,^{1}H) = 9.2 Hz, 2H, C^{2,6}-C*H*(SiMe$_3$)$_2$, Tbb$_X$), 2.55 (s, 6H, C^{2,6}-*Me*, Mes), 2.76 (s, ^{2}J(^{29}Si,^{1}H) = 9.2 Hz, 2H, C^{2,6}-C*H*(SiMe$_3$)$_2$, Tbb$_Y$), 5.06 (s, 5H, C$_5$*H$_5$*), 6.72 (s, 2H, C^{3,5}-*H*, Mes), 6.89 (s, 2H, C^{3,5}-*H*, Tbb$_X$), 6.96 (s, 2H, C^{3,5}-*H*, Tbb$_Y$), 11.25 (s, 1H, Ge−*H*).

^{13}C{^{1}H} NMR (125.8 MHz, (D$_6$)benzene, 298 K): δ (ppm) = 1.0 (s, 12C, C^{2,6}-CH(Si*Me$_3$*)$_2$, Tbb$_X$), 1.6 (s, 12C, C^{2,6}-CH(Si*Me$_3$*)$_2$, Tbb$_Y$), 21.3 (s, 1C, C^{4}-*Me*, Mes), 22.4 (s, 2C, C^{2,6}-*Me*, Mes), 29.9 (s, 2C, C^{2,6}-*C*H(SiMe$_3$)$_2$, Tbb$_Y$), 30.3 (s, 2C, C^{2,6}-*C*H(SiMe$_3$)$_2$, Tbb$_X$), 31.38 and 31.42 (each s, 6C, C^{4}-C*Me$_3$*, Tbb$_{X,Y}$), 34.5 (s, 2C, C^{4}-*C*Me$_3$, Tbb$_{X,Y}$), 80.4 (s, 5C, *C$_5$*H$_5$), 116.5 and 119.6 (s each, 1C each, Ge*CC*Mes), 121.9 (s, 1C, *C^{1}*, Mes), 122.0 (s, 2C, *C^{3,5}*-H, Tbb$_X$), 122.8 (s, 2C, *C^{3,5}*-H, Tbb$_Y$), 128.0 (s, 2C, *C^{3,5}*-H, Mes), *137.5 (s, 1C, *C^{4}*, Mes), 139.7 (s, 2C, *C^{2,6}*-Me, Mes), 145.4 (s, 2C, *C^{2,6}*, Tbb$_X$), 145.9 (s, 2C, *C^{2,6}*, Tbb$_Y$), 150.5 (s, 1C, *C^{4}*, Tbb$_Y$), 150.8 (s, 1C, *C^{4}*, Tbb$_X$), 151.3 (s, 1C, *C^{1}*, Tbb$_X$), 151.6 (s, 1C, *C^{1}*, Tbb$_Y$). *: this signal is masked by of that the deuterated solvent and was detected in the HMBC experiment.

4.5.15. [CpCo(Ge$_2$Tbb$_2$C$_2$PhNMe$_2$)] (14-Co)

Method A (from **1-Co**)

A brown solution of **1-Co•Et₂O** (300 mg, 0.236 mmol, 1 equiv.) in 15 mL of toluene was treated with an excess of 1-dimethylamino-2-phenylacetylene (342 mg, 2.36 mmol, 10 equiv.). The reaction mixture was heated for 24 h at 95 °C. The colour of the reaction solution became more reddish. Monitoring the progress of the reaction by ^{1}H NMR spectroscopy revealed very selective formation of **14-Co**. All attempts to isolate **14-Co** in pure form only by crystallization of the crude product from various solvents failed yielding always an oil containing **14-Co** and 1-dimethylamino-2-phenylacetylene. ***(Although use of CH_3CN/Et_2O work-up was not done here, but if tries, it might lead to the isolation of pure compound from this mixture).

Method B (from **3-Co**)

A 0.324 M stock solution of 1-dimethylamino-2-phenylacetylene in *n*-hexane (0.75 mL, 0.244 mmol, 1 equiv.) was added at ambient temperature to a red-brown solution of **3-Co** (285 mg, 0.244 mmol, 1 equiv.) in 10 mL of *n*-hexane. The reaction solution immediately darkened to reddish-brown. After stirring for 10 min an aliquot of the reaction solution was taken and analyzed by ^{1}H NMR spectroscopy. This showed a complete and selective conversion of the starting materials to **14-Co**. Afterwards all volatiles were removed in vacuo, the resulting dark brown residue was dissolved in 2 mL of Et_2O followed by layering of CH_3CN (3.5 mL) and storing overnight at ambient temperature. The dark brown microcrystals of **14-Co** were obtained and isolated by filtering off the brown mother liquor at ambient temperature using a filter cannula and then dried for 1 h at 40 °C under fine vacuum. Yield: 150 mg (0.114 mmol, 47 % of **3-Co**).

Properties: Compound **14-Co** is a highly air-sensitive, dark brown solid decolorizing immediately upon contact with air. It can be stored under argon atmosphere at ambient temperature for several months. It is very soluble in *n*-pentane, benzene, toluene, Et_2O and THF at room temperature, but insoluble in acetonitrile. Under strict exclusion of air, solution of **14-Co** in (D_6)benzene shows no sign of decomposition after at least 3 days.

Elemental analysis: 14-Co ($C_{63}H_{114}CoGe_2NSi_8$, 1314.42 g mol^{-1}): calcd./%: C 57.57, H 8.74, N 1.07; found/%: C 57.94, H 9.02, N, 1.14; **Melting Point:** 242°C (dec.).

^{1}H NMR (500.1 MHz, (D_6)benzene, 298 K): δ (ppm) = 0.15 (s, 18H, $C^{2,6}$-CH(Si*Me₃*)$_A$, Tbb_X), 0.29 (s, 18H, $C^{2,6}$-CH(Si*Me₃*)$_B$, Tbb_X), 0.30 (s, 18H, $C^{2,6}$-CH(Si*Me₃*)$_A$, Tbb_Y), 0.30 (s, 18H, $C^{2,6}$-CH(Si*Me₃*)$_B$, Tbb_Y), 1.34 (s, 9H, C^{4}-C*Me₃*, Tbb_Y), 1.42 (s, 9H, C^{4}-C*Me₃*,

Tbb_X), 2.28 (s, 6H, 2 × *Me*, NMe_2), 2.73 (s, $^2J(^{29}Si,^1H)$ = 9 Hz, 2H, $C^{2,6}$-C*H*$(SiMe_3)_{A,B}$, Tbb_X), 2.91 (s, $^2J(^{29}Si,^1H)$ = 9 Hz, 2H, $C^{2,6}$-C*H*$(SiMe_3)_{A,B}$, Tbb_Y), 5.03 (s, 5H, C_5H_5), 6.72 (m, 2H, $C^{2,6}$-*H*, Ph), 6.84 (m, 1H, C^4-*H*, Ph), 6.90 (m, 2H, $C^{3,5}$-*H*, Ph), 6.93 (s, 2H, $C^{3,5}$-*H*, Tbb_Y), 6.95 (s, 2H, $C^{3,5}$-*H*, Tbb_X).

$^{13}C\{^1H\}$ NMR (125.8 MHz, (D_6)benzene, 298 K): δ (ppm) = 1.9 (s, 6C, $C^{2,6}$-CH(Si*Me*$_3$)$_A$, Tbb_Y, 2.0 (s, 6C, $C^{2,6}$-CH(Si*Me*$_3$)$_B$, Tbb_Y), 2.2 (s, 6C, $C^{2,6}$-CH(Si*Me*$_3$)$_A$, Tbb_X), 2.5 (s, 6C, $C^{2,6}$-CH(Si*Me*$_3$)$_B$, Tbb_X), 28.7 (s, $^1J(^{29}Si,^{13}C)$ = 41 Hz, 2C, $C^{2,6}$-*C*H$(SiMe_3)_{A,B}$, Tbb_Y), 29.2 (s, $^1J(^{29}Si,^{13}C)$ = 41 Hz, 2C, $C^{2,6}$-*C*H$(SiMe_3)_{A,B}$, Tbb_X), 31.4 (s, 3C, C^4-C*Me*$_3$, Tbb_Y), 31.5 (s, 3C, C^4-C*Me*$_3$, Tbb_X), 34.52 (s, 1C, C^4-*C*Me_3, Tbb_Y), 34.54 (s, 1C, C^4-*C*Me_3, Tbb_X), 45.6 (br, 2 × *Me*, NMe_2), 80.2 (s, 5C, C_5H_5), 122.9 (s, 2C, $C^{3,5}$-H, Tbb_Y), 123.2 (s, 2C, $C^{3,5}$-H, Tbb_X), 123.9 (s, 1C, C^4-H, Ph), 127.2 (s, 2C, $C^{3,5}$-H, Ph), 129.8 (s, 2C, $C^{2,6}$-H, Ph), 137.6 (s, 1C, Me_2NCCPh), 143.2 (s, 1C, C^1, Ph), 145.2 (s, 2C, $C^{2,6}$, Tbb_Y), 146.6 (s, 2C, $C^{2,6}$, Tbb_X), 149.1 (s, 1C, C^1, Tbb_X), 150.5 (s, 1C, C^4, Tbb_X), 150.7 (s, 1C, C^4, Tbb_Y), 154.0 (s, 1C, C^1, Tbb_Y), 182.9 (s, 1C, Me_2NCCPh).

4.5.16. [CpCo($Ge_2Tbb_2C_2H_4$)] (**15-Co**)

Method A

To an orange-yellow suspension of $Ge_2Br_2Tbb_2$ (1.5 g, 1.24 mmol, 1 equiv.) in 40 mL of benzene, an orange-red solution of $CpCo(C_2H_4)_2$ (224 mg, 1.24 mmol, 1 equiv.) in 5 mL of benzene was added dropwise at ambient temperature. The colour of the reaction solution turned brown-purple immediately. After 2.5 hrs. of stirring at ambient temperature, KC_8 (342 mg, 2.53 mmol, 2.03 equiv.) was added to the reaction solution and the resulting suspension was vigorously stirred overnight. The colour of the reaction solution became more reddish-brown. Analysis of an aliquot by ^1H NMR spectroscopy revealed selective formation of **15-Co** along with some minor unknown Cp and Tbb containing compounds with unknown composition. The reaction mixture was worked up by filtering off the graphite and the obtained clear red-brown filtrate was evaporated to dryness. The resulting brown mass was dissolved in 2.5 mL of *n*-hexane and stored –30 °C for 3 days. Muddy brown precipitate of **15-Co** was isolated by filtering off the mother liquor at −30 °C using a filter cannula and then dried at 60 °C for 2.5 hrs. under fine vacuum. Yield: 676 mg (0.565 mmol, 45 % from $Ge_2Br_2Tbb_2$).

Method B

To a red-brown solution of **3-Co** (25 mg, 0.021 mmol, 1 equiv.) in 3 mL of *n*-hexane, ethylene gas was introduced after a freeze-pump-thaw. While, the frozen reaction mixture was warming up to room temperature, the colour became more brownish.

Analysis of an aliquot by ^{1}H NMR spectroscopy revealed complete consumption of **3-Co** and quantitative formation of **15-Co**. No work up was performed to obtain pure **15-Co** from this method.

Properties: Compound **15-Co** is an air-sensitive, brown solid which can be stored under argon atmosphere at ambient temperature for several months. It is very soluble in *n*-hexane, benzene and Et_2O at room temperature. Under strict exclusion of air, solution of **15-Co** in (D_6)benzene shows no sign of decomposition after at least 5 days.

Elemental analysis: 15-Co ($C_{55}H_{107}CoGe_2Si_8$, 1197.28 g mol^{-1}): calcd./%: C 55.17, H 9.00; found/%: C 54.67, H 9.19; **Melting Point:** 233°C (dec.).

^{1}H NMR (400.1 MHz, (D_6)benzene, 298 K): δ (ppm) = 0.15 (s, 36H, 2 × C^{2,6}-CH(Si*Me$_3$*)$_A$, 2 × Tbb), 0.28 (s, 36H, 2 × C^{2,6}-CH(Si*Me$_3$*)$_B$, 2 × Tbb), 1.39 (s, 18H, 2 × C*Me$_3$*, 2 × Tbb), 1.55 (s, 4H, C_2*H$_4$*), 2.43 (s, 4H, 2 × C^{2,6}-C*H*(SiMe$_3$)$_A$(SiMe$_3$)$_B$, 2 × Tbb), 5.11 (s, 5H, C_5*H$_5$*), 6.96 (s, 4H, 2 × C^{3,5}-*H*, 2 × Tbb).
^{13}C{^{1}H} NMR (100.6 MHz, (D_6)benzene, 298 K): δ (ppm) = 1.0 (s, 12C, 2 × C^{2,6}-CH(Si*Me$_3$*)$_A$, 2 × Tbb), 1.2 (s, 12C, 2 × C^{2,6}-CH(Si*Me$_3$*)$_B$, 2 × Tbb), 30.3 (s, 4C, 2 × C^{2,6}-*C*H(SiMe$_3$)$_A$(SiMe$_3$)$_B$, 2 × Tbb), 31.4(s, 6C, 2 × C*Me$_3$*, 2 × Tbb), 34.6 (s, 2C, 2 × *C*Me$_3$, 2 × Tbb), 36.7 (s, 2C, *C*$_2$H$_4$), 78.8 (s, 5C, *C*$_5$H$_5$), 121.8 (s, 4C, 2 × *C*^{3,5}-H, 2 × Tbb), 145.5 (s, 4C, 2 × *C*^{2,6}-CH(SiMe$_3$)$_A$(SiMe$_3$)$_B$, 2 × Tbb), 151.0 (s, 2C, 2 ×*C*^{4}, 2 × Tbb), 153.1 (s, 2C, 2 ×*C*^{1}, 2 × Tbb).

4.5.17. [CpCo{Ge$_2$Tbb$_2$C$_2$Me$_2$(CHSiMe$_3$)}] (16-Co)

A dark-green solution of **5-Co** (150 mg, 0.122 mmol, 1 equiv.) in 7 mL of *n*-hexane was treated with a stock solution (2 M in *n*-hexane) of $CHSiMe_3N_2$ (0.09 mL, 0.172 mmol, 1.4 equiv.). The reaction mixture was heated for 16 hrs. at 60 °C. The dark green reaction solution completely transformed to deep red. Monitoring the reaction progress by ^{1}H NMR spectroscopy revealed a complete consumption of **5-Co** and its quantitative transformation to **16-Co**. Afterwards all volatiles were removed in vacuo, the resulting dark red residue was dissolved in 1.5 mL of *n*-pentane and stored at –60 °C for 3 days. Dark-red microcrystals were isolated by filtering off the mother liquor at −60 °C using a filter cannula and then dried at 40 °C for 1.5 hrs. under fine vacuum to afford *n*-pentane solvate **16-Co•(C_5H_{12})$_{0.9}$**. Yield: 120 mg (0.087 mmol, 71 % from **5-Co**).

Attempts to obtain the solvate-free form upon drying of **16-Co•(C_5H_{12})$_{0.9}$** in fine vacuum for 6 hrs. at ambient temperature or at 70 °C for 5 hrs. failed leading only to partial loss of *n*-pentane with partial decomposition.

Properties: Compound **16-Co•(C_5H_{12})$_{0.9}$** is an air-sensitive, red solid which can be stored under argon atmosphere at ambient temperature for several months. It is very well soluble in *n*-hexane, benzene and Et_2O at room temperature. Under strict exclusion of air, a solution of **16-Co•(C_5H_{12})$_{0.9}$** in (D_6)benzene shows no sign of decomposition after at least 2 days.

Elemental analysis: **16-Co•(C_5H_{12})$_{0.9}$** ($C_{61}H_{119}CoGe_2Si_9(C_5H_{12})_{0.9}$, 1374.45 g mol^{-1}): calcd./%: C 57.24, H 9.52; found/%: C 56.98, H 9.44; **Melting Point:** 208°C (dec.).

^{1}H NMR (500.1 MHz, (D_6)benzene, 298 K): δ (ppm) = 0,18 (s, 9H, C^2-(Si*Me*$_3$)$_A$(SiMe$_3$)$_B$, Tbb$_X$), 0.20 (s, 9H, C^2-(SiMe$_3$)$_A$(Si*Me*$_3$)$_B$, Tbb$_X$), 0.21 (s, 9H, CoCHSi*Me*$_3$), 0.22 (s, C^2-(Si*Me*$_3$)$_A$(SiMe$_3$)$_B$, Tbb$_Y$), 0.25 (s, 9H, C^2-(SiMe$_3$)$_A$(Si*Me*$_3$)$_B$, Tbb$_Y$), 0.28 (s, 9H, C^6-(Si*Me*$_3$)$_A$(SiMe$_3$)$_B$, Tbb$_Y$), 0.30 (s, 9H, C^6-(SiMe$_3$)$_A$(Si*Me*$_3$)$_B$, Tbb$_Y$), 0.39 (s, 9H, C^6-(Si*Me*$_3$)$_A$(SiMe$_3$)$_B$, Tbb$_X$), 0.43 (s, 9H, C^6-(SiMe$_3$)$_A$(Si*Me*$_3$)$_B$, Tbb$_X$), 1.39 and 1.41 (each s, 18H, 2 × C*Me*$_3$, Tbb$_{X,Y}$), 1.80 (s, 3H, Ge$_1$-C*Me*CMe-Ge$_2$), 1.85 (s, 1H, C^2-C*H*(SiMe$_3$)$_{A,B}$, Tbb$_X$), 1.88 (s, 1H, CoC*H*SiMe$_3$), 1.90 (s, 3H, Ge$_1$-CMeC*Me*-Ge$_2$), 2.30 (s, 1H, C^6-C*H*(SiMe$_3$)$_{A,B}$, Tbb$_X$), 2.61 (s, 1H, C^2-C*H*(SiMe$_3$)$_{A,B}$, Tbb$_Y$), 3.73 (s, 1H, C^6-C*H*(SiMe$_3$)$_{A,B}$, Tbb$_Y$), 4.96 (s, 5H, C_5H_5), 6.91 (d, ^4J(^{1}H-^{1}H) = 1.6 Hz, 1H, C^3-*H*, Tbb$_X$), 6.96 (d, ^4J(^{1}H-^{1}H) = 1.6 Hz, 1H, C^5-*H*, Tbb$_X$), 7.04 (d, ^4J(^{1}H-^{1}H) = 1.6 Hz, 1H, C^3-*H*, Tbb$_Y$), 7.05 (d, ^4J(^{1}H-^{1}H) = 1.6 Hz, 1H, C^5-*H*, Tbb$_Y$).

^{13}C{^{1}H} NMR (125.8 MHz, (D_6)benzene, 298 K): δ (ppm) = 0.6 (s, 1C, Co*C*HSiMe$_3$), 1.9 (s, 3C, C^6-(Si*Me*$_3$)$_A$(SiMe$_3$)$_B$, Tbb$_X$), 2.0 (s, 3C, C^6-(SiMe$_3$)$_A$(Si*Me*$_3$)$_B$, Tbb$_X$), 2.11 (s, 3C, C^6-(Si*Me*$_3$)$_A$(SiMe$_3$)$_B$, Tbb$_Y$), 2.12 (s, 3C, C^6-(SiMe$_3$)$_A$(Si*Me*$_3$)$_B$, Tbb$_Y$), 2.15 (s, 3C, C^2-(Si*Me*$_3$)$_A$(SiMe$_3$)$_B$, Tbb$_X$), 2.4 (s, 3C, C^2-(SiMe$_3$)$_A$(Si*Me*$_3$)$_B$, Tbb$_X$), 2.56 (s, 3C, C^2-(Si*Me*$_3$)$_A$(SiMe$_3$)$_B$, Tbb$_Y$), 2.58 (s, 3C, C2-(SiMe$_3$)$_A$(Si*Me*$_3$)$_B$, Tbb$_Y$), 5.3 (s, 3C, CoCHSi*Me*$_3$), 20.9 (s, 1C, Ge$_1$-CMeC*Me*-Ge$_2$), 22.1 (s, 1C, Ge$_1$-C*Me*CMe-Ge$_2$), 29.68 (s, 1C, C^6- *C*H(SiMe$_3$)$_{A,B}$, Tbb$_X$), 29.75 (s, 1C, C^2- *C*H(SiMe$_3$)$_{A,B}$, Tbb$_X$), 30.1 (s, 1C, C^6-*C*H(SiMe$_3$)$_{A,B}$, Tbb$_Y$), 31.5 (s, 1C, C^2- *C*H(SiMe$_3$)$_{A,B}$, Tbb$_Y$), 31.23 and 31.32 (each s, 6C, 2 × C*Me*$_3$, Tbb$_{X,Y}$), 34.39 and 34.42 (each s, 2C, 2 × *C*Me$_3$, Tbb$_{X,Y}$), 123.2 (s, 1C, *C*^{3}-H, Tbb$_Y$), 124.3 (s, 1C, *C*^{5}-H, Tbb$_X$), 124.47 (s, 1C, *C*^{3}-H, Tbb$_X$), 124.53 (s, 1C, *C*^{5}-H, Tbb$_Y$), 133.8 (s, 1C, *C*^{1}, Tbb$_Y$), 145.7 (s, 1C, *C*^{2}, Tbb$_X$), 147.3 (s, 1C, *C*^{6}, Tbb$_X$), 148.5 and 149.4 (each s, 2C, 2 × *C*^{4}, Tbb$_{X,Y}$), 149.9 (s, 1C, *C*^{6}, Tbb$_Y$), 150.1 (s, 1C, *C*^{1}, Tbb$_X$), 151.2 (s, 1C, *C*^{2}, Tbb$_Y$), 165.7 (s, 1C, Ge$_1$-*C*MeCMe-Ge$_2$), 167.3 (s, 1C, Ge$_1$-CMe*C*Me-Ge$_2$).

4.5.18. Ge_2Tbb_2COD (17-Ge)

To an orange-red solution of Ge_2Tbb_2 (512 mg, 0.489 mmol, 1 equiv.) in 10 mL of *n*-hexane, 2 mL of *n*-hexane solution of 1,5-COD (53 mg, 0.489 mmol, 1 equiv.) was

added dropwise at ambient temperature. The colour of the reaction solution immediately turned dark red and then gradually became a pale orange suspension. After, half an hour of stirring at ambient temperature, an aliquot of the reaction mixture was analyzed by ^{1}H NMR spectroscopy revealed a complete consumption of Ge_2Tbb_2 and a selective formation of **17-Ge** along with some minor unknown compounds. The suspension was filtered off to separate small amount of yellow precipitate and the obtained orange filtrate was evaporated to dryness. The pale orange crude product was washed with 2 mL of precooled (–60°C) *n*-pentane at – 60°C followed by another washing with 2 mL of DCM at ambient temperature. The resulting colourless solid was dried for 6 hrs. at ambient temperature. Yield: 90 mg (0.078 mmol, 16 % from Ge_2Tbb_2).

Properties: Compound **17-Ge** is an air-stable, colourless solid, which is very well soluble in *n*-pentane, benzene, and Et_2O but poor soluble in DCM at ambient temperature.

Elemental analysis: 17-Ge ($C_{56}H_{110}Ge_2Si_8$, 1153.38 g mol^{-1}): calcd./%: C 58.31, H 9.61; found/%: C 57.73, H 9.49; **Melting Point:** 242°C (dec.).

^{1}H NMR (500.1 MHz, (D_6)benzene, 298 K): δ (ppm) = 0.24 (s, br, $\Delta\nu_{1/2}$ = 12 Hz, 72H, 2 × C^{2,6}-CH(Si*Me*$_3$)$_2$, 2 × Tbb), 1.31 (s, 18H, 2 × C*Me*$_3$, 2 × Tbb), 1.77 (m, br, 4H, 4 × H_A, COD), 2.33 (s, ^{2}J (^{29}Si-^{1}H) = 9 Hz, 4H, 2 × C^{2,6}-C*H*(SiMe$_3$)$_2$, 2 × Tbb), 2.52 (m, 4H, 4 × $H_{A'}$, COD), 3.15 (s, br, $\Delta\nu_{1/2}$ = 5.5 Hz, 4H, 4 × H_B, COD), 6.87 (s, 4H, 2 × C^{3,5}-*H*, 2 × Tbb).

^{13}C{^{1}H} NMR (125.8 MHz, (D_6)benzene, 298 K): δ (ppm) = 1.3 (s, br, $\Delta\nu_{1/2}$ = 11 Hz, 24C, 2 × C^{2,6}-CH(Si*Me*$_3$)$_2$, 2 × Tbb), 27.4 (s, 4C, 4 × C_A, COD), 30.1 (s, ^{1}J (^{29}Si-^{31}C) = 42 Hz, 4C, 2 × C^{2,6}-*C*H(SiMe$_3$)$_2$, 2 × Tbb), 31.2 (s, 6C, 2 × C*Me*$_3$, 2 × Tbb), 34.3 (s, 2C, 2 × *C*Me$_3$, 2 × Tbb), 47.0 (s, 4C, 4 × C_B, COD), 122.1 (s, 4C, 2 × *C*^{3,5}-H, 2 × Tbb), 137.5 (s, 2C, *C*^{1}, 2 × Tbb), 149.4 (s, 4C, 2 × *C*^{2,6}-CH(SiMe$_3$)$_2$, 2 × Tbb), 150.5 (s, 2 × *C*^{4}, 2 × Tbb).

4.5.19. [CpRh(CO)GeBrTbb] (18-Rh)

To a stirred orange yellow solution of $Ge_2Br_2Tbb_2$ (500 mg, 0.415 mmol, 1 equiv.) in 20 mL of *n*-pentane, a stock solution (0.2343 M in *n*-hexane) of $CpRh(CO)_2$ (3.54 mL, 0.830 mmol, 2 equiv.) was added dropwise at ambient temperature. The reaction solution was stirred for 2 hrs. at ambient temperature, and the colour gradually turned to dark orange. The progress the reaction solution was followed by ^{1}H NMR spectroscopy in (D_6)benzene, revealing a complete consumption of $Ge_2Br_2Tbb_2$ and the selective formation of **18-Rh**. All volatiles were removed in vacuo and the resulting

dark orange mass was dissolved in 2.6 mL of Et_2O and stored in – 30 °C for 1 day. Dark orange crystals of **18-Rh** were isolated by filtering off the mother liquor at – 30 °C and dried for 1.5 hrs. in fine vacuum at ambient temperature. Yield: 440 mg (0.551 mmol, 66 % from $Ge_2Br_2Tbb_2$).

Properties: Compound **18-Rh** is moderately air-sensitive, orange-red solid that can be stored under argon atmosphere at ambient temperature for several months. It is very well soluble in *n*-hexane, benzene, THF, fluorobenzene and Et_2O at room temperature. Under strict exclusion of air, a solution of **18-Rh** in (D_6)benzene shows very minute decomposition after 10 hrs. of heating at 80 °C.

Elemental analysis: 18-Rh ($C_{30}H_{54}BrGeORhSi_4$, 798.51 g mol^{-1}): calcd./%: C 45.12, H 6.82; found/%: C 45.08, H 6.70; **Melting Point:** 180°C.

IR (*n*-hexane): $\tilde{\nu}$ (cm^{-1}) = 2003 (m), and 1984 (vs) [ν(CO)], 1582 (w), 1542 (w) and 1528 (w) [$\nu(CC)_{aryl}$].
IR (THF): $\tilde{\nu}$ (cm^{-1}) = 1992 (w, sh) and 1978 (vs) [ν(CO)], 1582 (w), 1545 (w) and 1533 (w) [$\nu(CC)_{aryl}$].
ATR-IR (solid): $\tilde{\nu}$ (cm^{-1}) = 2951 (m, br), 2900 (m), 2865 (w), 2787 (w), 1976 (vs) and 1935 (w) [ν(CO)], 1581 (m), 1542 (m, sh) and 1532 (m) [$\nu(CC)_{aryl}$], 1475 (vw), 1461 (vw), 1422 (vw, sh), 1394 (m), 1362 (vw), 1260 (m, sh), 1248 (s), 1180 (w, sh), 1170 (m), 1010 (w), 993 (w), 962 (m), 936 (vw), 881 (m), 834 (vs, br), 796 (s, br), 762 (s, br), 738 (w), 721 (w), 688 (m), 662 (w), 644 (vw), 624 (vw), 609 (vw), 554 (vw), 539 (w), 497 (m), 465 (m br), 416 (w).
^{1}H NMR (500.1 MHz, (D_6)benzene, 298 K): δ (ppm) = 0.27 (s, br, $\Delta\nu_{1/2}$ = 4.5 Hz, 36H, $C^{2,6}$-CH(Si*Me*$_3$)$_{A,B}$, Tbb), 1.27 (s, 9H, C*Me*$_3$, Tbb), 2.43 (s, ^2J (^{29}Si-^{1}H) = 9 Hz, 2H, $C^{2,6}$-C*H*(SiMe$_3$)$_{A,B}$, Tbb), 5.07 (d, ^2J (^{103}Rh-^{1}H) = 0.7 Hz, 5H, C_5H_5), 6.83 (s, 2H, $C^{3,5}$-*H*, Tbb).
^{13}C{^{1}H} NMR (125.8 MHz, (D_6)benzene, 298 K): δ (ppm) = 1.0 (s, br, $\Delta\nu_{1/2}$ = 6.6 Hz, 6C, $C^{2,6}$-CH(Si*Me*$_3$)$_A$(SiMe$_3$)$_B$, Tbb), 1.3 (s, br, $\Delta\nu_{1/2}$ = 6.6 Hz, 6C, $C^{2,6}$-CH(SiMe$_3$)$_A$(Si*Me*$_3$)$_B$, Tbb), 31.1 (s, 3C, C*Me*$_3$, Tbb), 31.6 (s, ^1J (^{29}Si-^{31}C) = 42 Hz, 2C, $C^{2,6}$-*C*H(SiMe$_3$)$_{A,B}$, Tbb), 34.6 (s, 1C, *C*Me$_3$, Tbb), 88.02 (d, ^1J (^{103}Rh-^{13}C) = 3.7 Hz, 5C, C_5H_5), 122.2 (s, 2C, $C^{3,5}$-H, Tbb), 146.0 (s, 2C, $C^{2,6}$-CH(SiMe$_3$)$_{A,B}$, Tbb), 151.04 (d, ^2J (^{103}Rh-^{13}C) = 13.6 Hz, 1C, C^1, Tbb), 153.4 (s, 1C, C^4, Tbb), 195.16 (d, ^1J (^{103}Rh-^{13}C) = 83 Hz, 1C, Rh-*C*O).

4.5.20. [CpCo(CO){Si₂(CO)Tbb₂}] (19-Co)

To a stirred golden yellow solution of Si_2Tbb_2 (400 mg, 418 mmol, 1 equiv.) in 5 mL of *n*-pentane, 2 mL of a dark orange *n*-pentane solution of $CpCo(CO)_2$ (77 mg,

427 mmol, 1.02 equiv.) was added dropwise at ambient temperature. The colour of the reaction solution immediately turned brownish red. After 15 min of stirring at ambient temperature an aliquot of the reaction solution was analyzed by ^{1}H NMR spectroscopy, revealed complete consumption of Si_2Tbb_2 and formation of a mixture of compounds (**19-Co** (80 mole %), **20-Co** (6 mole %) and **21-Co** (14 mole %)) along with tiny unreacted $CpCo(CO)_2$. All volatiles were removed at 0 °C in vacuo and resulting brown mass was washed by precooled (–30 °C) *n*-pentane (2 × 2 mL) at –30 °C followed by drying at 0 °C for 30 min in fine vacuum. ^{1}H NMR spectroscopic analysis of the dark brown solid showed a (1:1:7.1) mixture** of **21-Co**, **20-Co** and **19-Co** respectively. **All attempts of obtaining **19-Co** in analytically pure form from this mixture by crystallization have remained unsuccessful.

The IR and NMR spectroscopic data of **19-Co** given below were derived from the NMR spectra of the mixture of **19-Co**, **20-Co**, and **21-Co** after comparison with the IR and the NMR spectra of pure **20-Co** and **21-Co** respectively.

IR (*n*-pentane): $\tilde{\nu}$ (cm^{-1}) = 1963 (s) [ν(CO)], 1578 (w) [ν(CO)], 1586 (w) and 1528 (w) [$\nu(CC)_{aryl}$].

IR (THF): $\tilde{\nu}$ (cm^{-1}) = 1961 (s) [ν(CO)], 1569 (m, br) [ν(CO)], 1586 (w) and 1528 (w) [$\nu(CC)_{aryl}$].

^{1}H NMR (500.1 MHz, (D_6)benzene, 298 K): δ (ppm) = 0.31 (s, 36H, 2 × $C^{2,6}$-CH($SiMe_3$)$_A$,($SiMe_3$)$_B$, 2 × Tbb), 0.32 (s, 36H, 2 × $C^{2,6}$-CH($SiMe_3$)$_A$,($SiMe_3$)$_B$, 2 × Tbb), 1.31 (s, 18H, 2 × CMe_3, 2 × Tbb), 2.42 (s, ^{2}J(^{29}Si-^{1}H) = 9 Hz, 4H, 2 × $C^{2,6}$-C*H*($SiMe_3$)$_{A,B}$, 2 × Tbb), 5.07 (s, 5H, C_5H_5), 6.93 (s, 4H, 2 × $C^{3,5}$-*H*, 2 × Tbb).

^{13}C{^{1}H} NMR (125.8 MHz, (D_6)benzene, 298 K): δ (ppm) = 1.29 (s, 12C, 2 × $C^{2,6}$-CH($SiMe_3$)$_A$,($SiMe_3$)$_B$, 2 × Tbb), 1.30 (s, 12C, 2 × $C^{2,6}$-CH($SiMe_3$)$_A$,($SiMe_3$)$_B$, 2 × Tbb), 31.1 (s, 6C, 2 × CMe_3, 2 × Tbb), 32.5 (s, ^{1}J(^{29}Si-^{31}C) = 41 Hz, 4C, 2 × $C^{2,6}$-*C*H($SiMe_3$)$_{A,B}$, 2 × Tbb), 34.6 (s, 2C, 2 × *C*Me_3, 2 × Tbb), 87.1 (s, 5C, C_5H_5), 122.1 (s, 4C, 2 × $C^{3,5}$-H, 2 × Tbb), 136.3 (s, 2C, 2 × C^{1}, 2 × Tbb), 149.3 (s, 4C, 2 × $C^{2,6}$-CH($SiMe_3$)$_{A,B}$, 2 × Tbb), 152.5 (s, 2C, 2 × C^{4}, 2 × Tbb), 203.8 (s, br, $\Delta\nu_{1/2}$ = 15 Hz, 1C, Co-*C*O), 221.1 (s, 1C, Si*C*OSi).

^{29}Si{^{1}H} NMR (99.3 MHz, (D_6)benzene, 298 K): δ (ppm) = 2.4 (s, 4Si, 4 × *Si*Me_3, 2 × $C^{2,6}$-CH(*Si*Me_3)$_A$($SiMe_3$)$_B$, 2 × Tbb), 2.6 (s, 4Si, 4 × *Si*Me_3, 2 × $C^{2,6}$-CH($SiMe_3$)$_A$(*Si*Me_3)$_B$, 2 × Tbb), 119.1 (s, 2Si, Co-*Si*-Tbb).

4.5.21. [CpCo(CO){Si₂(CO)₂Tbb₂}] (20-Co)

To a stirred golden yellow solution of Si_2Tbb_2 (2.2 g, 2.30 mmol, 1 equiv.) in 80 mL of *n*-hexane, 2 mL *n*-hexane solution of $CpCo(CO)_2$ (422 mg, 2.347 mmol, 1.02 equiv.)

was added dropwise at ambient temperature. The colour of the reaction solution immediately turned brownish red. After 10 minutes of stirring at ambient temperature, CO (0.4 bar) gas was introduced in to the reaction solution. Whereupon stirring in CO atmosphere, within 5 minutes, the colour of the reaction solution turned orange. The progress of the reaction was followed by FT-IR spectroscopy and ^{1}H NMR spectroscopy. The IR spectrum of the reaction solution indicated the selective formation of the complex **20-Co** (ν(CO) = 1987, 1663, and 1613 cm^{-1}) in addition to little unreacted $CpCo(CO)_2$ (ν(CO) = 2031 and 1971 cm^{-1}). Analysis of an aliquot of the reaction solution by ^{1}H NMR spectroscopy in (D_6)benzene revealed a complete consumption of Si_2Tbb_2 and the selective formation of **20-Co**. The reaction solution was worked up by evaporating the solvent to dryness in vacuum followed by crystallization of the crude product from Et_2O (15 mL) at −30 °C. The resulting orange microcrystals were isolated by filtration at −30 °C and dried under fine vacuum at 40 °C for 2 hours. Yield: 2.265 g (1.946 mmol, 84 % from Si_2Tbb_2).

Properties: Compound **20-Co** is an air-sensitive, orange solid. It is well soluble in *n*-hexane, benzene, toluene, THF and Et_2O at ambient temperature. Under strict exclusion of air, a solution of **20-Co** in (D_6)benzene does not show any sign of decomposition after 3 days at ambient temperature.

Elemental analysis: 20-Co ($C_{56}H_{103}CoO_3Si_{10}$, 1164.20 g mol^{-1}): calcd./%: C 57.77, H 8.92; found/%: C 57.76, H 9.07; **Melting Point:** 215°C(dec.).

IR (*n*-hexane): $\tilde{\nu}$ (cm^{-1}) = 1987 (s) [ν(CO)], 1663 (m) [ν(CO)], 1613 (m) [ν(CO)], 1587 (w) and 1530 (w) [$\nu(CC)_{Aryl}$].
IR (THF): $\tilde{\nu}$ (cm^{-1}) = 1984 (s) [ν(CO)], 1660 (m) [ν(CO)], 1611 (m) [ν(CO)], 1587 (w) and 1529 (w) [$\nu(CC)_{Aryl}$].
ATR-IR (solid): $\tilde{\nu}$ (cm^{-1}) = 2962 (m, sh), 2951 (m), 2899 (w), 2868 (vw), 1981 (s) [ν(CO)], 1661 (m) [ν(CO)], 1615 (m) [ν(CO)], 1587 (w) and 1529 (w) [$\nu(CC)_{Aryl}$], 1476 (vw), 1462 (vw, br), 1420 (vw, br), 1396 (m), 1360 (vw), 1260 (m), 1244 (s), 1172 (w), 1162 (w), 1137 (w), 1042 (vw), 1026 (vw), 1006 (w), 954 (m), 940 (w), 887 (m), 858 (m, sh), 853 (s, sh), 826 (vs), 771 (vw, br), 760 (vw, br), 741 (vw, br), 722 (vw, br), 682 (w), 662 (vw, br), 644 (vw, br), 626 (w), 606 (vw, br), 584 (w, br), 561 (vw, br), 538 (w), 499 (w), 448 (w, sh), 436 (m), 418 (w).
^{1}H NMR (500.1 MHz, (D_6)benzene, 298 K): δ (ppm) = 0.29 (s, 36H, 4 × Si*Me*$_3$, 2 × $C^{2,6}$-$CH(SiMe_3)_A(SiMe_3)_B$, 2 × Tbb), 0.31 (s, 36H, 4 × Si*Me*$_3$, 2 × $C^{2,6}$-$CH(SiMe_3)_A(SiMe_3)_B$, 2 × Tbb), 1.31 (s, 18H, 2 × C*Me*$_3$, 2 × Tbb), 2.34 (s, $^2J(^{29}Si,^1H)$ = 9 Hz, 4H, 2 × $C^{2,6}$-C*H*$(SiMe_3)_A(SiMe_3)_B$, 2 × Tbb), 4.81 (s, 5H, C_5H_5), 7.02 (s, 4H, 2 × $C^{3,5}$-*H*, 2 × Tbb).

$^{13}C\{^1H\}$ NMR (125.8 MHz, (D_6)benzene, 298 K): δ (ppm) = 0.7 (s, $^1J(^{29}Si,^{13}C)$ = 52 Hz, 12C, 4 × Si*Me*$_3$, 2 × C^{2,6}-CH(Si*Me*$_3$)$_A$(SiMe$_3$)$_B$, 2 × Tbb), 1.1 (s, $^1J(^{29}Si,^{13}C)$ = 52 Hz, 12C, 4 × Si*Me*$_3$, 2 × C^{2,6}-CH(SiMe$_3$)$_A$(Si*Me*$_3$)$_B$, 2 × Tbb), 31.1 (s, 6C, 2 × C*Me*$_3$, 2 × Tbb), 31.3 (s, 4C, 2 × C^{2,6}-*C*H(SiMe$_3$)$_A$(SiMe$_3$)$_B$, 2 × Tbb), 34.7 (s, 2C, 2 × *C*Me$_3$, 2 × Tbb), 87.7 (s, 5C, *C*$_5$H$_5$), 122.1 (s, 4C, 2 × *C*^{3,5}, 2 × Tbb), 129.4 (s, 2C, 2 × *C*^{1}, 2 × Tbb), 152.8 (s, 4C, 2 × *C*^{2,6}, 2 × Tbb), 153.5 (s, 2C, 2 × *C*^{4}, 2 × Tbb), 204.7 (s, 1C, Co-*C*O), 224.2 (s, 1C, Si-*C*O-Si), 239.2 (s, 1C, Si-*C*O-Si).

$^{29}Si\{^1H\}$ NMR (99.3 MHz, (D_6)benzene, 298 K): δ (ppm) = 2.7 (s, 4Si, 4 × *Si*Me$_3$, 2 × C^{2,6}-CH(*Si*Me$_3$)$_A$(SiMe$_3$)$_B$, 2 × Tbb), 2.8 (s, 4Si, 4 × *Si*Me$_3$, 2 × C^{2,6}-CH(SiMe$_3$)$_A$(*Si*Me$_3$)$_B$, 2 × Tbb), 49.2 (s, 2Si, Co-*Si*-Tbb).

4.5.22. [CpRh(CO){Si$_2$(CO)$_2$Tbb$_2$}] (20-Rh)

To a stirred golden yellow solution of Si_2Tbb_2(900 mg, 0.94 mmol, 1 equiv.) in 20 mL of *n*-hexane, a stock solution (0.391 M in *n*-hexane) of $CpRh(CO)_2$(2.48 mL, 0.97 mmol, 1.03 equiv.) was added dropwise at ambient temperature. The colour of the reaction solution immediately turned orange brown. After 10 minutes of stirring at ambient temperature, CO (0.4 bar) gas was introduced in to the reaction solution. Whereupon stirring in CO atmosphere, within 5 minutes, the colour of the reaction solution turned greenish yellow. The progress of the reaction was followed by FT-IR spectroscopy and ^{1}H NMR spectroscopy. The IR spectrum of the reaction solution indicated the selective formation of the complex **20-Rh** (ν(CO) = 2002, 1665, and 1620 cm^{-1}) in addition to little unreacted $CpRh(CO)_2$ (ν(CO) = 2049 and 1987 cm^{-1}). Analysis of an aliquot of the reaction solution by ^{1}H NMR spectroscopy in (D_6)benzene revealed a complete consumption of Si_2Tbb_2 and the selective formation of **20-Rh**. The reaction solution was worked up by evaporating the solvent to dryness in vacuum followed by crystallization of the crude product from Et_2O (8 mL) at −30 °C. The resulting greenish yellow microcrystals were isolated by filtration at −30 °C and dried under fine vacuum at ambient temperature for 30 min to afford the ether hemi-solvate **20-Rh•0.5 Et$_2$O**. Yield: 872 mg (0.70 mmol, 74 % from Si_2Tbb_2).

Attempts to obtain the solvate-free form upon drying of **20-Rh•0.5 Et$_2$O** in fine vacuum for 5 hrs. at ambient temperature or at 60 °C for 3 hrs. failed leading only to partial loss of Et_2O and extensive decomposition.

Properties: Compound **20-Rh•0.5 Et$_2$O** is an air-sensitive, greenish yellow solid. It is well soluble in *n*-hexane, benzene, toluene, THF and Et_2O at ambient temperature. Under strict exclusion of air, a solution of **20-Rh•0.5 Et$_2$O** in (D_6)benzene does not show any sign of decomposition after 2 days at ambient temperature.

Elemental analysis: 20-Rh•0.5 Et₂O ($C_{56}H_{103}O_3RhSi_{10}(C_4H_{10}O)_{0,5}$, 1245.23 g mol^{-1}): calcd./%: C 55.94, H 8.74; found/%: C 55.92, H 8.77; **Melting Point:** 205°C(dec.).

IR (*n*-hexane): $\tilde{\nu}$ (cm^{-1}) = 2002 (s) [ν(CO)], 1665 (m) [ν(CO)], 1620 (m) [ν(CO)], 1587 (w) and 1530 (w) [$\nu(CC)_{Aryl}$].
IR (THF): $\tilde{\nu}$ (cm^{-1}) = 1999 (s) [ν(CO)], 1661 (m) [ν(CO)], 1618 (m) [ν(CO)], 1587 (w) and 1530 (w) [$\nu(CC)_{Aryl}$].
ATR-IR (solid): $\tilde{\nu}$ (cm^{-1}) = 2953 (m), 2899 (w), 2870 (vw), 2000 (s), 1666 (s) and 1618 (s) [ν(CO)], 1587 (m) and 1529 (m) [$\nu(CC)_{Aryl}$], 1477 (vw), 1396 (m), 1361 (vw), 1260 (s), 1244 (s), 1172 (m), 1161 (m), 1137 (w), 1118 (vw), 1041 (vw), 1027 (w), 1002 (m), 956 (m), 940 (m), 887 (m),856 (s, sh), 834 (vs), 801 (s), 771 (m), 761 (m), 741 (m), 723 (w), 683 (m), 662 (w), 645 (vw), 626 (w), 607 (vw), 596 (vw), 585 (vw), 562 (w), 538 (vw), 512 (w), 482 (m), 453 (w), 436 (m), 419 (w).
^{1}H NMR (500.1 MHz, (D_6)benzene, 298 K): δ (ppm) = 0.28 (s, 36H, 4 × Si*Me*$_3$, 2 × C^{2,6}-CH(Si*Me*$_3$)$_A$(SiMe$_3$)$_B$, 2 × Tbb), 0.32 (s, 36H, 4 × Si*Me*$_3$, 2 × C^{2,6}-CH(SiMe$_3$)$_A$(Si*Me*$_3$)$_B$, 2 × Tbb), 1.30 (s, 18H, 2 × C*Me*$_3$, 2 × Tbb), 2.38 (s, ^2J(^{29}Si,^{1}H) = 9.5 Hz, 4H, 2 × C^{2,6}-C*H*(SiMe$_3$)$_A$(SiMe$_3$)$_B$, 2 × Tbb), 5.18 (s, 5H, C_5H_5), 7.01 (s, 4H, 2 × C^{3,5}-*H*, 2 × Tbb).
^{13}C{^{1}H} NMR (125.8 MHz, (D_6)benzene, 298 K): δ (ppm) = 0.8 (s, ^1J(^{29}Si,^{13}C) = 52 Hz, 12C, 4 × Si*Me*$_3$, 2 × C^{2,6}-CH(Si*Me*$_3$)$_A$(SiMe$_3$)$_B$, 2 × Tbb), 1.1 (s, ^1J(^{29}Si,^{13}C) = 52 Hz, 12C, 4 × Si*Me*$_3$, 2 × C^{2,6}-CH(SiMe$_3$)$_A$(Si*Me*$_3$)$_B$, 2 × Tbb), 31.1 (s, 6C, 2 × C*Me*$_3$, 2 × Tbb), 31.2 (s, 4C, 2 × C^{2,6}-*C*H(SiMe$_3$)$_A$(SiMe$_3$)$_B$, 2 × Tbb), 34.6 (s, 2C, 2 × *C*Me$_3$, 2 × Tbb), 92.45 (d, ^1J(^{103}Rh,^{13}C) = 3 Hz, 5C, C_5H_5), 122.1 (s, 4C, 2 × *C*^{3,5}, 2 × Tbb), 128.9 (s, 2C, 2 × *C*^{1}, 2 × Tbb), 152.5 (s, 4C, 2 × *C*^{2,6}, 2 × Tbb), 153.4 (s, 2C, 2 × *C*^{4}, 2 × Tbb), 192.8 (d, ^1J(^{103}Rh,^{13}C) = 79 Hz, 1C, Rh-*C*O), 227.9 (d, ^2J(^{103}Rh,^{13}C) = 7 Hz, 1C, Si-*C*O-Si), 240.6 (s, ^1J(^{29}Si,^{13}C) = 29 Hz, 1C, Si-*C*O-Si).
^{29}Si{^{1}H} NMR (99.3 MHz, (D_6)benzene, 298 K): δ (ppm) = 2.6 (s, 4Si, 4 × *Si*Me$_3$, 2 × C^{2,6}-CH(*Si*Me$_3$)$_A$(SiMe$_3$)$_B$, 2 × Tbb), 2.8 (s, 4Si, 4 × *Si*Me$_3$, 2 × C^{2,6}-CH(SiMe$_3$)$_A$(*Si*Me$_3$)$_B$, 2 × Tbb), 41.95 (d, ^1J(^{103}Rh,^{29}Si) = 28 Hz, 2Si, Rh-*Si*-Tbb).

4.5.23. [CpCo(Si₂COTbb₂)] (21-Co)

The orange solution of **20-Co** (1.5 g, 1.288 mmol) in 50 mL of toluene was refluxed for 5 hours. During the course of refluxing, the colour of the reaction solution gradually turned wine red. Analysis of an aliquot of the reaction solution by ^{1}H NMR spectroscopy in (D_6)benzene revealed a quantitative transformation of **20-Co** to the complex **21-Co**. The reaction solution was worked up by evaporating the solvent to dryness in vacuum followed by crystallization of the crude product from *n*-hexane (10 mL) at −30 °C. The resulting dark maroon crystals were isolated by filtration at

−30 °C and dried under fine vacuum at 60 °C for 3 hrs. to afford the complex **21-Co**. Yield: 1.25 g (1.128 mmol, 85 % from **20-Co**).

Properties: Compound **21-Co** is an extremely air-sensitive, dark maroon solid which is well soluble in *n*-hexane, benzene, toluene, THF and Et_2O at ambient temperature. Under strict exclusion of air, a solution of **21-Co** in (D_6)benzene does not show any sign of decomposition atleast after 2 days at ambient temperature.

Elemental analysis: 21-Co ($C_{54}H_{103}CoOSi_{10}$, 1108.18 g mol^{-1}): calcd./%: C 58.53, H 9.37; found/%: C 58.63, H 9.49; **Melting Point:** 194°C(dec.).

IR (*n*-hexane): $\tilde{\nu}$ (cm^{-1}) = 1615 (m) [ν(CO)], 1586 (w) and 1529 (w) [$\nu(CC)_{Aryl}$].
IR (THF): $\tilde{\nu}$ (cm^{-1}) = 1612 (m) [ν(CO)], 1586 (w) and 1528 (w) [$\nu(CC)_{Aryl}$].
ATR-IR (solid): $\tilde{\nu}$ (cm^{-1}) = 2962 (m, sh), 2951 (m), 2899 (w), 2869 (vw), 1613 (m) [ν(CO)], 1585 (w) and 1527 (w) [$\nu(CC)_{Aryl}$], 1476 (vw), 1462 (vw), 1421 (vw, br), 1394 (m), 1361 (vw), 1258 (m, sh), 1246 (s), 1165 (w), 1140 (vw), 1042 (vw), 1020 (vw), 1003 (w), 954 (m), 937 (w), 883 (m), 859 (m, sh), 836 (vs, br), 806 (s, sh), 771 (w), 760 (w), 742 (vw), 718 (vw, br), 684 (m), 661 (w), 643 (vw), 619 (vw), 598 (vw), 578 (vw), 556 (vw), 530 (vw), 472 (w, br), 430 (vw).
^{1}H NMR (500.1 MHz, (D_6)benzene, 298 K): δ (ppm) = 0.22 (s, 72H, 8 × Si*Me*$_3$, 2 × C^{2,6}-CH(Si*Me*$_3$)$_2$, 2 × Tbb), 1.36 (s, 18H, 2 × C*Me*$_3$, 2 × Tbb), 2.40 (s, ^2J(^{29}Si,^{1}H) = 9.5 Hz, 4H, 2 × C^{2,6}-C*H*(SiMe$_3$)$_2$, 2 × Tbb), 5.12 (s, 5H, C_5H_5), 6.97 (s, 4H, 2 × C^{3,5}-*H*, 2 × Tbb).
^{13}C{^{1}H} NMR (125.8 MHz, (D_6)benzene, 298 K): δ (ppm) = 1.0 (s, ^1J(^{29}Si,^{13}C) = 52 Hz, 24C, 8 × Si*Me*$_3$, 2 × C^{2,6}-CH(Si*Me*$_3$)$_2$, 2 × Tbb), 31.2 (s, 6C, 2 × C*Me*$_3$, 2 × Tbb), 32.6(s, ^1J(^{29}Si,^{13}C) = 42 Hz, 4C, 2 × C^{2,6}-*C*H(SiMe$_3$)$_2$, 2 × Tbb), 34.7 (s, 2C, 2 × *C*Me$_3$, 2 × Tbb), 78.6 (s, 5C, C_5H_5), 121.5 (s, 4C, 2 × *C*^{3,5}, 2 × Tbb), 139.1 (s, 2C, 2 × *C*^{1}, 2 × Tbb), 148.0 (s, 4C, 2 × *C*^{2,6}, 2 × Tbb), 153.1 (s, 2C, 2 × *C*^{4}, 2 × Tbb), 310.0 (s, 1C, Si-*C*O-Si).
^{29}Si{^{1}H} NMR (99.3 MHz, (D_6)benzene, 298 K): δ (ppm) = 2.2 (s, 8Si, 8 × *Si*Me$_3$, 2 × C^{2,6}-CH(*Si*Me$_3$)$_2$, 2 × Tbb), 290.7 (s, 2Si, Co-*Si*-Tbb).

4.5.24. [CpRh(Si$_2$COTbb$_2$)] (21-Rh)

The greenish yellow solution of **20-Rh•0.5 Et$_2$O** (400 mg, 0.32 mmol) in 35 mL of toluene was refluxed for 5 hours. During the course of refluxing, the colour of the reaction solution gradually turned yellowish brown. Analysis of an aliquot of the reaction solution by ^{1}H NMR spectroscopy in (D_6)benzene revealed a complete consumption of **20-Rh** and the selective formation of the complex **21-Rh**. The reaction solution was worked up by evaporating the solvent to dryness in vacuum followed by crystallization of the crude product from *n*-pentane (4.5 mL) at −30 °C.

The resulting brown black microcrystals were isolated by filtration at −30 °C and dried under fine vacuum at 60 °C for 1 h to afford the complex **21-Rh**. Yield: 250 mg (0.22 mmol, 68 % from **20-Rh•0.5 Et_2O**).

Properties: Compound **21-Rh** is an extremely air-sensitive, brown black solid which is well soluble in *n*-hexane, benzene, toluene, THF and Et_2O at ambient temperature. Under strict exclusion of air, a solution of **21-Rh** in (D_6)benzene does not show any sign of decomposition atleast after 16 hours at ambient temperature.

Elemental analysis: 21-Rh ($C_{54}H_{103}ORhSi_{10}$, 1152.16 g mol^{-1}): calcd./%: C 56.29, H 9.01; found/%: C 56.21, H 9.21; **Melting Point:** 209°C(dec.).

IR (*n*-hexane): $\tilde{\nu}$ (cm^{-1}) = 1623 (m) [ν(CO)], 1586 (w) and 1529 (w) [$\nu(CC)_{Aryl}$].
IR (THF): $\tilde{\nu}$ (cm^{-1}) = 1619 (m) [ν(CO)], 1586 (w) and 1529 (w) [$\nu(CC)_{Aryl}$].
ATR-IR (solid): $\tilde{\nu}$ (cm^{-1}) = 2952 (m), 2899 (w), 2868 (w), 2756 (vw), 1621 (m) [ν(CO)], 1586 (w) and 1529 (w) [$\nu(CC)_{Aryl}$], 1476 (vw), 1463 (vw), 1424 (vw), 1395 (m), 1362 (vw), 1258 (m), 1245 (s), 1169 (m), 1145 (vw), 1107 (vw), 1091 (vw), 1045 (vw), 1027 (w), 1005 (w), 955 (m), 938 (w), 884 (m), 854 (s, sh), 833 (vs), 787 (s), 770 (m), 762 (m), 743 (m), 718 (m), 685 (s), 661 (m), 645 (w), 622 (w), 608 (w), 600 (w), 578 (vw), 557 (w), 524 (vw), 484 (w), 470 (m), 449 (w, sh), 426 (w), 409 (vw).
^{1}H NMR (500.1 MHz, (D_6)benzene, 298 K): δ (ppm) = 0.22 (s, $^2J(^{29}Si,^1H)$ = 6.5 Hz, 72H, 8 × Si*Me*$_3$, 2 × $C^{2,6}$-CH(Si*Me*$_3$)$_2$, 2 × Tbb), 1.32 (s, 18H, 2 × C*Me*$_3$, 2 × Tbb), 2.28 (s, $^2J(^{29}Si,^1H)$ = 9.5 Hz, 4H, 2 × $C^{2,6}$-C*H*($SiMe_3$)$_2$, 2 × Tbb), 5.45 (s, 5H, C_5H_5), 6.90 (s, 4H, 2 × $C^{3,5}$-*H*, 2 × Tbb).
^{13}C{^{1}H} NMR (125.8 MHz, (D_6)benzene, 298 K): δ (ppm) = 1.0 (s, $^1J(^{29}Si,^{13}C)$ = 52 Hz, 24C, 8 × Si*Me*$_3$, 2 × $C^{2,6}$-CH(Si*Me*$_3$)$_2$, 2 × Tbb), 31.2 (s, 6C, 2 × C*Me*$_3$, 2 × Tbb), 32.7(s, $^1J(^{29}Si,^{13}C)$ = 42 Hz, 4C, 2 × $C^{2,6}$-*C*H($SiMe_3$)$_2$, 2 × Tbb), 34.6 (s, 2C, 2 × *C*Me_3, 2 × Tbb), 85.76 (d, $^1J(^{103}Rh,^{13}C)$ = 3 Hz, 5C, C_5H_5), 122.2 (s, 4C, 2 × $C^{3,5}$, 2 × Tbb), 138.05 (d, $^2J(^{103}Rh,^{13}C)$ = 8 Hz, 2C, 2 × C^1, 2 × Tbb), 148.0 (s, 4C, 2 × $C^{2,6}$, 2 × Tbb), 153.2 (s, 2C, 2 × C^4, 2 × Tbb), 302.41 (d, $^2J(^{103}Rh,^{13}C)$ = 32 Hz, 1C, Si-*C*O-Si).
^{29}Si{^{1}H} NMR (99.3 MHz, (D_6)benzene, 298 K): δ (ppm) = 2.2 (s, 8Si, 8 × *Si*Me_3, 2 × $C^{2,6}$-CH(*Si*Me_3)$_2$, 2 × Tbb), 281.2 (d, $^1J(^{103}Rh,^{29}Si)$ = 108 Hz, 2Si, Rh-*Si*-Tbb).

4.5.25. [CpCo(CNMes){Si_2(CO)(CNMes)Tbb_2}] (22-Co)

To a wine-red solution of **21-Co** (400 mg, 0.361 mmol, 1 equiv.) in 15 mL of *n*-hexane, 2 mL of *n*-hexane solution of MesNC (105 mg, 0.722 mmol, 2 equiv.) was dropwise added at ambient temperature. The colour of the reaction solution immediately changed to straw-yellow. After 15 min of stirring at ambient temperature, analysis of

an aliquot of the reaction solution by ^{1}H NMR spectroscopy revealed complete consumption of starting materials and very selective formation of **22-Co**. The reaction was worked up by evaporating the solvent to dryness in vacuo followed by a crystallization of the crude product from Et_2O (3 mL) at 4 °C overnight. Brown microcrystals were isolated by filtration at 4 °C and dried at 55 °C for 2 hours. Yield: 280 mg (0.20 mmol, 56 % from **21-Co**).

Properties: Compound **22-Co** is an air-sensitive, brown solid which is well soluble in *n*-hexane, benzene, toluene and Et_2O at ambient temperature. Under strict exclusion of air, a solution of **22-Co** in (D_6)benzene shows minute but unselective decomposition overnight at ambient temperature.

Elemental analysis: 22-Co ($C_{74}H_{125}CoN_2OSi_{10}$, 1398.58 g mol^{-1}): calcd./%: C 63.55, H 9.01, N 2.00; found/%: C 63.60, H 9.20, N 2.06; **Melting Point:** 203°C(dec.).

IR (*n*-hexane): $\tilde{\nu}$ (cm^{-1}) = 2085 (s) and 2074 (m, sh) [ν(CN)], 1645 (w) [ν(CO)], 1628 (w), 1614 (vw) and 1603 (vw) [ν(CN)], 1586 (vw) and 1528 (vw) [ν(CC)$_{Aryl}$].
IR (THF): $\tilde{\nu}$ (cm^{-1}) = 2086 (s) [ν(CN)], 1643 (w) [ν(CO)], 1626 (w), 1612 (w) and 1599 (vw) [ν(CN)], 1587 (w), 1578 (w, sh) and 1528 (w) [ν(CC)$_{Aryl}$].
ATR-IR (solid): $\tilde{\nu}$ (cm^{-1}) = 2956 (m, br), 2900 (w), 2864 (w, br), 2837 (vw), 2092 (s) [ν(CN)], 1643 (m) [ν(CO)], 1611 (w, sh) and 1596 (m) [ν(CN)], 1525 (w) [ν(CC)$_{Aryl}$], 1475 (w), 1462 (vw, sh), 1438 (vw, br), 1409 (vw, sh), 1393 (m), 1360 (vw), 1257 (m, sh), 1242 (s), 1200 (w), 1176 (w), 1159 (vw), 1148 (vw), 1139 (w), 1115 (vw), 1034 (vw, br), 1018 (vw), 1000 (vw, br), 989 (vw, br), 942 (w), 884 (w), 877 (w), 858 (s, sh), 833 (vs, br), 806 (s, sh), 763 (m), 744 (w), 713 (w), 681 (m, br), 664 (m), 643 (vw), 628 (w), 611 (vw), 596 (vw, br), 577 (vw, br), 565 (w, sh), 558 (w), 520 (w), 504 (vw), 482 (w), 472 (w), 457 (w), 422(w).
^{1}H NMR (500.1 MHz, (D_6)benzene, 298 K): δ (ppm) = 0.16 (s, br, $\Delta\nu_{1/2}$ = 6 Hz, 36H, 2 × C^{2,6}-CH(Si*Me*$_3$)$_A$(SiMe$_3$)$_B$, 2 × Tbb), 0.31 (s, br, $\Delta\nu_{1/2}$ = 4 Hz, 36H, 2 × C^{2,6}-CH(SiMe$_3$)$_A$(Si*Me*$_3$)$_B$, 2 × Tbb), 1.33 (s, 18H, 2 × C*Me*$_3$, 2 × Tbb), 1.93 (s, 3H, C^4-*Me*, Mes$_P$), 2.10 (s, 3H, C^4-*Me*, Mes$_Q$), 2.22 (s, 3H, C$^{2/6}$-*Me*, Mes$_Q$), 2.26 (s, 6H, C^{2,6}-*Me*, Mes$_P$), 2.36 (s, 3H, C$^{2/6}$-*Me*, Mes$_Q$), 3.02 (s, br, $\Delta\nu_{1/2}$ = 23 Hz, 4H, 2 × C^{2,6}-C*H*(SiMe$_3$)$_A$(SiMe$_3$)$_B$, 2 × Tbb), 5.24 (s, 5H, C$_5$*H*$_5$), 6.52 (s, 2H, C^{3,5}-*H*, Mes$_P$), 6.60 (s, br, $\Delta\nu_{1/2}$ = 4.5 Hz, 1H, C$^{3/5}$-*H*, Mes$_Q$), 6.71 (s, br, $\Delta\nu_{1/2}$ = 4.5 Hz, 1H, C$^{3/5}$-*H*, Mes$_Q$), 6.97 (s, br, $\Delta\nu_{1/2}$ = 5 Hz, 4H, 2 × C^{3,5}-*H*, 2 × Tbb).
^{13}C{^{1}H} NMR (125.8 MHz, (D_6)benzene, 298 K): δ (ppm) = 1.8 (s, 12C, 2 × C^{2,6}-CH(Si*Me*$_3$)$_A$(SiMe$_3$)$_B$, 2 × Tbb), 2.4 (s, br, $\Delta\nu_{1/2}$ = 10 Hz, 12C, 2 × C^{2,6}-CH(SiMe$_3$)$_A$(Si*Me*$_3$)$_B$, 2 × Tbb), 20.3 (s, 2C, C^{2,6}-*Me*, Mes$_P$), 20.7 (s, 1C, C^4-*Me*, Mes$_Q$),

20.9 (s, 1C, C^4-*Me*, Mes_P), 22.2 (s, 1C, $C^{2/6}$-*Me*, Mes_Q), 22.73(s, 1C, $C^{2/6}$-*Me*, Mes_Q), 30.5 (s, br, $\Delta\nu_{1/2}$ = 6 Hz, 4C, 2 × $C^{2,6}$-*C*H($SiMe_3$)$_A$($SiMe_3$)$_B$, 2 × Tbb), 31.2 (s, 6C, 2 × C*Me*$_3$, 2 × Tbb), 34.5 (s, 2C, 2 × *C*Me_3, 2 × Tbb), 87.1 (s, 5C, C_5H_5), 123.4 (s, 4C, 2 × $C^{3,5}$-H, 2 × Tbb), 126.1 (s, 1C, $C^{2/6}$, Mes_Q), 126.5 (s, 1C, $C^{2/6}$, Mes_Q), 128.2 **(s, 1C, C^1, Mes_P), 128.8 (s, 2C, $C^{3,5}$, Mes_P), 129.8 (s, 1C, $C^{3/5}$, Mes_Q), 130.2 (s, 1C, $C^{3/5}$, Mes_Q), 131.0 (s, 2C, 2 × C^1, 2 × Tbb), 132.0 (s, 1C, C^4, Mes_Q), 134.3 (s, 2C, $C^{2,6}$, Mes_P), 136.8 (s, 1C, C^4, Mes_P), 149.2 (s, 1C, C^1, Mes_Q), 150.9 (s, 2C, 2 × C^4, 2 × Tbb), 152.2 (s, br, $\Delta\nu_{1/2}$ = 38 Hz, 4C, 2 × $C^{2,6}$, 2 × Tbb), 165.7 (s, br, $\Delta\nu_{1/2}$ = 8 Hz, 1C, Co*C*NMes), 191.4 (s, 1C, Si*C*NMesSi), 239.0 (s, 1C, Si*C*OSi). ** this signal is masked by of that the deuterated solvent and was detected in the HMBC experiment

^{29}Si{^{1}H} NMR (99.3 MHz, (D_6)benzene, 298 K): δ (ppm) = 2.0 (s, 4Si, 2 × $C^{2,6}$-CH(*Si*Me_3)$_A$($SiMe_3$)$_B$, 2 × Tbb), 2.2 (s, 4Si, 2 × $C^{2,6}$-CH($SiMe_3$)$_A$(*Si*Me_3)$_B$, 2 × Tbb). ***no signal was detected for Co-*Si*-Tbb in ^{29}Si NMR, though one cross peak was found in (^{29}Si-^{1}H) HMBC experiment at 43 ppm.

^{29}Si{^{1}H} NMR (99.3 MHz, (D_8)toluene, 238 K): δ (ppm) = 40.7 (s, br, $\Delta\nu_{1/2}$ = 8 Hz, 1Si, Co-*Si*-Tbb), 47.1 (s, br, $\Delta\nu_{1/2}$ = 14 Hz, 1Si, Co-*Si*-Tbb). **signals correspond to *Si*Me_3 were extremely broad to pick.

4.5.26. [CpCo(CO){Si_2(CO)(CNMes)Tbb$_2$}] (23-Co)

An orange solution of **20-Co** (746 mg, 0.641 mmol, 1 equiv.) in 25 mL of benzene was treated with MesNC (98 mg, 673 mmol, 1.05 equiv.) at ambient temperature and the reaction mixture was heated for 84 hours at 60 °C. During the course of heating the colour of the reaction solution gradually became straw-brown. Monitoring the reaction progress by ^{1}H NMR spectroscopy revealed 97 % selective conversion of **20-Co** to **23-Co** along with small amount of MesNC. The reaction was stopped and worked up by evaporating the solvent to dryness in vacuo followed by a crystallization from *n*-hexane (8 mL) at –20 °C overnight. Straw-brown microcrystalline precipitate was isolated at –20 °C by filtering off the mother liquor and dried at 60 °C for 3 hours to afford the mono-hexane solvate **23-Co•C_6H_{14}**. Yield: 695 mg (0.508 mmol, 79 % from **20-Co**).

Properties: Compound **23-Co** is an air-sensitive, straw-brown solid which is well soluble in *n*-hexane, benzene, toluene, THF and Et_2O at ambient temperature. Under strict exclusion of air, a solution of **23-Co** in (D_6)benzene does not show any decomposition after one day at ambient temperature.

Elemental analysis: 23-Co•C_6H_{14} ($C_{65}H_{114}CoNO_2Si_{10}$•($C_6H_{14}$), 1367.57 g mol^{-1}): calcd./%: C 62.36, H 9.43, N 1.02; found/%: C 62.38, H 9.09, N 1.14; **Melting Point:** 171°C(dec.).

IR (*n*-heptane): $\tilde{\nu}$ (cm^{-1}) = 1979 (s) [ν(CO)], 1639 (w, br) [ν(CN)], 1617 (m) [ν(CO)], 1589 (vw) and 1528 (w) [ν(CC)$_{Aryl}$].
IR (THF): $\tilde{\nu}$ (cm^{-1}) = 1978 (s) [ν(CO)], 1637 (w, br) [ν(CN)], 1615 (m) [ν(CO)], 1589 (vw) and 1527 (w) [ν(CC)$_{Aryl}$].
ATR-IR (solid): $\tilde{\nu}$ (cm^{-1}) = 2963 (m, sh), 2952 (m), 2927 (w, br), 2901 (w), 2869 (vw), 1976(s) [ν(CO)], 1630 (m) [ν(CN)], 1613 (m) [ν(CO)], 1589 (w) and 1527 (w) [ν(CC)$_{Aryl}$], 1474 (w, br), 1412 (w, sh), 1394 (m), 1361 (w), 1259 (m, sh), 1241 (s), 1199 (w), 1176 (w), 1163 (w), 1147 (vw), 1139 (w), 1126 (vw, br), 1006 (w), 993 (w, sh), 949 (m), 942 (m, sh), 885 (m), 857 (s, sh), 833 (vs), 762 (s), 744 (m), 718 (m), 680 (s, br), 664 (m), 644 (w), 628 (w), 609 (w), 583 (m), 560 (w, br), 535 (m), 509 (m), 475 (w), 463 (w, sh), 455 (w, br), 431 (vw, br), 418 (m).
^{1}H NMR (500.1 MHz, (D_6)benzene, 298 K): δ (ppm) = –0.01, 0.31, 0.34 and 0.41 (each s, each br, $\Delta\nu_{1/2}$ = 8 Hz, 9 Hz, 9 Hz, and 12 Hz, 72H, 8 × Si*Me$_3$*, 2 × C^{2,6}-CH(Si*Me$_3$*)$_{A,B}$, 2 × Tbb), 1.31 (s, 18H, 2 × C*Me$_3$*, 2 × Tbb), 2.09 (s, 3H, C^4-*Me*, Mes), 2.29 (s, br, $\Delta\nu_{1/2}$ = 13 Hz, 2H, 2 × C^2-C*H*(SiMe$_3$)$_{A,B}$, 2 × Tbb), 2.34 (s, br, $\Delta\nu_{1/2}$ = 6 Hz, 3H, C$^{2/6}$-*Me*, Mes), 2.38 (s, br, $\Delta\nu_{1/2}$ = 6 Hz, 3H, C$^{2/6}$-*Me*, Mes), 3.23 (s, br, $\Delta\nu_{1/2}$ = 12 Hz, 2 × C^6-C*H*(SiMe$_3$)$_{A,B}$, 2 × Tbb), 4.71 (s, 5H, C_5H_5), 6.72 (s, 2H, C^{3,5}-*H*, Mes), 6.98 (s, 4H, 2 × C^{3,5}-*H*, Tbb).
^{13}C{^{1}H} NMR (125.8 MHz, (D_6)benzene, 298 K): δ (ppm) = 0.8, 1.2, 1.8 and 2.1 (each s, each br, $\Delta\nu_{1/2}$ = 13 Hz, 14 Hz, 14 Hz, and 13 Hz, 24C, 8 × Si*Me$_3$*, 2 × C^{2,6}-CH(Si*Me$_3$*)$_{A,B}$, 2 × Tbb), 20.7 (s, 1C, C^4-*Me*, Mes), 21.5 (s, 2C, C^{2,6}-*Me*, Mes), 29.7 (s, br, $\Delta\nu_{1/2}$ = 14 Hz, 2C, 2 × C^6-*C*H(SiMe$_3$)$_{A,B}$, 2 × Tbb), 31.1 (s, 6C, 2 × C*Me$_3$*, 2 × Tbb), 31.8 (s, br, $\Delta\nu_{1/2}$ = 16 Hz, 2C, 2 × C^2-*C*H(SiMe$_3$)$_{A,B}$, 2 × Tbb), 34.5 (s, 2C, 2 × *C*Me$_3$, 2 × Tbb), 88.2 (s, 5C, *C*$_5$H$_5$), 122.3 (s, br, $\Delta\nu_{1/2}$ = 14 Hz, 2C, 2 × C^3-*H*, 2 × Tbb), 124.0 (s, br, $\Delta\nu_{1/2}$ = 14 Hz, 2C, 2 × C^5-*H*, 2 × Tbb), 124.5 (s, br, $\Delta\nu_{1/2}$ = 5 Hz, 1C, *C$^{2/6}$*-Me, Mes), 125.0 (s, br, $\Delta\nu_{1/2}$ = 5 Hz, 1C, *C$^{2/6}$*-Me, Mes), 129.5 (s, br, $\Delta\nu_{1/2}$ = 6 Hz, 2C, *C^{3,5}*-H, Mes), 129.9 (s, br, $\Delta\nu_{1/2}$ = 6 Hz, 1C, *C^4*-Me, Mes), 131.0 (s, 2C, 2 × *C^6*, 2 × Tbb), 131.5 (s, 2C, 2 × *C^2*, 2 × Tbb), 148.8 (s, 1C, *C^1*, Mes), 151.9 (s, 2C, 2 × *C^4*, 2 × Tbb), 152.5 (s, br, $\Delta\nu_{1/2}$ = 10.5 Hz, 2C, 2 × *C^1*, 2 × Tbb), 192.8 (s, ^1J (^{29}Si-^{13}C) = 30 Hz, 1C, Si*C*NMesSi), 205.7 (s, br, $\Delta\nu_{1/2}$ = 9 Hz, 1C, Co-*C*O), 226.8 (s, ^1J (^{29}Si-^{13}C) = 21 Hz, 1C, Si*C*OSi).

^{29}Si{^{1}H} NMR (99.3 MHz, (D_6)benzene, 298 K): δ (ppm) = 2.6 (s, 4Si, 2 × $C^{2,6}$-CH($SiMe_3$)$_A$, 2 × Tbb), 2.7 (s, 4Si, 2 × $C^{2,6}$-CH($SiMe_3$)$_B$, 2 × Tbb), 33.4 (s, 2Si, Co-*Si*-Tbb).

4.5.27. [CpCo(Si₂CNMesTbb₂)] (24-Co)

The straw-brown solution of **23-Co•C_6H_{14}** (815 mg, 0.596 mmol) in 40 mL of *n*-heptane was refluxed for 5 hours. During the course of refluxing, the colour of the reaction solution gradually turned wine red. Analysis of an aliquot of the reaction solution by ^{1}H NMR spectroscopy in (D_6)benzene revealed a complete consumption of **23-Co** and the very selective formation of complex **24-Co**. The reaction solution was worked up by evaporating the solvent to dryness in vacuum followed by crystallization of the crude product from Et_2O (8 mL) at −30 °C. The resulting dark maroon microcrystals were isolated by filtration at −30 °C and dried under fine vacuum at 60 °C for 3 hrs. to afford the Et_2O hemi solvate **24-Co•0.25 Et_2O**. Yield: 532 mg (0.428 mmol, 72 % from **23-Co•C_6H_{14}**).

Attempts to obtain the solvate-free form upon drying of **24-Co•0.25 Et_2O** in fine vacuum for 5 hours at ambient temperature or at 75 °C for 3 hrs. failed leading only to partial loss of Et_2O and extensive decomposition.

Properties: Compound **24-Co** is an air-sensitive, dark maroon solid which is well soluble in *n*-hexane, benzene, toluene and Et_2O at ambient temperature. Under strict exclusion of air, a solution of **24-Co** in (D_6)benzene does not show any sign of decomposition after 2 days at ambient temperature.

Elemental analysis: 24-Co•0.25 Et_2O ($C_{63}H_{114}CoNSi_{10}$•$(C_4H_{10}O)_{0.25}$, 1243.90 g mol^{-1}): calcd./%: C 61.80, H 9.44, N 1.13; found/%: C 61.68, H 9.51, N 1.15; **Melting Point:** 130°C(dec.).

IR (*n*-hexane): $\tilde{\nu}$ (cm^{-1}) = 1610 (vw) [ν(CN)], 1587 (w), 1564 (vw), 1543 (vw) and 1527 (w) [ν(CC)$_{Aryl}$].
IR (THF): $\tilde{\nu}$ (cm^{-1}) = 1609 (vw) [ν(CN)], 1587 (w), 1564 (vw), 1542 (vw) and 1527 (w) [ν(CC)$_{Aryl}$].
ATR-IR (solid): $\tilde{\nu}$ (cm^{-1}) = 2959 (m, sh), 2952 (m), 2900 (w), 2866 (w), 2801 (vw), 1608 (vw) [ν(CN)], 1585 (m), 1543 (vw, sh) and 1524 (m) [ν(CC)$_{Aryl}$], 1476 (w), 1464 (w, br), 1421 (vw), 1393 (m), 1361 (w), 1352 (vw, sh), 1260 (m, sh), 1247 (s), 1200 (vw), 1171 (w, sh), 1160 (w), 1135 (w), 1114 (w), 1028 (w), 1006 (w), 987 (w, br), 947 (m), 937 (m, sh), 882 (m), 857 (s, sh), 833 (s, br), 803 (s), 771 (m, sh), 762 (m), 739 (w), 718

(m), 684 (s), 662 (m), 643 (vw), 625 (w), 605 (m), 591 (vw), 574 (vw), 555 (vw), 530 (w), 508 (vw, br), 469 (s), 457 (w, sh), 432 (vw, sh), 420 (w), 412 (w, sh).

^{1}H NMR (500.1 MHz, (D_6)benzene, 298 K): δ (ppm) = 0.09 (s, br, $\Delta\nu_{1/2}$ = 9 Hz, 36H, 2 × $C^{2,6}$-CH(Si*Me*$_3$)$_A$(SiMe$_3$)$_B$, 2 × Tbb), 0.34 (s, br, $\Delta\nu_{1/2}$ = 9 Hz, 36H, 2 × $C^{2,6}$-CH(SiMe$_3$)$_A$(Si*Me*$_3$)$_B$, 2 × Tbb), 1.35 (s, 18H, 2 × C*Me*$_3$, 2 × Tbb), 1.99 (s, 3H, C^4-*Me*, Mes), 2.11 (s, 6H, $C^{2,6}$-*Me*, Mes), 2.67 (s, ^2J (^{29}Si-^{1}H) = 9 Hz, 4H, 2 × $C^{2,6}$-C*H*(SiMe$_3$)$_A$(SiMe$_3$)$_B$, 2 × Tbb), 4.97 (s, 5H, C_5H_5), 6.59 (s, 2H, $C^{3,5}$-*H*, Mes), 6.94 (s, 4H, 2 × $C^{3,5}$-*H*, 2 × Tbb).

^{13}C{^{1}H} NMR (125.8 MHz, (D_6)benzene, 298 K): δ (ppm) = 1.5 (s, br, $\Delta\nu_{1/2}$ = 9 Hz, 12C, 2 × $C^{2,6}$-CH(Si*Me*$_3$)$_A$(SiMe$_3$)$_B$, 2 × Tbb), 2.0 (s, br, $\Delta\nu_{1/2}$ = 9 Hz, 12C, 2 × $C^{2,6}$-CH(SiMe$_3$)$_A$(Si*Me*$_3$)$_B$, 2 × Tbb), 20.9 (s, 1C, C^4-*Me*, Mes), 21.4 (s, 2C, $C^{2,6}$-*Me*, Mes), 31.2 (s, 6C, 2 × C*Me*$_3$, 2 × Tbb), 31.4 (s, 4C, 2 × $C^{2,6}$-*C*H(SiMe$_3$)$_A$(SiMe$_3$)$_B$, 2 × Tbb), 34.6 (s, 2C, 2 × *C*Me$_3$, 2 × Tbb), 79.8 (s, 5C, C_5H_5), 122.7 (s, 4C, 2 × $C^{3,5}$-H, 2 × Tbb), 123.0 (s, 2C, $C^{2,6}$-Me, Mes), 130,0 (s, 2C, $C^{3,5}$-H, Mes), 132.2 (s, 1C, C^4-Me, Mes), 140.3 (s, 2C, 2 × C^1, 2 × Tbb), 147.8 (s, 4C, 2 × $C^{2,6}$, 2 × Tbb), 149.4 (s, 1C, C^1, Mes), 151.8 (s, 2C, 2 × C^4, 2 × Tbb), 237.8 (s, 1C, Si*C*NMesSi).

^{29}Si{^{1}H} NMR (99.3 MHz, (D_6)benzene, 298 K): δ (ppm) = 2.1 (s, 8Si, 8 × *Si*Me$_3$, 2 × $C^{2,6}$-CH(*Si*Me$_3$)$_{A,B}$, 2 × Tbb), 269.2 (s, br, $\Delta\nu_{1/2}$ = 28 Hz, 2Si, Co-*Si*-Tbb).

4.5.28. [CpCo{Si$_2$(CNMes)$_2$Tbb$_2$}] (25-Co)

A wine-red solution of **24-Co•0.25 Et$_2$O** (256 mg, 0.206 mmol, 1 equiv.) in 5 mL of *n*-hexane was treated with 2 mL of a *n*-hexane solution of MesNC (33 mg, 0.226 mmol, 1.1 equiv.) at ambient temperature. The reaction solution was heated at 65 °C for 90 hours and during the course of heating the colour of the reaction solution gradually changed to red-brown. Analysis of an aliquot of the reaction solution by ^{1}H NMR spectroscopy revealed a complete consumption of **24-Co** and very selective formation of **25-Co** (97 mole %) along with 3 mole% of CpCo(MesNC)$_2$ and little unreacted MesNC. The reaction was worked up by evaporating the solvent to dryness in vacuo followed by crystallization of the crude product from Et_2O (2.8 mL) at –30 °C for 5 hours. The black microcrystals were separated from its mother liquor by filtration at –30 °C followed by drying at 40 °C for 2 hrs. to afford the Et_2O hemi-solvate **25-Co•1.4 Et$_2$O** as red-brown solid. Yield: 200 mg (0.136 mmol, 66 % from **24-Co•0.25 Et$_2$O**).

Attempts to obtain the solvate-free form upon drying of **25-Co•1.4 Et$_2$O** in fine vacuum at 65 °C for 3 hours failed leading only to partial loss of Et_2O and partial decomposition.

Properties: Compound **25-Co** is an air-sensitive, brown-red solid, which is well soluble in *n*-hexane, benzene, THF and Et_2O at ambient temperature. Under strict exclusion of air, a solution of **25-Co** in (D_6)benzene does not show any sign decomposition after 2 days at ambient temperature.

Elemental analysis: 25-Co•1.4 Et_2O ($C_{73}H_{125}CoN_2Si_{10}$•$(C_4H_{10}O)_{1.4}$, 1474.34 g mol^{-1}): calcd./%: C 64.03, H 9.50, N 1.90; found/%: C 64.13, H 9.37, N 1.93; **Melting Point:** 192°C(dec.).

IR (*n*-hexane): $\tilde{\nu}$ (cm^{-1}) = 1589 (w) and 1526 (w) [$\nu(CC)_{Aryl}$], 1558 (vw) and 1547 (vw), [ν(CN)].

IR (THF): $\tilde{\nu}$ (cm^{-1}) = 1588 (w) and 1526 (w) [$\nu(CC)_{Aryl}$], 1547 (vw), [ν(CN)].

^{1}H NMR (500.1 MHz, (D_6)benzene, 298 K): δ (ppm) = –0.03 (s, 18H, 2 × Si*Me*$_3$, 2 × C^2-CH(Si*Me*$_3$)$_A$(SiMe$_3$)$_B$, 2 × Tbb), 0.26 (s, 18H, 2 × Si*Me*$_3$, 2 × C^6-CH(Si*Me*$_3$)$_A$(SiMe$_3$)$_B$, 2 × Tbb), 0.27 (s, 18H, 2 × Si*Me*$_3$, 2 × C^2-CH(SiMe$_3$)$_A$(Si*Me*$_3$)$_B$, 2 × Tbb), 0.41 (s, 18H, 2 × Si*Me*$_3$, 2 × C^6-CH(SiMe$_3$)$_A$(Si*Me*$_3$)$_B$, 2 × Tbb), 1.14 (s, 6H, 2 × C^2-*Me*, 2 × Mes). 1.39 (s, 18H, 2 × C*Me*$_3$, 2 × Tbb), 2.16 (s, 6H, 2 × C^4-*Me*, 2 × Mes), 2.27 (s, 2H, 2 × C^2-C*H*(SiMe$_3$)$_A$(SiMe$_3$)$_B$, 2 × Tbb), 2.32 (s, 6H, 2 × C^6-*Me*, 2 × Mes), 2.54 (s, 2H, 2 × C^6-C*H*(SiMe$_3$)$_A$(SiMe$_3$)$_B$, 2 × Tbb), 4.78 (s, 5H, C$_5$*H*$_5$), 6.55 (s, br, $\Delta\nu_{1/2}$ = 4.5 Hz, 2H, 2 × C^3-*H*, 2 × Mes), 6.71 (s, $\Delta\nu_{1/2}$ = 4.5 Hz, 2H, 2 × C^5-*H*, 2 × Mes), 6.92 (d,^4J (^{1}H-^{1}H) = 1.3 Hz, 2H, 2 × C^5-*H*, 2 × Tbb), 6.99 (d,^4J (^{1}H-^{1}H) = 1.3 Hz, 2H, 2 × C^3-*H*, 2 × Tbb).

^{13}C{^{1}H} NMR (125.8 MHz, (D_6)benzene, 298 K): δ (ppm) = 1.3 (s, 6C, 2 × Si*Me*$_3$, 2 × C^2-CH(Si*Me*$_3$)$_A$(SiMe$_3$)$_B$, 2 × Tbb), 1.6 (s, 6C, 2 × Si*Me*$_3$, 2 × C^2-CH(SiMe$_3$)$_A$(Si*Me*$_3$)$_B$, 2 × Tbb), 2.5 (s, 6C, 2 × Si*Me*$_3$, 2 × C^6-CH(SiMe$_3$)$_A$(Si*Me*$_3$)$_B$, 2 × Tbb), 3.2 (s, 6C, 2 × Si*Me*$_3$, 2 × C^6-CH(Si*Me*$_3$)$_A$(SiMe$_3$)$_B$, 2 × Tbb), 18.0 (s, 2C, 2 × C^2-*Me*, 2 × Mes), 20.8 (s, 2C, 2 × C^4-*Me*, 2 × Mes), 23.4 (s, 2C, 2 × C^6-*Me*, 2 × Mes), 30.7 (s, 2C, 2 × C^2-*C*H(SiMe$_3$)$_A$(SiMe$_3$)$_B$, 2 × Tbb), 31.2 (s, 6C, 2 × C*Me*$_3$, 2 × Tbb), 34.1 (s, 2C, 2 × C^6-*C*H(SiMe$_3$)$_A$(SiMe$_3$)$_B$, 2 × Tbb), 34.5 (s, 2C, 2 × *C*Me$_3$, 2 × Tbb), 81.8 (s, 5C, *C*$_5$H$_5$), 121.5 (s, 2C, 2 × *C*^{6}, 2 × Mes), 122.6 (s, 2C, 2 × *C*^{3}, 2 × Tbb), 123.2 (s, 2C, 2 × *C*^{5}, 2 × Tbb), 128.4 (s, 2C, 2 × *C*^{5}, 2 × Mes), 129.0 (s, 2C, 2 ×*C*^{4}, 2 × Mes), 129.7 (s, 2C, 2 × *C*^{3}, 2 × Mes), 132.7 (s, 2C, 2 × *C*^{2}, 2 × Mes), 141.3 (s, 2C, 2 × *C*^{1}, 2 × Tbb), 147.4 (s, 2C, 2 × *C*^{6}, 2 × Tbb), 147.8 (s, 2C, 2 × *C*^{2}, 2 × Tbb), 150.6 (s, 2C, 2 × *C*^{1}, 2 × Mes), 151.3 (s, 2C, 2 × *C*^{4}, 2 × Tbb), 194.3 (s, 2C, 2 × N*C*Mes).

^{29}Si{^{1}H} NMR (99.3 MHz, (D_6)benzene, 298 K): δ (ppm) = 1.21 (s, 2Si, 2 × *Si*Me$_3$, 2 × C^6-CH(*Si*Me$_3$)$_A$(SiMe$_3$)$_B$, 2 × Tbb), 1.25 (s, 2Si, 2 × *Si*Me$_3$, 2 × C^2-CH(*Si*Me$_3$)$_A$(SiMe$_3$)$_B$, 2 × Tbb), 2.5 (s, 2Si, 2 × *Si*Me$_3$, 2 × C^6-CH(SiMe$_3$)$_A$(*Si*Me$_3$)$_B$, 2 × Tbb), 4.8 (s, 2Si, 2 × *Si*Me$_3$, 2 × C^2-CH(SiMe$_3$)$_A$(*Si*Me$_3$)$_B$, 2 × Tbb), 286.2 (s, br, $\Delta\nu_{1/2}$ = 19 Hz, 2Si, Co-*Si*-Tbb).

4.5.29. [CpCoCSi$_2$Me$_2$Tbb$_2$] (**26-Co**)

To a stirred 10 mL of wine-red *n*-pentane solution of **21-Co** (300 mg, 0.271 mmol, 1 equiv.), a stock solution (2 M in toluene) of AlMe3 (0.14 mL, 0.271 mmol, 1 equiv.) was added dropwise at ambient temperature. The colour of the reaction solution was changed immediately to light green. After 5 min of stirring at ambient temperature, an aliquot of the reaction solution was analyzed by ^{1}H NMR spectroscopy revealed complete consumption of **21-Co** and quantitative formation of **26-Co**. The reaction mixture was evaporated to dryness and the resulting light green mass was suspended in 3 mL of 1 : 1 (Et_2O : CH_3CN) mixture. The yellowish-green precipitate of **26-Co** was separated from off-white mother liquor by filtration at ambient temperature and dried at 45 °C for 2 hours. Yield: 200 mg (0.178 mmol, 66 % from **21-Co**).

Properties: Compound **26-Co** is a moderately air-sensitive, yellowish-green solid, which is well soluble in *n*-hexane, benzene, Et_2O at ambient temperature, but insoluble in CH_3CN. Under strict exclusion of air, a solution of **26-Co** in (D_6)benzene does not show any sign decomposition after one day at ambient temperature.

Elemental analysis: 26-Co ($C_{56}H_{109}CoSi_{10}$, 1122.25 g mol^{-1}): calcd./%: C 59.93, H 9.79; found/%: C 59.24, H 9.78; **Melting Point:** 208°C(dec.).

^{1}H NMR (500.1 MHz, (D_6)benzene, 298 K): δ (ppm) = 0.24 (s, 36H, 4 × Si*Me$_3$*, 2 × C^{2,6}-CH(Si*Me$_3$*)$_A$(SiMe$_3$)$_B$, 2 × Tbb), 0.29 (s, 36H, 4 × Si*Me$_3$*, 2 × C^{2,6}-CH(SiMe$_3$)$_A$(Si*Me$_3$*)$_B$, 2 × Tbb), 1.09 (s, 6H, 2 × *Me*, Si(*Me*)Tbb), 1.35 (s, 18H, 2 × C*Me$_3$*, 2 × Tbb), 3.04 (s, 4H, 2 × C^{2,6}-C*H*(SiMe$_3$)$_{A,B}$, 2 × Tbb), 4.93 (s, 5H, C_5H_5), 6.94 (s, 4H, 2 × C^{3,5}-*H*, 2 × Tbb).
^{13}C{^{1}H} NMR (125.8 MHz, (D_6)benzene, 298 K): δ (ppm) = 1.6 (s, 12C, 4 × Si*Me$_3$*, 2 × C^{2,6}-CH(Si*Me$_3$*)$_A$(SiMe$_3$)$_B$, 2 × Tbb), 1.8 (s, 12C, 4 × Si*Me$_3$*, 2 × C^{2,6}-CH(SiMe$_3$)$_A$(Si*Me$_3$*)$_B$, 2 × Tbb), 10.9 (s, ^1J (^{29}Si-^{13}C) = 56 Hz, 2C, 2 × *Me*, Si(*Me*)Tbb), 30.4 (s, ^1J (^{29}Si-^{13}C) = 43 Hz, 4C, 2 × C^{2,6}-*C*H(SiMe$_3$)$_{A,B}$, 2 × Tbb), 31.2 (s, 6C, 2 × C*Me$_3$*, 2 × Tbb), 34.4 (s, 2C, 2 × *C*Me$_3$, 2 × Tbb), 79.9 (s, 5C, *C$_5$*H$_5$), 122.6 (s, 4C, 2 × *C^{3,5}*-H, 2 × Tbb), 132.1 (s, 2C, 2 × *C^1*, 2 × Tbb), 150.0 (s, 2C, 2 ×*C^4*, 2 × Tbb), 150.4 (s, 4C, 2 × *C^{2,6}*, 2 × Tbb), 313.8 (s, 1C, Co=*C*).
^{29}Si{^{1}H} NMR (99.3 MHz, (D_6)benzene, 298 K): δ (ppm) = 1.9 (s, 4Si, 4 × *Si*Me$_3$, 2 × C^{2,6}-CH(*Si*Me$_3$)$_A$(SiMe$_3$)$_B$, 2 × Tbb), 2.0 (s, 4Si, 4 × *Si*Me$_3$, 2 × C^{2,6}-CH(SiMe$_3$)$_A$(*Si*Me$_3$)$_B$, 2 × Tbb), 6.6 (s, 2Si, Co-*Si*MeTbb).

4.5.30. [CpRhCSi$_2$Me$_2$Tbb$_2$] (**26-Rh**)

To a yellowish-brown solution of **21-Rh** (200 mg, 0.17 mmol, 1 equiv.) in 5 mL of *n*-pentane, a stock solution (2 M in toluene) of AlMe$_3$ (0.09 mL, 0.17 mmol, 1 equiv.)

was added dropwise at ambient temperature. The colour of the reaction solution was changed immediately to brownish-purple. Analysis of an aliquot of the reaction solution by ^{1}H NMR spectroscopy in (D_6)benzene revealed a complete consumption of **21-Rh** and the selective formation of the complex **26-Rh.** The reaction solution was worked up by evaporating the solvent to dryness in vacuum and the resulting brown mass was suspended in 4 mL of 3 : 1 (Et_2O : CH_3CN) mixture. The mink-brwon precipitate was separated from off-white mother liquor by filtration at ambient temperature and dried under fine vacuum at 40 °C for 2.5 hours. Yield: 145 mg (0.12 mmol, 72 % from **21-Rh**).

Properties: Compound **26-Rh** is a moderately air-sensitive, mink-brown solid, which is well soluble in *n*-hexane, benzene, Et_2O at ambient temperature, but insoluble in CH_3CN. Under strict exclusion of air, a solution of **26-Rh** in (D_6)benzene does not show any sign decomposition after 2 days at ambient temperature.

Elemental analysis: 26-Rh ($C_{56}H_{109}RhSi_{10}$, 1122.25 g mol^{-1}): calcd./%: C 57.67, H 9.42; found/%: C 57.83, H 9.43; **Melting Point:** 222°C(dec.).

^{1}H NMR (500.1 MHz, (D_6)benzene, 298 K): δ (ppm) = 0.22 (s, 36H, 4 × Si*Me*$_3$, 2 × C^{2,6}-CH(Si*Me*$_3$)$_A$(SiMe$_3$)$_B$, 2 × Tbb), 0.28 (s, 36H, 4 × Si*Me*$_3$, 2 × C^{2,6}-CH(SiMe$_3$)$_A$(Si*Me*$_3$)$_B$, 2 × Tbb), 1.14 (s, ^{2}J(^{29}Si-^{1}H) = 7.6 Hz), 6H, 2 × *Me*, 2 × Si(*Me*)Tbb), 1.34 (s, 18H, 2 × C*Me*$_3$, 2 × Tbb), 2.94 (s, ^{2}J(^{29}Si,^{1}H) = 9. Hz, 4H, 2 × C^{2,6}-C*H*(SiMe$_3$)$_A$(SiMe$_3$)$_B$, 2 × Tbb), 5.39 (s, 5H, C_5H_5), 6.90 (s, 4H, 2 × C^{3,5}-*H*, 2 × Tbb).

^{13}C{^{1}H} NMR (125.8 MHz, (D_6)benzene, 298 K): δ (ppm) = 1.6 (s, ^{1}J(^{29}Si,^{13}C) = 52 Hz, 12C, 4 × Si*Me*$_3$, 2 × C^{2,6}-CH(Si*Me*$_3$)$_A$(SiMe$_3$)$_B$, 2 × Tbb), 1.8 (s, ^{1}J(^{29}Si,^{13}C) = 52 Hz, 12C, 4 × Si*Me*$_3$, 2 × C^{2,6}-CH(SiMe$_3$)$_A$(Si*Me*$_3$)$_B$, 2 × Tbb), 12.2 (s, ^{1}J(^{29}Si,^{13}C) = 56 Hz, 2C, 2 × *Me*, 2 × Si(*Me*)Tbb), 30.2 (s, ^{1}J(^{29}Si,^{13}C) = 42 Hz, 4C, 2 × C^{2,6}-*C*H(SiMe$_3$)$_A$(SiMe$_3$)$_B$, 2 × Tbb), 31.2 (s, 6C, 2 × C*Me*$_3$, 2 × Tbb), 34.3 (s, 2C, 2 × *C*Me$_3$, 2 × Tbb), 85.25 (d, ^{1}J(^{103}Rh,^{13}C) = 3 Hz, 5C, *C*$_5$H$_5$), 122.4 (s, 4C, 2 × *C*^{3,5}, 2 × Tbb), 131.4 (s, 2C, 2 × *C*^{1}, 2 × Tbb), 150.1 (s, 2C, 2 × *C*^{4}, 2 × Tbb), 150.6 (s, 4C, 2 × *C*^{2,6}, 2 × Tbb), 318.6 (s, 1C, Rh=*C*).

^{29}Si{^{1}H} NMR (99.3 MHz, (D_6)benzene, 298 K): δ (ppm) = –2.21 (d, ^{1}J(^{103}Rh,^{29}Si) = 38 Hz, 2Si, Rh-*Si*MeTbb), 1.9 (s, 4Si, 4 × *Si*Me$_3$, 2 × C^{2,6}-CH(*Si*Me$_3$)$_A$(SiMe$_3$)$_B$, 2 × Tbb), 2.0 (s, 4Si, 4 × *Si*Me$_3$, 2 × C^{2,6}-CH(SiMe$_3$)$_A$(*Si*Me$_3$)$_B$, 2 × Tbb).

4.5.31. [CpRh(PMe$_3$){Si$_2$COTbb$_2$}] (27-Rh)

To a yellowish-brown solution of **21-Rh** (400 mg, 0.35 mmol, 1 equiv.) in 20 mL of *n*-pentane, colourless PMe$_3$ (0.35 mL, 3.5 mmol, 10 equiv.) was added dropwise at

ambient temperature. The reaction solution immediately turned slightly purple and upon stirring for 2 hours at ambient temperature, it gradually intensified to dark brownish purple. Analysis of an aliquot of the reaction solution by ^{1}H NMR and ^{31}P NMR spectroscopy revealed about selective formation of the complex **27-Rh** in addition to little unreacted **21-Rh** (2 mole% with respect to the product). Subsequently all volatiles were removed in vacuo. The crude product was suspended in 3 mL of *n*-pentane and kept at −30 °C for 2 hours. The resulting brownish-maroon precipitate was isolated by filtering off the purple brown mother liquor at −30 °C and dried in vacuo for 30 min at 0 °C. Yield: 370 mg (0.30 mmol, 87 % from **21-Rh**).

At ambient temperature, **27-Rh** dissociates in solution and forms back the starting complex **21-Rh** along with free PMe_3. Monitoring of this process by ^{1}H NMR spectroscopy in (D_6)benzene revealed a fast conversion at 25 °C (ca. 34 mole % of **21-Rh** after 4.5 h), which surprisingly does not change any further with time, probably indicating the presence of ligand dissociation equilibrium in solution.

Properties: Compound **27-Rh** is an extremely air-sensitive and thermolabile brownish-maroon solid. It is well soluble in *n*-hexane, benzene, toluene, THF and Et_2O at ambient temperature.

Elemental analysis: 27-Rh ($C_{57}H_{112}OPRhSi_{10}$, 1228.23 g mol^{-1}): calcd./%: C 55.74, H 9.19; found/%: C 55.54, H 9.15; **Melting Point:** 185°C(dec.).

IR (*n*-hexane): $\tilde{\nu}$ (cm^{-1}) = 1588 (w) [ν(CC)$_{Aryl}$], 1530 (m, br) [ν(CO) and ν(CC)$_{Aryl}$].
IR (THF): $\tilde{\nu}$ (cm^{-1}) = 1587 (w) [ν(CC)$_{Aryl}$], 1528 (m, br) [ν(CO) and ν(CC)$_{Aryl}$].
ATR-IR (Solid): $\tilde{\nu}$ (cm^{-1}) = 2951 (m), 2898 (w), 2868 (vw), 1589 (w) [ν(CC)$_{Aryl}$], 1529 (m) [ν(CO) and ν(CC)$_{Aryl}$], 1477 (w), 1460 (vw, br), 1433 (vw, br), 1415 (w, br), 1393 (m), 1360 (w), 1304 (vw), 1283 (w), 1258 (m), 1244 (s, br), 1205 (vw, br), 1175 (w, br), 1152 (w), 1133 (vw), 1012 (m, br), 994 (w, sh), 948 (s), 938(m, sh), 887 (m), 857 (s, br, sh), 883 (vs), 796 (m), 783 (m), 762 (m), 742 (w), 718 (w, br), 679 (m), 662 (m), 645 (w), 625 (w), 607 (w), 597 (vw), 577 (vw), 558 (m), 527 (m), 474 (vw, br), 437 (m), 420 (m).
^{1}H NMR (500.1 MHz, (D_6)benzene, 298 K): δ (ppm) = 0.29 (s, ^{2}J(^{29}Si-^{1}H) = 6 Hz, 36H, 4 × Si*Me*$_3$, 2 × C^{2,6}-CH(Si*Me*$_3$)$_A$(SiMe$_3$)$_B$, 2 × Tbb), 0.38 (s, ^{2}J(^{29}Si-^{1}H) = 6 Hz, 36H, 4 × Si*Me*$_3$, 2 × C^{2,6}-CH(SiMe$_3$)$_A$(Si*Me*$_3$)$_B$, 2 × Tbb), 1.28 (dd, ^{2}J(^{31}P-^{1}H) = 10 Hz, ^{3}J(^{103}Rh-^{1}H) = 1 Hz, 9H, Rh-P*Me*$_3$), 1.35 (s, 18H, 2 × C*Me*$_3$, 2 × Tbb), 2.97 (s, ^{2}J(^{29}Si,^{1}H) = 9. Hz, 4H, 2 × C^{2,6}-C*H*(SiMe$_3$)$_A$(SiMe$_3$)$_B$, 2 × Tbb), 5.43 (d, ^{2}J(^{103}Rh-^{1}H) = 1.5 Hz, 5H, C_5*H*$_5$), 6.97 (s, 4H, 2 × C^{3,5}-*H*, 2 × Tbb).

^{1}H NMR (500.1 MHz, (D_8)toluene, 298 K): δ (ppm) = 0.26 (s, 36H, 4 × Si*Me$_3$*, 2 × $C^{2,6}$-CH(Si*Me$_3$*)$_A$(SiMe$_3$)$_B$, 2 × Tbb), 0.34 (s, 36H, 4 × Si*Me$_3$*, 2 × $C^{2,6}$-CH(SiMe$_3$)$_A$(Si*Me$_3$*)$_B$, 2 × Tbb), 1.28 (dd, ^{2}J(^{31}P-^{1}H) = 10 Hz, ^{3}J(^{103}Rh-^{1}H) = 1 Hz, 9H, P*Me$_3$*), 1.34 (s, 18H, 2 × C*Me$_3$*, 2 × Tbb), 2.92 (s, ^{2}J(^{29}Si,^{1}H) = 9. Hz, 4H, 2 × $C^{2,6}$-C*H*(SiMe$_3$)$_A$(SiMe$_3$)$_B$, 2 × Tbb), 5.40 (d, ^{2}J(^{103}Rh-^{1}H) = 1.5 Hz, 5H, C_5H_5), 6.93 (s, 4H, 2 × $C^{3,5}$-*H*, 2 × Tbb).

^{1}H NMR (500.1 MHz, (D_8)toluene, 238 K): δ (ppm) = 0.29 (s, 36H, 4 × Si*Me$_3$*, 2 × $C^{2,6}$-CH(Si*Me$_3$*)$_A$(SiMe$_3$)$_B$, 2 × Tbb), 0.39 (s, 36H, 4 × Si*Me$_3$*, 2 × $C^{2,6}$-CH(SiMe$_3$)$_A$(Si*Me$_3$*)$_B$, 2 × Tbb), 1.18 (d, ^{2}J(^{31}P-^{1}H) = 10 Hz, 9H, P*Me$_3$*), 1.36 (s, 18H, 2 × C*Me$_3$*, 2 × Tbb), 2.96 (s, br, $\Delta\nu_{1/2}$ = 12 Hz, 4H, 2 × $C^{2,6}$-C*H*(SiMe$_3$)$_A$(SiMe$_3$)$_B$, 2 × Tbb), 5.37 (d, ^{2}J(^{103}Rh-^{1}H) = 1.5 Hz, 5H, C_5H_5), 6.96 (s, 4H, 2 × $C^{3,5}$-*H*, 2 × Tbb).

^{31}P{^{1}H} NMR (200.4 MHz, (D_6)benzene, 298 K): δ (ppm) = 1.82 (d, ^{1}J(^{103}Rh-^{31}P) = 159 Hz).

^{31}P{^{1}H} NMR (200.4 MHz, (D_8)toluene, 298 K): δ (ppm) = 1.86 (d, ^{1}J(^{103}Rh-^{31}P) = 159 Hz).

^{31}P{^{1}H} NMR (200.4 MHz, (D_8)toluene, 238 K): δ (ppm) = 2.73 (d, ^{1}J(^{103}Rh-^{31}P) = 158 Hz).

^{13}C{^{1}H} NMR (125.8 MHz, (D_6)benzene, 298 K): δ (ppm) = 1.79 (s, ^{1}J(^{29}Si,^{13}C) = 51 Hz, 12C, 4 × Si*Me$_3$*, 2 × $C^{2,6}$-CH(Si*Me$_3$*)$_A$(SiMe$_3$)$_B$, 2 × Tbb), 1.84 (s, ^{1}J(^{29}Si,^{13}C) = 51 Hz, 12C, 4 × Si*Me$_3$*, 2 × $C^{2,6}$-CH(SiMe$_3$)$_A$(Si*Me$_3$*)$_B$, 2 × Tbb), 25.71 (dd, ^{1}J(^{31}P-^{13}C) = 35 Hz, ^{2}J(^{103}Rh-^{13}C) = 1.4 Hz, 3C, P*Me$_3$*), 30.8 (s, ^{1}J(^{29}Si,^{13}C) = 42 Hz, 4C, 2 × $C^{2,6}$-*C*H(SiMe$_3$)$_A$(SiMe$_3$)$_B$, 2 × Tbb), 31.2 (s, 6C, 2 × C*Me$_3$*, 2 × Tbb), 34.5 (s, 2C, 2 × *C*Me$_3$, 2 × Tbb), 91.2 (m, 5C, C_5H_5), 122.6 (s, 4C, 2 × $C^{3,5}$, 2 × Tbb), 136.7 (m, 2C, 2 × C^{1}, 2 × Tbb), 149.7 (s, 4C, 2 × $C^{2,6}$, 2 × Tbb), 150.8 (s, 2C, 2 × C^{4}, 2 × Tbb), 225.95 (dd, ^{2}J(^{103}Rh-^{13}C) = 18 Hz, ^{3}J(^{31}P-^{13}C) = 13 Hz, 1C, *CO*).

^{13}C{^{1}H} NMR (125.8 MHz, (D_8)toluene, 238 K): δ (ppm) = 1.5 (s, ^{1}J(^{29}Si,^{13}C) = 51 Hz, 12C, 4 × Si*Me$_3$*, 2 × $C^{2,6}$-CH(Si*Me$_3$*)$_A$(SiMe$_3$)$_B$, 2 × Tbb), 1.6 (s, ^{1}J(^{29}Si,^{13}C) = 51 Hz, 12C, 4 × Si*Me$_3$*, 2 × $C^{2,6}$-CH(SiMe$_3$)$_A$(Si*Me$_3$*)$_B$, 2 × Tbb), 25.2 (d, ^{1}J(^{31}P-^{13}C) = 36 Hz, 3C, P*Me$_3$*), 30.3 (s, ^{1}J(^{29}Si,^{13}C) = 42 Hz, 4C, 2 × $C^{2,6}$-*C*H(SiMe$_3$)$_A$(SiMe$_3$)$_B$, 2 × Tbb), 31.1 (s, 6C, 2 × C*Me$_3$*, 2 × Tbb), 34.4 (s, 2C, 2 × *C*Me$_3$, 2 × Tbb), 92.0 (m, 5C, C_5H_5), 122.2 (s, 4C, 2 × $C^{3,5}$, 2 × Tbb), 136.2 (m, 2C, 2 × C^{1}, 2 × Tbb), 149.3 (s, br, $\Delta\nu_{1/2}$ = 54 Hz, 4C, 2 × $C^{2,6}$, 2 × Tbb), 150.6 (s, 2C, 2 × C^{4}, 2 × Tbb), 225.9 (dd, ^{2}J(^{103}Rh-^{13}C) = 19 Hz, ^{3}J(^{31}P-^{13}C) = 13 Hz, 1C, *CO*).

^{29}Si{^{1}H} NMR (99.3 MHz, (D_6)benzene, 298 K): δ (ppm) = 2.0 (s, 4Si, 4 × *Si*Me$_3$, 2 × $C^{2,6}$-CH(*Si*Me$_3$)$_A$(SiMe$_3$)$_B$, 2 × Tbb), 2.3 (s, 4Si, 4 × *Si*Me$_3$, 2 × $C^{2,6}$-CH(SiMe$_3$)$_A$(*Si*Me$_3$)$_B$, 2 × Tbb), 89.9 (dd, ^{1}J(^{103}Rh,^{29}Si) = 48 Hz, ^{2}J(^{31}P-^{29}Si) = 10 Hz, 2Si, Rh-*Si*Tbb).

4.5.32. [CpRh{Si_2(IMe_4)(CO)Tbb_2}] (**28-Rh**)

To a brown solution of **21-Rh** (230 mg, 0.2 mmol, 1 equiv.) in 15 mL of Et_2O, a suspension of IMe_4 in 3 mL of Et_2O was added at ambient temperature. The reaction mixture was immediately turning to a clear purple solution. After 5 mins of stirring at ambient temperature, an aliquot of the reaction mixture in (D_6)benzene was analyzed by ^{1}H NMR spectroscopy, revealing a complete consumption of starting materials and a very selective formation of **28-Rh**. The reaction solution was evaporated to dryness in vacuo obtaining a black mass, which was redissolved in 1.6 mL of *n*-hexane. The resulting purple solution was stored at –30 °C for 2 days. The black microcrystals of **28-Rh** were isolated by filtration at –30 °C and upon drying under fine vacuum at ambient temperature for 10 mins, affording *n*-hexane hemi-solvate **28-Rh•**1.4 **C_6H_{14}** as a black-brown solid. Yield: 160 mg (0.11 mmol, 57 % from **21-Rh**).

Attempts to obtain the solvate-free form upon drying of **28-Rh•**1.4 **C_6H_{14}** in fine vacuum for 2 hrs. at ambient temperature or at 50 °C for 2 hrs. failed leading only to partial loss of n-hexane and very-extensive decomposition into some unknown Cp containing products.

Properties: Compound **28-Rh** is highly air-sensitive, brown-black solid. It is well soluble in *n*-hexane, benzene, toluene, THF and diethyl ether at ambient temperature Under strict exclusion of air, a solution of **28-Rh** in (D_6)benzene shows minute decomposition after 12 hrs. at ambient temperature.

Elemental analysis: 29-Rh•1.4 **C_6H_{14}** ($C_{61}H_{115}N_2ORhSi_{10}(C_6H_{14})_{1,4}$, 1396.98 g mol^{-1}): calcd./%: C 59.67, H 9.71, N 2.01; found/%: C 59.44, H 9.68, N 2.01; **Melting Point:** 174°C(dec.).

^{1}H NMR (500.1 MHz, (D_6)benzene, 298 K): δ (ppm) = –0.16 (very br s, 9H, 1 × Si*Me*$_3$, C$^{2/6}$-CH(Si*Me*$_3$)$_A$(SiMe$_3$)$_B$, Tbb$_Y$), 0.12 (s, 18H, 2 × Si*Me*$_3$, C^{2,6}-CH(Si*Me*$_3$)$_A$(SiMe$_3$)$_B$, Tbb$_X$), 0.31 (s, 18H, 2 × Si*Me*$_3$, C^{2,6}-CH(SiMe$_3$)$_A$(Si*Me*$_3$)$_B$, Tbb$_X$), 0.40 (br s, $\Delta\nu_{1/2}$ = 30 Hz, 27H, 3 × Si*Me*$_3$, C$^{2/6}$-CH(Si*Me*$_3$)$_A$(SiMe$_3$)$_B$, and C^{2,6}-CH(SiMe$_3$)$_A$(Si*Me*$_3$)$_B$, Tbb$_Y$), 1.36 (s, 9H, C^4-C*Me*$_3$, Tbb$_X$), 1.40 (s, 9H, C^4-C*Me*$_3$, Tbb$_Y$), 1.42 (very br, 6H, 2 × *Me*, C^{4,5}-*Me*, IMe_4), 2.14 (very br s, $\Delta\nu_{1/2}$ = 34 Hz, 2H, C^{2,6}-C*H*(SiMe$_3$)$_{A,B}$, Tbb$_Y$), 2.61 (br s, $\Delta\nu_{1/2}$ = 17 Hz, 2H, C^{2,6}-C*H*(SiMe$_3$)$_{A,B}$, Tbb$_X$), 3.06 (very br s, $\Delta\nu_{1/2}$ = ca. 59 Hz, 3H, N-*Me*$_A$, IMe_4), 3.91 (very br s, $\Delta\nu_{1/2}$ = ca. 87 Hz, 3H, N-*Me*$_B$, IMe_4), 5.42 (s, 5H, C_5H_5), 6.86 (s, 2H, C^{3,5}-*H*, Tbb$_X$).*signal corresponds to C^{3,5}-*H* of Tbb$_Y$ were not detected.

^{1}H NMR (300.1 MHz, (D_8)toluene, 193 K): δ (ppm) = –0.23 (s, 9H, 1 × Si*Me*$_3$, C$^{2/6}$-CH(Si*Me*$_3$)$_{A/B}$, Tbb$_Y$), –0.01 (br s, $\Delta\nu_{1/2}$ = 15 Hz, 9H, 1 × Si*Me*$_3$, C$^{2/6}$-CH(Si*Me*$_3$)$_{A/B}$, Tbb$_X$), 0.15 (br s, $\Delta\nu_{1/2}$ = 15 Hz, 9H, 1 × Si*Me*$_3$, C$^{2/6}$-CH(Si*Me*$_3$)$_{A/B}$, Tbb$_X$), 0.25 (br s, $\Delta\nu_{1/2}$ = 14.4 Hz, 9H, 1 × Si*Me*$_3$, C$^{2/6}$-CH(Si*Me*$_3$)$_{A/B}$, Tbb$_X$), 0.37 (s, 9H, 1 × Si*Me*$_3$, C$^{2/6}$-CH(Si*Me*$_3$)$_{A/B}$, Tbb$_Y$), 0.38 (s, 9H, 1 × Si*Me*$_3$, C$^{2/6}$-CH(Si*Me*$_3$)$_{A/B}$, Tbb$_Y$), 0.55 (br s, 18H, 2 × Si*Me*$_3$, C$^{2/6}$-CH(Si*Me*$_3$)$_{A/B}$, Tbb$_Y$ and C$^{2/6}$-CH(Si*Me*$_3$)$_{A/B}$, Tbb$_X$), 1.27 (very br s, 3H, C$^{4/5}$-*Me*, IMe$_4$), 1.37 (very br s, 3H, C$^{4/5}$-*Me*, IMe$_4$), 1.38 (s, 9H, C^4-C*Me*$_3$, Tbb$_{X/Y}$), 1.44 (s, 9H, C^4-C*Me*$_3$, Tbb$_{X/Y}$), 1.89 (s, 1H, C$^{2/6}$-C*H*(SiMe$_3$)$_{A/B}$, Tbb$_{X/Y}$), 2.97 (s, 3H, N-*Me*$_A$, IMe$_4$), 3.61 (s, 3H, N-*Me*$_B$, IMe$_4$), 4.30 (s, 1H, C$^{2/6}$-C*H*(SiMe$_3$)$_{A/B}$, Tbb$_{X/Y}$), 5.51 (s, 5H, C$_5$*H*$_5$), 6.70 (br s, $\Delta\nu_{1/2}$ = 5 Hz, 1H, C$^{3/5}$-*H*, Tbb$_{X/Y}$), 6.75 (br s, $\Delta\nu_{1/2}$ = 10 Hz, 1H, C$^{3/5}$-*H*, Tbb$_{X/Y}$), 7.01 (br s, $\Delta\nu_{1/2}$ = 5.6 Hz, 1H, C$^{3/5}$-*H*, Tbb$_{X/Y}$), 7.03 (br s, $\Delta\nu_{1/2}$ = 6 Hz, 1H, C$^{3/5}$-*H*, Tbb$_{X/Y}$).* two Dsi-signals correspond to C$^{2/6}$-C*H*(SiMe$_3$)$_{A/B}$, Tbb$_{X/Y}$ were not detected.

^{13}C{^{1}H} NMR (125.8 MHz, (D_6)benzene, 298 K): δ (ppm) = 0.9 (s, 6C, 2 × Si*Me*$_3$, C^{2,6}-CH(Si*Me*$_3$)$_A$(SiMe$_3$)$_B$, Tbb$_X$), 1.5 (s, 6C, 2 × Si*Me*$_3$, C^{2,6}-CH(SiMe$_3$)$_A$(Si*Me*$_3$)$_B$, Tbb$_X$), 2.3 (very br s, $\Delta\nu_{1/2}$ = 39.8 Hz, 12C, 4 × Si*Me*$_3$, C^{2,6}-CH(Si*Me*$_3$)$_{A,B}$, Tbb$_Y$), 8.6 (very br, 2C, C^{4,5}-*Me*, IMe$_4$), 30.0 (s, 2C, C$^{2/6}$-*C*H(SiMe$_3$)$_{A/B}$, Tbb$_X$), 31.3 and 31.4 (each s, 6C, 2 × C*Me*$_3$, Tbb$_{X,Y}$), 34.2 and 34.5 (each s, 2C, 2 × *C*Me$_3$, Tbb$_{X,Y}$), 36.0 (very br, 2C, 2 × N-*Me*, IMe$_4$), 85.0 (s, 5C, *C*$_5$H$_5$), 121.6 (s, 2C, *C*^{3,5}-H, Tbb$_X$), 125.1 (s), 138.4 (very br), 140.2 (d, ^2J(^{103}Rh-^{13}C) = 8.3 Hz, 1C, C^1, Tbb$_X$), 148.0 (s, 2C, C^{2,6}- CH(SiMe$_3$)$_{A,B}$, Tbb$_X$), 150.2 (s, 1C, *C*^{4}, Tbb$_X$). *the missing peaks were not detected; **the assignment of few of the above mentioned signals is not done as no cross peaks were detected in their corresponding 2D NMR spectra.

^{13}C{^{1}H} NMR (75.5 MHz, (D_8)toluene, 193 K): δ (ppm) = 1.0 (very br, 24C, 8 × Si*Me*$_3$, 2 × C^{2,6}-CH(Si*Me*$_3$)$_{A,B}$, Tbb$_{X,Y}$), 31.1 and 31.2 (each very br s, 6C, 2 × C*Me*$_3$, Tbb$_{X,Y}$), 34.1 and 34.4 (each s, 2C, 2 × *C*Me$_3$, Tbb$_{X,Y}$), 85.0 (s, 5C, *C*$_5$H$_5$), 147.4 (s, 1C, *C*^{4}, Tbb$_{X/Y}$), 147.5 (s), 149.8 (s, 1C, *C*^{4}, Tbb$_{X/Y}$), 151.2 (s), 155.3 (s, 1C, *C*^{2}, IMe$_4$). *the missing peaks were not detected; **the assignment of few of the above mentioned signals is not done as no cross peaks were detected in their corresponding 2D NMR spectra.

^{29}Si{^{1}H} NMR (99.3 MHz, (D_6)benzene, 298 K): δ (ppm) = 1.25 (s, 2Si, 2 × *Si*Me$_3$, C^{2,6}-CH(*Si*Me$_3$)$_A$(SiMe$_3$)$_B$, Tbb$_X$), 1.72 (s, 2Si, 2 × *Si*Me$_3$, C^{2,6}-CH(SiMe$_3$)$_A$(*Si*Me$_3$)$_B$, Tbb$_X$), 15.8 (d, ^1J(^{103}Rh-^{29}Si) = 99 Hz, 1Si, Rh–*Si*-IMe$_4$), 210.5 (d, ^1J(^{103}Rh-^{29}Si) = 109 Hz, 1Si, Rh=*Si*-Tbb). *** signals correspond to *Si*Me$_3$ silicon atoms of Tbb$_Y$ were not detected.

^{29}Si{^{1}H} NMR (59.6 MHz, (D_8)toluene, 193 K): δ (ppm) = 0.64 (s), 1.70 (very br s), 2.57, 2.99 and 3.60 (total 8Si, 8 × *Si*Me3, 2 ×C^{2,6}-CH(*Si*Me$_3$)$_{A,B}$, Tbb$_{X,Y}$). ***signals correspond to metal coordinated silicon atoms were not detected.

4.5.33. [(PMe$_3$)$_2$Co{(GeClTbb)(GeTbb)}] (**29-Co**)

In a 200 mL Schlenk tube a blue solution of [Co(PMe$_3$)$_3$Cl] (124 mg, 0.38 mmol, 1 equiv.) in 5 mL of benzene was added to a reddish orange solution of Ge$_2$Tbb$_2$ (400 mg, 0.38 mmol, 1 equiv.) in 15 mL of benzene at ambient temperature. The colour of the reaction solution immediately turned brown. A ^{1}H NMR spectrum of an aliquot of the reaction solution in (D$_6$)benzene revealed the formation of a mixture of **29-Co**, [(PMe$_3$)$_3$Co≡GeTbb][vii] and TbbGeCl(PMe$_3$)[viii] in the approximate ratio of 1 : 2 : 3. The Schlenk tube was immersed in a preheated oil bath (80 °C) and stirred for 12 h under periodic vacuum. During this time the colour of the reaction solution gradually changed to barn-red. After 12 h of heating, a ^{1}H NMR spectrum of the reaction solution was recorded confirming a complete conversion and selective formation of **29-Co**. The solution was evaporated to dryness to give a barn-red mass, which was dissolved in Et$_2$O (1.3 mL). The obtained solution was stored at –60 °C for 6 days leading to a precipitation of **29-Co** as a dark red solid, which was isolated by filtration at –60 °C and dried under fine vacuum at 40 °C for 1 hour. Yield: 375 mg (0.29 mmol, 76 % from Ge$_2$Tbb$_2$).

Properties: Compound **29-Co** is highly air-sensitive, barn-red solid. It is well soluble in *n*-hexane, benzene, toluene and diethyl ether at ambient temperature, but insoluble in CH$_3$CN. Under strict exclusion of air, a solution of **29-Co** in (D$_6$)benzene does not show any sign of decomposition after 3 days at ambient temperature.

Elemental analysis: 29-Co (C$_{54}$H$_{116}$ClCoGe$_2$P$_2$Si$_8$, 1291.74 g mol^{-1}): calcd./%: C 50.21, H 9.05; found/%: C 49.95, H 9.18; **Melting Point:** 177°C.

^{1}H NMR (500.1 MHz, (D$_6$)benzene, 298 K): δ (ppm) = 0.31 (s, 72H, 2 × C^{2,6}-CH(Si*Me$_3$*)$_2$, 2 × Tbb), 1.31 (s, 18H, 2 × C^4-C*Me$_3$*, 2 × Tbb), 1.62 (d, ^2J(^{31}P,^{1}H) = 8 Hz, 18H, 2 × P*Me$_3$*), 2.80 (s, 4H, 2 × C^{2,6}-C*H*(SiMe$_3$)$_2$, 2 × Tbb), 6.84 (s, 4H, 2 × C^{3,5}-*H*, 2 × Tbb).
^{31}P{^{1}H} NMR (200.4 MHz, (D$_6$)benzene, 298 K): δ (ppm) = 6.76 (s, very br, $\Delta\nu_{1/2}$ = ca. 408 Hz, 2 × *P*Me$_3$).
^{13}C{^{1}H} NMR (125.8 MHz, (D$_6$)benzene, 298 K): δ (ppm) = 1.6 (s, 24C, 2 × C^{2,6}-CH(Si*Me$_3$*)$_2$, 2 × Tbb), 28.4 (dd, ^1J(^{31}P,^{13}C) = 23 Hz, ^3J(^{31}P,^{13}C) = 4 Hz, 6C, 2 × P*Me$_3$*), 29.8 (s, ^1J(^{29}Si,^{13}C) = 42 Hz, 4C, 2 × C^{2,6}-*C*H(SiMe$_3$)$_2$), 31.2 (s, 6C, 2 × C^4-C*Me$_3$*, 2 × Tbb), 34.6 (s, 2C, 2 × C^4-*C*Me$_3$, 2 × Tbb), 122.6 (s, 4C, 2 × *C*^{3,5}-H, 2 × Tbb), 146.0 (s, 4C, 2 × *C*^{2,6}-CH(SiMe$_3$)$_2$, 2 × Tbb), 150.3 (s, 2C, 2 × *C*^{4}-CMe$_3$, 2 × Tbb), 163.1(s, 2C, 2 × C^1, 2 × Tbb).

4.5.34. $[(PMe_3)_2Co(GeTbb)_2][B(Ar^F)_4]$ (**30-Co**)

A colourless solution of $Na[B(Ar^F)_4]$ (172 mg, 0.19 mmol, 1 equiv.) in 5 mL of fluorobenzene was added to a barn-red solution of **29-Co** (250 mg, 0.19 mmol, 1 equiv.) in 20 mL of fluorobenzene at ambient temperature. The colour of the reaction solution turned immediately orange-brown. After 15 min of stirring , a No- D[242] ^1H and $^{31}P\{^1H\}$ spectrum of an aliquot was recorded, revealing the quantitative conversion of **29-Co** to **30-Co.** Then petroleum ether (10 mL) was added to the reaction solution followed by a filtration from NaCl and evaporation of the filtrate to dryness. The resulting sticky orange-brown mass was triturated in 20 mL of petroleum ether. After removal of the liquid phase by filtration, the obtained wood-brown solid was washed with petroleum ether (2 × 20 mL) and dried in fine vacuum for one hour at 40 °C. Yield: 350 mg (0.16 mmol, 85 % from **29-Co**).

Properties: Compound **30-Co** is an air-sensitive wood-brown solid. It is well soluble in chlorobenzene, fluorobenzene, dichloromethane and diethyl ether at ambient temperature. Under strict exclusion of air a solution of **30-Co** in (D_2)dichloromethane does not show any sign of decomposition after at least 8 hours at ambient temperature.

Elemental analysis: 30-Co ($C_{86}H_{128}BCoF_{24}Ge_2P_2Si_8$, 2119.49 g mol^{-1}): calcd./%: C 48.73, H 6.09; found/%: C 48.59, H 5.86; **Melting Point:** 181°C (dec.).

^{1}H NMR (500.1 MHz, (D_2)dichloromethane, 298 K): δ (ppm) = 0.14 (s, $^2J(^{29}Si,^1H)$ = 6 Hz, 72H, 2 × $C^{2,6}$-CH(Si*Me$_3$)$_2$*, 2 × Tbb), 1.27 (s, 18H, 2 × C^4-C*Me$_3$*, 2 × Tbb), 1.72 (d, $^2J(^{31}P,^1H)$ = 8 Hz, 18H, 2 × P*Me$_3$*), 2.53 (s, 4H, 2 × $C^{2,6}$-C*H*$(SiMe_3)_2$, 2 × Tbb), 6.74 (s, 4H, 2 × $C^{3,5}$-*H*, 2 × Tbb), 7.56 (br, s, 4H, 4 × C^4-*H*, $B(Ar^F)_4$), 7.72 (br s, 8H, 4 × $C^{2,6}$-*H*, $B(Ar^F)_4$*)*.

^{31}P{^{1}H} NMR (200.4 MHz, (D_2)dichloromethane, 298 K): δ (ppm) = 5.6 (br, s, $\Delta\nu_{1/2}$ = ca. 106 Hz, 2 × *P*Me_3).

^{13}C{^{1}H} NMR (125.8 MHz, (D_2)dichloromethane, 298 K): δ (ppm) = 1.14 (s, $^1J(^{29}Si,^{13}C)$ = 52 Hz, 24C, 2 × $C^{2,6}$-CH(Si*Me$_3$)$_2$*, 2 × Tbb), 28.4 (m, 6C, 2 × P*Me$_3$*), 30.8 (s, 6C, 2 × C^4-C*Me$_3$*, 2 × Tbb), 32.3 (s, $^1J(^{29}Si,^{13}C)$ = 40 Hz, 4C, 2 × $C^{2,6}$-*C*H$(SiMe_3)_2$), 35.6 (s, 2C, 2 × C^4-*C*Me_3, 2 × Tbb), 117.8 (sept, $^4J(^{19}F.^1H)$ = 3.6 Hz, 4C, 4 × *C^4*-H, $B(Ar^F)_4$), 123.1 (s, 4C, 2 × *C^{3,5}*-H, 2 × Tbb), 125.0 (q, $^1J(^{19}F,^{13}C)$ = 273 Hz, 8C, 4 × $C^{3,5}$-*C*F_3, $B(Ar^F)_4$), 129.3 (qq, $^2J(^{19}F,^{13}C)$ = 32 Hz, $^3J(^{13}C,^{11}B)$ = 3 Hz, 8C, 4 × *C^{3,5}*-CF_3, $B(Ar^F)_4$), 135.2 (s, 8C, 4 × *C^{2,6}*-H, $B(Ar^F)_4$), 147.9 (s, 4C, 2 × *C^{2,6}*-$CH(SiMe_3)_2$, 2 × Tbb) 156.6 (s, 2C, *2* × *C^4*-CMe_3, 2 × Tbb), 162.4 (q, $^1J(^{13}C,^{11}B)$ = 50 Hz, 4C, 4 × *C^1*, $B(Ar^F)_4$), 168.8 (s, 2C, 2 × *C^1*, 2 × Tbb).

4.5.35. [(PMe$_3$)$_2$Ni(GeClTbb)$_2$] (**31-Ni**)

To a stirred orange-red solution of Ge_2Tbb_2 (350 mg, 0.335 mmol, 1 equiv.) in 15 mL of *n*-hexane, a red suspension of $(PMe_3)_2NiCl_2$ (94 mg, 0.335 mmol, 1 equiv.) in 3 mL of *n*-hexane was added at ambient temperature. The colour of the reaction solution was immediately changed to purple. After 1 h of stirring at ambient temperature an aliquot of the reaction solution in (D_6)benzene was analyzed by ^{1}H and 31P NMR spectroscopy revealed complete consumption of the starting materials and very selective formation of **31-Ni**.[vi] The reaction solution was evaporated to dryness in vacuo followed by a freeze-pump-thaw. Obtained purple mass was redissolved in 2.5 mL of *n*-hexane and stored at –60 °C overnight. Dark-violet crystals were isolated by filtration at –60 °C followed by drying at 45 °C for 2 hours. Yield: 310 mg (0.234 mmol, 70 % from Ge_2Tbb_2).

Properties: Compound **31-Ni** is highly air-sensitive, dark-violet solid. It is well soluble in *n*-hexane, benzene, toluene and diethyl ether at ambient temperature. Under strict exclusion of air, a solution of **31-Ni** in (D_6)benzene does not show any sign of decomposition after 2 days at ambient temperature.

^{1}H NMR (500.1 MHz, (D_6)benzene, 298 K): δ (ppm) = 0.35 (s, 72H, 2 × C^{2,6}-CH(Si*Me*$_3$)$_2$, 2 × Tbb), 1.33 (s, 18H, 2 × C^4-C*Me*$_3$, 2 × Tbb), 1.40 (d, ^2J(^{31}P-^{1}H) = 6 Hz, 18H, 2 × P*Me*$_3$), 2.39 (s, 4H, 2 × C^{2,6}-C*H*(SiMe$_3$)$_2$, 2 × Tbb), 6.87 (s, 4H, 2 × C^{3,5}-*H*, 2 × Tbb).
^{31}P{^{1}H} NMR (200.4 MHz, (D_6)benzene, 298 K): δ (ppm) = −19.5 (s, 2P, 2 × *P*Me$_3$).
^{13}C{^{1}H} NMR (125.8 MHz, (D_6)benzene, 298 K): δ (ppm) = 1.8 (s, 24C, 2 × C^{2,6}-CH(Si*Me*$_3$)$_2$, 2 × Tbb), 23.9 (dd, ^1J(^{31}P-^{13}C) = 15 Hz, ^3J(^{31}P-^{13}C) = 11 Hz, 6C, 2 × P*Me*$_3$), 30.0 (s, 4C, 2 × C^{2,6}-*C*H(SiMe$_3$)$_2$, 2 × Tbb), 31.3 (s, 6C, 2 × C^4-C*Me*$_3$, 2 × Tbb), 34.5 (s, 2C, 2 × C^4-*C*Me$_3$, 2 × Tbb), 122.6 (s, 4C, 2 × *C*^{3,5}-H, 2 × Tbb), 145.7 (s, 4C, 2 × *C*^{2,6}-CH(SiMe$_3$)$_2$, 2 × Tbb), 150.7 (s, 2C, 2 × C^4-CMe$_3$, 2 × Tbb), 158.2 (s, 2C, 2 × *C*^{1}, 2 × Tbb).

4.5.36. [(PMe$_3$)$_2$Ni{(GeClTbb)(GeTbb)}][B(Ar^F)$_4$] (**32-Ni**)

A colourless solution of Na[B(Ar^F)$_4$] (132 mg, 0.149 mmol, 1 equiv.) in 5 mL of fluorobenzene was added to a violet solution of **31-Ni** (210 mg, 0.149 mmol, 1 equiv.) in 20 mL of fluorobenzene at ambient temperature. The colour of the reaction solution turned immediately red-brown. After 30 min of stirring a No-D[242] ^{1}H and ^{31}P{^{1}H} spectrum of an aliquot was recorded, revealing the quantitative conversion of **31-Ni** to **32-Ni.** Then *n*-pentane (5 mL) was added to the reaction solution followed by a filtration from NaCl and evaporation of the filtrate to dryness. The resulting sticky

brown mass was triturated in 10 mL of *n*-pentane. After removal of the liquid phase by filtration, the obtained red-brown solid was washed with *n*-pentane (2 × 10 mL) and dried in fine vacuum for one hour at 40 °C. Yield: 220 mg (0.102 mmol, 64 % from **31-Ni**).

Properties: Compound **32-Ni** is an air-sensitive red-brown solid. It is well soluble in chlorobenzene, fluorobenzene, dichloromethane and diethyl ether at ambient temperature. Under strict exclusion of air a solution of **32-Ni** in (D_2)dichloromethane does not show any sign of decomposition after at least 24 hours at ambient temperature.

Elemental analysis: 32-Ni ($C_{86}H_{128}BClF_{24}Ge_2NiP_2Si_8$, 2154.71 g mol^{-1}): calcd./%: C 47.94, H 5.99; found/%: C 48.93, H 6.12; **Melting Point:** 156°C (dec.).

^{1}H NMR (500.1 MHz, (D_2)dichloromethane, 298 K): δ (ppm) = 0.16 (s, ^2J(^{29}Si,^{1}H) = 6 Hz, 72H, 2 × C^{2,6}-CH(Si*Me$_3$*)$_2$, 2 × Tbb), 1.28 (s, 18H, 2 × C^4-C*Me$_3$*, 2 × Tbb), 1.72 (m, 18H, 2 × P*Me$_3$*), 1.82 (s, ^2J (^{29}Si-^{1}H) = 8.5 Hz, 4H, 2 × C^{2,6}-C*H*(SiMe$_3$)$_2$, 2 × Tbb), 6.75 (s, 4H, 2 × C^{3,5}-*H*, 2 × Tbb), 7.56 (br, s, 4H, 4 × C^4-*H*, B(Ar^F)$_4$), 7.73 (m,br, 8H, 4 × C^{2,6}-*H*, B(Ar^F)$_4$*)*.

^{31}P{^{1}H} NMR (200.4 MHz, (D_2)dichloromethane, 298 K): δ (ppm) = –9.7 (s, 2P, 2 × *P*Me$_3$).

^{13}C{^{1}H} NMR (125.8 MHz, (D_2)dichloromethane, 298 K): δ (ppm) = 1.3 (s, ^1J(^{29}Si-^{13}C) = 52 Hz, 24C, 2 × C^{2,6}-CH(Si*Me$_3$*)$_2$, 2 × Tbb), 23.75 (m, 6C, 2 × P*Me$_3$*), 30.9 (s, 6C, 2 × C^4-C*Me$_3$*, 2 × Tbb), 33.0 (s, ^1J(^{29}Si-^{13}C) = 40 Hz, 4C, 2 × C^{2,6}-*C*H(SiMe$_3$)$_2$), 35.3 (s, 2C, 2 × C^4-*C*Me$_3$, 2 × Tbb), 117.9 (sept, ^4J(^{19}F-^{1}H) = 3.6 Hz, 4C, 4 × *C^4*-H, B(Ar^F)$_4$), 123.7 (s, 4C, 2 × *C^{3,5}*-H, 2 × Tbb), 125.0 (q, ^1J(^{19}F-^{13}C) = 272 Hz, 8C, 4 × C^{3,5}-*C*F$_3$, B(Ar^F)$_4$), 129.3 (qq, ^2J(^{19}F-^{13}C) = 32 Hz, ^3J(^{13}C-^{11}B) = 3 Hz, 8C, 4 × *C^{3,5}*-CF$_3$, B(Ar^F)$_4$), 135.2 (br m, 8C, 4 × *C^{2,6}*-H, B(Ar^F)$_4$), 147.4 ((s, 4C, 2 × *C^{2,6}*-CH(SiMe$_3$)$_2$, 2 × Tbb), 156.2 (s, 2C, *2* × *C^4*-CMe$_3$, 2 × Tbb), 161.0 (s, 2C, 2 × *C^1*, 2 × Tbb), 162.2 (q, ^1J(^{13}C,^{11}B) = 50 Hz, 4C, 4 × *C^1*, B(Ar^F)$_4$).

4.5.37. [(PMe$_3$)$_2$Fe(GeTbb)$_2$] (33-Fe)

Isolation of 33-Fe

In a Schlenk tube, yellow-orange Ge_2Tbb_2 (1.5 g, 1.44 mmol, 2 equiv) and grey (PMe_3)$_2FeCl_2$ (200 mg, 0.717 mmol, 1 equiv.) were taken together as solid and 20 mL of benzene was added in to it at ambient temperature. The colour of the reaction solution was dark-brown. After 10 min of stirring at ambient temperature an aliquot of the reaction solution was analyzed by ^{1}H and ^{31}P NMR spectroscopy revealed

complete consumption of Ge_2Tbb_2 and selective formation of **33-Fe** and $Ge_2Cl_2Tbb_2$ in almost 1 : 1 molar ratio. The reaction solution was evaporated to dryness and the brown mass was dissolved in 3.2 mL of Et_2O and stored at –60 °C overnight. The yellowish-brown precipitate was separated from its dark-brown mother liquor by filtration at –60 °C. The filtrate was evaporated to dryness in vacuo and resulting black mass was redissolved in 4.8 mL of 1 : 3 (CH_3CN : Et_2O) mixture and layered by 1.6 mL of CH_3CN. The whole mixture was kept for diffusion at ambient temperature for 2 days. The black needle like crystals were isolated by filtration at ambient temperature and drying at 45 °C for 2 hours obtained analytically pure **33-Fe**. Yield: 620 mg (0.495 mmol, 69 % from $(PMe_3)_2FeCl_2$).

Properties: Compound **33-Fe** is highly air-sensitive, black solid. It is well soluble in *n*-hexane, benzene, toluene and diethyl ether, but insoluble in acetonitrile at ambient temperature. Under strict exclusion of air, a solution of **33-Fe** in (D_6)benzene does not show any sign of decomposition after 3 days at ambient temperature.

Elemental analysis: 33-Fe ($C_{54}H_{116}FeGe_2P_2Si_8$, 1253.20 g mol^{-1}): calcd./%: C 51.75, H 9.33; found/%: C 51.50, H 9.43; **Melting Point:** 222°C (dec.).

^{1}H NMR (500.1 MHz, (D_6)benzene, 298 K): δ (ppm) = 0.30 (s, 72H, 2 × C^{2,6}-CH(Si*Me*$_3$)$_2$, 2 × Tbb), 1.31 (s, 18H, 2 × C^4-C*Me*$_3$, 2 × Tbb), 1.68 (d, ^2J(^{31}P-^{1}H) = 7 Hz, 18H, 2 × P*Me*$_3$), 3.69 (s, ^2J (^{29}Si-^{1}H) = 9 Hz, 4H, 2 × C^{2,6}-C*H*(SiMe$_3$)$_2$, 2 × Tbb), 6.86 (s, 4H, 2 × C^{3,5}-*H*, 2 × Tbb).

^{31}P{^{1}H} NMR (200.4 MHz, (D_6)benzene, 298 K): δ (ppm) = 18.2 (s, ^1J (^{31}P-^{13}C) = 67 Hz, 2P, 2 × *P*Me$_3$).

^{13}C{^{1}H} NMR (125.8 MHz, (D_6)benzene, 298 K): δ (ppm) = 1.2 (s, ^1J (^{29}Si-^{13}C) = 51 Hz, 24C, 2 × C^{2,6}-CH(Si*Me*$_3$)$_2$, 2 × Tbb), 29.7 (s, ^1J (^{29}Si-^{13}C) = 43 Hz, 4C, 2 × C^{2,6}-*C*H(SiMe$_3$)$_2$, 2 × Tbb), 31.2 (s, 6C, 2 × C^4-C*Me*$_3$, 2 × Tbb), 32.9 (m, 6C, 2 × P*Me*$_3$), 34.8 (s, 2C, 2 × C^4-*C*Me$_3$, 2 × Tbb), 121.8 (s, 4C, 2 × *C*^{3,5}-H, 2 × Tbb), 145.8 (s, 4C, 2 × *C*^{2,6}-CH(SiMe$_3$)$_2$, 2 × Tbb), 150.1 (s, 2C, 2 × C^4-CMe$_3$, 2 × Tbb), 167.7 (s, 2C, 2 × *C*^{1}, 2 × Tbb).

Isolation of $Ge_2Cl_2Tbb_2$

In a Schlenk tube, yellow-orange Ge_2Tbb_2 (1.5 g, 1.44 mmol, 2 equiv) and grey $(PMe_3)_2FeCl_2$ (200 mg, 0.717 mmol, 1 equiv.) were taken together as solid and 20 mL of benzene was added in to it at ambient temperature. The colour of the reaction solution was dark-brown. After 10 min of stirring at ambient temperature an aliquot of the reaction solution was analyzed by ^{1}H and ^{31}P NMR spectroscopy revealed

complete consumption of Ge_2Tbb_2 and selective formation of 33-Fe and **$Ge_2Cl_2Tbb_2$** in almost 1 : 1 molar ratio. The reaction solution was evaporated to dryness and the brown mass was dissolved in 3.2 mL of Et_2O and stored at –60 °C overnight. The yellowish-brown precipitate was separated from its dark-brown mother liquor by filtration at –60 °C and washed by precooled Et_2O (2 × 2.5 mL) at 0 °C. The obtained bright yellow powder of $Ge_2Cl_2Tbb_2$ was further dried at ambient temperature for 1 hour. Yield: 330 mg (0.269 mmol, 42 % from $(PMe_3)_2FeCl_2$).

Elemental analysis: $Ge_2Cl_2Tbb_2$ ($C_{48}H_{98}Cl_2Ge_2Si_8$, 1253.20 g mol^{-1}): calcd./%: C 51.65, H 8.85; found/%: C 51.11, H 9.22.

^{1}H NMR (500.1 MHz, (D_6)benzene, 298 K): δ (ppm) = 0.29 (s, 72H, 2 × $C^{2,6}$-CH(Si*Me*$_3$)$_2$, 2 × Tbb), 1.29 (s, 18H, 2 × C*Me*$_3$, 2 × Tbb), 2.45 (s, $^2J(^{29}Si,^1H)$ = 9 Hz, 4H, 2 × $C^{2,6}$-C*H*$(SiMe_3)_2$, 2 × Tbb), 6.99 (s, 4H, 2 × $C^{3,5}$-*H*, 2 × Tbb).
^{13}C{^{1}H} NMR (125.8 MHz, (D_6)benzene, 298 K): δ (ppm) = 1.12 (s, $^1J(^{29}Si,^{13}C)$ = 52 Hz, 24C, 2 × $C^{2,6}$-CH(Si*Me*$_3$)$_2$, 2 × Tbb), 31.1 (s, 6C, 2 × C*Me*$_3$, 2 × Tbb), 34.6 (s, 2C, 2 × *C*Me_3, 2 × Tbb), 35.2 (s, 4C, 2 × $C^{2,6}$-*C*H$(SiMe_3)_2$, 2 × Tbb), 122.3 (s, 4C, 2 × *C*^{3,5}-H, 2 × Tbb), 147.2 (s, 2C, 2 × Ge-*C*^{1}, 2 × Tbb), 148.6 (s, 4C, 2 × *C*^{2,6}, 2 × Tbb), 153.0 (s, 2C, 2 × *C*^{4}, 2 × Tbb).

4.5.38. $[(PMe_3)_2Fe(GeTbb)_2][B(Ar^F)_4]$ (34-Fe)

To a stirred brown solution of **33-Fe** (70 mg, 0.056 mmol, 1 equiv.) in 3 mL Et_2O, 2 mL Et_2O solution of $[Cp_2Fe][B(Ar^F)_4]$ (59 mg, 0.056 mmol, 1 equiv.) was added dropwise at ambient temperature. No considerable colour change was observed. After stirring the reaction mixture for 1 hour at ambient temperature an aliquot was analyzed by ^{31}P NMR spectroscopy. Absence of any signal in the NMR spectra revealed complete consumption of **33-Fe** and probably formation of an open shell compound. The reaction solution was evaporated to dryness in vacuo. The resulting sticky brown mass was triturated in 5 mL of *n*-hexane. After removal of the liquid phase by filtration, the obtained wood-brown solid was washed with *n*-hexane (3 × 5 mL) and dried in fine vacuum for one hour at ambient temperature to obtain **34-Fe** as analytically pure. Yield: 84 mg (0.040 mmol, 71 % from **33-Fe**).

Properties: Compound **34-Fe** is highly air-sensitive, wood-brown solid. It is partially soluble in *n*-hexane but very well soluble in diethyl ether and fluorobenzene at ambient temperature. Under strict exclusion of air, a sample solution of **34-Fe** in fluorobenzene starts to deteriorate after few hours at ambient temperature.

Elemental analysis: 34-Fe ($C_{86}H_{128}BF_{24}FeGe_2P_2Si_8$, 2116.41 g mol^{-1}): calcd./%: C 48.81, H 6.10; found/%: C 48.86, H 6.17; **Melting Point:** 180°C (dec.).

4.5.39. (caac^{Me})SiBrGeTbb (35-Si)

Method A

A dark purple solution of $Si_2Br_2(caac^{Me})_2$ (398 mg, 0.506 mmol, 1.00 equiv.) in 5 mL of toluene was added at ambient temperature to a stirred reddish orange solution of Ge_2Tbb_2 (750 mg, 0.718 mmol, 1.42 equiv.) in 10 mL of toluene. The drak-purple reaction mixture was stirred for 4 hours at 90 °C, whereupon its colour changed from dark-purple to dark greenish-blue. An aliquot of the reaction solution was analyzed by ^{1}H NMR spectroscopy in (D_6)benzene, revealed complete consumption of the starting materials and selective formation of **35-Si** along with some minute unknown side-products. After evaporation of the solvent to dryness in vacuo, the greenish-blue residue was dissolved in *n*-hexane (4 mL) and stored at −60 °C for one day. The obtained dark-blue, microcrystalline solid was recrystallized again from 3 mL of *n*-hexane at −30 °C. The resulting dark blue single crystals of **35-Si** as hexane solvate **35-Si•C_6H_{14}** were isolated after a filtration at −30 °C dried under fine-vacuum for 1 h at 40 °C. Yield: 615 mg (0.614 mmol, 61 % from $Si_2Br_2(caac^{Me})_2$).

Method B

A dark-red solution of $SiBr_2(caac^{Me})$ (566 mg, 1.195 mmol, 2.00 equiv.) in 5 mL of benzene was added dropwise to a stirred yellow-orange suspension of $Ge_2Br_2Tbb_2$ (750 mg, 0.597 mmol, 1.00 equiv.) in 15 mL of benzene at ambient temperature. A rapid reaction occurred leading to a brown solution, which was stirred for 1 hour at ambient temperature. ^{1}H NMR spectroscopic analysis of an aliquot of the reaction solution revealed complete consumption of the staring materials and selective formation of **36-Si**. Afterwards, KC_8 (326 mg, 2.42 mmol, 2.02 equiv.) was added in one portion to that brown solution and the reaction mixture was stirred for 16 hrs. at ambient temperature. During the course of stirring the colour of the reaction solution gradually changed to greenish-blue. An analysis of an aliquot of the reaction mixture by ^{1}H NMR spectroscopy revealed the very selective formation of **35-Si**. The dark-blue solution was separated from the black insoluble part by filtration and evaporated to dryness in vacuo. The obtained blue mass was dissolved in 4 mL of *n*-hexane and stored for one day at −60 °C. The dark blue microcrystals of **35-Si** as mono-hexane solvate **35-Si•C_6H_{14}** were separated from the greenish-blue mother liquor by filtration at −60 °C and dried for 1 h at ambient temperature in fine vacuum. Yield: 780 mg (0.778 mmol, 65 % of $SiBr_2(caac^{Me})$).

Attempts to obtain the solvate-free form upon drying **35-Si•C_6H_{14}** in fine vacuum either at ambient temperature or at 80 °C for 4 h failed leading only to partial loss of *n*-hexane and minute decomposition.

Although **35-Si•C_6H_{14}** was extremely pure by NMR spectroscopy, for unknown reason repeated sample measurements for EA could never obtain the correct CHN analysis. To obtain **35-Si** pure by elemental analysis, **35-Si•C_6H_{14}** had to be recrystallized from toluene and obtained as toluene solvate **35-Si•tol** and thereafter got the correct (CHN) analysis.

Properties: Compound **35-Si•C_6H_{14}** / **35-Si•tol** is an extremely air sensitive dark blue solid turning immediately colourless upon contact with air. It can be stored under argon atmosphere at ambient temperature for several months. It is very well soluble in toluene, benzene, Et_2O, THF and *n*-hexane at ambient temperature. Under strict exclusion of air, a sample solution of **35-Si•C_6H_{14}** / **35-Si•tol** in (D_6)benzene does not show any sign of decomposition after at least 2 days at ambient temperature.

Elemental analysis: 35-Si•tol ($C_{44}H_{80}BrGeNSi_5$•(C_7H_8), 1008.19 g mol^{-1}): calcd./%: C 60.76, H 8.80, N 1.39; found/%: C 60.74, H 8.94, N 1.26; **Melting Point:** 133°C (dec.).

^{1}H NMR (**35-Si•C_6H_{14}**)(500.1 MHz, (D_6)benzene, 298 K): δ (ppm) = 0.30 (s, 36H, $C^{2,6}$-CH(Si*Me*$_3$)$_2$, Tbb), 1.02 (s, 6H, C^5-*Me*$_2$, caac^{Me}), 1.14 (d, ^3J(^{1}H-^{1}H) = 6.6 Hz, 6H, $C^{2,6}$-CH*Me*$_A$Me$_B$, Dipp), 1.39 (s, 9H, C*Me*$_3$, Tbb), 1.40 (s, 2H, $C^{2,6}$-C*H*(SiMe$_3$)$_2$, Tbb), 1.62 (d, ^3J(^{1}H-^{1}H) = 6.6 Hz, 6H, $C^{2,6}$-CHMe$_A$*Me*$_B$, Dipp), 1.70 (s, 2H, C^4*H*$_2$, caac^{Me}), 1.83 (s, 6H, C^3*Me*$_2$, caac^{Me}), 2.97 (sept, ^3J(^{1}H-^{1}H) = 6.6 Hz, 2H, $C^{2,6}$-C*H*Me$_A$Me$_B$, Dipp), 6.85 (s, 2H, $C^{3,5}$-*H*, Tbb), 7.12 − 7.14 (m, 3H, $C^{3,4,5}$-*H*, Dipp).

^{1}H NMR (**35-Si•C_6H_{14}**) (500.1 MHz, (D_8)THF, 298 K): δ (ppm) = 0.03 (s, 36H, $C^{2,6}$-CH(Si*Me*$_3$)$_2$, Tbb), 1.20 (s, 2H, $C^{2,6}$-C*H*(SiMe$_3$)$_2$, Tbb), 1.25 (s, 9H, C*Me*$_3$, Tbb), 1.30 (d, ^3J(^{1}H-^{1}H) = 6.7 Hz, 6H, $C^{2,6}$-CH*Me*$_A$Me$_B$, Dipp), 1.46 (s, 6H, C^5-*Me*$_2$, caac^{Me}), 1.53 (d, ^3J(^{1}H-^{1}H) = 6.7 Hz, 6H, $C^{2,6}$-CHMe$_A$*Me*$_B$, Dipp), 1.91 (s, 6H, C^3-*Me*$_2$, caac^{Me}), 2.29 (s, 2H, C^4-*H*$_2$, caac^{Me}), 3.10 (sept, ^3J(^{1}H-^{1}H) = 6.7 Hz, 2H, $C^{2,6}$-C*H*Me$_A$Me$_B$, Dipp), 6.56 (s, 2H, $C^{3,5}$-*H*, Tbb), 7.32 (s, 3H, $C^{3,4,5}$-*H*, Dipp).

^{1}H NMR (**35-Si•tol**) (500.1 MHz, (D_8)THF, 298 K): δ (ppm) = 0.03 (s, 36H, $C^{2,6}$-CH(Si*Me*$_3$)$_2$, Tbb), 1.20 (s, 2H, $C^{2,6}$-C*H*(SiMe$_3$)$_2$, Tbb), 1.25 (s, 9H, C*Me*$_3$, Tbb), 1.30 (d, ^3J(^{1}H-^{1}H) = 6.7 Hz, 6H, $C^{2,6}$-CH*Me*$_A$Me$_B$, Dipp), 1.46 (s, 6H, C^5-*Me*$_2$, caac^{Me}), 1.53 (d, ^3J(^{1}H-^{1}H) = 6.7 Hz, 6H, $C^{2,6}$-CHMe$_A$*Me*$_B$, Dipp), 1.91 (s, 6H, C^3-*Me*$_2$, caac^{Me}), 2.29 (s, 2H, C^4-*H*$_2$, caac^{Me}), 3.10 (sept, ^3J(^{1}H-^{1}H) = 6.7 Hz, 2H, $C^{2,6}$-C*H*Me$_A$Me$_B$, Dipp), 6.56 (s, 2H, $C^{3,5}$-*H*, Tbb), 7.32 (s, 3H, $C^{3,4,5}$-*H*, Dipp).

$^{13}C\{^1H\}$ NMR (35-Si•C_6H_{14}) (125.8 MHz, (D_8)THF, 298 K): δ (ppm) = 1.54 (s, 12C, $C^{2,6}$-CH(Si*Me*$_3)_2$, Tbb), 25.7 (s, 2C, $C^{2,6}$-CH*Me*$_A$Me$_B$, Dipp), 29.2 (s, 2C, C^5-*Me*$_2$, caac^{Me}), 30.0 (s, 4C, $C^{2,6}$-CHMe$_A$*Me*$_B$ and $C^{2,6}$-*C*HMe$_A$Me$_B$, Dipp), 31.8 (s, 3C, C^4-C*Me*$_3$, Tbb), 32.0 (s, 2C, $C^{2,6}$-*C*H(SiMe$_3)_2$, Tbb), 32.5 (s, 2C, C^3-*Me*$_2$, caac^{Me}), 34.6 (s, 1C, *C*Me$_3$, Tbb), 52.3 (s, 1C, *C*^{3}-Me$_2$, caac^{Me}), 56.9 (s, 1C, *C*^{4}-H$_2$, caac^{Me}), 74.3 (s, 1C, *C*^{5}-Me$_2$, caac^{Me}), 122.3 (s, 2C, *C*^{3,5}-H, Tbb), 128.2 (s, 2C, *C*^{3,5}-H, Dipp), 130.8 (s, 1C, *C*^{4}-H, Dipp), 136.2 (s, 1C, *C*^{1}, Dipp), 145.6 (s, 2C, *C*^{2,6}, Tbb), 146.8 (s, 2C, *C*^{2,6}, Dipp), 149.3 (s, 1C, *C*^{4}, Tbb), 155.6 (s, 1C, *C*^{1}, Tbb), 208.4 (s, 1C, *C*^{2}N).

$^{29}Si\{^1H\}$ NMR (35-Si•C_6H_{14}) (99.3 MHz, (D_8)THF, 298 K): δ (ppm) = 1.5 (s, 4Si, $C^{2,6}$-CH(*Si*Me$_3)_2$, Tbb), 84.6 (very br, 1Si, (caac^{Me})*Si*).

$^{29}Si\{^1H\}$ NMR (35-Si•C_6H_{14}) (99.3 MHz, (D_8)THF, 239 K): δ (ppm) = 0.8 (very br, s, 2Si, $C^{2,6}$-CH(*Si*Me$_3)_A$(SiMe$_3)_B$, Tbb), 2.3 (very br s, 2Si, $C^{2,6}$-CH(SiMe$_3)_A$(*Si*Me$_3)_B$, Tbb), 85.7 (s, 1Si, (caac^{Me})*Si*).

^1H-^{15}N HMBC (35-Si•C_6H_{14})(500.1 MHz, 50.7 MHz, (D_8)THF, 298 K): δ (ppm) = 177.0 (1N, C^2*N*).

4.5.40. (SIDipp)SiBrGeTbb (37-Si)

In a 250 mL schlenk tube, Purple solid of (SIDipp)SiCNAr^{Mes} (1.900 g, 2.51 mmol, 1 equiv.) and orange-yellow solid of $Ge_2Br_2Tbb_2$ (1.542 g, 1.28 mmol, 0.5 equiv.) were suspended in 70 mL of toluene and stirred at ambient temperature. Whereupon, after 10 min of stirring, the colour of the suspension turned dark-blue and the stirring was further continued for next 5 hours. Afterwards, an aliquot of the reaction was analyzed by ^{1}H NMR spectroscopy mixture in (D_6)benzene, revealing the selective formation of **37-Si** along with free Ar^{Mes}NC almost in 1 : 1 ratio. All volatiles were removed in vacuo and the crude product was dried under fine vacuum at 60 °C for 1 hour. To the obtained purple-black residue, $B(C_6F_5)_3$ (1.285 g, 2.51 mmol, 1 equiv.) was added along with 50 mL of *n*-hexane and the resulting blue suspension was stirred for 1 h at ambient temperature. Purple-black residue was separated from blue mother liquor and washed with 36 mL (4 × 9mL) of a mixture of *n*-pentane : Et_2O (2 : 1) followed by additional washing with *n*-pentane (3 × 10 mL) at ambient temperature. Drying the obtained mass in fine vacuum for 1 h at 40 °C afforded **37-Si** as deep purple-black powder. Yield: 1.6 g (1.57 mmol, 63 % from (SIDipp)SiCNAr^{Mes}).

Properties: Compound **37-Si** is an extremely air sensitive black-purple solid decolorizes immediately upon contact with air. It can be stored under argon atmosphere at ambient temperature for several months. It is sparingly soluble in *n*-hexane, moderately soluble in Et_2O and well soluble in toluene, benzene and THF at

ambient temperature. Under strict exclusion of air, a sample solution of **37-Si** in (D_6)benzene does not show any sign of decomposition after at least 3 days at ambient temperature.

Elemental analysis: 37-Si ($C_{51}H_{87}BrGeN_2Si_5$, 1021.19 g mol^{-1}): calcd./%: C 59.98, H 8.59, N 2.74; found/%: C 59.20, H 8.54, N 2.62; **Melting Point:** 193°C (dec.).

^{1}H NMR (500.1 MHz, (D_6)benzene, 298 K): δ (ppm) = 0.27 (s, 36H, C^{2,6}-CH(Si*Me*$_3$)$_2$, Tbb), 1.18 (d, ^3J(^{1}H-^{1}H) = 6.8 Hz, 12H, 2 × C^{2,6}-CH*Me*$_A$Me$_B$, 2 × Dipp), 1.36 (s, 9H, C^4-C*Me*$_3$, Tbb), 1.61 (d, ^3J(^{1}H-^{1}H) = 6.8 Hz, 12H, 2 × C^{2,6}-CHMe$_A$*Me*$_B$, 2 × Dipp), 1.90 (s, 2H, C^{2,6}-C*H*(SiMe$_3$)$_2$, Tbb), 3.24 (sept, ^3J(^{1}H-^{1}H) = 6.8 Hz, 4H, 2 × C^{2,6}-C*H*Me$_A$Me$_B$, 2 × Dipp), 3.44 (s, 4H, C^{4,5}-*H*$_2$, SIDipp), 6.79 (s, 2H, C^{3,5}-*H*, Tbb) 7.05 (d, ^3J(^{1}H-^{1}H) = 7.8 Hz, 4H, 2 × C^{3,5}-*H*, 2 × Dipp), 7.17 (t, ^3J(^{1}H-^{1}H) = 7.8 Hz, 2H, 2 × C^4-*H*, 2 × Dipp).
^{13}C{^{1}H} NMR (125.8 MHz, (D_6)benzene, 298 K): δ (ppm) = 1.5 (s, 12C, C^{2,6}-CH(Si*Me*$_3$)$_2$, Tbb), 25.4 (s, 4C, 2 × C^{2,6}-CHMe$_A$*Me*$_B$, 2 × Dipp), 25.6 (s, 2C, 2 × C^{2,6}-CH*Me*$_A$Me$_B$, 2 × Dipp), 29.3 (s, 4C, 2 × C^{2,6}-*C*HMe$_A$Me$_B$, 2 × Dipp), 31.6 (s, 5C, C^4-C*Me*$_3$ + 2 × C^{2,6}-*C*H(SiMe$_3$)$_2$, Tbb), 34.2 (s, 1C, C^4-*C*Me$_3$, Tbb), 54.0 (s, 2C, *C*^{4,5}-H$_2$, SIDipp), 121.6 (s, 2C, *C*^{3,5}-H, Tbb), 125.5 (s, 4C, 2 × *C*^{3,5}-H, 2 × Dipp), 130.4 (s, 2C, 2 × *C*^{4}-H, 2 × Dipp), 135.6 (s, 2C, 2 × *C*^{1}, 2 × Dipp), 145.8 (s, 1C, *C*^{1}, Tbb), 146.8 (s, 4C, 2 × *C*^{2,6}, 2 × Dipp), 148.0 (s, 1C, *C*^{4}, Tbb), 153.4 (s, 2C, *C*^{2,6}-CH(SiMe$_3$)$_2$, Tbb), 185.8 (s, 1C, *C*^{2}, N*C*^{2}N, SIDipp).
^{29}Si{^{1}H} NMR (99.3 MHz, (D_6)benzene, 298 K): δ (ppm) = 1.3 (s, 4Si, C^{2,6}-CH(*Si*Me$_3$)$_2$, Tbb), 48.2 (s, 1Si, (SIDipp)*Si*).
**No cross peak was found in (^{15}N-^{1}H) HMBC experiment

4.5.41. (caac^{Me}SiMesGeTbb) (38-Si)

To a greenish-blue solution of **35-Si•C$_6$H$_{14}$** (1 g, 0.998 mmol, 1 equiv.) in 10 mL of Et_2O, a colourless suspension of MesLi•0.09(Et_2O) (133 mg, 0,998 mmol, 1 equiv.) in 3 mL of Et_2O was added at ambient temperature. No considerable colour change was observed. After 1 h of stirring at ambient temperature an aliquot of the reaction mixture was analyzed by ^{1}H NMR spectroscopy in (D_6)benzene, revealing complete consumption of **35-Si** and very selective formation of **38-Si**. All volatiles were removed in vacuo followed by a freeze-pump-thaw. The obtained dark-blue mass was re-suspended in 20 mL *n*-pentane at ambient temperature and filtered from off-white precipitate. Afterwards the greenish-blue filtrate was evaporated to dryness in fine vacuum followed by crystallization of the crude product from *n*-pentane (2 mL) at –60 °C for 2 days. Dark-blue precipitate of **38-Si** was isolated by filtration at –60 °C and dried at 40 °C for 3 hours. Yield: 823 mg (0.861 mmol, 86 % from **35-Si•C$_6$H$_{14}$**).

Properties: Compound **38-Si** is an extremely air sensitive dark blue solid turning immediately colourless upon contact with air. It can be stored under argon atmosphere at ambient temperature for several months. It is very well soluble in toluene, benzene, Et_2O, and *n*-hexane at ambient temperature. Under strict exclusion of air, a sample solution of **38-Si** in (D_6)benzene does not show any sign of decomposition after at least 4 days at ambient temperature.

Elemental analysis: 38-Si ($C_{53}H_{91}GeNSi_5$, 955.33 g mol^{-1}): calcd./%: C 66.63, H 9.60, N 1.47; found/%: C 66.48, H 9.86, N 1.41; **Melting Point:** 207°C.

^{1}H NMR (500.1 MHz, (D_6)benzene, 298 K): δ (ppm) = 0.20 (s, 36H, C^{2,6}-CH(Si*Me$_3$*)$_2$, Tbb), 1.12 (s, 6H, C^5-*Me$_2$*, caac^{Me}), 1.23 (pseudo t, 14H, C^{2,6}-CH*Me$_A$*Me$_B$, Dipp + C^{2,6}-C*H*(SiMe$_3$)$_2$, Tbb + C^3-*Me$_2$*, caac^{Me}), 1.33 (s, 9H, C*Me$_3$*, Tbb), 1.70 (s, 2H, C^4-*H$_2$*, caac^{Me}), 1.72 (d, ^3J(^{1}H-^{1}H) = 6.6 Hz, 6H, C^{2,6}-CHMe$_A$*Me$_B$*, Dipp), 2.07 (s, 3H, C^4-*Me*, Mes), 2.72 (s, 6H, C^{2,6}-*Me*, Mes), 3.16 (sept, ^3J(^{1}H-^{1}H) = 6.6 Hz, 2H, C^{2,6}-C*H*Me$_A$Me$_B$, Dipp), 6.77 (s, 2H, C^{3,5}-*H*, Mes), 6.78 (s, 2H, C^{3,5}-*H*, Tbb), 7.20 − 7.26 (m, 3H, C^{3,4,5}-*H*, Dipp).

^{13}C{^{1}H} NMR (125.8 MHz, (D_6)benzene, 298 K): δ (ppm) = 1.8 (s, 12C, C^{2,6}-CH(Si*Me$_3$*)$_2$, Tbb), 21.2 (s, 1C, s, 3H, C^4-*Me*, Mes), 25.6 (s, 2C, C^3-*Me$_2$*, caac^{Me}), 28.6 (s, 2C, C^5-*Me$_2$*, caac^{Me}), 28.7 (s, 2C, C^{2,6}-*Me*, Mes), 29.4 (s, 2C, C^{2,6}-*C*HMe$_A$Me$_B$, Dipp), 30.7 (s, 2C, C^{2,6}-CHMe$_A$*Me$_B$*, Dipp), 31.18 (s, 2C, C^{2,6}-CH*Me$_A$*Me$_B$, Dipp), 31.23 (s, 2C, C^{2,6}-*C*H(SiMe$_3$)$_2$, Tbb), 31.6 (s, 3C, C*Me$_3$*, Tbb), 34.1 (s, 1C, *C*Me$_3$, Tbb), 51.8 (s, 1C, *C*^{3}-Me$_2$, caac^{Me}), 56.6 (s, 1C, *C*^{4}-H$_2$, caac^{Me}), 71.5 (s, 1C, *C*^{5}-Me$_2$, caac^{Me}), 122.2 (s, 2C, *C*^{3,5}-H, Tbb), 128.3 (s, 2C, *C*^{3,5}-H, Dipp), 128.4 (s, 2C, *C*^{3,5}-H, Mes), 130.1 (s, 1C, *C*^{4}-H, Dipp), 137.4 (s, 1C, *C*^{1}, Dipp), 138.4 (s, 1C, *C*^{4}-Me, Mes), 142.1 (s, 1C, *C*^{1}, Mes), 143.8 (s, 2C, *C*^{2,6}-Me, Mes), 144.6 (s, 2C, *C*^{2,6}-CH(SiMe$_3$)$_2$, Tbb), 145.7 (s, 2C, *C*^{2,6}-CHMe$_A$Me$_B$, Dipp), 147.8 (s, 1C, *C*^{4}, Tbb), 158.5 (s, 1C, *C*^{1}, Tbb), 208.6 (s, 1C, *C*^{2}, caac^{Me})

^{29}Si{^{1}H} NMR (99.3 MHz, (D_6)benzene, 298 K): δ (ppm) = 1.3 (s, 4Si, C^{2,6}-CH(*Si*Me$_3$)$_2$, Tbb), 105.4 (s, 1Si, (caac^{Me})*Si*).

^{1}H-^{15}N HMBC (500.1 MHz, 50.7 MHz, (D_6)benzene, 298 K): δ (ppm) = 171.6 (1N, C^2*N*).

4.5.42. [(caac^{Me})SiTbbGe][B(Ar^F)$_4$] (39-Si)

To a greenish-blue solution of **35-Si•C$_6$H$_{14}$** (1.2 g, 1.197 mmol, 1 equiv.) in 40 mL of fluorobenzene, colourless NaB(Ar^F)$_4$ (1.06 g, 1.197 mmol, 1 equiv.) was added at ambient temperature. The reaction mixture was stirred for 3 hours at ambient temperature, whereupon the colour gradually changed from greenish-blue to ink-blue. An aliquot of the reaction mixture was analysed by ^{1}H No-D NMR spectroscopy, revealing the quantitative transformation of **35-Si** to **39-Si**. Afterwards, *n*-pentane

(15 mL) was added to the reaction mixture followed by a filtration from NaCl and evaporation of the filtrate to dryness. The resulting sticky blue mass was triturated in 25 mL of *n*-pentane. After removal of the liquid phase by filtration, the obtained ink-blue solid was washed with *n*-pentane (3 × 10 mL) and dried in fine vacuum for half an hour at 40 °C. Yield: 1.8 g (1.059 mmol, 88 % from **35-Si•C_6H_{14}**).

Properties: Compound **39-Si** is an extremely air sensitive dark blue solid, turns colourless upon contact with air. It can be stored under argon atmosphere at ambient temperature for several years. It is very well soluble in fluorobenzene, Et_2O and dichloromethane, but insoluble in aliphatic solvents at ambient temperature. Under strict exclusion of air, a sample solution of **39-Si** in (D_2)dichloromethane shows partial decomposition after 8 hours at ambient temperature.

Elemental analysis: 39-Si ($C_{76}H_{92}BF_{24}GeNSi_5$, 1699.36 g mol^{-1}): calcd./%: C 53.72, H 5.46, N 0.82; found/%: C 53.88, H 5.62, N 0.76; **Melting Point:** 171°C (dec.).

^{1}H NMR (500.1 MHz, (D_2)dichloromethane, 298 K): δ (ppm) = 0.03 (s, 18H, $C^{2,6}$-CH(Si*Me*$_3$)$_A$(SiMe$_3$)$_B$, Tbb), 0.17 (s, 18H, $C^{2,6}$-CH(SiMe$_3$)$_A$(Si*Me*$_3$)$_B$, Tbb), 1.29 (s, 9H, C^4-C*Me*$_3$, Tbb), 1.42 (s, 6H, C^5-*Me*$_2$, caac^{Me}), 1.45 (s, 6H, C^3-*Me*$_2$, caac^{Me}), 1.48 (d, ^3J (^{1}H-^{1}H) = 6.7 Hz, 6H, $C^{2,6}$-CH*Me*$_A$Me$_B$, Dipp), 1.86 (d, ^3J (^{1}H-^{1}H) = 6.7 Hz, 6H, $C^{2,6}$-CHMe$_A$*Me*$_B$, Dipp), 2.09 (s, ^2J (^{29}Si-^{1}H) = 8 Hz, 2H, $C^{2,6}$-C*H*(SiMe$_3$)$_A$(SiMe$_3$)$_B$, Tbb), 2.40 (s, 2H, C^4-*H*$_2$, caac^{Me}), 2.91 (sept, ^3J(^{1}H-^{1}H) = 6.6 Hz, 2H, $C^{2,6}$-C*H*Me$_A$Me$_B$, Dipp), 6.75 (s, 2H, $C^{3,5}$-*H*, Tbb), 7.57 (br s, 4H, 4 × C^4-*H*, B(Ar^F)$_4$), 7.58 (t, ^3J(^{1}H-^{1}H) = 7.9 Hz, 1H, C^4-*H*, Dipp), 7.73 (br m, 8H, 4 × $C^{2,6}$-*H*, B(Ar^F)$_4$), 8.10 (d, ^3J(^{1}H-^{1}H) = 7.9 Hz, 2H, $C^{3,5}$-*H*, Dipp)

^{13}C{^{1}H} NMR (125.8 MHz, (D_2)dichloromethane, 298 K): δ (ppm) = 0.7 (s, ^1J (^{29}Si-^{13}C) = 52 Hz, 6C, $C^{2,6}$-CH(Si*Me*$_3$)$_A$(SiMe$_3$)$_B$, Tbb), 2.1 (s, ^1J (^{29}Si-^{13}C) = 52 Hz, 6C, $C^{2,6}$-CH(SiMe$_3$)$_A$(Si*Me*$_3$)$_B$, Tbb), 25.3 (s, 2C, $C^{2,6}$-CH*Me*$_A$Me$_B$, Dipp), 30.0 (s, 4C, $C^{2,6}$-*C*HMe$_A$Me$_B$, Dipp + C^5-*Me*$_2$, caac^{Me}), 30.9 (s, 3C, C^4-C*Me*$_3$, Tbb), 31.8 (s, 2C, C^3-*Me*$_2$, caac^{Me}), 32.0 (s, 2C, $C^{2,6}$-CHMe$_A$*Me*$_B$, Dipp), 34.7 (s, 1C, C^4-*C*Me$_3$, Tbb), 35.0 (s, 2C, $C^{2,6}$-*C*H(SiMe$_3$)$_A$(SiMe$_3$)$_B$, Tbb), 49.9 (s, 1C, *C*^{3}-Me$_2$, caac^{Me}), 54.1 (s, 1C, *C*^{4}-H$_2$, caac^{Me}), 79.0 (s, 1C, *C*^{5}-Me$_2$, caac^{Me}), 117.86 (sept, ^4J(^{19}F-^{1}H) = 3.6 Hz, 4C, 4 × *C*^{4}-H, B(Ar^F)$_4$), 124.1 (s, 2C, *C*^{3,5}-H, Tbb), 125.0 (q, ^1J(^{19}F-^{13}C) = 272 Hz, 8C, 4 × $C^{3,5}$-*C*F$_3$, B(Ar^F)$_4$), 126.0 (s, 1C, *C*^{1}, Tbb), 129.3 (qq, ^2J(^{19}F-^{13}C) = 32 Hz, ^3J(^{13}C-^{11}B) = 3 Hz, 8C, 4 × *C*^{3,5}-CF$_3$, B(Ar^F)$_4$), 135.2 (br m, 8C, 4 × *C*^{2,6}-H, B(Ar^F)$_4$), 135.6 (s, 1C, *C*^{1}, Dipp), 136.0 (s, 1C, *C*^{4}-H, dipp), 138.2 (s, 2C, *C*^{3,5}-H, Dipp), 143.5 (s, 2C, *C*^{2,6}-CHMe$_A$Me$_B$, Dipp), 151.3 (s, 2C, *C*^{2,6}-CH(SiMe$_3$)$_2$, Tbb), 153.8 (s, 1C, *C*^{4}, Tbb), 162.2 (q, ^1J(^{13}C,^{11}B) = 50 Hz, 4C, 4 × *C*^{1}, B(Ar^F)$_4$), 235.6 (s, 1C, *C*^{2}, caac^{Me}).

^{29}Si{^{1}H} NMR (99.3 MHz, (D_2)dichloromethane, 298 K): δ (ppm) = 2.4 (s, 2Si, $C^{2,6}$-CH(SiMe$_3$)$_A$(SiMe$_3$)$_B$, Tbb), 2.8 (s, 2Si, $C^{2,6}$-CH(SiMe$_3$)$_A$(SiMe$_3$)$_B$, Tbb), 182.7 (s, 1Si, (caac^{Me})*Si*).
^{1}H-^{15}N HMBC (500.1 MHz, 50.7 MHz, (D_2)dichloromethane, 298 K): δ (ppm) = 193.8 (1N, C^2*N*).

4.5.43. (caac^{Me})SiKGeTbb (40-Si)

To a vigorously stirred greenish-blue solution of **35-Si•C$_6$H$_{14}$** (280 mg, 0.279 mmol, 1 equiv.) in 20 mL of benzene, KC_8 (76 mg, 0.564 mmol, 2.02 equiv.) was added in one portion at ambient temperature. The colour of the reaction mixture turned immediately dark green. After one hour of stirring at ambient temperature an aliquot of the reaction mixture was analysed by ^{1}H NMR spectroscopy in (D_6)benzene and revealed the complete consumption of **35-Si** and the selective formation of **40-Si** along with some minute side products. The dark green solution was separated from the black insoluble part by filtration and evaporated to dryness in vacuo. The obtained green solid was washed with *n*-pentane (2 × 3 mL) at ambient temperature followed by a drying at 40 °C for 1 hour. Yield: 170 mg (0.194 mmol, 69 % from **35-Si•C$_6$H$_{14}$**).

Properties: Compound **40-Si** is an extremely air sensitive, dark green, pyrophoric solid, which turns colourless immediately upon contact with air. It can be stored under argon atmosphere at –30 °C for several months. It is sparingly soluble in aliphatic solvents and very well soluble in benzene, toluene, and Et_2O at ambient temperature. Under strict exclusion of air, a sample solution of **40-Si** in (D_6)benzene does not show any sign of decomposition after 8 hours at ambient temperature.

Elemental analysis: 40-Si ($C_{44}H_{80}GeKNSi_5$, 875.24 g mol^{-1}): calcd./%: C 60.38, H 9.21, N 1.60; found/%: C 59.87, H 9.00, N 1.48; **Melting Point:** 178°C (dec.).

^{1}H NMR (500.1 MHz, (D_6)benzene, 298 K): δ (ppm) = 0.21 (s, 36H, $C^{2,6}$-CH(SiMe_3)$_2$, Tbb), 1.22 (s, 6H, C^5-Me_2, caac^{Me}), 1.29 (s, 9H, CMe_3, Tbb), 1.31 (d, ^3J(^{1}H-^{1}H) = 6.7 Hz, 6H, $C^{2,6}$-CHMe_AMe$_B$, Dipp), 1.56 (d, ^3J(^{1}H-^{1}H) = 6.3 Hz, 6H, $C^{2,6}$-CHMe$_A$$Me_B$, Dipp), 2.02 (s, 2H, C^4-H_2, caac^{Me}), 2.28 (s, 6H, C^3-Me_2, caac^{Me}), 3.24 (sept, ^3J(^{1}H-^{1}H) = 6.5 Hz, 2H, $C^{2,6}$-CHMe$_A$Me$_B$, Dipp), 3.47 (s, 2H, $C^{2,6}$-CH(SiMe$_3$)$_2$, Tbb), 6.70 (s, 2H, $C^{3,5}$-H, Tbb), 7.08 (d, ^3J(^{1}H-^{1}H) = 7.3 Hz, 2H, $C^{3,5}$-H, Dipp), **7.13 (t, 1H, C^4-H, Dipp). ** due to overlapping the signal with the signal of deuterated benzene the ^3J(^{1}H-^{1}H) coupling constant could not be obtained.

$^{13}C\{^1H\}$ NMR (125.8 MHz, (D_6)benzene, 298 K): δ (ppm) = 2.2 (s, 1J (29Si-13C) = 51 Hz, 12C, $C^{2,6}$-CH(Si*Me*$_3$)$_2$, Tbb), 24.8 (s, 2C, $C^{2,6}$-CH*Me*$_A$Me$_B$, Dipp), 28.9 (s, 2C, $C^{2,6}$-C*H*Me$_A$Me$_B$, Dipp), 29.5 (s, 2C, $C^{2,6}$-CHMe$_A$*Me*$_B$, Dipp), 30.0 (s, 2C, C^5-*Me*$_2$, caac^{Me}), 31.4 (s, 2C, $C^{2,6}$-*C*H(SiMe$_3$)$_2$, Tbb), 31.8 (s, 3C, C*Me*$_3$, Tbb), 33.9 (s, 1C, *C*Me$_3$, Tbb), 34.3 (s, 2C, C^3-*Me*$_2$, caac^{Me}), 50.6 (s, 1C, *C*^{3}-Me$_2$, caac^{Me}), 55.7 (s, 1C, *C*^{4}-H$_2$, caac^{Me}), 69.9 (s, 1C, *C*^{5}-Me$_2$, caac^{Me}), 120.3 (s, 2C, *C*^{3,5}-H, Tbb), 124.7 (s, 2C, *C*^{3,5}-H, Dipp), 128.5 (s, 1C, *C*^{4}-H, Dipp), 137.6 (s, 1C, C^1, Dipp), 146.0 (s, 1C, *C*^{4}, Tbb), 147.7 (s, 2C, *C*^{2,6}-CH(SiMe$_3$)$_2$, Tbb), 149.0 (s, 2C, *C*^{2,6}-CHMe$_A$Me$_B$, Dipp), 173.8 (s, 1C, *C*^{1}, Tbb), 234.8 (s, 1C, *C*^{2}, caac^{Me}).

$^{29}Si\{^1H\}$ NMR (99.3 MHz, (D_6)benzene, 298 K): δ (ppm) = 1.3 (s, 4Si, $C^{2,6}$-CH(*Si*Me$_3$)$_2$, Tbb), 219.5 (s, 1Si, (caac^{Me})*Si*).

^1H-^{15}N HMBC (500.1 MHz, 50.7 MHz, (D_6)benzene, 298 K): δ (ppm) = 166.8 (1N, C^2*N*).

4.5.44. [CpMo(CO)$_2$GeTbb] (41-Mo)

Method A

To a stirred colourless suspension of Li[CpMo(CO)$_3$] (13 mg, 0.050 mmol, 1 equiv.) in 3 mL of toluene, a dark blue solution of **35-Si•C$_6$H$_{14}$** (50 mg, 0.050 mmol, 1 equiv.) in 3 mL of toluene was dropwise added at ambient temperature. No considerable colour change was observed, thereafter the reaction mixture was heated at 80 °C for 2 hours. During the course of heating, the reaction mixture gradually turned to a black suspension. The progress of the reaction was analyzed by IR and ^{1}H NMR spectroscopy. the IR spectrum of the reaction mixture indicated the selective formation of a cis-dicarbonyl complex [(ν(CO) = 1931 and 1870 cm^{-1}] and the analysis of an aliquot of the reaction mixture by ^{1}H NMR spectroscopy in (D_6)benzene revealed complete consumption of starting materials and very selective formation of **41-Mo**. Isolation of pure **41-Mo** upon doing further work up the reaction mixture from this method was not performed.

Method B

To a stirred colourless suspension of Li[CpMo(CO)$_3$] (210 mg, 0.830 mmol, 2 equiv.) in 10 mL of toluene, a yellow-orange suspension of Ge$_2$Br$_2$Tbb$_2$ (500 mg, 0.415 mmol, 1 equiv.) in 10 mL of toluene was added at ambient temperature. No considerable colour change was observed, thereafter the reaction mixture was heated at 80 °C for 2 hours. During the course of heating, the reaction mixture gradually turned to a dark red suspension. An analysis of an aliquot of the reaction mixture by ^{1}H NMR spectroscopy in (D_6)benzene revealed complete consumption of starting materials and very selective formation of **41-Mo.** The clear dark red solution was separated from

off-white residue by filtration at ambient temperature followed by an evaporation to dryness in vacuo. The resulting red mass was crystallized from *n*-hexane (2.5 mL) at –30 °C overnight. Obtained dark red crystals of **41-Mo** were separated from its mother liquor by filtration at –30 °C and dried in fine vacuum at 50 °C for one hour. Yield: 350 mg (0.473 mmol, 57 % from Li[CpMo(CO)$_3$]).

Properties: Compound **41-Mo** is an air sensitive dark red solid. It can be stored under argon atmosphere at ambient temperature for several years. It is very well soluble in Et_2O, THF, *n*-hexane, benzene and toluene at ambient temperature. Under strict exclusion of air, a sample solution of **41-Mo** in (D_6)benzene does not show any sign of decomposition after one week at ambient temperature.

Elemental analysis: 41-Mo ($C_{31}H_{54}GeMoO_2Si_4$, 739.65 g mol^{-1}): calcd./%: C 50.33, H 7.35; found/%: C 49.55, H 7.26; **Melting Point:** 183°C.

IR (*n*-hexane): $\tilde{\nu}$ (cm^{-1}) = 1940 (s) and 1880 (s) [ν(CO)], 1580 (w), 1546 (vw, br) and 1533 (w) [$\nu(CC)_{Aryl}$].
IR (*n*-toluene): $\tilde{\nu}$ (cm^{-1}) = 1931 (s) and 1880 (s) [ν(CO)].
^{1}H NMR (500.1 MHz, (D_6)benzene, 298 K): δ (ppm) = 0.22 (s, ^2J (^{29}Si-^{1}H) = 6 Hz, ^1J (^{13}C-^{1}H) = 119 Hz, 36H, C^{2,6}-CH(Si*Me*$_3$)$_2$, Tbb), 1.20 (s, 9H, C^4-C*Me*$_3$, Tbb), 3.01 (s, ^2J (^{29}Si-^{1}H) = 10 Hz, 2H, C^{2,6}-C*H*(SiMe$_3$)$_2$, Tbb), 4.99 (s, 5H, C$_5$*H*$_5$), 6.83 (s, 2H, C^{3,5}-*H*, Tbb).
^{13}C{^{1}H} NMR (125.8 MHz, (D_6)benzene, 298 K): δ (ppm) = 0.4 (s, ^1J (^{29}Si-^{13}C) = 52 Hz, 12C, C^{2,6}-CH(Si*Me*$_3$)$_2$, Tbb), 31.0 (s, 3C, C^4-C*Me*$_3$, Tbb), 31.4 (s, ^1J (^{29}Si-^{13}C) = 41 Hz, 2C, C^{2,6}-*C*H(SiMe$_3$)$_2$, Tbb), 34.9 (s, 1C, C^4-*C*Me$_3$, Tbb), 87.1 (s, 5C, *C*$_5$H$_5$), 121.7 (s, 2C, *C*^{3,5}-H, Tbb), 146.8 (s, 2C, *C*^{2,6}-CH(SiMe$_3$)$_2$, Tbb), 153.9 (s, 1C, *C*^{4}, Tbb), 163.4 (s, 1C, *C*^{1}, Tbb), 231.5 (s, 2C, 2 × *C*O, Mo-*C*O).

4.5.45. (caac^{Me})GeBrTbb (42-Ge)

Method A

To a stirred yellow-orange suspension of $Ge_2Br_2Tbb_2$ (300 mg, 0.249 mmol, 1 equiv.) in 10 mL of toluene, a dark purple solution of $Si_2(caac^{Me})_2$ (156 mg, 0.249 mmol, 1 equiv.) in 5 mL of toluene was added dropwise at ambient temperature. The colour of the reaction solution was immediately changed first to dark green then within 2-3 min it changed to orange-red. An analysis of an aliquot of the reaction solution by ^{1}H NMR spectroscopy in (D_6)benzene revealed complete consumption of starting materials and selective formation of **42-Ge** along with some minor compounds with unknown composition. The reaction was worked up by evaporating the solvent to

dryness in vacuo followed by a crystallization of the crude product from *n*-hexane at –60 °C for 2 days. The orange-red microcrystals of **42-Ge** were isolated by filtration at –60 °C and dried in fine vacuum at 40 °C for 2 hours. Yield: 232 mg (0.261 mmol, 52 % from $Ge_2Br_2Tbb_2$).

Method B

To a stirred yellow-orange suspension of $Ge_2Br_2Tbb_2$ (500 mg, 415 mmol, 1 equiv.) in 10 mL of benzene, a colourless solution of $caac^{Me}$ (237 mg, 830 mmol, 2 equiv.) in 5 mL of benzene was dropwise added at ambient temperature. The yellow-orange suspension immediately become a clear orange-red solution. After stirring for half an hour at ambient temperature an aliquot of the reaction solution was analyzed by ^1H NMR spectroscopy in (D_6)benzene revealing complete consumption of starting materials and very selective formation of **42-Ge**. All volatiles were removed in vacuo followed a crystallization of the crude product from 5 mL of Et_2O : THF (1.5 : 1) mixture at –30 °C for 16 hours. Orange-red crystals of **42-Ge** were isolated by filtration from its mother liquor at –30 °C and dried in fine vacuum for one hour at 50 °C. Yield: 400 mg (0.450 mmol, 54 % from $caac^{Me}$).

Properties: Compound **42-Ge** is an air sensitive orange-red solid. It can be stored under argon atmosphere at ambient temperature for several days. It is well soluble in Et_2O, THF, *n*-hexane, benzene and toluene at ambient temperature. Under strict exclusion of air, a sample solution of **42-Ge** in (D_6)benzene either after one week at ambient temperature or heating at 80 °C for 3 hrs. does not show any sign of decomposition.

Elemental analysis: 42-Ge ($C_{44}H_{80}BrGeNSi_4$, 887.97 g mol^{-1}): calcd./%: C 59.51, H 9.08, N 1.58; found/%: C 59.70, H 9.09, N 1.39; **Melting Point:** 168°C (dec.).

^1H NMR (500.1 MHz, (D_6)benzene, 298 K): δ (ppm) = 0,32 (s, ^2J (^{29}Si-^1H) = 6 Hz, 36H, $C^{2,6}$-CH(Si*Me*$_3$)$_2$, Tbb), 0.98 (s, 6H, C^5-*Me*$_2$, $caac^{Me}$), 1.18 (d, ^3J(^1H-^1H) = 6.6 Hz, 6H, $C^{2,6}$-CH*Me*$_A$Me$_B$, Dipp), 1.38 (s, 9H, C^4-C*Me*$_3$, Tbb), 1.46 (s, 6H, C^3-*Me*$_2$, $caac^{Me}$), 1.47 (s, 2H, C^4-*H*$_2$, $caac^{Me}$), 1.74 (d, ^3J(^1H-^1H) = 6.6 Hz, 6H, $C^{2,6}$-CHMe$_A$*Me*$_B$, Dipp), 2.98 (sept, ^3J(^1H-^1H) = 6.6 Hz, 2H, $C^{2,6}$-C*H*Me$_A$Me$_B$, Dipp), 3.47 (s, ^2J (^{29}Si-^1H) = 9 Hz, 2H, $C^{2,6}$-C*H*(SiMe$_3$)$_2$, Tbb), 6.94 (s, 2H, $C^{3,5}$-*H*, Tbb), 7.10 (d, ^3J(^1H-^1H) = 7.7 Hz, 2H, $C^{3,5}$-*H*, Dipp), 7.22 (m, 1H, C^4-*H*, Dipp).

$^{13}C\{^1H\}$ NMR (125.8 MHz, (D_6)benzene, 298 K): δ (ppm) = 2.3 (s, ^1J (^{29}Si-^{13}C) = 51 Hz, 12C, $C^{2,6}$-CH(Si*Me*$_3$)$_2$, Tbb), 25.6 (s, 2C, $C^{2,6}$-CH*Me*$_A$Me$_B$, Dipp), 27.5 (s, 2C, $C^{2,6}$-CHMe$_A$*Me*$_B$, Dipp), 29.3 (s, 2C, $C^{2,6}$-*C*HMe$_A$Me$_B$, Dipp), 29.4 (s, 2C, C^5-*Me*$_2$, $caac^{Me}$),

29.9 (s, ^{1}J (^{29}Si-^{13}C) = 43 Hz, 2C, C^{2,6}-*C*H(SiMe$_3$)$_2$, Tbb), 31.4 (s, 3C, C^4-C*Me$_3$*, Tbb), 33.6 (s, 2C, C^3-*Me$_2$*, caac^{Me}), 34.3 (s, 1C, C^4-*C*Me$_3$, Tbb), 52.3 (s, 1C, *C^4*-H$_2$, caac^{Me}), 53.8 (s, 1C, *C^3*-Me$_2$, caac^{Me}), 77.4 (s, 1C, *C^5*-Me$_2$, caac^{Me}), 123.6 (s, 2C, *C^{3,5}*-H, Tbb), 125.7 (s, 2C, *C^{3,5}*-H, Dipp), 129.7 (s, 1C, *C^4*-H, Dipp), 134.0 (s, 1C, *C^1*, Dipp), 144.7 (s, 1C, *C^1*, Tbb), 147.0 (s, 2C, *C^{2,6}*-CHMe$_A$Me$_B$, Dipp), 149.1 (s, 1C, *C^4*, Tbb), 150.6 (s, 2C, *C^{2,6}*-CH(SiMe$_3$)$_2$, Tbb), 239.7 (s, 1C, *C^2*, caac^{Me}).

^{1}H-^{15}N HMBC (500.1 MHz, 50.7 MHz, (D$_6$)benzene, 298 K): δ (ppm) = 202.3 (1N, C^2*N*).

4.5.46. (caac^{Me})SiTbbGeBr (**43-Si**)

To an ink-blue solution of **39-Si** (1.02 g, 0.600 mmol, 1 equiv.) in 30 mL of fluorobenzene, solid NEt$_4$Br (126 mg, 0.600 mmol, 1 equiv.) was added and the mixture was stirred for 4 hrs. at ambient temperature. During the course of stirring, the colour of the reaction mixture gradually changed from blue to greenish-blue and finally to pine-green. Analysis of an aliquot of the reaction solution by ^{1}H no-D NMR spectroscopy revealed about complete consumption of starting materials and very selective formation of **43-Si**. After removing all the volatiles in vacuo, an extraction of the dark-green mass by 20 mL of *n*-pentane at ambient temperature was done which obtained a clear pine-green filtrate and a beige solid as residue. The filtrate was evaporated to dryness in vacuo and the resulting dark green residue was washed by 6 mL (2 × 3 mL) of Et$_2$O : CH$_3$CN (1 : 2, v/v) mixture at –30 °C. The obtained green solid was further dried in fine vacuum at 45 °C for 1.5 hours. Yield: 480 mg (0.524 mmol, 87 % from **39-Si**).

Properties: Compound **43-Si** is an air sensitive pine-green solid. It can be stored under argon atmosphere at ambient temperature for several days. It is well soluble in Et$_2$O, THF, *n*-hexane, benzene and toluene, but insoluble in acetonitrile at ambient temperature. Under strict exclusion of air, a sample solution of **43-Si** in (D$_6$)benzene does not show any sign of decomposition atleast after 3 days at ambient temperature.

Elemental analysis: 43-Si (C$_{44}$H$_{80}$BrGeNSi$_5$, 916.05 g mol^{-1}): calcd./%: C 57.69, H 8.80, N 1.59; found/%: C 58.31, H 8.78, N 1.56; **Melting Point:** 122°C (dec.).

^{1}H NMR (500.1 MHz, (D$_6$)benzene, 298 K): δ (ppm) = 0.29 (s, ^{2}J (^{29}Si-^{1}H) = 6 Hz, 18H, C^{2,6}-CH(Si*Me$_3$*)$_A$(SiMe$_3$)$_B$, Tbb), 0.37 (s, ^{2}J (^{29}Si-^{1}H) = 6 Hz, 18H, C^{2,6}-CH(SiMe$_3$)$_A$(Si*Me$_3$*)$_B$, Tbb), 1.01 (s, 6H, C^5-*Me$_2$*, caac^{Me}), 1.13 (s, 6H, C^3-*Me$_2$*, caac^{Me}), 1.15 (d, ^{3}J(^{1}H-^{1}H) = 6.7 Hz, 6H, C^{2,6}-CH*Me$_A$*Me$_B$, Dipp), 1.36 (s, 9H, C^4-C*Me$_3$*, Tbb), 1.58 (d, ^{3}J(^{1}H-^{1}H) = 6.7 Hz, 6H, C^{2,6}-CHMe$_A$*Me$_B$*, Dipp), 1.68 (s, 2H, C^4-*H$_2$*, caac^{Me}), 2.90 (s, ^{2}J (^{29}Si-^{1}H) = 9 Hz, 2H, C^{2,6}-C*H*(SiMe$_3$)$_2$, Tbb), 3.14 (sept, ^{3}J(^{1}H-^{1}H) = 6.6 Hz,

2H, $C^{2,6}$-C*H*Me_AMe_B, Dipp), 6.93 (s, 2H, $C^{3,5}$-*H*, Tbb), 7.05 (t, $^3J(^1H\text{-}^1H)$ = 7.8 Hz, 1H, C^4-*H*, Dipp), 7.26 (d, $^3J(^1H\text{-}^1H)$ = 7.8 Hz, 2H, $C^{3,5}$-*H*, Dipp).

$^{13}C\{^1H\}$ NMR (125.8 MHz, (D_6)benzene, 298 K): δ (ppm) = 2.4 (s, ^1J ($^{29}Si\text{-}^{13}C$) = 51 Hz, 6C, $C^{2,6}$-CH(Si*Me*$_3)_A(SiMe_3)_B$, Tbb), 3.2 (s, ^1J ($^{29}Si\text{-}^{13}C$) = 51 Hz, 6C, $C^{2,6}$-CH$(SiMe_3)_A$(Si*Me*$_3)_B$, Tbb), 25.0 (s, 2C, $C^{2,6}$-CH*Me*$_A$Me$_B$, Dipp), 28.7 (s, 2C, $C^{2,6}$-*C*HMe_AMe_B, Dipp), 29.7 (s, 2C, C^5-*Me*$_2$, caac^{Me}), 30.5 (s, 2C, $C^{2,6}$-CHMe_A*Me*$_B$, Dipp), 31.28 (s, 3C, C^4-C*Me*$_3$, Tbb), 31.33 (s, 2C, $C^{2,6}$-*C*H$(SiMe_3)_2$, Tbb), 31.4 (s, 2C, C^3-*Me*$_2$, caac^{Me}), 34.4 (s, 1C, C^4-*C*Me$_3$, Tbb), 50.4 (s, 1C, *C*^{3}-Me$_2$, caac^{Me}), 53.0 (s, 1C, C^4-*H*$_2$, caac^{Me}), 71.4 (s, 1C, *C*^{5}-Me$_2$, caac^{Me}), 123.6 (s, 2C, *C*^{3,5}-H, Tbb), 131.0 (s, 1C, *C*^{4}-H, Dipp), 131.4 (s, 2C, *C*^{3,5}-H, Dipp), 135.7 (s, 1C, *C*^{1}, Tbb), 136.6 (s, 1C, *C*^{1}, Dipp), 146.2 (s, 2C, *C*^{2,6}-CHMe_AMe_B, Dipp), 149.9 (s, 1C, *C*^{4}, Tbb), 151.4 (s, 2C, *C*^{2,6}-CH$(SiMe_3)_A(SiMe_3)_B$, Tbb), 211.1 (s, 1C, *C*^{2}, caac^{Me}).

$^{29}Si\{^1H\}$ NMR (99.3 MHz, (D_6)benzene, 298 K): δ (ppm) = 0.4 (s, ^1J ($^{29}Si\text{-}^{13}C$) = 51 Hz, 2Si, $C^{2,6}$-CH(*Si*Me$_3)_A(SiMe_3)_B$, Tbb,), 3.8 (s, ^1J ($^{29}Si\text{-}^{13}C$) = 51 Hz, 2Si, $C^{2,6}$-CH$(SiMe_3)_A$(*Si*Me$_3)_B$, Tbb), 127.1 (s, 1Si, (caac^{Me})*Si*).

$^1H\text{-}^{15}N$ HMBC (500.1 MHz, 50.7 MHz, (D_6)benzene, 298 K): δ (ppm) = 157.9 (1N, C^2*N*).

4.5.47. (caac^{Me})GeSiBrTbb (**44-Si**)

In a 50 mL schlenk tube, **43-Si** (120 mg, 0.131 mmol) was dissolved in 5 mL of toluene at ambient temperature and the resulting green solution was heated at 105 °C for 1 hour. The colour of the solution gradually changed from green to dark blue. Analysis of an aliquot of the reaction solution by ^1H NMR spectroscopy revealed complete consumption of **43-Si** and its selective transformation to **44-Si**[xiii] along with some minor unknown side products. The reaction solution was worked up by evaporating the solvent to dryness in vacuo followed by a crystallization from *n*-pentane (1.5 mL) at –60 °C for 2 days. Isolation of the dark blue crystals by filtration at –60 °C and drying for 2 hrs. at 45 °C obtained **44-Si** in NMR spectroscopically pure form. Yield: 37 mg (0.040 mmol, 31 % from **43-Si**).

Properties: Compound **44-Si** is an air sensitive, pyrophoric dark blue solid. It can be stored under argon atmosphere at ambient temperature for several months. It is well soluble in Et_2O, *n*-hexane, benzene and toluene at ambient temperature. Under strict

[xiii] Using different methodology, synthesis and complete characterization of this compound is already been reported in a PhD thesis which can be found as "Silicon Compounds in Low Oxidation States Supported by a Cyclic (Alkyl)(Amino)Carbene: Synthesis, Structure and Reactivity", Fabian Gstrein, *PhD-dissertation*, **2023**, Rheinische Friedrich-Wilhelms-Universität Bonn.

exclusion of air, a sample solution of **44-Si** in (D_6)benzene does not show any sign of decomposition atleast after 2 days at ambient temperature.

^{1}H NMR (500.1 MHz, (D_6)benzene, 298 K): δ (ppm) = 0.30 (s, 36H, $C^{2,6}$-CH(Si*Me*$_3$)$_2$, Tbb), 0.93 (s, 6H, C^5-*Me*$_2$, caac^{Me}), 1.13 (d, ^3J(^{1}H-^{1}H) = 6.6 Hz, 6H, $C^{2,6}$-CH*Me*$_A$Me$_B$, Dipp), 1.33 (s, 9H, C^4-C*Me*$_3$, Tbb), 1.59 (s, 2H, C^4-*H*$_2$, caac^{Me}), 1.64 (d, ^3J(^{1}H-^{1}H) = 6.6 Hz, 6H, $C^{2,6}$-CHMe$_A$*Me*$_B$, Dipp), 1.73 (s, 6H, C^3-*Me*$_2$, caac^{Me}), 2.76 (sept, ^3J(^{1}H-^{1}H) = 6.5 Hz, 2H, $C^{2,6}$-C*H*Me$_A$Me$_B$, Dipp), 3.40 (s, ^2J(^{29}Si-^{1}H) = 9.6 Hz, 2H, $C^{2,6}$-C*H*(SiMe$_3$)$_2$, Tbb), 6.96 (s, 2H, $C^{3,5}$-*H*, Tbb), 7.04 (d, ^3J(^{1}H-^{1}H)= 7.7 Hz, 2H, $C^{3,5}$-*H*, Dipp), 7.15** (m, 1H, C^4-*H*, Dipp). **The signal overlaps with the residual proton signal of the deuterated benzene.

^{13}C{^{1}H} NMR (125.8 MHz, (D_6)benzene, 298 K): δ (ppm) = 1.39 (s, 12C, $C^{2,6}$-CH(Si*Me*$_3$)$_2$, Tbb), 24.5 (s, 2C, $C^{2,6}$-CH*Me*$_A$Me$_B$, Dipp), 28.2 (s, 2C, $C^{2,6}$-CHMe$_A$*Me*$_B$, Dipp), 28.8 (s, 2C, C^5-*Me*$_2$, caac^{Me}), 29.2 (s, 2C, $C^{2,6}$-*C*HMe$_A$Me$_B$, Dipp), 31.4 (s, 3C, C^4-C*Me*$_3$, Tbb), 32.6 (s, 2C, C^3-*Me*$_2$, caac^{Me}), 33.7 (s, 2C, $C^{2,6}$-*C*H(SiMe$_3$)$_2$, Tbb), 34.5 (s, 1C, C^4-*C*Me$_3$, Tbb), 51.7 (s, 1C, *C*^{4}-H$_2$, caac^{Me}), 54.2 (s, 1C, *C*^{3}-Me$_2$, caac^{Me}), 76.6 (s, 1C, *C*^{5}-Me$_2$, caac^{Me}), 120.6 (s, 2C, *C*^{3,5}-H, Tbb), 125.8 (s, 2C, *C*^{3,5}-H, Dipp), 129.9 (s, 1C, *C*^{4}-H, Dipp), 134.0 (s, 1C, *C*^{1}, Dipp), 139.9 (s, 1C, *C*^{1}, Tbb), 146.3 (s, 2C, *C*^{2,6}-CHMe$_A$Me$_B$, Dipp), 150.1 (s, 2C, *C*^{2,6}-CH(SiMe$_3$)$_2$, Tbb), 151.7 (s, 1C, *C*^{4}, Tbb), 255.4 (s, 1C, *C*^{2}, caac^{Me}).

^{29}Si{^{1}H} NMR (99.3 MHz, (D_6)benzene, 298 K): δ (ppm) = 2.3 (s, 4Si, $C^{2,6}$-CH(*Si*Me$_3$)$_2$, Tbb), 120.4 (s, 1Si, *Si*(Br)Tbb).

^{1}H-^{15}N HMBC (500.1 MHz, 50.7 MHz, (D_6)benzene, 298 K): δ (ppm) = 205.5 (1N, C^2*N*).

4.5.48. [(caac^{Me})SiTbbGeCNMes][B(Ar^F)$_4$] (45-Si)

To an ink blue solution of **39-Si** (300 mg, 0.177 mmol, 1 equiv) in 25 mL of fluorobenzene, a colourless solution of MesNC (25 mg, 0,177 mmol, 1 equiv.) in 2 mL of fluorobenzene was added at ambient temperature. The colour of the reaction solution was immediately changed from ink blue to cyan. After 15 min of stirring at ambient temperature an aliquot of the reaction solution was analyzed by ^{1}H no-D NMR spectroscopy, revealing very selective and complete transformation of **39-Si** into **45-Si**. The reaction was worked up by evaporating the solvent to dryness in vacuo followed by a trituration of the cyan residue in 10 mL of *n*-pentane. After removal of the liquid phase by filtration, the obtained cyan powder was washed with *n*-pentane (2 × 10 mL) at ambient temperature and dried in fine vacuum for an hour at 40 °C. Yield: 296 mg (0.160 mmol, 91 % from **39-Si**).

Properties: Compound **45-Si** is an air sensitive cyan solid. It is well soluble in Et_2O, fluorobenzene and dichloromethane, but insoluble in aliphatic solvents at ambient temperature. Under strict exclusion of air, a sample solution of **45-Si** in (D_2)dichloromethane shows minute decomposition after 5 hrs. at ambient temperature.

Elemental analysis: 45-Si ($C_{86}H_{103}BF_{24}GeN_2Si_5$, 1844.56 g mol^{-1}): calcd./%: C 56.00, H 5.63, N 1.52; found/%: C 55.61, H 5.70, N 1.33; **Melting Point:** 157°C (dec.).

ATR-IR (solid): $\tilde{\nu}$ (cm^{-1}) = 2985 (w, sh), 2966 (m), 2952 (w, sh), 2929 (vw, sh), 2906 (vw), 2870 (vw), 2824 (vw), 2127 (m) [ν(CN)], 1610 (w, br), 1586 (w) and 1521 (w) [$\nu(CC)_{Aryl}$], 1475 (vw, br, sh), 1461 (vw, br), 1394 (m), 1385 (m), 1355 (s), 1277 (vs), 1257 (s, sh), 1177 (s), 1165 (s), 1123 (vs, br), 1106 (s, sh), 1051 (w), 1041 (w), 1007 (m), 997 (w, sh), 978 (vw, br), 935 (m), 887 (s), 851 (s, sh), 837 (vs, br), 806 (m), 771 (vw, br), 760 (vw, br), 744 (w), 713 (m), 681 (s), 668 (s), 632 (vw), 608 (vw), 572 (vw, sh), 564 (vw), 504 (w), 481 (w), 467 (w), 447 (w), 418 (w).

^{1}H NMR (500.1 MHz, (D_2)dichloromethane, 298 K): δ (ppm) = 0.06 (s, ^2J (^{29}Si-^{1}H) = 6 Hz, 18H, $C^{2,6}$-CH(Si*Me*$_3$)$_A$(SiMe$_3$)$_B$, Tbb), 0.10 (s, ^2J (^{29}Si-^{1}H) = 6 Hz, 18H, $C^{2,6}$-CH(SiMe$_3$)$_A$(Si*Me*$_3$)$_B$, Tbb), 1.31 (s, 9H, C^4-C*Me*$_3$, Tbb), 1.40 (d, ^3J (^{1}H-^{1}H) = 6.6 Hz, 6H, $C^{2,6}$-CH*Me*$_A$Me$_B$, Dipp), 1.54 (s, 6H, C^5-*Me*$_2$, caac^{Me}), 1.59 (s, 6H, C^3-*Me*$_2$, caac^{Me}), 1.63 (d, ^3J (^{1}H-^{1}H) = 6.7 Hz, 6H, $C^{2,6}$-CHMe$_A$*Me*$_B$, Dipp), 2.02 (s, 6H, $C^{2,6}$-*Me*, Mes), 2.04 (s, 2H, $C^{2,6}$-C*H*(SiMe$_3$)$_A$(SiMe$_3$)$_B$, Tbb), 2.27 (s, 3H, C^4-*Me*, Mes), 2.30 (s, 2H, C^4-*H*$_2$, caac^{Me}), 2.92 (sept, ^3J(^{1}H-^{1}H) = 6.6 Hz, 2H, $C^{2,6}$-C*H*Me$_A$Me$_B$, Dipp), 6.88 (s, 2H, $C^{3,5}$-*H*, Tbb), 6.92 (s, 2H, $C^{3,5}$-*H*, Mes), 7.56 (br s, 4H, 4 × C^4-*H*, B(Ar^F)$_4$), 7.58 (m, 1H, C^4-*H*, Dipp), 7.65 (m, 2H, $C^{3,5}$-*H*, Dipp), 7.73 (br m, 8H, 4 × $C^{2,6}$-*H*, B(Ar^F)$_4$).

^{13}C{^{1}H} NMR (125.8 MHz, (D_2)dichloromethane, 298 K): δ (ppm) = 2.4 (s, ^1J (^{29}Si-^{13}C) = 52 Hz, 6C, $C^{2,6}$-CH(Si*Me*$_3$)$_A$(SiMe$_3$)$_B$, Tbb), 2.8 (s, ^1J (^{29}Si-^{13}C) = 52 Hz, 6C, $C^{2,6}$-CH(SiMe$_3$)$_A$(Si*Me*$_3$)$_B$, Tbb), 18.9 (s, 2C, $C^{2,6}$-*Me*, Mes), 21.5 (s, 1C, C^4-*Me*, Mes), 25.7 (s, 2C, $C^{2,6}$-CH*Me*$_A$Me$_B$, Dipp), 29.6 (s, 2C, C^5-*Me*$_2$, caac^{Me}), 29.9 (s, 2C, $C^{2,6}$-*C*HMe$_A$Me$_B$, Dipp), 30.1 (s, 2C, $C^{2,6}$-CHMe$_A$*Me*$_B$, Dipp), 31.2 (s, 3C, C^4-C*Me*$_3$, Tbb), 32.4 (s, 1C, *C*^{3}-Me$_2$, caac^{Me}), 34.1 (s, 2C, $C^{2,6}$-*C*H(SiMe$_3$)$_A$(SiMe$_3$)$_B$, Tbb), 34.8 (s, 1C, C^4-*C*Me$_3$, Tbb), 52.6 (s, 1C, *C*^{4}-H$_2$, caac^{Me}), 52.8 (s, 1C, *C*^{3}-Me$_2$, caac^{Me}), 80.7 (s, 1C, *C*^{5}-Me$_2$, caac^{Me}), 117.9 (sept, ^4J(^{19}F-^{1}H) = 3.6 Hz, 4C, 4 × *C*^{4}-H, B(Ar^F)$_4$), **122.0 (s, very br, 1C, *C*^{1}, Mes), 124.1 (s, 2C, *C*^{3,5}-H, Tbb), 125.03 (q, ^1J(^{19}F-^{13}C) = 272 Hz, 8C, 4 × $C^{3,5}$-*C*F$_3$, B(Ar^F)$_4$), 129.3 (qq, ^2J(^{19}F-^{13}C) = 32 Hz, ^3J(^{13}C-^{11}B) = 3 Hz, 8C, 4 × *C*^{3,5}-CF$_3$, B(Ar^F)$_4$), 129.7 (s, 2C, *C*^{3,5}-H, Mes), 131.8 (s, 2C, *C*^{3,5}-H, Dipp), 133.0 (s, 1C, *C*^{4}-H, dipp), 134.2 (s, 1C, *C*^{1}, Tbb), 134.6 (s, 1C, *C*^{1}, Dipp), 135.2 (br m, 8C, 4 × *C*^{2,6}-H, B(Ar^F)$_4$), 136.0 (s, 2C, *C*^{2,6}-Me, Mes), 143.1 (s, 1C, *C*^{4}-Me, Mes), 143.7 (s, 2C, *C*^{2,6}-CHMe$_A$Me$_B$, Dipp),

150.9 (s, 2C, $C^{2,6}$-$CH(SiMe_3)_2$, Tbb), 153.1 (s, 1C, C^4, Tbb), 162.2 (q, $^1J(^{13}C,^{11}B)$ = 50 Hz, 4C, 4 × C^1, $B(Ar^F)_4$), **218.9 (s very br, 1C, C^2, $caac^{Me}$). **The exact value of full width at half maximum could not be determined. ***Signal corresponds to Mes*N**C* was not observed.

^{29}Si{^{1}H} NMR (99.3 MHz, (D_2)dichloromethane, 298 K): δ (ppm) = 2.1 (s, 2Si, $C^{2,6}$-$CH(SiMe_3)_A(SiMe_3)_B$, Tbb), 3.5 (s, 2Si, $C^{2,6}$-$CH(SiMe_3)_A(SiMe_3)_B$, Tbb), 175.7 (s, 1Si, $(caac^{Me})Si$).

^{1}H-^{15}N HMBC (500.1 MHz, 50.7 MHz, (D_2)dichloromethane, 298 K): δ (ppm) = 209.4 (1N, C^2N).

4.5.49. [Cp*(CO)$_3$TiSiTbb] (46-Ti)

Isolation of [Cp*(CO)$_3$TiSi(Tbb)(4-dmap)][xiv]

A mixture of $Si_2Br_2Tbb_2$ (1 g, 0.896 mmol, 1 equiv.) and 4-dmap (219 mg, 1.792 mmol, 2 equiv.) was suspended in 30 mL toluene and the resulting bright yellow suspension was stirred at ambient temperature. After 30 min a deep-orange solution was formed, which was added dropwise under exclusion of light to a stirred red solution of the titanate $[NEt_4][Cp^*Ti(CO)_4]$ (762 mg, 1.791 mmol, 2 equiv.) in 70 mL toluene at −30 °C. The reaction solution was stirred at this temperature for 1 h during which the color of the solution turned to purplish-brown. The reaction solution was allowed to warm up to ambient temperature and stirred for an additional 1.5 h while the purplish-brown color turned dark purple. The progress of the reaction was analyzed by FT-IR spectroscopy, which revealed complete consumption of the titanate and selective formation of [Cp*(CO)$_3$TiSi(Tbb)(4-dmap)]. The reaction solution was worked up by evaporating the solvent to dryness under fine vacuum, extracting the crude purple solid with 3 × 20 mL of benzene at ambient temperature, evaporating the combined benzene extracts to dryness and crystallizing the resulting NEt_4Br free purple solid from 10 mL of Et_2O at –30 °C for one day. The purple microcrystalline solid of [Cp*(CO)$_3$TiSi(Tbb)(4-dmap)] was isolated by filtering off the brown supernatant solution using a filter cannula at –30 °C followed by drying the solid under fine vacuum at ambient temperature for 1 hour. Yield: 828 mg (0.955 mmol, 53 % of $NEt_4[Cp^*Ti(CO)_4]$).

Properties: Compound [Cp*(CO)$_3$TiSi(Tbb)(4-dmap)] is highly air sensitive purple solid, which turns brown immediately upon exposer to air. It can be stored under

[xiv] Synthesis and complete characterization of **46-Ti** was first done in the research group of Prof. Filippou by Dr. Ujjal Das and later on, a similar chemistry was developed by Dr. Niklas Wienkenhöver, which can be found in reference [229].

argon without any exposer to light for several days. It is stable in solution for at least one day at room temperature under complete exclusion of light. Upon exposure to day light its purple (D_6)benzene solution turned within 12 hrs. into a dark-brown solution, which according to ^{1}H NMR spectroscopy showed an unselective decomposition. It is poorly soluble in *n*-hexane, moderately soluble in Et_2O, well-soluble in benzene, toluene and THF.

Elemental analysis: [Cp*(CO)$_3$TiSi(Tbb)(4-dmap)] ($C_{44}H_{74}N_2O_3Si_5Ti$, 867.37 g mol^{-1}): calcd./%: C 60.93, H 8.60, N 3.23; found/%: C 60.26, H 8.75, N 3.17; **Melting Point:** 157°C (dec.).

IR (THF): $\tilde{\nu}$ (cm^{-1}) = 1909 (vs) [CO], 1845 (m) [CO], 1814 (m) [CO], 1761 (w) [CO], 1626 (m) [CN].

IR (toluene): $\tilde{\nu}$ (cm^{-1}) = 1915 (vs) [CO], 1852 (m) [CO], 1811 (m) [CO], 1762 (w) [CO], 1624 (m) [CN].

ATR-IR (solid): $\tilde{\nu}$ (cm^{-1}) = 2949 (m), 2896 (m), 2852 (m), 1899 (vs) [CO], 1848 (vs) [CO], 1731 (s) [CO], 1618 (s) [CN], 1584 (w), 1544 (m), 1521 (m), 1477 (w), 1441 (m), 1391 (m), 1361 (vw), 1342 (vw), 1247 (m), 1226 (m), 1156 (w), 1122 (w), 1048 (w), 1027 (vw), 1005 (s), 943 (m), 885 (m), 858 (sh), 836 (vs), 815 (vs), 761 (m), 746 (m), 720 (w), 685 (m), 662 (m), 644 (vw), 624 (w), 605 (w), 573 (w), 550 (m), 521 (m), 492 (m), 482 (m), 470 (m), 442 (m), 418 (m).

^{1}H NMR (300.1 MHz, (D_6)benzene, 298 K): δ (ppm) = 0.23 (br s, $\Delta\nu_{1/2}$ = 15 Hz, 36H, C^{2,6}-CH(Si*Me*$_3$)$_2$, Tbb), 1.34 (s, 9H, C^4-C*Me*$_3$, Tbb), 1.90 (br s, $\Delta\nu_{1/2}$ = 23 Hz, 6H, C^4-N*Me*$_2$, 4-dmap), 2.17 (s, 15H, C$_5$*Me*$_5$), 2.73 (br s, $\Delta\nu_{1/2}$ = 19 Hz, 2H, C^{2,6}-C*H*(SiMe$_3$)$_2$, Tbb), 5.91 (br s, $\Delta\nu_{1/2}$ = 12 Hz, 2H, C^{3,5}-*H*, 4-dmap), 6.91 (s, 2H, C^{3,5}-*H*, Tbb), 8.28 (br s, $\Delta\nu_{1/2}$ = 16 Hz, 2H, C^{2,6}-*H*, 4-dmap).

^{1}H NMR (300.1 MHz, (D_8)toluene, 298 K): δ (ppm) = 0.20 (s, $\Delta\nu_{1/2}$ = 9 Hz, 36H, C^{2,6}-CH(Si*Me*$_3$)$_2$, Tbb), 1.39 (s, 9H, C^4-C*Me*$_3$, Tbb), 1.96 (s, $\Delta\nu_{1/2}$ = 6 Hz, 6H, C^4-N*Me*$_2$, 4-dmap), 2.21 (s, 15H, C$_5$*Me*$_5$), 2.74 (br s, $\Delta\nu_{1/2}$ = 13 Hz, 2H, C^{2,6}-C*H*(SiMe$_3$)$_2$, Tbb), 5.95 (br d, $\Delta\nu_{1/2}$ = 4 Hz, ^3J (^{1}H-^{1}H) = 6 Hz, 2H, C^{3,5}-*H*, 4-dmap), 6.91 (s, 2H, C^{3,5}-*H*, Tbb), 8.20 (br d, $\Delta\nu_{1/2}$ = 7 Hz, ^3J (^{1}H-^{1}H) = 6 Hz, 2H, C^{2,6}-*H*, 4-dmap).

^{1}H NMR (300.1 MHz, (D_8)toluene, 203 K): δ (ppm) = = 0.11, 0.53 (each s, 9H each, C^2-CH(Si*Me*$_3$)$_A$(Si*Me*$_3$)$_B$, Tbb), 0.23, 0.40 (each s, 9H each, C^6-CH(Si*Me*$_3$)$_A$(Si*Me*$_3$)$_B$, Tbb), 1.37 (br, 6H, C^4-N*Me*$_2$, 4-dmap), 1.47 (s, 9H, C^4-C*Me*$_3$, Tbb), 2.35 (s, 15H, C$_5$*Me*$_5$), 2.47 (s, 1H, C^2-C*H*(SiMe$_3$)$_A$(SiMe$_3$)$_B$), 3.16 (s, 1H, C^6-C*H*(SiMe$_3$)$_A$(SiMe$_3$)$_B$, Tbb), 4.85, 6.09 (each very br s, 1H each, C^3-*H* + C^5-*H* , 4-dmap), 6.92, (br, 1H, C$^{2/6}$-H, 4-dmap), 6.99 (s, 2H, C^{3,5}-*H*, Tbb), 9.46 (br, 1H, C$^{2/6}$-*H*, 4-dmap).

$^{13}C\{^1H\}$ NMR (75.5 MHz, (D_8)toluene, 298 K): **δ** (ppm) = 1.6 (s, 12C, $C^{2,6}$-CH(Si*Me*$_3$)$_2$, Tbb), 12.5 (s, 5C, C_5*Me*$_5$), 29.9 (s, 2C, $C^{2,6}$-*C*H(SiMe$_3$)$_2$, Tbb), 31.4 (s, 3C, C^4-C*Me*$_3$, Tbb), 34.5 (s, 1C, C^4-*C*Me$_3$, Tbb), 38.2 (s, 2C, C^4-N*Me*$_2$, 4-dmap), 105.8 (s, 2C, *C*^{3,5}-H, 4-dmap), 106.4 (s, 5C, *C*$_5$Me$_5$), 122.5 (s, 2C, *C*^{3,5}-H, Tbb), 143.1 (br, 1C, *C*^{1}-Si, Tbb), 147.4 (br, *C*^{2,6}-CH(SiMe$_3$)$_2$, Tbb), 149.5 (s, 2C, *C*^{2,6}-H, 4-dmap), 150.6 (s, 1C, *C*^{4}-CMe$_3$, Tbb), 154.6 (s, 1C, *C*^{4}-NMe$_2$, 4-dmap).**No carbonyl carbon signal was observed in the $^{13}C\{^1H\}$ NMR spectrum.

$^{13}C\{^1H\}$ NMR (75.5 MHz, (D_8)toluene, 203 K): **δ** (ppm) = 1.1, 1.9 (each s, 3C each, C^2-CH(Si*Me*$_3$)$_A$(Si*Me*$_3$)$_B$), 1.3, 1.4 (each s, 3C each, C^6-CH(Si*Me*$_3$)$_A$(Si*Me*$_3$)$_B$, Tbb), 12.7 (s, 5C, C_5*Me*$_5$), 28.9 (br, 2C, $C^{2,6}$-*C*H(SiMe$_3$)$_A$(SiMe$_3$)$_B$, Tbb), 31.2 (s, 3C, C^4-C*Me*$_3$, Tbb), 34.3 (s, 1C, C^4-*C*Me$_3$, Tbb), 37.8 (br, 2C, C^4-N*Me*$_2$, 4-dmap), 105.7 (s, 5C, *C*$_5$Me$_5$), 121.9 and 122.4 (each br s, 1C each, *C*^{3}-H + *C*^{5}-H, Tbb), 141.6 (s, 1C, *C*^{1}-Si, Tbb), 148.7 and 149.7 (each s, 1C each, *C*^{2}-CH(SiMe$_3$)$_A$(SiMe$_3$)$_B$ + *C*^{6}-CH(SiMe$_3$)$_A$(SiMe$_3$)$_B$, Tbb), 149.9 (s, 1C, *C*^{4}-CMe$_3$, Tbb), 153.9 (s, 1C, *C*^{4}-NMe$_2$, 4-dmap), 271.2 (s, 1C, *C*O), 284.1 (s, 1C, *C*O), 285.9 (s, 1C, *C*O). **The signals of the $C^{2,3,5,6}$ carbon atoms of the 4-dmap ligand were not detected in the $^{13}C\{^1H\}$ NMR spectrum.

$^{29}Si\{^1H\}$ NMR (59.6 MHz, (D_8)toluene, 203 K): **δ** (ppm) = 0.58, 0.61, 4.0, 4.5 (each s, 1Si each, C^2-CH(*Si*Me$_3$)$_A$(*Si*Me$_3$)$_B$ + C^6-CH(*Si*Me$_3$)$_A$(*Si*Me$_3$)$_B$, Tbb), 255.8 (s, 1Si, Ti*Si*Tbb).

Isolation of [Cp*(CO)$_3$TiSiTbb] (46-Ti) from [Cp*(CO)$_3$TiSi(Tbb)(4-dmap)]

A solution of B(*p*-Tol)$_3$ (202 mg, 0.710 mmol, 1 equiv.) in 10 mL of toluene was added to a pre-cooled solution of [Cp*(CO)$_3$TiSi(Tbb)(4-dmap)] (615 mg, 0.710 mmol, 1 equiv.) in 30 mL of toluene at –60 °C, whereupon the purple colour of the solution immediately changed to brownish-purple. The reaction solution was stirred at this temperature for 1 h and then warmed to room temperature. After stirring at ambient temperature for 1 h, an aliquot of the solution was taken and studied by FT-IR spectroscopy, which showed complete consumption of [Cp*(CO)$_3$TiSi(Tbb)(4-dmap)] and selective formation of **46-Ti**. The reaction solution was worked up by evaporating the solvent to dryness under fine-vacuum to obtain a crude deep-brown solid, extracting the crude product with 3 × 5 mL of pre-cooled *n*-hexane at –60 °C leaving the colourless adduct B(p-Tol)$_3$(4-dmap) as insoluble solid. After concentrating the volume of the combined purplish-brown extracts to 5 mL under fine-vacuum and upon storing it at –60 °C for two days obtained dark brown microcrystals of **46-Ti**. The crystals were isolated by cannula filtration of the greenish-brown supernatant solution at –60 °C and dried under fine vacuum at ambient temperature for 1 h to

afford **46-Ti** in analytically pure form. Yield: 313 mg (0.420 mmol, 59 % from [Cp*(CO)$_3$TiSi(Tbb)(4-dmap)]).

Properties: Compound **46-Ti** is highly air sensitive dark brown solid, decolorizing immediately upon contact with air. It is soluble in *n*-hexane, benzene, and toluene, but decomposes completely within three days in dry, deoxygenated THF at ambient temperature. A sample solution of **46-Ti** in (D_6)benzene does not show any sign of decomposition atleast after 16 hrs. at ambient temperature.

Elemental analysis: 46-Ti ($C_{37}H_{64}O_3Si_5Ti$, 745.20 g mol^{-1}): calcd./%: C 59.63, H 8.66; found/%: C 59.10, H 8.78; **Melting Point:** 162°C (dec.).

IR (*n*-hexane): $\tilde{\nu}$ (cm^{-1}) = 1980 (vs) [CO], 1918 (w) [CO], 1866 (vw, br) [CO], 1811 (w) [CO].
IR (THF): $\tilde{\nu}$ (cm^{-1}) = 1972 (vs) [CO], 1918 (w) [CO], 1859 (vw, br) [CO], 1803 (w) [CO].
ATR-IR (solid): $\tilde{\nu}$ (cm^{-1}) = 2952 (m), 2901 (m), 2861 (w), 1968 (vs) [CO], 1905 (s) [CO], 1807 (vs) [CO], 1632 (vw), 1583 (m), 1525 (m), 1475 (w), 1458 (w), 1420 (w), 1395 (m), 1377 (m), 1360 (w), 1259 (m) [SiMe$_3$], 1245 (s), 1166 (m), 1136 (w), 1043 (w), 1027 (w), 1011 (m), 959 (m), 939 (w), 886 (m), 856 (sh), 834 (vs) [SiMe$_3$], 770 (sh), 761 (m), 741 (m), 721 (m), 685 (m), 658 (w), 647 (w), 620 (vw), 606 (w), 577 (vw), 562 (w), 546 (w), 520 (m), 500 (m), 463 (vw), 436 (w), 417 (m).
^{1}H NMR (300.1 MHz, (D_6)benzene, 298 K): δ (ppm) = 0.23 (s, ^2J (^{29}Si-^{1}H) = 6 Hz, 36H, C^{2,6}-CH(Si*Me$_3$*)$_2$, Tbb), 1.23 (s, 9H, C^4-C*Me$_3$*, Tbb), 2.01 (s, 15H, C$_5$*Me$_5$*), 2.56 (s, ^2J (^{29}Si-^{1}H) = 12 Hz, 2H, C^{2,6}-C*H*(SiMe$_3$)$_2$, Tbb), 6.81 (s, 2H, C^{3,5}-*H*, Tbb).
^{13}C{^{1}H} NMR (75.5 MHz, (D_6)benzene, 298 K): δ (ppm) = 0.54 (s, ^1J (^{29}Si-^{13}C) = 52 Hz, 12C, C^{2,6}-CH(Si*Me$_3$*)$_2$, Tbb), 12.5 (s, 5C, C$_5$*Me$_5$*), 31.0 (s, 3C, C^4-C*Me$_3$*, Tbb), 32.4 (s, ^1J (^{29}Si-^{13}C) = 41 Hz, 2C, C^{2,6}-*C*H(SiMe$_3$)$_2$, Tbb), 34.8 (s, 1C, C^4-*C*Me$_3$, Tbb), 110.9 (s, 5C, *C*$_5$Me$_5$), 121.2 (s, 2C, *C*^{3,5}-H, Tbb), 148.09 (s, 2C, *C*^{2,6}-CH(SiMe$_3$)$_2$, Tbb), 148.1 (s, 1C, *C*^{1}-Si, Tbb), 154.6 (s, 1C, *C*^{4}-CMe$_3$, Tbb), 247.5 (s, 1C, *C*O$_{diag}$), 270.2 (s, 2C, 2 × *C*O$_{lat}$).
^{29}Si{^{1}H} NMR (59.6 MHz, (D_8)toluene, 203 K): δ (ppm) = 1.8 (s, 4Si, C^{2,6}-CH(*Si*Me$_3$)$_2$, Tbb), 433.8 (s, 1Si, Ti*Si*Tbb).

4.5.50. [Cp*(CO)$_3$TiGeTbb] (47-Ti)

A mixture of titanate NEt$_4$(Cp*Ti(CO)$_4$) (530 mg, 1.246 mmol, 1 equiv.) and Ge$_2$Br$_2$Tbb$_2$ (1.5 g, 1.245 mmol, 1 equiv.) was treated with 15 mL of benzene and the resulting dark purplish-brown solution was stirred at ambient temperature. An aliquot of the reaction solution was taken after 4 hrs. and analyzed by ^{1}H NMR

spectroscopy in (D_6)benzene, which showed complete consumption of starting materials and selective formation of **47-Ti** and [NEt_4][$GeBr_2$Tbb] in a 1 : 1 molar ratio. The reaction solution was worked up by evaporating the solvent to dryness at 40 °C under fine vacuum, extraction of **47-Ti** from obtained brown crude solid with *n*-hexane (3 × 15 mL) at ambient temperature left the insoluble [NEt_4][$GeBr_2$(Tbb)] as white solid. Upon concentrating the combined *n*-hexane extracts to 5 mL under fine vacuum and storing the solution at –60 °C for one day obtained dark brown crystals of **47-Ti**, which were isolated by filtering off the purplish-brown supernatant solution with a filter cannula at –60 °C followed by drying the crystals under fine vacuum for 2 hrs. at 55 °C. The *n*-pentane insoluble white solid was dried under fine vacuum for 1 h at 55 °C to obtain [NEt_4][$GeBr_2$Tbb] as spectroscopically pure white solid. Yield of **47-Ti**: 700 mg (0.886 mmol, 71% from NEt_4[Cp*Ti$(CO)_4$]) and Yield of [NEt_4][$GeBr_2$Tbb]: 715 mg (0.88 mmol, 71% from $Ge_2Br_2Tbb_2$).

Properties: Compound **47-Ti** is highly air sensitive solid, decolorizing immediately upon contact to air. It is well soluble *n*-hexane and highly soluble in benzene and THF. A sample solution of **47-Ti** in (D_6)benzene does not show any sign of decomposition atleast after 16 hrs. at ambient temperature.

Elemental analysis: 47-Ti ($C_{37}H_{64}GeO_3Si_4Ti$, 789.72 g mol^{-1}): calcd./%: C 56.27, H 8.17; found/%: C 55.85, H 8.38; **Melting Point:** 185°C.

IR (*n*-hexane): $\tilde{\nu}$ (cm^{-1}) = 1980 (vs), 1915 (vw, br), 1873 (m) and 1856 (m, sh) [CO], 1581 (w) and 1531 (w) [CC_{Aryl}].
IR (THF): $\tilde{\nu}$ (cm^{-1}) = 1970 (vs), 1914 (vw, br), 1861 (m, br) and 1849 (m, br) [CO], 1580 (w) and 1532 (w) [CC_{Aryl}].
ATR-IR (solid): $\tilde{\nu}$ (cm^{-1}) = 2952 (w), 2901 (w), 2866 (w), 1965 (s) [CO], 1904 (w) [CO], 1843 (m) [CO], 1580 (w) and 1530 (w) [CC_{Aryl}], 1477 (w), 1460 (w), 1395 (w), 1378 (w), 1362 (w), 1259 (w) [$SiMe_3$], 1245 (m) [$SiMe_3$], 1167 (w), 1025 (sh), 1013 (w), 961 (w), 935 (w), 886 (w), 834 (s) [$SiMe_3$], 770 (sh), 761 (m), 738 (w), 722 (w), 685 (m), 659 (w), 643 (w), 622 (w), 609 (w), 556 (w), 539 (w), 521 (w), 499 (w), 432 (w), 412 (m).
^{1}H NMR (500.1 MHz, (D_6)benzene, 298 K): δ (ppm) = 0.23 (s, ^2J (^{29}Si-^{1}H) = 6 Hz, 36H, $C^{2,6}$-CH(Si*Me*$_3$)$_2$, Tbb), 1.25 (s, 9H, C^4-C*Me*$_3$, Tbb), 1.99 (s, 15H, C_5*Me*$_5$), 2.36 (s, ^2J (^{29}Si-^{1}H) = 9.5 Hz, 2H, $C^{2,6}$-C*H*($SiMe_3$)$_2$, Tbb), 6.85 (s, 2H, $C^{3,5}$-*H*, Tbb).
^{13}C{^{1}H} NMR (125.8 MHz, (D_6)benzene, 298 K): δ (ppm) = 0.45 (s, ^1J (^{29}Si-^{13}C) = 51 Hz, 12C, $C^{2,6}$-CH(Si*Me*$_3$)$_2$, Tbb), 12.7 (s, 5C, C_5*Me*$_5$), 31.1 (s, 3C, C^4-C*Me*$_3$, Tbb), 31.6 (s, 2C, ^1J (^{29}Si-^{13}C) = 42 Hz, $C^{2,6}$-*C*H($SiMe_3$)$_2$, Tbb), 34.8 (s, 1C, C^4-*C*Me$_3$, Tbb), 110.6 (s, 5C, *C*$_5$Me$_5$), 121.6 (s, 2C, *C*^{3,5}-H, Tbb), 144.7 (s, 2C, *C*^{2,6}-CH($SiMe_3$)$_2$, Tbb), 153.3 (s,

1C, *C*^{1}-Si, Tbb), 165.5 (s, 1C, *C*^{4}-CMe_3, Tbb), 248.8 (s, 1C, *C*O_{diag}), 268.1 (s, 2C, 2 × *C*O_{lat}).

Spectroscopic data of [NEt_4][$GeBr_2$Tbb]

^{1}H NMR (300.1 MHz, (D_8)THF, 298 K): δ (ppm) = 0.08 (s, 36H, ^{2}J (^{29}Si-^{1}H) = 6 Hz, C^{2,6}-CH(Si*Me*$_3$)$_2$, Tbb), 1.26 (s, 9H, C^{4}-C*Me*$_3$, Tbb), 1.43 (tt, ^{3}J (^{1}H-^{1}H) = 7.3 Hz, ^{3}J (^{14}N-^{1}H) = 1.9 Hz, 12H, N(CH_2*CH*$_3$)$_4$), 3.54 (q, ^{3}J (^{1}H-^{1}H) = 7.3 Hz, 8H, N(*CH*$_2$$CH_3$)$_4$), 3.63 (s, ^{2}J (^{29}Si-^{1}H) = 9.5 Hz, 2H, C^{2,6}-C*H*($SiMe_3$)$_2$, Tbb), 6.55 (s, 2H, C^{3,5}-*H*, Tbb).
^{13}C{^{1}H} NMR (75.5 MHz, (D_8)THF, 298 K): δ (ppm) = 1.5 (s, ^{1}J (^{29}Si-^{13}C) = 51 Hz, 12C, C^{2,6}-CH(Si*Me*$_3$)$_2$, Tbb), 8.5 (s, 4C, N(CH_2*CH*$_3$)$_4$), 27.0 (s, 2C, C^{2,6}-*C*H($SiMe_3$)$_2$, Tbb), 31.8 (s, 3C, C^{4}-C*Me*$_3$, Tbb), 34.6 (s, 1C, C^{4}-*C*Me_3, Tbb), 54.0 (s, 4C, N(*CH*$_2$$CH_3$)$_4$), 122.0 (s, 2C, *C*^{3,5}-H, Tbb), 148.5 (s, 1C, *C*^{4}-CMe_3, Tbb), 150.1 (s, 2C, *C*^{2,6}-CH($SiMe_3$)$_2$, Tbb), 152.8 (s, 1C, *C*^{1}-Si, Tbb).

4.5.51. [Cp*(CO)$_2$(PMe_3)TiSiTbb] (**48-Ti**)

To a solution of **46-Ti** (450 mg, 0.603 mmol, 1 equiv.) in 15 mL of *n*-hexane, a stock solution (0.88 M in *n*-hexane) of PMe_3 (0.72 mL, 0.627 mmol, 1.04 equiv.) was added at ambient temperature and the resulting brownish-purple solution was heated at 60 °C in a closed Schlenk tube. The colour of the reaction solution gradually changed to dark red. After 2 hrs. of heating the reaction solution was cooled to room temperature and an aliquot was analysed by solution IR and ^{1}H NMR spectroscopy, which showed complete consumption of **46-Ti** and quantitative formation of **48-Ti**. The reaction solution was worked up by evaporating the solvent to dryness under fine-vacuum to obtain a dark red solid and crystallizing it from 2 mL of *n*-hexane at −60 °C for one day obtained dark red microcrystals of **48-Ti**. The microcrystalline solid was isolated by filtering off the red supernatant followed by drying under fine-vacuum at 50 °C for 1 h affording **48-Ti** as an analytically pure solid. Yield: 360 mg (0.450 mmol, 76% from **46-Ti**).

Properties: Compound **48-Ti** is highly air sensitive dark red solid, decolorizing immediately upon contact with air. It is well soluble in *n*-hexane, diethyl ether, benzene and toluene at ambient temperature. A sample solution of **48-Ti** in (D_6)benzene does not show any sign of decomposition atleast after 24 hrs. at ambient temperature.

Elemental analysis: 47-Ti ($C_{39}H_{73}O_2PSi_5Ti$, 793.26 g mol^{-1}): calcd./%: C 59.05, H 9.28; found/%: C 59.02, H 9.52; **Melting Point:** 185°C (dec.).

IR (*n*-hexane): $\tilde{\nu}$ (cm^{-1}) = 1861 (m), 1792 (s, br) and 1767 (m, sh) [CO], 1584 (w) and 1530 (w) [CC_{Aryl}].

IR (THF): $\tilde{\nu}$ (cm^{-1}) = 1858 (m), 1785 (s, br) and 1763 (s, sh) [CO], 1584 (w) and 1526 (w) [CC_{Aryl}].

ATR-IR (solid): $\tilde{\nu}$ (cm^{-1}) = 2951 (m), 2900 (m), 2858 (w), 2807 (w) 1835 (w) [CO], 1780 (s) [CO], 1583 (w) and 1527 (w) [CC_{Aryl}], 1477 (w), 1458 (w), 1423 (w), 1396 (w), 1375 (m), 1362 (w), 1302 (w), 1281 (w), 1260 (m) [$SiMe_3$], 1243 (m) [$SiMe_3$], 1218 (w), 1164 (w), 1016 (w), 959 (sh), 950 (w), 937 (sh), 889 (w), 856 (sh), 835 (vs) [$SiMe_3$], 763 (w), 743 (w), 722 (w), 686 (w), 661 (w), 643 (w), 623 (w), 609 (w), 563 (w), 540 (w), 524 (w), 498 (w), 453 (w), 433 (w), 419 (w).

^{1}H NMR (500.1 MHz, (D_6)benzene, 298 K): δ (ppm) = 0.32 (s, ^2J (^{29}Si-^{1}H) = 6 Hz, 36H, $C^{2,6}$-CH(Si*Me*$_3$)$_2$, Tbb), 0.99 (d, ^2J (^{31}P-^{1}H) = 6.5 Hz, 9H, P*Me*$_3$) 1.30 (s, 9H, C^4-C*Me*$_3$, Tbb), 2.08 (s, 15H, C_5*Me*$_5$), 2.40 (s, ^2J (^{29}Si-^{1}H) = 9.5 Hz, 2H, $C^{2,6}$-C*H*($SiMe_3$)$_2$, Tbb), 6.88 (s, 2H, $C^{3,5}$-*H*, Tbb).

^{31}P{^{1}H} NMR (200.4 MHz, (D_6)benzene, 298 K): δ (ppm) = 14.43 (s, 1P, *P*Me_3).

^{13}C{^{1}H} NMR (125.8 MHz, (D_6)benzene, 298 K): δ (ppm) = 0.7 (s, ^1J (^{29}Si-^{13}C) = 51.5 Hz, 12C, $C^{2,6}$-CH(Si*Me*$_3$)$_2$, Tbb), 13.4 (s, 5C, C_5*Me*$_5$), 17.3 (d, ^1J (^{31}P-^{13}C) = 17.8 Hz, 3C, P*Me*$_3$), 30.8 (s, ^1J (^{29}Si-^{13}C) = 42 Hz, 2C, $C^{2,6}$-*C*H($SiMe_3$)$_2$, Tbb), 31.2 (s, 3C, C^4-C*Me*$_3$, Tbb), 34.6 (s, 1C, C^4-*C*Me_3, Tbb), 110.3 (s, 5C, *C*$_5$$Me_5$), 121.4 (s, 2C, *C*^{3,5}-H, Tbb), 146.4 (s, 2C, *C*^{2,6}-CH($SiMe_3$)$_2$, Tbb), 150.1 (s, 1C, *C*^{1}, Tbb), 152.4 (s, 1C, *C*^{4}-CMe_3, Tbb), 281.6 (d, ^2J (^{31}P-^{13}C) = 21.9 Hz, 2C, 2 × *C*O_{lat}).

^{29}Si{^{1}H} NMR (99.3 MHz, (D_6)benzene, 298 K): δ (ppm) = 2.1 (s, 4Si, $C^{2,6}$-CH(*Si*Me_3)$_2$, Tbb), 446.8 (s, ^2J (^{31}P-^{29}Si) = 32.3 Hz, 1Si, Ti*Si*Tbb).

4.5.52. [Cp*(CO)$_2$(PMe_3)TiGeTbb] (**49-Ti**)

To a solution of **47-Ti** (530 mg, 0.671 mmol, 1 equiv.) in 20 mL of *n*-hexane, a stock solution (0.88 M in *n*-hexane) of PMe_3 (0.8 mL, 0.705 mmol, 1.05 equiv.) was added at ambient temperature and the resulting brownish-purple solution was heated at 60 °C in a closed Schlenk tube. The colour of the reaction solution gradually changed to maroon. After 3 hrs. of heating the reaction solution was cooled to room temperature and an aliquot was analysed by solution IR and ^{1}H NMR spectroscopy, which showed complete consumption of **47-Ti** and quantitative formation of **49-Ti**. The reaction solution was worked up by evaporating the solvent to dryness under fine-vacuum to obtain a dark maroon solid and crystallizing it from 2 mL of *n*-hexane at −60 °C for one day obtained maroon-red microcrystals which were isolated by filtering off the red supernatant followed by drying under fine-vacuum at 50 °C for 1 hour. Yield: 400 mg (0.477 mmol, 71 % from **47-Ti**).

Properties: Compound **49-Ti** is highly air sensitive dark maroon solid, decolorizing immediately upon contact with air. It is well soluble in *n*-hexane, diethyl ether, benzene and toluene at ambient temperature. A sample solution of **49-Ti** in (D_6)benzene does not show any sign of decomposition atleast after 24 hrs. at ambient temperature.

Elemental analysis: 49-Ti ($C_{39}H_{73}GeO_2PSi_4Ti$, 837.79 g mol^{-1}): calcd./%: C 55.91, H 8.78; found/%: C 55.89, H 8.61; **Melting Point:** 224°C (dec.).

IR (*n*-hexane): $\tilde{\nu}$ (cm^{-1}) = 1860 (m, br) and 1815 (s) [CO], 1582 (w), 1544 (vw, br) and 1530 (w) [CC_{Aryl}].
IR (THF): $\tilde{\nu}$ (cm^{-1}) = 1861 (m, br) and 1809 (s) [CO], 1580 (w), 1542 (vw, br) and 1530 (w) [CC_{Aryl}].
ATR-IR (solid): $\tilde{\nu}$ (cm^{-1}) = 2950 (m), 2901 (m), 2859 (w), 2809 (vw, br), 1851 (m) [CO], 1802 (s) [CO], 1580 (w), 1544 (vw, br) and 1531 (w) [CC_{Aryl}], 1484 (vw), 1475 (vw), 1457 (vw), 1433 (vw, sh), 1421 (w), 1395 (w), 1375 (w), 1361 (vw), 1302 (vw), 1282 (w), 1258 (m), 1244 (s), 1216 (vw), 1163 (w), 1019 (m), 959 (m, sh), 949 (m), 938 (m, sh), 887 (m), 858 (s, sh), 835 (vs, br), 826 (vs, sh), 802 (m, sh), 770 (w, sh), 762 (m), 740 (w), 720 (w), 685 (m), 661 (m), 641 (w), 622 (vw), 609 (vw), 555 (vw), 535 (w), 510 (vw), 449 (w), 416 (m).
^{1}H NMR (500.1 MHz, (D_6)benzene, 298 K): δ (ppm) = 0.32 (s, ^2J(^{29}Si-^{1}H) = 6.5 Hz, 36H, $C^{2,6}$-CH(Si*Me*$_3$)$_2$, Tbb), 0.96 (d, ^2J (^{31}P-^{1}H) = 6.5 Hz, 9H, P*Me*$_3$) 1.31 (s, 9H, C^4-C*Me*$_3$, Tbb), 2.06 (s, 15H, C_5*Me*$_5$), 2.27 (s, ^2J (^{29}Si-^{1}H) = 9.5 Hz, 2H, $C^{2,6}$-C*H*(SiMe$_3$)$_2$, Tbb), 6.92 (s, 2H, $C^{3,5}$-*H*, Tbb).
^{31}P{^{1}H} NMR (200.4 MHz, (D_6)benzene, 298 K): δ (ppm) = 11.2 (s, 1P, *P*Me$_3$).
^{13}C{^{1}H} NMR (125.8 MHz, (D_6)benzene, 298 K): δ (ppm) = 0.7 (s, ^1J(^{29}Si-^{13}C) = 51.5 Hz, 12C, $C^{2,6}$-CH(Si*Me*$_3$)$_2$, Tbb), 13.6 (s, 5C, C_5*Me*$_5$), 17.47 (d, ^1J (^{31}P-^{13}C) = 17.8 Hz, 3C, P*Me*$_3$), 30.4 (s, ^1J (^{29}Si-^{13}C) = 42 Hz, 2C, $C^{2,6}$-*C*H(SiMe$_3$)$_2$, Tbb), 31.4 (s, 3C, C^4-C*Me*$_3$, Tbb), 34.6 (s, 1C, C^4-*C*Me$_3$, Tbb), 110.0 (s, 5C, *C*$_5$Me$_5$), 121.6 (s, 2C, *C*^{3,5}-H, Tbb), 143.5 (s, 2C, *C*^{2,6}-CH(SiMe$_3$)$_2$, Tbb), 151.2 (s, 1C, *C*^{4}-CMe$_3$, Tbb), 165.6 (s, 1C, *C*^{1}, Tbb), 280.87 (d, ^2J (^{31}P-^{13}C) = 20.4 Hz, 2C, 2 × *C*O$_{lat}$).

4.5.53. [Cp*(CO)(CNMes)$_2$TiGeTbb] (50-Ti)

To a brown solution of **47-Ti** (500 mg, 0.630 mmol, 1 equiv.) in 10 mL of *n*-hexane, a solution of MesNC (188 mg, 1.290 mmol, 2.05 equiv.) in 5 mL *n*-hexane was added at ambient temperature. The resulting brown solution was heated at 50 °C in a closed Schlenk tube during which the brown color the solution gradually turned to dark green. After 30 hrs. of heating, the reaction solution was cooled to ambient

temperature and an aliquot was taken for solution FT-IR spectroscopic analysis, which revealed complete consumption of the **47-Ti** and selective formation of the monocarbonyl-diisonitrile complex **50-Ti** along with tiny unreacted MesNC. The reaction solution was worked up by evaporating the solvent to dryness under fine-vacuum and followed by crystallization of the crude green solid from 2 mL Et_2O at –60 °C for three days afforded dark green microcrystals of **50-Ti**, which were isolated by filtering off the green supernatant solution followed by drying under fine vacuum for 1 h at 50 °C. Yield: 366 mg (0.352 mmol, 56% of **47-Ti**).

Properties: Compound **50-Ti** is highly air sensitive dark green solid, decolorizing immediately upon contact with air. It is well soluble in *n*-hexane, diethyl ether, benzene and toluene at ambient temperature. A sample solution of **50-Ti** in (D_6)benzene does not show any sign of decomposition atleast after 12 hrs. at ambient temperature.

Elemental analysis: 50-Ti ($C_{55}H_{86}GeN_2OSi_4Ti$, 1024.10 g mol^{-1}): calcd./%: C 64.50, H 8.46, N 2.74; found/%: C 63.98, H 8.58, N 2.61; **Melting Point:** 118°C (dec.).

IR (*n*-hexane): $\tilde{\nu}$ (cm^{-1}) = 2054 (s) [CN], 2029 (m) [CN], 1827 (w) [CO], 1778 (w) [CO].
IR (THF): $\tilde{\nu}$ (cm^{-1}) = 2060 (s) [CN], 2039 (m) [CN], 1817 (w) [CO], 1768 (w) [CO].
ATR-IR (solid): $\tilde{\nu}$ (cm^{-1}) = 2949 (w), 2896 (w), 2859 (w), 2051 (s) [CN], 2027 (s) [CN], 1813 (w) [CO], 1764 (m) [CO], 1608 (w), 1580 (w) [CC_{Aryl}], 1527 (w) [CC_{Aryl}], 1474 (w), 1393 (w), 1374 (w), 1360 (m), 1257 (w) [$SiMe_3$], 1244 (m) [$SiMe_3$], 1204 (w), 1161 (w), 1143 (w), 1024 (w), 957 (w), 935 (w), 885 (w), 835 (s) [$SiMe_3$], 762 (w), 730 (w), 716 (w), 685 (m), 662 (w), 641 (w), 622 (w), 608 (w), 591 (w), 565 (w), 554 (w), 525 (w), 488 (m), 462 (w), 436 (w), 416 (w).
^{1}H NMR (500.1 MHz, (D_6)benzene, 298 K): δ (ppm) = 0.23 (s, ^2J(^{29}Si-^{1}H) = 6.5 Hz, 18H, $C^{2,6}$-CH(Si*Me*$_3$)$_A$(SiMe$_3$)$_B$, Tbb), 0.25 (s, ^2J (^{29}Si-^{1}H) = 6.5 Hz, 18H, $C^{2,6}$-CH(SiMe$_3$)$_A$(Si*Me*$_3$)$_B$, Tbb), 1.32 (s, 9H, C^4-C*Me*$_3$, Tbb), 1.95 (s, 3H, C^4-*Me*, Mes$_X$, CNMes), 1.98 (s, 3H, C^4-*Me*, Mes$_Y$, CNMes), 2.31 (s, 15H, C_5*Me*$_5$), 2.40 (s, 6H, $C^{2,6}$-*Me*, Mes$_Y$, CNMes), 2.42 (s, 6H, $C^{2,6}$-*Me*, Mes$_X$, CNMes), 2.94 (s, ^2J(^{29}Si-^{1}H) = 9.8 Hz, 2H, $C^{2,6}$-C*H*(SiMe$_3$)$_2$, Tbb), 6.55 (s, 2H, $C^{3,5}$-*H*, Mes$_X$, CNMes), 6.58 (s, 2H, $C^{3,5}$-*H*, Mes$_Y$, CNMes), 6.89 (s, 2H, $C^{3,5}$-*H*, Tbb).
^{13}C{^{1}H} NMR (125.8 MHz, (D_6)benzene, 298 K): δ (ppm) = 0.82 (s, 6C, $C^{2,6}$-CH(Si*Me*$_3$)$_A$(SiMe$_3$)$_B$, Tbb), 0.84 (s, 6C, $C^{2,6}$-CH(SiMe$_3$)$_A$(Si*Me*$_3$)$_B$, Tbb), 13.6 (s, 5C, C_5*Me*$_5$), 19.3 (s, 2C, $C^{2,6}$-*Me*, Mes$_X$, CNMes), 19.4 (s, 2C, $C^{2,6}$-*Me*, Mes$_Y$, CNMes), 20.91 and 20.94 (each s, 1C each, 2 × C^4-*Me*, Mes$_{X,Y}$, 2 × CNMes), 30.9 (s, ^1J(^{29}Si-^{13}C) = 43 Hz, 2C, $C^{2,6}$-*C*H(SiMe$_3$)$_A$(SiMe$_3$)$_B$, Tbb), 31.4 (s, 3C, C^4-C*Me*$_3$, Tbb), 34.6 (s, 1C, C^4-

*C*Me$_3$, Tbb), 109.7 (s, 5C, *C*$_5$Me$_5$), 121.3 (s, 2C, *C*^{3,5}-H, Tbb), 126.1 (s, 1C, *C*^{1}, Mes$_X$, CNMes), 126.9 (s, 1C, *C*^{1}, Mes$_Y$, CNMes), 128.8 (s, 2C, *C*^{3,5}-H, Mes$_Y$, CNMes), 128.9 (s, 2C, *C*^{3,5}-H, Mes$_X$, CNMes), 132.6 (s, 2C, *C*^{2,6}, Mes$_Y$, CNMes), 133.6 (s, 2C, *C*^{2,6}, Mes$_X$, CNMes), 136.9 (s, 1C, *C*^{4}, Mes$_Y$, CNMes), 137.7 (s, 1C, *C*^{4}, Mes$_X$, CNMes), 144.2 (s, 2C, *C*^{2,6}-CH(SiMe$_3$)$_A$(SiMe$_3$)$_B$, Tbb), 150.5 (s, 1C, *C*^{4}-CMe$_3$, Tbb), 164.9 (s, 1C, *C*^{1}, Tbb), 204.4 and 207.8 (each s, 1C each, 2 × *C*NMes$_{X,Y}$), 290.4 (s, 2C, *C*O).

4.5.54. $Si_2Tbb_2(PMe_3)$ (51-Si)

A colorless stock solution (0.468 M in *n*-hexane) of PMe_3 (0.7 mL, 0.329 mmol, 1.05 equiv.) was added dropwise to a yellow solution of Si_2Tbb_2 (300 mg, 0.314 mmol, 1 equiv.) in 20 mL of *n*-hexane at ambient temperature. The color of the reaction solution immediately changed to dark orange. Analysis of an aliquot of the reaction solution by ^{1}H NMR and ^{31}P NMR spectroscopy in (D_6)benzene revealed the selective formation of **51-Si**. The reaction solution was concentrated up to 1/6th of the total volume and stored at −10 °C overnight. The fluffy feather like orange mass was crashed out, which were isolated by filtration at −10 °C and dried at ambient temperature for one hour to obtain **51-Si** as *n*-hexane hemi solvate **51-Si•0.5 C_6H_{14}**. Yield: 200 mg (0.186 mmol, 59 % from Si_2Tbb_2).

Attempts to obtain the solvate-free form upon drying of **51-Si•0.5 C_6H_{14}** in fine vacuum for 3 hrs. at ambient temperature or at 50 °C for 2 hrs. failed leading only to partial loss of *n*-hexane and extensive decomposition.

Properties: Compound **51-Si•0.5 C_6H_{14}** is a highly air-sensitive, orange-red solid, decolorizes immediately upon exposure to air. It is well soluble in *n*-hexane, diethyl ether, benzene and toluene at ambient temperature. Under strict exclusion of air, a solution of **51-Si** in (D_6)benzene shows no sign of decomposition after 12 hours at ambient temperature.

Elemental analysis: **51-Si•0.5 C_6H_{14}** ($C_{51}H_{107}PSi_{10}$•0.5 C_6H_{14}, 1075.31 g mol^{-1}): calcd./%: C 60.31, H 10.69; found/%: C 60.02, H 10.80; **Melting Point:** 147 °C (dec.).

^{1}H NMR (500.1 MHz, (D_6)benzene, 298 K): δ (ppm) = 0.36 (br s, $\Delta\nu_{1/2}$ = ca. 28.5 Hz, 72H, 2 × C^{2,6}-CH(Si*Me*$_3$)$_2$, Tbb$_{X,Y}$), 1.03 (d, ^2J (^{31}P-^{1}H) = 10.6 Hz, 9H, P*Me*$_3$), 1.37 (br s, $\Delta\nu_{1/2}$ = ca. 21 Hz, 9H, C^4-C*Me*$_3$, Tbb$_Y$), 1.44 (br s, $\Delta\nu_{1/2}$ = ca. 21 Hz, 9H, C^4-C*Me*$_3$, Tbb$_X$), 2.74 (br s, $\Delta\nu_{1/2}$ = ca. 13.5 Hz, 2H, C^{2,6}-C*H*(SiMe$_3$)$_2$, Tbb$_X$), 3.63 (br s, $\Delta\nu_{1/2}$ = ca. 13 Hz, 2H, C^{2,6}-C*H*(SiMe$_3$)$_2$, Tbb$_Y$), 6.88 (br s, $\Delta\nu_{1/2}$ = ca. 13.1 Hz, 2H, C^{3,5}-*H*, Tbb$_X$), 7.05 (br s, $\Delta\nu_{1/2}$ = ca. 13.4 Hz, 2H, C^{3,5}-*H*, Tbb$_Y$).

^{1}H NMR (500.1 MHz, (D_8)toluene, 298 K): δ (ppm) = 0.32 (br s, $\Delta\nu_{1/2}$ = ca. 12.6 Hz, 72H, 2 × $C^{2,6}$-CH(Si*Me*$_3$)$_2$, $Tbb_{X,Y}$), 1.06 (d, ^{2}J (^{31}P-^{1}H) = 10.5 Hz, 9H, P*Me*$_3$), 1.38 and 1.40 (each very br s, each 9H, 2 × C^{4}-C*Me*$_3$, $Tbb_{X,Y}$), 2.71 (br s, $\Delta\nu_{1/2}$ = ca. 13.5 Hz, 2H, $C^{2,6}$-C*H*(SiMe$_3$)$_2$, Tbb_X), 3.60 ($\Delta\nu_{1/2}$ = ca. 13 Hz, 2H, $C^{2,6}$-C*H*(SiMe$_3$)$_2$, Tbb_Y), 6.84 (very br s, 2H, $C^{3,5}$-*H*, Tbb_X), 7.02 (very br s, 2H, $C^{3,5}$-*H*, Tbb_Y).

^{1}H NMR (500.1 MHz, (D_8)toluene, 238 K): δ (ppm) = 0.29 (s, 18H, $C^{2,6}$-CH(Si*Me*$_3$)$_A$(SiMe$_3$)$_B$, Tbb_X), 0.35 (s, 18H, $C^{2,6}$-CH(Si*Me*$_3$)$_A$(SiMe$_3$)$_B$, Tbb_Y), 0.39 (s, 18H, $C^{2,6}$-CH(SiMe$_3$)$_A$(Si*Me*$_3$)$_B$, Tbb_Y), 0.40 (s, 18H, $C^{2,6}$-CH(SiMe$_3$)$_A$(Si*Me*$_3$)$_B$, Tbb_X), 0.97 (d, ^{2}J (^{31}P-^{1}H) = 11 Hz, 9H, P*Me*$_3$), 1.37 (s, 9H, C^{4}-C*Me*$_3$, Tbb_Y), 1.45 (s, 9H, C^{4}-C*Me*$_3$, Tbb_X), 2.77 (s, ^{2}J (^{29}Si-^{1}H) = 9 Hz, 2H, $C^{2,6}$-C*H*(SiMe$_3$)$_2$, Tbb_X), 3.62 (s, ^{2}J (^{29}Si-^{1}H) = 9 Hz, 2H, $C^{2,6}$-C*H*(SiMe$_3$)$_2$, Tbb_Y), 6.87 (s, 2H, $C^{3,5}$-*H*, Tbb_X), 7.07 (s, 2H, $C^{3,5}$-*H*, Tbb_Y).

^{31}P{^{1}H} NMR (202.5 MHz, (D_6)benzene, 298 K): δ (ppm) = –43.6 (s, ^{1}J (^{31}P-^{29}Si) = 233 Hz, *P*Me$_3$).

^{31}P{^{1}H} NMR (202.5 MHz, (D_8)toluene, 298 K): δ (ppm) = –43.6 (s, *P*Me$_3$).

^{31}P{^{1}H} NMR (202.5 MHz, (D_8)toluene, 238 K): δ (ppm) = –42.5 (s, ^{1}J (^{31}P-^{29}Si) = 224.5 Hz, *P*Me$_3$).

^{13}C{^{1}H} NMR (125.8 MHz, (D_6)benzene, 298 K): δ (ppm) = 1.7, 2.2, 2.5 and 3.4 (each very br s, each 6C, 2 × $C^{2,6}$-CH(Si*Me*$_3$)$_2$, $Tbb_{X,Y}$), 15.3 (d, ^{1}J (^{31}P-^{13}C) = 30.5 Hz, 3C, P*Me*$_3$), 31.4 (br s, $\Delta\nu_{1/2}$ = ca. 17.5 Hz, 3C, C^{4}-C*Me*$_3$, Tbb_X), 31.6 (br s, $\Delta\nu_{1/2}$ = ca. 13 Hz, 3C, C^{4}-C*Me*$_3$, Tbb_Y), 32.3 (br s, $\Delta\nu_{1/2}$ = ca. 15.4 Hz, 2C, $C^{2,6}$-*C*H(SiMe$_3$)$_2$, Tbb_X), 33.5 (br s, $\Delta\nu_{1/2}$ = ca. 14 Hz, 2C, $C^{2,6}$-*C*H(SiMe$_3$)$_2$, Tbb_Y), 34.2 and 34.4 (very br s, each 1C, 2 × C^{4}-*C*Me$_3$, $Tbb_{X,Y}$), 121.9 (br s, $\Delta\nu_{1/2}$ = ca. 11 Hz, 2C, $C^{3,5}$-H, Tbb_Y), 122.2 (br s, $\Delta\nu_{1/2}$ = ca. 12 Hz, 2C, $C^{3,5}$-H, Tbb_X), 132.9 (very br s, 1C, C^{1}, Tbb_Y), 145.6 (very br s, 1C, C^{1}, Tbb_X), 146.3 (br s, $\Delta\nu_{1/2}$ = ca. 7 Hz, 2C, $C^{2,6}$, Tbb_X), 147.5 (very br s, 1C, C^{4}, Tbb_X), 149.6 (very br s, 1C, C^{4}, Tbb_Y), 152.1 (br s, $\Delta\nu_{1/2}$ = ca. 12 Hz, 2C, $C^{2,6}$, Tbb_Y).

^{13}C{^{1}H} NMR (125.8 MHz, (D_8)toluene, 238 K): δ (ppm) = 1.4 (s, ^{1}J (^{29}Si-^{13}C) = 51 Hz, 6C, $C^{2,6}$-CH(Si*Me*$_3$)$_{A/B}$, Tbb_X), 1.9 (s, ^{1}J (^{29}Si-^{13}C) = 51 Hz, 6C, $C^{2,6}$-CH(Si*Me*$_3$)$_{A/B}$, Tbb_Y), 2.4 (s, ^{1}J (^{29}Si-^{13}C) = 51 Hz, 6C, $C^{2,6}$-CH(Si*Me*$_3$)$_{A/B}$, Tbb_Y), 3.3 (s, ^{1}J (^{29}Si-^{13}C) = 51 Hz, 6C, $C^{2,6}$-CH(Si*Me*$_3$)$_{A/B}$, Tbb_X), 14.67 (d, ^{1}J (^{31}P-^{13}C) = 31.6 Hz, 3C, P*Me*$_3$), 31.3 (s, 3C, C^{4}-C*Me*$_3$, Tbb_Y), 31.6 (s, 3C, C^{4}-C*Me*$_3$, Tbb_X), 31.8 (s, 2C, $C^{2,6}$-*C*H(SiMe$_3$)$_2$, Tbb_X), 33.0 (s, 2C, $C^{2,6}$-*C*H(SiMe$_3$)$_2$, Tbb_Y), 34.1 (s, 1C, C^{4}-*C*Me$_3$, Tbb_X), 34.4 (s, 1C, C^{4}-*C*Me$_3$, Tbb_Y), 121.6 (s, 2C, $C^{3,5}$-H, Tbb_Y), 122.0 (s, 2C, $C^{3,5}$-H, Tbb_X), 132.52 (d, ^{2}J (^{31}P-^{13}C) = 10.7 Hz, 1C, C^{1}, Tbb_Y), 145.48 (d, ^{3}J (^{31}P-^{13}C) = 7.7 Hz, 1C, C^{1}, Tbb_X), 145.9 (s, 2C, $C^{2,6}$, Tbb_X), 147.1 (s, 1C, C^{4}, Tbb_X), 149.34 (d, ^{5}J (^{31}P-^{13}C) = 1.7 Hz, 1C, C^{4}, Tbb_Y), 151.48 (d, ^{3}J (^{31}P-^{13}C) = 3.2 Hz, 2C, $C^{2,6}$, Tbb_Y).

^{29}Si{^{1}H} NMR (99.3 MHz, (D_6)benzene, 298 K): δ (ppm) = –7.4 (very br d, ^{1}J (^{31}P-^{29}Si) = ca. 235 Hz, 1Si, PMe_3-*Si*), 2.2 (very br, 8Si, 2 × C^{2,6}-CH(*Si*Me_3)$_2$, $Tbb_{X,Y}$), 268.8 (very br s, 1Si, PMe_3-Si*Si*Tbb).

^{29}Si{^{1}H} NMR (99.3 MHz, (D_8)toluene, 238 K): δ (ppm) = –6.3 (d, ^{1}J (^{31}P-^{29}Si) = 224.4 Hz, 1Si, PMe_3-*Si*), 0.5 (s, ^{1}J (^{29}Si-^{13}C) = 51 Hz, 2Si, C^{2,6}-CH(*Si*Me_3)$_{A/B}$, Tbb_Y), 1.3 (s, ^{1}J (^{29}Si-^{13}C) = 51 Hz, 2Si, C^{2,6}-CH(*Si*Me_3)$_{A/B}$, Tbb_X), 2.4 (s, ^{1}J (^{29}Si-^{13}C) = 51 Hz, 2Si, C^{2,6}-CH(*Si*Me_3)$_{A/B}$, Tbb_X), 4.9 (s, ^{1}J (^{29}Si-^{13}C) = 51 Hz, 2Si, C^{2,6}-CH(*Si*Me_3)$_{A/B}$, Tbb_Y), 265.0 (br d, ^{1}J (^{31}P-^{29}Si) = 7.7 Hz, 1Si, PMe_3-Si*Si*Tbb).

4.5.55. $Ge_2Tbb_2(PMe_3)$ (51-Ge)

A colorless stock solution (1 M in THF) of PMe_3 (0.72 mL, 0.72 mmol, 2.5 equiv.) was added to an orange-red solution of Ge_2Tbb_2 (300 mg, 0.29 mmol, 1 equiv.) in 15 mL of *n*-pentane at ambient temperature. The color of the reaction solution immediately changed to red-brown. Analysis of an aliquot of the reaction solution by ^{1}H NMR and ^{31}P NMR spectroscopy in (D_6)benzene revealed the selective formation of **51-Ge** along with little TbbH (ca. 4 mol%). The reaction solution was evaporated to dryness in vacuo. The red-brown mass obtained was dissolved in 6 mL of *n*-pentane and the solution was stored overnight at –30 °C. The compound **51-Ge** crystallized as dark red-brown crystals, which were isolated by filtration at –30 °C and dried in vacuo at ambient temperature for 30 minutes. Yield: 297 mg (0.26 mmol, 92 % from Ge_2Tbb_2).

Properties: Compound **51-Ge** is a highly air-sensitive, reddish-brown solid. It is well soluble in *n*-hexane, diethyl ether, benzene and toluene at ambient temperature giving reddish-brown solutions. Under strict exclusion of air, a solution of **51-Ge** in (D_6)benzene shows no signs of decomposition after 12 hours at ambient temperature.

Elemental analysis: 51-Ge ($C_{51}H_{107}Ge_2PSi_8$, 1121.27 g mol^{-1}): calcd./%: C 54.63, H 9.62; found/%: C 54.53, H 9.83; **Melting Point:** 165°C (dec.).

^{1}H NMR (500.1 MHz, (D_6)benzene, 298 K): δ (ppm) = 0.33 (s, 72H, 2 × C^{2,6}-CH(Si*Me$_3$*)$_2$, 2 × Tbb), 1.11 (d, ^{2}J (^{31}P-^{1}H) = 10 Hz, 9H, P*Me$_3$*), 1.39 (s, 18H, 2 × C^{4}-C*Me$_3$*, 2 × Tbb), 3.17 (br s, $\Delta\nu_{1/2}$ = ca. 37 Hz, 4H, 2 × C^{2,6}-C*H*($SiMe_3$)$_2$, 2 × Tbb), 6.96 (s, 4H, 2 × C^{3,5}-*H*, 2 × Tbb).

^{1}H NMR (300.1 MHz, (D_8)toluene, 213 K): δ (ppm) = 0.30 (s, 18H, C^{2,6}-CH(Si*Me$_3$*)$_A$($SiMe_3$)$_B$, Tbb_Y), 0.37 (s, 18H, C^{2,6}-CH(Si*Me$_3$*)$_A$($SiMe_3$)$_B$, Tbb_X), 0.38 (s, 18H, C^{2,6}-CH($SiMe_3$)$_A$(Si*Me$_3$*)$_B$, Tbb_X), 0.41 (s, 18H, C^{2,6}-CH($SiMe_3$)$_A$(Si*Me$_3$*)$_B$, Tbb_Y), 1.01 (d, ^{2}J (^{31}P-^{1}H) = 11 Hz, 9H, P*Me$_3$*), 1.38 (s, 9H, C^{4}-C*Me$_3$*, Tbb_X), 1.46 (s, 9H, C^{4}-C*Me$_3$*, Tbb_Y), 2.95 (s, 2H, ^{2}J (^{29}Si-^{1}H) = 9.2 Hz, C^{2,6}-C*H*($SiMe_3$)$_A$($SiMe_3$)$_B$, Tbb_Y), 3.53 (s, 2H,

^{2}J (^{29}Si-^{1}H) = 8.8 Hz, C^{2,6}-C*H*(SiMe$_3$)$_A$(SiMe$_3$)$_B$, Tbb$_X$), 6.89 (s, 2H, C^{3,5}-*H*, Tbb$_Y$), 7.07 (s, 2H, C^{3,5}-*H*, Tbb$_X$).

^{31}P{^{1}H} NMR (202.5 MHz, (D$_6$)benzene, 298 K): δ (ppm) = –27.0 (brs, $\Delta\nu_{1/2}$ = ca. 169 Hz, *P*Me$_3$).

^{31}P{^{1}H} NMR (121.5 MHz, (D$_8$)toluene, 213 K): δ (ppm) = –24.0 (s, *P*Me$_3$).

^{13}C{^{1}H} NMR (125.8 MHz, (D$_6$)benzene, 298 K): δ (ppm) = 2.2 (s, 24C, 2 × C^{2,6}-CH(Si*Me$_3$*)$_2$, 2 × Tbb), 16.1 (d, ^{1}J (^{31}P-^{13}C) = 23 Hz, 3C, P*Me$_3$*), 31.5 (s, 6C, 2 × C^{4}-C*Me$_3$*, 2 × Tbb), 33.3 (br s, $\Delta\nu_{1/2}$ = ca. 17 Hz, 4C, 2 × C^{2,6}-*C*H(SiMe$_3$)$_2$, 2 × Tbb), 34.3 (s, 2C, 2 × C^{4}-*C*Me$_3$, 2 × Tbb), 121.8 (s, 4C, 2 × *C^{3,5}*-H, 2 × Tbb), 148.5 (br s, $\Delta\nu_{1/2}$ = ca. 14 Hz, 2C, *2* × *C^{4}*, 2 × Tbb), 148.8 (br s, 2C, 2 × *C^{1}*, 2 × Tbb); **the C^{2,6} signal of Tbb was not observed.

^{13}C{^{1}H} NMR (75.5 MHz, (D$_8$)toluene, 213 K): δ (ppm) = 1.1 (s, 6C, C^{2,6}-CH(Si*Me$_3$*)$_A$(SiMe$_3$)$_B$, Tbb$_Y$), 1.7 (s, 6C, C^{2,6}-CH(Si*Me$_3$*)$_A$(SiMe$_3$)$_B$, Tbb$_X$), 2.2 (s, 6C, C^{2,6}-CH(SiMe$_3$)$_A$(Si*Me$_3$*)$_B$, Tbb$_X$), 2.9 (s, 6C, C^{2,6}-CH(SiMe$_3$)$_A$(Si*Me$_3$*)$_B$, Tbb$_Y$), 15.2 (d, ^{1}J (^{31}P-^{13}C) = 26 Hz, 3C, P*Me$_3$*), 31.3 (s, 3C, C^{4}-C*Me$_3$*, Tbb$_X$), 31.5 (s, 3C, C^{4}-C*Me$_3$*, Tbb$_Y$), 31.7 (s, 2C, C^{2,6}-*C*H(SiMe$_3$)$_A$(SiMe$_3$)$_B$, Tbb$_Y$), 33.1 (s, 2C, C^{2,6}-*C*H(SiMe$_3$)$_A$(SiMe$_3$)$_B$, Tbb$_X$), 34.0 (s, 1C, C^{4}-*C*Me$_3$, Tbb$_Y$), 34.2 (s, 1C, C^{4}-*C*Me$_3$, Tbb$_X$), 121.2 (s, 2C, *C^{3,5}*-H, Tbb$_X$), 121.7 (s, 2C, *C^{3,5}*-H, Tbb$_Y$), 142.0 (d, 1C, ^{2}J (^{31}P-^{13}C) = 1 Hz, *C^{1}*, Tbb$_X$), 147.0 (s, 2C, *C^{2,6}*-CH(SiMe$_3$)$_A$(SiMe$_3$)$_B$, Tbb$_Y$), 147.1 (s, 1C, *C^{4}*-CMe$_3$, Tbb$_Y$), 148.7 (d, 1C, ^{5}J (^{31}P-^{13}C) = 2 Hz, *C^{4}*-CMe$_3$, Tbb$_X$), 149.8 (d, 2C, ^{3}J (^{31}P-^{13}C) = 4 Hz, *C^{2,6}*-CH(SiMe$_3$)$_A$(SiMe$_3$)$_B$, Tbb$_X$), 152.7 (d, 1C, ^{3}J (^{31}P-^{13}C) = 8 Hz, *C^{1}*, Tbb$_Y$).

4.5.56. Tbb(Me)SiSi(AlMe$_2$)Tbb (52-Si)

To a golden yellow solution of Si$_2$Tbb$_2$ (300 mg, 0.314 mmol, 1 equiv.) in 6 mL of *n*-pentane, a stock solution (2 M in toluene) of AlMe$_3$ (0.16 mL, 0.314 mmol, 1 equiv.) was added dropwise at ambient temperature. The colour of the reaction solution was immediately changed to lemon yellow. After 5 min of stirring at ambient temperature, an aliquot of the reaction solution was analyzed by ^{1}H NMR spectroscopy, revealing the complete consumption of Si$_2$Tbb$_2$ and the selective formation of **52-Si**. The reaction solution was concentrated to half of its volume in vacuum and stored at –30 °C overnight. The yellow crystals of **52-Si** were isolated by filtration at –30 °C followed by drying at 50 °C for 1 hour in fine vacuum. Yield: 140 mg (0.136 mmol, 43 % from Si$_2$Tbb$_2$).

Properties: Compound **52-Si** is moderately air-sensitive, lemon yellow solid that is well soluble in *n*-hexane, diethyl ether, benzene and toluene at ambient temperature.

Under strict exclusion of air, a sample solution of **52-Si** in (D_6)benzene does not show any sign of decomposition after 2 days at ambient temperature.

Elemental analysis: 52-Si ($C_{51}H_{107}AlSi_{10}$, 1028.23 g mol^{-1}): calcd./%: C 59.57, H 10.49; found/%: C 59.83, H 10.61; **Melting Point:** 166 °C (dec.).

^{1}H NMR (500.1 MHz, (D_6)benzene, 298 K): δ (ppm) = –0.22 (s, 6H, Al*Me*$_2$), 0.13 (s, ^2J (^{29}Si-^{1}H) = 6 Hz, 18H, C^{2,6}-CH(Si*Me*$_3$)$_A$(SiMe$_3$)$_B$, Tbb$_X$), 0.24 (s, 18H, C^{2,6}-CH(Si*Me*$_3$)$_A$(SiMe$_3$)$_B$, Tbb$_Y$), 0.33 (s, 18H, C^{2,6}-CH(SiMe$_3$)$_A$(Si*Me*$_3$)$_B$, Tbb$_Y$), 0.45 (s, ^2J (^{29}Si-^{1}H) = 6 Hz, 18H, C^{2,6}-CH(SiMe$_3$)$_A$(Si*Me*$_3$)$_B$, Tbb$_X$), 1.14 (s, ^2J (^{29}Si-^{1}H) = 6 Hz, ^3J (^{29}Si-^{1}H) = 4.5 Hz, 3H, TbbSi*Me*), 1.32 (s, 9H, C^4-C*Me*$_3$, Tbb$_X$), 1.37 (s, 9H, C^4-C*Me*$_3$, Tbb$_Y$), 2.88 (s, ^2J (^{29}Si-^{1}H) = 9 Hz, 2H, C^{2,6}-C*H*(SiMe$_3$)$_{A,B}$, Tbb$_X$), 3.29 (s, ^2J (^{29}Si-^{1}H) = 9 Hz, 2H, C^{2,6}-C*H*(SiMe$_3$)$_{A,B}$, Tbb$_Y$), 6.98 (s, 2H, C^{3,5}-*H*, Tbb$_X$), 6.99 (s, 2H, C^{3,5}-*H*, Tbb$_Y$).
^{13}C{^{1}H} NMR (125.8 MHz, (D_6)benzene, 298 K): δ (ppm) = 0.0 (br s, $\Delta\nu_{1/2}$ = ca. 5.5 Hz, 2C, Al*Me*$_2$), 1.4 (s, 6C, C^{2,6}-CH(Si*Me*$_3$)$_A$(SiMe$_3$)$_B$, Tbb$_X$), 1.7 (s, 6C, C^{2,6}-CH(Si*Me*$_3$)$_A$(SiMe$_3$)$_B$, Tbb$_Y$), 2.0 (s, 6C, C^{2,6}-CH(SiMe$_3$)$_A$(Si*Me*$_3$)$_B$, Tbb$_Y$), 3.1 (s, 6C, C^{2,6}-CH(SiMe$_3$)$_A$(Si*Me*$_3$)$_B$, Tbb$_X$), 6.8 (s, ^1J (^{29}Si-^{13}C) = 36.6 Hz, 1C, TbbSi*Me*), 31.26 (s, 3C, C^4-C*Me*$_3$, Tbb$_X$), 31.33 (s, 3C, C^4-C*Me*$_3$, Tbb$_Y$), 33.5 (s, ^1J (^{29}Si-^{13}C) = 42 Hz, 2C, C^{2,6}-*C*H(SiMe$_3$)$_{A,B}$, Tbb$_X$), 34.0 (s, ^1J (^{29}Si-^{13}C) = 42 Hz, 2C, C^{2,6}-*C*H(SiMe$_3$)$_{A,B}$, Tbb$_Y$), 34.3 and 34.6 (each s, 2C, 2 × C^4-*C*Me$_3$, Tbb$_{X,Y}$), 121.8 and 122.0 (each s, 4C, 2 × *C*^{3,5}-H, Tbb$_{X,Y}$), 130.8 (s, 1C, *C*^{1}, Tbb$_Y$), 133.6 (s, 1C, *C*^{1}, Tbb$_X$), 149.3 (s, 1C, *C*^{4}, Tbb$_Y$), 150.2 (s, 2C, *C*^{2,6}, Tbb$_X$), 151.0 (s, 2C, *C*^{2,6}, Tbb$_Y$), 151.6 (s, 1C, *C*^{4}, Tbb$_X$).
^{29}Si{^{1}H} NMR (99.3 MHz, (D_6)benzene, 298 K): δ (ppm) = 2.0 (br s, $\Delta\nu_{1/2}$ = 5 Hz, 2Si, C^{2,6}-CH(*Si*Me$_3$)$_A$(SiMe$_3$)$_B$, Tbb$_Y$), 2.2 (br s, $\Delta\nu_{1/2}$ = 4 Hz, 2Si, C^{2,6}-CH(SiMe$_3$)$_A$(*Si*Me$_3$)$_B$, Tbb$_Y$), 2.6 (s, 4Si, C^{2,6}-CH(*Si*Me$_3$)$_{A,B}$, Tbb$_X$), 45.8 (br s, $\Delta\nu_{1/2}$ = ca. 10.8 Hz, 1Si, *Si*AlMe$_2$), 145.0 (s, 1Si, TbbSi*Me*).

5. Appendices

5.1. List of Synthesized compounds

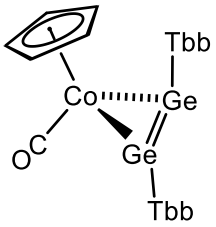

1-Co

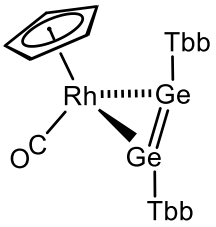

1-Rh

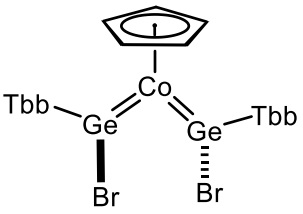

2-Co

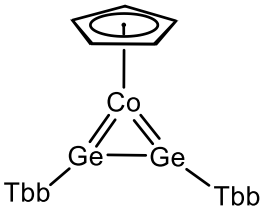

3-Co

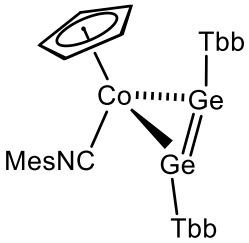

4-Co

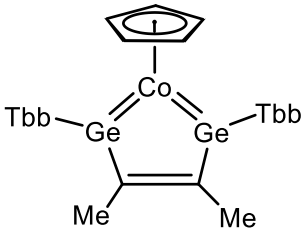

5-Co

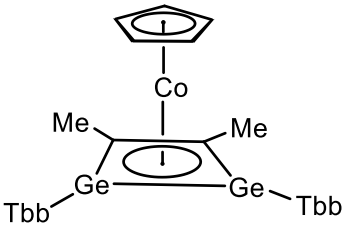

6-Co

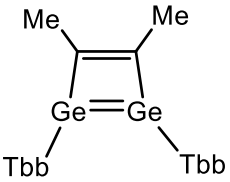

7-Ge

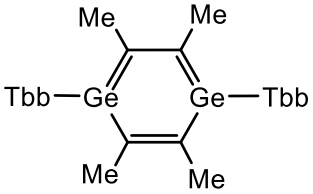

8-Ge

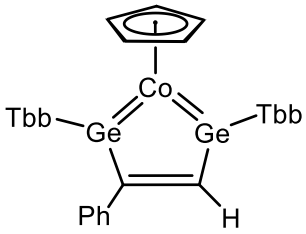

9-Co

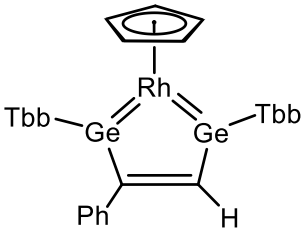

9-Rh

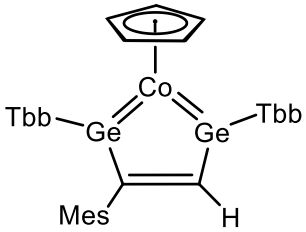

10-Co

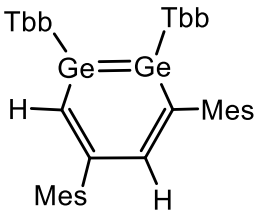

11-Ge

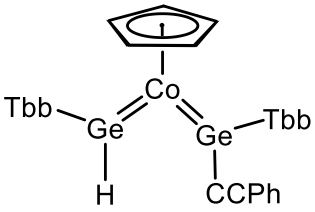

12-Co

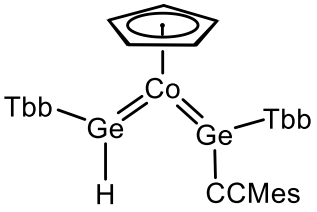

13-Co

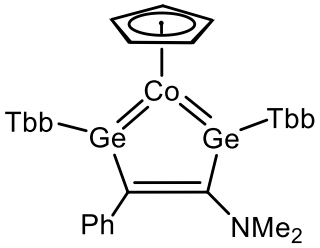

14-Co

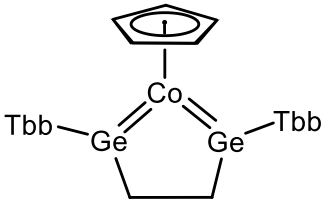

15-Co

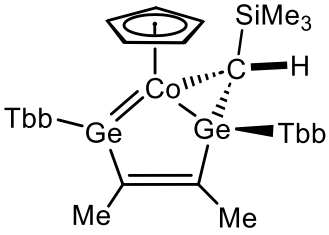

16-Co

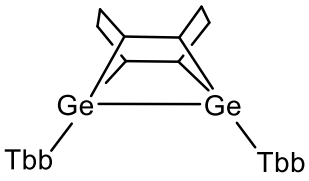

17-Ge

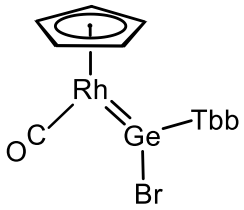

18-Rh

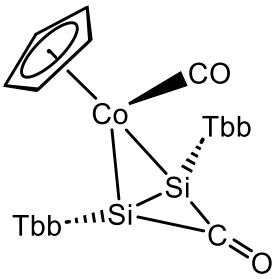

19-Co

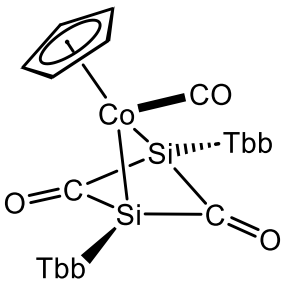

20-Co

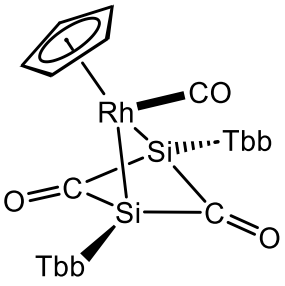

20-Rh

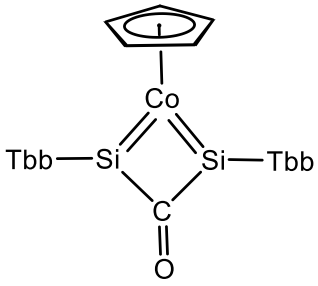

21-Co

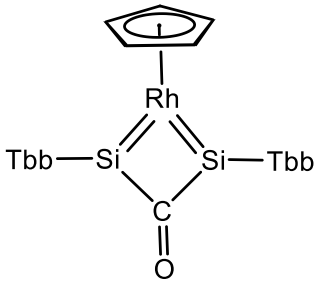

21-Rh

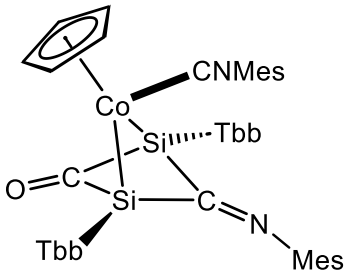

22-Co

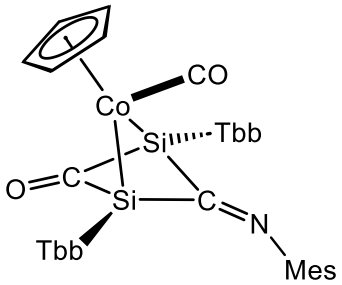

23-Co

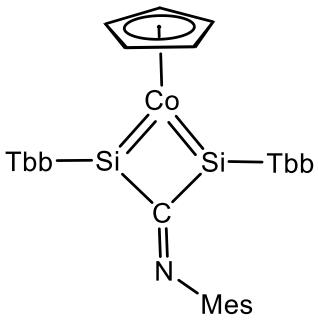

24-Co

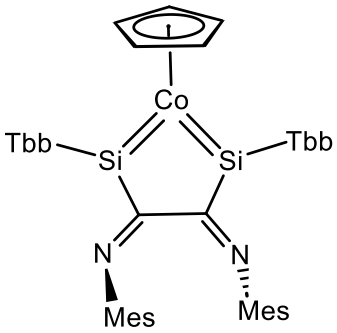

25-Co

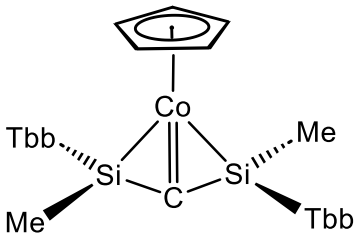

26-Co

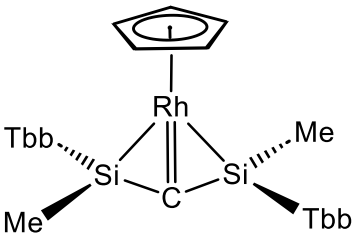

26-Rh

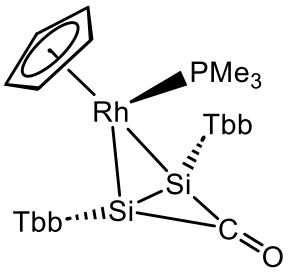

27-Rh

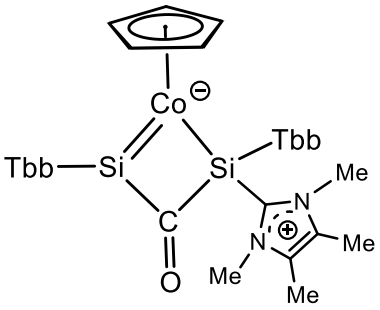

28-Co

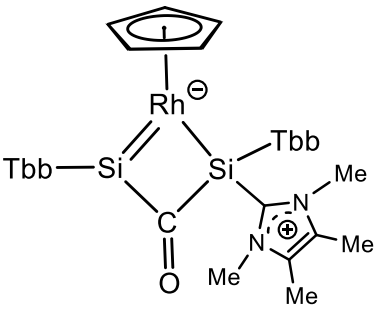

28-Rh

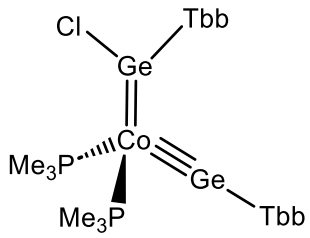

29-Co

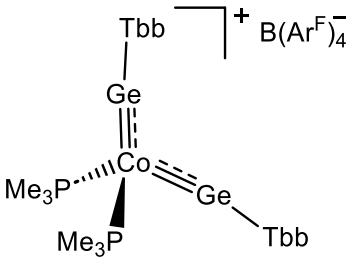

30-Co

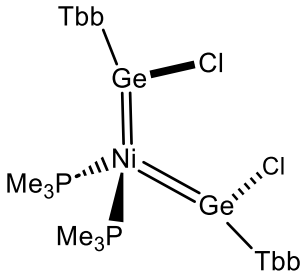

31-Ni

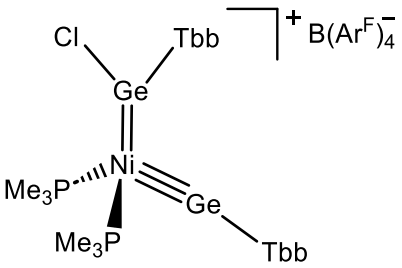

32-Ni

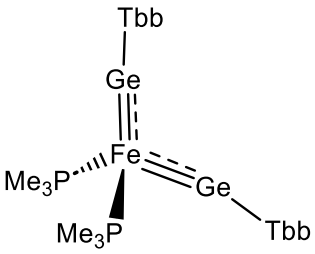

33-Fe

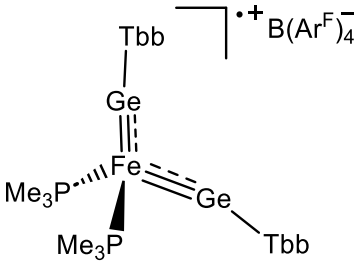

34-Fe

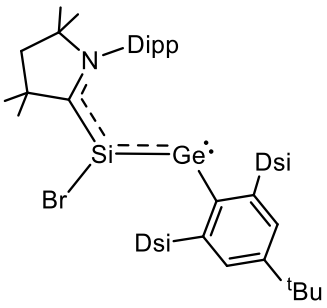

35-Si

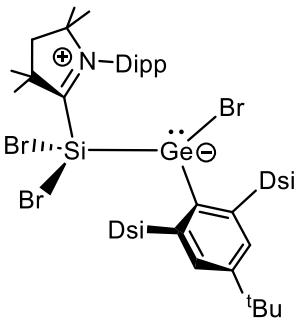

36-Si

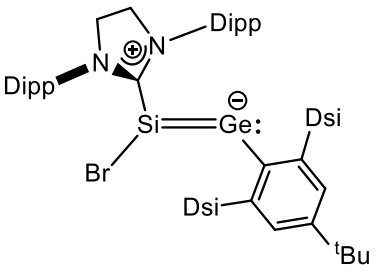

37-Si

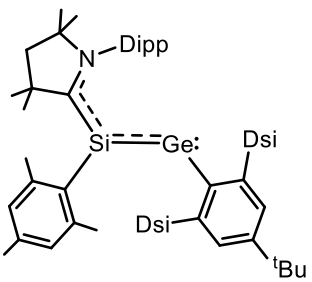

38-Si

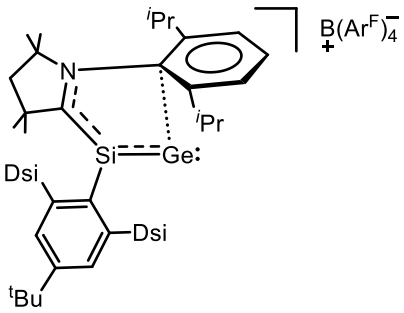

39-Si

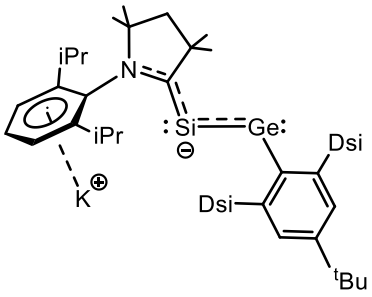

40-Si

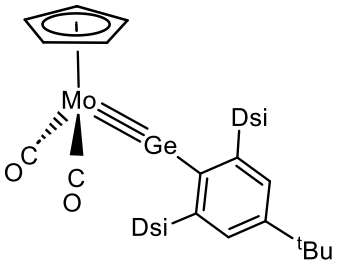

41-Mo

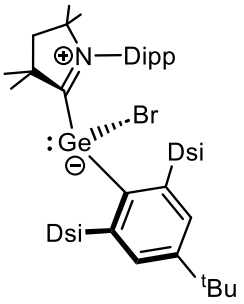

42-Ge

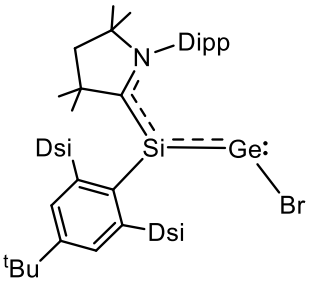

43-Si

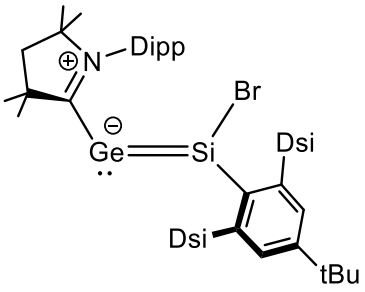

44-Si

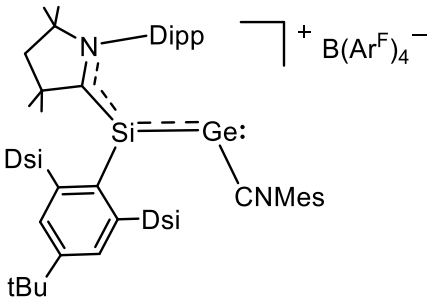

45-Si

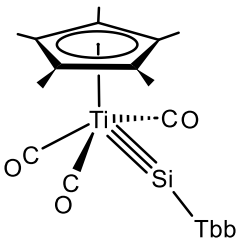

46-Ti

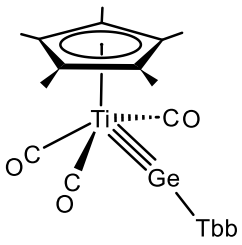

47-Ti

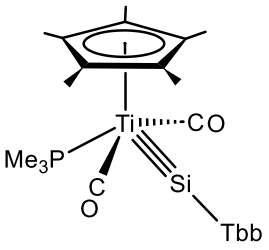

48-Ti

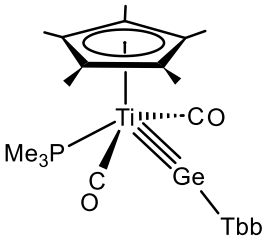

49-Ti

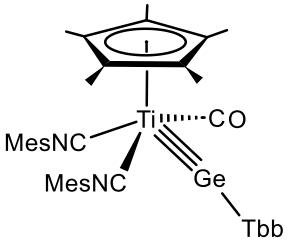

50-Ti

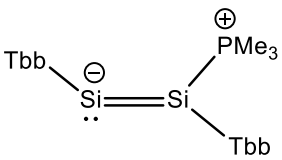

51-Si

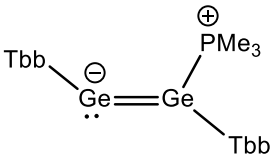

51-Ge

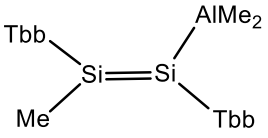

52-Si

5.2. Crystallographic data of synthesized compounds

Table 9. Crystal data and structure refinement parameters of [CpCo(CO)Ge_2Tbb_2] (**1-Co**) and [CpRh(CO)Ge_2Tbb_2] (**1-Rh**).

	1-Co	**1-Rh**
Crystal Habitus	clear dark brown block	clear green block
Device Type	Bruker X8-KappaApexII	Bruker D8 Venture
Empirical formula	$C_{58}H_{113}CoGe_2O_2Si_8$	$C_{58}H_{113}Ge_2O_2RhSi_8$
Moiety formula	$C_{54}H_{103}CoGe_2OSi_8$, $C_4H_{10}O$	$C_{54}H_{103}Ge_2ORhSi_8$, $C_4H_{10}O$
Formula weight	1271.31	1315.29
Temperature/K	100	100
Crystal system	monoclinic	monoclinic
Space group	$P2_1/c$	$P2_1/c$
a/Å	17.2923(8)	17.2739(11)
b/Å	12.4200(6)	12.5345(8)
c/Å	33.4736(16)	33.483(2)
α/°	90	90
β/°	100.1254(15)	100.146(2)
γ/°	90	90
Volume/Å^3	7077.2(6)	7136.4(8)
Z	4	4
ρ_{calc}g/cm^3	1.193	1.224
μ/mm^{-1}	1.246	4.391
F(000)	2720.0	2792.0
Crystal size/mm^3	0.18 × 0.09 × 0.08	0.32 × 0.28 × 0.12
Absorption correction	empirical	multi-scan
Tmin; Tmax	0.6446; 0.7462	0.6550; 0.7461
Radiation	MoKα (λ = 0.71073)	CuKα (λ = 1.54178)
2Θ range for data collection/°	3.504 to 55.998°	7.546 to 145.106°
Completeness to theta	0.998	0.999
Index ranges	-22 ≤ h ≤ 22, -16 ≤ k ≤ 16, -44 ≤ l ≤ 44	-21 ≤ h ≤ 21, -15 ≤ k ≤ 15, -41 ≤ l ≤ 41
Reflections collected	154198	137642
Independent reflections	17062 [R_{int} = 0.0348, R_{sigma} = 0.0182]	14146 [R_{int} = 0.0329, R_{sigma} = 0.0228]
Data/restraints/parameters	17062/103/734	14146/810/768
Goodness-of-fit on F^2	1.028	1.065
Final R indexes [I>=2σ (I)]	R_1 = 0.0424, wR_2 = 0.1111	R_1 = 0.0437, wR_2 = 0.1076
Final R indexes [all data]	R_1 = 0.0482, wR_2 = 0.1152	R_1 = 0.0438, wR_2 = 0.1076
Largest diff. peak/hole / e Å^{-3}	1.97/-1.16	1.69/-1.29

Table 10. Crystal data and structure refinement parameters of [CpCo(GeBrTbb)$_2$] (**2-Co**) and [CpCo(Ge$_2$Tbb$_2$)] (**3-Co**).

	2-Co	**3-Co**
Crystal Habitus	clear orangish brown plate	clear brown plate
Device Type	Bruker X8-KappaApexII	Bruker X8-KappaApexII
Empirical formula	$C_{53}H_{103}Si_8CoGe_2Br_2$	$C_{53}H_{103}Si_8CoGe_2$
Moiety formula	$C_{53}H_{103}Br_2CoGe_2Si_8$	$C_{53}H_{103}CoGe_2Si_8$
Formula weight	1329.00	1169.18
Temperature/K	100.0	100
Crystal system	triclinic	monoclinic
Space group	P-1	$P2_1/c$
a/Å	13.1912(10)	12.7213(8)
b/Å	17.1939(16)	30.8609(16)
c/Å	17.8012(16)	18.1568(11)
α/°	103.922(2)	90
β/°	110.594(2)	109.078(2)
γ/°	102.759(3)	90
Volume/Å^3	3454.9(5)	6736.7(7)
Z	2	4
ρ_{calc}g/cm^3	1.278	1.153
μ/mm^{-1}	2.427	1.302
F(000)	1388.0	2496.0
Crystal size/mm^3	0.6 × 0.2 × 0.02	0.19 × 0.18 × 0.06
Absorption correction	empirical	empirical
Tmin; Tmax	0.5124; 0.7460	0.5431; 0.7461
Radiation	MoKα (λ = 0.71073)	MoKα (λ = 0.71073)
2Θ range for data collection/°	4.4 to 50.5°	4.91 to 55.998°
Completeness to theta	0.978	0.998
Index ranges	-15 ≤ h ≤ 13, -20 ≤ k ≤ 20, -21 ≤ l ≤ 21	-16 ≤ h ≤ 16, -40 ≤ k ≤ 40, -23 ≤ l ≤ 23
Reflections collected	27514	127077
Independent reflections	12241 [R_{int} = 0.0660, R_{sigma} = 0.0964]	16250 [R_{int} = 0.0604, R_{sigma} = 0.0370]
Data/restraints/parameters	12241/0/625	16250/54/638
Goodness-of-fit on F^2	0.996	1.031
Final R indexes [I>=2σ (I)]	R_1 = 0.0448, wR_2 = 0.0890	R_1 = 0.0415, wR_2 = 0.0885
Final R indexes [all data]	R_1 = 0.0801, wR_2 = 0.1014	R_1 = 0.0559, wR_2 = 0.0952
Largest diff. peak/hole / e Å^{-3}	0.97/-0.60	1.71/-0.77

Table 11. Crystal data and structure refinement parameters of [CpCo(MesNC)Ge_2Tbb$_2$] (**4-Co**) and [CpCo(Ge_2Tbb$_2$$C_2$$Me_2$)] (**5-Co**).

	4-Co	**5-Co**
Crystal Habitus	clear orangish brown plate	clear green plate
Device Type	Bruker D8 Venture	Bruker D8 Venture
Empirical formula	$C_{63}H_{114}CoGe_2NSi_8$	$C_{126}H_{246}Co_2Ge_4NO_{2.5}Si_{16}$
Moiety formula	$C_{63}H_{114}CoGe_2NSi_8$	2($C_{57}H_{109}CoGe_2Si_8$), 2.5($C_4H_{10}O$), C_2H_3N
Formula weight	1314.38	2672.88
Temperature/K	100.0	100.0
Crystal system	monoclinic	triclinic
Space group	$P2_1/n$	P-1
a/Å	17.1360(8)	12.3115(3)
b/Å	12.3899(6)	17.8208(5)
c/Å	35.5637(18)	19.4041(5)
α/°	90	66.525(2)
β/°	98.110(3)	79.764(2)
γ/°	90	87.291(2)
Volume/Å^3	7475.1(6)	3841.46(18)
Z	4	1
ρ_{calc}g/cm^3	1.168	1.155
μ/mm^{-1}	4.144	4.048
F(000)	2808.0	1435.0
Crystal size/mm^3	0.32 × 0.3 × 0.01	0.24 × 0.09 × 0.03
Absorption correction	empirical	empirical
Tmin; Tmax	0.5397; 0.7536	0.4938; 0.7536
Radiation	CuKα (λ = 1.54178)	CuKα (λ = 1.54178)
2Θ range for data collection/°	5.02 to 139.998°	5.042 to 135.5°
Completeness to theta	0.999	0.999
Index ranges	-20 ≤ h ≤ 20, -15 ≤ k ≤ 15, -43 ≤ l ≤ 43	-14 ≤ h ≤ 14, -21 ≤ k ≤ 21, -23 ≤ l ≤ 23
Reflections collected	113703	137356
Independent reflections	14157 [R_{int} = 0.0838, R_{sigma} = 0.0491]	13926 [R_{int} = 0.0862, R_{sigma} = 0.0398]
Data/restraints/parameters	14157/762/737	13926/160/776
Goodness-of-fit on F^2	1.182	1.043
Final R indexes [I>=2σ (I)]	R_1 = 0.1056, wR_2 = 0.2429	R_1 = 0.0515, wR_2 = 0.1242
Final R indexes [all data]	R_1 = 0.1123, wR_2 = 0.2455	R_1 = 0.0669, wR_2 = 0.1348
Largest diff. peak/hole / e Å^{-3}	1.48/-1.49	1.52/-1.36

Table 12. Crystal data and structure refinement parameters of [CpCo($Ge_2Tbb_2C_2Me_2$)cbd] (**6-Co**) and ($Ge_2Tbb_2C_2Me_2$) (**7-Ge**).

	6-Co	**7-Ge**
Crystal Habitus	clear brown plate	clear green plate
Device Type	STOE IPDS-2T	Bruker X8-KappaApexII
Empirical formula	$C_{57}H_{109}CoGe_2Si_8$	$C_{52}H_{104}Si_8Ge_2$
Moiety formula	$C_{57}H_{109}CoGe_2Si_8$	$C_{52}H_{104}Ge_2Si_8$
Formula weight	1223.27	1099.25
Temperature/K	123(2)	100
Crystal system	monoclinic	orthorhombic
Space group	$P2_1/c$	Pbca
a/Å	12.9794(6)	16.6046(9)
b/Å	31.6336(13)	25.1885(13)
c/Å	17.9064(8)	31.4036(17)
α/°	90	90
β/°	108.135(3)	90
γ/°	90	90
Volume/$Å^3$	6986.9(5)	13134.4(12)
Z	4	8
$\rho_{calc}g/cm^3$	1.163	1.112
μ/mm^{-1}	1.258	1.090
F(000)	2616.0	4736.0
Crystal size/mm^3	0.18 × 0.15 × 0.04	0.16 × 0.14 × 0.06
Absorption correction	integration	empirical
Tmin; Tmax	0.7255; 0.9371	0.5606; 0.7461
Radiation	MoKα (λ = 0.71073)	MoKα (λ = 0.71073)
2Θ range for data collection/°	5.064 to 51.988°	5.59 to 56°
Completeness to theta	0.974	0.997
Index ranges	-11 ≤ h ≤ 16, -31 ≤ k ≤ 38, -22 ≤ l ≤ 15	-21 ≤ h ≤ 21, -33 ≤ k ≤ 33, -41 ≤ l ≤ 41
Reflections collected	30805	106131
Independent reflections	13316 [R_{int} = 0.0923, R_{sigma} = 0.1892]	15808 [R_{int} = 0.0477, R_{sigma} = 0.0310]
Data/restraints/parameters	13316/1636/807	15808/7/591
Goodness-of-fit on F^2	0.904	1.030
Final R indexes [I>=2σ (I)]	R_1 = 0.0870, wR_2 = 0.2004	R_1 = 0.0330, wR_2 = 0.0759
Final R indexes [all data]	R_1 = 0.1779, wR_2 = 0.2343	R_1 = 0.0472, wR_2 = 0.0816
Largest diff. peak/hole / e $Å^{-3}$	1.33/-1.07	0.78/-0.29

Table 13. Crystal data and structure refinement parameters of ($Ge_2Tbb_2C_2Me_2$) (**8-Ge**) and [$CpCo(Ge_2Tbb_2C_2HPh)$] (**9-Co**).

	8-Ge	**9-Co**
Crystal Habitus	clear orange block	clear dark green plate
Device Type	Bruker X8-KappaApexII	STOE IPDS-2T
Empirical formula	$C_{62}H_{124}Ge_2Si_8$	$C_{61}H_{109}CoGe_2Si_8$
Moiety formula	$C_{56}H_{110}Ge_2Si_8$, C_6H_{14}	$C_{61}H_{109}CoGe_2Si_8$
Formula weight	1239.50	1271.31
Temperature/K	100	123(2)
Crystal system	monoclinic	triclinic
Space group	$P2_1/n$	P-1
a/Å	10.5997(4)	13.0993(6)
b/Å	20.6965(8)	17.5083(7)
c/Å	17.4013(7)	17.8754(8)
α/°	90	97.647(3)
β/°	105.9819(12)	105.809(3)
γ/°	90	109.057(3)
Volume/Å^3	3669.9(2)	3615.6(3)
Z	2	2
ρ_{calc}g/cm^3	1.122	1.168
μ/mm^{-1}	0.983	1.218
F(000)	1344.0	1356.0
Crystal size/mm^3	0.18 × 0.17 × 0.16	0.3 × 0.14 × 0.06
Absorption correction	empirical	integration
Tmin; Tmax	0.6681; 0.7462	0.7794; 0.8867
Radiation	MoKα (λ = 0.71073)	MoKα (λ = 0.71073)
2Θ range for data collection/°	5.252 to 55.998°	5.492 to 56°
Completeness to theta	0.998	0.988
Index ranges	-14 ≤ h ≤ 14, -27 ≤ k ≤ 27, -22 ≤ l ≤ 22	-17 ≤ h ≤ 17, -22 ≤ k ≤ 23, -23 ≤ l ≤ 23
Reflections collected	76965	35466
Independent reflections	8821 [R_{int} = 0.0367, R_{sigma} = 0.0185]	17253 [R_{int} = 0.0859, R_{sigma} = 0.1481]
Data/restraints/parameters	8821/24/364	17253/41/700
Goodness-of-fit on F^2	1.039	0.783
Final R indexes [I>=2σ (I)]	R_1 = 0.0354, wR_2 = 0.0982	R_1 = 0.0499, wR_2 = 0.0952
Final R indexes [all data]	R_1 = 0.0418, wR_2 = 0.1031	R_1 = 0.1126, wR_2 = 0.1079
Largest diff. peak/hole / e Å^{-3}	1.02/-0.75	0.90/-1.14

Table 14. Crystal data and structure refinement parameters of [CpRh($Ge_2Tbb_2C_2HPh$)] (**9-Rh**) and [CpCo($Ge_2Tbb_2C_2HMes$)] (**10-Co**).

	9-Rh	**10-Co**
Crystal Habitus	clear greenish brown planks	clear bluish green plates
Device Type	Stadivari	STOE STADIVARI
Empirical formula	$C_{61}H_{109}Ge_2RhSi_8$	$C_{64}H_{115}CoGe_2Si_8$
Moiety formula	$C_{61}H_{109}Ge_2RhSi_8$	$C_{64}H_{115}CoGe_2Si_8$
Formula weight	1315.33	1313.38
Temperature/K	100	100
Crystal system	triclinic	monoclinic
Space group	P-1	$P2_1/c$
a/Å	13.0890(4)	27.4671(10)
b/Å	17.5207(6)	13.3895(4)
c/Å	18.0398(6)	20.8522(7)
α/°	97.468(3)	90
β/°	105.941(3)	100.778(3)
γ/°	109.023(3)	90
Volume/$Å^3$	3649.41(22)	7533.5(4)
Z	2	4
$\rho_{calc}g/cm^3$	1.197	1.158
μ/mm^{-1}	4.27	4.108
F(000)	1392.0	2808.0
Crystal size/mm^3	0.48 × 0.193 × 0.02	0.4 × 0.177 × 0.01
Absorption correction	multi-scan	multi-scan
Tmin; Tmax	0.2035; 0.2680	0.6116; 0.7793
Radiation	CuKα (λ = 1.54186)	Cu Kα (λ = 1.54186)
2Θ range for data collection/°	7.498 to 142.704°	7.888 to 141.414°
Completeness to theta	0.994	0.995
Index ranges	-15 ≤ h ≤ 12, -21 ≤ k ≤ 20, -21 ≤ l ≤ 21	-33 ≤ h ≤ 32, -16 ≤ k ≤ 7, -25 ≤ l ≤ 24
Reflections collected	123922	70497
Independent reflections	13696 [R_{int} = 0.0983, R_{sigma} = 0.0428]	14181 [R_{int} = 0.0986, R_{sigma} = 0.0741]
Data/restraints/parameters	13696/46/719	14181/702/740
Goodness-of-fit on F^2	1.033	1.047
Final R indexes [I>=2σ (I)]	R_1 = 0.0696, wR_2 = 0.1744	R_1 = 0.0778, wR_2 = 0.1757
Final R indexes [all data]	R_1 = 0.0924, wR_2 = 0.1962	R_1 = 0.1235, wR_2 = 0.2034
Largest diff. peak/hole / e $Å^{-3}$	2.70/-1.48	1.78/-0.84

Table 15. Crystal data and structure refinement parameters of ($Ge_2Tbb_2C_4H_2Mes_2$) (**11-Ge**) and [CpCo{(GeHTbb)(GeCCMesTbb)}] (**12-Co**).

	11-Ge	**12-Co**
Crystal Habitus	clear yellowish orange plate	clear orangish brown plate
Device Type	STOE STADIVARI	STOE IPDS-2T
Empirical formula	$C_{70}H_{122}Ge_2Si_8$	$C_{68}H_{117}CoGe_2Si_8$
Moiety formula	$C_{70}H_{122}Ge_2Si_8$	$C_{61}H_{109}CoGe_2Si_8$, C_7H_8
Formula weight	1333.57	1363.44
Temperature/K	100	123
Crystal system	monoclinic	triclinic
Space group	$P2_1/n$	P-1
a/Å	15.4582(3)	13.3078(14)
b/Å	22.4395(6)	16.7470(17)
c/Å	22.7763(5)	21.0303(18)
α/°	90	103.116(7)
β/°	98.315(2)	101.818(7)
γ/°	90	109.419(8)
Volume/Å^3	7817.5(3)	4099.7(7)
Z	4	2
ρ_{calc}g/cm^3	1.133	1.104
μ/mm^{-1}	2.380	1.078
F(000)	2872.0	1456.0
Crystal size/mm^3	0.1 × 0.1 × 0.1	0.36 × 0.18 × 0.02
Absorption correction	multi-scan	integration
Tmin; Tmax	0.4142; 0.9156	0.4390; 0.8473
Radiation	CuKα (λ = 1.54186)	MoKα (λ = 0.71073)
2Θ range for data collection/°	6.498 to 135.5°	5.17 to 51.998°
Completeness to theta	0.995	0.972
Index ranges	-18 ≤ h ≤ 16, -26 ≤ k ≤ 26, -27 ≤ l ≤ 21	-16 ≤ h ≤ 16, -20 ≤ k ≤ 20, -23 ≤ l ≤ 25
Reflections collected	97964	32316
Independent reflections	14101 [R_{int} = 0.1378, R_{sigma} = 0.0731]	15646 [R_{int} = 0.1546, R_{sigma} = 0.2698]
Data/restraints/parameters	14101/678/757	15646/228/760
Goodness-of-fit on F^2	1.041	0.756
Final R indexes [I>=2σ (I)]	R_1 = 0.0859, wR_2 = 0.2016	R_1 = 0.0690, wR_2 = 0.1340
Final R indexes [all data]	R_1 = 0.1372, wR_2 = 0.2399	R_1 = 0.1941, wR_2 = 0.1719
Largest diff. peak/hole / e Å^{-3}	2.07/-0.71	0.54/-0.88

Table 16. Crystal data and structure refinement parameters of [CpCo($Ge_2Tbb_2C_2PhNMe_2$)] (**14-Co**) and [CpCo($Ge_2Tbb_2C_2H_4$)] (**15-Co**).

	14-Co	**15-Co**
Crystal Habitus	dark brown blocks	clear brown block
Device Type	STOE IPDS 2T	Bruker X8-KappaApexII
Empirical formula	$C_{63}H_{114}CoGe_2NSi_8$	$C_{61}H_{113}CoGe_2Si_8$
Moiety formula	$C_{63}H_{114}CoGe_2NSi_8$	$C_{55}H_{107}CoGe_2Si_8$, $2(C_3H_3)$
Formula weight	1314.38	1275.34
Temperature/K	123(2)	100
Crystal system	monoclinic	triclinic
Space group	$P2_1/c$	P-1
a/Å	17.8050(9)	13.4005(9)
b/Å	22.7743(8)	17.1233(12)
c/Å	19.9727(11)	17.4220(11)
α/°	90	88.500(3)
β/°	106.755(4)	78.723(3)
γ/°	90	72.934(3)
Volume/$Å^3$	7755.0(7)	3745.8(4)
Z	4	2
$\rho_{calc}g/cm^3$	1.126	1.131
μ/mm^{-1}	1.138	1.176
F(000)	2808.0	1364.0
Crystal size/mm^3	0.6 × 0.32 × 0.16	0.19 × 0.16 × 0.1
Absorption correction	integration	empirical
Tmin; Tmax	0.7510; 0.9016	0.5083; 0.7461
Radiation	Mo Kα (λ = 0.71073)	MoKα (λ = 0.71073)
2Θ range for data collection/°	4.97 to 51°	2.384 to 56°
Completeness to theta	0.969	0.993
Index ranges	-20 ≤ h ≤ 21, -25 ≤ k ≤ 27, -24 ≤ l ≤ 17	-17 ≤ h ≤ 17, -22 ≤ k ≤ 22, -23 ≤ l ≤ 23
Reflections collected	27532	138314
Independent reflections	13992 [R_{int} = 0.0613, R_{sigma} = 0.0870]	17742 [R_{int} = 0.0657, R_{sigma} = 0.0470]
Data/restraints/parameters	13992/1027/830	17742/417/679
Goodness-of-fit on F^2	0.973	1.192
Final R indexes [I>=2σ (I)]	R_1 = 0.0710, wR_2 = 0.1868	R_1 = 0.2122, wR_2 = 0.4160
Final R indexes [all data]	R_1 = 0.1084, wR_2 = 0.2025	R_1 = 0.2213, wR_2 = 0.4201
Largest diff. peak/hole / e $Å^{-3}$	0.95/-1.45	5.49/-2.31

Table 17. Crystal data and structure refinement parameters of [CpCo{$Ge_2Tbb_2C_2Me_2(CHSiMe_3)$}] (**16-Co**) and ($Ge_2Tbb_2COD$) (**17-Ge**).

	16-Co	**17-Ge**
Crystal Habitus	clear red cube	clear colourless plate
Device Type	Bruker D8 Venture	Bruker X8-KappaApexII
Empirical formula	$C_{61}H_{119}CoGe_2Si_9$	$C_{56}H_{110}Ge_2Si_8$
Moiety formula	$2(C_{30.5}H_{59.5}Co_{0.5}GeSi_{4.5})$	$C_{56}H_{110}Ge_2Si_8$
Formula weight	1309.47	1153.33
Temperature/K	100.00	100
Crystal system	monoclinic	monoclinic
Space group	C2/c	$P2_1/n$
a/Å	33.8140(18)	17.0861(9)
b/Å	13.6278(7)	18.5879(10)
c/Å	16.8069(9)	22.0469(11)
α/°	90	90
β/°	90.658(2)	96.496(3)
γ/°	90	90
Volume/$Å^3$	7744.3(7)	6957.0(6)
Z	4	4
$\rho_{calc}g/cm^3$	1.123	1.101
μ/mm^{-1}	1.154	1.032
F(000)	2808.0	2488.0
Crystal size/mm^3	0.4 × 0.24 × 0.24	0.52 × 0.24 × 0.04
Absorption correction	none	empirical
Tmin; Tmax	0.6951; 0.7460	0.6378; 0.7461
Radiation	MoKα (λ = 0.71073)	MoKα (λ = 0.71073)
2Θ range for data collection/°	4.024 to 60.072°	2.874 to 53.998°
Completeness to theta	0.999	0.999
Index ranges	-47 ≤ h ≤ 47, -19 ≤ k ≤ 19, -23 ≤ l ≤ 23	-21 ≤ h ≤ 21, -23 ≤ k ≤ 23, -27 ≤ l ≤ 28
Reflections collected	68232	500153
Independent reflections	11335 [R_{int} = 0.0460, R_{sigma} = 0.0291]	15187 [R_{int} = 0.0784, R_{sigma} = 0.0255]
Data/restraints/parameters	11335/474/457	15187/0/656
Goodness-of-fit on F^2	1.119	1.034
Final R indexes [I>=2σ (I)]	R_1 = 0.0536, wR_2 = 0.1219	R_1 = 0.0436, wR_2 = 0.1070
Final R indexes [all data]	R_1 = 0.0624, wR_2 = 0.1269	R_1 = 0.0596, wR_2 = 0.1173
Largest diff. peak/hole / e $Å^{-3}$	0.75/-0.75	2.13/-0.70

Table 18. Crystal data and structure refinement parameters of [CpRh(CO)GeBrTbb] (**18-Rh**) and [CpCo(CO){$Si_2(CO)_2Tbb_2$}] (**20-Co**).

	18-Rh	**20-Co**
Crystal Habitus	clear orange block	clear light orange prism
Device Type	Bruker D8 Venture	STOE IPDS-2T
Empirical formula	$C_{30}H_{54}BrGeORhSi_4$	$C_{116}H_{216}Co_2O_7Si_{20}$
Moiety formula	$C_{30}H_{54}BrGeORhSi_4$	$2(C_{56}H_{103}CoO_3Si_{10})$, $C_4H_{10}O$
Formula weight	798.50	2402.54
Temperature/K	100	123
Crystal system	monoclinic	triclinic
Space group	$P2_1/n$	P-1
a/Å	8.7028(11)	13.4559(4)
b/Å	13.0357(17)	16.9287(5)
c/Å	33.925(4)	17.8532(6)
α/°	90	102.956(2)
β/°	94.860(4)	102.364(2)
γ/°	90	108.034(2)
Volume/$Å^3$	3834.8(8)	3587.8(2)
Z	4	1
$\rho_{calc}g/cm^3$	1.383	1.112
μ/mm^{-1}	2.401	0.444
F(000)	1640.0	1302.0
Crystal size/mm^3	0.545 × 0.532 × 0.234	0.6 × 0.24 × 0.22
Absorption correction	multi-scan	integration
Tmin; Tmax	0.3110; 0.9685	0.1624; 0.9237
Radiation	MoKα (λ = 0.71073)	MoKα (λ = 0.71073)
2Θ range for data collection/°	4.75 to 58.5°	5.328 to 56°
Completeness to theta	0.971	0.989
Index ranges	-11 ≤ h ≤ 11, -17 ≤ k ≤ 17, -46 ≤ l ≤ 46	-17 ≤ h ≤ 17, -22 ≤ k ≤ 21, -23 ≤ l ≤ 23
Reflections collected	46676	52152
Independent reflections	46676 [R_{int} = ?, R_{sigma} = 0.0980]	17043 [R_{int} = 0.1657, R_{sigma} = 0.1470]
Data/restraints/parameters	46676/501/450	17043/20/686
Goodness-of-fit on F^2	1.053	0.887
Final R indexes [I>=2σ (I)]	R_1 = 0.1204, wR_2 = 0.2868	R_1 = 0.0723, wR_2 = 0.1574
Final R indexes [all data]	R_1 = 0.1359, wR_2 = 0.2962	R_1 = 0.1034, wR_2 = 0.1658
Largest diff. peak/hole / e $Å^{-3}$	3.79/-1.79	2.21/-1.33

Table 19. Crystal data and structure refinement parameters of [CpRh(CO){$Si_2(CO)_2Tbb_2$}] (**20-Rh**) and [$CpCo(Si_2COTbb_2)$] (**21-Co**).

	20-Rh	**21-Co**
Crystal Habitus	clear yellow prism	clear orange prism
Device Type	Bruker D8 Venture	Bruker APEX-II CCD
Empirical formula	$C_{116}H_{216}O_7Rh_2Si_{20}$	$C_{54}H_{103}OSi_{10}Co$
Moiety formula	$2(C_{56}H_{103}O_3RhSi_{10})$, $C_4H_{10}O$	$C_{54}H_{103}CoOSi_{10}$
Formula weight	2490.50	1108.19
Temperature/K	100.0	100.0
Crystal system	triclinic	triclinic
Space group	P-1	P-1
a/Å	12.0864(6)	12.8914(7)
b/Å	15.6044(6)	17.3383(7)
c/Å	20.5938(12)	17.4026(8)
α/°	83.05	95.803(2)
β/°	73.19	107.538(2)
γ/°	74.08	109.950(2)
Volume/$Å^3$	3571.8(3)	3394.9(3)
Z	1	2
$\rho_{calc}g/cm^3$	1.158	1.084
μ/mm^{-1}	0.444	0.461
F(000)	1338.0	1204.0
Crystal size/mm^3	0.4 × 0.24 × 0.2	0.28 × 0.26 × 0.12
Absorption correction	multi-scan	none
Tmin; Tmax	0.6985; 0.7484	0.6946; 0.7460
Radiation	MoKα (λ = 0.71073)	MoKα (λ = 0.71073)
2Θ range for data collection/°	3.67 to 57°	3.884 to 54°
Completeness to theta	0.997	0.999
Index ranges	-16 ≤ h ≤ 16, -20 ≤ k ≤ 20, -27 ≤ l ≤ 27	-16 ≤ h ≤ 16, -22 ≤ k ≤ 22, -22 ≤ l ≤ 22
Reflections collected	153729	123188
Independent reflections	18076 [R_{int} = 0.0338, R_{sigma} = 0.0211]	14836 [R_{int} = 0.0755, R_{sigma} = 0.0385]
Data/restraints/parameters	18076/1088/874	14836/697/684
Goodness-of-fit on F^2	1.123	1.031
Final R indexes [I>=2σ (I)]	R_1 = 0.0261, wR_2 = 0.0653	R_1 = 0.0359, wR_2 = 0.0866
Final R indexes [all data]	R_1 = 0.0281, wR_2 = 0.0670	R_1 = 0.0450, wR_2 = 0.0941
Largest diff. peak/hole / e $Å^{-3}$	0.85/-0.54	1.22/-0.39

Table 20. Crystal data and structure refinement parameters of [CpRh(Si$_2$COTbb$_2$)] (**21-Rh**) and [CpCo(CNMes){Si$_2$(CO)(CNMes)Tbb$_2$}] (**22-Co**).

	21-Rh	**22-Co**
Crystal Habitus	clear orangish brown prisms	clear orangish brown prism
Device Type	STOE STADIVARI	STOE STADIVARI
Empirical formula	$C_{54}H_{103}ORhSi_{10}$	$C_{74}H_{125}CoN_2OSi_{10}$
Moiety formula	$C_{54}H_{103}ORhSi_{10}$	$C_{74}H_{125}CoN_2OSi_{10}$
Formula weight	1152.16	1398.58
Temperature/K	100	100
Crystal system	triclinic	monoclinic
Space group	P-1	$P2_1/n$
a/Å	12.91132(21)	17.4026(2)
b/Å	17.0885(3)	18.8807(3)
c/Å	17.8002(3)	26.2227(3)
α/°	98.4358(14)	90
β/°	106.3869(13)	105.9830(10)
γ/°	109.5021(13)	90
Volume/Å^3	3423.34(10)	8283.01(19)
Z	2	4
ρ_{calc}g/cm^3	1.118	1.122
μ/mm^{-1}	3.93	3.307
F(000)	1240.0	3032.0
Crystal size/mm^3	0.32 × 0.187 × 0.1	0.24 × 0.12 × 0.1
Absorption correction	multi-scan	multi-scan
Tmin; Tmax	0.2206; 0.2871	0.5367; 0.5776
Radiation	CuKα (λ = 1.54186)	CuKα (λ = 1.54186)
2Θ range for data collection/°	7.77 to 135.496°	5.848 to 141.978°
Completeness to theta	0.994	1.000
Index ranges	-15 ≤ h ≤ 15, -20 ≤ k ≤ 14, -21 ≤ l ≤ 21	-21 ≤ h ≤ 16, -20 ≤ k ≤ 23, -32 ≤ l ≤ 31
Reflections collected	107874	324427
Independent reflections	12339 [R_{int} = 0.0298, R_{sigma} = 0.0161]	15906 [R_{int} = 0.0964, R_{sigma} = 0.0262]
Data/restraints/parameters	12339/258/772	15906/831/861
Goodness-of-fit on F^2	1.024	1.068
Final R indexes [I>=2σ (I)]	R_1 = 0.0476, wR_2 = 0.1133	R_1 = 0.0424, wR_2 = 0.0902
Final R indexes [all data]	R_1 = 0.0518, wR_2 = 0.1162	R_1 = 0.0576, wR_2 = 0.1009
Largest diff. peak/hole / e Å^{-3}	1.38/-0.93	0.33/-0.32

Table 21. Crystal data and structure refinement parameters of [CpCo(CO){Si_2(CO)(CNMes)Tbb$_2$}] (**23-Co**) and [CpCo(Si_2CNMes)Tbb$_2$] (**24-Co**).

	23-Co	**24-Co**
Crystal Habitus	clear brown block	clear brown block
Device Type	Bruker D8 Venture	Bruker D8 Venture
Empirical formula	$C_{71}H_{128}NO_2Si_{10}Co$	$C_{67}H_{123}CoNOSi_{10}$
Moiety formula	$C_{65}H_{114}CoNO_2Si_{10}$, C_6H_{14}	$C_{63}H_{114}CoNSi_{10}$, C_4H_9O
Formula weight	1367.57	1298.49
Temperature/K	100	100.0
Crystal system	monoclinic	triclinic
Space group	$P2_1/n$	P-1
a/Å	17.0137(6)	12.9806(8)
b/Å	16.0703(6)	17.2137(11)
c/Å	30.9138(10)	19.5426(12)
α/°	90	97.056(3)
β/°	100.2820(10)	94.832(3)
γ/°	90	108.548(2)
Volume/Å^3	8316.6(5)	4073.1(4)
Z	4	2
ρ_{calc}g/cm^3	1.092	1.059
μ/mm^{-1}	3.287	0.393
F(000)	2976.0	1414.0
Crystal size/mm^3	0.48 × 0.28 × 0.16	0.21 × 0.12 × 0.06
Absorption correction	empirical	empirical
Tmin; Tmax	0.6250; 0.7543	0.5651; 0.7461
Radiation	CuKα (λ = 1.54178)	MoKα (λ = 0.71073)
2Θ range for data collection/°	5.552 to 159.942°	3.712 to 55.998°
Completeness to theta	0.999	0.994
Index ranges	-21 ≤ h ≤ 21, -20 ≤ k ≤ 17, -38 ≤ l ≤ 39	-17 ≤ h ≤ 17, -22 ≤ k ≤ 22, -25 ≤ l ≤ 25
Reflections collected	214796	64961
Independent reflections	17977 [R_{int} = 0.0427, R_{sigma} = 0.0209]	19554 [R_{int} = 0.0457, R_{sigma} = 0.0518]
Data/restraints/parameters	17977/1/801	19554/720/756
Goodness-of-fit on F^2	1.030	1.028
Final R indexes [I>=2σ (I)]	R_1 = 0.0420, wR_2 = 0.1156	R_1 = 0.0587, wR_2 = 0.1610
Final R indexes [all data]	R_1 = 0.0433, wR_2 = 0.1166	R_1 = 0.0847, wR_2 = 0.1834
Largest diff. peak/hole / e Å^{-3}	0.73/-0.49	1.24/-0.97

Table 22. Crystal data and structure refinement parameters of [CpCo{Si_2($CNMes)_2$$Tbb_2$}] (**25-Co**) and [CpCo$CSi_2Me_2Tbb_2$] (**26-Co**).

	25-Co	**26-Co**
Crystal Habitus	clear dark green plank	clear green plank
Device Type	STOE STADIVARI	STOE STADIVARI
Empirical formula	$C_{85}H_{153}CoN_2Si_{10}$	$C_{56}H_{109}CoSi_{10}$
Moiety formula	$C_{73}H_{125}CoN_2Si_{10}$, 2($C_6H_{14}$)	$C_{56}H_{109}CoSi_{10}$
Formula weight	1542.91	1122.26
Temperature/K	100	100.0
Crystal system	triclinic	triclinic
Space group	P-1	P-1
a/Å	16.1275(5)	9.2552(5)
b/Å	16.9644(5)	16.4139(8)
c/Å	20.1536(6)	23.9608(12)
α/°	65.5238(22)	105.288(4)
β/°	76.0824(23)	89.939(4)
γ/°	77.5337(23)	104.278(4)
Volume/$Å^3$	4828.75(25)	3394.7(3)
Z	2	2
$\rho_{calc}g/cm^3$	1.061	1.098
μ/mm^{-1}	2.82	3.900
F(000)	1688.0	1224.0
Crystal size/mm^3	0.13 × 0.1 × 0.09	0.6 × 0.467 × 0.32
Absorption correction	multi-scan	multi-scan
Tmin; Tmax	0.4168; 0.6587	0.0873; 0.1680
Radiation	CuKα (λ = 1.54186)	CuKα (λ = 1.54186)
2Θ range for data collection/°	6.848 to 135.498°	7.668 to 135.496°
Completeness to theta	0.988	0.991
Index ranges	-12 ≤ h ≤ 19, -19 ≤ k ≤ 20, -24 ≤ l ≤ 24	-10 ≤ h ≤ 3, -19 ≤ k ≤ 19, -28 ≤ l ≤ 28
Reflections collected	75936	69247
Independent reflections	17297 [R_{int} = 0.0875, R_{sigma} = 0.0752]	12184 [R_{int} = 0.0816, R_{sigma} = 0.0482]
Data/restraints/parameters	17297/64/923	12184/6/636
Goodness-of-fit on F^2	1.031	1.091
Final R indexes [I>=2σ (I)]	R_1 = 0.0756, wR_2 = 0.1791	R_1 = 0.0954, wR_2 = 0.2411
Final R indexes [all data]	R_1 = 0.1193, wR_2 = 0.2122	R_1 = 0.1209, wR_2 = 0.2627
Largest diff. peak/hole / e $Å^{-3}$	0.98/-0.57	1.69/-1.20

Table 23. Crystal data and structure refinement parameters of [CpRhCSi$_2$Me$_2$Tbb$_2$] (**26-Rh**) and [CpRh(PMe$_3$)(Si$_2$COTbb$_2$)] (**27-Rh**).

	26-Rh	**27-Rh**
Crystal Habitus	clear red plank	clear red block
Device Type	Bruker D8 Venture	Bruker D8 Venture
Empirical formula	$C_{56}H_{109}RhSi_{10}$	$C_{57}H_{112}OPRhSi_{10}$
Moiety formula	$C_{56}H_{109}RhSi_{10}$	$C_{57}H_{112}OPRhSi_{10}$
Formula weight	1166.24	1228.24
Temperature/K	100.0	100.0
Crystal system	monoclinic	monoclinic
Space group	$P2_1/c$	$P2_1/n$
a/Å	23.1955(13)	12.0816(8)
b/Å	9.4315(5)	24.6452(17)
c/Å	32.7452(17)	23.9789(15)
α/°	90	90
β/°	107.368(2)	91.318(3)
γ/°	90	90
Volume/Å^3	6837.0(6)	7137.9(8)
Z	4	4
ρ_{calc}g/cm^3	1.133	1.143
μ/mm^{-1}	0.456	0.463
F(000)	2520.0	2648.0
Crystal size/mm^3	0.26 × 0.13 × 0.08	0.46 × 0.32 × 0.2
Absorption correction	multi-scan	multi-scan
Tmin; Tmax	0.6397; 0.7461	0.6515; 0.7474
Radiation	MoKα (λ = 0.71073)	MoKα (λ = 0.71073)
2Θ range for data collection/°	3.822 to 56°	3.756 to 56°
Completeness to theta	0.998	0.999
Index ranges	-28 ≤ h ≤ 30, -12 ≤ k ≤ 12, -43 ≤ l ≤ 41	-15 ≤ h ≤ 15, -32 ≤ k ≤ 32, -31 ≤ l ≤ 31
Reflections collected	80245	154309
Independent reflections	16500 [R_{int} = 0.0247, R_{sigma} = 0.0215]	17203 [R_{int} = 0.0645, R_{sigma} = 0.0318]
Data/restraints/parameters	16500/2/636	17203/264/807
Goodness-of-fit on F^2	1.065	1.035
Final R indexes [I>=2σ (I)]	R_1 = 0.0254, wR_2 = 0.0620	R_1 = 0.0283, wR_2 = 0.0689
Final R indexes [all data]	R_1 = 0.0284, wR_2 = 0.0636	R_1 = 0.0319, wR_2 = 0.0712
Largest diff. peak/hole / e Å^{-3}	0.44/-0.57	0.47/-0.48

Table 24. Crystal data and structure refinement parameters of [CpRh{Si_2IMe_4(CO)Tbb$_2$}] (**28-Rh**).

	28-Rh
Crystal Habitus	clear brown plate
Device Type	Bruker D8 Venture
Empirical formula	$C_{69}H_{135}N_2O_3RhSi_{10}$
Moiety formula	$C_{61}H_{115}N_2ORhSi_{10}$, 2($C_4H_{10}O$)
Formula weight	1424.59
Temperature/K	100.0
Crystal system	monoclinic
Space group	$P2_1/n$
a/Å	22.7928(11)
b/Å	17.6889(7)
c/Å	23.3841(11)
α/°	90
β/°	117.555(2)
γ/°	90
Volume/Å^3	8358.5(7)
Z	4
ρ_{calc}g/cm^3	1.132
μ/mm^{-1}	0.388
F(000)	3088.0
Crystal size/mm^3	0.22 × 0.12 × 0.06
Absorption correction	multi-scan
Tmin; Tmax	0.6525; 0.7459
Radiation	MoKα (λ = 0.71073)
2Θ range for data collection/°	3.93 to 56°
Completeness to theta	1.000
Index ranges	-29 ≤ h ≤ 30, -23 ≤ k ≤ 22, -30 ≤ l ≤ 30
Reflections collected	140477
Independent reflections	20175 [R_{int} = 0.0991, R_{sigma} = 0.0810]
Data/restraints/parameters	20175/19/864
Goodness-of-fit on F^2	1.071
Final R indexes [I>=2σ (I)]	R_1 = 0.0459, wR_2 = 0.1187
Final R indexes [all data]	R_1 = 0.0739, wR_2 = 0.1462
Largest diff. peak/hole / e Å^{-3}	0.75/-1.11

Table 25. Crystal data and structure refinement parameters of [(PMe$_3$)$_2$Co{(GeClTbb)(GeTbb)}] (**29-Co**) and [(PMe$_3$)$_2$Co(GeTbb)$_2$][B(Ar^F)$_4$] (**30-Co**).

	29-Co	**30-Co**
Crystal Habitus	clear dark violet plank	clear dark pink plank
Device Type	STOE IPDS-2T	STOE IPDS-2T
Empirical formula	$C_{58}H_{125}ClCoGe_2OP_2Si_8$	$C_{91}H_{140}BCoF_{24}Ge_2P_2Si_8$
Moiety formula	$C_{54}H_{116}ClCoGe_2P_2Si_8$, C_4H_9O	$C_{54}H_{116}CoGe_2P_2Si_8$, $C_{32}H_{12}BF_{24}$, C_5H_{12}
Formula weight	1364.79	2191.60
Temperature/K	123(2)	123
Crystal system	triclinic	triclinic
Space group	P-1	P-1
a/Å	13.7247(4)	13.3522(4)
b/Å	16.8753(5)	19.3482(5)
c/Å	17.9749(5)	23.8403(7)
α/°	82.683(2)	108.285(2)
β/°	80.016(2)	96.402(2)
γ/°	76.353(2)	97.637(2)
Volume/Å^3	3968.0(2)	5718.8(3)
Z	2	2
ρ_{calc}g/cm^3	1.142	1.273
μ/mm^{-1}	1.186	0.855
F(000)	1462.0	2280.0
Crystal size/mm^3	0.6 × 0.32 × 0.12	0.31 × 0.09 × 0.03
Absorption correction	integration	integration
Tmin; Tmax	0.6661; 0.8537	0.7916; 0.9487
Radiation	MoKα (λ = 0.71073)	MoKα (λ = 0.71073)
2Θ range for data collection/°	5.162 to 56°	5.234 to 53.998°
Completeness to theta	0.998	0.958
Index ranges	-18 ≤ h ≤ 18, -22 ≤ k ≤ 22, -20 ≤ l ≤ 23	-17 ≤ h ≤ 15, -24 ≤ k ≤ 24, -30 ≤ l ≤ 30
Reflections collected	52492	44951
Independent reflections	19132 [R_{int} = 0.0668, R_{sigma} = 0.0730]	23494 [R_{int} = 0.0579, R_{sigma} = 0.1151]
Data/restraints/parameters	19132/6/696	23494/180/1284
Goodness-of-fit on F^2	0.856	0.847
Final R indexes [I>=2σ (I)]	R_1 = 0.0325, wR_2 = 0.0694	R_1 = 0.0465, wR_2 = 0.0824
Final R indexes [all data]	R_1 = 0.0559, wR_2 = 0.0735	R_1 = 0.0982, wR_2 = 0.0932
Largest diff. peak/hole / e Å^{-3}	0.70/-0.58	0.76/-0.42

Table 26. Crystal data and structure refinement parameters of $[(PMe_3)_2Ni\{(GeClTbb)(GeTbb)\}][B(Ar^F)_4]$ (**32-Ni**) and $[(PMe_3)_2Fe(GeTbb)_2]$ (**33-Fe**).

	32-Ni	**33-Fe**
Crystal Habitus	clear dark red plate	clear brown plate
Device Type	STOE Stadivari	STOE IPDS-2T
Empirical formula	$C_{86}H_{128}BClF_{24}Ge_2NiP_2Si_8$	$C_{61}H_{124}FeGe_2P_2Si_8$
Moiety formula	$C_{54}H_{116}ClGe_2NiP_2Si_8$, $C_{32}H_{12}BF_{24}$	$C_{54}H_{116}FeGe_2P_2Si_8$, C_7H_8
Formula weight	2154.69	1345.28
Temperature/K	100	123(2)
Crystal system	monoclinic	triclinic
Space group	$P2_1/c$	P-1
a/Å	16.3821(5)	12.8143(6)
b/Å	12.9644(3)	15.3832(7)
c/Å	50.5284(15)	20.5227(8)
α/°	90	97.483(3)
β/°	93.184(2)	93.378(3)
γ/°	90	97.692(3)
Volume/Å^3	10714.9(5)	3963.0(3)
Z	4	2
ρ_{calc}g/cm^3	1.336	1.127
μ/mm^{-1}	2.938	1.127
F(000)	4464.0	1444.0
Crystal size/mm^3	0.12 × 0.083 × 0.03	0.3 × 0.21 × 0.1
Absorption correction	multi-scan	integration
Tmin; Tmax	0.3308; 0.4293	0.4287; 0.8535
Radiation	CuKα (λ = 1.54186)	MoKα (λ = 0.71073)
2Θ range for data collection/°	6.274 to 142.028°	5.142 to 51.998°
Completeness to theta	0.997	0.940
Index ranges	-17 ≤ h ≤ 20, -15 ≤ k ≤ 9, -61 ≤ l ≤ 60	-13 ≤ h ≤ 15, -18 ≤ k ≤ 18, -25 ≤ l ≤ 25
Reflections collected	125968	31421
Independent reflections	20481 [R_{int} = 0.0599, R_{sigma} = 0.0417]	14551 [R_{int} = 0.1124, R_{sigma} = 0.0901]
Data/restraints/parameters	20481/24/1210	14551/114/745
Goodness-of-fit on F^2	1.073	1.057
Final R indexes [I>=2σ (I)]	R_1 = 0.0810, wR_2 = 0.2159	R_1 = 0.0615, wR_2 = 0.1618
Final R indexes [all data]	R_1 = 0.1114, wR_2 = 0.2506	R_1 = 0.0811, wR_2 = 0.1723
Largest diff. peak/hole / e Å^{-3}	1.08/-0.93	1.41/-0.91

Table 27. Crystal data and structure refinement parameters of $[(PMe_3)_2Fe(GeTbb)_2][B(Ar^F)_4]$ (**34-Fe**) and $(caac^{Me})SiBrGeTbb$ (**35-Si**).

	34-Fe	**35-Si**
Crystal Habitus	clear dark brown prism	clear bluish green block
Device Type	STOE IPDS-2T	STOE IPDS-2T
Empirical formula	$C_{86}H_{128}BF_{24}FeGe_2P_2Si_8$	$C_{49}H_{92}BrGeNSi_5$
Moiety formula	$C_{54}H_{116}FeGe_2P_2Si_8$, $C_{32}H_{12}BF_{24}$	$C_{44}H_{80}BrGeNSi_5$, C_5H_{12}
Formula weight	2116.38	988.18
Temperature/K	173.0	123
Crystal system	monoclinic	monoclinic
Space group	$P2_1/c$	$P2_1/n$
a/Å	16.9970(4)	9.8325(3)
b/Å	32.8022(5)	39.5649(12)
c/Å	19.8896(5)	14.7058(4)
α/°	90	90
β/°	94.630(2)	94.341(2)
γ/°	90	90
Volume/Å^3	11053.0(4)	5704.5(3)
Z	4	4
ρ_{calc}g/cm^3	1.272	1.151
μ/mm^{-1}	0.864	1.372
F(000)	4388.0	2120.0
Crystal size/mm^3	0.6 × 0.467 × 0.32	0.6 × 0.32 × 0.3
Absorption correction	integration	integration
Tmin; Tmax	0.6639; 0.8905	0.8263; 0.8940
Radiation	MoKα (λ = 0.71073)	MoKα (λ = 0.71073)
2Θ range for data collection/°	4.59 to 51.998°	4.968 to 51.996°
Completeness to theta	0.998	0.999
Index ranges	-14 ≤ h ≤ 20, -30 ≤ k ≤ 40, -24 ≤ l ≤ 24	-12 ≤ h ≤ 10, -48 ≤ k ≤ 48, -18 ≤ l ≤ 16
Reflections collected	51554	44762
Independent reflections	21691 [R_{int} = 0.0749, R_{sigma} = 0.0543]	11200 [R_{int} = 0.0920, R_{sigma} = 0.1166]
Data/restraints/parameters	21691/1161/1240	11200/94/569
Goodness-of-fit on F^2	1.014	0.882
Final R indexes [I>=2σ (I)]	R_1 = 0.0600, wR_2 = 0.1350	R_1 = 0.0527, wR_2 = 0.1092
Final R indexes [all data]	R_1 = 0.0825, wR_2 = 0.1496	R_1 = 0.1155, wR_2 = 0.1259
Largest diff. peak/hole / e Å^{-3}	1.21/-1.27	0.88/-0.77

Table 28. Crystal data and structure refinement parameters of (caac^{Me})SiBr$_2$GeBrTbb (**36-Si**) and (SIDipp)SiBrGeTbb (**37-Si**).

	36-Si	**37-Si**
Crystal Habitus	clear brown block	clear reddish brown prism
Device Type	STOE IPDS-2T	STOE IPDS-2T
Empirical formula	$C_{54}H_{104}Br_3GeNSi_5$	$C_{112}H_{198}Br_2Ge_2N_4OSi_{10}$
Moiety formula	$C_{44}H_{80}Br_3GeNSi_5$, 2(C_5H_{12})	2($C_{51}H_{87}BrGeN_2Si_5$), $C_4H_{10}O$, C_6H_{14}
Formula weight	1220.15	2202.63
Temperature/K	123	123(2)
Crystal system	triclinic	monoclinic
Space group	P-1	$P2_1/n$
a/Å	12.1448(5)	15.0003(10)
b/Å	15.6094(5)	18.1466(10)
c/Å	18.6297(6)	24.6468(17)
α/°	98.151(3)	90
β/°	107.455(3)	98.222(5)
γ/°	98.300(3)	90
Volume/Å^3	3269.1(2)	6640.0(7)
Z	2	2
ρ_{calc}g/cm^3	1.240	1.102
μ/mm^{-1}	2.425	1.186
F(000)	1284.0	2360.0
Crystal size/mm^3	0.15 × 0.12 × 0.11	0.6 × 0.22 × 0.2
Absorption correction	integration	integration
Tmin; Tmax	0.4135; 0.6726	0.4688; 0.9363
Radiation	MoKα (λ = 0.71073)	MoKα (λ = 0.71073)
2Θ range for data collection/°	5.38 to 51.994°	5.262 to 50.5°
Completeness to theta	0.998	0.959
Index ranges	-14 ≤ h ≤ 14, -19 ≤ k ≤ 19, -22 ≤ l ≤ 22	-18 ≤ h ≤ 17, -21 ≤ k ≤ 21, -29 ≤ l ≤ 29
Reflections collected	170402	62147
Independent reflections	170402 [R_{int} = ?, R_{sigma} = 0.1469]	62147 [R_{int} = ?, R_{sigma} = 0.2035]
Data/restraints/parameters	170402/133/636	62147/376/669
Goodness-of-fit on F^2	0.853	0.841
Final R indexes [I>=2σ (I)]	R_1 = 0.0763, wR_2 = 0.1778	R_1 = 0.0763, wR_2 = 0.1576
Final R indexes [all data]	R_1 = 0.1670, wR_2 = 0.2100	R_1 = 0.1538, wR_2 = 0.1821
Largest diff. peak/hole / e Å^{-3}	2.59/-1.35	1.08/-0.85

Table 29. Crystal data and structure refinement parameters of (caac^{Me})SiMesGeTbb (**38-Si**) and [(caac^{Me})SiTbbGe][B(Ar^{F})$_4$] (**39-Si**).

	38-Si	**39-Si**
Crystal Habitus	clear greenish blue block	clear dark blue plate
Device Type	STOE IPDS-2T	STOE IPDS-2T
Empirical formula	$C_{53}H_{91}GeNSi_5$	$C_{76}H_{92}BF_{24}GeNSi_5$
Moiety formula	$C_{53}H_{91}GeNSi_5$	$C_{44}H_{80}GeNSi_5$, $C_{32}H_{12}BF_{24}$
Formula weight	955.30	1699.35
Temperature/K	123	123
Crystal system	monoclinic	monoclinic
Space group	$P2_1/c$	$P2_1/c$
a/Å	11.9649(3)	14.2969(3)
b/Å	28.7479(6)	15.8411(2)
c/Å	17.2457(4)	36.7944(8)
α/°	90	90
β/°	107.510(2)	91.726(2)
γ/°	90	90
Volume/Å^3	5657.1(2)	8329.4(3)
Z	4	4
ρ_{calc}g/cm^3	1.122	1.355
μ/mm^{-1}	0.680	0.534
F(000)	2072.0	3512.0
Crystal size/mm^3	0.48 × 0.28 × 0.24	0.3 × 0.2 × 0.15
Absorption correction	integration	integration
Tmin; Tmax	0.7488; 0.8887	0.7262; 0.9032
Radiation	MoKα (λ = 0.71073)	MoKα (λ = 0.71073)
2Θ range for data collection/°	5.12 to 56°	5.144 to 55.996°
Completeness to theta	0.998	0.995
Index ranges	-15 ≤ h ≤ 15, -37 ≤ k ≤ 37, -22 ≤ l ≤ 22	-18 ≤ h ≤ 18, -20 ≤ k ≤ 20, -48 ≤ l ≤ 46
Reflections collected	53044	111689
Independent reflections	13594 [R_{int} = 0.0353, R_{sigma} = 0.0542]	20032 [R_{int} = 0.0477, R_{sigma} = 0.0279]
Data/restraints/parameters	13594/0/567	20032/102/1052
Goodness-of-fit on F^2	0.895	1.035
Final R indexes [I>=2σ (I)]	R_1 = 0.0291, wR_2 = 0.0584	R_1 = 0.0457, wR_2 = 0.1192
Final R indexes [all data]	R_1 = 0.0508, wR_2 = 0.0610	R_1 = 0.0570, wR_2 = 0.1261
Largest diff. peak/hole / e Å^{-3}	0.38/-0.27	1.15/-0.50

Table 30. Crystal data and structure refinement parameters of (caac^{Me})SiKGeTbb (**40-Si**) and [CpMo(CO)$_2$GeTbb] (**41-Mo**).

	40-Si	**41-Mo**
Crystal Habitus	clear dark green plank	clear orange block
Device Type	Bruker X8-KappaApexII	STOE IPDS-2T
Empirical formula	$C_{50}H_{86}GeKNSi_5$	$C_{31}H_{54}GeMoO_2Si_4$
Moiety formula	$C_{44}H_{80}GeKNSi_5$, C_6H_6	$C_{31}H_{54}GeMoO_2Si_4$
Formula weight	953.33	739.63
Temperature/K	100	123.0
Crystal system	monoclinic	monoclinic
Space group	$P2_1/c$	$P2_1/c$
a/Å	14.698(4)	9.0745(6)
b/Å	23.919(7)	26.3724(11)
c/Å	17.096(5)	16.7938(12)
α/°	90	90
β/°	101.891(8)	104.328(5)
γ/°	90	90
Volume/Å^3	5881(3)	3894.0(4)
Z	4	4
ρ_{calc}g/cm^3	1.077	1.262
μ/mm^{-1}	0.723	1.240
F(000)	2056.0	1544.0
Crystal size/mm^3	0.33 × 0.11 × 0.1	0.15 × 0.14 × 0.06
Absorption correction	empirical	integration
Tmin; Tmax	0.4933; 0.7460	0.5800; 0.7756
Radiation	MoKα (λ = 0.71073)	MoKα (λ = 0.71073)
2Θ range for data collection/°	2.832 to 56°	5.24 to 50.496°
Completeness to theta	0.988	0.974
Index ranges	-18 ≤ h ≤ 19, -30 ≤ k ≤ 31, -22 ≤ l ≤ 22	-10 ≤ h ≤ 10, -30 ≤ k ≤ 31, -20 ≤ l ≤ 17
Reflections collected	53421	17421
Independent reflections	13973 [R_{int} = 0.3011, R_{sigma} = 0.3427]	6869 [R_{int} = 0.1452, R_{sigma} = 0.1040]
Data/restraints/parameters	13973/97/577	6869/72/417
Goodness-of-fit on F^2	1.020	1.051
Final R indexes [I>=2σ (I)]	R_1 = 0.1252, wR_2 = 0.2678	R_1 = 0.0830, wR_2 = 0.2071
Final R indexes [all data]	R_1 = 0.2931, wR_2 = 0.3458	R_1 = 0.1089, wR_2 = 0.2269
Largest diff. peak/hole / e Å^{-3}	1.49/-1.38	1.20/-1.73

Table 31. Crystal data and structure refinement parameters of (caac^{Me})GeBrTbb (**42-Ge**) and (caac^{Me})SiTbbGeBr (**43-Si**).

	42-Ge	**43-Si**
Crystal Habitus	clear orangish red plank	clear blue plate
Device Type	Bruker X8-KappaApexII	STOE STADIVARI
Empirical formula	$C_{44}H_{80}NSi_4GeBr$	$C_{106}H_{202}Br_2Ge_2N_2Si_{10}$
Moiety formula	$C_{44}H_{80}BrGeNSi_4$	$2(C_{44}H_{80}BrGeNSi_5)$, $3(C_6H_{14})$
Formula weight	887.95	2090.6233
Temperature/K	100	100
Crystal system	monoclinic	triclinic
Space group	$P2_1/n$	P-1
a/Å	9.0838(14)	16.23255(22)
b/Å	24.271(4)	18.2557(3)
c/Å	22.365(4)	21.8590(3)
α/°	90	75.4745(12)
β/°	92.081(5)	74.5290(10)
γ/°	90	89.9333(12)
Volume/Å^3	4927.7(14)	6028.35(15)
Z	4	2
ρ_{calc}g/cm^3	1.197	1.152
μ/mm^{-1}	1.558	2.644
F(000)	1896.0	2252.0
Crystal size/mm^3	0.3 × 0.12 × 0.1	0.16 × 0.1 × 0.01
Absorption correction	empirical	multi-scan
Tmin; Tmax	0.5437; 0.7461	0.3991; 0.8292
Radiation	MoKα (λ = 0.71073)	CuKα (λ = 1.54186)
2Θ range for data collection/°	3.644 to 55.998°	5.664 to 141.216°
Completeness to theta	0.998	0.988
Index ranges	-12 ≤ h ≤ 12, -32 ≤ k ≤ 32, -29 ≤ l ≤ 29	-19 ≤ h ≤ 18, -22 ≤ k ≤ 14, -26 ≤ l ≤ 25
Reflections collected	87517	237534
Independent reflections	11860 [R_{int} = 0.1166, R_{sigma} = 0.0747]	22660 [R_{int} = 0.0590, R_{sigma} = 0.0276]
Data/restraints/parameters	11860/36/514	22660/978/1151
Goodness-of-fit on F^2	1.033	1.050
Final R indexes [I>=2σ (I)]	R_1 = 0.0460, wR_2 = 0.0864	R_1 = 0.0771, wR_2 = 0.2119
Final R indexes [all data]	R_1 = 0.0789, wR_2 = 0.0956	R_1 = 0.0838, wR_2 = 0.2216
Largest diff. peak/hole / e Å^{-3}	0.59/-0.55	2.49/-1.55

Table 32. Crystal data and structure refinement parameters of [(caac^{Me})SiTbbGeCNMes][B(Ar^{F})$_4$] (**45-Si**) and [Cp*(CO)$_3$TiGeTbb] (**47-Ti**).

	45-Si	**47-Ti**
Crystal Habitus	clear blue block	clear reddish violet block
Device Type	STOE IPDS-2T	STOE IPDS-2T
Empirical formula	$C_{92}H_{109}BF_{24}GeN_2Si_5$	$C_{37}H_{64}GeO_3Si_4Ti$
Moiety formula	$C_{54}H_{91}GeN_2Si_5$, $C_{32}H_{12}BF_{24}$, C_6H_6	$C_{37}H_{64}GeO_3Si_4Ti$
Formula weight	1922.66	789.73
Temperature/K	123	123
Crystal system	monoclinic	monoclinic
Space group	$P2_1/c$	$P2_1/n$
a/Å	18.4389(4)	14.1586(7)
b/Å	16.7580(2)	20.8998(10)
c/Å	30.8572(5)	15.5514(7)
α/°	90	90
β/°	90.081(2)	102.544(4)
γ/°	90	90
Volume/Å^3	9534.8(3)	4492.0(4)
Z	4	4
ρ_{calc}g/cm^3	1.339	1.168
μ/mm^{-1}	0.476	0.983
F(000)	3992.0	1680.0
Crystal size/mm^3	0.48 × 0.46 × 0.32	0.6 × 0.46 × 0.12
Absorption correction	integration	integration
Tmin; Tmax	0.5257; 0.7747	0.7725; 0.9562
Radiation	MoKα (λ = 0.71073)	MoKα (λ = 0.71073)
2Θ range for data collection/°	5.038 to 50.5°	5.258 to 51.996°
Completeness to theta	0.998	0.999
Index ranges	-22 ≤ h ≤ 22, 0 ≤ k ≤ 20, 0 ≤ l ≤ 36	-17 ≤ h ≤ 17, -25 ≤ k ≤ 25, -17 ≤ l ≤ 19
Reflections collected	17206	32851
Independent reflections	17206 [R_{int} = 0.0730, R_{sigma} = 0.0677]	8827 [R_{int} = 0.0508, R_{sigma} = 0.0461]
Data/restraints/parameters	17206/114/1168	8827/20/435
Goodness-of-fit on F^2	1.021	0.980
Final R indexes [I>=2σ (I)]	R_1 = 0.0894, wR_2 = 0.2452	R_1 = 0.0346, wR_2 = 0.0777
Final R indexes [all data]	R_1 = 0.1209, wR_2 = 0.2634	R_1 = 0.0508, wR_2 = 0.0815
Largest diff. peak/hole / e Å^{-3}	1.06/-1.13	0.68/-0.49

Table 33. Crystal data and structure refinement parameters of [Cp*(CO)$_2$(PMe$_3$)TiSiTbb] (**48-Ti**) and [Cp*(CO)$_2$(PMe$_3$)TiGeTbb] (**49-Ti**).

	48-Ti	**49-Ti**
Crystal Habitus	clear red plate	clear red block
Device Type	STOE IPDS-2T	STOE IPDS-2T
Empirical formula	$C_{39}H_{73}O_2PSi_5Ti$	$C_{39}H_{73}GeO_2PSi_4Ti$
Moiety formula	$C_{39}H_{73}O_2PSi_5Ti$	$C_{39}H_{73}GeO_2PSi_4Ti$
Formula weight	793.29	837.79
Temperature/K	150.0	123(2)
Crystal system	monoclinic	triclinic
Space group	C2/c	P-1
a/Å	21.2304(7)	12.0363(8)
b/Å	11.9100(3)	12.6571(8)
c/Å	41.1517(14)	18.8777(13)
α/°	90	97.026(5)
β/°	110.920(2)	103.433(5)
γ/°	90	117.046(5)
Volume/Å^3	9719.4(5)	2403.5(3)
Z	8	2
ρ_{calc}g/cm^3	1.084	1.158
μ/mm^{-1}	0.360	0.953
F(000)	3440.0	896.0
Crystal size/mm^3	0.48 × 0.42 × 0.08	0.48 × 0.393 × 0.3
Absorption correction	integration	integration
Tmin; Tmax	0.8125; 0.9434	0.7823; 0.9033
Radiation	MoKα (λ = 0.71073)	MoKα (λ = 0.71073)
2Θ range for data collection/°	5.252 to 54°	5.026 to 53.998°
Completeness to theta	0.997	0.998
Index ranges	-27 ≤ h ≤ 25, -11 ≤ k ≤ 14, -35 ≤ l ≤ 51	-15 ≤ h ≤ 13, -16 ≤ k ≤ 16, -24 ≤ l ≤ 24
Reflections collected	23729	24245
Independent reflections	10460 [R_{int} = 0.0339, R_{sigma} = 0.0568]	10471 [R_{int} = 0.0487, R_{sigma} = 0.0538]
Data/restraints/parameters	10460/12/456	10471/734/597
Goodness-of-fit on F^2	0.910	1.091
Final R indexes [I>=2σ (I)]	R_1 = 0.0369, wR_2 = 0.0780	R_1 = 0.0581, wR_2 = 0.1602
Final R indexes [all data]	R_1 = 0.0677, wR_2 = 0.0843	R_1 = 0.0883, wR_2 = 0.1750
Largest diff. peak/hole / e Å^{-3}	0.34/-0.29	1.08/-1.07

Table 34. Crystal data and structure refinement parameters of [Cp*(CO)(CNMes)$_2$TiGeTbb] (**50-Ti**) and Si$_2$Tbb$_2$(PMe$_3$) (**51-Si**).

	50-Ti	**51-Si**
Crystal Habitus	dark green blocks	clear orange plate
Device Type	STOE IPDS-2T	STOE IPDS-2T
Empirical formula	$C_{63}H_{106}GeN_2O_3Si_4Ti$	$C_{55}H_{117}OPSi_{10}$
Moiety formula	$C_{55}H_{86}GeN_2OSi_4Ti$, 2($C_4H_{10}O$)	$C_{51}H_{107}PSi_{10}$, $C_4H_{10}O$
Formula weight	1172.34	1106.35
Temperature/K	123(2)	123
Crystal system	monoclinic	monoclinic
Space group	$P2_1/n$	$P2_1/n$
a/Å	14.3347(4)	21.8729(8)
b/Å	16.4420(4)	14.2467(6)
c/Å	29.3583(9)	22.9704(8)
α/°	90	90
β/°	90.707(2)	90.353(3)
γ/°	90	90
Volume/Å^3	6919.0(3)	7157.8(5)
Z	4	4
ρ_{calc}g/cm^3	1.125	1.027
μ/mm^{-1}	0.659	0.237
F(000)	2528.0	2440.0
Crystal size/mm^3	0.36 × 0.313 × 0.28	0.3 × 0.1 × 0.05
Absorption correction	integration	integration
Tmin; Tmax	0.7304; 0.9552	0.9665; 0.9937
Radiation	Mo Kα (λ = 0.71073)	MoKα (λ = 0.71073)
2Θ range for data collection/°	4.954 to 51.422°	5.626 to 52°
Completeness to theta	0.999	0.970
Index ranges	-17 ≤ h ≤ 17, -20 ≤ k ≤ 20, -35 ≤ l ≤ 35	-24 ≤ h ≤ 26, -17 ≤ k ≤ 17, -28 ≤ l ≤ 28
Reflections collected	109489	56456
Independent reflections	13032 [R_{int} = 0.0948, R_{sigma} = 0.0473]	13627 [R_{int} = 0.1223, R_{sigma} = 0.1651]
Data/restraints/parameters	13032/831/784	13627/109/660
Goodness-of-fit on F^2	1.235	0.945
Final R indexes [I>=2σ (I)]	R_1 = 0.0986, wR_2 = 0.2166	R_1 = 0.0927, wR_2 = 0.2153
Final R indexes [all data]	R_1 = 0.1148, wR_2 = 0.2271	R_1 = 0.1902, wR_2 = 0.2575
Largest diff. peak/hole / e Å^{-3}	1.09/-0.62	1.47/-0.79

Table 35. Crystal data and structure refinement parameters of $Ge_2Tbb_2(PMe_3)$ (**51-Ge**) and Tbb(Me)SiSi($AlMe_2$)Tbb (**52-Si**).

	51-Ge	**52-Si**
Crystal Habitus	clear red block	clear yellow plate
Device Type	Bruker X8-KappaApexII	Bruker D8 Venture
Empirical formula	$C_{61}H_{131}Ge_2PSi_8$	$C_{51}H_{107}AlSi_{10}$
Moiety formula	$C_{51}H_{107}Ge_2PSi_8$, 2(C_5H_{12})	$C_{51}H_{107}AlSi_{10}$
Formula weight	1265.52	1028.24
Temperature/K	100	100.0
Crystal system	monoclinic	triclinic
Space group	$P2_1$	P-1
a/Å	12.0437(16)	13.7757(8)
b/Å	24.143(3)	16.4213(9)
c/Å	13.561(2)	17.9165(10)
α/°	90	105.442(2)
β/°	103.445(4)	103.989(2)
γ/°	90	112.577(2)
Volume/Å^3	3834.9(9)	3327.0(3)
Z	2	2
ρ_{calc}g/cm^3	1.096	1.026
μ/mm^{-1}	0.961	0.239
F(000)	1376.0	1132.0
Crystal size/mm^3	0.18 × 0.1 × 0.09	0.21 × 0.12 × 0.07
Absorption correction	empirical	multi-scan
Tmin; Tmax	0.5805; 0.7460	0.7005; 0.7461
Radiation	MoKα (λ = 0.71073)	MoKα (λ = 0.71073)
2Θ range for data collection/°	4.846 to 55.996°	4.768 to 55.998°
Completeness to theta	0.999	0.999
Index ranges	-15 ≤ h ≤ 15, -31 ≤ k ≤ 31, -17 ≤ l ≤ 17	-18 ≤ h ≤ 18, -21 ≤ k ≤ 21, -23 ≤ l ≤ 23
Reflections collected	69707	99568
Independent reflections	18466 [R_{int} = 0.1842, R_{sigma} = 0.2123]	16047 [R_{int} = 0.0716, R_{sigma} = 0.0462]
Data/restraints/parameters	18466/35/686	16047/99/671
Goodness-of-fit on F^2	1.023	1.027
Final R indexes [I>=2σ (I)]	R_1 = 0.0876, wR_2 = 0.1714	R_1 = 0.0598, wR_2 = 0.1378
Final R indexes [all data]	R_1 = 0.1818, wR_2 = 0.2038	R_1 = 0.0846, wR_2 = 0.1602
Largest diff. peak/hole / e Å^{-3}	0.95/-1.19	1.45/-1.01
Flack parameter	0.412(8)	

5.3. Supplementary molecular structures

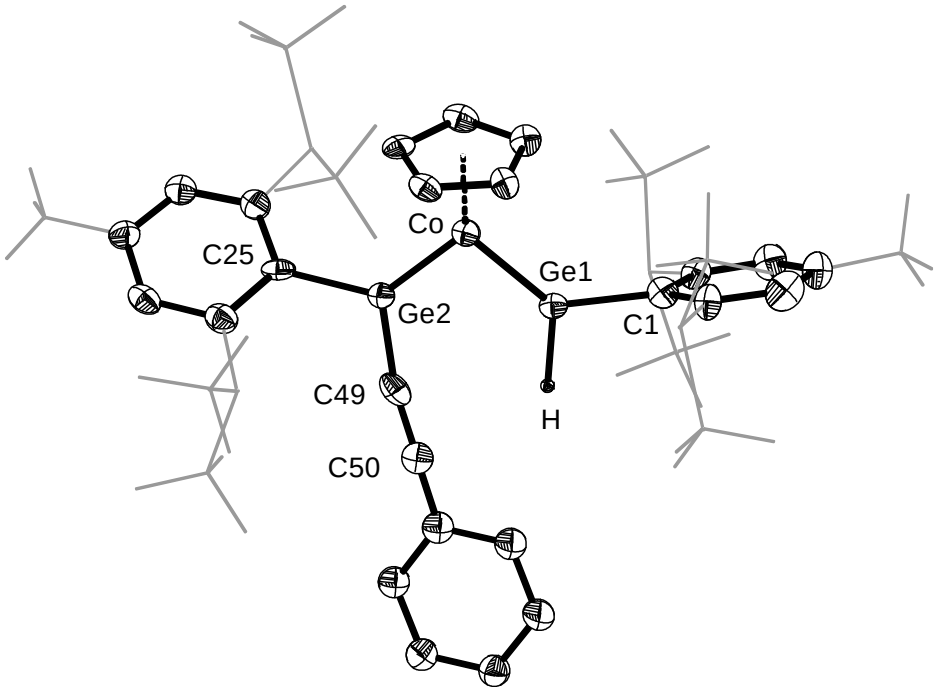

Figure 92. DIAMOND plot of the molecular structure of **12-Co**. Thermal ellipsoids are set at 30 % probability level. Hydrogen atoms are omitted and the Dsi and ^{t}Bu substituents of the Tbb ligand are presented in wire-frame for clarity. Selected bond lengths [Å] and bond angles [°]: Co-Ge1 2.1759(15), Co-Ge2 2.1830(14), Ge2-C49 1.897(15), C49-C50 1.185(19), Co-Ge2-C25 130.9(2), Co-Ge2-C49 122.6(4), C25-Ge2-C49 106.4(5).

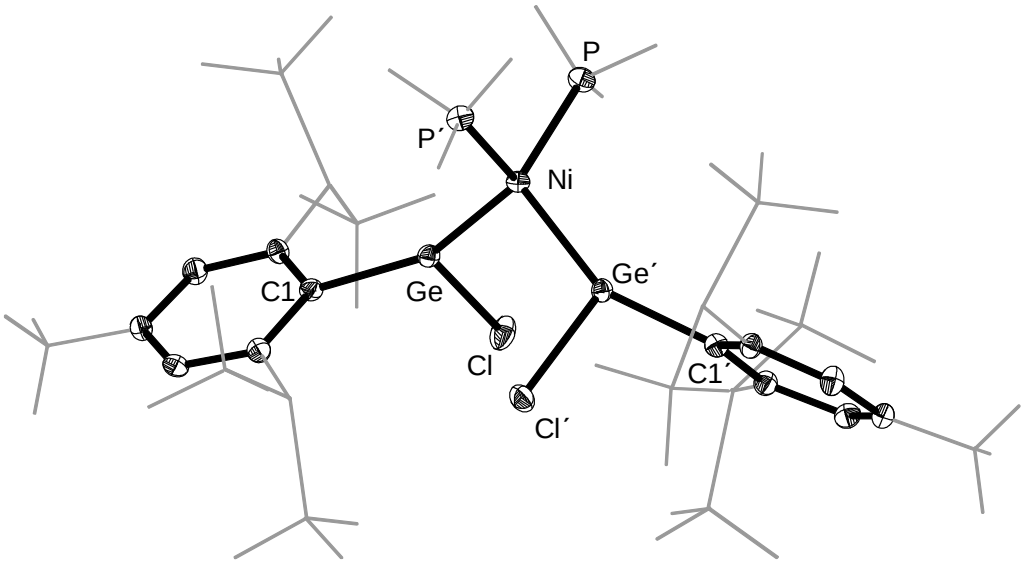

Figure 93. DIAMOND plot of the molecular structure of **31-Ni**. Thermal ellipsoids are set at 30 % probability level. Hydrogen atoms are omitted, the Dsi and ^{t}Bu substituents of the Tbb ligand and methyl groups of PMe_3 are presented in wire-frame for clarity. Selected bond lengths [Å] and bond angles: Ge-Ni 2.2120(7), Ge-Cl 2.2578(14), Ge-C1 1.991(5), Ni-P 2.1906(13), Ni-Ge-Cl 110.55(5), Ni-Ge-C1 153.01(14), C1-Ge-Cl: 96.35(15), Ge-Ni-Ge 98.37(4), P-Ni-P 105.43(8).

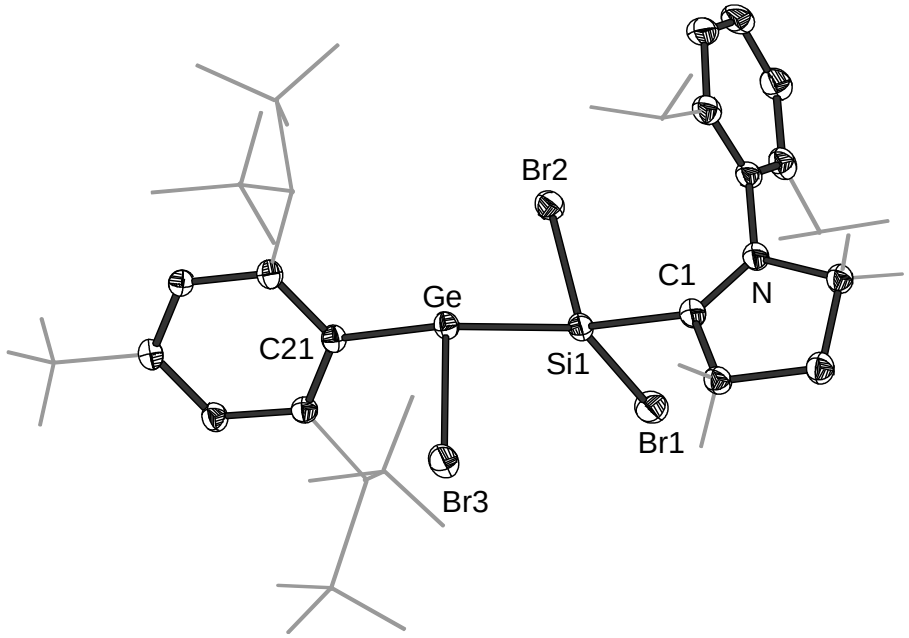

Figure 94. DIAMOND plot of the molecular structure of **36-Si**. Thermal ellipsoids are set at 30 % probability level. Hydrogen atoms are omitted, the Dsi and ^{t}Bu substituents of the Tbb ligand, ^{i}Pr substituents of Dipp group and $C^{3,5}$ Methyl groups of CAAC are presented in wire-frame for clarity. Selected bond lengths [Å], bond angles [°] and torsion angles [°]: Si1-Ge 2.474(2), Si1-C1 1.972(8), Si1-Ge-C21 110.4(2), C21-Ge-Br3 98.2(2), Si1-Ge-Br3 105.66(6), Ge-Si1-C1-N –119.135(7), C21-Ge-Si1-C1 179.776(4).

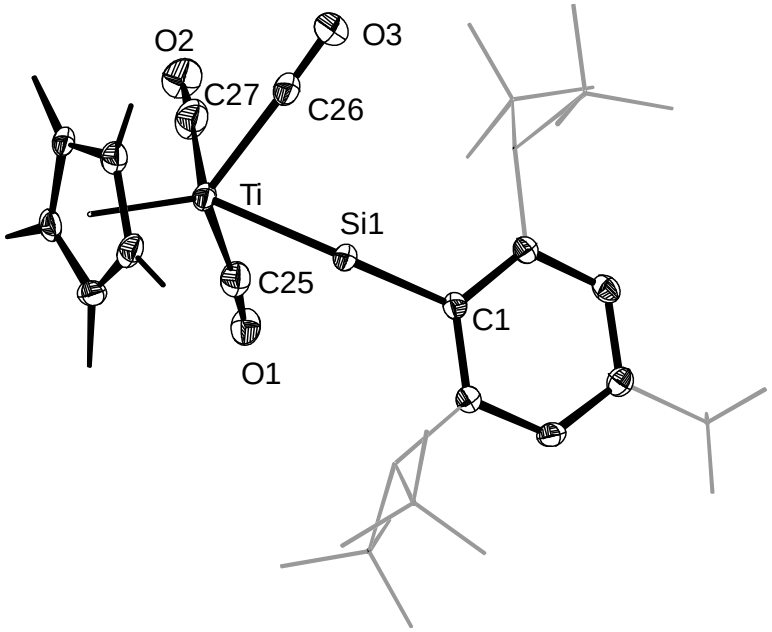

Figure 95. DIAMOND plot of the molecular structure of **46-Ti**. Thermal ellipsoids are set at 30 % probability level. Hydrogen atoms are omitted, the Dsi and ^{t}Bu substituents of the Tbb ligand and methyl groups of Cp* are presented in wire-frame for clarity. Selected bond lengths [Å] and bond angles: Ti-Si1 2.2845(6), Ti-C25 2.021(2), Ti-C26 2.056(2), Ti-C27 2.063 (2), Ti-Si1-C1 162.94(6), C27-Ti-Si1 109.40(6).

5.4. Cyclic Voltammetric studies of compounds

Table 36. Criteria for electrochemical processes in cyclic voltammetry.

Process	Criteria
E_r	i) Nicholson criteria: ΔE_p = 57 – 64 mV for one electron redox event.[a)] ii) Randles-Sevcik criteria: i_p versus $\upsilon^{1/2}$plot is linear at constant temperature. iii) i_{pa}/i_{pc} = 1 iv) ΔE_p is constant at all scan rates.
E_q	v) Nicholson criteria: ΔE_p = 65 – 160 mV for one electron redox event. vi) Randles-Sevcik criteria: i_p versus $\upsilon^{1/2}$plot is almost linear at constant temperature. vii) i_{pa}/i_{pc} = 1 viii) ΔE_p increases as the scan rate increases.
E_i	ix) only one peak potential is observed at all scan rate.
E_rC_i	x) one peak potential at lower scan rates but two peak potentials at higher scan rates. xi) criteria-(i) to (iv) are satisfied at higher scan rates.

ΔE_p = separation between the peak potential, i_p = peak current, i_{pa} = anodic peak current, i_{pc} = cathodic peak current, υ = scan rate. a) A higher range of ΔE_p of 57 – 100 mV was considered in our studies due to incomplete iR-drop compensation. The electrochemical processes - reversible (E_r), quasi-reversible (E_q), irreversible (E_i) and a reversible electrochemical process coupled with irreversible chemical reaction (E_rC_i) were distinguished according to the criteria given in reference [247,248].

CV studies of [CpCo(CO)Ge$_2$Tbb$_2$] (**1-Co**)

Complex **1-Co** displays two reversible voltammetric waves (E_r-process) at a $E_{1/2}$ = –1.366 V for the redox couple **1-Co**/**1-Co**$^{\bullet-}$ and at a $E_{1/2}$ = +0.462 V for the redox couple **1-Co**/**1-Co**$^{\bullet+}$. In addition, it undergoes two irreversible electron transfers (E_i-process) at a peak potential of E_{pc} = –2.273 V and E_{pa} = +1.367 V for reduction and oxidation, respectively. The assignment is backed up by determining the open circuit potential (OCP) = –0.708 V vs. DMFc$^{+/0}$.

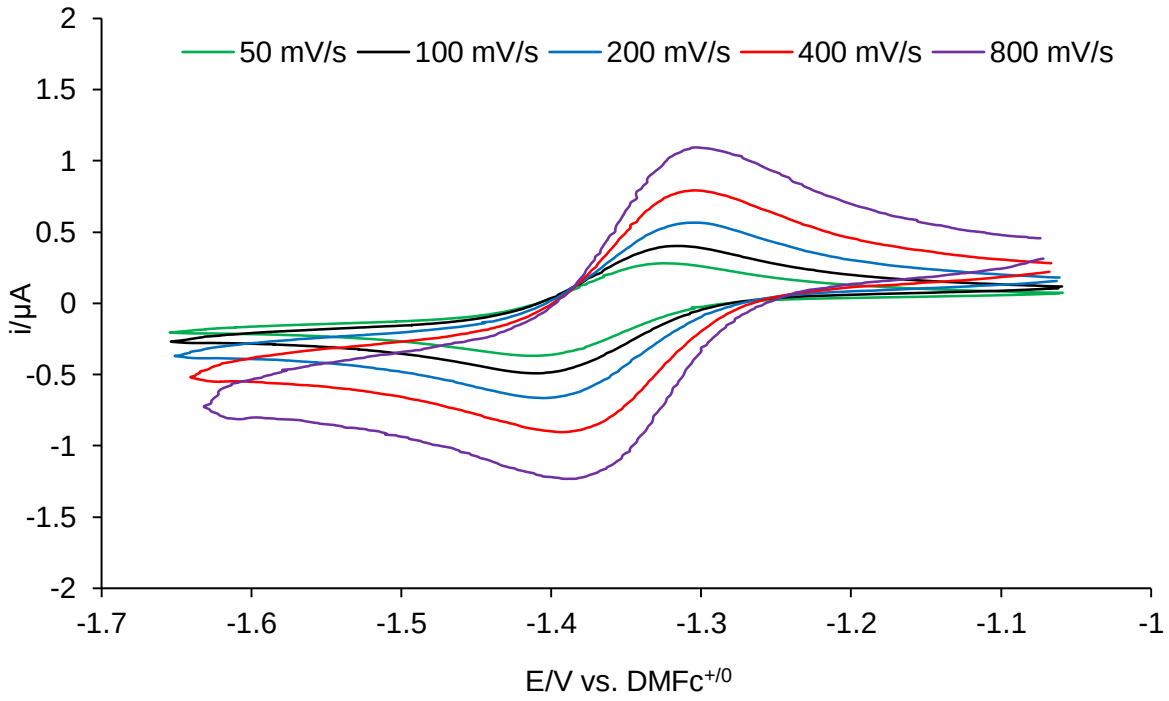

Figure 96. Cyclic voltammograms of **1-Co** measured between the initial potential of –1.05 V and switching potential of –1.65 V at different scan rates in fluorobenzene at ambient temperature. A reversible reduction at $E_{1/2}$ = –1.366 V vs. DMFc$^{+/0}$ is observed.

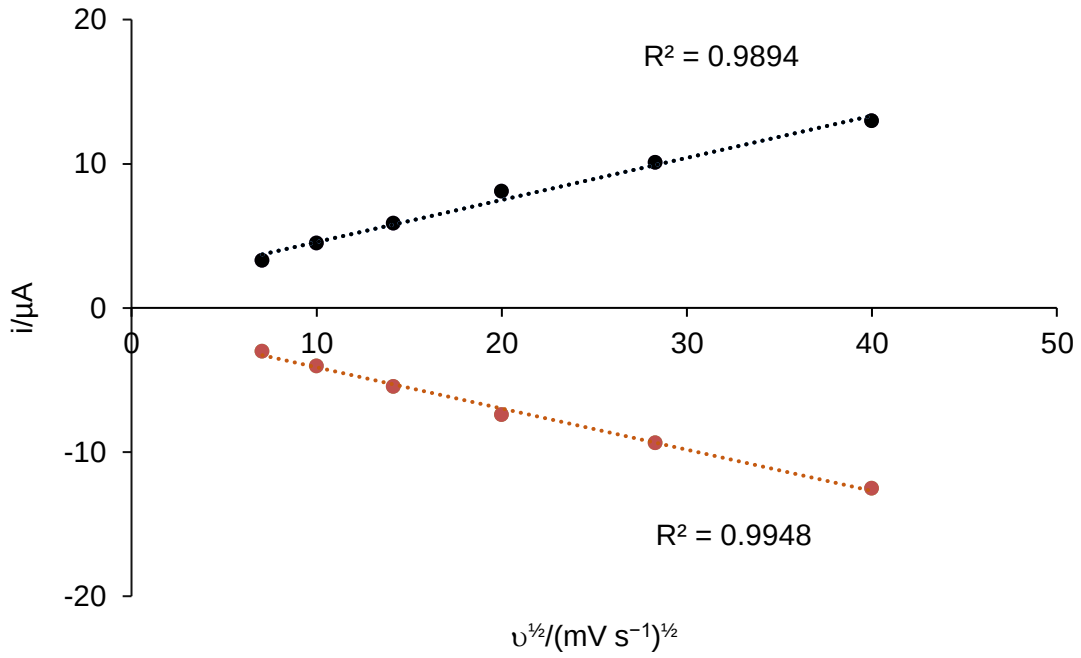

Figure 97. Randles-Sevcik plot (i_p versus $\upsilon^{1/2}$) of the **1-Co/1-Co$^{\bullet-}$** redox couple at ambient temperature.

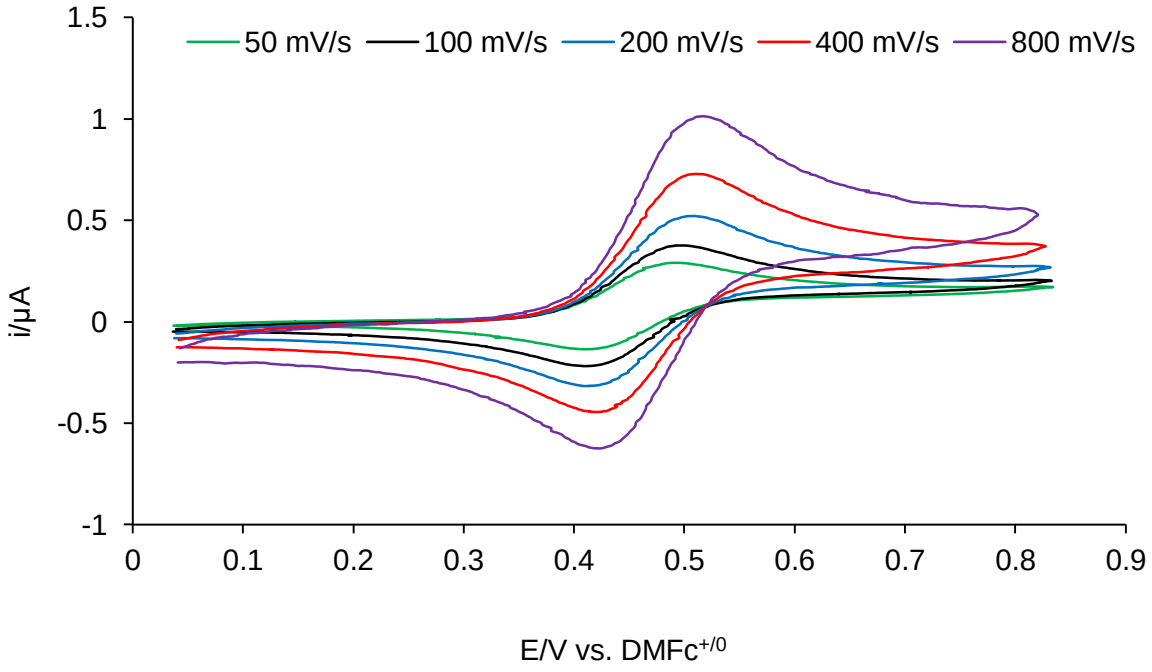

Figure 98. Cyclic voltammograms of **1-Co** measured between the initial potential of −0.05 V and switching potential of 0.85 V at different scan rates in fluorobenzene at ambient temperature. A reversible oxidation at $E_{1/2}$ = 0.462 V vs. DMFc$^{+/0}$ is observed.

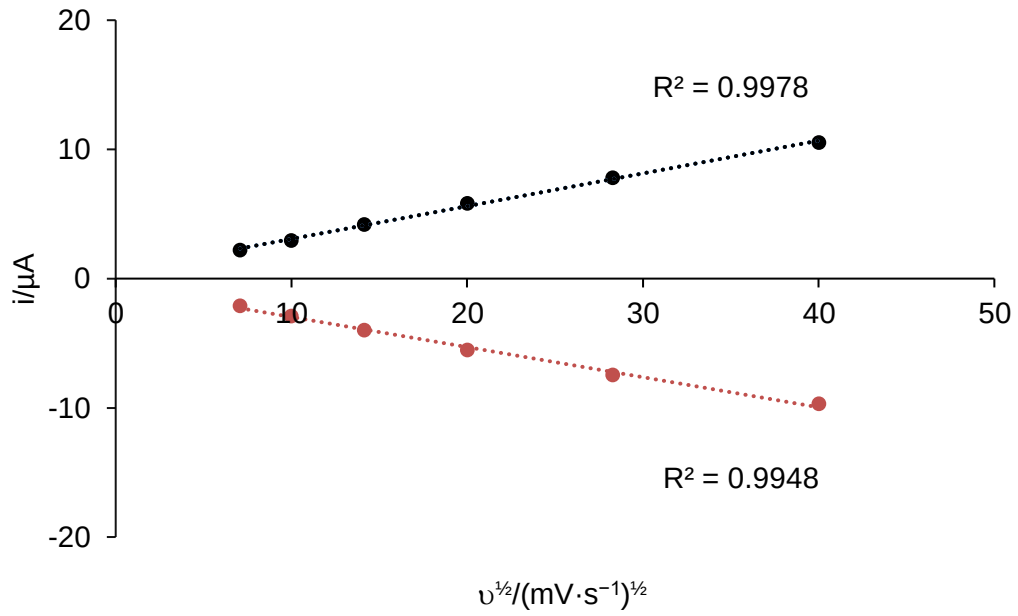

Figure 99. Randles-Sevcik plot (i_p versus $\upsilon^{1/2}$) of the **1-Co/1-Co$^{\bullet+}$** redox couple at ambient temperature.

Table 37. Results of the cyclic voltammetric experiments of **1-Co**.

υ (mV s^{-1})	i_{pa} (µA)	i_{pc} (µA)	i_{pa}/i_{pc}	E_{pa} (V)	E_{pc} (V)	ΔE_p (mV)	$E_{1/2}$ (V)
			E_r-process for **1-Co/1-Co$^{\bullet-}$**				
50	3.29	-2.99	1.10	-1.336	-1.397	61	-1.367
100	4.48	-4.03	1.11	-1.327	-1.405	78	-1.366
200	5.87	-5.45	1.08	-1.325	-1.407	82	-1.366
400	8.08	-7.40	1.09	-1.330	-1.402	72	-1.366
800	10.07	-9.35	1.08	-1.337	-1.395	58	-1.366
			E_r-process for **1-Co/1-Co$^{\bullet+}$**				
50	2.22	-2.09	1.06	0.491	0.433	58	0.462
100	2.95	-2.90	1.02	0.497	0.427	70	0.462
200	4.19	-4.00	1.05	0.502	0.422	80	0.462
400	5.81	-5.51	1.05	0.497	0.427	70	0.462
800	7.82	-7.48	1.05	0.505	0.419	86	0.462

υ: scan rate; I_{pa}: anodic peak-current; I_{pc}: cathodic peak-current; I_{pa}/I_{pc}: ratio of anodic and cathodic peak current; E_{pa}: anodic peak potential; E_{pc}: cathodic peak potential; $\Delta E_p = |E_{pa} - E_{pc}|$ = peak potential separation; $E_{1/2} = (E_{pa} + E_{pc})/2$ = half wave potential. All potentials are given versus the $[Fe(C_5Me_5)_2]^{+1/0}$ reference electrode.

CV studies of [CpCo(Ge$_2$Tbb$_2$)] (3-Co)

Complex **3-Co** shows two reversible voltammetric response at the $E_{1/2}$ = −1.484 V and +0.149 V for the **3-Co/3-Co$^{\bullet-}$** and **3-Co/3-Co$^{\bullet+}$** redox couple, respectively. In addition, it undergoes an irreversible electron transfer (E_i-process) at a peak potential of E_{pa} = +0.828 V. The assignment is backed up by determining the open circuit potential (OCP) = −0.767 V vs. $DMFc^{+/0}$.

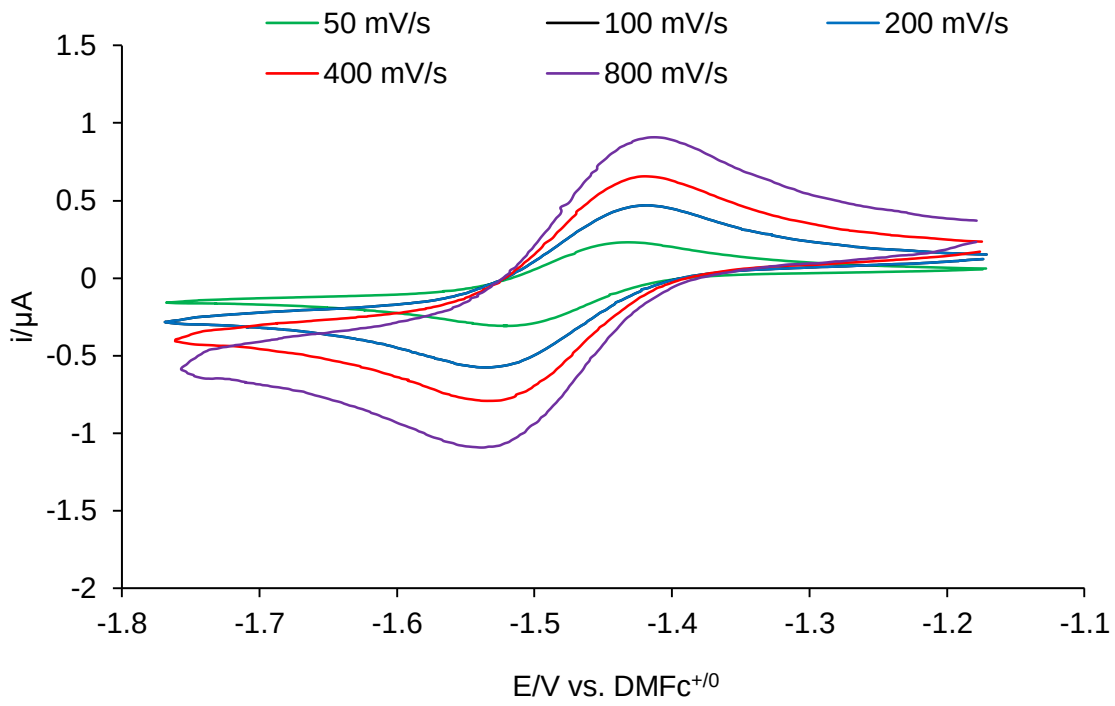

Figure 100. Cyclic voltammograms of **3-Co** measured between the initial potential of −1.15 V and switching potential of −1.75 V at different scan rates in fluorobenzene at ambient temperature. A reversible reduction at $E_{1/2}$ = −1.484 V vs. DMFc$^{+/0}$ is observed.

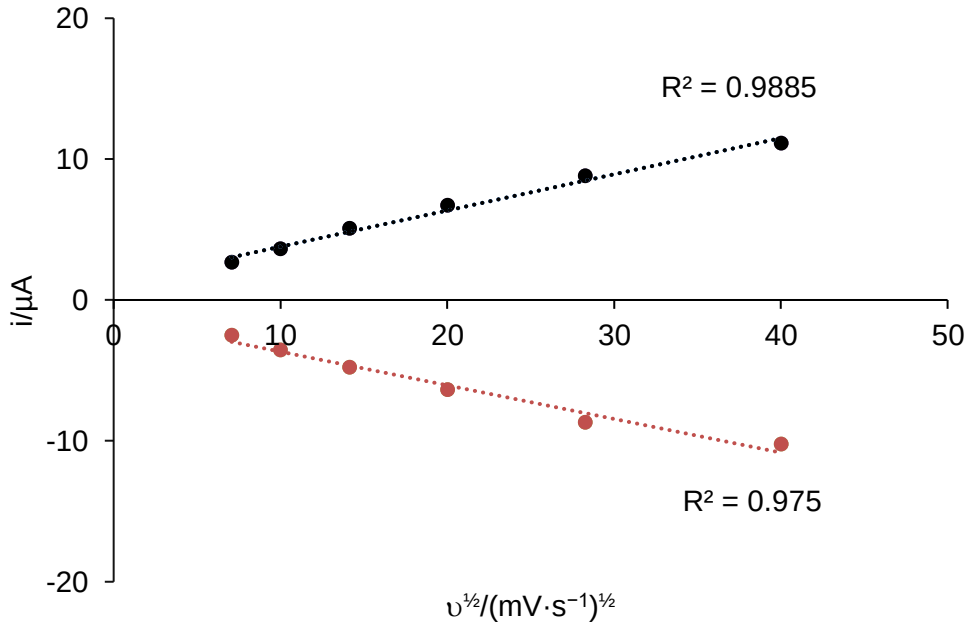

Figure 101. Randles-Sevcik plot (i_p versus $\upsilon^{1/2}$) of the **3-Co**/**3-Co**$^{\bullet-}$ redox couple at ambient temperature.

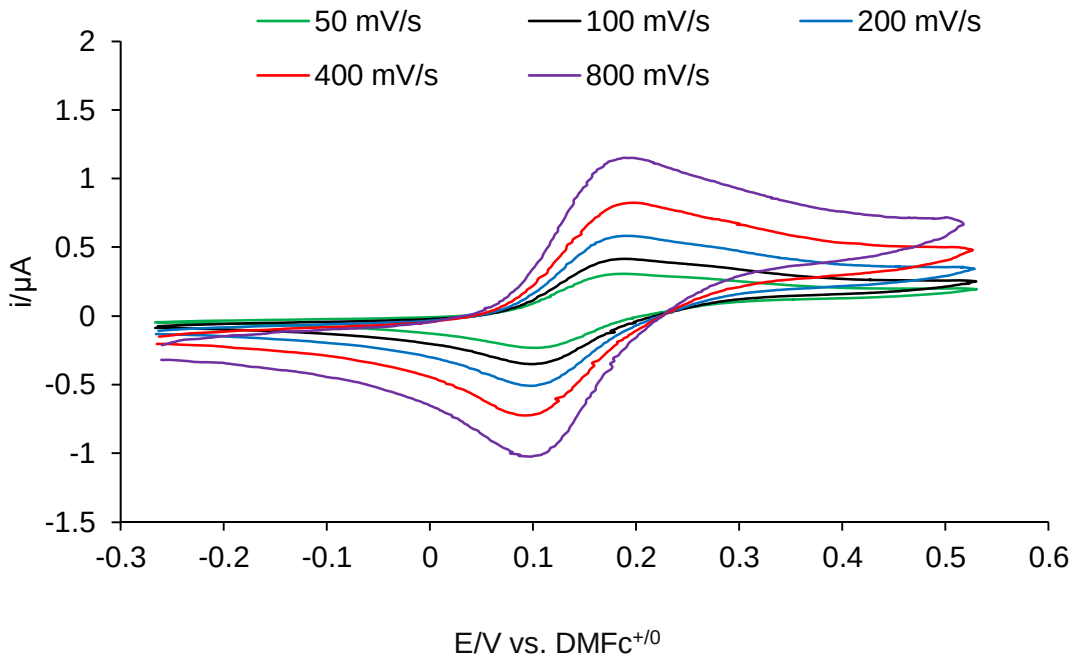

Figure 102. Cyclic voltammograms of **3-Co** measured between the initial potential of −0.25 V and switching potential of 0.55 V at different scan rates in fluorobenzene at ambient temperature. A possibly reversible oxidation at $E_{1/2}$ = 0.149 V vs. DMFc$^{+/0}$ is observed. The ratio of oxidative and reductive currents $-i_{pa}/i_{pc}$ is not significantly dependent on the scan rate and both currents are linearly dependent on the square root of the scan rate, fulfilling two criteria of reversibility. However, the oxidative current is always too low, which is the reason the current ratio does not reach 1. This may be due to some underlying secondary oxidative process, which may be indicated by the somewhat unusually linear shape of the oxidative current above 0.2 V vs. DMFc$^{+/0}$.

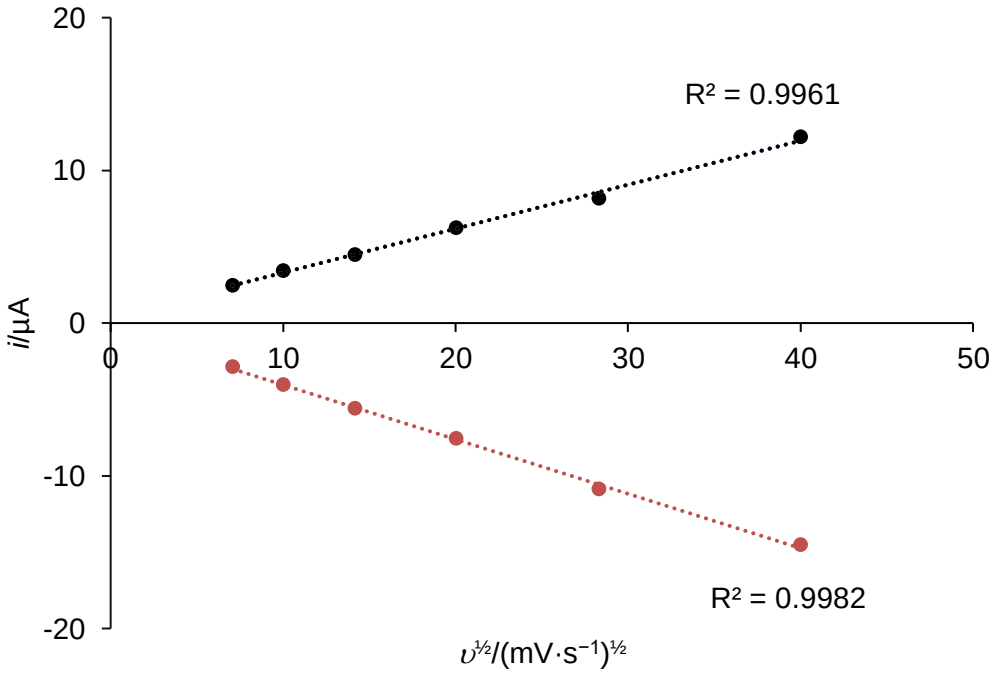

Figure 103. Randles-Sevcik plot (i_p versus $\upsilon^{1/2}$) of the **3-Co/3-Co$^{+\bullet}$** redox couple at ambient temperature.

Table 38. Results of the cyclic voltammetric experiments of **3-Co**.

υ (mV s^{-1})	i_{pa} (µA)	i_{pc} (µA)	i_{pa}/i_{pc}	E_{pa} (V)	E_{pc} (V)	ΔE_p (mV)	$E_{½}$ (V)
			E_r-process for **3-Co**/**3-Co**$^{\bullet-}$				
50	2.66	-2.53	1.05	-1.445	-1.524	79	-1.485
100	3.64	-3.56	1.02	-1.445	-1.523	78	-1.484
200	5.06	-4.78	1.06	-1.440	-1.528	88	-1.484
400	6.70	-6.39	1.05	-1.439	-1.529	90	-1.484
800	8.82	-8.71	1.01	-1.441	-1.527	86	-1.484
			E_r-process for **3-Co**/**3-Co**$^{\bullet+}$				
50	2.46	-2.86	0.86	0.178	0.121	57	0.150
100	3.44	-4.06	0.85	0.182	0.117	65	0.150
200	4.49	-5.59	0.80	0.186	0.112	74	0.149
400	6.21	-7.57	0.82	0.188	0.110	78	0.149
800	8.15	-10.89	0.75	0.182	0.117	65	0.150

υ: scan rate; I_{pa}: anodic peak-current; I_{pc}: cathodic peak-current; I_{pa}/I_{pc}: ratio of anodic and cathodic peak current; E_{pa}: anodic peak potential; E_{pc}: cathodic peak potential; $\Delta E_p = |E_{pa} - E_{pc}|$ = peak potential separation; $E_{1/2} = (E_{pa} + E_{pc})/2$ = half wave potential. All potentials are given versus the $[Fe(C_5Me_5)_2]^{+1/0}$ reference electrode.

CV studies of [CpCo(Ge$_2$Tbb$_2$C$_2$Me$_2$)] (**5-Co**)

Compound **5-Co** shows quasi-reversible (E_q-process) voltammetric waves at a $E_{1/2}$ = −1.983 V for the redox couple **5-Co**/**5-Co**$^{\bullet-}$ and at a $E_{1/2}$ = +0.337 V for the redox couple **5-Co**/**5-Co**$^{\bullet+}$. The assignment is made based on the determination of the open circuit potential (OCP) = −0.132 V vs. DMFc$^{+/0}$.

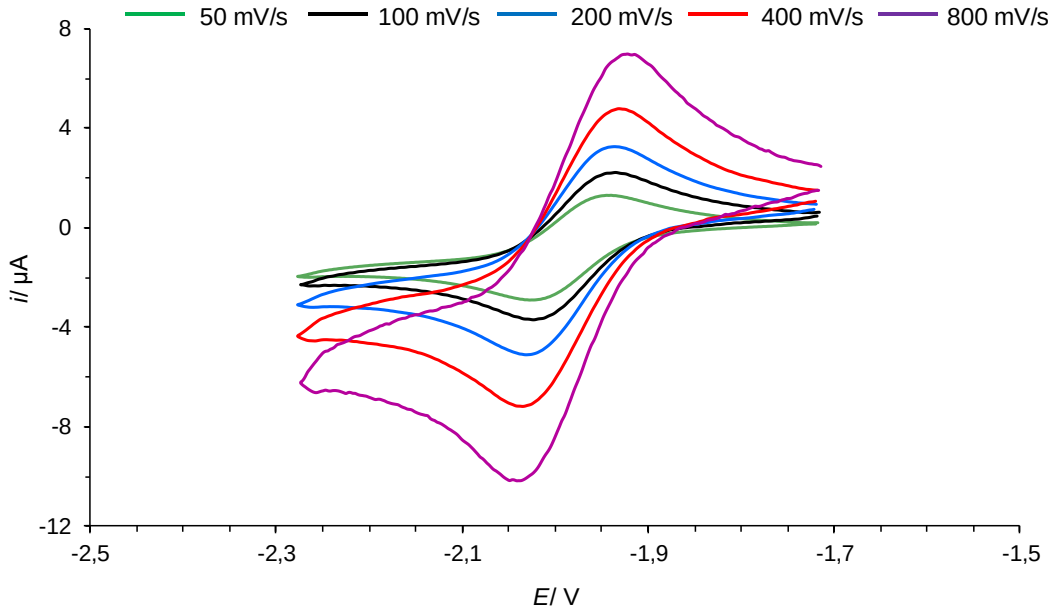

Figure 104. Cyclic voltammograms of **5-Co** measured between the initial potential of −1.70 V and switching potential of −2.30 V at different scan rates in fluorobenzene at ambient temperature. A quasi-reversible reduction at $E_{1/2}$ = −1.983 V vs. DMFc$^{+/0}$ is observed.

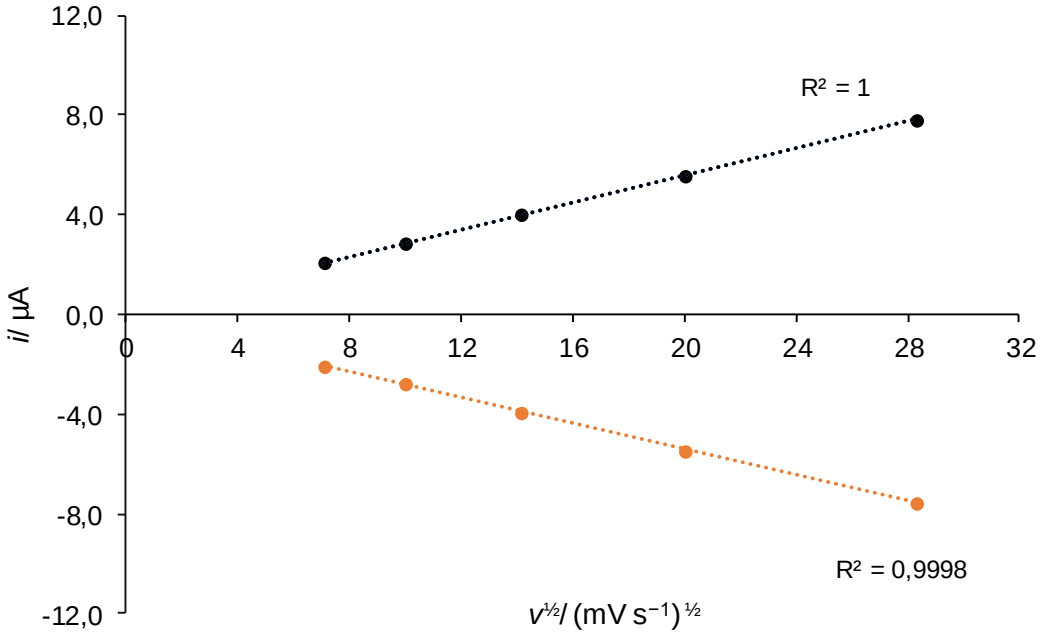

Figure 105. Randles-Sevcik plot (i_p versus $\upsilon^{1/2}$) of the **5-Co/5-Co$^{\bullet-}$** redox couple at ambient temperature.

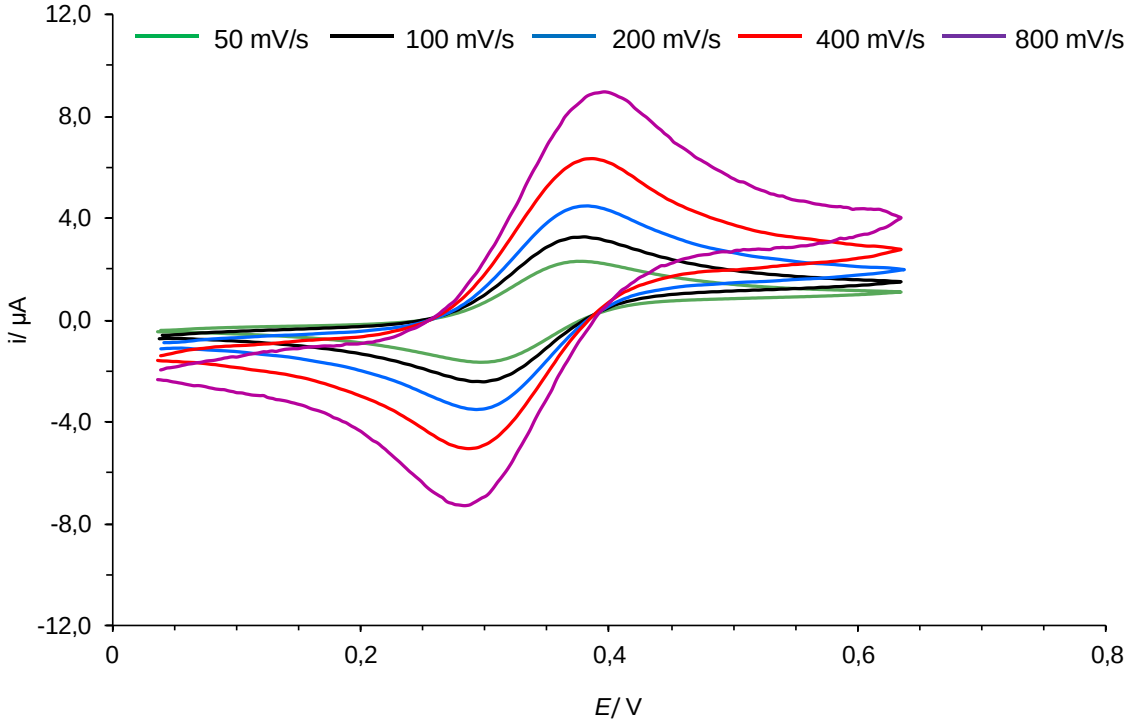

Figure 106. Cyclic voltammograms of **5-Co** measured between the initial potential of −0.05 V and switching potential of 0.65 V at different scan rates in fluorobenzene at ambient temperature. A quasi-reversible oxidation at $E_{1/2}$ = 0.337 V vs. $DMFc^{+/0}$ is observed.

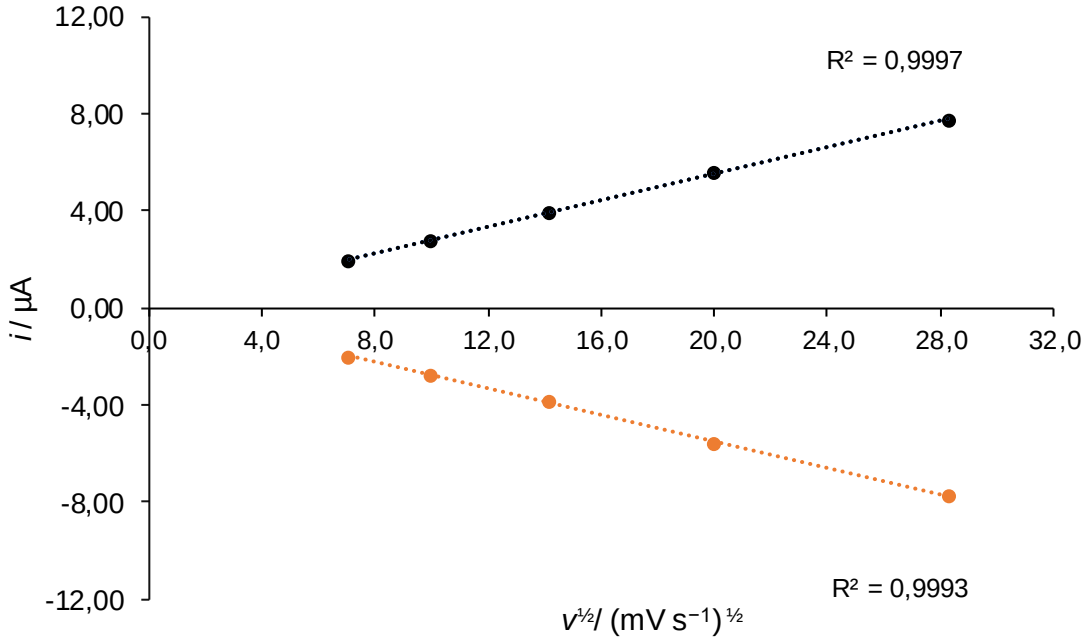

Figure 107. Randles-Sevcik plot (i_p versus $\upsilon^{1/2}$) of the **5-Co/5-Co$^{\bullet+}$** redox couple at ambient temperature.

Table 39. Results of the cyclic voltammetric experiments of **5-Co**.

υ (mV s^{-1})	i_{pa} (µA)	i_{pc} (µA)	i_{pa}/i_{pc}	E_{pa} (V)	E_{pc} (V)	ΔE_p (mV)	$E_{1/2}$ (V)
			E_q-process for **5-Co/5-Co$^{\bullet-}$**				
50	2.07	-2.09	0.99	-1.946	-2.020	73	-1.983
100	2.86	-2.78	1.03	-1.943	-2.023	81	-1.983
200	4.00	-3.91	1.02	-1.940	-2.026	86	-1.983
400	5.58	-5.45	1.02	-1.939	-2.027	88	-1.983
800	7.82	-7.53	1.04	-1.932	-2.034	103	-1.983
			E_q-process for **5-Co/5-Co$^{\bullet+}$**				
50	1.96	-1.99	0.99	0.374	0.300	73	0.337
100	2.80	-2.76	1.01	0.372	0.302	71	0.337
200	3.94	-3.86	1.02	0.376	0.298	78	0.337
400	5.58	-5.60	1.00	0.382	0.292	90	0.337
800	7.74	-7.70	1.00	0.388	0.286	103	0.337

υ: scan rate; I_{pa}: anodic peak-current; I_{pc}: cathodic peak-current; I_{pa}/I_{pc}: ratio of anodic and cathodic peak current; E_{pa}: anodic peak potential; E_{pc}: cathodic peak potential; $\Delta E_p = |E_{pa} - E_{pc}|$ = peak potential separation; $E_{1/2} = (E_{pa} + E_{pc})/2$ = half wave potential. All potentials are given versus the $[Fe(C_5Me_5)_2]^{+1/0}$ reference electrode.

CV studies of [(PMe$_3$)$_2$Co{(GeClTbb)(GeTbb)}] (**29-Co**)

Complex **29-Co** shows an one electron E_rC_i oxidation at $E_{1/2}$ of +0.137 V and a reversible one-electron oxidation at a $E_{1/2}$ of +1.292 V. It also shows an irreversible reduction at a cathodic peak potential E_{pc} of −2.200 V. The assignment is backed up by the determination of the open circuit potential at −0.437 V vs. $DMFc^{+/0}$.

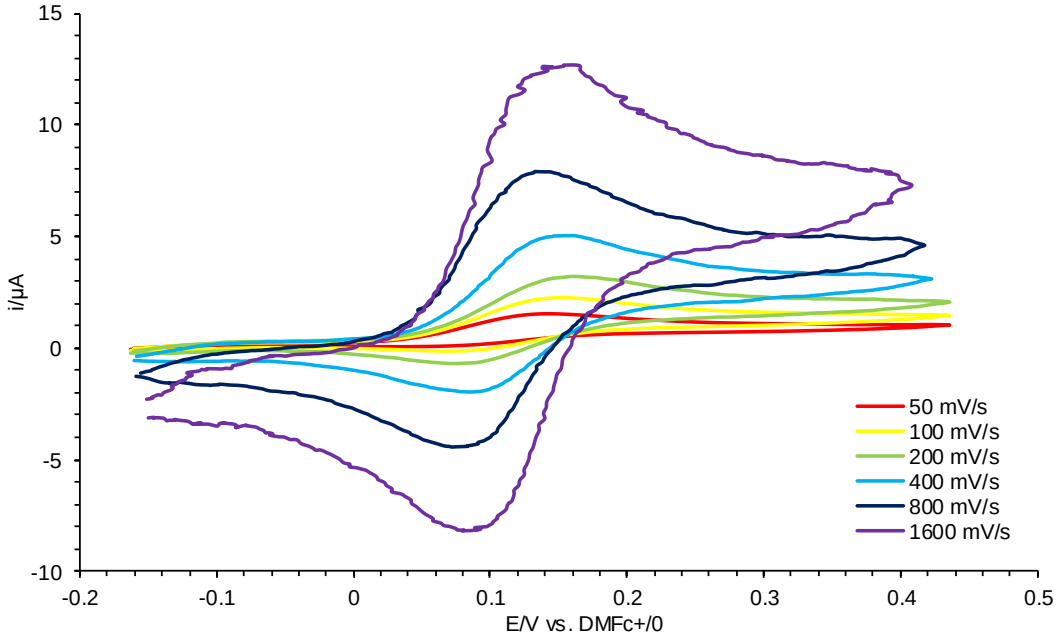

Figure 108. Cyclic voltammograms of **29-Co** in fluorobenzene measured at ambient temperature at different scan rates between the initial potential of −0.180 V and switching potential of +0.380 V. An oxidation (E_rC_i process) at $E_{1/2}$ = 0.137 V vs. $DMFc^{+/0}$ is observed.

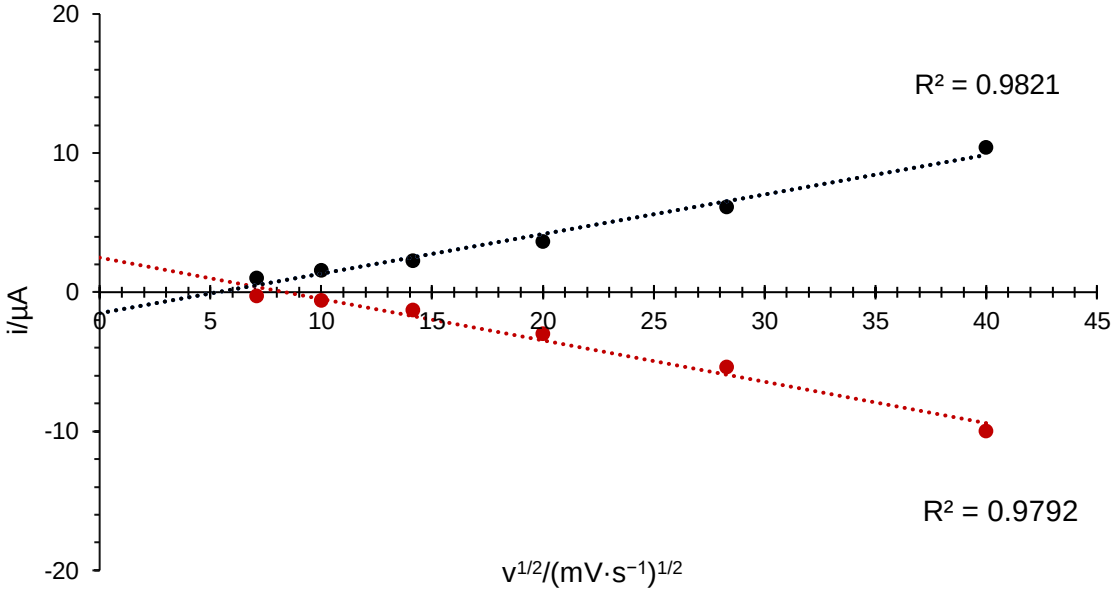

Figure 109. Randles-Sevcik plot of the [**29-Co**]/[**29-Co**]$^{\bullet+}$ redox couple at ambient temperature.

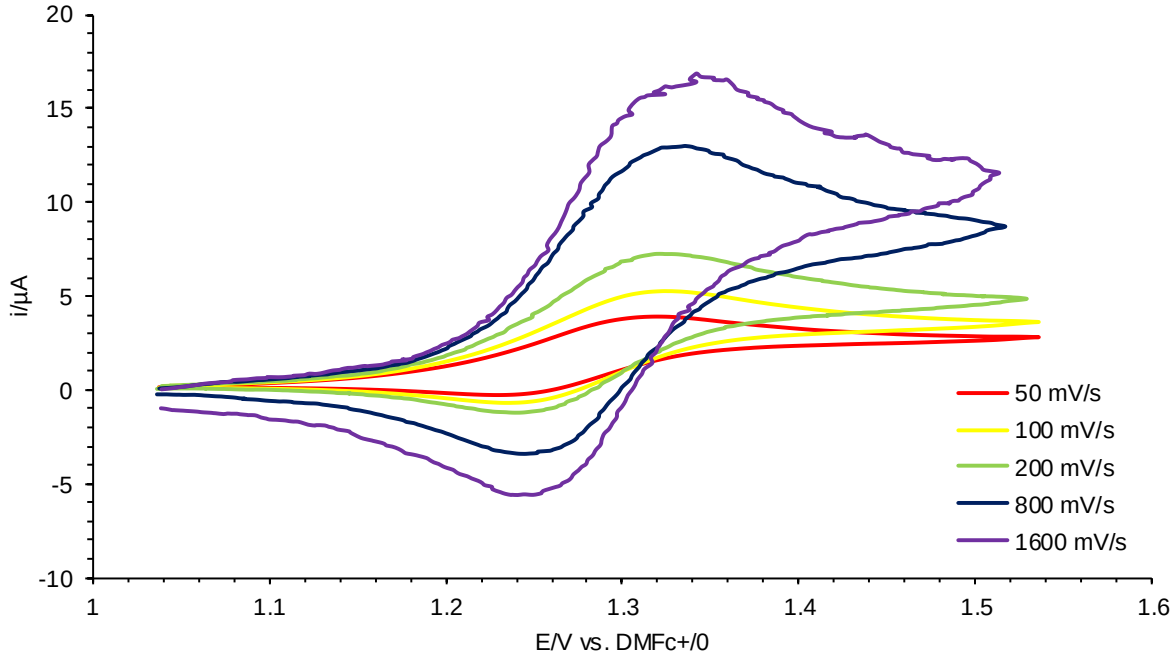

Figure 110. Cyclic voltammograms of **29-Co** in fluorobenzene measured at ambient temperature at different scan rates between the initial potential of +1.040 V and switching potential of +1.520 V. A reversible oxidation at $E_{1/2}$ = 1.292 V vs. $DMFc^{+/0}$ is observed.

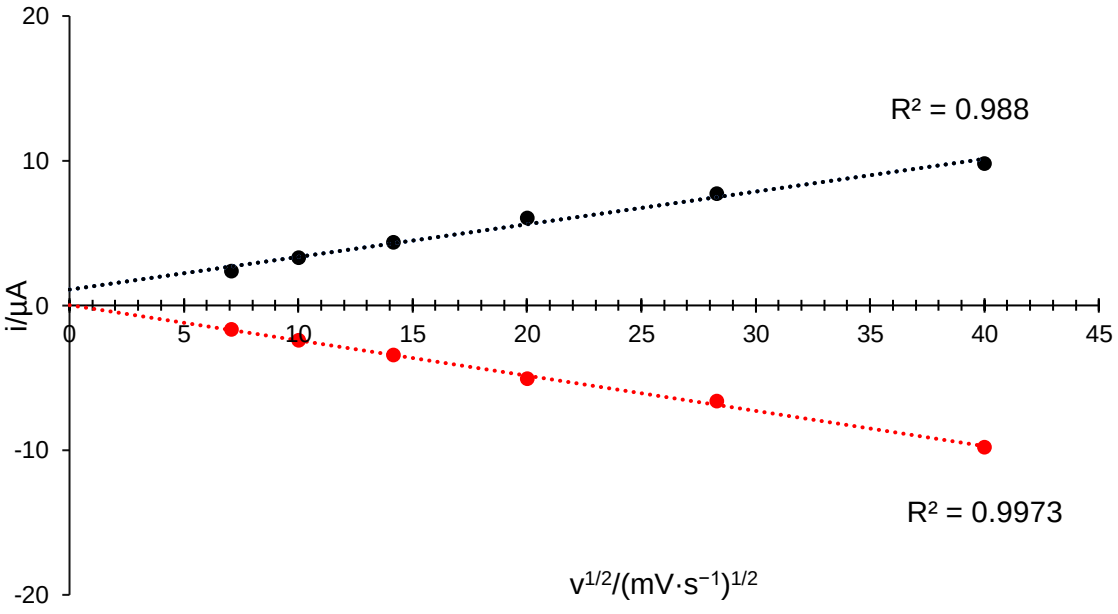

Figure 111. Randles-Sevcik plot of the $[\mathbf{29\text{-}Co}]^{+\bullet}/[\mathbf{29\text{-}Co}]^{2+}$ redox couple at ambient temperature.

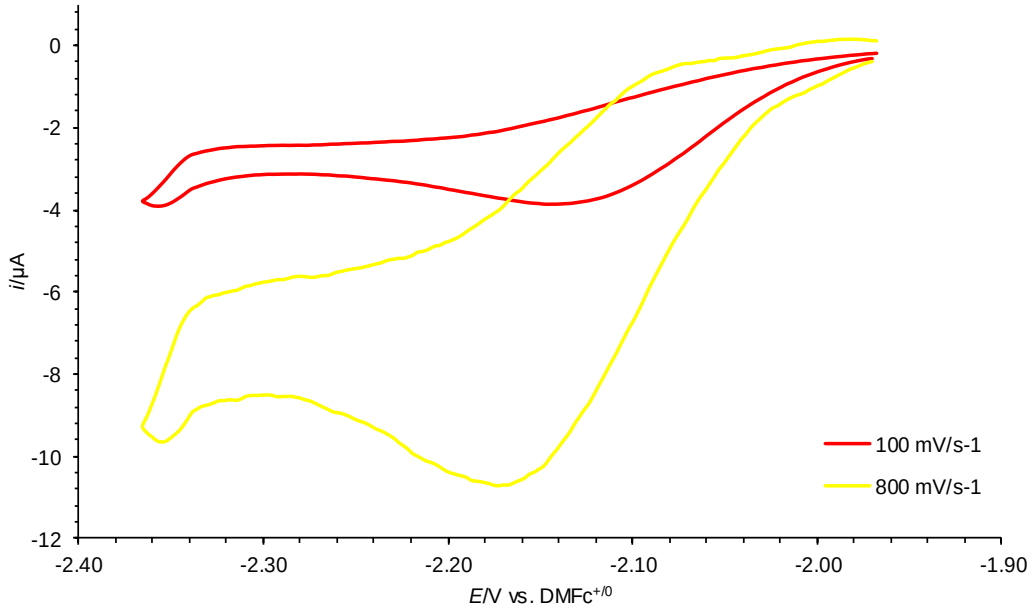

Figure 112. Cyclic voltammograms of **29-Co** in fluorobenzene measured at ambient temperature at two different scan rates between the initial potential of −2.000 V. An irreversible reduction at E_{pc} = −1.638 V vs. $DMFc^{+/0}$ (at 100 mV·s^{-1}) is observed.

Table 40. Results of the cyclic voltammetric experiments of **29-Co**.

υ (mV s^{-1})	i_{pa} (µA)	i_{pc} (µA)	i_{pa}/i_{pc}	E_{pa} (V)	E_{pc} (V)	ΔE_p (mV)	$E_{½}$ (V)
			E_rC_i-process for **29-Co**/**29-Co**$^{\bullet+}$				
50	1.01	−0.28	3.61	0.171	0.103	68	0.137
100	1.54	−0.62	2.50	0.170	0.104	66	0.137
200	2.25	−1.31	1.72	0.171	0.103	68	0.137
400	3.64	−3.02	1.21	0.167	0.107	59	0.137
800	6.10	−5.40	1.13	0.166	0.108	58	0.137
			E_r-process for **29-Co**$^{\bullet+}$/**29-Co**$^{2+}$				
50	2.35	−1.66	1.42	1.326	1.258	68	1.292
100	3.29	−2.42	1.36	1.327	1.257	71	1.292
200	4.36	−3.42	1.27	1.324	1.260	64	1.292
400	6.05	−5.08	1.19	1.328	1.256	72	1.292
800	7.70	−6.61	1.16	1.327	1.257	71	1.292

υ: scan rate; I_{pa}: anodic peak-current; I_{pc}: cathodic peak-current; I_{pa}/I_{pc}: ratio of anodic and cathodic peak current; E_{pa}: anodic peak potential; E_{pc}: cathodic peak potential; $\Delta E_p = |E_{pa} - E_{pc}|$ = peak potential separation; $E_{1/2} = (E_{pa} + E_{pc})/2$ = half wave potential. All potentials are given versus the $[Fe(C_5Me_5)_2]^{+1/0}$ reference electrode.

CV studies of $[(PMe_3)_2Co(GeTbb)_2][B(Ar^F)_4]$ (30-Co)

The investigated complex **30-Co** features one quasi-reversible one electron oxidation at a $E_{1/2}$ = 1.306 V and a quasi-reversible one electron reduction at a $E_{1/2}$ = −1.215 V vs. $DMFc^{+/0}$. The assignment is backed up by the determination of the open circuit potential of −0.43 V vs. $DMFc^{+/0}$.

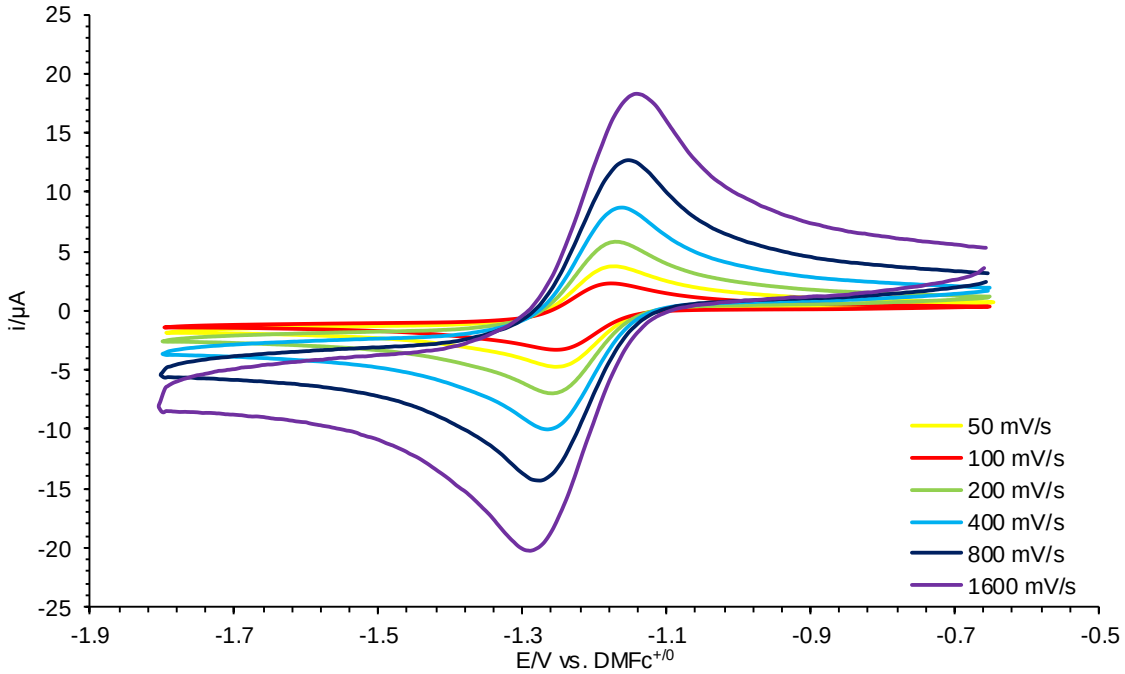

Figure 113. Cyclic voltammograms of **30-Co** in fluorobenzene measured at ambient temperature at different scan rates between the initial potential of −1.800 V and switching potential of −0.700 V. A quasi-reversible reduction at $E_{1/2}$ = −1.215 V vs. $DMFc^{+/0}$ is observed.

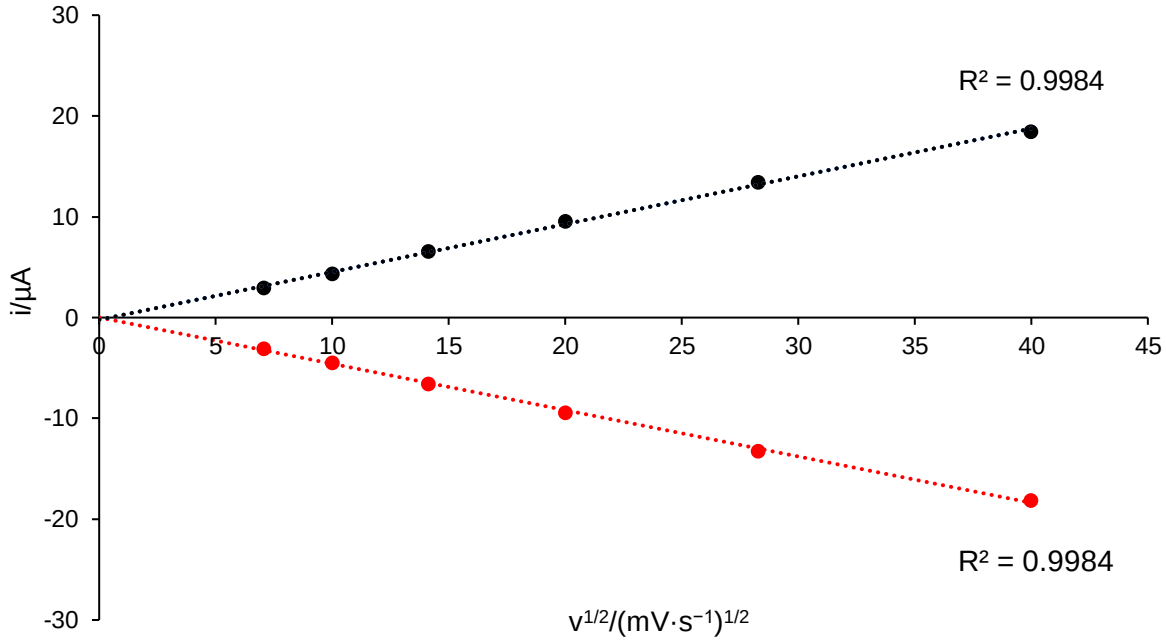

Figure 114. Randles-Sevcik plot of the **30-Co**/**30-Co**$^{neu.}$ redox couple at room temperature.

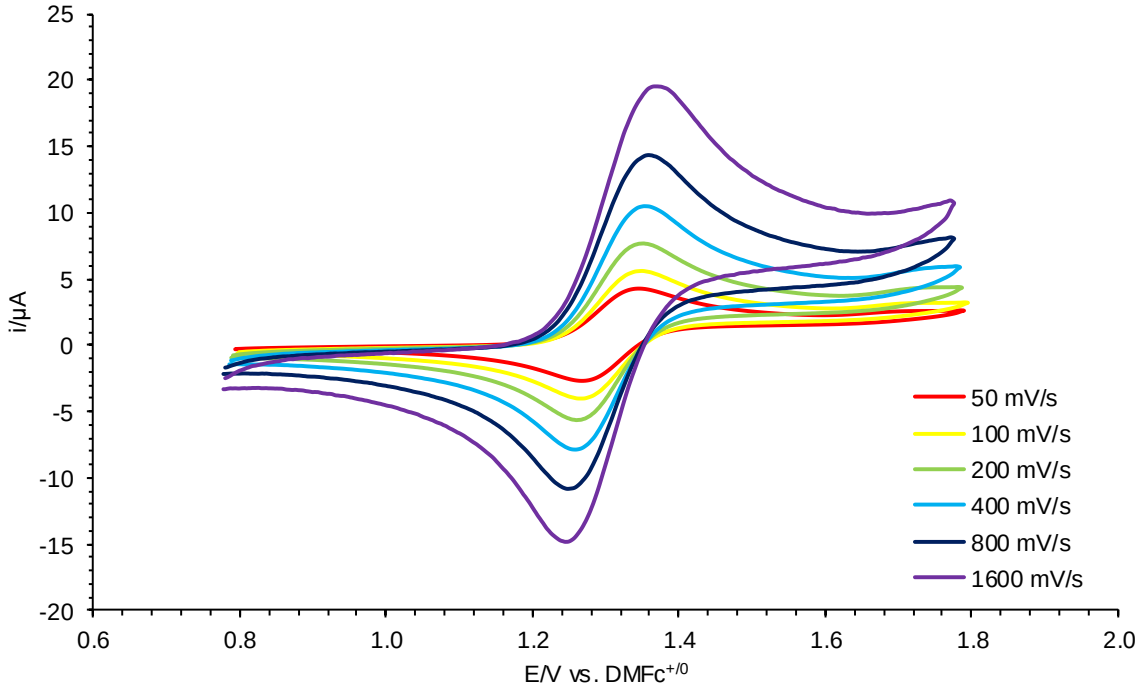

Figure 115. Cyclic voltammograms of **30-Co** in fluorobenzene measured at ambient temperature at different scan rates between the initial potential of +0.800 V and switching potential of +1.800 V. A quasi-reversible oxidation at $E_{1/2}$ = 1.306 V vs. $DMFc^{+/0}$ is observed.

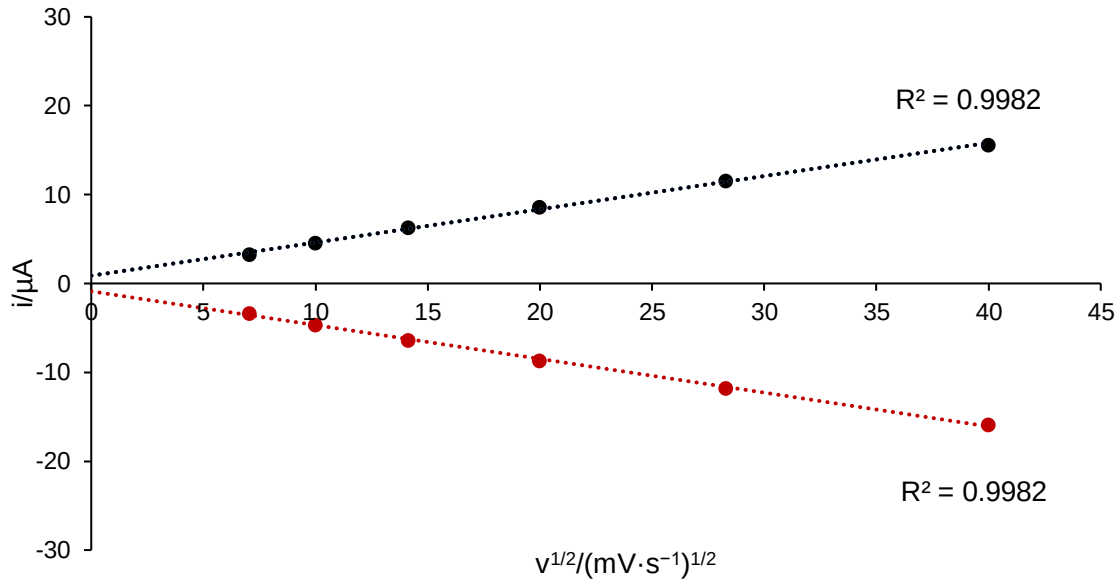

Figure 116. Randles-Sevcik plot of the **30-Co**/**30-Co**$^{\bullet+}$ redox couple at ambient temperature.

Table 41. Results of the cyclic voltammetric experiments of **30-Co**.

υ (mV s^{-1})	i_{pa} (µA)	i_{pc} (µA)	i_{pa}/i_{pc}	E_{pa} (V)	E_{pc} (V)	ΔE_p (mV)	$E_{½}$ (V)
			E_q-process for **30-Co**/**30-Co**$^{neu.}$				
50	2.96	−3.05	0.97	−1.178	−1.251	73	−1.215
100	4.38	−4.45	0.98	−1.178	−1.251	73	−1.215
200	6.56	−6.56	1.00	−1.172	−1.257	86	−1.215
400	9.55	−9.45	1.01	−1.165	−1.265	100	−1.215
800	13.45	−13.22	1.02	−1.155	−1.274	120	−1.215
			E_q-process for **30-Co**/**30-Co**$^{\bullet+}$				
50	3.29	−3.34	0.98	1.342	1.342	71	1.306
100	4.54	−4.62	0.98	1.342	1.342	73	1.306
200	6.27	−6.38	0.98	1.345	1.345	78	1.306
400	8.62	−8.72	0.99	1.350	1.350	88	1.306
800	11.56	−11.81	0.98	1.355	1.355	98	1.306

υ: scan rate; I_{pa}: anodic peak-current; I_{pc}: cathodic peak-current; I_{pa}/I_{pc}: ratio of anodic and cathodic peak current; E_{pa}: anodic peak potential; E_{pc}: cathodic peak potential; $\Delta E_p = |E_{pa} - E_{pc}|$ = peak potential separation; $E_{1/2} = (E_{pa} + E_{pc})/2$ = half wave potential; neu.: neutral. All potentials are given versus the $[Fe(C_5Me_5)_2]^{+1/0}$ reference electrode.

CV studies of $[(PMe_3)_2Fe(GeTbb)_2]$ (**33-Fe**)

Complex **33-Fe** features two reversible voltammetric response at the $E_{1/2}$ = 0.330 V and 0.910 V for the **33-Fe**/**33-Fe**$^{\bullet+}$ and **33-Fe**$^{\bullet+}$/**33-Fe**$^{2+}$ redox couple, respectively. The assignment is confirmed by the determination of the open circuit potential at −0.603 V vs. $DMFc^{+/0}$.

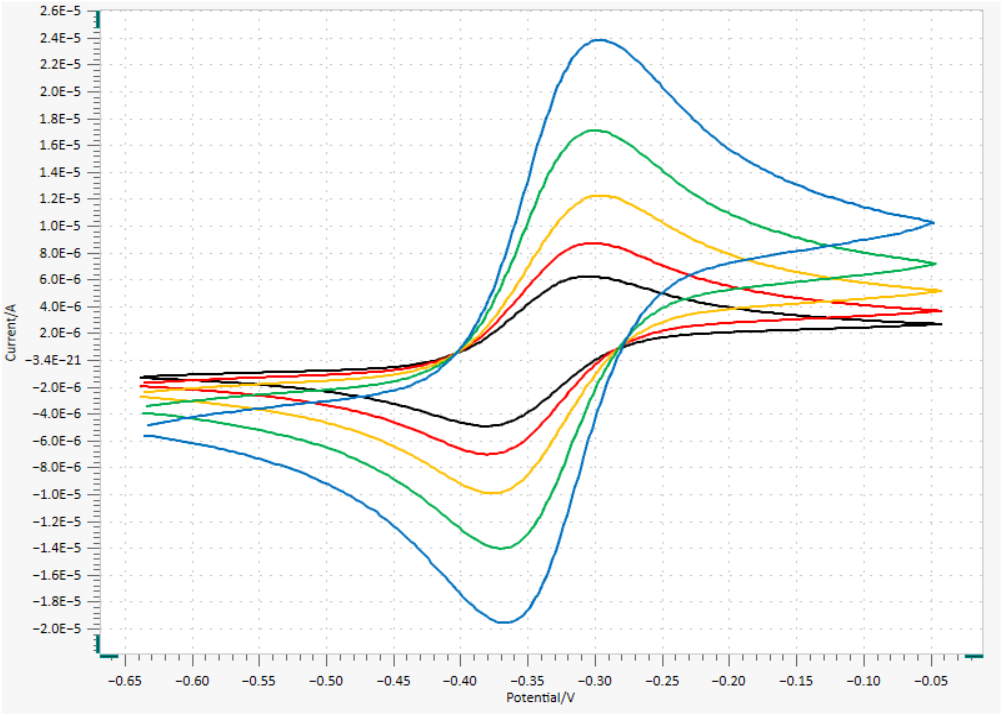

Figure 117. Cyclic voltammograms: measurements at 50 mV·s^{-1} (black), 100 mV·s^{-1} (red), 200 mV·s^{-1} (yellow), 400 mV·s^{-1} (green), and 800 mV·s^{-1} (blue) vs. $DMFc^{+/0}$. A reversible oxidation at $E_{1/2}$ = −0.330 V vs. $DMFc^{+/0}$ is observed.

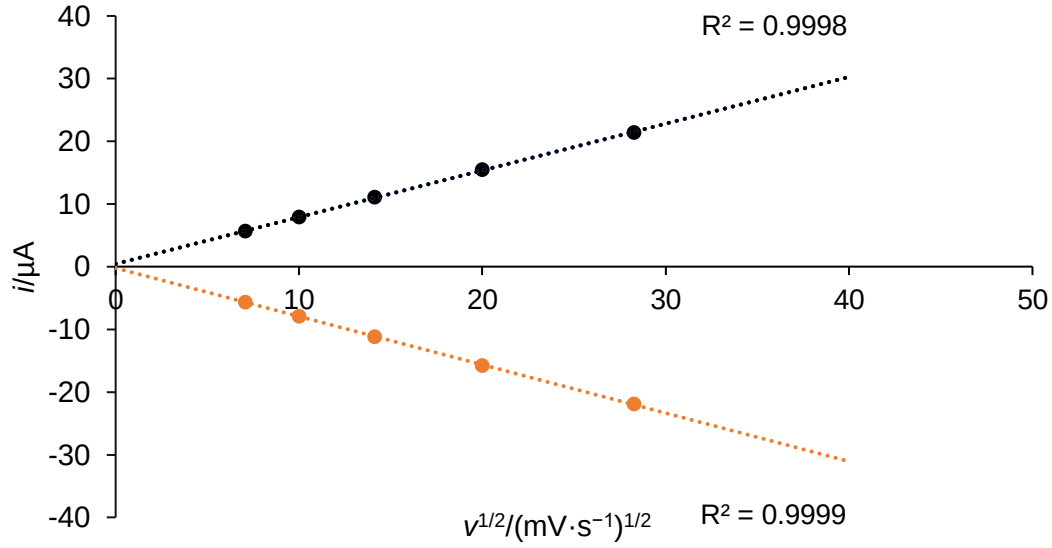

Figure 118. Randles-Sevcik plot of the **33-Fe**/**33-Fe**$^{\bullet+}$ redox couple at ambient temperature.

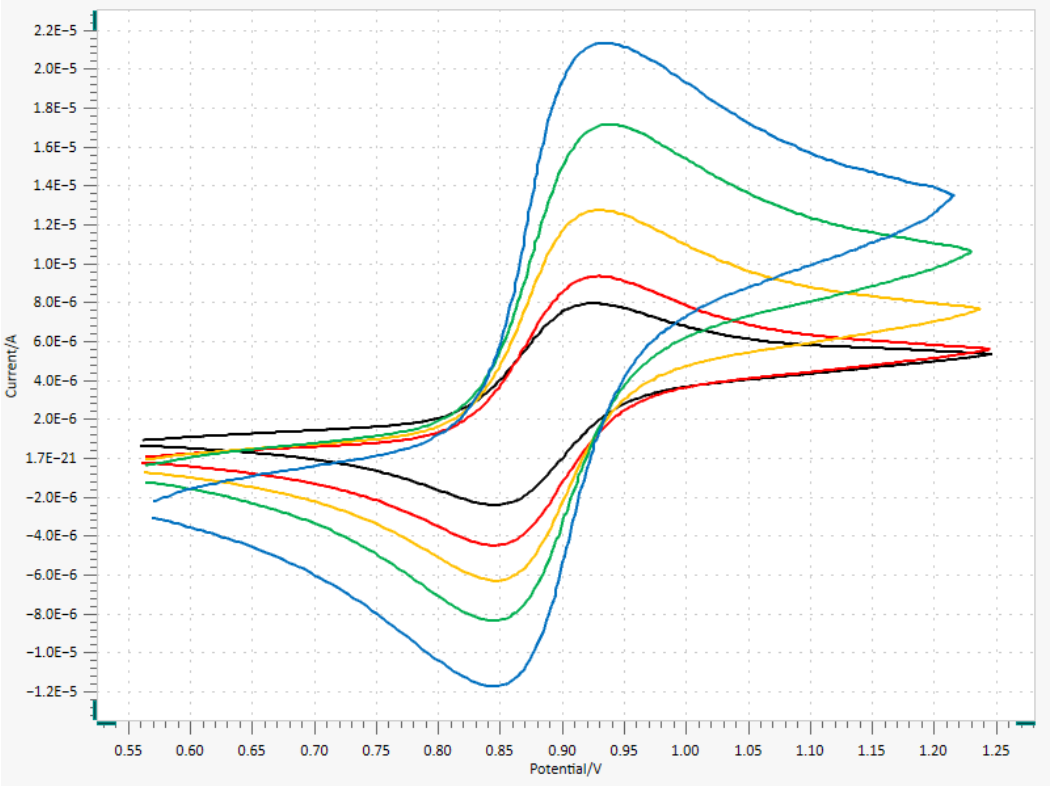

Figure 119. Cyclic voltammograms: measurements at 50 mV·s^{-1} (black), 100 mV·s^{-1} (red), 200 mV·s^{-1} (yellow), 400 mV·s^{-1} (green), and 800 mV·s^{-1} (blue) vs. DMFc$^{+/0}$. A reversible oxidation at $E_{1/2}$ = 0.910 V vs. DMFc$^{+/0}$ is observed.

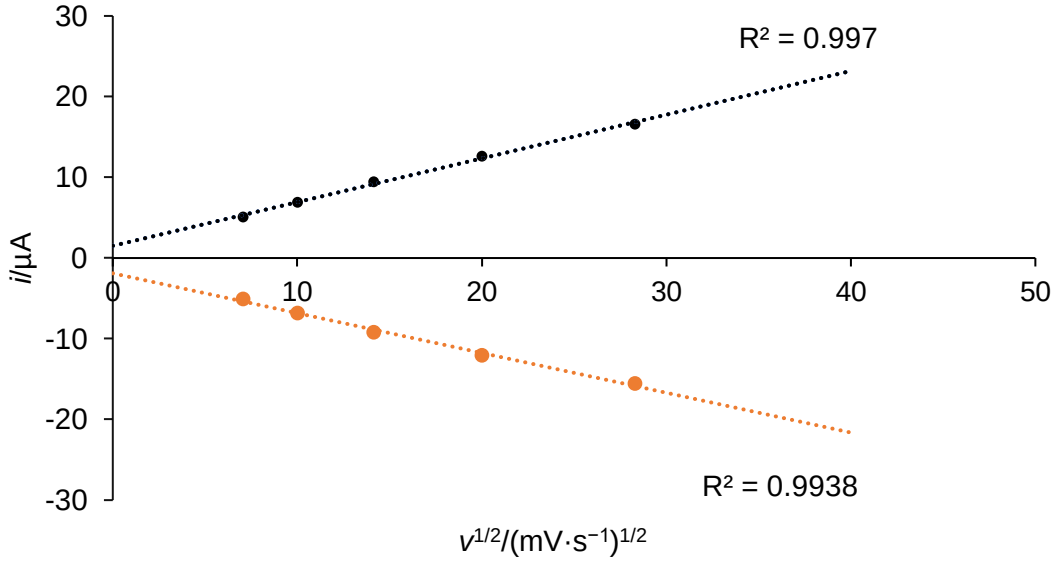

Figure 120. Randles-Sevcik plot of the **33-Fe**$^{\bullet+}$/**33-Fe**$^{2+}$ redox couple at ambient temperature.

Table 42. Results of the cyclic voltammetric experiments of **33-Fe**.

υ (mV s^{-1})	i_{pa} (µA)	i_{pc} (µA)	i_{pa}/i_{pc}	E_{pa} (V)	E_{pc} (V)	ΔE_p (mV)	$E_{½}$ (V)
			E_r-process for **33-Fe**/**33-Fe**$^{\bullet+}$				
50	5.63	−5.64	1.00	−0.296	−0.364	68	−0.330
100	7.89	−7.92	1.00	−0.295	−0.365	71	−0.330
200	11.03	−11.15	0.99	−0.293	−0.367	73	−0.330
400	15.49	−15.78	0.98	−0.299	−0.361	62	−0.330
800	21.43	−21.97	0.98	−0.298	−0.362	63	−0.330
			E_r-process for **33-Fe**$^{\bullet+}$/**33-Fe**$^{2+}$				
50	5.08	−5.06	1.00	0.945	0.875	70	0.910
100	6.91	−6.80	1.02	0.947	0.873	75	0.910
200	9.44	−9.21	1.03	0.946	0.874	72	0.910
400	12.58	−12.10	1.04	0.949	0.871	78	0.910
800	16.60	−15.54	1.07	0.946	0.874	72	0.910

υ: scan rate; I_{pa}: anodic peak-current; I_{pc}: cathodic peak-current; I_{pa}/I_{pc}: ratio of anodic and cathodic peak current; E_{pa}: anodic peak potential; E_{pc}: cathodic peak potential; $\Delta E_p = |E_{pa} - E_{pc}|$ = peak potential separation; $E_{1/2} = (E_{pa} + E_{pc})/2$ = half wave potential.; All potentials are given versus the $[Fe(C_5Me_5)_2]^{+1/0}$ reference electrode.

CV studies of [Cp*(CO)$_3$TiSiTbb] (**46-Ti**)

Complex **46-Ti** displays two reversible one-electron voltammetric waves at a $E_{1/2}$ = +0.625 V and −1.767 V for the redox couple **46-Ti**/**46-Ti**$^{\bullet+}$ and **46-Ti**/**46-Ti**$^{\bullet-}$, respectively. In addition, an E_rC_i process was found for the voltammetric wave of the **46-Ti**$^{\bullet-}$/**46-Ti**$^{2-}$ redox pair with an $E_{1/2}$ of −2.236 V, which was coupled with an irreversible chemical reaction of the dianion **46-Ti**$^{2-}$. The assignment is confirmed by the determination of the open circuit potential at −0.515 V vs. $DMFc^{+/0}$.

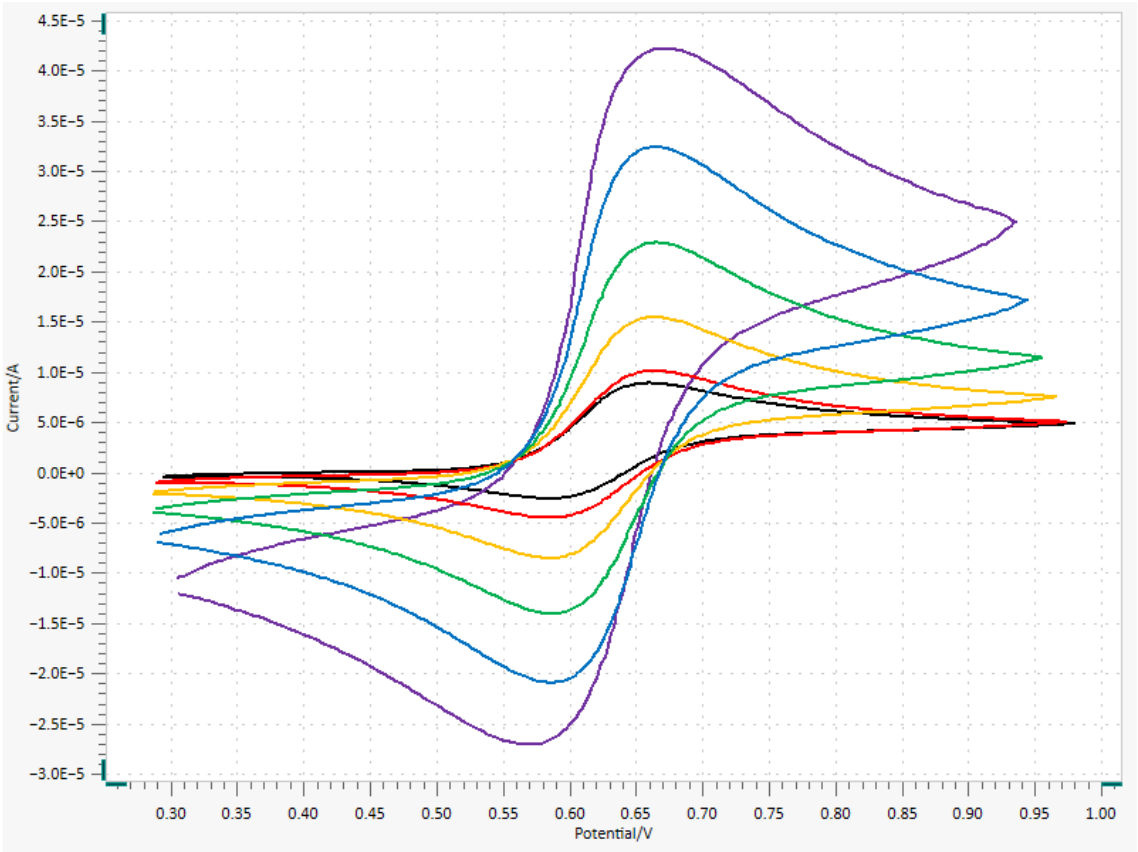

Figure 121. Cyclic voltammograms: measurements at 50 mV·s^{-1} (black), 100 mV·s^{-1} (red), 200 mV·s^{-1} (yellow), 400 mV·s^{-1} (green), 800 mV·s^{-1} (blue), and 1600 mV·s^{-1} (purple) vs. DMFc$^{+/0}$. A reversible oxidation at $E_{1/2}$ = 0.625 V vs. DMFc$^{+/0}$ is observed.

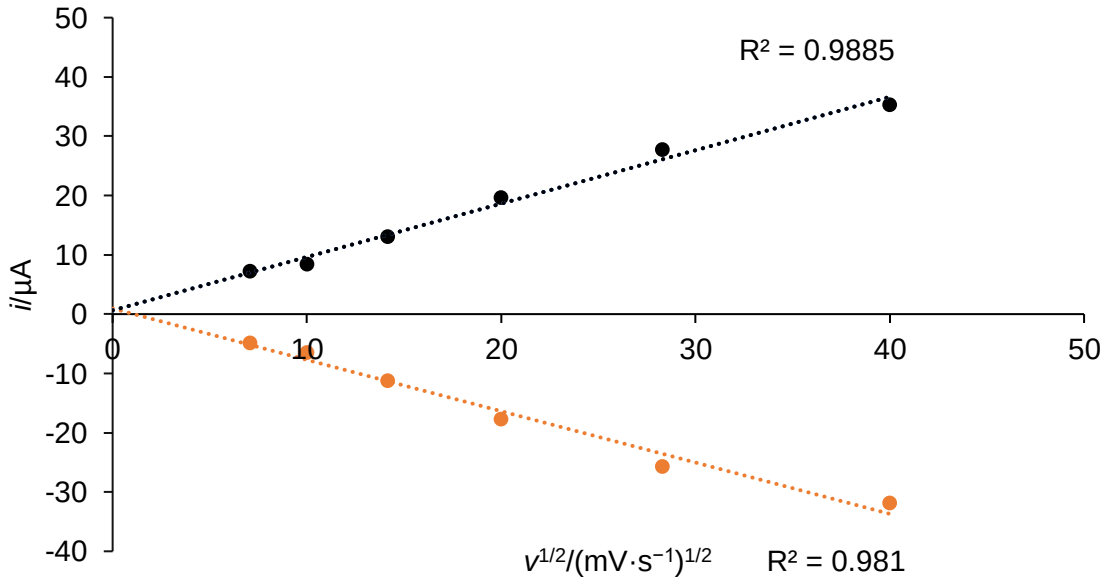

Figure 122. Randles-Sevcik plot of the **46-Ti**/**46-Ti**$^{\bullet+}$ redox couple at ambient temperature.

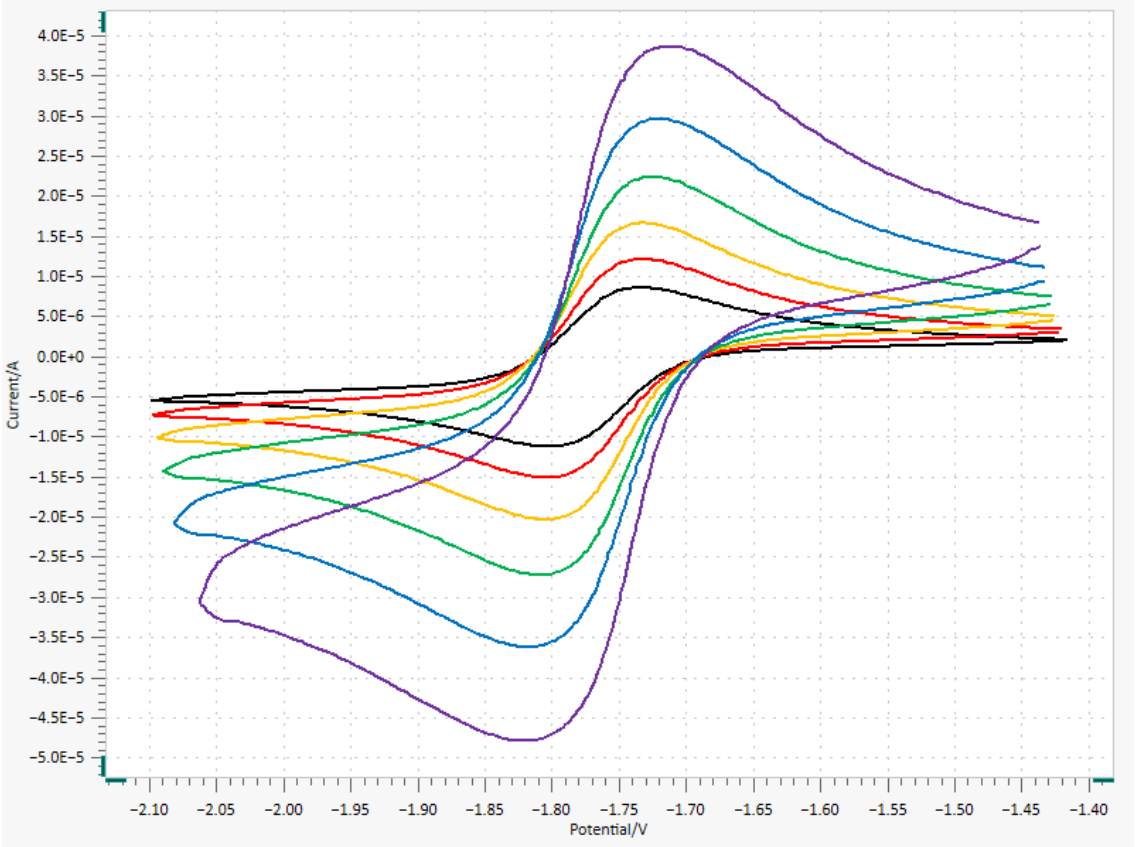

Figure 123. Cyclic voltammograms: measurements at 50 mV·s^{-1} (black), 100 mV·s^{-1} (red), 200 mV·s^{-1} (yellow), 400 mV·s^{-1} (green), 800 mV·s^{-1} (blue), and 1600 mV·s^{-1} (purple) vs. DMFc$^{+/0}$. A reversible oxidation at $E_{1/2}$ = −1.767 V vs. DMFc$^{+/0}$ is observed.

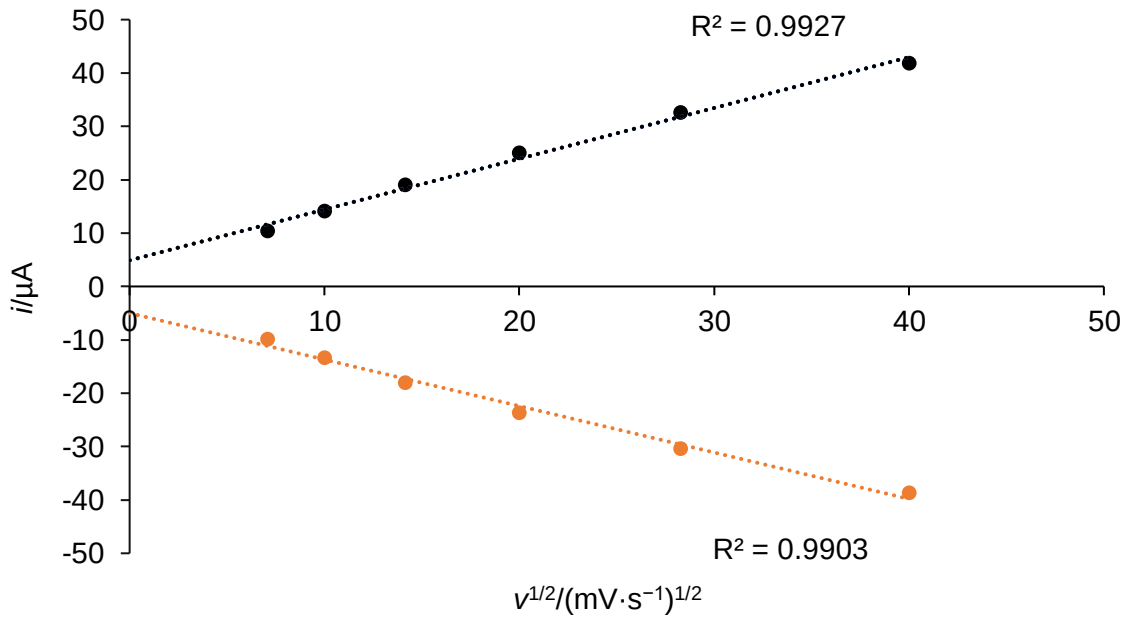

Figure 124. Randles-Sevcik plot of the **46-Si**/**46-Si**$^{\bullet-}$ redox couple at ambient temperature.

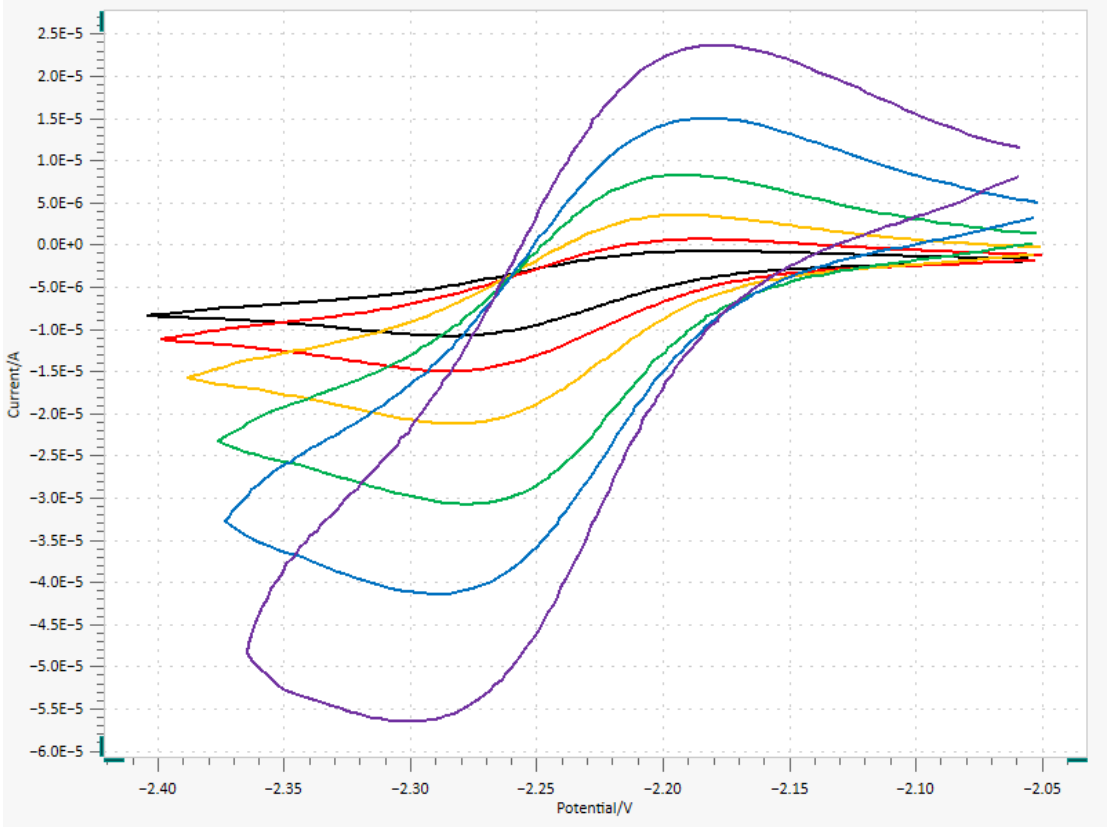

Figure 125. Cyclic voltammograms: measurements at 50 mV·s^{-1} (black), 100 mV·s^{-1} (red), 200 mV·s^{-1} (yellow), 400 mV·s^{-1} (green), 800 mV·s^{-1} (blue), and 1600 mV·s^{-1} (purple) vs. DMFc$^{+/0}$. A reduction associated with an irreversible chemical reaction at $E_{1/2}$ = −2.236 V vs. DMFc$^{+/0}$ is observed.

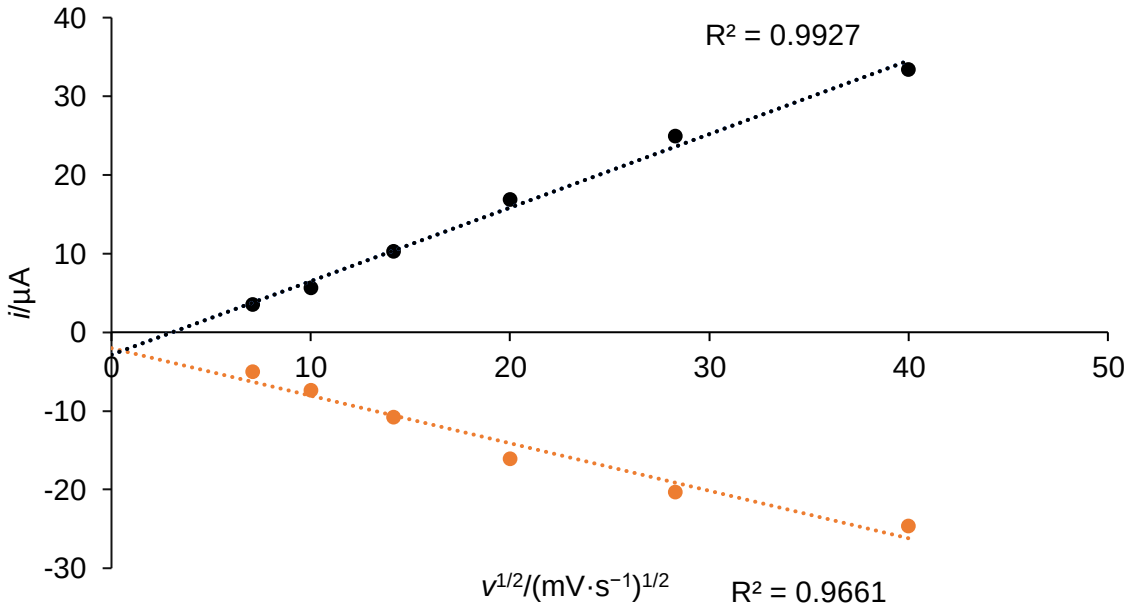

Figure 126. Randles-Sevcik plot of the **46-Ti**$^{2-}$/**46-Ti**$^{\bullet-}$ redox couple at ambient temperature.

Table 43. Cyclic voltammetric results of **46-Ti**.

υ (mV s^{-1})	i_{pa} (µA)	i_{pc} (µA)	i_{pa}/i_{pc}	E_{pa} (V)	E_{pc} (V)	ΔE_p (mV)	$E_{½}$ (V)
			E_r-process for **46-Ti**/**46-Ti**$^{\bullet+}$				
50	7.18	−4.83	1.49	0.659	0.592	67	0.625
100	8.36	−6.45	1.30	0.656	0.594	63	0.625
200	13.07	−11.22	1.17	0.657	0.593	65	0.625
400	19.63	−17.68	1.11	0.656	0.594	63	0.625
800	27.78	−25.69	1.08	0.654	0.596	59	0.625
1600	35.33	−31.92	1.11	0.658	0.592	65	0.625
			E_r-process for **46-Ti**/**46-Ti**$^{\bullet-}$				
50	10.39	−9.82	1.06	−1.737	−1.797	61	−1.767
100	14.12	−13.40	1.05	−1.736	−1.798	63	−1.767
200	19.06	−18.03	1.06	−1.735	−1.799	64	−1.767
400	25.05	−23.63	1.06	−1.736	−1.798	62	−1.767
800	32.60	−30.40	1.07	−1.730	−1.804	73	−1.767
1600	41.90	−38.70	1.08	−1.730	−1.804	75	−1.767
			E_rC_i-process for **46-Ti**$^{\bullet-}$/**46-Ti**$^{2-}$				
50	3.50	−5.04	0.69	−2.201	−2.271	71	−2.236
100	5.66	−7.43	0.76	−2.201	−2.271	71	−2.236
200	10.28	−10.84	0.95	−2.202	−2.270	68	−2.236
400	16.83	−16.07	1.05	−2.207	−2.265	57	−2.236
800	24.93	−20.35	1.23	−2.204	−2.268	64	−2.236
1600	33.36	−24.63	1.35	−2.198	−2.274	76	−2.236

υ: scan rate; I_{pa}: anodic peak-current; I_{pc}: cathodic peak-current; I_{pa}/I_{pc}: ratio of anodic and cathodic peak current; E_{pa}: anodic peak potential; E_{pc}: cathodic peak potential; $\Delta E_p = |E_{pa} - E_{pc}|$ = peak potential separation; $E_{1/2} = (E_{pa} + E_{pc})/2$ = half wave potential.; All potentials are given versus the $[Fe(C_5Me_5)_2]^{+1/0}$ reference electrode.

CV studies of [Cp*(CO)$_3$TiGeTbb] (**47-Ti**)

The investigated titanium-germylidyne complex **47-Ti** features two reductive and two oxidative processes in PhF/(NBu$_4$)[Al(OC(CF$_3$)$_3$)$_4$] at ambient temperature. The first reduction takes place at $E_{1/2}$ = −1.776 V vs. DMFc$^{+/0}$ and is reversible. The second reduction takes place at $E_{1/2}$ = −2.192 V vs. DMFc$^{+/0}$ and is possibly reversible since the oxidative currents of this process could not be correctly determined due to the close proximity to the previous reductive process. The first oxidation takes place at $E_{1/2}$ = 0.571 V vs. DMFc$^{+/0}$ and is quasi-reversible. The second oxidation takes place at E_{pa} = 1.310 V vs. DMFc$^{+/0}$ and is irreversible. The assignment is backed up by the determination of the open circuit potential (OCP) = −0.551 V vs. DMFc$^{+/0}$).

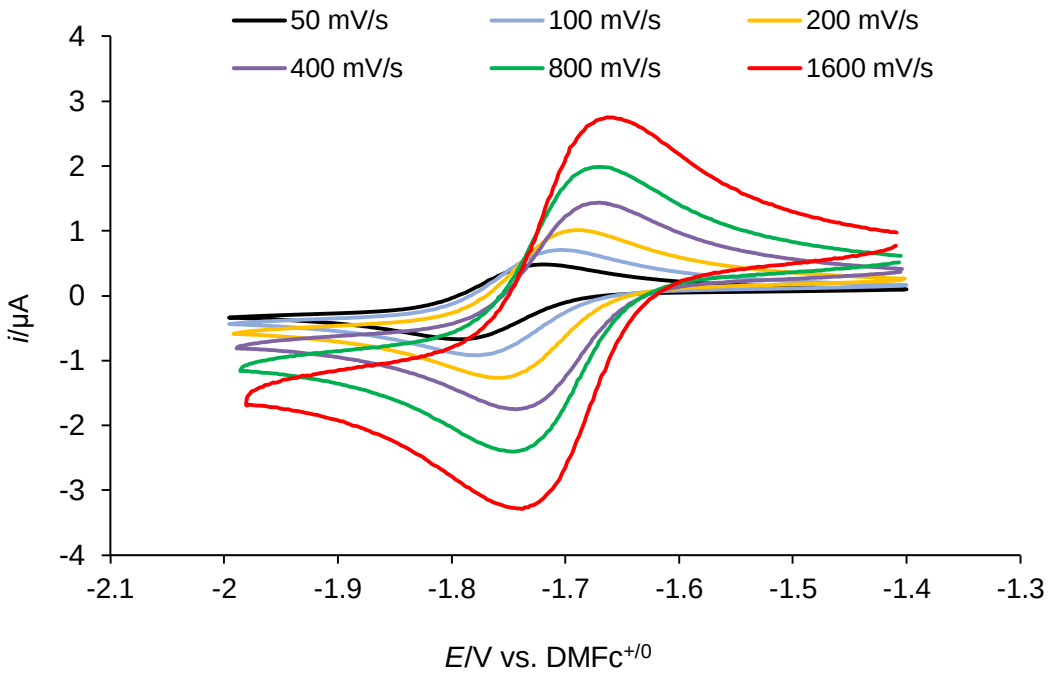

Figure 127. Cyclic voltammograms of **47-Ti** in fluorobenzene measured at ambient temperature at different scan rates between the initial potential of −1.42 V and switching potential of −1.98 V. A reversible reduction at $E_{1/2}$ = −1.776 V vs. $DMFc^{+/0}$ is observed.

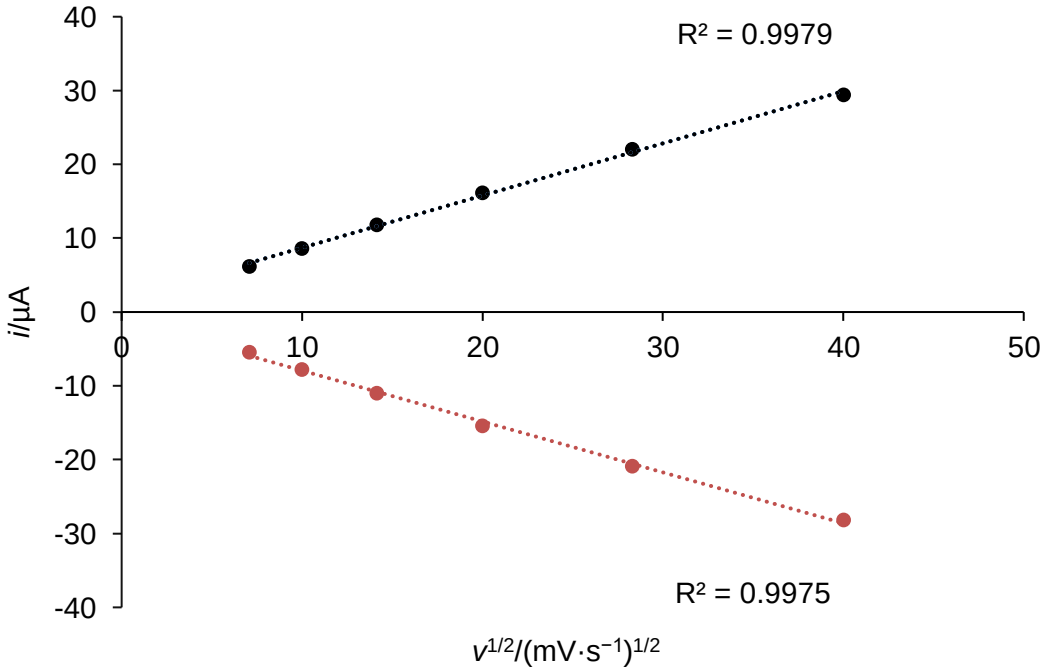

Figure 128. Randles-Sevcik plot of the **47-Ti**/**47-Ti**$^{\bullet-}$ redox couple at ambient temperature.

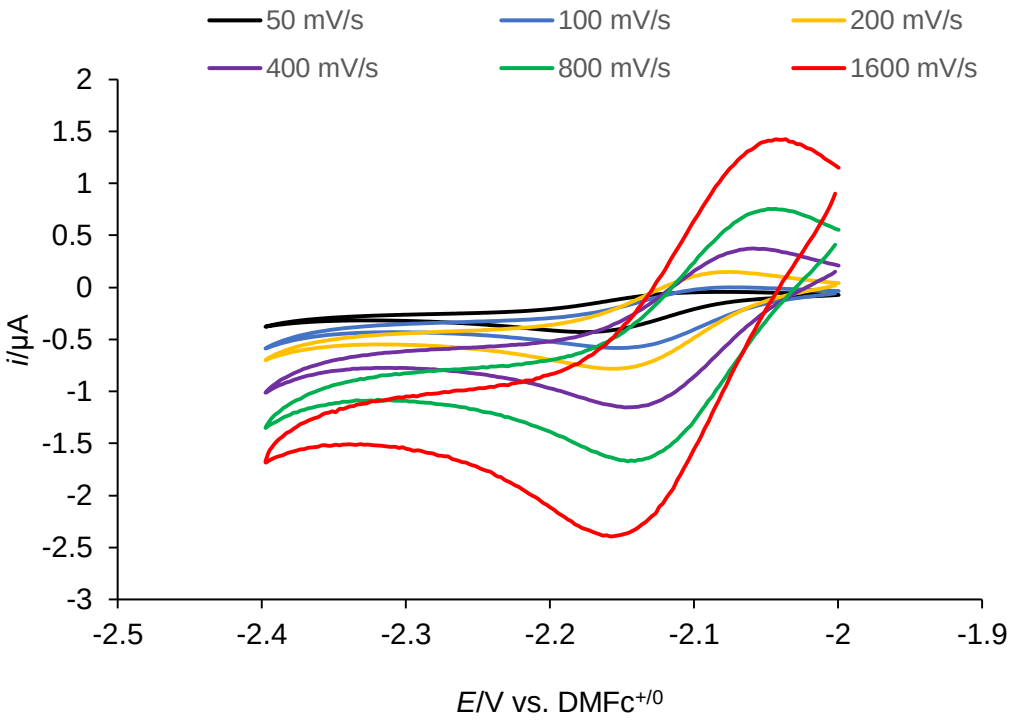

Figure 129. Cyclic voltammograms of **47-Ti** in fluorobenzene measured at ambient temperature at different scan rates between the initial potential of –2.0 V and switching potential of –2.4 V. A possibly reversible reduction at $E_{1/2}$ = −2.192 V vs. $DMFc^{+/0}$ is observed. Due to the close proximity to the previous reduction, it is practically not possible to obtain the correct measurement of the oxidative current of this redox process. However, the ratio of oxidative and reductive currents $-i_{pa}/i_{pc}$ is not significantly dependent on the scan rate, but both currents are linearly dependent on the square root of the scan rate, fulfilling two criteria of reversibility.

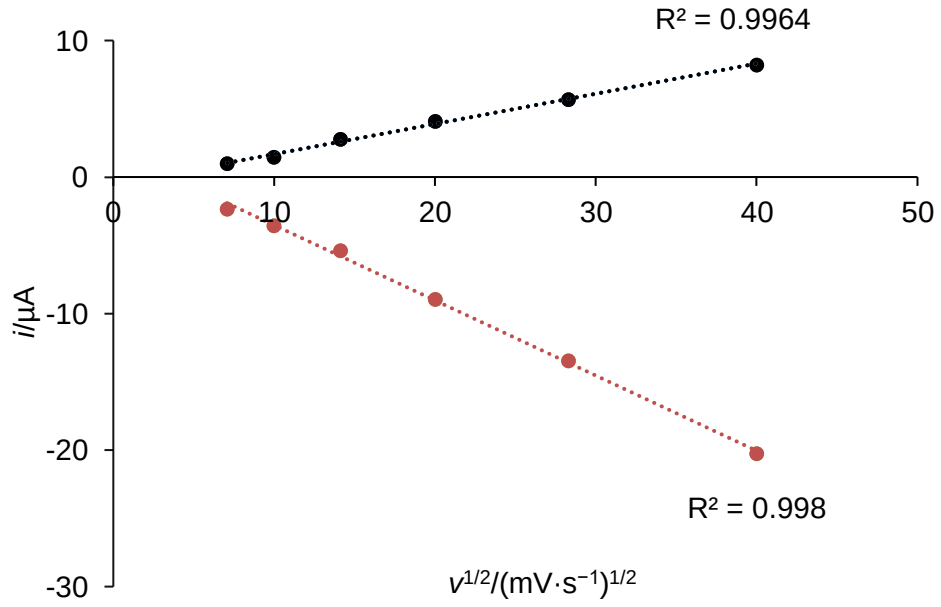

Figure 130. Randles-Sevcik plot of the **47-Ti**$^{\bullet-}$/**47-Ti**$^{2-}$ redox couple at ambient temperature.

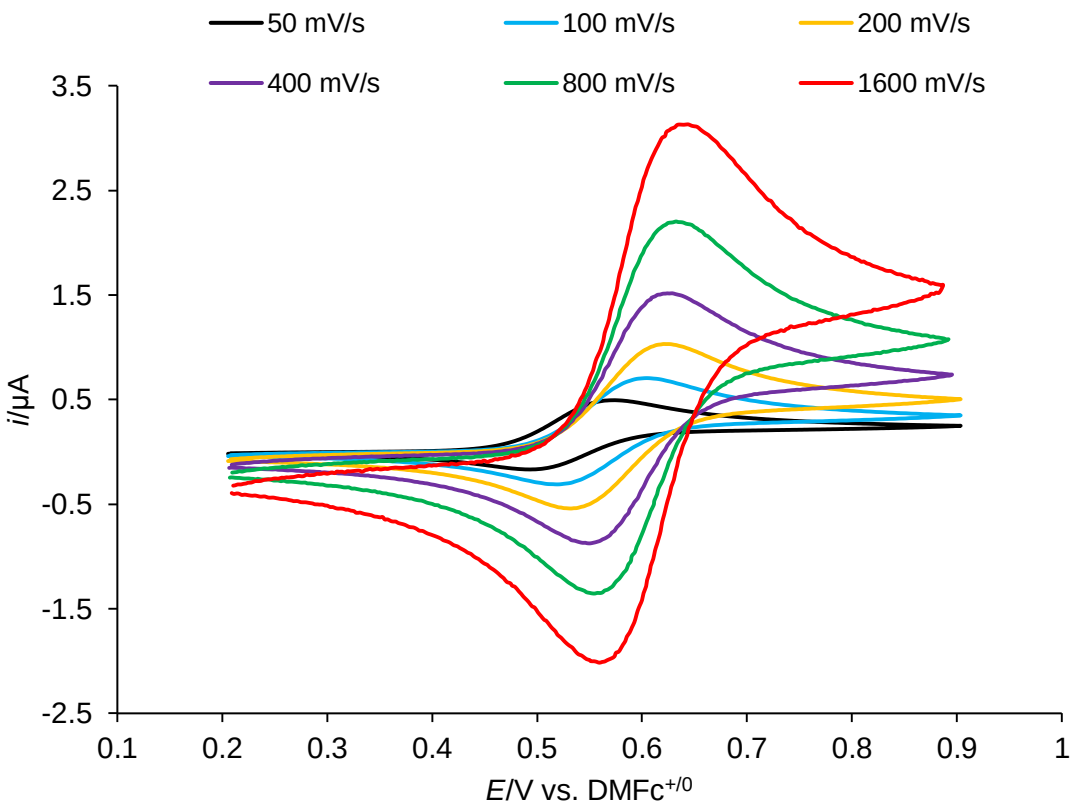

Figure 131. Cyclic voltammograms of **47-Ti** in fluorobenzene measured at ambient temperature at different scan rates between the initial potential of +0.2 V and switching potential of +0.9 V. A quasi-reversible oxidation at $E_{1/2}$ = 0.571 V vs. $DMFc^{+/0}$ is observed.

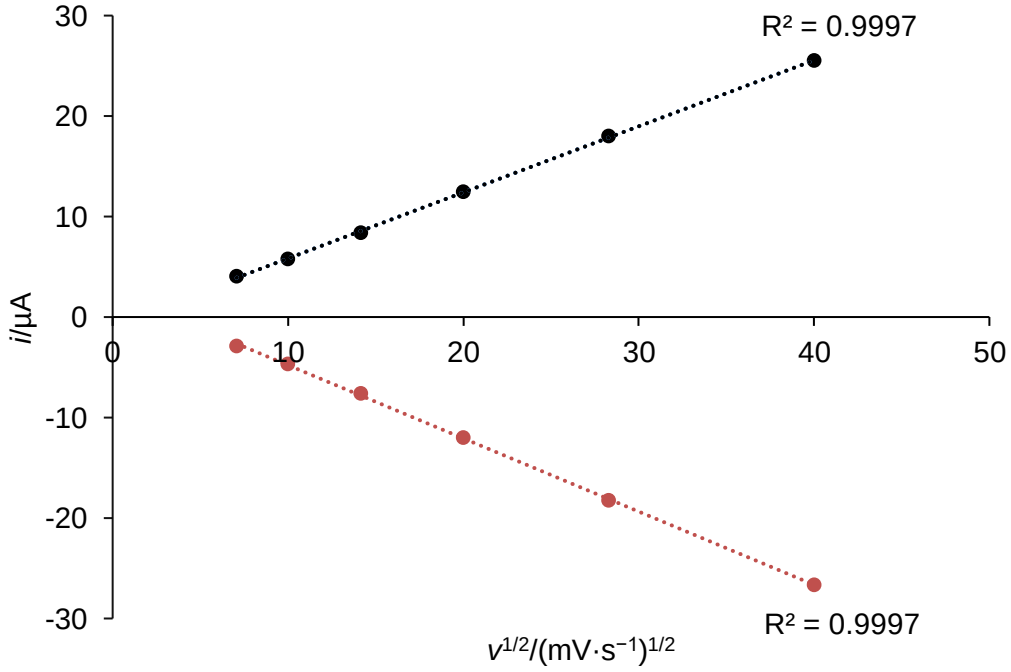

Figure 132. Randles-Sevcik plot of the **47-Ti**/**47-Ti**$^{\bullet+}$ redox couple at ambient temperature.

Table 44. Cyclic voltammetric results of **47-Ti**.

υ (mV s^{-1})	i_{pa} (μA)	i_{pc} (μA)	i_{pa}/i_{pc}	E_{pa} (V)	E_{pc} (V)	ΔE_p (mV)	$E_{½}$ (V)
			E_r-process for **47-Ti**/**47-Ti**$^{\bullet+}$				
50	4.05	−2.87	1.41	0.606	0.536	70	0.571
100	5.75	−4.71	1.22	0.611	0.531	80	0.571
200	8.36	−7.62	1.10	0.613	0.529	84	0.571
400	12.46	−12.01	1.04	0.606	0.536	70	0.571
800	17.99	−18.23	0.99	0.603	0.539	64	0.571
1600	25.49	−26.64	0.96	0.606	0.536	70	0.571
			E_r-process for **47-Ti**/**47-Ti**$^{\bullet-}$				
50	6.21	−5.47	1.14	−1.742	−1.810	68	−1.776
100	8.58	−7.74	1.11	−1.741	−1.811	70	−1.776
200	11.84	−11.01	1.08	−1.746	−1.806	60	−1.776
400	16.15	−15.41	1.05	−1.746	−1.806	60	−1.776
800	22.09	−20.83	1.06	−1.743	−1.809	66	−1.776
1600	29.44	−28.17	1.05	−1.739	−1.813	74	−1.776
			E_q-process for **47-Ti**$^{\bullet-}$/**47-Ti**$^{2-}$				
50	0.98	−2.35	0.42	−2.163	−2.221	58	−2.192
100	1.45	−3.54	0.41	−2.164	−2.220	56	−2.192
200	2.77	−5.37	0.52	−2.163	−2.221	58	−2.192
400	4.10	−8.94	0.46	−2.159	−2.225	66	−2.192
800	5.69	−13.46	0.42	−2.158	−2.226	68	−2.192
1600	8.23	−20.27	0.41	−2.151	−2.234	83	−2.193

υ: scan rate; I_{pa}: anodic peak-current; I_{pc}: cathodic peak-current; I_{pa}/I_{pc}: ratio of anodic and cathodic peak current; E_{pa}: anodic peak potential; E_{pc}: cathodic peak potential; $\Delta E_p = |E_{pa} - E_{pc}|$ = peak potential separation; $E_{1/2} = (E_{pa} + E_{pc})/2$ = half wave potential.; All potentials are given versus the $[Fe(C_5Me_5)_2]^{+1/0}$ reference electrode.

CV studies of [Cp*(CO)$_2$(PMe$_3$)TiSiTbb] (**48-Ti**)

The investigated titanium silylidyne complex [Cp*(PMe$_3$)(CO)$_2$Ti≡SiTbb] (**48-Ti**) features two major oxidations in PhF/(NBu$_4$)[Al(OC(CF$_3$)$_3$)$_4$]. The assignment is backed up by the determination of the open circuit potential (OCP) = −0.851 V vs. DMFc$^{+/0}$). The first oxidation takes place at $E_{1/2}$ = 0.183 V vs. DMFc$^{+/0}$ and is reversible. The second oxidation takes place at E_{pa} = 1.165 V vs. DMFc$^{+/0}$ at 100 mV/s and is irreversible. Due to the irreversible nature of the second oxidation, the third oxidative process at E_{pa} = 1.541 V vs. DMFc$^{+/0}$ at 100 mV/s is most likely caused by a reaction product of the double oxidized silylidyne complex and is not further investigated.

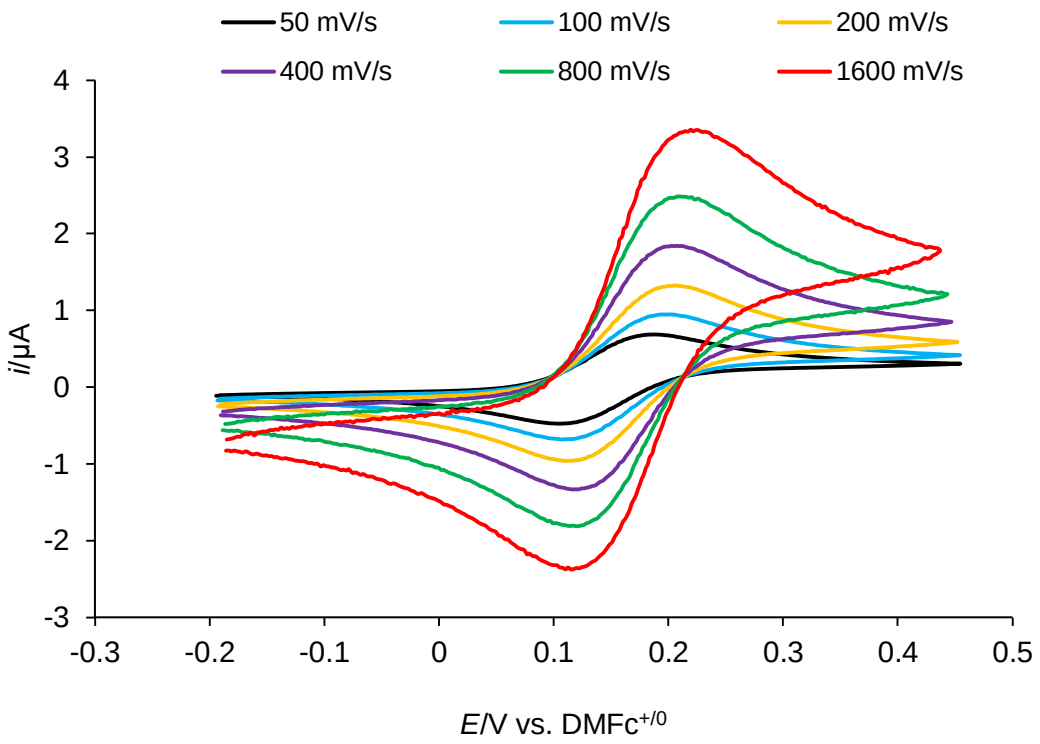

Figure 133. Cyclic voltammograms of Cp*(CO)$_2$(PMe$_3$)Ti≡Si−Tbb (**48-Ti**) in fluorobenzene measured at ambient temperature at different scan rates between the initial potential of −0.200 V and switching potential of +0.450 V referenced versus the [Fe(C$_5$Me$_5$)$_2$]$^+$/[Fe(C$_5$Me$_5$)$_2$] couple. A reversible oxidation at $E_{1/2}$ = 0.183 V vs. DMFc$^{+/0}$ is observed.

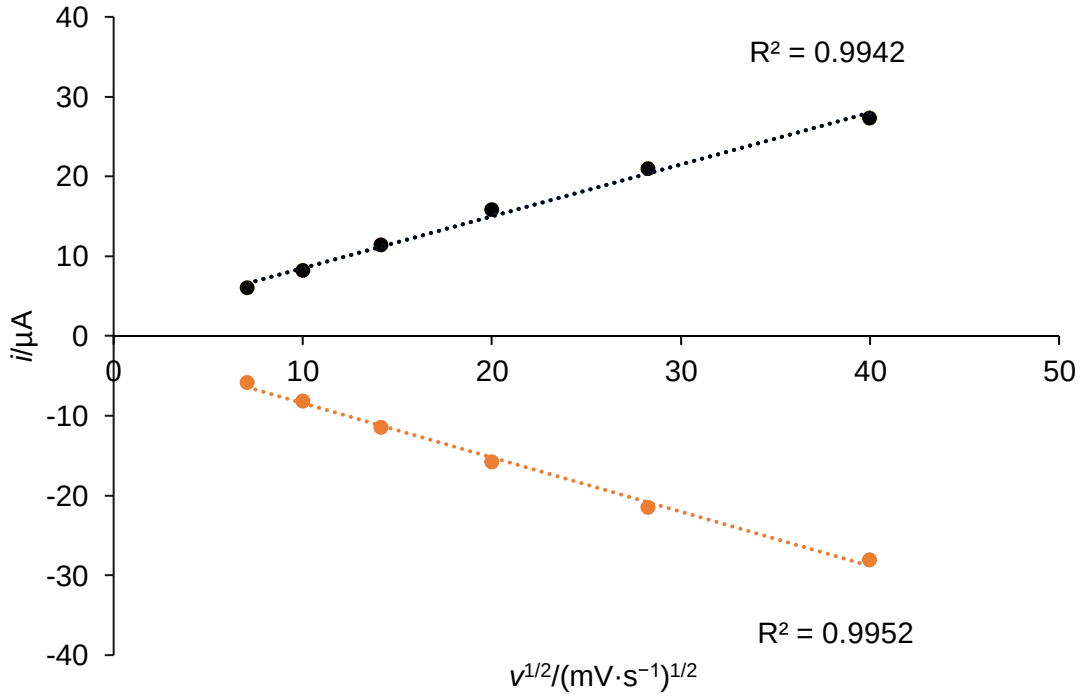

Figure 134. Randles-Sevcik plot of the **48-Ti**/**48-Ti**$^{\bullet+}$ redox couple at ambient temperature.

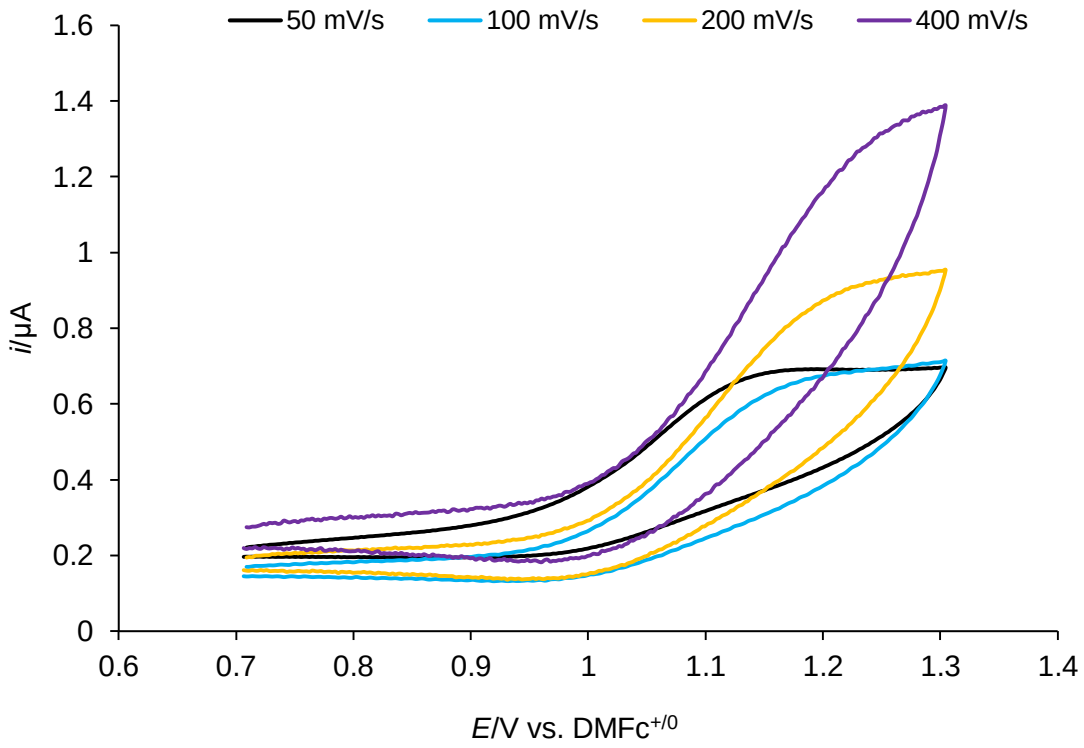

Figure 135. Cyclic voltammograms of Cp*(CO)$_2$(PMe$_3$)Ti≡Si–Tbb (**48-Ti**) in fluorobenzene measured at ambient temperature at different scan rates between the initial potential of +0.710 V and switching potential of +1.320 V referenced versus the $[Fe(C_5Me_5)_2]^+/[Fe(C_5Me_5)_2]$ couple. An irreversible oxidation at E_{pa} = +1.165 V vs. DMFc$^{+/0}$ is observed.

Table 45. Cyclic voltammetric results of **48-Ti**.

υ (mV s^{-1})	i_{pa} (µA)	i_{pc} (µA)	i_{pa}/i_{pc}	E_{pa} (V)	E_{pc} (V)	ΔE_p (mV)	$E_{½}$ (V)
E_r-process for **48-Ti**/**48-Ti**$^{\bullet+}$							
50	5.99	–5.86	1.02	0.220	0.146	74	0.183
100	8.22	–8.16	1.01	0.221	0.144	77	0.183
200	11.43	–11.47	1.00	0.224	0.141	83	0.183
400	15.79	–15.81	1.00	0.221	0.145	76	0.183
800	20.93	–21.52	0.97	0.223	0.144	79	0.184
1600	27.31	–28.13	0.97	0.227	0.140	87	0.184

υ: scan rate; I_{pa}: anodic peak-current; I_{pc}: cathodic peak-current; I_{pa}/I_{pc}: ratio of anodic and cathodic peak current; E_{pa}: anodic peak potential; E_{pc}: cathodic peak potential; $\Delta E_p = |E_{pa} - E_{pc}|$ = peak potential separation; $E_{1/2} = (E_{pa} + E_{pc})/2$ = half wave potential.; All potentials are given versus the $[Fe(C_5Me_5)_2]^{+1/0}$ reference electrode.

5.5. UV-Vis NIR spectroscopic studies of compounds

UV-Vis-NIR spectra of 5-Co

The UV-Vis-NIR spectra of **5-Co** were recorded in toluene at ambient temperature and are depicted in ***Figure 136***. The absorption maxima and corresponding molar extinction coefficients (**ε**) are summarized in ***Table 46***. The absorption bands were determined by means of band deconvolution assuming a Gaussian line profile. The corresponding deconvoluted absorption bands are displayed in ***Figure 137*** and the parameters used for the band deconvolution are summarized in ***Table 47***.

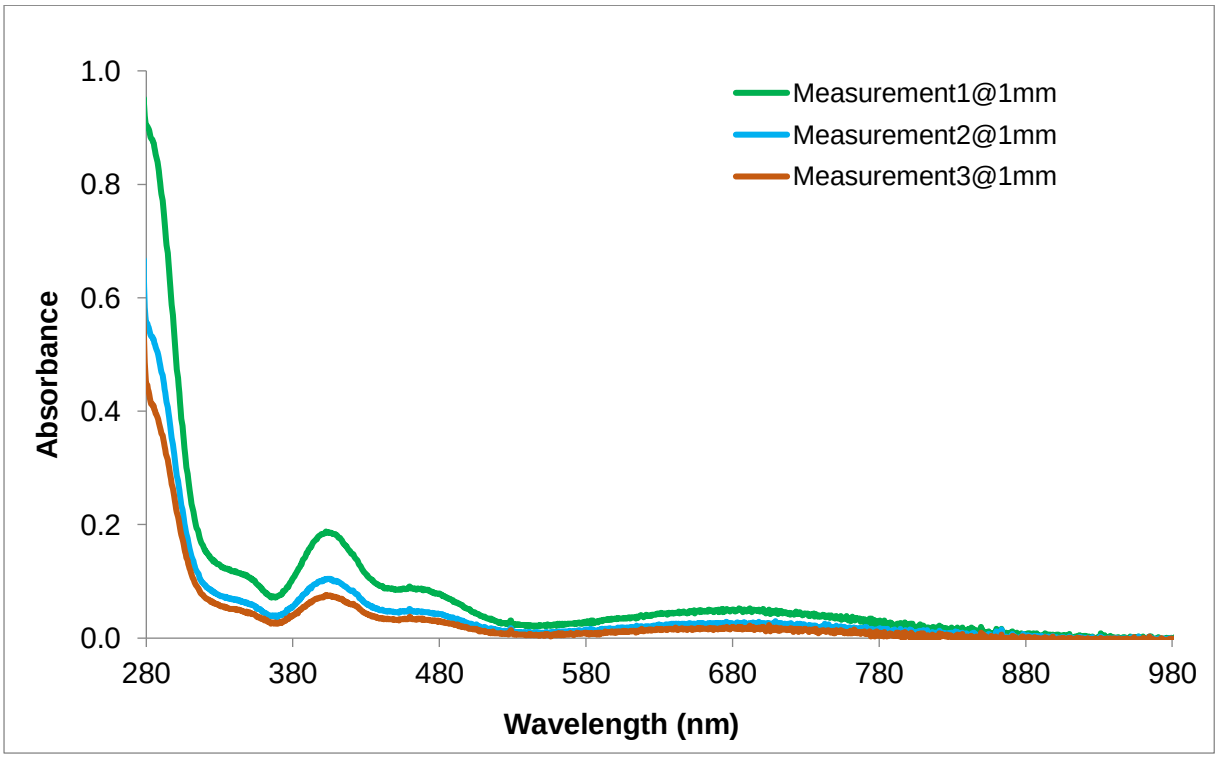

Figure 136. Experimental UV-Vis-NIR spectra of **5-Co** in *n*-hexane from 280 – 980 nm at different concentrations.

Table 46. Absorption maxima of the UV-Vis-NIR spectra of **5-Co** depicted in ***Figure 136*** and their corresponding molar extinction coefficients.

λ_{max}/nm	677	471	403	345	330	311	285
ε / $L \cdot mol^{-1} \cdot cm^{-1}$	2162	3802	8116	4899	5426	9944	35862

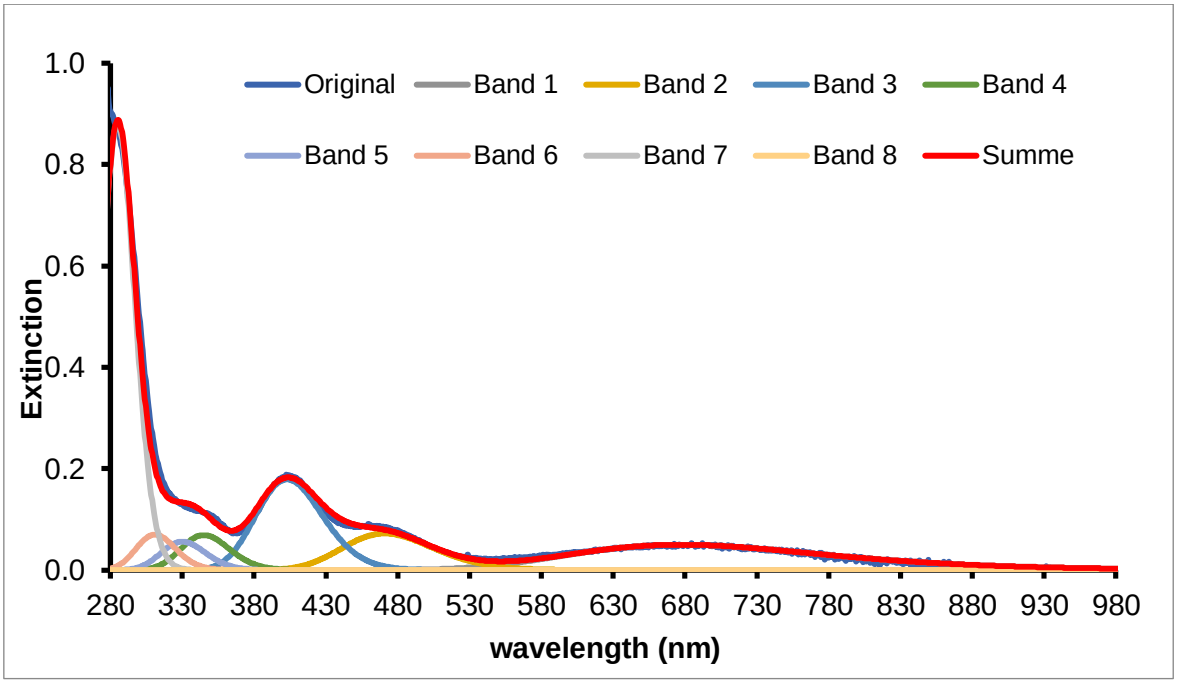

Figure 137. Deconvoluted and experimental UV-Vis-NIR spectra of **5-Co** in toluene at c = 24 µmol L^{-1} and d = 1 mm.

Table 47. Parameters used for the band deconvolution of the UV-Vis-NIR spectrum depicted in ***Figure 137***.

		Band 1	Band 2	Band 3	Band 4	Band 5	Band 6	Band 7
Absorbance	$\mathbf{A_{max}}$	0.050	0.072	0.179	0.069	0.056	0.070	0.880
Bandwidth	σ_{max}	2700	2000	2000	2000	2000	2000	2000
Wavelength	λ_{max}	677	471	403	345	330	311	285

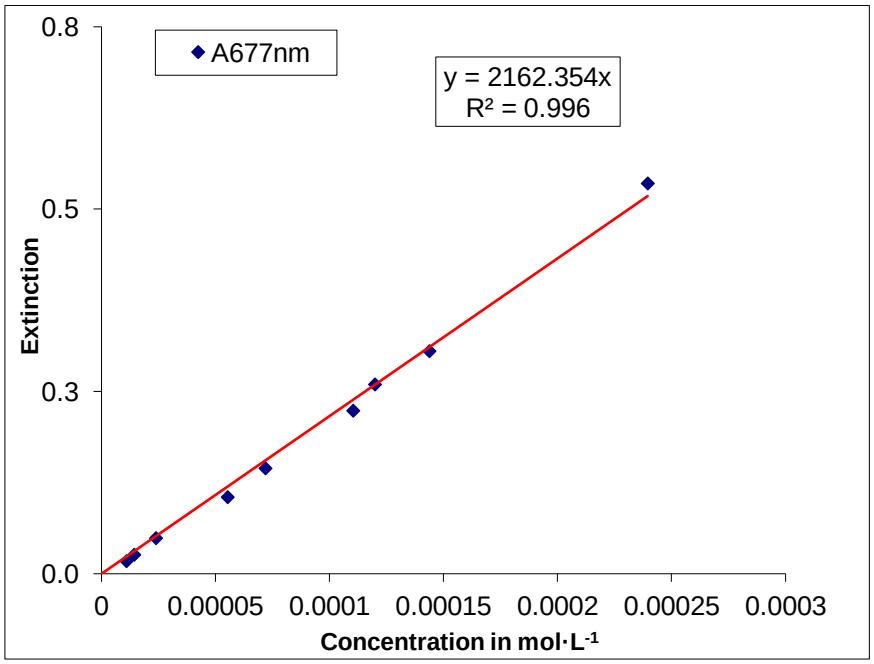

Figure 138. Plot of extinction vs concentration for the band at λ_{max} = 677 nm in the UV-Vis spectrum of **5-Co**.

UV-Vis-NIR spectra of **10-Co**

The UV-Vis-NIR spectra of **10-Co** were recorded in toluene at ambient temperature and are depicted in ***Figure 139***. The absorption maxima and corresponding molar extinction coefficients (**ε**) are summarized in ***Table 48***. The absorption bands were determined by means of band deconvolution assuming a Gaussian line profile. The corresponding deconvoluted absorption bands are displayed in ***Figure 140*** and the parameters used for the band deconvolution are summarized in ***Table 49***.

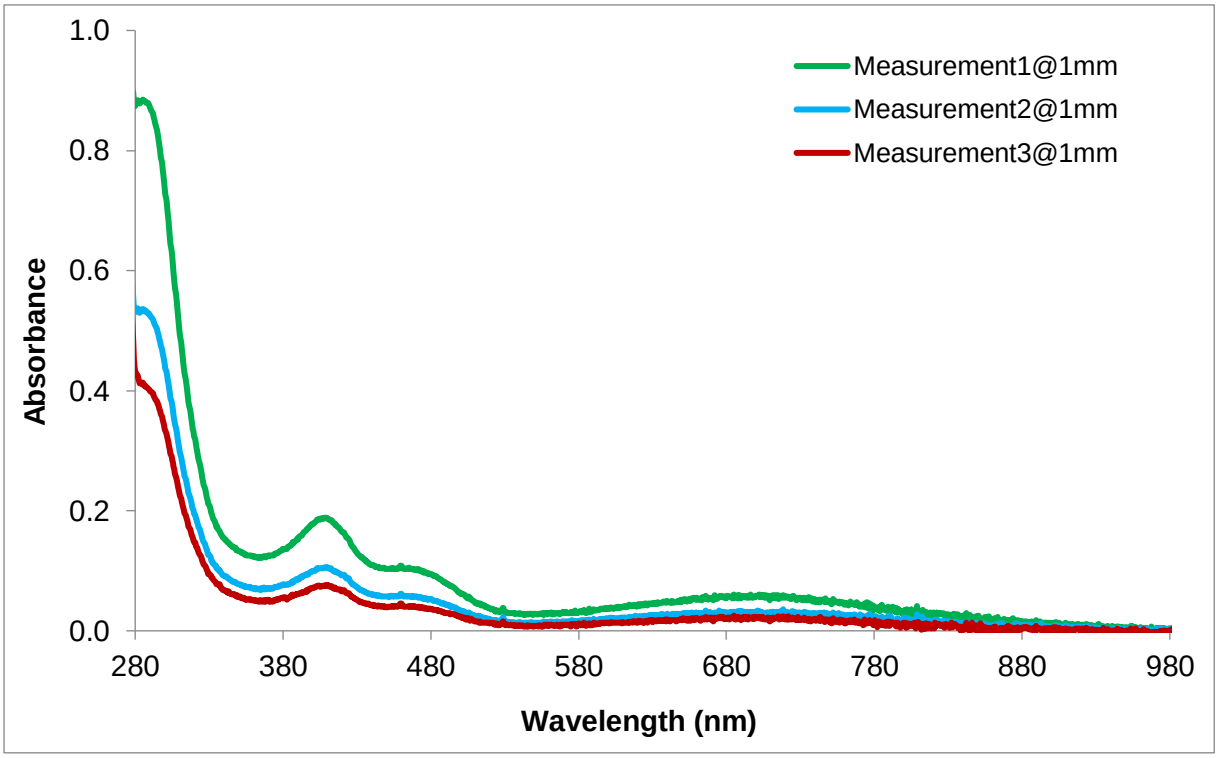

Figure 139. Experimental UV-Vis-NIR spectra of **10-Co** in toluene from 280 – 980 nm at different concentrations.

Table 48. Absorption maxima of the UV-Vis-NIR spectra of **10-Co** depicted in ***Figure 139*** and their corresponding molar extinction coefficients.

λ_{max}/nm	693	550	473	405	353	286
ε / L·mol^{-1}·cm^{-1}	1692	932	3047	5528	3888	24774

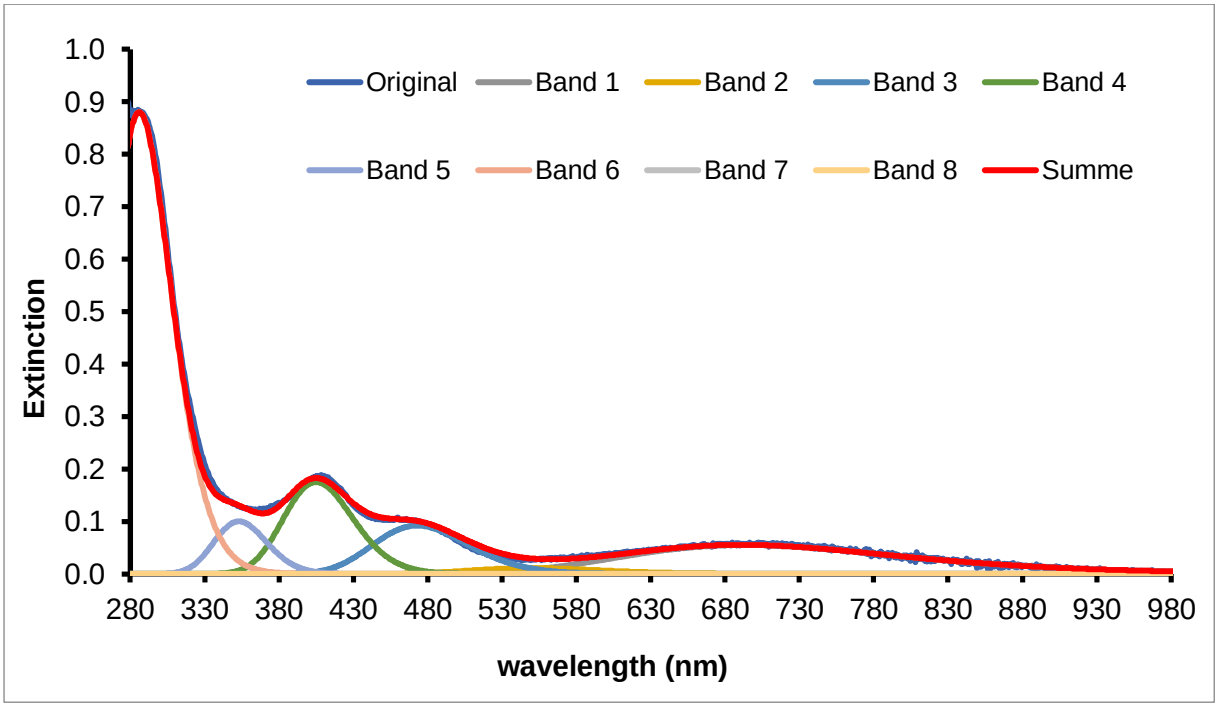

Figure 140. Deconvoluted and experimental UV-Vis-NIR spectra of **10-Co** in toluene at c = 35 µmol L^{-1} and d = 1 mm.

Table 49. Parameters used for the band deconvolution of the UV-Vis-NIR spectrum depicted in ***Figure 140***.

		Band 1	Band 2	Band 3	Band 4	Band 5	Band 6
Absorbance	$\mathbf{A_{max}}$	0.055	0.011	0.092	0.175	0.100	0.880
Bandwidth	$\mathbf{\sigma_{max}}$	2700	2000	2000	2000	2000	3500
Wavelength	$\mathbf{\lambda_{max}}$	693	550	473	405	353	286

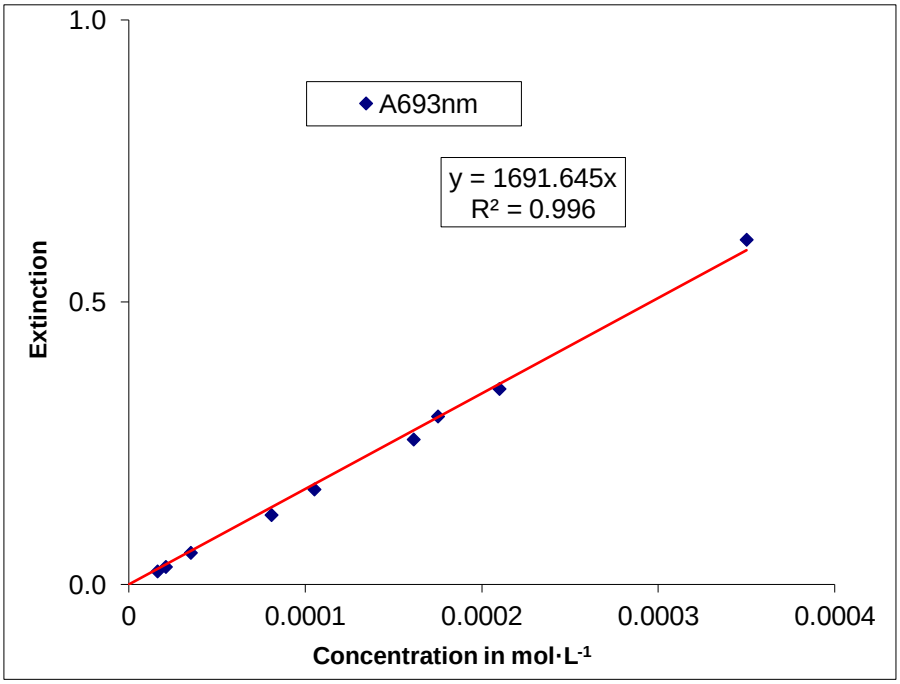

Figure 141. Plot of extinction vs concentration for the band at λ_{max} = 693 nm in the UV-Vis spectrum of **10-Co**.

UV-Vis-NIR spectra of 14-Co

The UV-Vis-NIR spectra of **14-Co** were recorded in toluene at ambient temperature and are depicted ***Figure 142***. The absorption maxima and corresponding molar extinction coefficients (**ε**) are summarized in ***Table 50***. The absorption bands were determined by means of band deconvolution assuming a Gaussian line profile. The corresponding deconvoluted absorption bands are displayed in ***Figure 143*** and the parameters used for the band deconvolution are summarized in ***Table 51***.

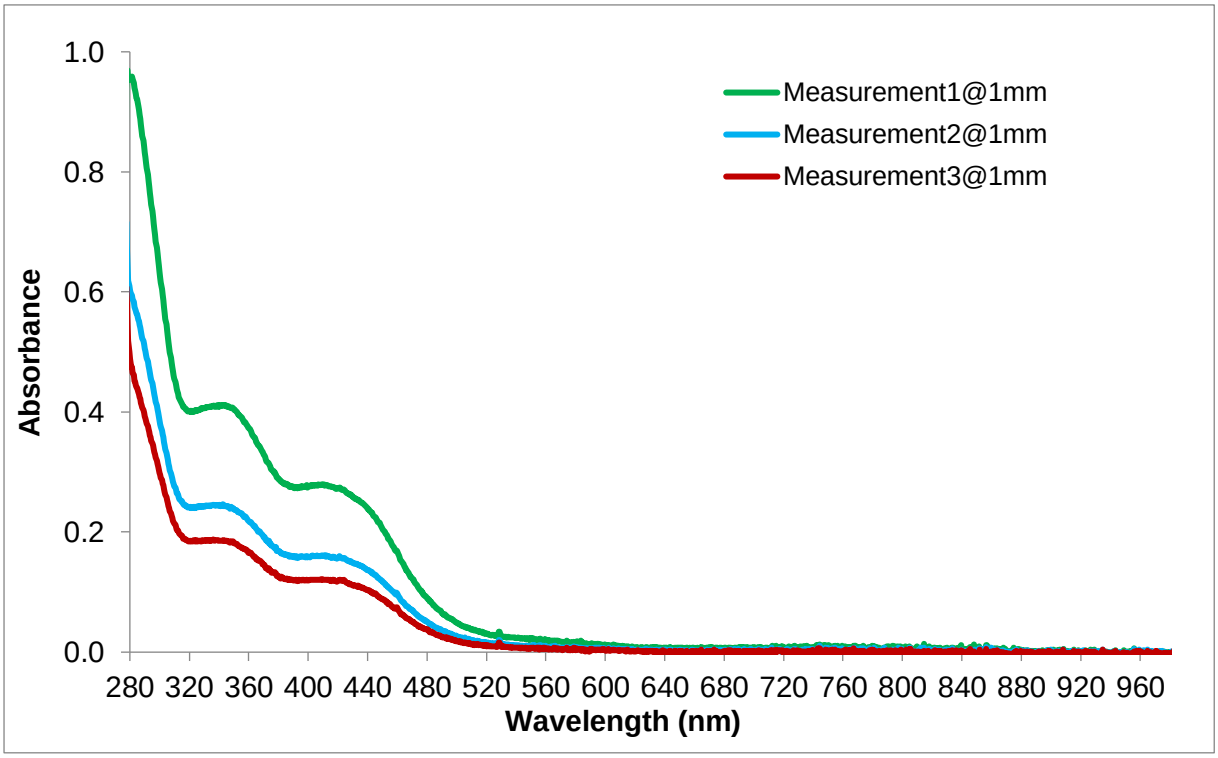

Figure 142. Experimental UV-Vis-NIR spectra of **14-Co** in toluene from 280 – 970 nm at different concentrations.

Table 50. Absorption maxima of the UV-Vis-NIR spectra of **14-Co** depicted in ***Figure 142*** and their corresponding molar extinction coefficients.

λ_{max}/nm	538	437	392	352.5	328	281
ε / $L \cdot mol^{-1} \cdot cm^{-1}$	873	7565	8458	12120	12195	29436

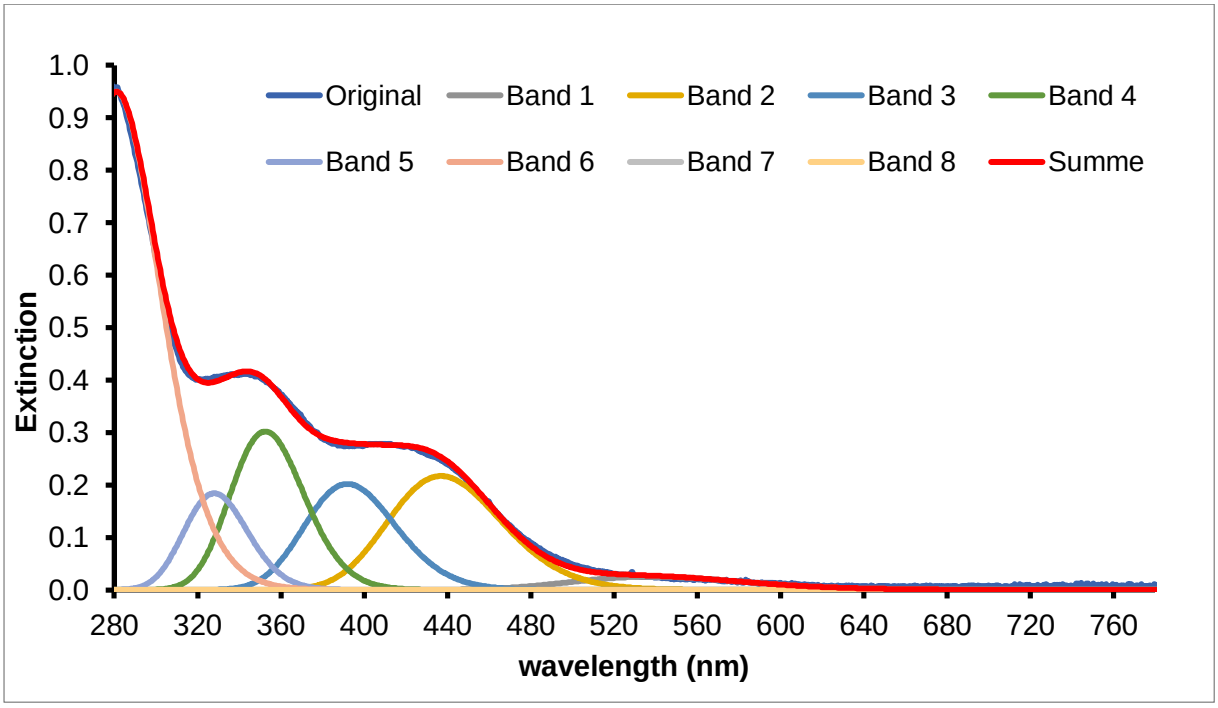

Figure 143. Deconvoluted and experimental UV-Vis-NIR spectra of **14-Co** in toluene at c = 33 µmol L^{-1} and d = 1 mm.

Table 51. Parameters used for the band deconvolution of the UV-Vis-NIR spectrum depicted in ***Figure 143***.

		Band 1	Band 2	Band 3	Band 4	Band 5	Band 6
Absorbance	$\mathbf{A_{max}}$	0.025	0.217	0.202	0.302	0.184	0.950
Bandwidth	$\boldsymbol{\sigma_{max}}$	2000	2000	2000	2000	2000	3500
Wavelength	$\boldsymbol{\lambda_{max}}$	538.0	437.0	392.0	352.5	328.0	281.0

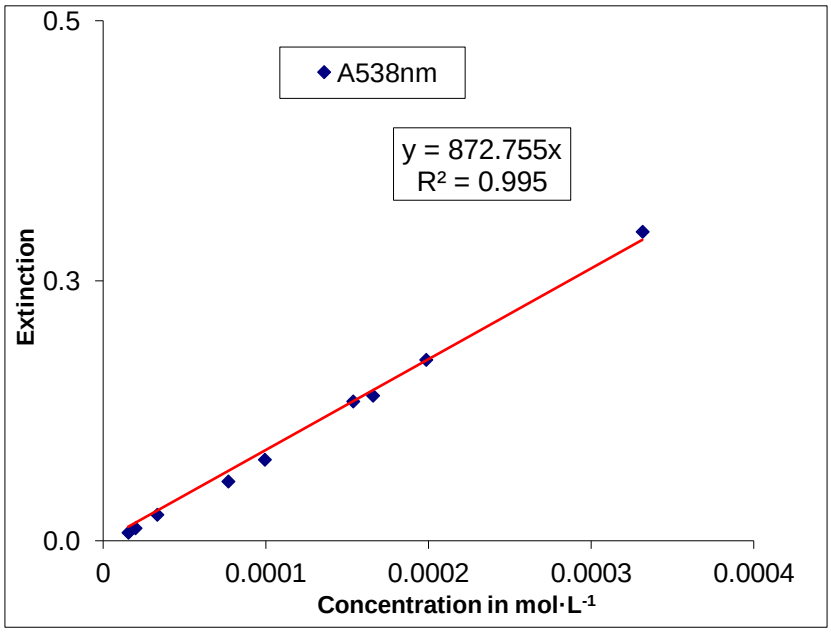

Figure 144. Plot of extinction vs concentration for the band at λ_{max} = 538 nm in the UV-Vis spectrum of **14-Co**.

5.6. Computational details

Level of Theory

level of theory (**I**)	B97-D3(BJ)ATM/def2-TZVP	
functional set	B97-D	GGA
basis set	def2-TZVP	polarized triple-ζ
resolution of identity	RI-J	
auxiliary basis set	def2/J	Coulomb fitting basis
effective core potentials	def2-ECP	for Rb-Rn
dispersion correction	D3(BJ)	D3 with Becke-Johnson damping
three-body dispersion	ATM	Axilrod-Teller-Muto correction

Types of Calculations

structure optimization			
program	ORCA 5.0.0		
level of theory	B97-D3(BJ)ATM/def2-TZVP		
grid settings	DEFGRID2		grid for exchange-correlation
convergence criteria	ΔEmax	= 5 · 10−6 EH	max. energy change
	gmax	= 3 · 10−4 EH/Bohr	max. gradient
	RMS(g)max	= 3 · 10−4 EH/Bohr	max. RMS gradient
	Δxmax	= 4 · 10−3 Bohr	max. displacement
	RMS(Δx)max	= 2 · 10−3 Bohr	max. RMS displacement

NBO/NRT analysis	
program	NBO 7.0.10
level of theory	B97-D3(BJ)ATM/def2-TZVP

frequency calculation		
program	ORCA 5.0.0	
level of theory	B97-D3(BJ)ATM/def2-TZVP	
grid settings	DEFGRID2	grid for exchange-correlation
frequencies	harmonic, derived from two-sided numerical differentiation of the analytical gradients	

Ro-vibrational corrections to obtain free energies were obtained from quasi rigid rotor harmonic oscillator (Quasi-RRHO) statistical treatment (T = 298.15 K, p = 1 atm) based on harmonic frequencies calculated at the structure optimization level (B97-D3(BJ)ATM/def2-TZVP). To avoid errors in the harmonic approximation, frequencies with wave numbers below 100 cm-1 were treated partially as rigid rotors.

All mentioned theoretical calculations in this dissertation were performed either by Leonard R. Maurer or by Dr. Gregor Schnakenburg.

5.7. Study of the dynamics of compounds by VT ^{1}H NMR spectroscopy

VT ^{1}H NMR spectra and line shape analysis of 1-Co

The digermyne complex **1-Co** exists in solution as a racemic mixture of two C_1-symmetric enantiomers featuring an (***R,R***) and (***S,S***) configuration of the two pyramidal coordinated Ge centers, respectively.

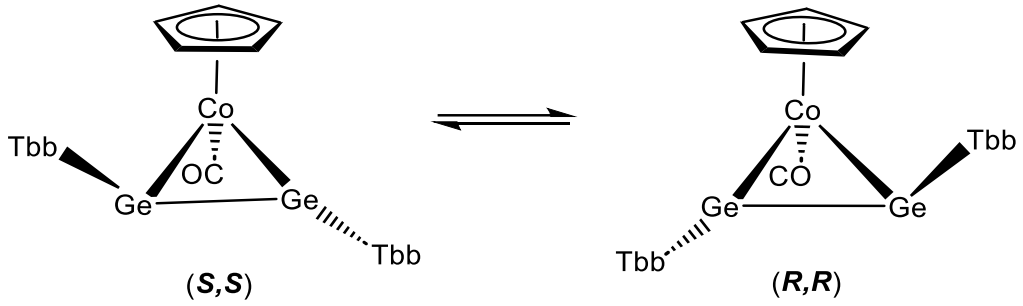

Figure 145. The two C_1-symmetric enantiomers of complex **1-Co** undergoing stereomutaiton in solution.

This stereochemical arrangement is a result of the *trans*-bent, ideally C_{2h} symmetric structure of the digermyne Ge_2Tbb_2 and its coordination to the Co center via its out of plane π bond, which renders the Tbb substituents diastereotopic. The one Tbb substituent denoted arbitrarily as Tbb_x points in the direction of the CO ligand (away from the Cp ligand) and the other Tbb substituent denoted as Tbb_Y points in the opposite direction (towards the Cp ligand). Therefore, a separate set of signals is observed for each Tbb substituent in the slow exchange limit ^{1}H NMR spectra, e.g. one singlet for each of the ^{t}Bu methyl protons at δ = 1.33 ppm and 1.38 ppm at 213 K. In addition, rotation of one Tbb substituent (presumably Tbb_x) about the respective Ge-C_{Tbb} bond is frozen out at low temperatures, whereas rotation of the other Tbb substituent (presumably Tbb_Y) about the respective Ge-C_{Tbb} bond occurs rapidly on the NMR time scale even at low temperatures. This leads to a double set of proton signals for the C^2/C^6 bonded Dsi substituents and the C^3/C^5 bonded protons of the Tbb_x substituent in the slow exchange limit ^{1}H NMR spectra, whereas one set of signals is observed for the related protons of the Tbb_Y substituent.

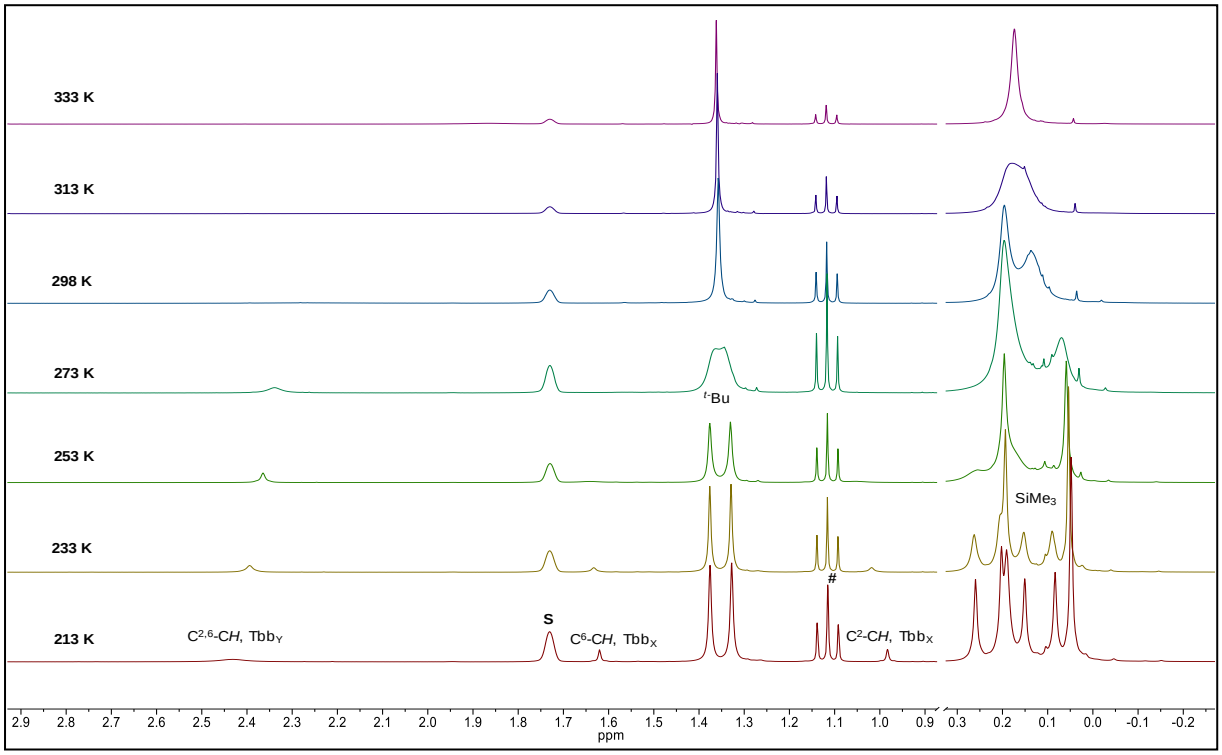

Figure 146. Excerpt of the VT ^{1}H NMR spectra (300.1 MHz) of **1-Co** in (D_8)THF (chemical shift range: 0 – 2.9 ppm); the residual proton signal of the deuterated solvent is marked with the letter S and the quartet signal of Et_2O with the symbol #.

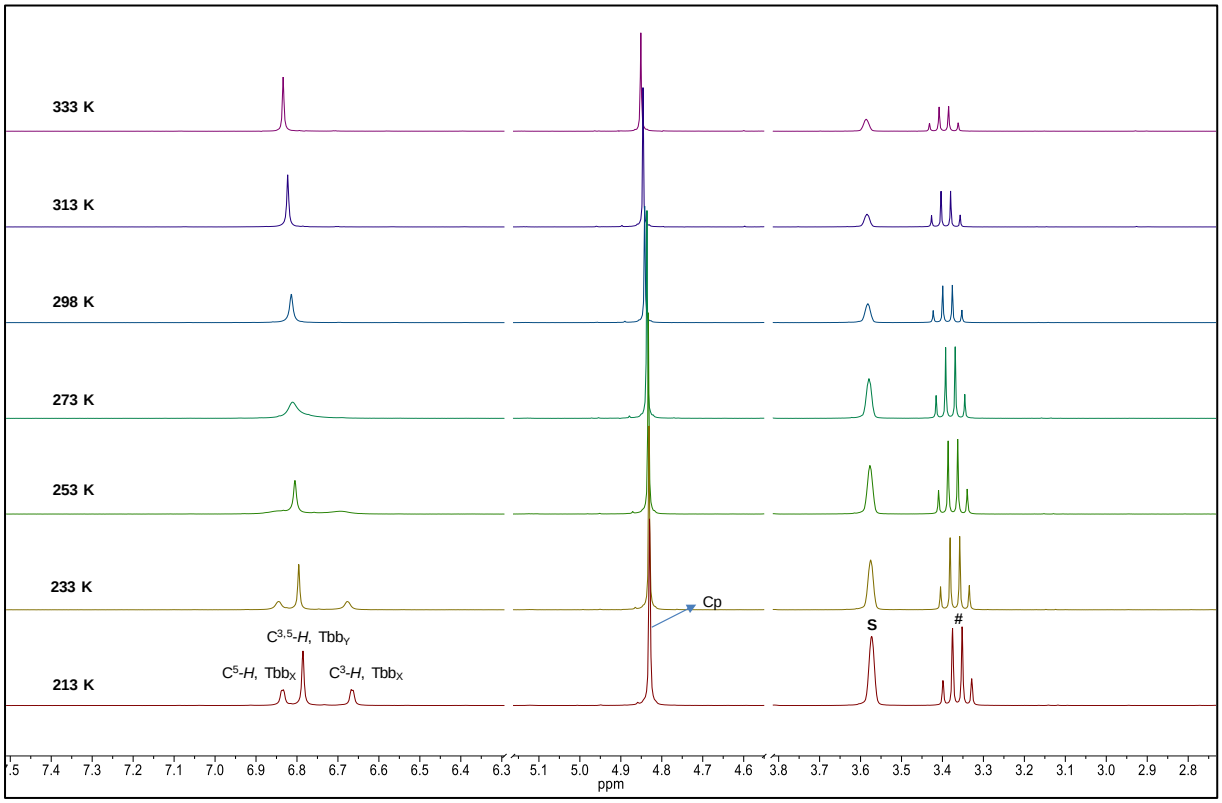

Figure 147. Excerpt of the VT ^{1}H NMR spectra (300.1 MHz) of **1-Co** in (D_8)THF (chemical shift range: 2.8 – 7.5 ppm); the residual proton signal of the deuterated solvent is marked with the letter S and the quartet signal of Et_2O with the symbol #.

For example, one singlet is observed for each of the Dsi C-*H* protons of the Tbb_X substituent at δ = 0.99 ppm and 1.62 ppm (T = 213 K), but only one broadened singlet for the Dsi C-*H* protons of the Tbb_Y substituent at δ = 2.43 ppm. The intensity ratio of these signals is 1:1:2. Similarly, two doublets are observed at T = 213 K for the C^3/C^5 bonded aromatic protons of the Tbb_X substituent at δ = 6.67 ppm and 6.84 ppm in the ratio of 1 : 1, but one singlet of double intensity for the $C^{3,5}$-*H* protons of the Tbb_Y substituent at δ = 6.79 ppm. Two dynamics processes were resolved using VT ^{1}H NMR spectroscopy in the temperature range 213 K – 333 K. The one process proceeding via a lower activation barrier involves the rotation of the Tbb_x substituent about the Ge-C_{Tbb} bond. The second process involves an enantiomerization interchanging the positions of two Tbb substituents. The first process was analyzed taking advantage of the C^3-*H* and C^5-*H* proton signals of the Tbb_X substituent, which broaden with increasing temperature, coalesce at $T_C \approx 263$ K and then merge with the $C^{3,5}$-*H* protons of the Tbb_Y substituent to a narrow singlet at 333 K due to fast positional exchange of the Tbb substituents.

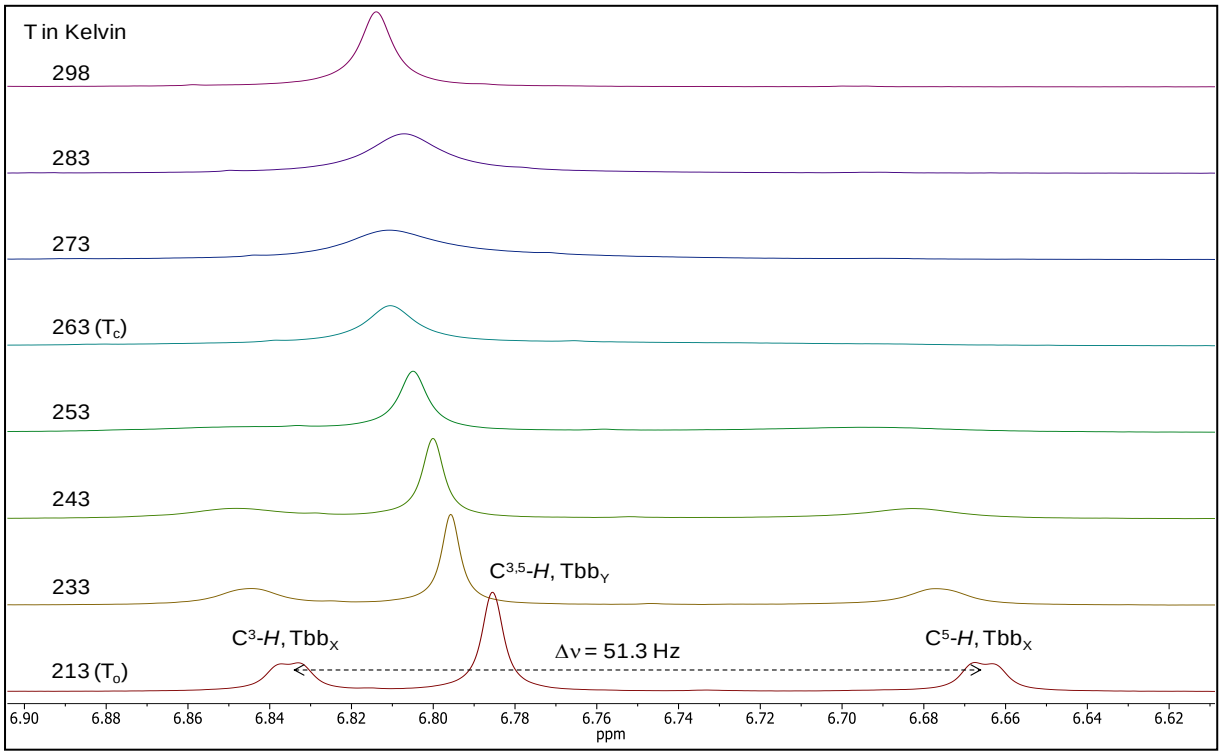

Figure 148. Excerpt (6.62 – 6.90 ppm) of the VT-^{1}H NMR spectra (300.1 MHz) of **1-Co** in (D_8)THF from 213 – 298 K.

The Gibbs energy of activation ($\Delta G^{\ddagger}$) for the rotation process at the coalescence temperature T_c was obtained from the modified Eyring equation (eq. 1) with $k = 2.22 \cdot \Delta\nu$, where k is the exchange rate constant at T_c and $\Delta\nu$ is the separation of the exchanging signals in Hz in the low temperature limit spectrum (T_o = 213 K), where

no exchange is assumed to occur (k = 0) and Δν/J is larger than 3,[266] using the values of T_C = 263 K and Δν = 51.3 Hz, $\Delta G^{\ddagger}(T_C)$ was calculated to 53.8 kJ/mol.

$$\Delta G^{\ddagger} = 0.01915 \cdot T_c \cdot \left[9.972 + \log\left(\frac{T_c}{\Delta\nu}\right)\right] [\mathrm{kJ\ mol^{-1}}] \quad (\mathrm{eq.}\ 1)$$

The second process was studied taking advantage of the interchanging of ^{t}Bu methyl protons, which upon warming first broaden, then coalesce at ≈ 273 K and finally merge to a sharp singlet at 333 K.

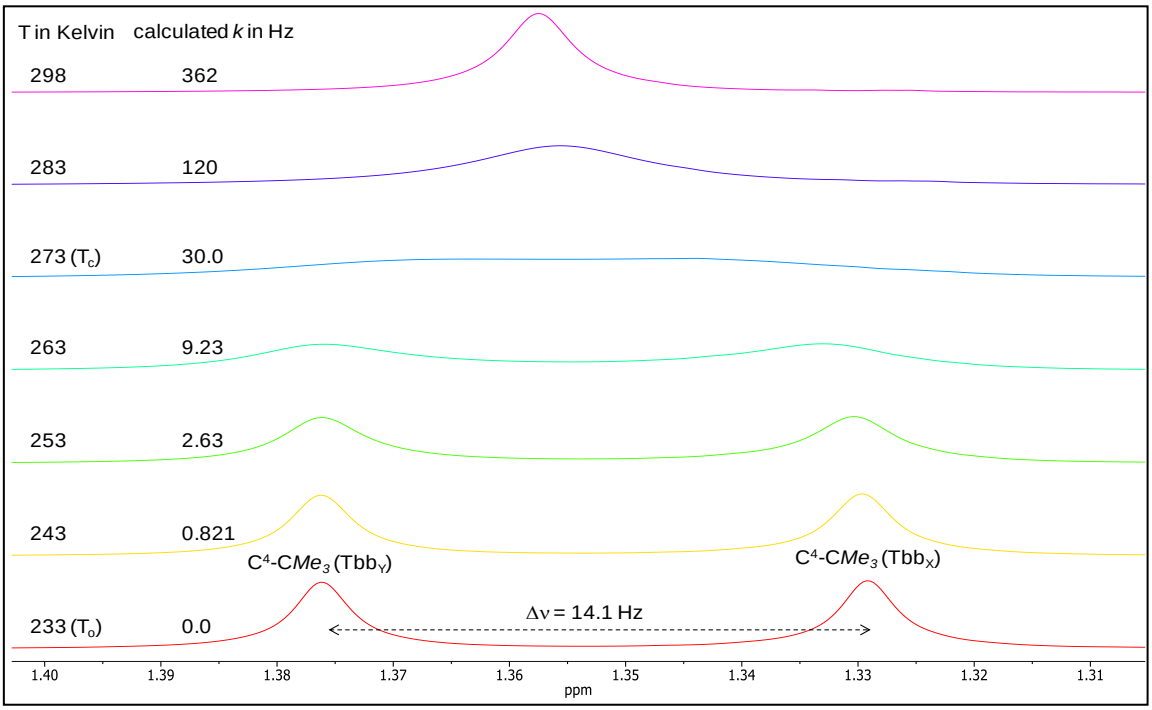

Figure 149. Excerpt of the VT-^{1}H NMR spectra (300.1 MHz) of **1-Co** in (D_8)THF from 233 K – 298 K showing the exchanging C^4-C*Me*$_3$ signals of the Tbb_X and Tbb_Y substituents.

This dynamic process (enantiomerization) is an example of an equally populated two-site chemical exchange. Full line-shape analysis of the signals in the temperature range 233 K – 298 K using the NMR simulation programme gNMR afforded the first order rate constants for the chemical exchange of the Tbb_X and Tbb_Y substituents listed in ***Table 52***.

Table 52. Rate constants (k[Hz]) for the enationmerization process in **1-Co** at different temperatures.

T[a)]	k[Hz]	σ (k)	k/T	ln(k/T)	1/T
243	0.821	1.13	0.0034	–5.6903	0.00412
253	2.63	1.16	0.0104	–4.5664	0.00395
263	9.23	1.03	0.0351	–3.3497	0.00380
273	30	1.23	0.1099	–2.2083	0.00366
283	120	1.07	0.4240	–0.8580	0.00353
298	362	1.07	1.2148	0.1946	0.00336

[a)] The average error of the temperature was estimated to σ(T) = 0.2 K.

The temperature dependence of the exchange rate constant k was derived from a modified form of the linearized Eyring equation (eq. 2, k_B = Boltzmann constant, h = Planck´s constant, R = gas constant) assuming that the transmission coefficient κ is equal 1 and that the activation enthalpy ($\Delta H^{\ddagger}$) is constant over the temperature interval of the experiment ($\Delta C_p^{\ddagger} = d(\Delta H^{\ddagger})/dT = 0$, $\Delta C_p^{\ddagger}$ = heat capacity of activation).

$$\ln\left(\frac{k}{T}\right) = \ln\left(\frac{k_B}{h}\right) + \left(\frac{\Delta S^{\ddagger}}{R}\right) + \left(-\frac{\Delta H^{\ddagger}}{R}\right) \cdot \frac{1}{T} \qquad \text{(eq. 2)}$$

$$\Delta H^{\ddagger} = -R \cdot \text{slope} \; [\text{J mol}^{-1}] \qquad \text{(eq. 3)}$$

$$\Delta S^{\ddagger} = R \cdot \left(\text{Intercept} - \ln\left(\frac{k_B}{h}\right)\right) \; [\text{J K}^{-1}\,\text{mol}^{-1}] \qquad \text{(eq. 4)}$$

$$\Delta G^{\ddagger} = \Delta H^{\ddagger} - T \cdot \Delta S^{\ddagger} \qquad \text{(eq. 5)}$$

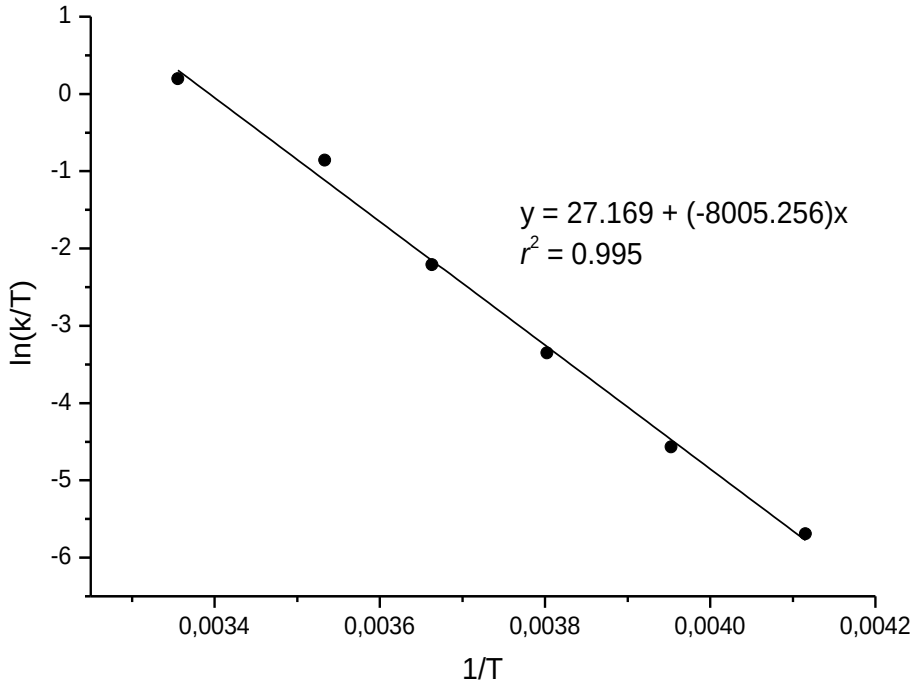

Figure 150. Eyring plot of ln(k/T) vs 1/T for the enantiomerization process of complex **1-Co**; the standard errors of the linear fit are σ(slope) = 261.68 and σ(intercept) = 0.98.

The enthalpy of activation ($\Delta H^{\ddagger}$) and entropy of activation ($\Delta S^{\ddagger}$) were obtained from the slope and the intercept of the linear fit, using equations 3 and 4 and $\Delta G^{\ddagger}$ was calculated from *equation 5*. The activation parameters are summarized in ***Table 53***.

Table 53. Activation parameters for the enantiomerization process of **1-Co** obtained from full-line shape iteration.

Activation parameter	Estimated value[xv]
$\Delta G^{\ddagger}$(273 K)	58.8 (±3) kJ mol^{-1}
$\Delta H^{\ddagger}$	66.5 (±2) kJ mol^{-1}
$\Delta S^{\ddagger}$	28(±8) J K^{-1} mol^{-1}

The free Gibbs energy of activation for the enatiomerization process was also calculated using equation 1, where T_c is the coalescence temperature (273 K) and $\Delta\nu$ is the chemical shift difference of the exchanging ^{t}Bu singlets in the low-temperature limit spectrum (233 K), where no exchange is assumed to occur (k = 0). The $\Delta G^{\ddagger}$ value of 58.9 kJ/mol was obtained with $T_c \approx 273$ K and $\Delta\nu = 14.1$ Hz, which compares very well with that obtained from full line-shape analysis ($\Delta G^{\ddagger}$ = 58.8 kJ/mol).

[xv] The error was calculated using the variance formula: H. H. Ku, *J. Res. Nat. Stand. Sec. C: Engineering and Instrumentation*, **1966**, *70C*, 262.

5.8. List of abbreviations

4-dmap	4-dimethylaminopyridine
ATR	Attenuated total reflection
br	broad
ca.	circa
calcd.	calculated
CAAC	cyclic(alkyl)(amino)carbene
caac^{Me}	:C[N(Dipp)(CMe_2)(CH_2)(CR_2)] R = Me
Cp	cyclopentadienyl
Cp*	pentamethylcyclopentadienyl
CV	Cyclic voltammetry
$\Delta\nu_{1/2}$	half height width
d	doublet
dec.	decomposition
DEPT	distortionless enhancement by polarisation transfer
DFT	Density functional theory
Dipp	2,6-$^{i}Pr_2$-C_6H_3
DME	dimethoxyethane
dmfc	Decamethylferrocene, [η^5-$C_5Me_5)_2$Fe]
Dsi	Disyl, $CH(SiMe_3)_2$
EA	elemental analysis
Eind	1,1,3,3,5,5,7,7-octaethyl-s-hydrindacen-4-yl
EMind	1,1,7,7-tetraethyl-3,3,5,5-tetramethyl-s-hydrindacen-4-yl
equiv.	equivalent(s)
EPR	electron paramagnetic resonance
Et_2O	diethylether
et al.	And others
FT	Fourier-transform
Fig.	figure
HMBC	Heteronuclear multiple bond correlation

HMQC	Heteronuclear multiple quantum coherence
HOMO	Highest occupied molecular orbital
in situ	in the reaction mixture
^{i}Pr	isopropyl
IMe_4	1,3,4,5-tetramethylimidazol-2-ylidene
IDipp	1,3-bis(2,6-diisopropylphenyl)imidazol-2-ylidene
IR	Infra red
Mes	mesityl, 2,4,6-Me_3-C_6H_2
NBO	natural bond orbital
NHC	N-heterocyclic carbene
NHI	N-heterocylcic imine
NMR	nuclear magnetic resonance
NRT	natural resonance theory
OTf	triflate, $OSO_2(CF_3)$
Ph	phenyl substituent
SIDipp	1,3-bis(2,6-diisopropylphenyl)imidazolidin-2-ylidene
t	triplet
Tbb	2,4-Dsi_2-4-^{t}Bu-C_6H_2
Tbt	2,4,6-$(CH(SiMe_3)_2)_3$-C_6H_2
^{t}Bu	tert.-butyl
THF	tetrahydrofuran
Tip	2,4,6-$^{i}Pr_2$-C_6H_3
TMS	$SiMe_3$
UV	ultra violet
Vis	visible
vs	very strong
vw	very weak
X	halogen

5.9. Scientific Contributions

Conference contributions

"Si=Ge Double Bonds: Synthesis and Reactivity of a caac^{Me}-supported Germasilyne".

Prasenjit Palui, Fabian Gstrein, Leonard R. Maurer, Ujjal Das, and Alexander C. Filippou. 21st Conference on Inorganic Chemistry, Marburg, Germany, 26th – 28th September, **2022**, Book of Abstracts, W 100.

Scientific Lectures

"Non-alkyne Like Reactivity of Ditetrelynes E_2R_2 (E = Si, Ge)"- presented at the Inorganic Chemistry Colloquium, University of Bonn, 21st December, **2023**.

6. Oath of compliance with the principles of scientific integrity

I hereby affirm that this dissertation was prepared independently at the Institute of Inorganic Chemistry, University of Bonn under the supervision of Prof. Dr. A. C. Filippou, and that all references and additional sources have been appropriately cited.

Prasenjit Palui

Bonn, 2024

7. References

[1] A. F. Holleman, E. Und Nils Wiberg, G. Fischer, *Lehrbuch Der Anorganischen Chemie*, Walter De Gruyter, Berlin • New York, **2007**.

[2] P. Siffert, E. F. Krimmel, Eds. , *Silicon*, Springer Berlin Heidelberg, Berlin, Heidelberg, **2004**.

[3] D. Benedikovic, L. Virot, G. Aubin, J.-M. Hartmann, F. Amar, X. Le Roux, C. Alonso-Ramos, É. Cassan, D. Marris-Morini, J.-M. Fédéli, F. Boeuf, B. Szelag, L. Vivien, *Nanophotonics* **2021**, *10*, 1059–1079.

[4] W. Kutzelnigg, *Angew. Chem. Int. Ed. Engl.* **1984**, *23*, 272–295.

[5] R. Janoschek, *Chemie in unserer Zeit* **1988**, *22*, 128–138.

[6] P. P. Power, *Chem. Commun.* **2003**, 2091.

[7] T. Tsukada, Y. Shoji, K. Takenouchi, H. Taka, T. Fukushima, *Chem. Commun.* **2022**, *58*, 4973–4976.

[8] L. Pu, B. Twamley, P. P. Power, *J. Am. Chem. Soc.* **2000**, *122*, 3524–3525.

[9] M. Stender, A. D. Phillips, R. J. Wright, P. P. Power, *Angew. Chem. Int. Ed.* **2002**, *41*, 1785–1787.

[10] A. D. Phillips, R. J. Wright, M. M. Olmstead, P. P. Power, *J. Am. Chem. Soc.* **2002**, *124*, 5930–5931.

[11] A. Sekiguchi, R. Kinjo, M. Ichinohe, *Science* **2004**, *305*, 1755–1757.

[12] N. Wiberg, W. Niedermayer, H. Nöth, M. Warchhold, *Z. anorg. allg. Chem.* **2001**, *627*, 1717–1722.

[13] N. Wiberg, W. Niedermayer, G. Fischer, H. Nöth, M. Suter, *Eur. J. Inorg. Chem.* **2002**, *2002*, 1066–1070.

[14] E. A. Carter, W. A. Goddard, *J. Phys. Chem.* **1986**, *90*, 998–1001.

[15] G. Trinquier, J. P. Malrieu, *J. Am. Chem. Soc.* **1987**, *109*, 5303–5315.

[16] J. P. Malrieu, G. Trinquier, *J. Am. Chem. Soc.* **1989**, *111*, 5916–5921.

[17] H. B. Wedler, P. Wendelboe, P. P. Power, *Organometallics* **2018**, *37*, 2929–2936.

[18] T. Sasamori, K. Hironaka, Y. Sugiyama, N. Takagi, S. Nagase, Y. Hosoi, Y. Furukawa, N. Tokitoh, *J. Am. Chem. Soc.* **2008**, *130*, 13856–13857.

[19] Y. Murata, M. Ichinohe, A. Sekiguchi, *J. Am. Chem. Soc.* **2010**, *132*, 16768–16770.

[20] S. Ishida, R. Sugawara, Y. Misawa, T. Iwamoto, *Angew. Chem.* **2013**, *125*, 13107–13111.

[21] T. Sugahara, J.-D. Guo, D. Hashizume, T. Sasamori, S. Nagase, N. Tokitoh, *Dalton Trans.* **2018**, *47*, 13318–13322.

[22] Y. Ding, J. Zhang, Y. Li, C. Cui, *J. Am. Chem. Soc.* **2022**, *144*, 20566–20570.

[23] Y. Sugiyama, T. Sasamori, Y. Hosoi, Y. Furukawa, N. Takagi, S. Nagase, N. Tokitoh, *J. Am. Chem. Soc.* **2006**, *128*, 1023–1031.

[24] Y. Peng, R. C. Fischer, W. A. Merrill, J. Fischer, L. Pu, B. D. Ellis, J. C. Fettinger, R. H. Herber, P. P. Power, *Chem. Sci.* **2010**, *1*, 461.

[25] J. Li, C. Schenk, C. Goedecke, G. Frenking, C. Jones, *J. Am. Chem. Soc.* **2011**, *133*, 18622–18625.

[26] T. J. Hadlington, M. Hermann, J. Li, G. Frenking, C. Jones, *Angew. Chem. Int. Ed.* **2013**, *52*, 10199–10203.

[27] T. Sugahara, J.-D. Guo, T. Sasamori, Y. Karatsu, Y. Furukawa, A. E. Ferao, S. Nagase, N. Tokitoh, *BCSJ* **2016**, *89*, 1375–1384.

[28] J. A. Kelly, M. Juckel, T. J. Hadlington, I. Fernández, G. Frenking, C. Jones, *Chemistry A European J* **2019**, *25*, 2773–2785.

[29] A. Caise, L. P. Griffin, A. Heilmann, C. McManus, J. Campos, S. Aldridge, *Angew Chem Int Ed* **2021**, *60*, 15606–15612.

[30] R. C. Fischer, L. Pu, J. C. Fettinger, M. A. Brynda, P. P. Power, *J. Am. Chem. Soc.* **2006**, *128*, 11366–11367.

[31] T. J. Hadlington, C. Jones, *Chem. Commun.* **2014**, *50*, 2321.

[32] L. G. Perla, J. M. Kulenkampff, J. C. Fettinger, P. P. Power, *Organometallics* **2018**, *37*, 4048–4054.

[33] J. Guo, T. Sasamori, *Chemistry An Asian Journal* **2018**, *13*, 3800–3817.

[34] T. Sugahara, J. Guo, T. Sasamori, S. Nagase, N. Tokitoh, *Angew Chem Int Ed* **2018**, *57*, 3499–3503.

[35] W. A. Herrmann, Ed. , *Transition Metals Part 1*, Georg Thieme Verlag, Stuttgart, **1997**.

[36] M. Cui, R. Lin, G. Jia, *Chemistry An Asian Journal* **2018**, *13*, 895–912.

[37] W. Ma, C. Yu, T. Chen, L. Xu, W.-X. Zhang, Z. Xi, *Chem. Soc. Rev.* **2017**, *46*, 1160–1192.

[38] J. R. Bleeke, *Acc. Chem. Res.* **1991**, *24*, 271–277.

[39] C. W. Landorf, M. M. Haley, *Angew. Chem. Int. Ed.* **2006**, *45*, 3914–3936.

[40] S. Ishida, T. Iwamoto, *Coordination Chemistry Reviews* **2016**, *314*, 34–63.

[41] M. Suginome, H. Oike, Y. Ito, *Organometallics* **1994**, *13*, 4148–4150.

[42] M. Suginome, H. Oike, S.-S. Park, Y. Ito, *BCSJ* **1996**, *69*, 289–299.

[43] M. Zirngast, M. Flock, J. Baumgartner, C. Marschner, *J. Am. Chem. Soc.* **2009**, *131*, 15952–15962.

[44] C. Kayser, G. Kickelbick, C. Marschner, *Angew. Chem. Int. Ed.* **2002**, *41*, 989–992.

[45] M. Tanabe, N. Ishikawa, M. Hanzawa, K. Osakada, *Organometallics* **2008**, *27*, 5152–5158.

[46] K. Mochida, H. Karube, M. Nanjo, Y. Nakadaira, *Organometallics* **2005**, *24*, 4734–4741.

[47] M. Tanabe, J. Jiang, H. Yamazawa, K. Osakada, T. Ohmura, M. Suginome, *Organometallics* **2011**, *30*, 3981–3991.

[48] C. Y. Lee, Y. Wang, C. S. Liu, *Inorg. Chem.* **1991**, *30*, 3893–3899.

[49] X. Wang, Y. Peng, M. M. Olmstead, H. Hope, P. P. Power, *J. Am. Chem. Soc.* **2010**, *132*, 13150–13151.

[50] Y. Wang, M. Karni, S. Yao, Y. Apeloig, M. Driess, *J. Am. Chem. Soc.* **2019**, *141*, 1655–1664.

[51] A. Jana, V. Huch, H. S. Rzepa, D. Scheschkewitz, *Organometallics* **2015**, *34*, 2130–2133.

[52] P. K. Majhi, M. Zimmer, B. Morgenstern, V. Huch, D. Scheschkewitz, *J. Am. Chem. Soc.* **2021**, *143*, 13350–13357.

[53] P. K. Majhi, M. Zimmer, B. Morgenstern, D. Scheschkewitz, *J. Am. Chem. Soc.* **2021**, *143*, 8981–8986.

[54] A. Jana, M. Majumdar, V. Huch, M. Zimmer, D. Scheschkewitz, *Dalton Trans.* **2014**, *43*, 5175–5181.

[55] T. Yoshimoto, H. Hashimoto, M. Ray, N. Hayakawa, T. Matsuo, J. Chakrabarti, H. Tobita, *Chem. Lett.* **2020**, *49*, 311–314.

[56] P. G. Hayes, Z. Xu, C. Beddie, J. M. Keith, M. B. Hall, T. D. Tilley, *J. Am. Chem. Soc.* **2013**, *135*, 11780–11783.

[57] B. Baars, *Synthese und Reaktivität von kationischen Metallosilylidinen und Metallosilylenen*, Mensch Und Buch Verlag, Berlin, **2017**.

[58] Y. N. Lebedev, *Multiple Bonding of Low-Valent Silicon and Germanium to Group 6 and 9 Metals*, Verl. Dr. Hut, München, **2015**.

[59] L. Arizpe, *Synthesis and Characterization of Complexes Featuring Tantalum-Germanium Multiple Bonds*, Mensch & Buch, Berlin, **2019**.

[60] R. Hoffmann, C. N. Wilker, O. Eisenstein, *J. Am. Chem. Soc.* **1982**, *104*, 632–634.

[61] A. C. Filippou, W. Grünleitner, C. Völkl, P. Kiprof, *Angew. Chem. Int. Ed. Engl.* **1991**, *30*, 1167–1169.

[62] A. C. Filippou, C. Völkl, W. Grünleitner, P. Kiprof, *Journal of Organometallic Chemistry* **1992**, *434*, 201–223.

[63] D. L. M. Suess, J. C. Peters, *J. Am. Chem. Soc.* **2013**, *135*, 12580–12583.

[64] J. A. Buss, T. Agapie, *J. Am. Chem. Soc.* **2016**, *138*, 16466–16477.

[65] S. Saini, A. Agarwal, S. K. Bose, *Dalton Trans.* **2020**, *49*, 17055–17075.

[66] H. Hashimoto, K. Nagata, *Chem. Lett.* **2021**, *50*, 778–787.

[67] L. R. Maurer, J. Rump, A. C. Filippou, *Inorganics* **2023**, *11*, 129.

[68] I. Papazoglou, *Unprecedented Tetrylidyne Complexes of Group 6 and 10 Metals*, Dr. Hut, München, **2017**.

[69] U. Chakraborty, Multiple Bonds between Group 7 Transition Metals and Heavier Tetrel Elements (Ge –Pb), Dissertation, University of Bonn, **2013**.

[70] J. Morvan, M. Mauduit, G. Bertrand, R. Jazzar, *ACS Catal.* **2021**, *11*, 1714–1748.

[71] S. G. Patra, N. K. Das, *Polyhedron* **2021**, *200*, 115096.

[72] H. Albright, A. J. Davis, J. L. Gomez-Lopez, H. L. Vonesh, P. K. Quach, T. H. Lambert, C. S. Schindler, *Chem. Rev.* **2021**, *121*, 9359–9406.

[73] D. S. Belov, G. Tejeda, K. V. Bukhryakov, *ChemPlusChem* **2021**, *86*, 924–937.

[74] A. Fürstner, *J. Am. Chem. Soc.* **2021**, *143*, 15538–15555.

[75] M. Cui, G. Jia, *J. Am. Chem. Soc.* **2022**, *144*, 12546–12566.

[76] A. S. Goldman, A. H. Roy, Z. Huang, R. Ahuja, W. Schinski, M. Brookhart, *Science* **2006**, *312*, 257–261.

[77] R. C. Fischer, P. P. Power, *Chem. Rev.* **2010**, *110*, 3877–3923.

[78] F. Hanusch, L. Groll, S. Inoue, *Chem. Sci.* **2021**, *12*, 2001–2015.

[79] K. Kishikawa, N. Tokitoh, R. Okazaki, *Chem. Lett.* **1998**, *27*, 239–240.

[80] M. Takahashi, S. Tsutsui, K. Sakamoto, M. Kira, T. Müller, Y. Apeloig, *J. Am. Chem. Soc.* **2001**, *123*, 347–348.

[81] K. Suzuki, T. Matsuo, D. Hashizume, K. Tamao, *J. Am. Chem. Soc.* **2011**, *133*, 19710–19713.

[82] T. Agou, N. Hayakawa, T. Sasamori, T. Matsuo, D. Hashizume, N. Tokitoh, *Chemistry A European J* **2014**, *20*, 9246–9249.

[83] L. Klemmer, A.-L. Thömmes, M. Zimmer, V. Huch, B. Morgenstern, D. Scheschkewitz, *Nat. Chem.* **2021**, *13*, 373–377.

[84] M. L. McCrea-Hendrick, C. A. Caputo, J. Linnera, P. Vasko, C. M. Weinstein, J. C. Fettinger, H. M. Tuononen, P. P. Power, *Organometallics* **2016**, *35*, 2759–2767.

[85] J. D. Queen, A. C. Phung, C. A. Caputo, J. C. Fettinger, P. P. Power, *J. Am. Chem. Soc.* **2020**, *142*, 2233–2237.

[86] A. Sekiguchi, *Pure and Applied Chemistry* **2008**, *80*, 447–457.

[87] J.-J. Maudrich, F. Diab, S. Weiß, M. Widemann, T. Dema, H. Schubert, K. M. Krebs, K. Eichele, L. Wesemann, *Inorg. Chem.* **2019**, *58*, 15758–15768.

[88] R. S. Ghadwal, H. W. Roesky, S. Merkel, J. Henn, D. Stalke, *Angewandte Chemie* **2009**, *121*, 5793–5796.

[89] A. C. Filippou, O. Chernov, G. Schnakenburg, *Angewandte Chemie* **2009**, *121*, 5797–5800.

[90] A. C. Filippou, O. Chernov, B. Blom, K. W. Stumpf, G. Schnakenburg, *Chem. Eur. J.* **2010**, *16*, 2866–2872.

[91] G. Frenking, M. Hermann, D. M. Andrada, N. Holzmann, *Chem. Soc. Rev.* **2016**, *45*, 1129–1144.

[92] M. Soleilhavoup, G. Bertrand, *Acc. Chem. Res.* **2015**, *48*, 256–266.

[93] M. Melaimi, R. Jazzar, M. Soleilhavoup, G. Bertrand, *Angew Chem Int Ed* **2017**, *56*, 10046–10068.

[94] S. Khan, H. W. Roesky, *Chemistry A European J* **2019**, *25*, 1636–1648.

[95] S. Karwasara, L. R. Maurer, B. Peerless, G. Schnakenburg, U. Das, A. C. Filippou, *J. Am. Chem. Soc.* **2021**, *143*, 14780–14794.

[96] A. Jana, V. Huch, D. Scheschkewitz, *Angew. Chem. Int. Ed.* **2013**, *52*, 12179–12182.

[97] K. M. Krebs, D. Hanselmann, H. Schubert, K. Wurst, M. Scheele, L. Wesemann, *J. Am. Chem. Soc.* **2019**, *141*, 3424–3429.

[98] P. Ghana, M. I. Arz, U. Das, G. Schnakenburg, A. C. Filippou, *Angew. Chem.* **2015**, *127*, 10118–10123.

[99] R. Kobayashi, S. Ishida, T. Iwamoto, *Organometallics* **2021**, *40*, 843–847.

[100] S. Kundu, S. Sinhababu, V. Chandrasekhar, H. W. Roesky, *Chem. Sci.* **2019**, *10*, 4727–4741.

[101] T. Sasamori, T. Sugahara, T. Agou, J.-D. Guo, S. Nagase, R. Streubel, N. Tokitoh, *Organometallics* **2015**, *34*, 2106–2109.

[102] C. Benisch, J. Chávez, R. Gleiter, B. Nuber, H. Irngartinger, T. Oeser, H. Pritzkow, F. Rominger, *Eur. J. Inorg. Chem.* **1998**, *1998*, 629–632.

[103] H. G. Schuster-Woldan, F. Basolo, *J. Am. Chem. Soc.* **1966**, *88*, 1657–1663.

[104] A. Wojcicki, F. Basolo, *Journal of Inorganic and Nuclear Chemistry* **1961**, *17*, 77–83.

[105] A. Krebs, J. Wilke, in *Wittig Chemistry*, Springer-Verlag, Berlin/Heidelberg, **1983**, pp. 189–233.

[106] K. K. Baldridge, K. D. Bunker, C. L. Vélez, R. L. Holland, A. L. Rheingold, C. E. Moore, J. M. O'Connor, *Organometallics* **2013**, *32*, 5473–5480.

[107] L. Salem, *Acc. Chem. Res.* **1971**, *4*, 322–328.

[108] S. Bajo, M. G. Alférez, M. M. Alcaide, J. López-Serrano, J. Campos, *Chemistry A European J* **2020**, *26*, 16833–16845.

[109] A. Sekiguchi, M. Tsukamoto, M. Ichinohe, *Science* **1997**, *275*, 60–61.

[110] Y. Yamamoto, T. Mise, H. Yamazaki, *BCSJ* **1978**, *51*, 2743–2744.

[111] K. Costuas, J.-Y. Saillard, *Organometallics* **1999**, *18*, 2505–2512.

[112] M. Mantina, A. C. Chamberlin, R. Valero, C. J. Cramer, D. G. Truhlar, *J. Phys. Chem. A* **2009**, *113*, 5806–5812.

[113] A. Doddi, C. Gemel, M. Winter, R. A. Fischer, C. Goedecke, H. S. Rzepa, G. Frenking, *Angew. Chem. Int. Ed.* **2013**, *52*, 450–454.

[114] M. Ma, L. Shen, H. Wang, Y. Zhao, B. Wu, X.-J. Yang, *Organometallics* **2020**, *39*, 1440–1447.

[115] T. Henneberger, W. Klein, J. V. Dums, T. F. Fässler, *Chem. Commun.* **2018**, *54*, 12381–12384.

[116] D. Nied, W. Klopper, F. Breher, *Angew Chem Int Ed* **2009**, *48*, 1411–1416.

[117] A. Jana, V. Huch, M. Repisky, R. J. F. Berger, D. Scheschkewitz, *Angew. Chem. Int. Ed.* **2014**, *53*, 3514–3518.

[118] E. Hupf, F. Kaiser, P. A. Lummis, M. M. D. Roy, R. McDonald, M. J. Ferguson, F. E. Kühn, E. Rivard, *Inorg. Chem.* **2020**, *59*, 1592–1601.

[119] E. D. Glendening, C. R. Landis, F. Weinhold, *WIREs Comput Mol Sci* **2012**, *2*, 1–42.

[120] C. R. Landis, F. Weinhold, *J Comput Chem* **2007**, *28*, 198–203.

[121] C. R. Landis, F. Weinhold, *J Comput Chem* **2016**, *37*, 237–241.

[122] J. I.-C. Wu, P. V. R. Schleyer, *Pure and Applied Chemistry* **2013**, *85*, 921–940.

[123] C. Cui, M. M. Olmstead, J. C. Fettinger, G. H. Spikes, P. P. Power, *J. Am. Chem. Soc.* **2005**, *127*, 17530–17541.

[124] L. Zhao, C. Jones, G. Frenking, *Chem. Eur. J.* **2015**, *21*, 12405–12413.

[125] T. Sugahara, J.-D. Guo, D. Hashizume, T. Sasamori, N. Tokitoh, *J. Am. Chem. Soc.* **2019**, *141*, 2263–2267.

[126] J. P. Lomont, S. C. Nguyen, M. C. Zoerb, A. D. Hill, J. P. Schlegel, C. B. Harris, *Organometallics* **2012**, *31*, 3582–3587.

[127] C. Benisch, R. Gleiter, T. H. Staeb, B. Nuber, T. Oeser, H. Pritzkow, F. Rominger, *Journal of Organometallic Chemistry* **2002**, *641*, 102–112.

[128] A. Spencer, H. Werner, *Journal of Organometallic Chemistry* **1979**, *171*, 219–228.

[129] A. Roglans, A. Pla-Quintana, M. Solà, *Chem. Rev.* **2021**, *121*, 1894–1979.

[130] M. Widemann, S. Jeggle, M. Auer, K. Eichele, H. Schubert, C. P. Sindlinger, L. Wesemann, *Chem. Sci.* **2022**, *13*, 3999–4009.

[131] E. J. Baerends, O. V. Gritsenko, R. Van Meer, *Phys. Chem. Chem. Phys.* **2013**, *15*, 16408.

[132] G. Albertin, S. Antoniutti, J. Castro, *Journal of Organometallic Chemistry* **2012**, *718*, 108–116.

[133] W. A. Herrmann, C. Bauer, J. M. Huggins, H. Pfisterer, M. L. Ziegler, *Journal of Organometallic Chemistry* **1983**, *258*, 81–99.

[134] P. Diversi, G. Ingrosso, A. Lucherini, W. Porzio, M. Zocchi, *Inorg. Chem.* **1980**, *19*, 3590–3597.

[135] T. Sasamori, T. Sugahara, T. Agou, K. Sugamata, J.-D. Guo, S. Nagase, N. Tokitoh, *Chem. Sci.* **2015**, *6*, 5526–5530.

[136] K. Takeuchi, M. Ichinohe, A. Sekiguchi, J. Guo, S. Nagase, *J of Physical Organic Chem* **2010**, *23*, 390–394.

[137] A. Kirschning, S. Luiken, A. Migliorini, M. Loreto, M. Vogt, *Synlett* **2009**, *2009*, 429–432.

[138] J. S. McIndoe, B. K. Nicholson, *Journal of Organometallic Chemistry* **1999**, *577*, 181–188.

[139] F. Hoffmann, J. Wagler, U. Böhme, G. Roewer, *Journal of Organometallic Chemistry* **2012**, *705*, 59–69.

[140] R. S. Ghadwal, R. Azhakar, K. Pröpper, J. J. Holstein, B. Dittrich, H. W. Roesky, *Inorg. Chem.* **2011**, *50*, 8502–8508.

[141] N. Parvin, B. Mishra, A. George, M. Neralkar, J. Hossain, P. Parameswaran, S. Hotha, S. Khan, *Chem. Commun.* **2020**, *56*, 7625–7628.

[142] Y. Kang, K. Kim, S.-O. Kang, J. Ko, B. T. Heaton, J. V. Barkley, *Journal of Organometallic Chemistry* **1997**, *532*, 79–82.

[143] S. Xie, Y. Dong, X. Du, Q. Fan, H. Yang, X. Li, H. Sun, O. Fuhr, D. Fenske, *Organometallics* **2021**, *40*, 286–293.

[144] M. Brookhart, B. E. Grant, C. P. Lenges, M. H. Prosenc, P. S. White, *Angew. Chem. Int. Ed.* **2000**, *39*, 1676–1679.

[145] R. Azhakar, R. S. Ghadwal, H. W. Roesky, J. Hey, D. Stalke, *Chem. Asian J.* **2012**, *7*, 528–533.

[146] K. Narasaka, N. Saito, Y. Hayashi, H. Ichida, *Chem. Lett.* **1990**, *19*, 1411–1414.

[147] N. Nakata, T. Oikawa, T. Matsumoto, Y. Kabe, A. Sekiguchi, *Organometallics* **2005**, *24*, 3368–3370.

[148] R. Jones, D. J. Williams, Y. Kabe, S. Masamune, *Angew. Chem. Int. Ed. Engl.* **1986**, *25*, 173–174.

[149] N. Wiberg, H. Schuster, A. Simon, K. Peters, *Angew. Chem. Int. Ed. Engl.* **1986**, *25*, 79–80.

[150] D. Nied, R. Köppe, W. Klopper, H. Schnöckel, F. Breher, *J. Am. Chem. Soc.* **2010**, *132*, 10264–10265.

[151] S. Kyushin, Y. Kurosaki, K. Otsuka, H. Imai, S. Ishida, T. Kyomen, M. Hanaya, H. Matsumoto, *Nat Commun* **2020**, *11*, 4009.

[152] S. Bourg, B. Boury, F. H. Carré, R. J. P. Corriu, *Organometallics* **1998**, *17*, 167–172.

[153] M. Aizenberg, J. Ott, C. J. Elsevier, D. Milstein, *Journal of Organometallic Chemistry* **1998**, *551*, 81–92.

[154] K. Osakada, K. Hataya, T. Yamamoto, *Inorganica Chimica Acta* **1997**, *259*, 203–211.

[155] S. N. Heaton, M. G. Partridge, R. N. Perutz, S. J. Parsons, F. Zimmermann, *J. Chem. Soc., Dalton Trans.* **1998**, 2515–2520.

[156] M. J. Fernandez, P. M. Bailey, P. O. Bentz, J. S. Ricci, T. F. Koetzle, P. M. Maitlis, *J. Am. Chem. Soc.* **1984**, *106*, 5458–5463.

[157] K. S. Cook, C. D. Incarvito, C. E. Webster, Y. Fan, M. B. Hall, J. F. Hartwig, *Angew. Chem.* **2004**, *116*, 5590–5593.

[158] D. Zhu, D. J. Kozera, K. D. Enns, P. H. M. Budzelaar, *Angew. Chem. Int. Ed.* **2012**, *51*, 12211–12214.

[159] P. C. B. Page, S. S. Klair, S. Rosenthal, *Chem. Soc. Rev.* **1990**, *19*, 147.

[160] P. PyykkÃ¶, M. Atsumi, *Chem. Eur. J.* **2009**, *15*, 12770–12779.

[161] J. Zhang, B. J. Foley, N. Bhuvanesh, J. Zhou, D. E. Janzen, M. T. Whited, O. V. Ozerov, *Organometallics* **2018**, *37*, 3956–3962.

[162] W. Wang, S. Inoue, S. Enthaler, M. Driess, *Angew. Chem. Int. Ed.* **2012**, *51*, 6167–6171.

[163] Y. Li, Q. Fan, H. Yang, S. Xie, W. Huang, X. Li, H. Sun, O. Fuhr, D. Fenske, *New J. Chem.* **2021**, *45*, 19950–19956.

[164] C. Ganesamoorthy, J. Schoening, C. Wölper, L. Song, P. R. Schreiner, S. Schulz, *Nat. Chem.* **2020**, *12*, 608–614.

[165] D. Reiter, R. Holzner, A. Porzelt, P. Frisch, S. Inoue, *Nat. Chem.* **2020**, *12*, 1131–1135.

[166] A. Rosas-Sánchez, I. Alvarado-Beltran, A. Baceiredo, N. Saffon-Merceron, S. Massou, V. Branchadell, T. Kato, *Angew Chem Int Ed* **2017**, *56*, 10549–10554.

[167] S. Takahashi, J. Sekiguchi, A. Ishii, N. Nakata, *Angew Chem Int Ed* **2021**, *60*, 4055–4059.

[168] E. Neumann, A. Pfaltz, *Organometallics* **2005**, *24*, 2008–2011.

[169] S. Takahashi, E. Bellan, A. Baceiredo, N. Saffon-Merceron, S. Massou, N. Nakata, D. Hashizume, V. Branchadell, T. Kato, *Angew Chem Int Ed* **2019**, *58*, 10310–10314.

[170] A.-M. Dechert-Schmitt, M. R. Garnsey, H. M. Wisniewska, J. I. Murray, T. Lee, D. W. Kung, N. Sach, D. G. Blackmond, *ACS Catal.* **2019**, *9*, 4508–4515.

[171] Y. Ito, S. Nishimura, M. Ishikawa, *Tetrahedron Letters* **1987**, *28*, 1293–1294.

[172] Y. Ito, M. Suginome, T. Matsuura, M. Murakami, *J. Am. Chem. Soc.* **1991**, *113*, 8899–8908.

[173] M. Weidenbruch, E. Kroke, K. Peters, H. G. Von Schnering, *Journal of Organometallic Chemistry* **1993**, *461*, 35–38.

[174] H. B. Yokelson, A. J. Millevolte, K. J. Haller, R. West, *J. Chem. Soc., Chem. Commun.* **1987**, 1605.

[175] S. Mukhopadhyay, A. G. Patro, R. S. Vadavi, S. Nembenna, *Eur J Inorg Chem* **2022**, *2022*, e202200469.

[176] T. Oikawa, N. Nakata, T. Matsumoto, Y. Kabe, A. Sekiguchi, *Heteroatom Chem.* **2008**, *19*, 87–92.

[177] P. Garg, D. Dange, Y. Jiang, C. Jones, *Dalton Trans.* **2022**, *51*, 7838–7844.

[178] Y. Ohmori, M. Ichinohe, A. Sekiguchi, M. J. Cowley, V. Huch, D. Scheschkewitz, *Organometallics* **2013**, *32*, 1591–1594.

[179] K. Takeuchi, M. Ichinohe, A. Sekiguchi, *J. Am. Chem. Soc.* **2008**, *130*, 16848–16849.

[180] T. Abe, T. Iwamoto, C. Kabuto, M. Kira, *J. Am. Chem. Soc.* **2006**, *128*, 4228–4229.

[181] J. Liu, Z. Liu, P. Liao, L. Zhang, T. Tu, X. Bi, *Angew. Chem. Int. Ed.* **2015**, *54*, 10618–10622.

[182] M. Peplow, *Nature* **2023**, *618*, 21–24.

[183] T. Iwamoto, T. Abe, K. Sugimoto, D. Hashizume, H. Matsui, R. Kishi, M. Nakano, S. Ishida, *Angew Chem Int Ed* **2019**, *58*, 4371–4375.

[184] P. Pyykkö, *J. Phys. Chem. A* **2015**, *119*, 2326–2337.

[185] G. E. Miracle, J. L. Ball, D. R. Powell, R. West, *J. Am. Chem. Soc.* **1993**, *115*, 11598–11599.

[186] S. Spirk, F. Belaj, J. H. Albering, R. Pietschnig, *Organometallics* **2010**, *29*, 2981–2986.

[187] M. Trommer, G. E. Miracle, B. E. Eichler, D. R. Powell, R. West, *Organometallics* **1997**, *16*, 5737–5747.

[188] M. M. Moeng, F. P. Malan, S. Lotz, D. I. Bezuidenhout, *Journal of Molecular Structure* **2022**, *1252*, 132093.

[189] A. C. Filippou, E. Herdtweck, H. G. Alt, *Journal of Organometallic Chemistry* **1988**, *355*, 437–447.

[190] E. Bleuel, O. Gevert, M. Laubender, H. Werner, *Organometallics* **2000**, *19*, 3109–3114.

[191] H. Werner, P. Schwab, E. Bleuel, N. Mahr, B. Windmüller, J. Wolf, *Chem. Eur. J.* **2000**, *6*, 4461–4470.

[192] T. Pechmann, C. D. Brandt, H. Werner, *Organometallics* **2003**, *22*, 3004–3006.

[193] D. J. D. Wilson, S. A. Couchman, J. L. Dutton, *Inorg. Chem.* **2012**, *51*, 7657–7668.

[194] A. Sekiguchi, V. Ya. Lee, *Chem. Rev.* **2003**, *103*, 1429–1448.

[195] T. Nukazawa, T. Iwamoto, *J. Am. Chem. Soc.* **2020**, *142*, 9920–9924.

[196] J. Chatt, L. A. Duncanson, *J. Chem. Soc.* **1953**, 2939.

[197] T. Iwamoto, D. Yin, C. Kabuto, M. Kira, *J. Am. Chem. Soc.* **2001**, *123*, 12730–12731.

[198] R. A. Jones, F. M. Real, G. Wilkinson, A. M. R. Galas, M. B. Hursthouse, K. M. A. Malik, *J. Chem. Soc., Dalton Trans.* **1980**, 511.

[199] A. K. Kakkar, G. Stringer, N. J. Taylor, T. B. Marder, *Can. J. Chem.* **1995**, *73*, 981–988.

[200] Y. Heider, P. Willmes, D. Mühlhausen, L. Klemmer, M. Zimmer, V. Huch, D. Scheschkewitz, *Angew Chem Int Ed* **2019**, *58*, 1939–1944.

[201] G. Dübek, F. Hanusch, S. Inoue, *Inorg. Chem.* **2019**, *58*, 15700–15704.

[202] B. J. Guddorf, M. Feldt, A. Hepp, C. G. Daniliuc, F. Lips, *Organometallics* **2020**, *39*, 4387–4394.

[203] L. Yang, D. R. Powell, R. P. Houser, *Dalton Trans.* **2007**, 955–964.

[204] K. Suzuki, Y. Numata, N. Fujita, N. Hayakawa, T. Tanikawa, D. Hashizume, K. Tamao, H. Fueno, K. Tanaka, T. Matsuo, *Chem. Commun.* **2018**, *54*, 2200–2203.

[205] B. Blom, Reactivity of Ylenes at Late Transition Metal Centers, Dissertation, University of Bonn, **2011**.

[206] Y. Wang, Y. Xie, P. Wei, R. B. King, H. F. Schaefer, P. Von R. Schleyer, G. H. Robinson, *Science* **2008**, *321*, 1069–1071.

[207] M. I. Arz, D. Geiß, M. Straßmann, G. Schnakenburg, A. C. Filippou, *Chem. Sci.* **2015**, *6*, 6515–6524.

[208] M. I. Arz, *Molekulare Si(0)- und Si(I)-Verbindungen: Synthese, Struktur und Reaktivität* **2015**.

[209] L. N. Zelenina, T. P. Chusova, Yu. G. Stenin, G. A. Berezovskii, *Russ. J. Phys. Chem.* **2006**, *80*, 1911–1914.

[210] R. Becerra, R. Walsh, in *Organosilicon Compounds*, Elsevier, **2017**, pp. 79–113.

[211] M. Igarashi, M. Ichinohe, A. Sekiguchi, *Heteroatom Chem.* **2008**, *19*, 649–653.

[212] J. Z. Xiong, D. Jiang, C. E. Dixon, K. M. Baines, T. K. Sham, *Can. J. Chem.* **1996**, *74*, 2229–2239.

[213] A. Rit, J. Campos, H. Niu, S. Aldridge, *Nature Chem* **2016**, *8*, 1022–1026.

[214] H. F. T. Klare, L. Albers, L. Süsse, S. Keess, T. Müller, M. Oestreich, *Chem. Rev.* **2021**, *121*, 5889–5985.

[215] D. Pinchuk, J. Mathew, A. Kaushansky, D. Bravo-Zhivotovskii, Y. Apeloig, *Angew Chem Int Ed* **2016**, *55*, 10258–10262.

[216] L. Zborovsky, R. Dobrovetsky, M. Botoshansky, D. Bravo-Zhivotovskii, Y. Apeloig, *J. Am. Chem. Soc.* **2012**, *134*, 18229–18232.

[217] D. M. Jenkins, W. Teng, U. Englich, D. Stone, K. Ruhlandt-Senge, *Organometallics* **2001**, *20*, 4600–4606.

[218] M. M. Siddiqui, S. Sinhababu, S. Dutta, S. Kundu, P. N. Ruth, A. Münch, R. Herbst-Irmer, D. Stalke, D. Koley, H. W. Roesky, *Angew. Chem. Int. Ed.* **2018**, *57*, 11776–11780.

[219] A. C. Filippou, K. W. Stumpf, O. Chernov, G. Schnakenburg, *Organometallics* **2012**, *31*, 748–755.

[220] H. Schumann, M. Glanz, F. Girgsdies, F. E. Hahn, M. Tamm, A. Grzegorzewski, *Angew. Chem. Int. Ed. Engl.* **1997**, *36*, 2232–2234.

[221] P. A. Rupar, M. C. Jennings, P. J. Ragogna, K. M. Baines, *Organometallics* **2007**, *26*, 4109–4111.

[222] N. Katir, D. Matioszek, S. Ladeira, J. Escudié, A. Castel, *Angew. Chem. Int. Ed.* **2011**, *50*, 5352–5355.

[223] C. Gendy, J. Mikko Rautiainen, A. Mailman, H. M. Tuononen, *Chemistry A European J* **2021**, *27*, 14405–14409.

[224] P. Fritsch, *Justus Liebigs Ann. Chem.* **1894**, *279*, 319–323.

[225] W. P. Buttenberg, *Justus Liebigs Ann. Chem.* **1894**, *279*, 324–337.

[226] H. Wiechell, *Justus Liebigs Ann. Chem.* **1894**, *279*, 337–344.

[227] N. Pavliček, P. Gawel, D. R. Kohn, Z. Majzik, Y. Xiong, G. Meyer, H. L. Anderson, L. Gross, *Nature Chem* **2018**, *10*, 853–858.

[228] Z. D. Brown, P. Vasko, J. C. Fettinger, H. M. Tuononen, P. P. Power, *J. Am. Chem. Soc.* **2012**, *134*, 4045–4048.

[229] N. Wienkenhöver, 1,2-Dibromodisilenes: A Rich Source for Titanium Silylidyne Complexes, Acyclic Silylenes and Disilyne Dianions, Dissertation, University of Bonn, **2017**.

[230] A. Lülsdorf, *Tetrylidin-Komplexe des Titans*, Mensch & Buch, Berlin, **2021**.

[231] P. P. Power, *Acc. Chem. Res.* **2011**, *44*, 627–637.

[232] T. Yamaguchi, A. Sekiguchi, M. Driess, *J. Am. Chem. Soc.* **2010**, *132*, 14061–14063.

[233] B. D. Shepherd, D. R. Powell, R. West, *Organometallics* **1989**, *8*, 2664–2669.

[234] R. Holzner, A. Porzelt, U. S. Karaca, F. Kiefer, P. Frisch, D. Wendel, M. C. Holthausen, S. Inoue, *Dalton Trans.* **2021**, *50*, 8785–8793.

[235] M. Schormann, K. S. Klimek, H. Hatop, S. P. Varkey, H. W. Roesky, C. Lehmann, C. Röpken, R. Herbst-Irmer, M. Noltemeyer, *Journal of Solid State Chemistry* **2001**, *162*, 225–236.

[236] A. Purath, H. Schnöckel, *Journal of Organometallic Chemistry* **1999**, *579*, 373–375.

[237] H. Watanabe, K. Takeuchi, N. Fukawa, M. Kato, M. Goto, Y. Nagai, *Chem. Lett.* **1987**, *16*, 1341–1344.

[238] D. Scheschkewitz, *Angew. Chem. Int. Ed.* **2004**, *43*, 2965–2967.

[239] D. B. G. Williams, M. Lawton, *J. Org. Chem.* **2010**, *75*, 8351–8354.

[240] R. Inoue, M. Yamaguchi, Y. Murakami, K. Okano, A. Mori, *ACS Omega* **2018**, *3*, 12703–12706.

[241] J. Geier, H. Rüegger, H. Grützmacher, *Dalton Trans.* **2006**, 129–136.

[242] T. R. Hoye, B. M. Eklov, T. D. Ryba, M. Voloshin, L. J. Yao, *Org. Lett.* **2004**, *6*, 953–956.

[243] R. K. Harris, E. D. Becker, S. M. Cabral De Menezes, P. Granger, R. E. Hoffman, K. W. Zilm, *Pure and Applied Chemistry* **2008**, *80*, 59–84.

[244] I. Noviandri, K. N. Brown, D. S. Fleming, P. T. Gulyas, P. A. Lay, A. F. Masters, L. Phillips, *J. Phys. Chem. B* **1999**, *103*, 6713–6722.

[245] I. Raabe, K. Wagner, K. Guttsche, M. Wang, M. Grätzel, G. Santiso-Quiñones, I. Krossing, *Chemistry A European J* **2009**, *15*, 1966–1976.

[246] M. P. Stewart, L. M. Paradee, I. Raabe, N. Trapp, J. S. Slattery, I. Krossing, W. E. Geiger, *Journal of Fluorine Chemistry* **2010**, *131*, 1091–1095.

[247] J. Heinze, *Angew. Chem. Int. Ed. Engl.* **1984**, *23*, 831–847.

[248] N. Elgrishi, K. J. Rountree, B. D. McCarthy, E. S. Rountree, T. T. Eisenhart, J. L. Dempsey, *J. Chem. Educ.* **2018**, *95*, 197–206.

[249] J. Kouvetakis, A. Haaland, D. J. Shorokhov, H. V. Volden, G. V. Girichev, V. I. Sokolov, P. Matsunaga, *J. Am. Chem. Soc.* **1998**, *120*, 6738–6744.

[250] M. Tashiro, T. Yamato, *J. Chem. Soc., Perkin Trans. 1* **1979**, 176.

[251] K. Nagata, T. Agou, N. Tokitoh, *Angew. Chem. Int. Ed.* **2014**, *53*, 3881–3884.

[252] K. Fredenhagen, G. Cadenbach, *Z. Anorg. Allg. Chem.* **1926**, *158*, 249–263.

[253] W. Rüdorff, E. Schulze, *Zeitschrift anorg allge chemie* **1954**, *277*, 156–171.

[254] S. R. Bahr, P. Boudjouk, *J. Org. Chem.* **1992**, *57*, 5545–5547.

[255] N. A. Yakelis, R. G. Bergman, *Organometallics* **2005**, *24*, 3579–3581.

[256] J. E. Borger, M. S. Bakker, A. W. Ehlers, M. Lutz, J. Chris Slootweg, K. Lammertsma, *Chem. Commun.* **2016**, *52*, 3284–3287.

[257] J. A. McCleverty, G. Wilkinson, L. G. Lipson, M. L. Maddox, H. D. Kaesz, in *Inorganic Syntheses* (Ed.: H.F. Holtzlaw), Wiley, **1966**, pp. 211–214.

[258] L. F. Dahl, C. Martell, D. L. Wampler, *J. Am. Chem. Soc.* **1961**, *83*, 1761–1762.

[259] Herrmann, Salzer, Eds. , *Synthetic Methods of Organometallic and Inorganic Chemistry: Volume 1: Literature, Laboratory Techniques, and Common Starting Materials*, Georg Thieme Verlag, Stuttgart, **1996**.

[260] H. F. Klein, H. H. Karsch, *Inorg. Chem.* **1975**, *14*, 473–477.

[261] Y. Nagata, Y.-Z. Ke, M. Suginome, *Chem. Lett.* **2015**, *44*, 53–55.

[262] J. W. Rathke, E. L. Muetterties, *J. Am. Chem. Soc.* **1975**, *97*, 3272–3273.

[263] N. Kuhn, T. Kratz, *Synthesis* **1993**, *1993*, 561–562.

[264] M. L. Luetkens, A. P. Sattelberger, H. H. Murray, J. D. Basil, J. P. Fackler, R. A. Jones, D. E. Heaton, in *Inorganic Syntheses* (Ed.: H.D. Kaesz), Wiley, **1989**, pp. 7–12.

[265] P. Patil, M. Ahmadian-Moghaddam, A. Dömling, *Green Chem.* **2020**, *22*, 6902–6911.

[266] H. Kessler, *Angew. Chem. Int. Ed. Engl.* **1970**, *9*, 219–235.